VDI Wissensforum

VDI-Berichte 2373

20th International VDI Congress
Dritev

June 24 and 25, 2020

Main topics:

- New series solutions from international OEs
- Integration of regulatory measures in the development
- Optimized mechanical components for hybrids and electric drives
- Concepts for conventional and electrified drives
- Data optimized development methods
- Challenges in systemic integration

VDI-BERICHTE
Herausgeber:
VDI Wissensforum GmbH

Bibliographische Information der Deutschen Nationalbibliothek
Die Deutsche Nationalbibliothek verzeichnet diese Publikation in der Deutschen Nationalbibliographie; detaillierte bibliographische Daten sind im Internet unter www.dnb.de abrufbar.

Bibliographic information published by the Deutsche Nationalbibliothek (German National Library)
The Deutsche Nationalbibliothek lists this publication in the Deutsche Nationalbibliographie (German National Bibliography); detailed bibliographic data is available via Internet at www.dnb.de.

Der VDI-Bericht, der die Vorträge der Tagung enthält, erscheint als nichtredigierter Manuskriptdruck.
Die einzelnen Beiträge geben die auf persönlichen Erkenntnissen beruhenden Ansichten und Erfahrungen der jeweiligen Vortragenden bzw. Autoren wieder. Printed in Germany.

ISSN 0083-5560
ISBN 978-3-18-092373-4

Content

New series solutions

System integration

Powertrain concepts

Components

New series solutions

Powertrain concepts

Drive solutions

Regulations

Methods

Online-Shopping für Ingenieure: Die Technische Literatur, die Sie brauchen!

Hier sichern Sie sich topaktuelles Ingenieurwissen aus den wichtigsten technischen Bereichen:

- 23 Reihen „Fortschritt-Berichte VDI“ mit aktuellen Dissertationen zu den relevanten technisch-wissenschaftlichen Themen
- Zahlreiche Titel zur Auswahl
- Tagungsbände „VDI-Berichte“ mit topaktuellem Ingenieurwissen und neuesten Forschungsergebnissen
- Sonderpublikationen, z. B. zum Thema Ingenieureinkommen

Willkommen im VDI nachrichten-Shop!

www.vdi-nachrichten.com/shop

VDI nachrichten
Die journalistische Heimat der Ingenieure.

Many thanks to the Gold-Sponsors of the Congress:

www.zf.com

www.castrol.com

Ford MACH-E Primary Electric Drive Unit

Greg Gardner, Ford Motor Company, Livonia Michigan, USA

Abstract

Full electrification of vehicles requires developing new electric drive units to transfer motor power to the wheels. For Ford's first BEV application we have chosen a concentric transverse mounted architecture to provide primary drive functions. Ford has worked with several supplier partners to develop an integrated e-transaxle consisting of a high voltage motor, inverter and system controller, final drive gearing, lubrication system, and a mechanical park mechanism for securing the vehicle. This architecture is flexible and "plugs and plays" into a range of 4x2 vehicles (single drive unit) and AWD/4X4 vehicles (two separate drive units). This paper will explore the development goals around Ford's first all-electric propulsion system.

Drive for Electrification

As global CO_2 standards become more and more stringent vehicle manufacturers will need to increase levels of electrification, both in the form of hybrid electric vehicles as well as full battery electric vehicles. In order to provide full electrification manufactures will need to develop all new propulsion systems that integrate the electric motor with appropriate gearing to transfer torque to the road.

Ford MACH-E Primary Drive Unit (PDU) Concept

The Ford MACH-E vehicle required the development of a transverse mounted PDU mounted at the rear of the vehicle and a transfer mounted SDU mounted in the front of AWD vehicles. This paper focuses on the PDU which was developed in conjunction with Borg Warner for the gearbox design and final assembly with an oil cooled e-motor manufactured by LG and an inverter system and controller manufactured by Denso. For package efficiency in Ford's vehicle the PDU utilizes a concentric in-line architecture utilizing a stepped planetary final drive arrangement. Cost efficiency is delivered by utilizing some key modules from Ford's electrified hybrid and conventional planetary automatic transmissions. These include an integrated park module developed with Stoneridge, an e-pump developed with GHSP, and an integrated cooler developed with Korens. Figure 1 provides a schematic of the PDU.

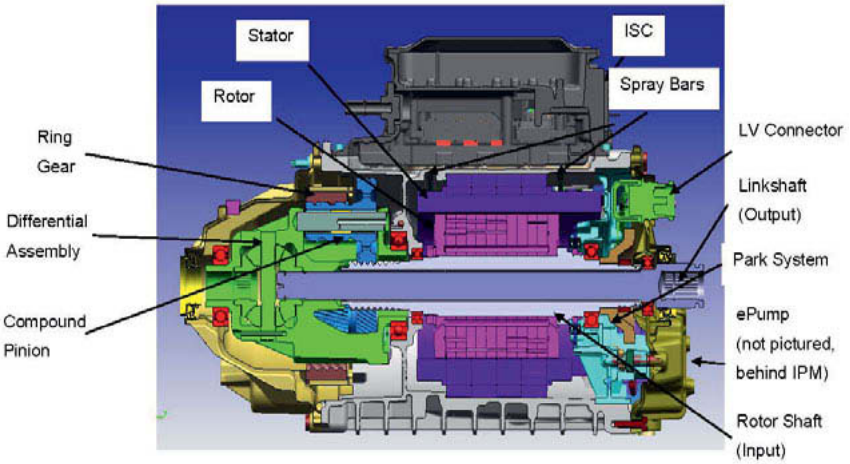

Fig. 1: Ford Mach-E PDU

Ford MACH-E Primary Drive Unit Design Features

The in-line PDU requires a stepped planetary arrangement in order to deliver its 9.05:1 final drive ratio. The final drive carrier is integrated into a cast iron differential for package efficiency utilizing full complement pinion bearings for maximum power density as shown in Figure 2. To provide for efficient cooling the Mach-E PDU features an integrated water to oil cooler assembly that mounts directly to the transmission case as shown in Figure 3. The integrated cooler is used to cool the ultra-low viscosity PDU fluid that is used to provide lubrication and cooling to the mechanical gear box components and cooling ot the motor assembly. To provide shorter electric wire paths, reduced resistance, and reduced electrical costs the inverter and motor controls are integrated into a common module that is direct mounted to the transmission as shown in Figure 4 and Figure 5. An integrated e-pump is incorporated into the PDU to provide lubrication and cooling functions. To keep cost low the e-pump is based off of the 10R80MHT pump design with a unique manifold and filter assembly provided by Filtran. The pump and filter assembly are shown in Figure 6. A permanent magnet oil cooled motor developed with LG serves as the propulsion mechanism in the PDU. The rotor and stator assemblies are shown in Figure 7.

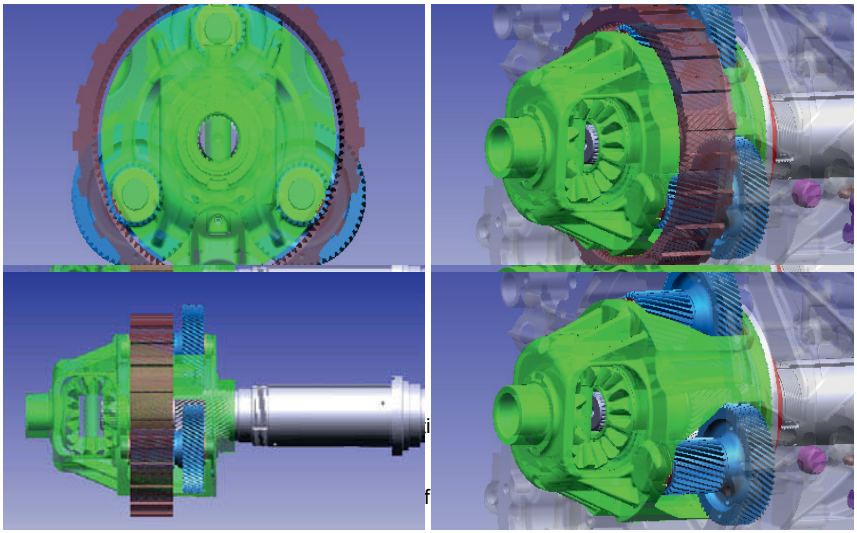

Fig. 2: Ford Mach-E Stepped Planetary and Differential Assembly

Fig. 3: Ford Mach-E Integrated Cooler

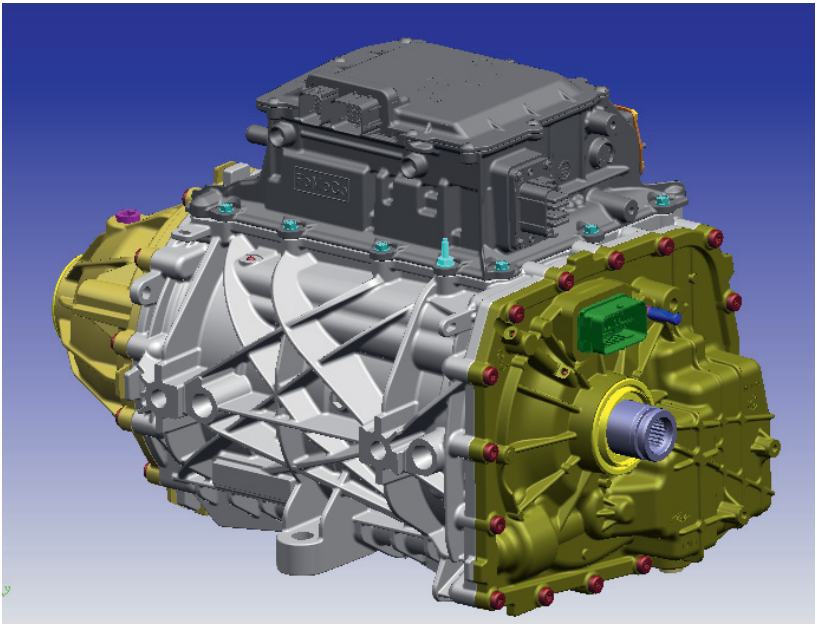

Fig. 4: Ford Mach-E Integrated Inverter and Motor Controls

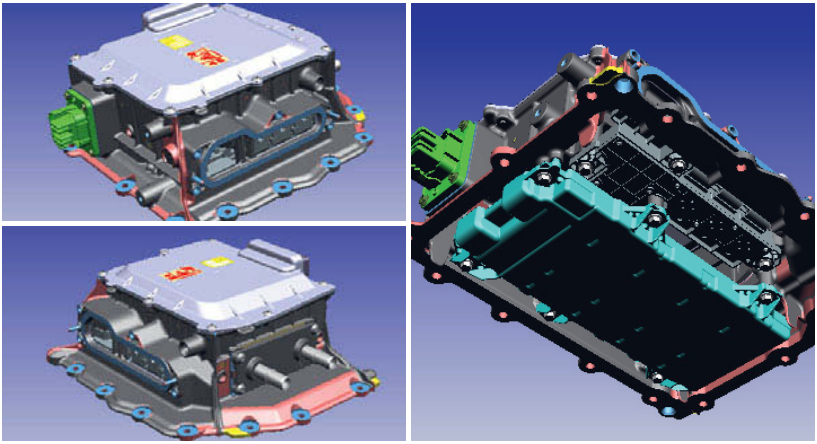

Fig. 5: Ford Mach-E Integrated Inverter and Motor Controls

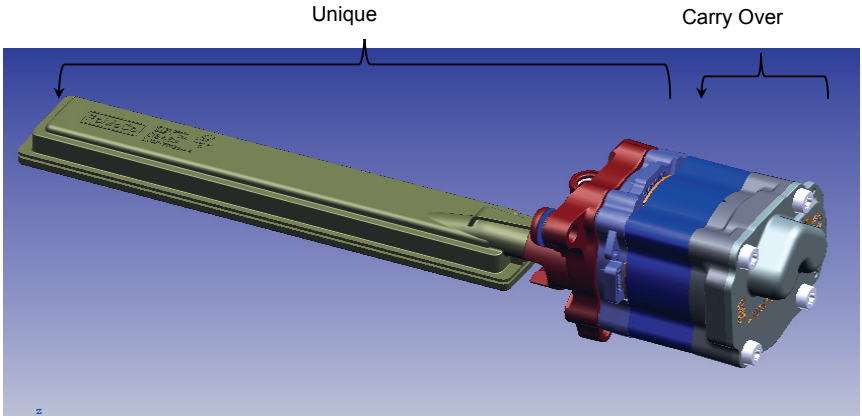

Fig. 6: Ford Mach-E E-Pump and Filter Assembly

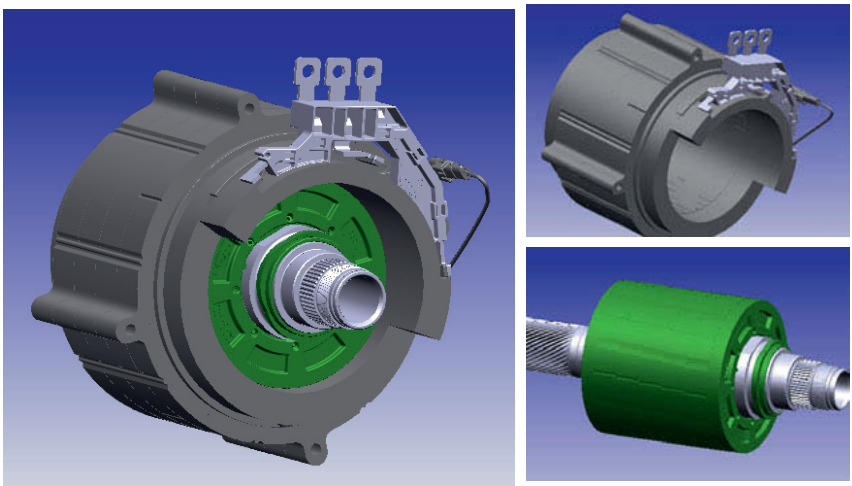

Fig. 7: Ford Mach-E Roter and Stator Assembly

In order to secure the vehicle when parked, a conventional automatic transmission park mechanism is integrated into the design. The park mechanism is actuated using an integrated internal park module unit which enables shift by wire functionality while delivering key safety requirements including automated return to park utilizing a Ford proprietary driver presence strategy and a default to park feature in the event of a loss of power state. For cost efficiency the internal park actuator is shared with the Ford hybrid portfolio. The internal park mechanism is shown in Figure 8. The use of an efficient in-line design results in an 111 kg PDU weight and features 210 kW and 430 NM of motor torque.

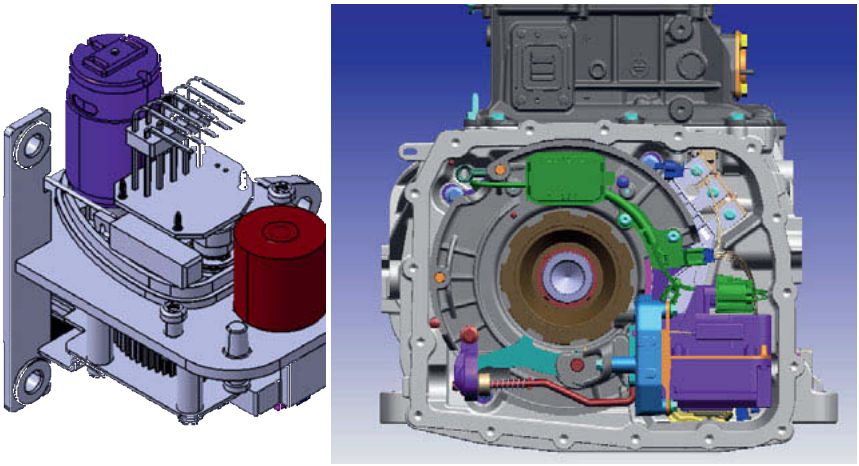

Fig. 8: Ford Mach-E Integrated Park Module

Conclusion

The in-line Mach-E PDU enables Ford to deliver a no compromise rear wheel drive battery electric vehicle architecture. This architecture offers efficient package efficiency while utilizing key catalog components that are shared across the Ford BEV and Hybrid portfolio. In addition the design is modular and can be utilized in both the primary drive position with an integrated park module or in the secondary drive position on all wheel drive vehicles without the integrated park system.

The front-axle drive of the MEB – Volkswagen expands the e-drive portfolio

Dipl.-Ing. **Peter Lück**, Dr. rer. nat. **Karsten Bennewitz**,
Dr.-Ing. **Jonas Tousen**, Dr.-Ing. **Johannes Peter**,
Volkswagen AG, Wolfsburg

Zusammenfassung

Der modulare elektrische Antriebsbaukasten (MEB) von Volkswagen [1] ist die Technologie-Plattform für die vollelektrischen Fahrzeuge der ID. Familie von VW und auch der Konzernmarken Seat, Audi, Skoda und VW Nutzfahrzeuge. Das erste auf dieser Plattform entwickelte Elektrofahrzeug ist der ID. 3, der derzeit in den Markt eingeführt wird. Mit dem ID. 4 wird die Elektro-Offensive von Volkswagen konsequent weiter vorangetrieben. Es ist das nächste von insgesamt 27 MEB-Fahrzeugen für emissionsfreie Mobilität auf den Markt, die beginnend ab Ende 2022 von verschiedenen Konzernmarken weltweit hergestellt werden. Neue Einblicke in den Allradantrieb des ID. 4 werden detailliert vorgestellt. Neben dem Hauptantrieb mit einer 150 kW Elektromaschine an der Hinterachse [2], [3] ist nun auch die Vorderachse elektrifiziert. Dafür kommt ein neu entwickelter Antrieb mit einer 75 kW Elektromaschine zum Einsatz. Die auf beide Achsen verteilte Gesamtleistung von bis zu 225 kW (306 PS) bietet ein beeindruckendes Allradantriebserlebnis.

Abstract

The Volkswagen modular electric drive matrix (MEB) [1] is the technology platform for the all- electric vehicles of the ID. family of VW and also the group brands Seat, Audi, Skoda and VW commercial vehicles. The first electric vehicle developed based on this platform, the ID. 3, is currently being launched. The electric vehicle push by Volkswagen is being systematically driven further forward with the ID. 4. This is the next vehicle to enter the market out of a total of 27 MEB vehicles that will be produced by various group brands worldwide starting from the end of 2022, with the goal to establish zero-emission mobility. Within this paper, new insights into the all-wheel drive train of the ID. 4 are presented in detail. In addition to the main drive with a 150 kW electric machine on the rear axle [2], [3], the front axle is also electrified. A newly developed drive with a 75 kW electric motor is used for this purpose. The total power of up to 225 kW (306 HP) distributed between both axes provides an impressive all-wheel drive experience.

1. Introduction

With the ID. family, Volkswagen is introducing a diverse fleet of zero-emission vehicles that customers will find attractive and it is a consistent and systematic way to advance the development and establishment of carbon-neutral mobility. Some ID. family members have already been presented to the public as concept cars. As the first model from the ID. family, the ID. 3 will be available on the market this year (2020) – a carbon-neutral, four-door electric compact car (fig. 1) with full connectivity, impressive driving dynamics and a range of up to 550 kilometres. The sales price enables a wide range of customers to enter the world of electric mobility.

Fig. 1: The ID. 3

New models in other segments will soon follow the ID. 3. All models have in common that the high-voltage battery is located at the centre of the vehicle between the axles. The HV battery is scalable, adaptable for various cell types, and features integrated liquid cooling. This means that it is relatively easy to integrate it into the various ID. models performance levels. Accordingly, ranges of approx. 330 km to over 500 km are possible depending on the battery size and the ID. model. An AC charger with a charging power of up to 11 kW is integrated, and a DC charging power of up to 125 kW is possible using combined charging system (CCS) equipment.

Two drives can be used in the MEB platform. The ID. 4 will be the first vehicle on the market with an MEB electric drive offered on the front axle in addition to the rear-axle drive. Volkswagen uses a permanent-magnet (PM) synchronous machine with a power of up to 150 kW (204 HP) on the rear axle. For models with all-wheel drive, like for the ID. 4 powertrain (fig. 2), Volkswagen is expanding the MEB portfolio to include an induction machine on the front axle. This machine delivers up to 75 kW (102 HP). In order to get smooth power output, both electric machines are combined with a single-speed transmission. In contrast to the rear machine, with its 310 Nm transmitted in a parallel-axis design, the front machine uses a coaxial design for its 160 Nm.

Fig. 2: MEB floor assembly in the ID. 4

The rear axle drive (PM synchronous machine) is characterized by high efficiency and high power density as well as constant power output over a wide speed range, which makes it possible to cover normal driving completely. The front-axle drive (induction machine), in contrast, is characterized by its ability to handle short-term overloads, as well as by low losses when it is driven through the road by the rear-axle machine. Accordingly, it is extraordinarily suitable as a boost drive, which in addition to the rear-axle drive handles four-wheel drive functionality, too. The coaxial design of the induction machine enables integration into the vehicle front end. As a result of the specific design, the front end in the MEB platform is relatively compact due to the short overhang.

2. High-voltage battery

The high-voltage battery (HV battery) is a system with multiple modules that are connected in parallel and in series. The individual modules, in turn, are made up of multiple battery cells. A powerful cooling system ensures that operation remains in the optimal temperature range of 25 to 35°C even under high loads or low ambient temperatures. Cell module controllers and a central battery energy management system monitor the currents, voltages and temperatures. This ensures that the MEB's high-performance lithium-ion HV battery, which is designed for a wide range of operating and temperature conditions, remains highly suitable for daily use with a long service life. In addition, it is characterized by a reproducibly high power output for the electric drives in a wide range of temperature and state-of-charge (SOC) levels.

The MEB takes full advantage of the technological possibilities offered by electric mobility. The HV battery is integrated centrally into the vehicle floor assembly in a compact manner that saves space. The vehicle was practically developed around the HV battery. This design approach has yielded numerous advantages in terms of positioning of powertrain components and ancillaries. In addition, the flat design of the HV battery allows a spacious vehicle interior between the axles. They also enable a weight distribution of almost 50 percent per axle. In combination with a low centre of gravity, this ensures the best possible conditions for all-wheel drive and the best possible driving characteristics.

A crash frame integrated into the HV battery housing protects the HV battery modules and ensures optimal stability. This means that the housing itself can be made of aluminium, which results in significant weight savings. Underbody cladding that is also made of aluminium is provided on the vehicle underbody as an additional protective element. It also optimizes the aerodynamics of the vehicle.

3. Charging technology

Current forecasts suggest that most of the ID. fleet is charged only once a week. It is estimated that 50 percent of charging will take place at home. Accordingly, MEB-based vehicles come with a type 2 vehicle inlet as standard which can be used for charging from an AC source. Possible charging powers are either 2.3 kW via a standard domestic outlet or 11 kW via a wall-box. AC charging via the wall-box provides enough power to fully charge the vehicle battery overnight. Since DC power is generally required to charge the HV battery, an 11 kW charger is integrated into the vehicle. This charger converts the alternating current from the outlet, wall-box, or AC charging station into direct current.

The optional CCS vehicle inlet enables significantly shorter charging times. In this case, the standard type 2 vehicle connector is combined with two additional power contacts for DC charging (fig. 3). With this vehicle inlet, the HV battery can be charged with a charging power of up to 125 kW. This makes it possible to recharge 80 percent of the HV battery energy within 30 minutes.

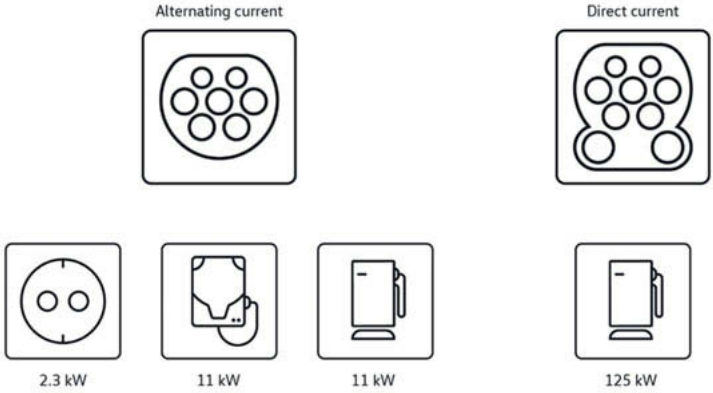

Fig. 3. Overview of MEB charging technology

In the long-term, the MEB is also ready for inductive charging. This charging method does not require any cables or connectors. The vehicle simply parks over a charging pad that charges the HV battery.

4. Electric axle drives for the MEB

For the MEB, two newly developed electric axle drives are available. A PM synchronous machine on the rear axle serves as the main drive. The drive consists of the electric machine, a power inverter and a single-speed transmission in a parallel-axis configuration. The PM synchronous machine delivers 150 kW of power, 310 Nm of torque and a maximum speed of 16,000 rpm. It is characterized by high power density, high efficiency and constant power output over a wide speed range. This drive was already presented in detail at the 19th International VDI-Congress in Bonn [3].

Depending on the specific vehicle design, MEB vehicles can also be driven by a front-axle drive. In this case, an induction machine with a power inverter and a single-speed transmission in a coaxial configuration is used for boost and all-wheel drive functionality (fig. 4). The induction machine has 75 kW of power, 160 Nm of torque, and a maximum speed of 13,500 rpm. This type of machine is characterized by its ability to handle short-term overloads, as well as by low losses when not being actively operated but is driven through the road by the rear-axle drive.

The design of the induction machine front-axle drive is described below. The principal differences between a PM synchronous machine and an induction machine are discussed, and the technical characteristics and performance specifications for the new machine in the ID. 4 are presented.

4.1 Induction machine front axle drive

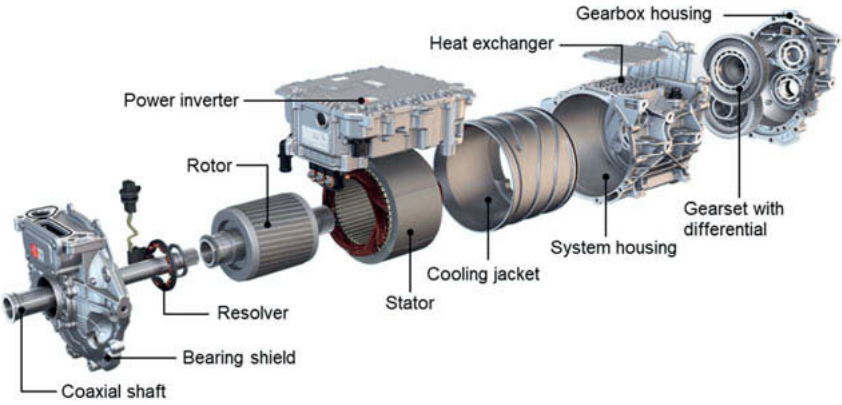

Fig. 4: Exploded view of MEB front-axle drive

The electric drive for the front axle is designed as a three-phase induction machine with two pole pairs and an aluminium squirrel cage in the rotor. It consists of the following main assemblies: power inverter, housing, stator, rotor, resolver with a temperature sensor, and a two-step single-speed transmission in a coaxial design.

The stator and the rotor are integrated in a cast housing in which the cooling system of the drive is also integrated. The rotor bearings are located in the system housing on the transmission side (A side) and in a bolted bearing shield on the opposite side (B side).

The openings and the terminal board for the three-phase connection, the resolver for determining the rotor speed, the temperature sensor system for determining the winding temperature and the signal connector are located on the bearing shield on the B side. The bearing shield on the B side is closed by a bearing shield cover. The signals from the resolver and the temperature sensor are transmitted to the power electronics via a connector.

The single-speed transmission reduces the speed of the electric machine for driving the wheels. The gear set, including the differential, is enclosed by the transmission case and bolted onto the system housing. Overall, the highly integrated components result in a very compact, relatively lightweight drive (fig. 5).

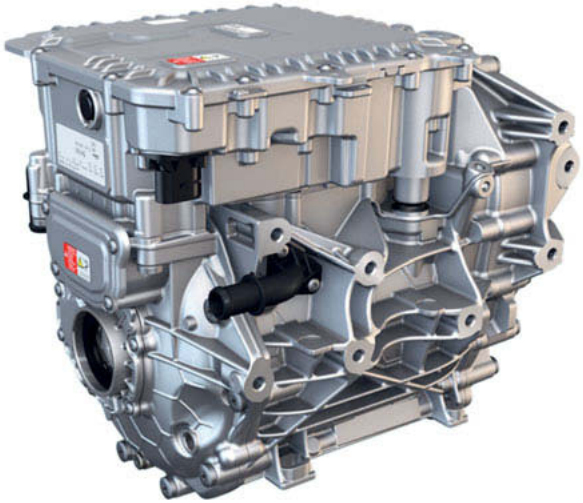

Fig. 5: MEB front axle drive

4.2 Power inverter

The three-phase current for the MEB front axle drive's induction machine is generated by a liquid-cooled power inverter that is mounted directly on the electric machine. Figure 6 shows an exploded view of the power inverter.

Three insulated-gate bipolar transistors (IGBTs) are connected inside the power inverter to form a B6 bridge. The IGBTs are kept at a constant temperature by the coolant circuit via a nickel-plated copper cooling plate and are enclosed in the module carrier so that the driver board can be plugged onto and therefore connected to the contact pins on the power module. Before the coolant in the power inverter housing is conveyed to the electric machine, it flows across the DC link capacitor, cooling it down as well. The connection between the coolant circuit and the machine is implemented by means of an interface with the help of a connecting and sealing element when positioning and bolting the power inverter. The controller board is

mounted above the module carrier and the gate driver board in order to save space. Additional assemblies in the power inverter include the electromagnetic compatibility (EMC) filter unit for the DC input and the busbars for the electric machine's AC connection.

The power inverter's modular design is intended for the industrialization of large quantities. Moreover, the power inverter's fully automated production ensures both assembly and functional quality even with large quantities. Of particular note is the compact and space-optimized design for the greatest possible integration density in the MEB front end, which no longer has a classic engine compartment.

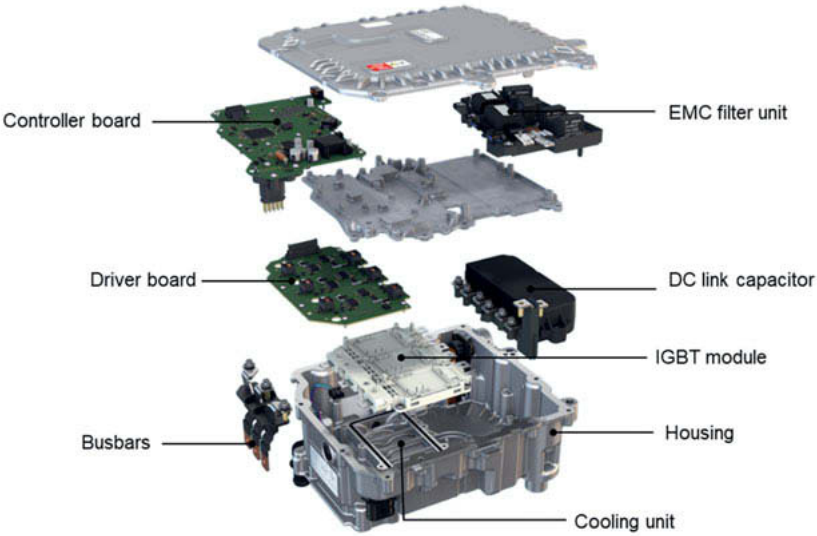

Fig. 6. Power inverter assembly

Some vehicle functions, such as vibration damping and anti-slip control functions were integrated directly into the power inverter. This makes it possible to implement interventions without any delay and without bus communications. The integration of individual vehicle functions in the power inverter results in more direct options for modifications during the development process and driving characteristics that are optimally tuned for the vehicle.

4.3 Electric machine

Driven by the power inverter accordingly, an electric machine converts the electrical energy into mechanical energy. First, the operating principle of the induction machine will be differentiated from that of a PM synchronous machine, and then the components of the induction machine will be presented.

Operating principle of the PM synchronous machine

The current in the stator's three-phase copper windings generates a rotating magnetic flux ("rotating field"). The exciter magnetic field in the rotor is generated without losses by permanent magnets and permeates the stator. This results in a circumferential force when the rotor's rotational speed and the stator's rotating field are identical (synchronous) (fig. 7, left).

Operating principle of the induction machine

The current in the stator's three-phase copper windings generates a rotating magnetic flux ("rotating field") that permeates the rotor with its squirrel-cage windings. The induction machine's rotor rotates during operation with a slightly slower speed than the stator's rotating field (asynchronous). This induces a voltage into the squirrel-cage windings that in turn results in a current. The magnetic field that this produces in the rotor results in a circumferential force that acts as torque on the rotor shaft (fig. 7, right).

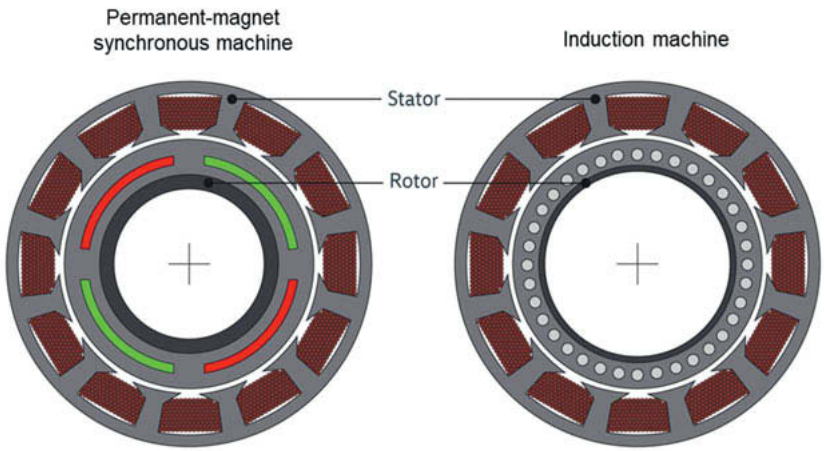

Fig. 7: Schematic diagram of a PM synchronous (left) and an induction machine (right)

Stator assembly

The stator essentially consists of the laminated core and the three-phase round-wire winding (fig. 8). The laminated core consists of individually welded and stacked laminations with an outer diameter of 200 mm. The sheet metal used to produce the laminations has a high magnetic permeability, a thickness of 0.27 mm, and is coated on both sides with an electrical insulating layer.

A special production equipment unit is used to automatically pull the coils into the stator slots, to produce the ultimate shape of the winding overhang and to connect the cable lugs to the three phases. The temperature sensor system is buried in the winding overhang. To achieve additional insulation and a better thermal connection and strength for the winding, the stator is impregnated with resin. The finished stator goes through automated test processes and is joined with the stator carrier in a shrinkage process. The water jacket for the stator consists of the intermediate space that is located between the stator carrier and the system housing and is sealed with O-rings after they have been bolted together.

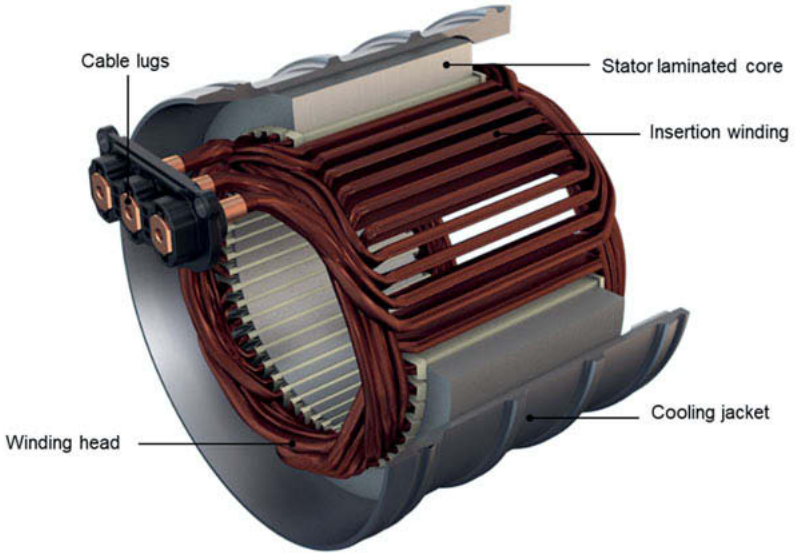

Fig. 8: Induction machine stator

Rotor assembly

The rotor is made up of a shaft with integrated teeth, balancing discs, a resolver rotor and a pressed-on rotor laminated core of individual laminations with a sheet thickness of 0.27 mm, which are evenly offset in relation to each other so that, for the squirrel cage's bars, there is a continuous angle over the length of the rotor (fig. 9). This ensures that torque will be produced in a more even manner and that optimized acoustic characteristics will be achieved. The individual bars are electrically connected via the short-circuit rings, which are located on both sides of the laminated core and that complete the squirrel cage's aluminium casting.

The rotor shaft with its gearing is mounted in a cantilever position and designed as a hollow shaft through which the transmission output shaft is guided coaxially. Friction-optimized, oil-lubricated deep-groove ball bearings are used for the rotor shaft, as well as for all shaft bearings. In terms of the vehicle's total range, minimizing the front axle drive's mechanical losses is of considerable importance, since this influences the overall road load, including during pure rear-wheel drive (two-wheel drive) operation.

The number and design of the slots in the rotor core cut section have been optimized in terms of the following important target factors in connection with the stator core cut section: performance, efficiency, and acoustics.

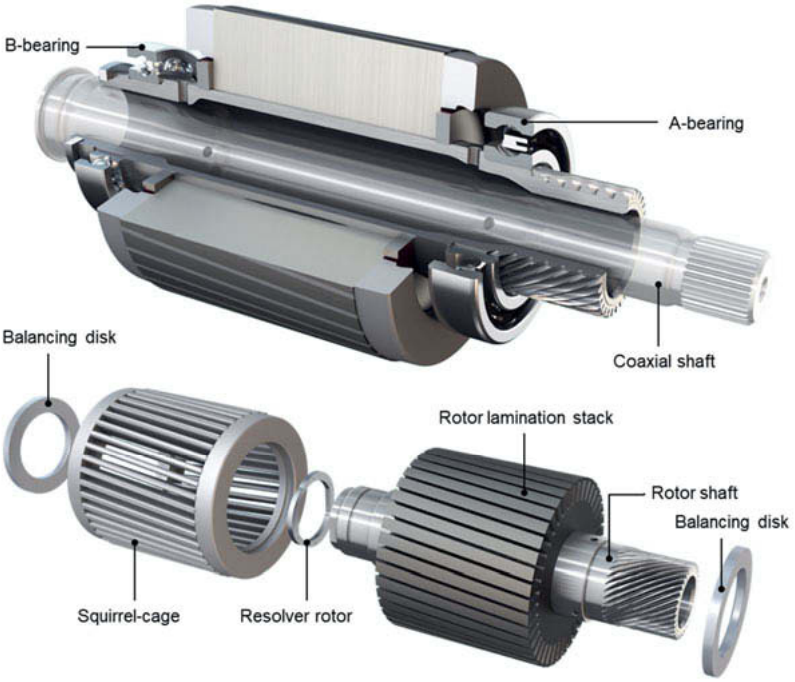

Fig. 9: Induction machine rotor
Top: Assembled rotor with guided-through coaxial shaft and bearing
Bottom: Exploded view of rotor components

4.4 Single-speed transmission

In order to drive the wheels, the torque and speed (maximum 13,500 rpm) of the electric machine are converted by the single-speed transmission. The overall gear ratio is achieved with a two-step spur-gear system via an intermediate shaft. The output is ultimately coaxial as a result of the transmission output shaft is guided through the hollow rotor shaft (fig. 10).

In addition to the pure torque and speed conversion, the transmission is largely responsible for acoustically perfect operation. For this purpose, the macro and micro geometries of the gear tooth system and the housing have been optimized in terms of their acoustic properties. The transmission components are supplied with oil that is factory-filled for life. In addition to

the pure lubrication function, the oil also takes care of the cooling function for the electric machine. A gear pump is required for the oil circuit, which is driven via the transmission's intermediate shaft and which is housed in the intermediate shaft bearing on the machine side.

In order to achieve friction-optimized operation, a deflector is used in a targeted manner to keep the oil away from the areas where the gear tooth system would otherwise cause splashing during operation. In addition, only easily-running deep-groove ball bearings are used in order to minimize losses when being driven by the other machine. The overall gear ratio is 9.95:1 and enables the ID. 4 to reach a top speed of 180 km/h.

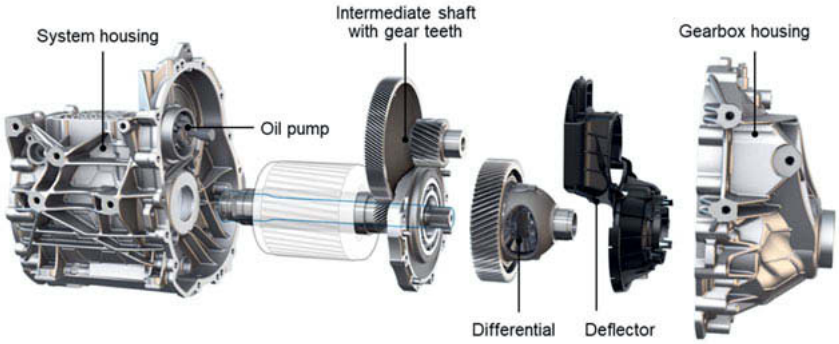

Fig. 10: Single-speed transmission of ID. 4 front-axle drive

4.5 Electric axle-drive cooling system

Heat is dissipated from the electric axle-drive by liquid coolant and oil cooling. The coolant is first conveyed through the power inverter so that there will be the greatest possible difference in temperature between the semiconductors and the coolant. After the coolant flows through the power inverter, the coolant enters the electric machine housing's water jacket via a sealing connecting element.

The losses in the stator are dissipated onto the electric machine housing's water jacket via the laminated core. The heat loss in the windings must first overcome the thermal resistance of the insulation system. Heat is also dissipated from the rotor to the water jacket via the air gap to the stator. The coolant is conveyed in a spiral pattern in cooling channels that are located between the stator carrier and the outer housing and that are optimized for pressure losses. It is then conveyed into the vehicle's outer coolant circuit through a coolant distributor at the end of the water jacket (fig. 11).

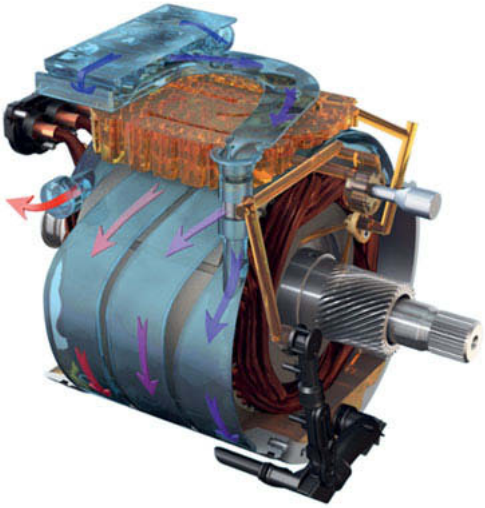

Fig. 11. Coolant flow through the power inverter and the induction machine's water jacket

Since heat is dissipated from the windings in the stator and the squirrel cage in the rotor to the water jacket via multiple thermal resistances, the achievable heat flow from the components into the coolant is limited. To be able to place a higher load on the induction machine, the electric machine components with an electromagnetic effect require additional cooling. This cooling is achieved via direct contact with the oil that is also used to lubricate the bearings and the gear tooth system parts. There is a shared oil management strategy in the group formed by the electric machine and the transmission.

The oil is sucked in via an oil pump that is integrated into the intermediate shaft's gear and is then pumped through an oil/coolant heat exchanger that is integrated into the cast housing, which is sealed with a cover and is located between the electric machine and the power inverter. After this, the cooled-down oil is directed towards the rotor's short circuit rings via the channels in the cast housing intended for this purpose. From the short circuit rings, the oil is hurled by the centrifugal force of the rotating rotor towards the stator's winding overhangs so that the oil can absorb the heat loss produced in the coils (fig. 11). Afterwards, the now heated oil is collected at the lowest point of the housing and is then sucked in again by the oil pump (fig. 12).

Fig. 12. Oil cooling of the rotor and stator

The combined coolant and oil cooling makes it possible to significantly expand the drive's operating limits. In particular, the constant power output of the induction machine benefits from the direct oil cooling of the rotor and stator.

4.6 Technical specifications for the electric drives in the ID. 4

The MEB axle-drives for the ID. vehicle family deliver remarkable drive power over a wide speed range. Both drives have an integrated power inverter. Due to their specific requirements,

they differ significantly in terms of design. The following table shows a comparison between the two drives.

Table 1: Drives in the ID. 4

		MEB rear-axle drive	MEB front-axle drive
Machine type		PM synchronous machine	Induction machine
Design voltage	[V]	320	320
Power (peak, 30 s)	[kW]	150	75
Max. torque	[Nm]	310	160
Max. speed	[1/min]	16,000	13,500
Gear ratio		11.5 : 1	9.95 : 1
Design		Parallel-axis	Coaxial
Power inverter		Integrated	Integrated
Total weight	[kg]	90	60

Figure 13 shows the characteristics for both electric machines, which indicate the maximum torque and power over the respective speed range. These characteristics make it clear that both electric machines are limited at their rated power. The total power and the power curve may vary depending on the ID. models.

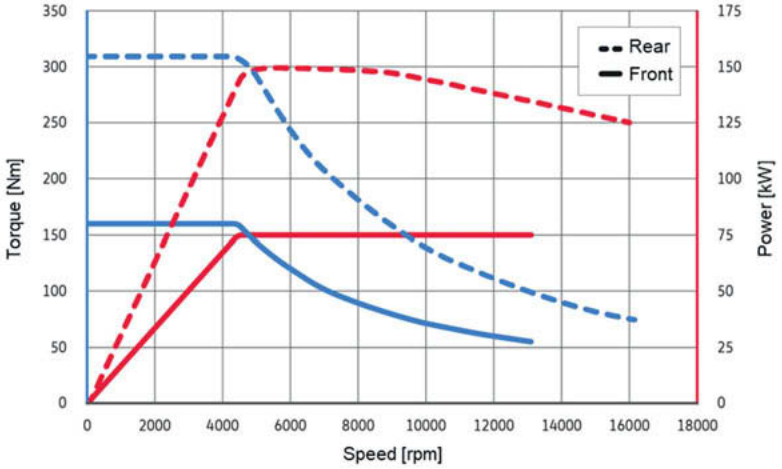

Fig. 13: Full-load diagram for PM synchronous (rear axle) and induction machine (front axle)

Below, figure 14 shows a characteristic map with the overall efficiency for the electric drive (power inverter, electric machine, transmission). There is a large efficiency zone in the range around 90%, which makes it possible to achieve long ranges in all-wheel drive operation.

The electric drives for the rear and front axle are designed for maximum efficiency according to their operating strategies in the all-wheel drive train. For various driving cycles, the ranges of maximum energy conversion are detected in the drive characteristic map and then the efficiency within these ranges is optimized to enable the greatest possible range for ID. 4 all-wheel drive vehicles. While low internal friction losses are important for both drives, the focus for the primary drive on the rear axle is on the highest possible efficiency in the low-load range and at moderate speeds in order to minimize the total energy consumption in the relevant driving cycles. The secondary front axle drive only switches on for sporty driving styles when the rear-axle drive hits its operating limits. This operating strategy ensures that the all-wheel drive train in the ID. 4 is used in the most efficient manner.

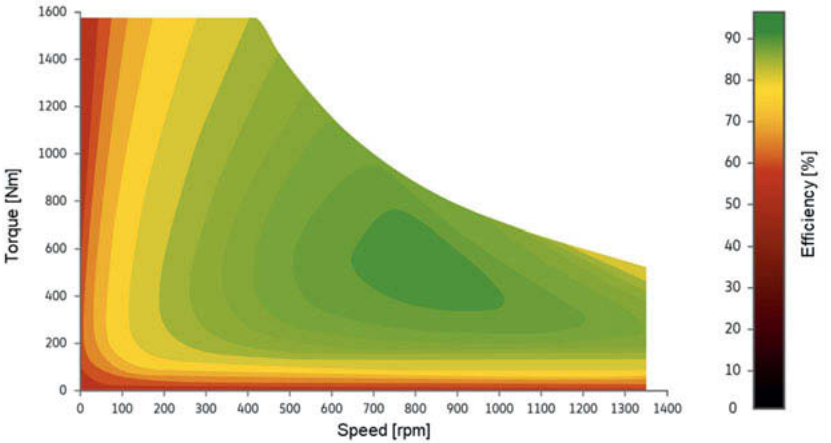

Fig. 14. Efficiency characteristic map of front-axle drive

5. Summary

The drive systems in the Volkswagen MEB are part of a modular assembly matrix with components that enable various powertrain configurations for electric vehicles.

For the ID. 4, an innovative front-axle drive is being developed that makes it possible to have powerful electric all-wheel drive operation that is optimal in terms of power consumption in combination with the rear-axle drive. The specific technological highlights of this front-axle drive include the highly integrated and compact design of its components as well as its efficient dual cooling system. The combination of liquid coolant and oil cooling achieves a high available power and high utilization of the active parts of the induction machine.

The new all-wheel drive powertrain extends the drive portfolio in the Volkswagen Group for future models in the ID. family. The modular assembly matrix makes it possible to achieve large quantities for the various individual components, which in turn can reduce direct costs. Together with the attractive driving characteristics of the new all-wheel drive train, this further increases the attractiveness of electric mobility.

Literature

[1] F. Welsch.
ID. Volkswagen – einfach elektrisch
40th Vienna Motor Symposium, Vienna, 2019

[2] K. Blumenröder, K. Bennewitz, P. Lück, et.al.
Der neue Modulare E-Antriebs-Baukasten von Volkswagen
40th Vienna Motor Symposium, Vienna, 2019

[3] K. Bennewitz, P. Lück, J. Tousen
Volkswagen's electric drivetrains of the new modular e-drive kit (MEB)
DRITEV – 19th International VDI-Congress, Bonn, 10./11.07.2019

The highly integrated ModulED drive module

Holistic concept design

Dipl.-Ing. **Daniel Kieninger**, **Jonas Hemsen**, M.Sc.,
Gordon Witham, M.Sc., Institute for Automotive Engineering (ika),
RWTH Aachen University, Aachen

1 Zusammenfassung

Innerhalb des EU Förderprojekts “ModulED” forschen 9 Partner aus 6 Nationen an einem hochintegrierten elektrischen Antriebsmodul für Straßenfahrzeuge. Es hat eine Spitzenleistung von 157 kW und vereint innovative Technologien im Bereich der elektrischen Maschinen, der Leistungselektronik und des Getriebes: Es verfügt über eine Hochdrehzahl-Hybridsynchronmaschine mit sechs Phasen und eingespritzten Polymermagneten, ein hochübersetztes Zweiganggetriebe mit doppeltem Planetenradsatz (Ravigneaux-Zahnradsatz) und eine Leistungselektronik aus Galliumnitrid (GaN) mit Wicklungsumschaltung. Die Kombination dieser Komponenten in einem einzigen Gehäuse macht das Antriebsmodul flexibel integrierbar in reinelektrische oder hybride Antriebsstrukturen. Derzeit befinden sich Prototypen im Aufbau, welche Mitte 2020 getestet werden sollen.

Zusätzlich zur Hardware wird vom Institut für Kraftfahrzeuge (ika) der RWTH Aachen eine innovative, ganzheitliche Auslegungsmethodik für Antriebssysteme entwickelt. Durch eine integrierte und automatisierte Komponentenauslegung wird es möglich, die komplexen physikalischen Abhängigkeiten zwischen den Komponenten schon bei der Auslegung zu erfassen und so anwendungsoptimale und abgestimmte Antriebsmodulkonzepte zu ermitteln.

2 Abstract

Within the EU funded project "ModulED", 9 partners from 6 nations research on a highly integrated electric drive train module for road vehicles. It has a peak power of 157 kW and combines innovative technologies in the field of electric machines, power electronics and transmission: It features a high-speed hybrid synchronous machine with six phases and injection mold polymer-bonded magnets, a high-ratio dual-speed transmission with double planetary gear set (Ravigneaux gear set) and gallium nitride (GaN) power electronics with winding reconfiguration capability. The combination of these components in a single housing makes the drive module

flexible to integrate in electric or hybrid drivetrain structures. Prototypes are currently under construction and will be tested in mid of 2020.

In addition to the hardware, an innovative holistic drivetrain design methodology is being developed by the Institute for Automotive Engineering (ika) of RWTH Aachen University. By means of an integrated and automated component design it is possible to detect the complex physical dependencies between the components already during the design phase and thus to determine application-optimal and coordinated drive module concepts.

3 ModulED – Technology and Status

Within the EU funded project "ModulED", 9 partners from 6 nations research on a highly integrated electric drive train module for electric vehicles using innovative technologies and new design methods. This module and its research and development areas are shown in Fig. 1. After a brief description of the technologies used in the prototype, the holistic design method developed within ModulED is presented in more detail.

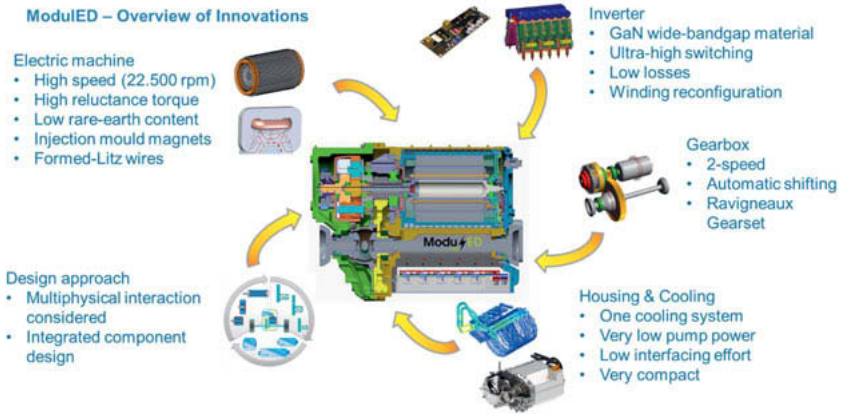

Fig. 1: ModulED drive module

The electric machine is a 6 pole, 6 phase hybrid synchronous permanent magnet machine for high speeds up to 22,500 rpm. The stator windings are made from a special wire type called *"formed litz wire"*. The permanent magnets are injection molded into the rotor sheet stack. To reach the full potential of polymer-bonded magnets, the injection has to be performed under an intense magnetic field to order magnetic particles in the same direction.

The inverter is based on gallium nitride (GaN) switches. The advantage of very low losses of the GaN switches comes with the drawback of reduced current capability in comparison with classical (silicon) IGBTs. Here, per switch, four GaN switches are operated in parallel to increase current capability. The six-phase configuration enables so called *"winding reconfiguration",* where two phases can be supplied either in series or individually. By dynamically switching between these two modes, the best operation behavior can be achieved at any time.

The herein used transmission is a 2-speed automatic transmission with ratios of 21.9 and 12.2. The challenge in transmission design is to achieve these high ratios with good efficiency, NVH, costs and compact dimensions. Within this project, numerous combinations of cylindrical gears and planetary gear sets have been investigated and evaluated regarding their suitability for the given task. The identified setup is a shiftable Ravigneaux gear set, followed by a cylindrical gear reduction stage.

The cooling subsystems of the motor and inverter run in parallel to reduce the required coolant pump power. The motor cooling itself uses several parallel channels. Having only one cooling circuit and all components integrated in one housing leads to a very compact overall design.
The integration of motor, inverter and transmission into a single housing unit simplifies the powertrain assembly in the vehicle and reduces the cost of interfacing by eliminating connectors, cables and covers. At the same time, a modular approach allows exchanging individual parts for repair. Further information on the developed drive module has been published in [1].

The development of the ModulED drive module was accompanied by a holistic concept design. For this purpose, a design environment has been created at the Institute for Automotive Engineering (ika) of RWTH Aachen University, with which drive modules can be designed and evaluated holistically based on vehicle requirements. This development approach and the resulting method will be presented in the following.

4 Holistic Concept Design of Drive Modules

The properties of electric drive modules result from the multiphysical interaction of the components. As an example, the size and costs of the electrical machine can be reduced by high-speed concepts, but this requires higher transmission ratios and therefore additional effort on the transmission side. In addition to the geometric properties, this also influences the resulting total losses and the thermal management of the module. Due to the complexity of interactions, an optimization on component level will only lead to a local optimum.

Furthermore, the knowledge of the design processes is often distributed over the individual component development sections or divided in classical domains (e.g. mechanical, electrical, magnetic, thermal or NVH), which complicates the optimization of the overall design. The design process is therefore done mostly sequential and iterative, which extends the development time and makes it more difficult to find the best overall drive system design.

In order to overcome these problems, a holistic approach targeting system optimization is required. The efforts and benefits on component level should be weighed up against each other on system level. To enable a holistic conception and optimization of electric vehicle drives, the Institute for Automotive Engineering (ika) of RWTH Aachen University developed the method of integrated component design.

4.1 Design Process

The developed design method consists of two main stages, the "*rough layout*" and the *"fine layout*". The full process was introduced in [3] and [4] is illustrated in Fig. 2.

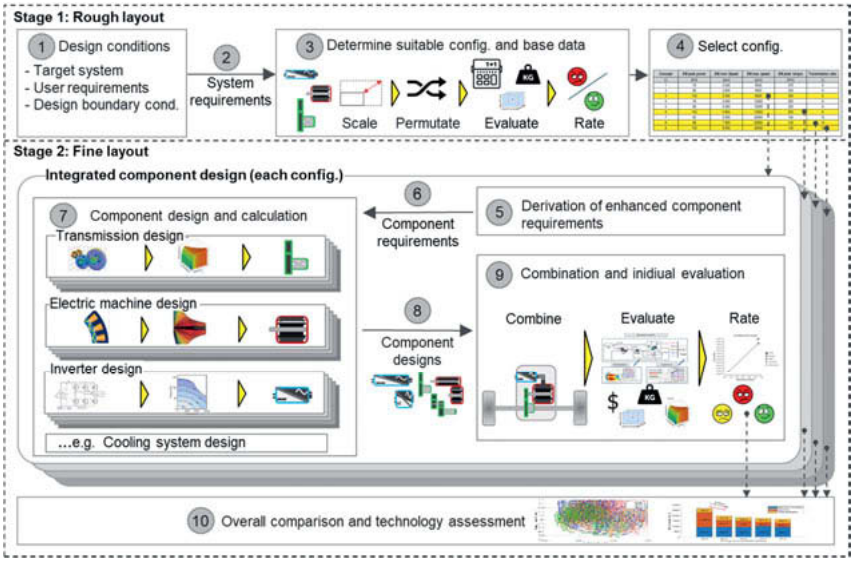

Fig. 2: Holistic concept design method for drive modules

The first stage is a rough layout, which results in pre-filtering to relevant component configurations. Various scaled component parameter sets are tested against the driving requirements and rated (1 - 3). The determination of vehicle characteristics is done with simplified component models and fast analytical calculations. Promising rough design variants are selected for further evaluation (4). The basic parameters of their components (power, torque, etc.) are a result from the first concept stage. This procedure corresponds to the state of the art. Stage 2 represents the fine design procedure using the integrated component design (5 - 9). This process runs in parallel for each selected concept from the rough layout. On vehicle level, enhanced component requirements based on the results of the rough design are derived (5). Suitable transmission, electric machine and inverter setups are created at component level by the integrated design modules (7). The vehicle level combines the component variants to drive modules and determines the resulting system properties such as costs, mass, volume and more. Furthermore, performance data and energy consumption for representative drive cycles are evaluated by means of longitudinal dynamic vehicle simulations (9). Advantages and disadvantages of e.g. high-speed concepts or multi-gear concepts and their effects on the other components are considered in this way to quantify the advantages on system level. After all design processes have run through, the multiple variants of each considered concept (selected rough designs) are compared against each other in an overall evaluation (10). This results in global optima and general trends of different concepts can be derived. The successful concepts of each rough design variant are then compared with each other (e.g. best high speed vs. best high torque concepts). The suitability of different technologies for concepts (e.g. SiC material for high-speed concepts) or optimization targets (high-speed for low loss suitable) can be evaluated.

4.2 Transmission: Design and Calculation Process

The aim of the design process is to determine promising transmission concepts while maintaining the service life requirements. For these transmission concepts, the relevant transmission properties at vehicle level, which are essentially the dimensions, masses and transmission losses, must be determined. This results in the requirement to carry out the design process until these properties are determined with high accuracy. This process is presented in detail in [2].

Fig. 3 shows the integrated transmission design process. The requirements (A) derived from an analytical rough design on vehicle level serve as input. The transmission load collectives, relevant for the service life and efficiency evaluation are determined from a defined sequence of driving cycles from the vehicle level.

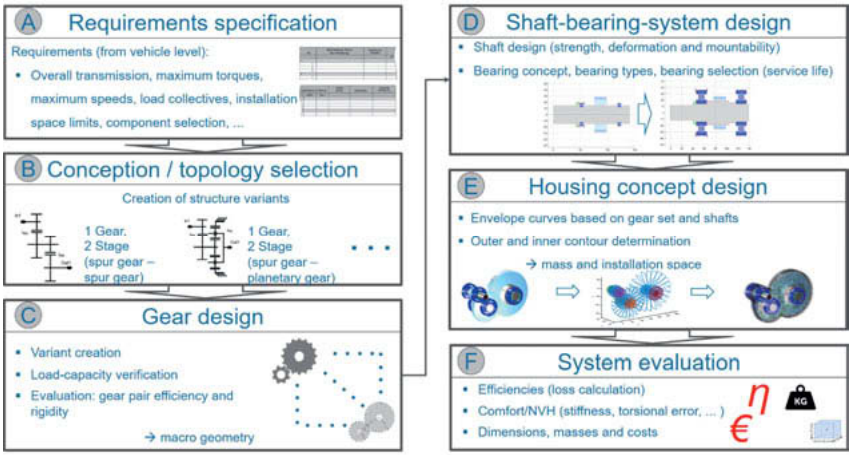

Fig. 3: Transmission design process

If no gear topology is specified, a topology selection is made (B). In next step, gearing variants are formed and the load carrying capacity is verified (C). A macro geometry variant is selected for further analysis. Based on the gearing geometry, the gear forces and thus all shaft bearing systems can be calculated and designed (D). At the end of the concept creation, a housing is created based on the envelopes of the gear elements (E). The detailed concept up to this step enables an analytical efficiency evaluation of the transmission. This is done by integrating all losses of the individual components for which data and load conditions are now known (F).

Each of these design steps in turn consists of several functions and process chains to fulfill the subtask. Fig. 4 exemplarily shows the sub-process of the housing design. The housing design process generates a suitable housing based on the transmission designed up to this point and evaluates its characteristic properties such as mass and installation space. The sub-processes have been presented in detail in [1].

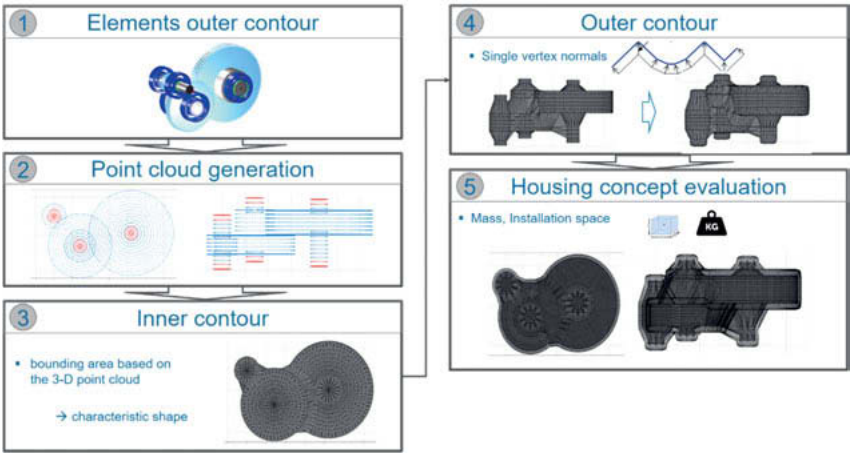

Fig. 4: Housing design process

4.3 Electric Machine: Design- and Calculation Process

The design and calculation process for the electric motor is shown in Fig. 5

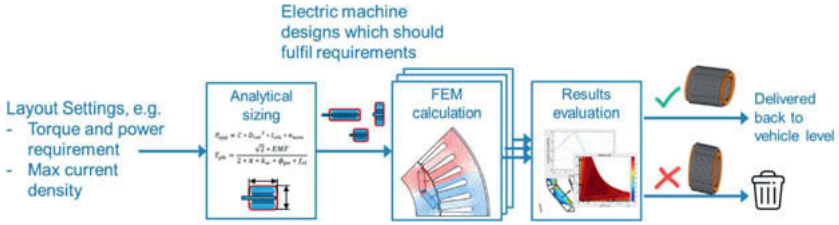

Fig. 5: Design and calculation process of electric machine

In a first step, the *"analytical sizing",* multiple PMSM designs are generated, which can be taken as basis for the electromagnetic performance calculations. The geometry, materials and electrical parameters of the different machine designs are estimated from torque and power requirements. The basis for the analytical rough design is empiric relations, experiences, expert knowledge and basic electrical and mechanical equations.

Subsequently, the machine designs are precisely calculated with the help of electromagnetic numerical FEM calculations and post-processing functions. Results are typical performance parameters of electric machines such as torque, power, torque ripple, efficiency, mass and more.

4.4 Inverter: Design- and Calculation Process

The design and calculation process for the inverter is shown in Fig. 6

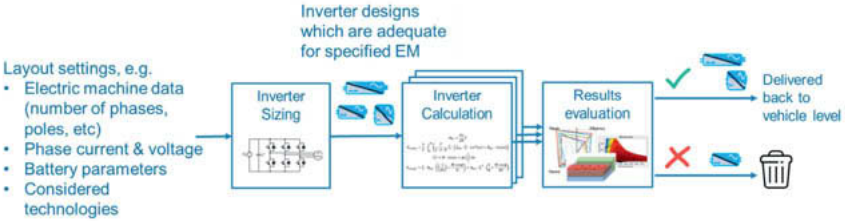

Fig. 6: Design and calculation process of inverter

The design process of inverter resembles the one from the electric machines in terms of having a *"sizing"* and a *"calculation"* step. In the *"sizing"* process, multiple inverter designs are created which are able to fulfil the requirements: For various chip technologies (e.g. Si IGBT, SiC MOSFET, GaN HEMT), the ideal switching frequency is determined as well as the number of required parallel chips and the DC link capacitors size.
In the subsequent step, the inverter designs are calculated precisely and their volume, weight, cost, efficiency and current ripple are determined and evaluated.

5 Sample Application in ModulED

The following is an extract from the application of the holistic drive module design from the ModulED project [5]. Here, the full process was run through for a passenger car of the C-segment. The reference vehicle is a Volvo C30 electric. The designed drive concepts had to fulfill the specifications of the reference vehicle, such as driving performance like acceleration capability or maximum weight. Exemplary results from the process are given in the following chapters.

5.1 Rough Layout

Within the vehicle rough design, a full factorial test plan was formed within the design space defined by the reference vehicle and the ModulED project. An extract of the vehicle requirements and base conditions is given in Fig. 7.

Parameter	Value
Vehicle test mass (incl. drive module)	1,690 kg
Maximum velocity	≥ 150 km/h
Acceleration 0 - 50 km/h	4.5 s
Acceleration 0 - 100 km/h	10.7 s
Launch gradeability	35 %
Min. lifetime resp. lifetime distance	5,000 h resp. 200,000 km

Fig. 7: Requirements and base conditions of vehicle

Based on the reference vehicle, the design process was performed for a battery electric vehicle with central drive and single-speed transmission. The mechanical and electric parameters (e.g. maximum speed, maximum power) of the components electric motor, inverter and transmission were varied within the design space. The battery and the basic vehicle parameters (e.g. battery supply voltage, vehicle drag coefficient) are taken over from the reference vehicle.

This results in almost 200,000 propulsion concepts. From this amount, 33,000 variants met all the defined performance requirements. The following four different maximum speed levels of the electric machine were selected for further consideration:

- 8,000 rpm
- 12,000 rpm
- 16,000 rpm
- 20,000 rpm

The highest speed is limited by the maximum speed of the bearings available from a database used for the transmission design process. For these maximum speed levels, valid concepts were taken from the result space. An extract of the concept results is given in Fig. 8.

Concept	EM peak output power	EM max. speed	EM nom. Speed	EM peak max. torque	Transmission ratio
Speed 1	102 kW	8,000 rpm	3,200 rpm	305 Nm	6
Speed 2	102 kW	12,000 rpm	4,800 rpm	200 Nm	9
Speed 3	102 kW	16,000 rpm	6,400 rpm	150 Nm	12
Speed 4	102 kW	20,000 rpm	8,000 rpm	120 Nm	15

Fig. 8: Rough layout results

Each of these concepts is individually further analyzed in the following fine design process with the integrated component design process.

5.2 Fine Design

Prior to the interpretation of the vehicle level results, the results at component level are explained, since their properties, characteristics, advantages and disadvantages influence the overall properties.

5.2.1 Transmission Design

For each concept derived from the rough layout, two- and three-stage spur gear transmissions were designed. For these transmission concepts, populations of 200 individuals were generated and calculated over 60 generations using a genetic algorithm. This process was run in parallel with four weighting functions. These weighting functions forced the optimizations towards high efficiency, low cost, low mass and a trade-off solution. To cover all possible transmission ratios, more than 150 million macro geometries were analytically calculated in advance.

The component results were examined for differences between the two-stage and three-stage topologies. For this purpose, the distribution of the transmission results over energy loss and mass is divided according to the respective transmission ratio and topology in the Fig. 9.

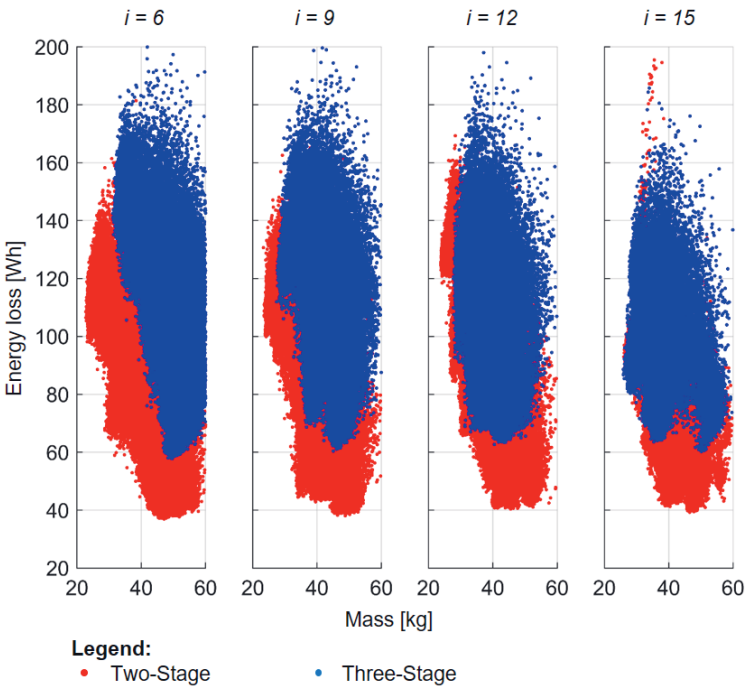

Fig. 9: Two-stage and three-stage transmissions over energy loss and mass

The results in the figure provide information on how the designed transmissions are distributed in terms of energy loss and mass. The trend is that three-stage helical gear transmissions are both heavier and create higher losses at low overall ratios. As expected, the disadvantages decrease with increasing total ratio. The overall transmission ratio for which three-stage transmissions are superior to two-stage version is not reached in this investigation and on the basis of the available results. The limiting factor for the maximum total gear ratio of 15 here is the available bearing catalogue, which only contained common transmission bearings with maximum speed up to approximately 22,000 rpm.

5.2.2 Electric Machine Design

The results for the required electric machine maximum speeds of 8,000 to 20,000 rpm is shown in Fig. 10.

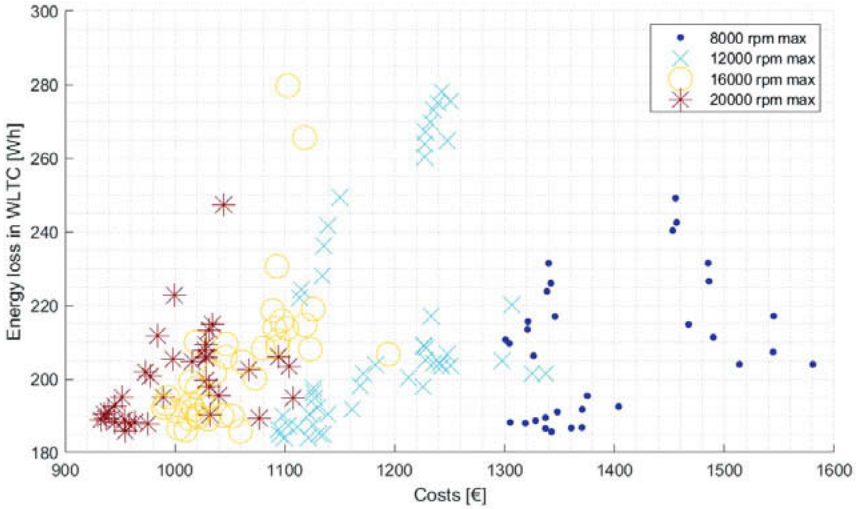

Fig. 10: Losses over costs of all calculated electric machines, sorted by maximum speed

The most evident result is the lower costs of high-speed EM versus low-speed EM. This is due to high speed machines being more compact and requiring less material. Additionally it can be seen that the energy losses in WLTC are not significantly lower when going to higher speeds, the best individuals per speed requirement have almost same losses. This means with a good design, also the low-speed EM can be very effective.

5.2.3 Inverter Design

The inverters are designed with a variation of three different parameters:

- The goal was to have IGBT as well as MOSFET transistors in the selection and also different chip materials: Si, SiC and GaN.
- Parallel chips: The minimum number of chips to reach current rating and higher numbers (in order to see an effect of more parallel devices, e.g. higher costs and higher/lower losses) are chosen
- Switching frequency: Around the ideal switching frequency (best compromise between losses, ripple and volume), a lower and a higher switching frequency are applied.

A result is shown below in Fig. 11.

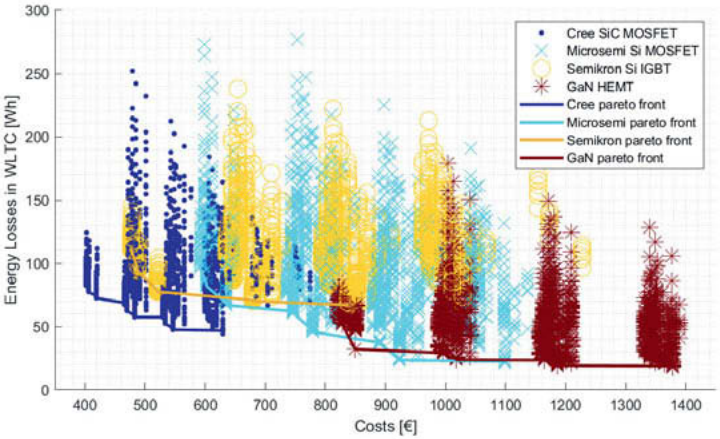

Fig. 11: Losses over cost of all laid out inverters sorted by switch type

From the plot it can be seen that with higher costs, the inverter WLTC cycle losses can be reduced. This results from more parallel chips as well as a slower switching frequency favoring lower losses. More parallel chips decrease losses because the current splits up among more devices and is lower in each individual device. This reduces the operation temperature and the on-resistance. At the same time the costs rise due to material cost per device. The cheapest inverters (down to 400 €) result with the Cree SiC MOSFET devices with still acceptable cycle losses (down to 42 Wh) whereas the most effective inverters result with the GaN HEMTs with cycle losses down to 18 Wh, these inverters are however relatively expensive. A compromise between those two is provided by the Microsemi Si MOSFETS and the Semikron Si IGBTs with SiC Diodes. However, the price analysis is a snapshot at mid-project, as the prices for Sic and GaN chips have in some cases further reduced (to varying degrees).

5.2.4 Configuration and Overall Assessment

For all selected propulsion system concepts, the component design process was executed, creating target-oriented component designs for the electric machine, inverter and transmission. The vehicle level then had a pool of possible component variants available for each selected rough design variant.

The genetic algorithm, already used for the transmission design, was used to find target-oriented drive modules. For this purpose, the designed components (electric machines, inverters

and transmissions) were virtually assembled, integrated and the resulting vehicle's overall properties were determined. For each propulsion system concept, three searches with different weighting functions for high efficiency, low costs and a trade-off solution were run through. Over the course of 60 generations, 150 individuals were calculated and evaluated. In total, 108,000 drive modules were evaluated. Of these, almost 80,000 variants successfully passed the evaluation process, of which 50,000 variants were unique.

The bar chart in Fig. 12 shows the cumulative component costs for five drive modules, which are on the Pareto front of the "Speed 2" (max. electric machine speed of 12,000 rpm) variants. The selected modules represent the 25 %, 50 % and 75 % quantile of the energy demand as well as the most efficient and the lowest cost variant.

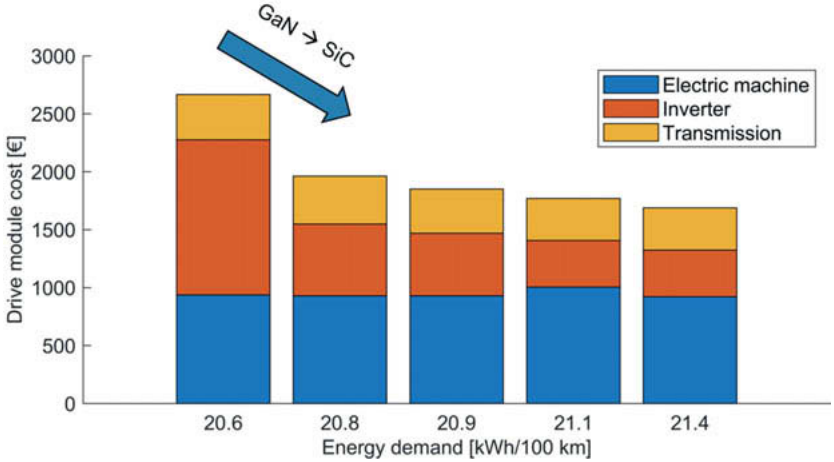

Fig. 12: Distribution of module costs depending on energy demand

Based on the above results, it can be derived for the examined design space that the component costs of the electric machine and transmission remain practically constant over the cycle energy demand. In contrast, the inverters show the possibility to increase the efficiency with additional investments. At the drive module level, GaN inverters also show the highest efficiency at higher costs, while SiC inverters achieve lower costs at higher losses.

In the last step, the results of all chosen concepts are compared with each other. Fig. 13 shows the distribution of the designed drive modules as a function of energy demand and module costs.

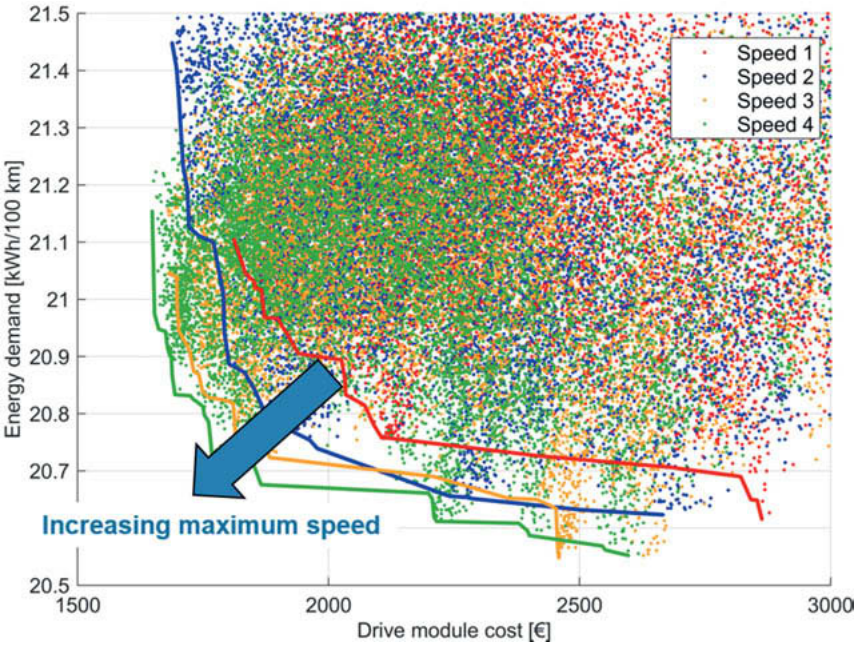

Fig. 13: Overall comparison of different speed levels on vehicle level

The Pareto lines of the different speed levels show a trend of decreasing losses and simultaneously decreasing costs for the high-speed variants (increasing maximum rotational machine speed). This can primarily be attributed to the electric machines, as already discussed in the component results. The lower energy consumption and costs can mainly be derived from the use of smaller electric machines. Chapter 5.2.1 showed that there were no significant disadvantages of versions with higher ratios in terms of costs and efficiency.

6 Conclusions

The developed, holistic drive module design process was successfully carried out on a reference vehicle within the ModulED project. In the process, various insights were gained at all levels of the process concerning the overall module as well as the individual components. Interdependencies between powertrain components during concept can be analyzed at vehicle level. For the target vehicle and technologies under review it was found that high speed concepts are suitable for reducing both losses and costs. Thus the technical approach chosen for the final drive module within the ModulED project can be confirmed as effective. The execution

shows that this process enables the system engineer to evaluate hundreds of thousands of design variants in a relatively short time (approx. two weeks + pre/post-processing) with a high level of detail and thus supports a well-founded concept decision.

7 Funding

This research was funded by the European Commission under the Horizon 2020 program, grant number 769953

8 References

[1] Hemsen, J., Kieninger, D., Eckstein, L. et al. *Innovative and Highly Integrated Modular Electric Drivetrain*. World Electr. Veh. J. (2019). https://doi.org/10.3390/wevj10040089

[2] Kieninger, D., Hemsen, J., Köller, S. et al. *Automated Design and Optimization of Transmissions for Electric Vehicles*. MTZ Worldwide 80, 88–93 (2019). https://doi.org/10.1007/s38313-019-0126-9

[3] Kieninger, D., Köller, S., Hemsen, J. et al. D2.1: Specifications of the propulsion system design. Modular Electric Drivetrains (ModulED), GV-04-2017: Next generation electric drivetrains for fully electric vehicles, focusing on high efficiency and low cost. Grant Agreement n° 769953

[4] Kieninger, D., Hemsen, J. Köller, S. D2.2: Holistic design environment. Modular Electric Drivetrains (ModulED), GV-04-2017: Next generation electric drivetrains for fully electric vehicles, focusing on high efficiency and low cost. Grant Agreement n° 769953

[5] Kieninger, D., Hemsen, J. Witham, G. D2.3: Sample Application for the specified target vehicle. Modular Electric Drivetrains (ModulED), GV-04-2017: Next generation electric drivetrains for fully electric vehicles, focusing on high efficiency and low cost. Grant Agreement n° 769953

e-FDU: Concept, Develop & Industrialization of a novel P4 powertrain

From Concept to Industrialization of a novel P4 powertrain in 24 month

Eng. **Alessandro Manelli**, Eng. **Fabio Filippo Irato**,
Eng. **Carlo Cavallino**, Eng. **Roberto Gay**,
Dana Graziano S.R.L., Rivoli, Italy

1 Abstract

Reduction on CO2 and polluting emissions on light vehicles is a key objective on which the automotive market is focusing during these years.
Hybrid and pure electric technologies are both solutions that the OEM are following to meet international regulations, for sport cars segment hybrid technologies allows to meet other important objectives, more customer oriented, which can be summarized in fuel economy, performance enhancement, driving pleasure.
For tier one companies these requirements can be translated in products that must focus on the improvement of efficiencies, power density, respect of the vehicle installation constraints and introduction of new features to allow a more controllable system.
Dana Graziano, under request and targets given by Ferrari, along with technological centre Vocis part of the Dana group, achieved the objective of developing and put in to industrialization in less than 24 months a novel p4 pure electric powertrain, in the form of a dual electric motor front axle.
Each unit drives the front wheels of the vehicle independently, i.e. a complete torque vectoring of the front wheels, allowing at the same time to have a full electric drive, improvement of traction capabilities and vehicle dynamics and a reduction of the fuel consumption.
Electric drive of the vehicle can be completely achieved, in both front and reverse manoeuvres.
The e-axle can be considered as two independent symmetric units, called left and right and kept together with a central housing, each unit is composed by a high revolution (25000 RPM) and high power density (up to 81KW) electric motor, a gear reduction stage (first stage cylindrical and a second planetary gear set) and an innovative linear electromagnetic actuator which undertake the function of disconnect system.

2 Keywords

E - Axle, P4 Powertrain Configuration, Linear Electromagnetic Actuator; Symmetrical Axle; Independent Front Wheels Drive; Torque Vectoring; High Speed Revolution; HV E-Motors; HEV; BEV.

Index

3 Introduction

Electrification is a fundamental aspect for automotive OEM to be able to meet the upcoming legislation targets regarding polluting emission, at the same time allows an improvement of fuel consumption and driving pleasure.
Dana Graziano P4 full electric powertrain layout, called e-FDU (Front Drive Unit), developed for Ferrari, represent the state of art to these demands, the e-FDU is a twin layout powertrain which integrates for each side an high speed e-motor, gear reduction stage and a smart actuator for the disconnect function (see Fig.1)
To meet and switch between all the functionalities required, of both pure electric and hybrid driving mode, special control strategies have been implemented.

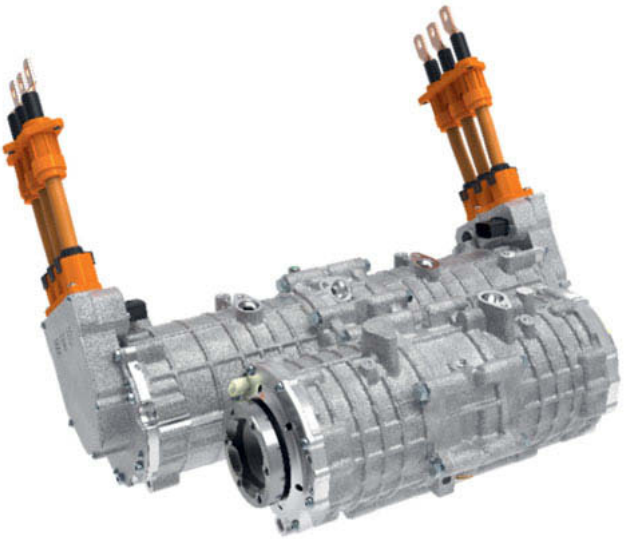

Fig. 1: e-FDU Overview

EMA, acronym of Electro Magnetic Actuator, is a smart actuator developed for this application, which allows to connect and dis-connect two rotating elements, acting on a shifting element placed at the output stage of the e-axle (see Fig. 2).
EMA can be defined as a smart actuator due to the fact that integrates all the elements to allow the function of disconnect system, in particular the electronic with its dedicated ECU, drive

stage and bobbins, and half of the necessary mechanic for the disconnect function, all integrated in the same package.

The electrical connection to the vehicle is hence performed with a low voltage line, for powering up the device, and a standard communication protocol used in the automotive sector, for driving it, the mechanical connection to the e-axle is simply performed through the use of screws.

Fig. 2: EMA Installed in the e-FDU

4 E-Axle Characteristics and Layout

The architecture and layout of the e-FDU has been developed to meet the objectives imposed by the customer, with a particular focus on efficiency, weight and space optimization.
Main system requirements are:

- Max. e-drive speed 135km/h
- Max hybrid drive speed 210km/h.
- Longitudinal acceleration in e-drive conditions ≥ 0.4 g.
- Max overall e-FDU weight of 60 Kg, e-motors, mechanics and disconnect included.
- Active Torque Vectoring capabilities.
- Disconnection of e-motors and gear mesh from wheels capabilities.
- Vehicle installation constraints (i.e. steering rack, air conditioning circuit, etc…).

To meet all these targets a symmetric layout, with independent e-motors, cinematic chain and disconnect system for each side has been choose. (see Fig. 3).

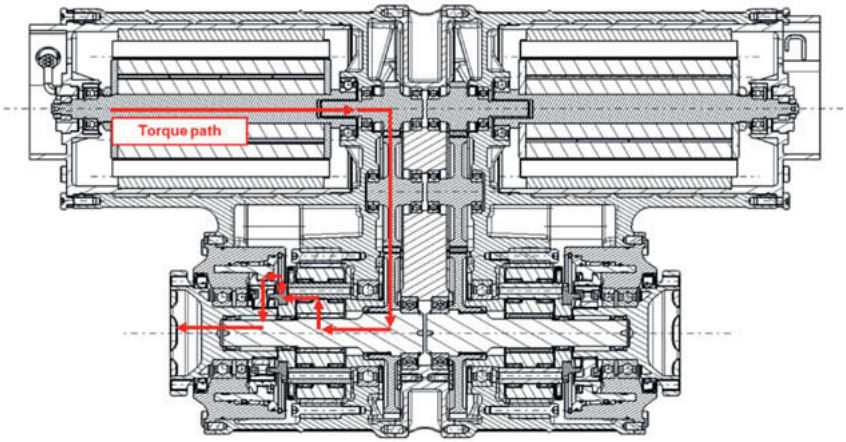

Fig. 3: Section of e-FDU final layout

5 E – Machines and gear ratio sizing

E– machines and gear ratio sizing has been sized together to meet all the requirements.
In particular each e-machine provides 81KW of power, in continuous conditions independently from the battery SOC, a maximum torque of 85Nm and reaches a maximum speed of 25000RPM, all referenced at the input stage of the e-FDU.
The gear mesh is composed of two reduction stages, a first reduction stage made by cylindrical gears and a second reduction stage made with a planetary gear set, in the configuration of input from sun shaft, output on the planet carrier and crown gear fixed to the chassis.
These 2 stages combined allows to reach a total gear ratio of 14.576:1, with the e-motors contribution it allows to meet completely the performance objective given.
The remaining function to disconnect the gear mesh and the e-motors from the wheels after a calibratable vehicle speed, to avoid an overspeed of the e-motors and allow a reduction of the drag-torques over a certain speed, is mechanically performed with a dog clutch mechanism.
The clutch body ring is directly welded on the planet carrier of the epicyclic gear set, while the sleeve, capable of linear motion, is directly placed inside the EMA, allowing to connect and disconnect the output flange, and hence to transmit or not torque, from the gear mesh.
The space boundary conditions given by installation requirements, minimum distance from all the surrounding elements like steering rack, air conditioning circuit and chassis (see Fig. 4), led to the decision to use an “8” shape like layout, as visible in Fig. 3, and to use an external oil cooling circuit driven by a dedicated electric pump for guarantee an optimal lubrication and cooling of the e-FDU.

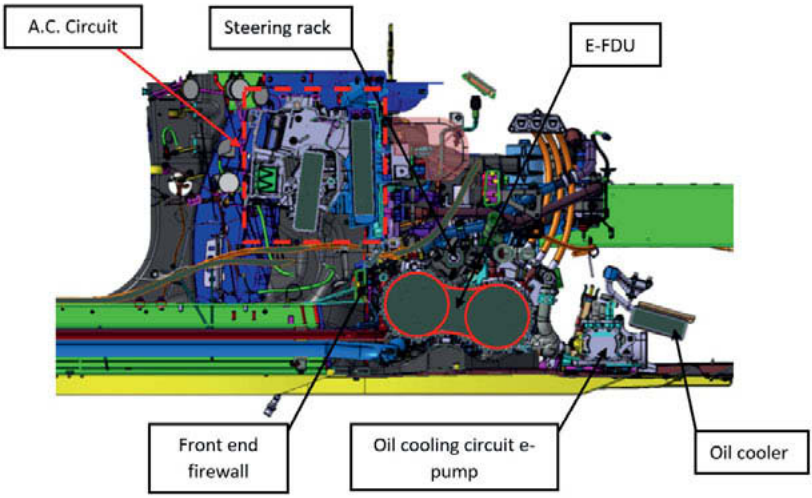

Fig. 4: e-FDU axle installation in vehicle

6 Disconnect system overview

During vehicle definition, by the customer, has been evaluated to not require all wheel drive on all the speed range, this lead to the requirement to disconnect the front gear mesh and e-motors system, allowing to optimize the power profile given by the front E-axle.

The mechanical concept of the disconnect system derives from a dog clutch layout in which:

- The output flange meshes through a spline with an hub, these are rigidly bound together with a locknut system.
- The hub meshes with the sleeve through an another spline, these are not rigidly bound but a linear movement of the sleeve is possible along the spline.

All the above elements are contained in the EMA

- Thanks to the linear movement the sleeve engages with the clutch body ring welded on the planet carrier through dog teeth, present on both sleeve and clutch body ring.

Thanks to the contribution of the e-motor during the engagement phase is possible to keep a constant indexing speed of the sleeve and the clutch body ring, allowing a fast engagement with reduced impulsive torque at the wheel NVH effects for the driver.

The design of the dog teeth has been choose in order to minimize angular clearance and hence improve backlash noise during standard torque transfer on this particular coupling.

The first concept of disconnect system, developed by the customer, used an hydraulic actuator.

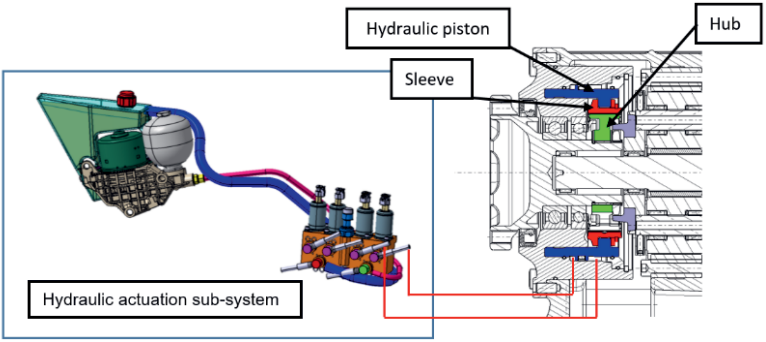

Fig. 5: E-FDU hydraulic actuation system layout.

Like all the classic actuator systems it was constituted by a pump, an accumulator, valves for pressure control of the actuator and of the whole circuit, and finally the hydraulic piston with a sensor to have a feedback on the position feed to a dedicated ECU installed outside the E-Axle.

EMA substituted the whole hydraulic circuit allowing to meet key benefits:

1. Space saving: no external actuation circuit and no external ECU are needed, since all the key elements are contained in the EMA
2. Electric power instead of hydraulic power: this allows to avoid the use of a dedicated hydraulic oil.
3. Weight saving: up to 5Kg of weight reduction
4. Installation simplification: no need to install external elements for the functioning of the e-FDU
5. Same performance: engagement time remains in the order of 100 ms.

6.1 Disconnect system: EMA (Electro Magnetic Actuator)

Coupling and decoupling the torque path from the e-machines to wheels, i.e. disconnect function, is demanded to the EMA, which is located at the output stage of the transmission.

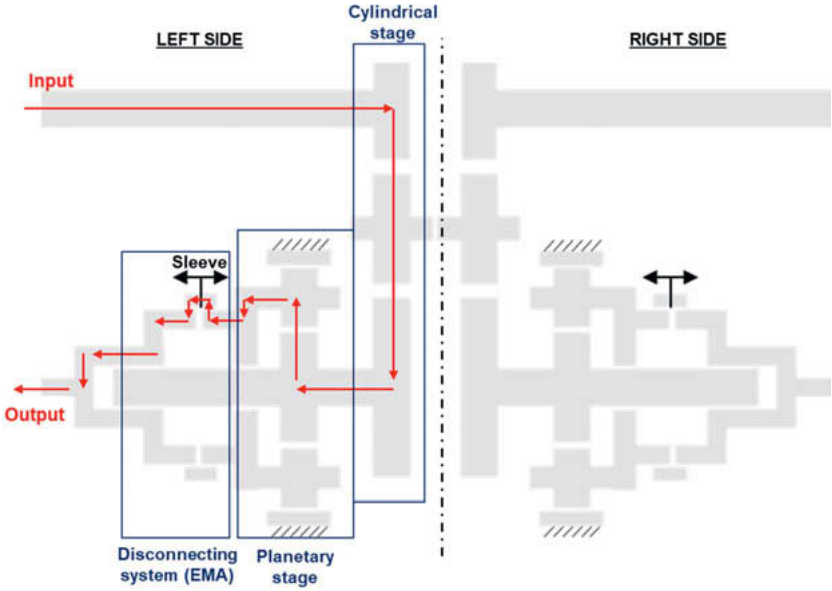

Fig. 6: e-FDU Layout and Overview of the main sub-systems

Due to the twin nature of the e-FDU two EMAs are needed, one for the left side and one for the right side of the e-axle, giving the possibility to use fully independently the left and right side of the front drive.

The mechanics, integrated electronic and electric drivers can be seen in Fig. 7 – 8 – 9:

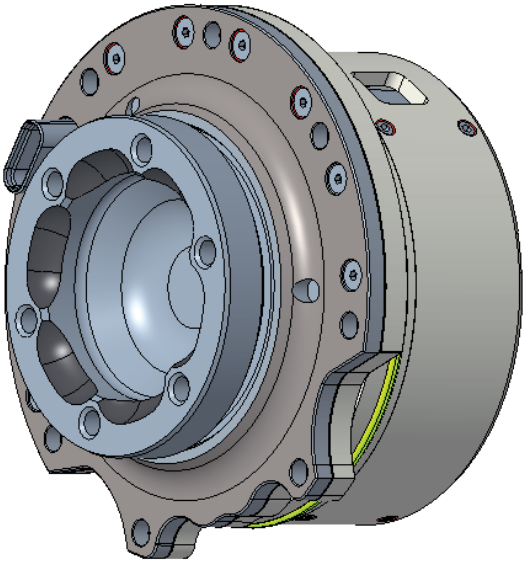

Fig. 7: CAD representation of the envelope of the EMA

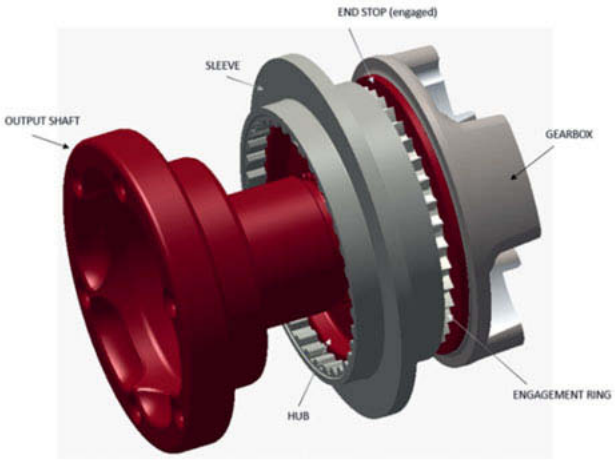

Fig. 8: Mechanical elements which undergo to the disconnect function

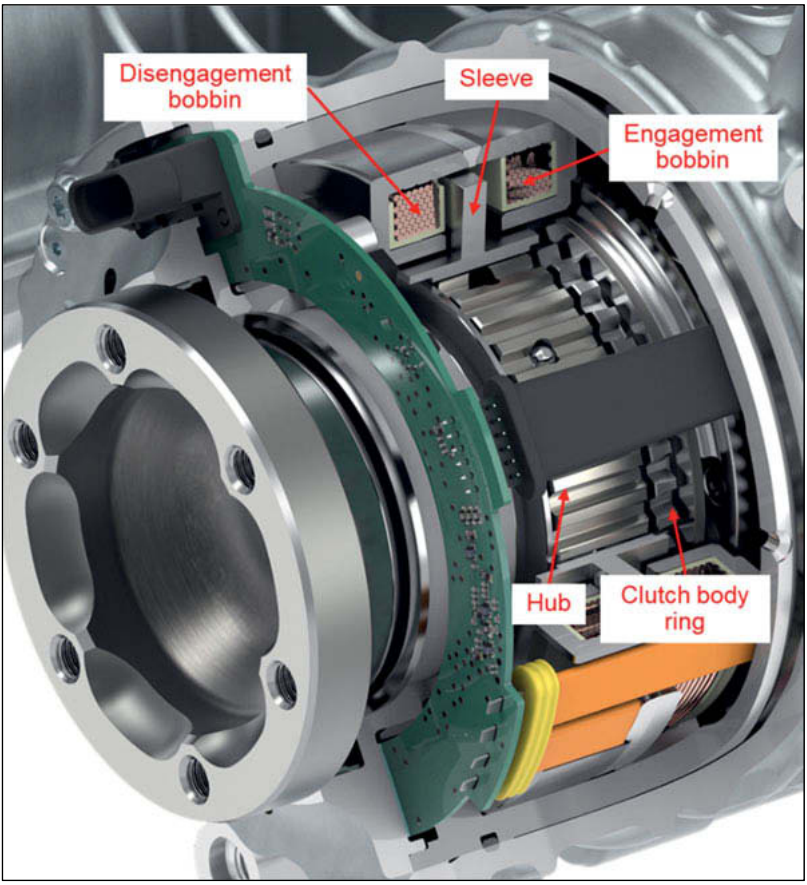

Fig. 9: Section of the EMA installed in the e-FDU

From Fig. 8 is possible to see all the mechanical components which are responsible of the torque flow, in particular the engagement ring or clutch body ring, sleeve with its linear movement capabilities on the spline that creates the coupling with the hub, which is coupled to the output shaft with an another spline.

To avoid the impact of the sleeve against the bobbins its stroke is limited thanks to the use of end stops, one used for the disengaged position placed inside the EMA and the one for the engaged position placed behind the engagement ring.

To constrain the magnetic flux inside the EMA and maximize the force on the sleeve non-magnetic steel has been used for both end-stops.

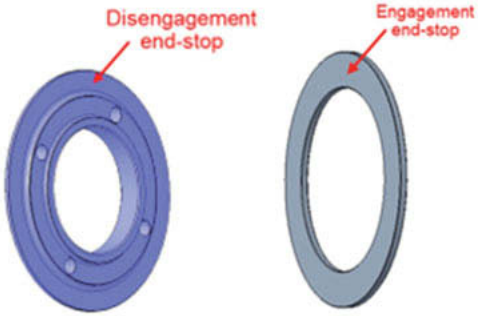

Fig. 10: CAD representation of disengagement, left, and engagement, right, end-stops

An important design feature requested to the EMA is to have an intrinsic bi-stable nature, both for disengaged and engaged position.
To guarantee this feature a retention system has been designed, in order to avoid undesired axial movements when not explicitly requested.

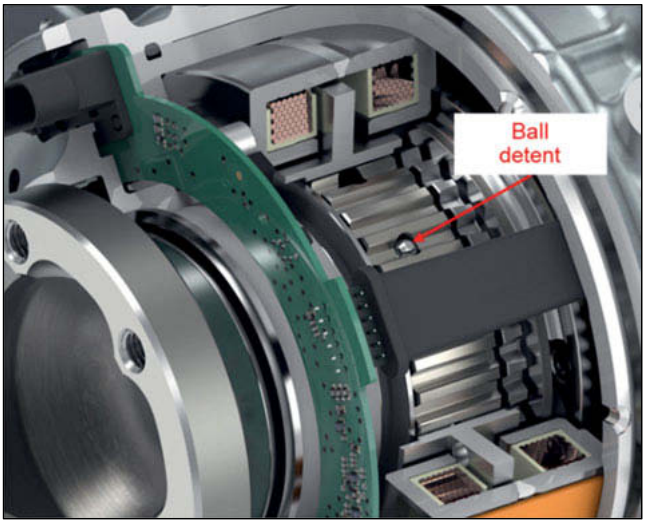

Fig. 11: EMA retention system

The retention system, derived from synchronizers, is placed in the spline interface between the hub and the sleeve, and is composed of a groove with two vanes, spheres and springs housed inside the hub.

When the spheres are inside one of the vanes undesired movements are neglected.

Core elements of the EMA are the disengagement and engagement bobbin, which are the elements responsible for the generation of magnetomotive force which pulls the sleeve in engaged or disengaged position.

Each bobbin is driven by a dedicated current driver, directly installed in the integrated PCB, which allow to drive and regulate the proper amount of current, improving actuation performances and the thermal management of the current driver.

Each bobbin is composed by four key elements:

1 Copper Coil, through which electrical current can flow
2 Spool, which supports the coil
3 Stator, made in magnetic steel
4 Connector, which allows the electrical connection to the PC

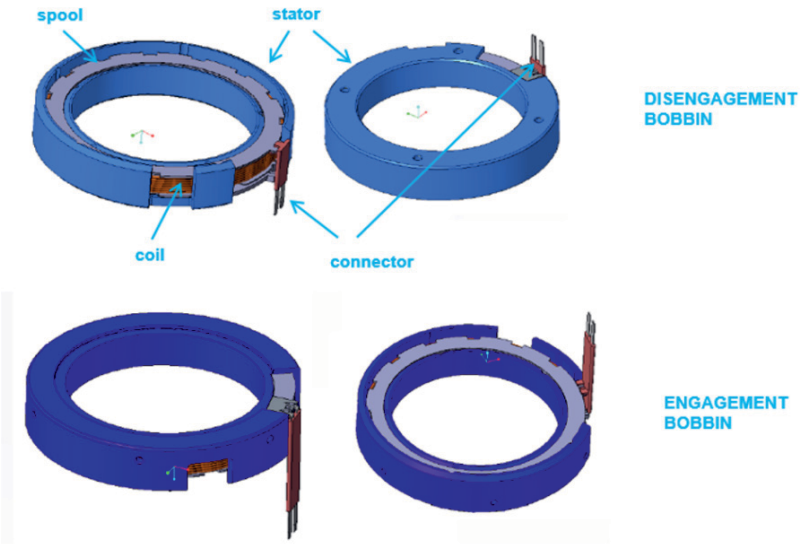

Fig. 12: CAD representation of Disengagement and Engagement Bobbin

Use of FEM methods, performed in a preliminary phase with 2D tools and subsequently with 3D tools, allowed to optimize key aspects of the bobbin assembly, like force generated on the sleeve along its stroke and weight reduction of the overall assembly.

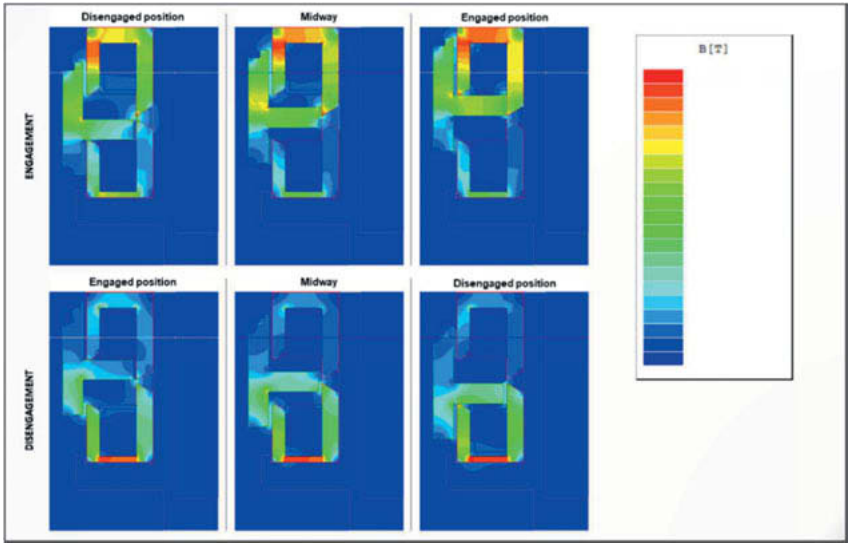

Fig. 13: 2D FEM Simulation, magnetic flux behavior prediction

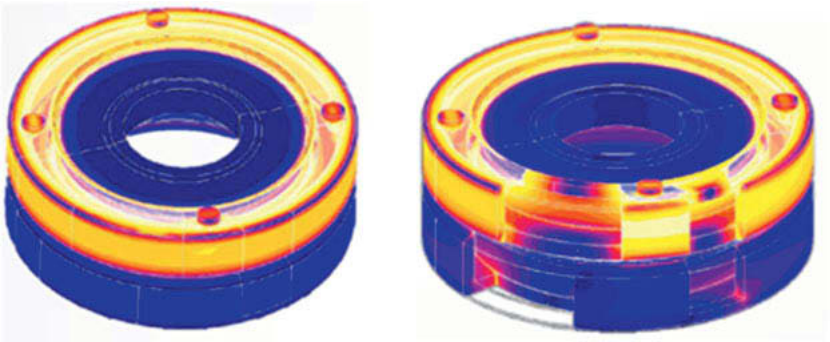

Fig. 14: 3D FEM Simulation, magnetic flux behaviour prediction

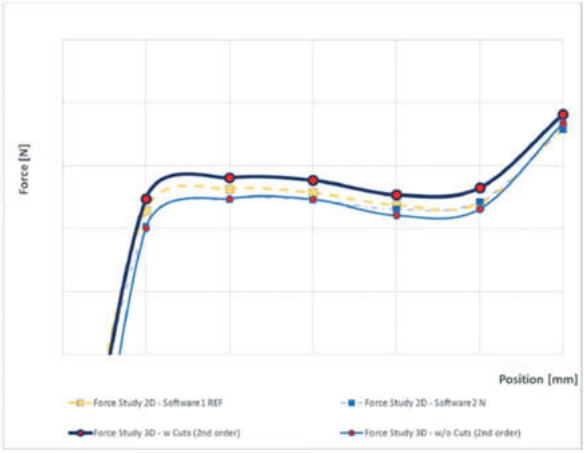

Fig. 15: Force profile predicted by simulations

To close the loop for the implementation of a position control on the sleeve, a non-contact, inductive, proportional position sensor has been designed and integrated in the EMA.

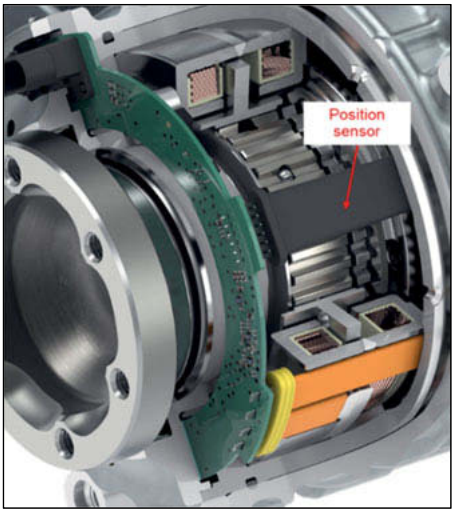

Fig. 16: EMA Position Sensor

The electrical signal is directly feed in to the integrated PCB, allowing a real time control of the mechanical state of the sleeve, and a more precise control during actuations.

Main electrical characteristics requested by the customer are shown below:

Table 1: EMA electrical characteristics

Characteristic	Value	Unit
Supply Voltage	9-16	[V]
Sleep Current	≤10	[µA]
Wake-Up Current	≤75	[mA]
Max Current on Bobbin	30	[A]

For driving the actuator and allowing the communication with all the ECUs present inside the vehicle CAN protocol has been choose and implemented.

Along with the proper commands to request an actuation, in engaged state or in disengaged state, key aspects and statuses are feedbacked by the EMA:

- Current level of voltage supply
- Current level of current absorption
- PCB temperature
- Linear Position of the sleeve
- Mechanical status of the coupling
- Health status of the EMA (fault state and cause of the fault)

All these information are necessary to guarantee optimal performances during shifting phase and a known and safe state of the coupling during standard operation of the vehicle.

Since the EMA can be considered as stand-alone component, integrable inside an e-axle for connect and disconnect functions, has been decided with the customer to perform a validation of the component as stand-alone, following a standard sets of test for an assessment on the electronic reliability, but also as an integrated component, for an assessment on the mechanical, integration reliability.

EMA patent utility model deposit has been released on 28.11.2017 (Reference number: 202017000136703; Title: “Dispositivo d’innesto ad azionamento elettromagnetico”).

6.2 Disengagement and engagement manoeuvre

Slave nature logic implemented inside the EMA software allows to disengage and engage the gear mesh to the wheels whenever is desired.

In this case disengagements are requested to remove the AWD at high speeds, which will cause an over-speed on the e-machines, but also for energy saving strategies which requires the front axle disconnection.

Instead, when is desired to have the possibility to have a torque path on the front axle, the ECU can simply command the reconnection of the e-axle.

To complete in the shortest time possible the disengagement and engagement phases (down to 50 ms) and without affecting driver comfort (no torque and NVH pulses during the actuations), particular strategies, which involves several control units like EMAs, e-machine drivers (HV inverters), wheel speed sensors and ECU, have been firstly tested on Dana Graziano test benches and subsequently implemented in vehicle.

An overview of the involved control units during these manoeuvres is presented in Fig. 17

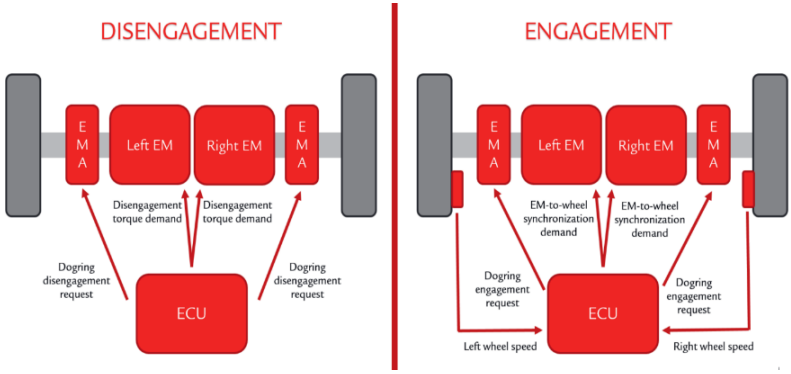

Fig. 17: Overview of the involved control units

6.3 Disengagement Maneuver

During a disengagement the key point to have good performances is to erase the torque that flows trough the dog clutch, which depends on vehicle speed and acceleration.

A specific torque profile generation is hence requested to the e-machines (inverters) while a request of disengagement is performed to the EMA.

In Fig. 18 the expected evolution of e-machine (P4) velocity, wheel velocity, EMA (dog ring) status and torque are showed.

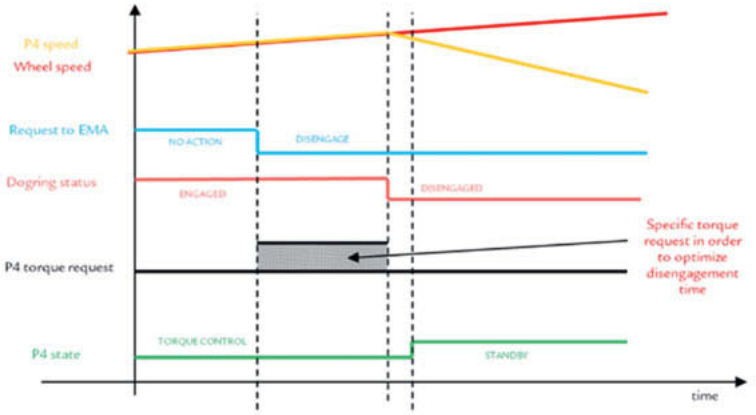

Fig. 18: Disengement Phase. in orange P4 speed, in red wheel speed, in blue command to EMA, in light red dog clutch status, in black P4 torque profile request, in green P4 state

6.4 Engagement Maneuver

Due to the nature of a dog clutch the function of mechanical synchronization is not present, to avoid torque pulses phenomena and long engagements time the synchronization of the speeds of the sleeve and of the clutch body ring is demanded to the speed control of the e-machines, i.e. the inverter.

Key parameter during an engagement of a dog clutch mechanism is the relative speed of the rotating elements, in particular two general statements are true:

- Lowering the relative speed increases the engagement time with benefits of driver comfort.
- Increasing the relative speed decreases the engagement time with a reduction on the benefits of driver comfort.

So different relative speeds are used depending on driving conditions.

In particular the mechanic of the EMA allows engagements inside a range of relative speeds between 20 and 80 RPM, allowing in these ranges to meet the maximum requested engagement time.

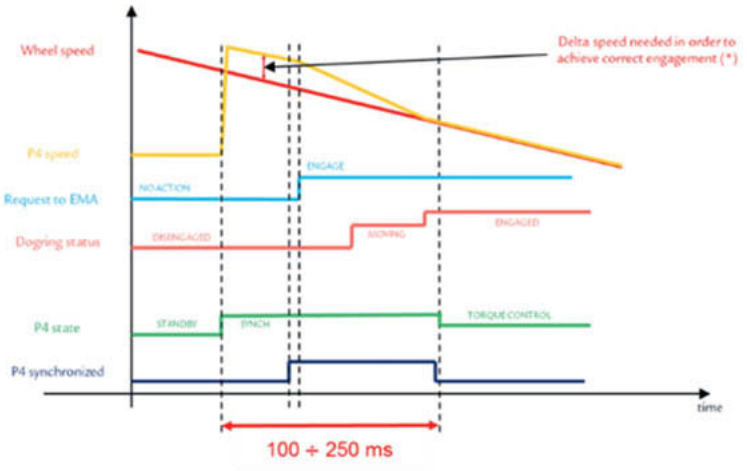

Fig. 19: Engagement Strategy, in orange P4 speed, in red the wheel speed, in blue request to EMA, in light red the dog-clutch status, in green the inverter state and in dark-blue the synchronization flag of P4

7 e-FDU Validation

As mentioned in the previous chapters the e-FDU can be considered as a twin layout, with a left side symmetrical to the right side.

If this can be considered true from an architecture point of view it must be considered that from a component and lubrication point of view this statement is no more true:

- Central housing, which connects left side to the right side, allows a share of oil for lubrication between the two sides.
- To have benefits in terms of cost and parts management it has been decided to use the same helix gears on both sides.
- To have benefits in terms of cost and industrialization capabilities, left and right housing are symmetrical.

From a technical point of view the combination of these decisions led to the following challenges:

- Having the same helix gear on both sides complicates the optimization of micro-geometry on the gear flanks, due to the fact that on a gear in which the flank works in “drive” condition on one side, will work in “coast” condition on the other side.
- The combination of having the same helix gears and symmetrical housing creates a non-symmetrical lubrication oil splashing behaviour inside the e-axle, which may cause to have a side that works in a “dry” condition respect to the other.

Thanks to specific software for virtual validation of the NVH behaviour of the axle, specific tests performed on Dana Graziano test benches, all these key points have been addressed leading to:

- An optimization of the inlet and outlet position for the external oil recirculation circuit but also of the internal oil splashing of the e-axle on the whole speed range and driving conditions, simulation of external accelerations has also been taken in account.
- An optimization of the micro-geometry on all the gears, allowing to satisfy the specification shared by the customer on all the speed and torque range which the axle must cover.

To have a complete understanding of the e-FDU behaviour almost all tests have been performed with original e-machines and their dedicated HV inverters, this decision lead to the possibility to detect side effects that cannot be easily predicted with the use of simulation tools and at the same time to optimize not only the mechanic of the e-FDU but also the software that govern the behaviour of the EMAs and of the inverter.

The following tests has been performed at a system level, meaning e-FDU and inverters together, test benches should therefore provide HV DC power, through the use of a battery simulator, and mechanical power, through the use of two dynos placed connected to the output shafts of the e-FDU with drive shafts.

7.1 Under load contact pattern

Purpose of this test is to evaluate the contact pattern of the various gear meshing, allowing a direct comparison with the results obtained with the virtual validation tools for micro-geometry optimization.
To perform this test all the gears are coated with a special marker, which allows to visually indicate the contact between the gears, and then the e-FDU is driven in coast and drive conditions at different level of torque, in both symmetrical and torque vectoring conditions.
Pictures of the contact are taken in each condition, subsequent image post-processing allows a comparison with virtual predicted results

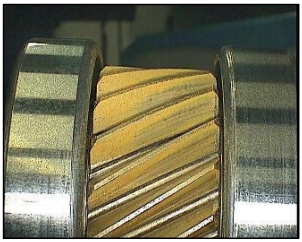

Fig. 20: Example of contact pattern at a certain level

7.2 Gears fatigue test

Purpose of this test is to verify the e-FDU, and all its subcomponents, reliability and durability by completing a fatigue cycle which is representative of the mission profile that the vehicle will sustain.
In this test the whole system is tested, e-FDU + inverters, and all the necessary auxiliary systems, like lubrication oil circulation circuit and inverter/e-motors cooling circuits, are replicated on the bench.
The e-axle is mounted on a proper clamping plate, and connected to two dynos through drive shafts.
With this layout natural torque flow and throughput is respected, since the elements that defines the torque level are the e-FDU e-machines.

Speed and torque are measured not only by the feedbacks of the e-FDU integrated e-machines but also thanks to speed and torque sensors placed at the output stage.

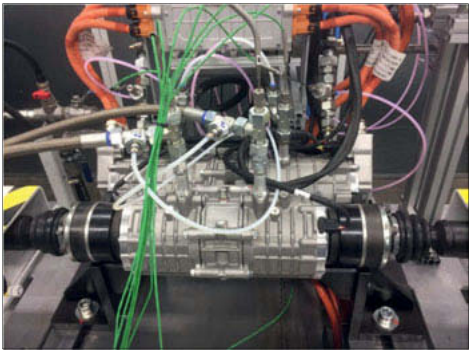

Fig. 21: Fatigue Test bench set-up

As per customer specification, the entire duty cycle performed doubles the mission profile that the vehicle shall attend.

7.3 EMA durability test

Purpose of this test is to evaluate the performances of engagements and disengagements manoeuvres, in terms of actuation time, over vehicle lifetime, taking in consideration all the components involved during the sequences.
Several actuations at different temperatures have been done in order to verify the overall capacity, EMA firstly, to respect the given targets.
Main obstacle of this test has been the necessity to reproduce the logic described in 3.2 on a test bench, taking in consideration also the response time that all the control units put in place.

7.4 Efficiency test

Purpose of this test is to verify the efficiency of the e-FDU, overall system, gears and e-motors, during symmetrical and torque vectoring working conditions.
Power meters have been installed to measure voltage and current on the 3 phases of each motor and DC common line for the inverters.

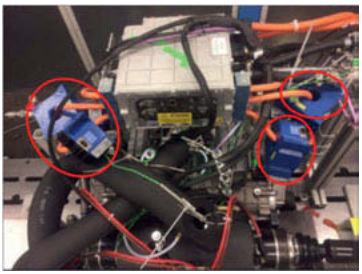

Fig. 22: Efficiency test current and voltage sensor for HV characterization

8 Industrialization and assembly line:

Assembly and EOL bench for e-FDU project has been designed and developed considering the following key principles:

1. Safe and Ergonomic
2. Material from outside of Aline
3. Balanced stations
4. Process/Logistic: SEPARATED
5. First Time Quality > 99%
6. One Piece Flow
7. «U» shape

During the design phase has been possible to divide the assembly line in to three main stations (see Fig. 23):

Fig. 23: Assembly line overview

8.1 Station #1 - Subcomponents assembly

Station #1 is dedicated to subcomponents preparation, see Fig. 24, in particular:

- Planetary gear set subassembly
- Bearings pressfit on shafts
- Snap rings installation
- Cylindrical gears coupling
- EMA preassembly

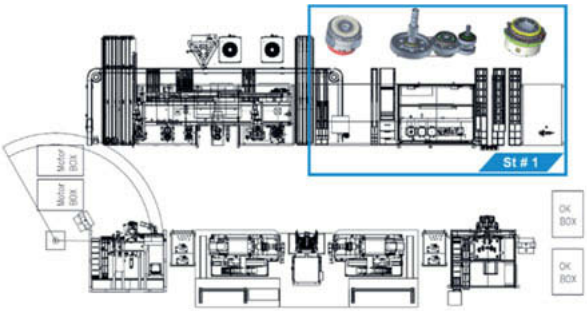

Fig. 24: Station #1 section

The pressing machine uses automatic pressing tools changeover (revolver, sliding, etc.) and is equipped with state of art sensors, like vision systems, to ensure presence and correct installation of all managed components (see Fig. 25).

Fig. 25: Pressing machine for bearings installation.

EMA subassembly is completely assembled in this station before fitting in the e-FDU, in specific bearings, output flange, hub, detents installation and locknut tightening are performed in this station (see Fig. 26).

Fig. 26: EMA assembly area

EMA is partially assembled by the supplier which have followed its industrialization, in which a first EOL is performed to fully characterize it's key characteristics.

8.2 Station #2 – Full assembly of the e-FDU

The station # 2 is dedicated to install all the subcomponents in to the central housing, by heating bearing seats with induction heater and introducing dowel pins with pressing machine for successive coupling of the lateral housing with the central one, which is done by firstly applying liquid seal (done automatically with a track following feeder), check of liquid pattern with vision system and finally closing the housings together (see Fig. 27 and Fig. 28).

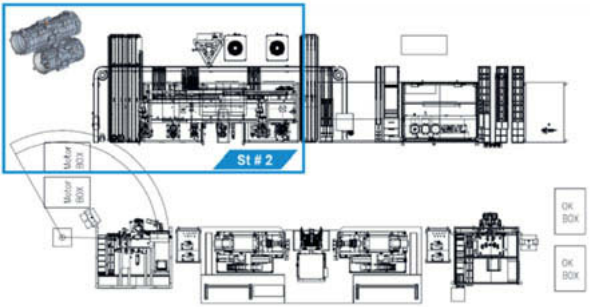

Fig. 27 Station #2 section

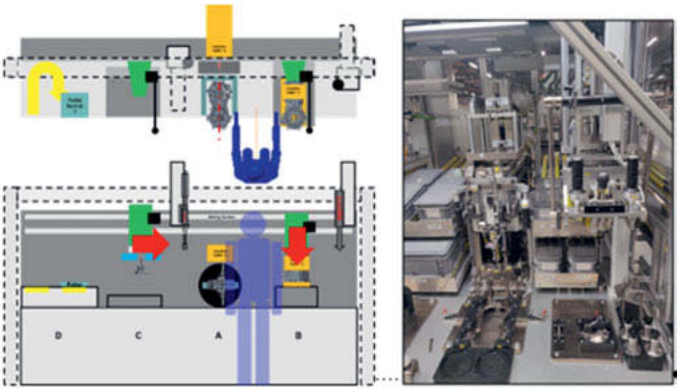

Fig. 28 Station #2 layout and detail

The assembly ends with the installation of EMAs and e-machines in to lateral housings, managed with specific Dalmec alignment system, and screw tightening, with torque angle controls (see Fig. 29 and Fig. 30).

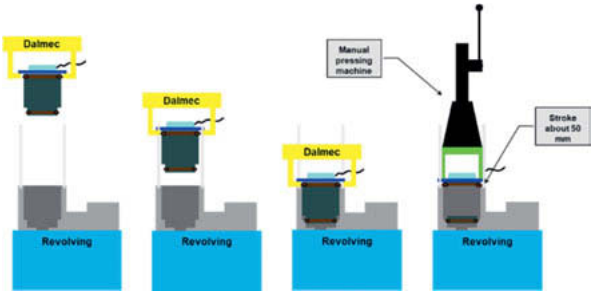

Fig. 29: Dalmec system for e-machine handling layout

Fig. 30: Dalmec system for e-machine handling

8.3 Station #3 + EOL

Station #3 is dedicated to installation of pre-assembled transmission on revolving station, for allowing external component assembly necessary for the EOL bench (i.e. oil plug, , water plugs, etc.), leakage test of oil and water circuits (this one is done for each transmission side), electrical insulation test on the e-motors, and finally EOL test.

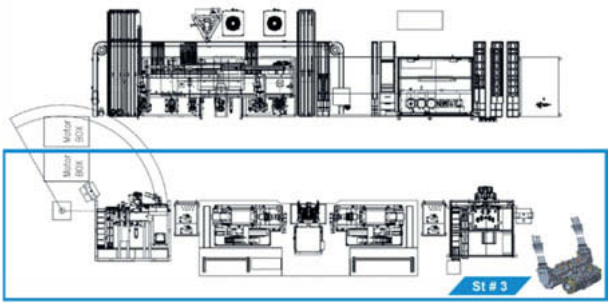

Fig. 31: Station #3 section

Fig. 32: Leakage test machine (oil and water circuits) and electric insulation machine

The EOL test bench is equipped with two dynamos able to cover the maximum power curve of the e-FDU, installed on a sliding axis in order to be automatically connected and disconnected to the tested unit. A battery emulator, supplies power to a gold inverter that drives the e-machines of the e-FDU (see Fig. 33).

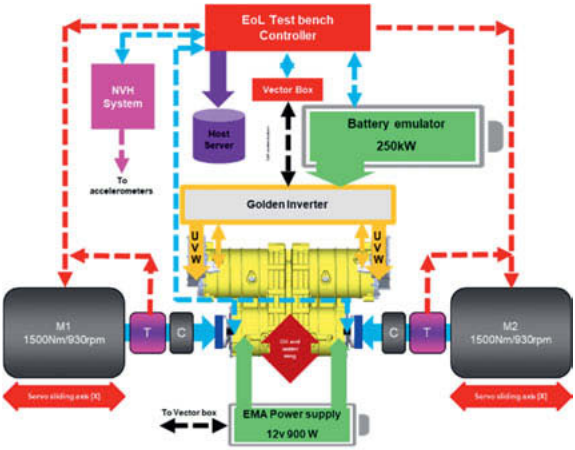

Fig. 33: EOL bench layout

The EOL bench reads directly from assembly line servers all the necessary data that has to be feed to the inverter to properly drive each pair of e-machines installed in the e-FDU.
It can apply different torque\speed ramps to the e-machines, required for different tests performed during the EOL cycles and automatically manages oil and water temperatures, heating and cooling the flow rates imposed to the e-FDU for depending on the test performed during the EOL.

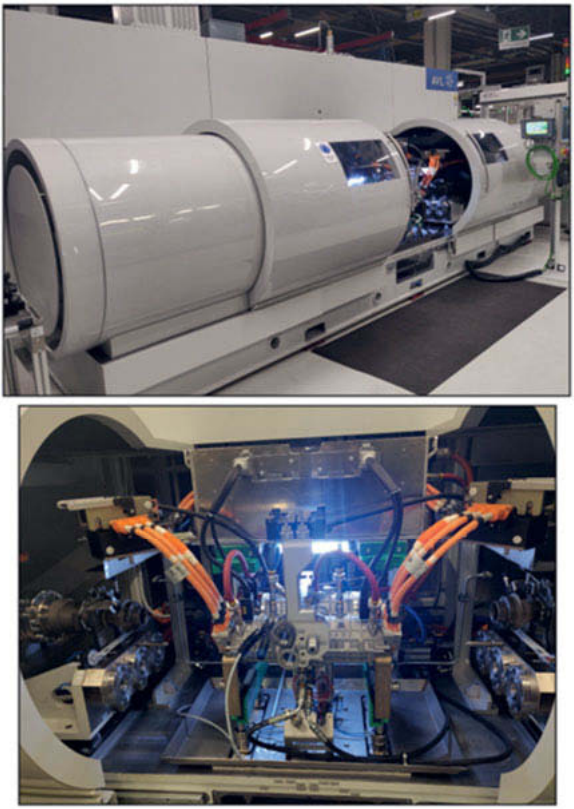

Fig. 34: EOL bench overview

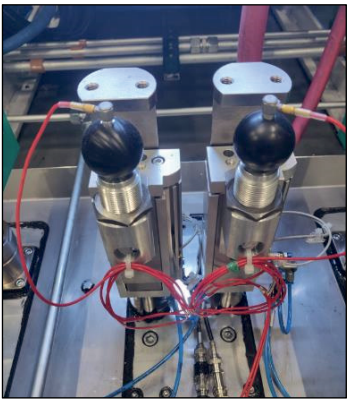

Fig. 35 EOL bench accelerometers for NVH acquisition

All the key aspects of the e-FDU are tested and characterized during the EOL cycle:

- Engagements & dis-engagements performances at different temperatures
- Retention system capabilities
- Torque unbalance between the left and right side
- NVH complete characterization

For each e-FDU all the data are stored, under customer request these can be directly shared.

9 Conclusions

Twin independent disconnectable transmissions driven by two high revolution (25000rpm) and high-power density electric motors (up to 162 kW in total).
Full electric drive in reverse gear.
Vehicle dynamics and torque vectoring optimization.
Specific vehicle control strategies have been developed to meet hybrid functionality and vehicle dynamic performances.
EMA as disconnect device for Ferrari series production high performance PHEV.
Smart actuator with integrated electronic hardware and compact design.
Precise sensor feedback for precise actuation control.
Contactless shifting powered by electromagnetic flux.
Actuation time less than 100 ms @ 20°C.
Semi-automatic assembly line with complete PLC management (all process controlled and managed by Host server).
Full power (up to 162 kW) EOL of complete powertrain (E-motors + Transmission + Disconnect).

10 References

[1]. Furlich J., Blough J., and Robinette D.: Torsional Vibration Analysis of Six Speed MT Transmission and Driveline from Road to Lab. SAE International, 2017-01-1845 (2017).
[2]. Galvagno E., Gutierrez P., Velardocchia M., and Vigliani A.: A Theoretical Investigation of the Influence of Powertrain Mounts on Transmission Torsional Dynamics. SAE International, 2017-01-1124 (2017).
[3]. Parmar, V., Di Rocco D., Sopouch M., and Albertini P.: Multi-Physics Simulation Model for Noise and Vibration Effects in Hybrid Vehicle Powertrain. SAE International, 2014-01-2093 (2014).

Development of the new chain CVT for middle capacity

Kentaro Sakai, Takuya Kishimoto, Takahiro Kobayashi, Takuya Maekawa, Tsuyoshi Shinohara, Masato Ogawa,
SUBARU CORPORATION, Tokyo, Japan

Abstract

The newly developed chain CVT for middle capacity, which is characterized by compactness, higher torque density and higher efficiency, has chased to achieve high levels of environmental friendliness and dynamic quality with NVH and driving performance. The CVT has realized the target performance by variator which has enlarged ratio coverage and new hydraulic system. This article introduces devices and those features of the new CVT.

1. Preface

The chain CVT for middle capacity has been much improved on its performance for the new vehicle launched in 2019 summer, which was launched in 2011 and improved in 2016. This article introduces the development of it.

2. Aim of Development

The configuration improvement of the CVT has been chased to meet the larger requirement for ‘Environmental Friendliness’ and ‘Dynamic Quality’ also in terms of low cost, which has features of chain CVT like compactness, high torque density, and constantly high transmission efficiency over the overall ratio. As a result, the base configuration was determined which fully realized the seamless CVT feature by covering all the ratio by one variator to realize considerable environmental friendliness and NV improvement.

The envelope dimension or its axle layout was kept to prevent from having any effect on vehicle compartment, however, approximately 80% components are newly designed. Its main configuration is shown in Fig.1, and its main cross section in Fig.2.

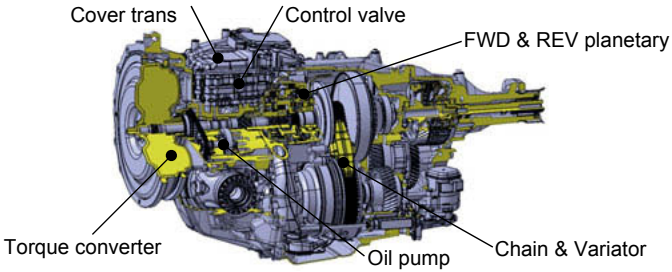

Fig. 1: Main configuration

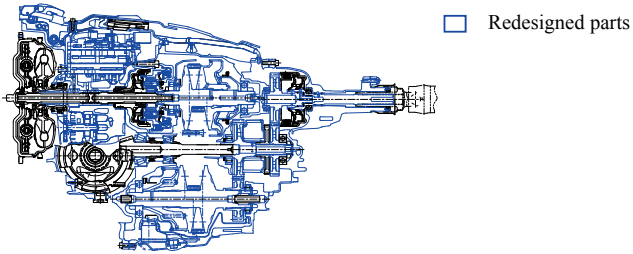

Fig. 2: Main cross section

2.1. Improvement on Environmental Friendliness

Targeting to realize class top performance on environmental friendliness, its ratio coverage was enlarged (8.1□7.0) to reduce engine rotational speed at high way by reducing overdrive ratio, furthermore, its power loss was reduced by 22% compared to the previous CVT by reducing hydraulic and stirring loss (Fig3, 4).

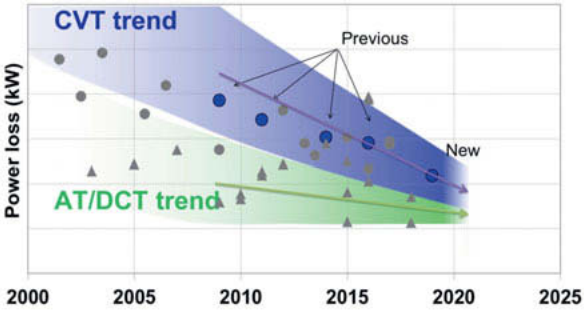

Fig. 3: Transmission power loss forecast as of 2016 (80km/h road load)

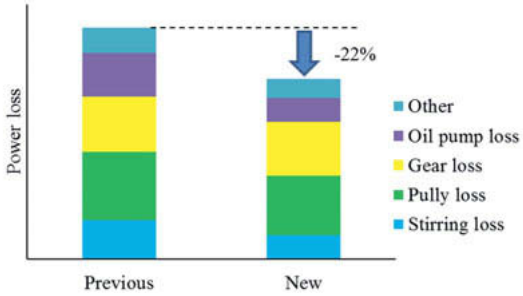

Fig. 4: Breakdown for transmission power loss (80km/h road load)

2.2 Dynamic Quality Improvement

Reduction gear ratio was enlarged, in addition to the enlarged low ratio by the larger ratio coverage, to improve launch and acceleration performance. Drive ability was also improved with the 8-speed manual mode (□previous 7-speed). In terms of NV performance, the vane-type oil pump and the optimized gear specification contributed to much better quietness.

3. Configuration and Feature of the New CVT

Table 1 shows the main specification of the new CVT.

Table.1 Main specification

		Previous	New
maximum input torque		250Nm	
gear ratio	ratio coverage	7.0	8.1
	pulley ratio	2.683~ 0.382	2.893~ 0.358
	reduction ratio	1.342	1.405
	final ratio(2type)	3.900/4.111	3.700 / 3.900

3.1. Enlarged Ratio Coverage

The target ratio coverage was determined on the point of ensuring launch ability by the low ratio and improving fuel economy by the od ratio, as well as on the point of ensuring traction at partial acceleration. In order to reach to the target, running radii at primary and secondary pulley were optimized with the same pulley axle distance to enlarge ratio coverage by 16% compared to the previous CVT. The ratio coverage- 8.1 which is a top-runner value without an auxiliary transmission was achieved (Fig. 5).

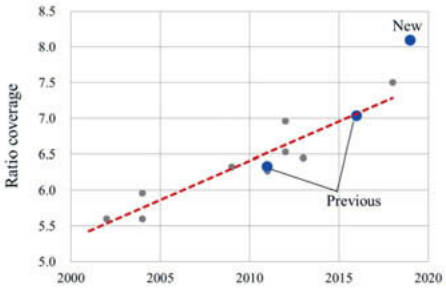

Fig. 5: CVT ratio coverage forecast as of 2016 for middle torque capacity

Since chain load should rise due to smaller running radii of the chain, shape change of rocker pins, optimum arrange of link plates, and further improved production process were done to strengthen the chain. Moreover, while diameters of pulley shafts being reduced to realize the smaller running radii, strength and stiffness of the shaft were secured for larger torque input at secondary side by adding shot peening process and optimizing back shape of pulley sheaves (Fig. 6, 7).

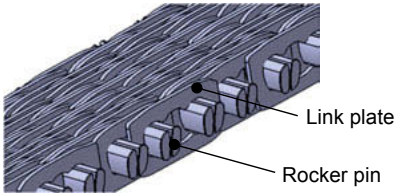

Fig.6 CVT chain

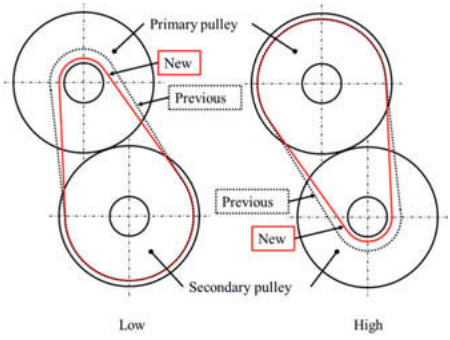

Fig. 7: Running radii comparison

3.2. Renewal of Hydraulic System

The CVT renewed its hydraulic system by implementing an independent hydraulic control between line and secondary pressure, and a 2-port oil pump to reduce power loss (Fig. 8).

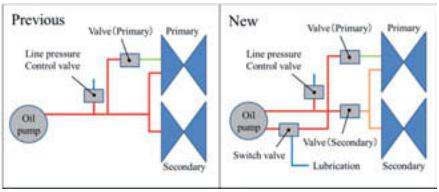

Fig. 8: Hydraulic system chart

3.2.1. Independent Hydraulic Control of Secondary pressure

Independent hydraulic control of secondary pressure was adopted to realize precise control which shared line pressure in the previous model. Thus, optimum secondary pressure was realized in the area where pressure was previously too much due to factors other than the variator. Power loss with variator clamping pressure was reduced by 14% at 80km/h road load.

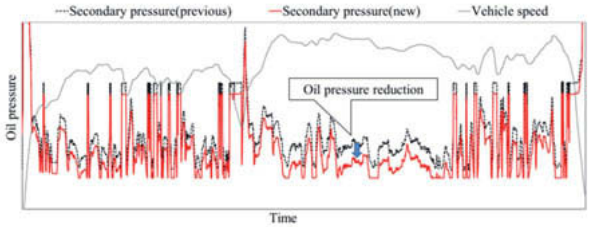

Fig. 9: Hydraulic pressure reduction in US highway mode

3.2.2. Oil Pump with 2-Port Discharge

The previous oil pump had some mechanical power loss since oil flow would excess necessary volume due to the 1-port discharge when necessary volume was small at low load condition. The new oil pump has 2-port discharge to change their ports depending on driving conditions. When big oil volume is requested from line pressure to each circuit, e.g. in acceleration, hydraulic pressure is supplied from 2 ports, and when small one being done in constant driving condition, the 1 port is switched to low pressure to reduce the oil pump load. The oil pump torque with the 1 port is reduced by 30% compared to that with the 2 ports. Power loss at 80km/h road load is reduced by 45% compared to the previous hydraulic system.

3.3. Reduction of Mechanical Loss

Friction loss torque was reduced by optimization internal specification of the taper roller bearings (Fig. 10).

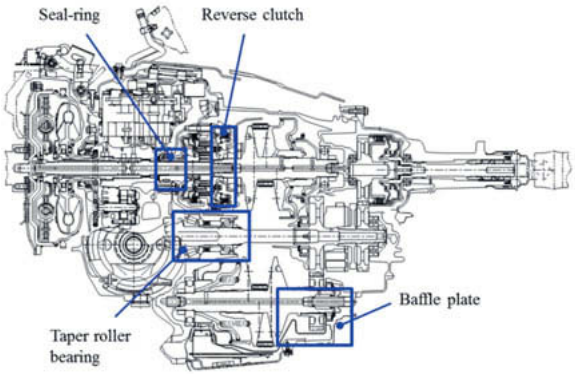

Fig.10: Items for mechanical loss reduction

Pocket shape at side faces of seal ring being optimized, its friction loss torque was reduced with forming an oil film by dynamic pressure effect (Fig. 11). Drag torque was reduced by improving oil drain ability with the change of facing paper shape at the reverse clutch (Fig. 12). Furthermore, viscosity of the CVT fluid being lowered at overall temperature range from low to high (Fig. 13), and oil inflow being suppressed with shape change of its pulley baffle plate (Fig. 14), stirring loss was reduced. The stirring loss becomes 37% less than that of the previous at 80km/h road load.

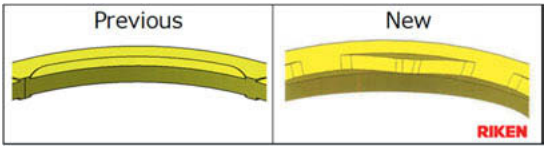

Fig. 11: Seal ring pocket shape

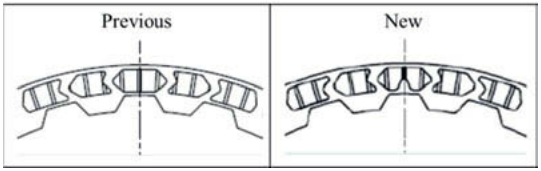

Fig. 12: Facing paper shape at reverse clutch

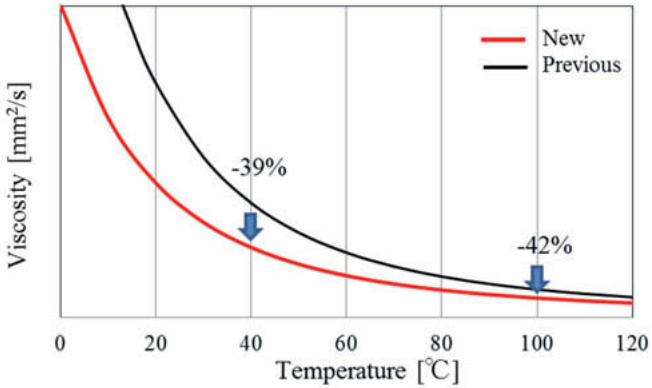

Fig. 13: CVT fluid viscosity

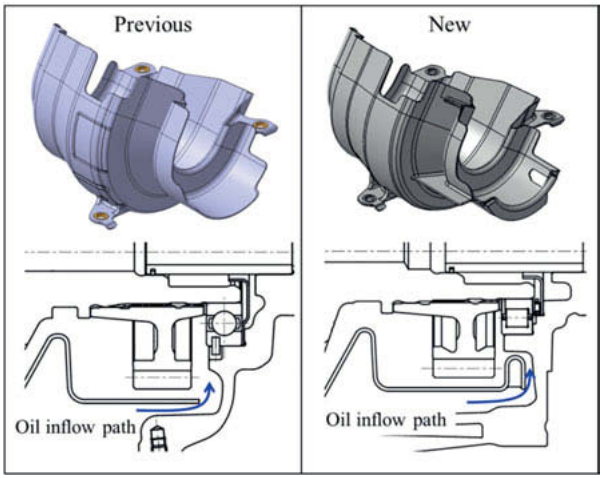

Fig. 14: Baffle plate for variator

3.4. Reduction of Oil Pump Noise

Vane type oil pump was adopted instead of internal gear type in the previous, and an oil guide, which was newly designed, was installed at upper stream of the suction port. With the rectification effect by the oil guide at its return circuit, absolute value of vacuum pressure being reduced to suppress generation of air bubbles, oil pump noise was reduced by 5dB (Fig. 16).

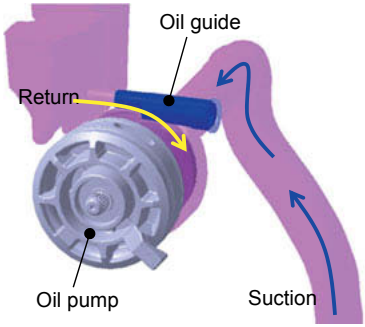

Fig. 15: Suction circuit for oil pump

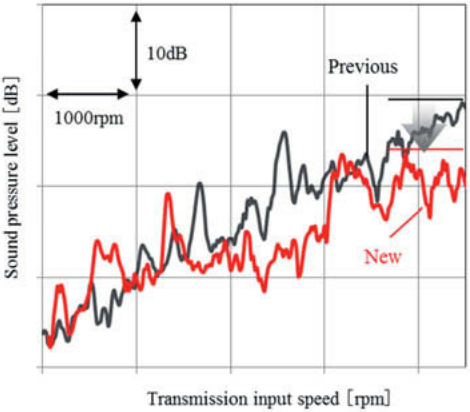

Fig. 16: Oil pump noise comparison

3.5. Reduction of Planetary Gear Noise

Gear meshing was designed to be in the same phase so as not to excite structural modes which much contributed to planetary gear noise, and, vectors of reaction forces being changed, sound pressure level of radiation was reduced by 10dB compared to the previous (Fig. 17).

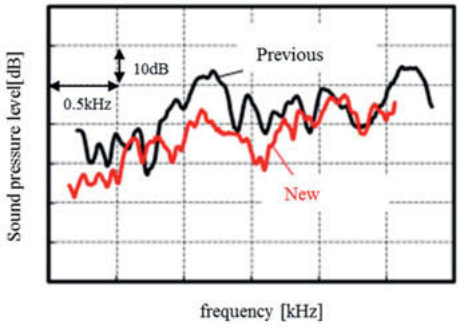

Fig. 17: Planetary gear noise comparison

3.6. Weight Reduction

Material changes being implemented like the oil sump plate from metal to aluminum, as well as the cover-trans from aluminum to plastic, each 64% and 44% weight reduction were realized together with their shape changes.

4. Summary

The new chain CVT for middle capacity has contributed to realizing considerable 'Environmental Friendliness' of the new vehicle with the ratio coverage- 8.1 which is the best in CVTs without an auxiliary transmission, and with the 22% reduction of power loss in total by its mechanical loss reduction. Moreover, in addition to better launch ability by its enlarged ratio coverage, the CVT has done to improving NV performance with their specification changes of the oil pump and the planetary gear set, etc.

The development for better 'Environmental Friendliness' and 'Dynamic Quality' will be continued to meet customers expectation all over the world.

Reference

[1] Shunsuke, Kijima. et al. Development of Lineartronic for New IMPREZA, SUBARU Technical Review No.44 (2017), P48-52

[2] Hiroko, Aoki. et al. Development of Design Procedure for the Planetary Gear Noise, SUBARU Technical Review No.43 (2016), P68-72

Cost efficient PHEV powertrain solution based on dedicated hybrid transmission

Cost efficiency for small and mid-size plug in hybrid vehicle

Dr.-Ing. **Kiarash Sabzewari**, **Magdalena Vieracker**,
Joerg Sagstetter, Vitesco Technologies, Regensburg

Zusammenfassung

Im Rahmen dieses Beitrags wird ein innovativer Ansatz für einen hybriden Antriebsstrang vorgestellt. Der Fokus liegt in der Realisierung eines kosteneffizienten Antriebsstrangs, um insbesondere Plug-In Hybride für das untere Fahrzeugsegment attraktiver zu gestalten. Dies wird durch die konsequente Vereinfachung des Verbrennungsmotors und Getriebes ermöglicht, die unter anderem Verzicht auf Motoraufladung, Anfahrelemente, mechanische Synchronisierungseinheiten sowie Rückwärtsgang beinhaltet. Durch Synergieeffekte aus der Elektrifizierung mit zwei Elektromotoren können diese Getriebefunktionen entfallen wobei gleichzeitig alle Fahrbarkeitsanforderungen erfüllt werden. Dieses Prinzip wird dedicated hybrid transmission (DHT) genannt. Abhängig von den Fahreranforderungen werden durch die Drehmomentverteilung zwischen drei Antrieben verschiedene Betriebsarten realisiert und die dynamische und komfortable Umsetzung der Anforderungen in allen Fahrsituationen erreicht. Erläutert wird zudem das innovative Regelungskonzept basierend auf dem Raddrehmoment, wodurch das Potenzial dieses neuen Antriebskonzeptes voll ausgeschöpft wird.

Abstract

This paper discusses an innovative powertrain approach for a PHEV. The focus lies on higher cost efficiency for the powertrain system in order to make plug-in hybrids more attractive for lower vehicle segments. Key measures are consequent simplification of the combustion engine and transmission by removal of engine turbocharging, drive off elements, mechanical gear synchronization and the reverse gear. The synergies of electrification are used to fulfill the drivability requirement and decontenting of the transmission, which is defined as a dedicated hybrid transmission (DHT). As a result, the new powertrain approach is capable of various driving modes, depending on the driver's request, by distributing the torque between three available drives in the vehicle. Consequently, fast dynamic response and high driving comfort

are achieved in all driving situations. An advanced control concept based on wheel torque is described, which fully exploits the potential of this sophisticated powertrain approach.

1. Introduction

The fulfillment of the driveability requirements as well as the realization of adequate electric driving range are fundamental challenges in the development of PHEVs. PHEVs on the market can be classified in parallel hybrids, such as P2 and P4 and power-split hybrids. The parallel hybrid approaches are based on conventional powertrains, considering existing powertrain components and packaging space. Thus, the maximum synergies between electric motor and internal combustion engine (ICE) can hardly be utilized. Furthermore, these solutions often entail additional costs, arising from extra electrical components without any simplification of components and systems such as ICE or transmission. Most of the currently available solutions confirm this fact. This is the main reason, why PHEVs have remained a niche on the market so far. An alternative solution to benefit from the synergy of electrification is shown by power split PHEVs. Using an electronic continuously variable transmission (eCVT) with port fuel injection engine (PFI) reduces the powertrain system cost. However, two cost-intensive permanent magnet electric motors (PSM) are the main disadvantage of such a power-split concept [1].

2. Powertrain approach

As a system supplier, Vitesco Technologies continuously analyses the impact of electrification on drivetrain development. As a part of this analysis a study has conducted preliminary studies to understand the impact of electrification on drivetrain development. Therefore, a concept has been developed for PHEV's based on a C-class vehicle. The proposed approach provides full hybrid functionality and aims to meet rigorous cost targets as well as key performance indicators for comfort. For a proper comparison of various PHEV concepts, the main

requirements are defined. These main requirements are summarized in Table 1.

Table 1 - Overview of PHEV main requirements

Scope	Description
Cost	Overall cost shall be significantly lower than existing P2/P4 PHEV
Vehicle category	C-segment, < 1500 kg
Evaluation basis	Worldwide Harmonized Light-Duty Vehicles Test Procedure (WLTP)
CO_2-emissions and pollutant	<50 g/km (weighted); Euro 6d
Driveability	Automated drivetrain
	No torque interruption during shifting
	Pure electric driving range more than 50 km
	Pure electric driving with sufficient potential for typical accelerations
	Maximum speed: 130 km/h purely electric; 160 km/h in hybrid mode
Electric power supply auxiliaries	3 kW 12 V power supply + 5 kW EACC at $SOC_{min:}$ and any other condition such as during vehicle standstill, creeping etc.

2.1. Architecture

To realize the dedicated hybrid transmission concept, three torque sources were arranged around the 4-gear automated manual transmission as shown in **Figure 1**. A crankshaft mounted starter generator (SG) is connected to the internal combustion engine (ICE) with a defined transmission ratio. The ICE and SG can be decoupled from the drivetrain by the sliding

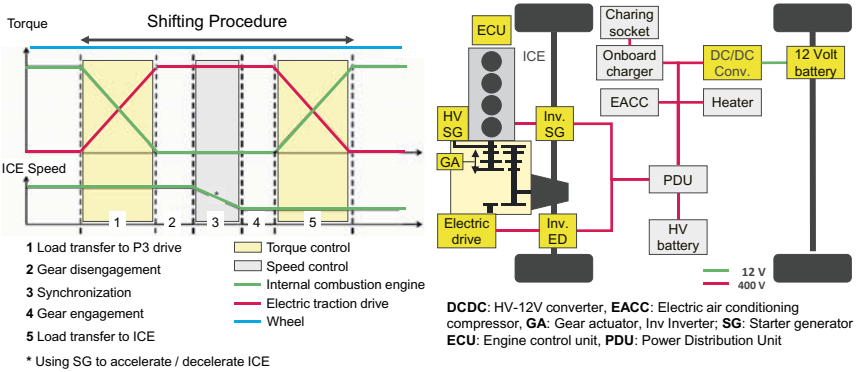

Figure 1 - Left: shifting procedure for DHT based on torque assist and synchronization by electric drives in five steps with respect to ICE speed and various torques. Right: principal architecture of Cost Efficient PHEV with proposed dedicated hybrid transmission

dog clutches. Furthermore, there is an electric traction machine (ED) on the gear output shaft, connected permanently to the wheel by a fixed ratio gear.
In order to achieve the maximum cost efficiency, the transmission architecture is simplified by removing launch elements, such as friction clutches, the conventional reverse gear, as well as any mechanical synchronization units. Consequently, any launch maneuver or backward driving is done by the ED. The ICE can be coupled to the drivetrain in any desired gear, as soon as the appropriate crankshaft speed corresponds to the vehicle speed and can close the drivetrain without an NVH issue. In addition to starting the engine, the starter generator is used to synchronize the crankshaft, both before coupling the engine in any gear and during up- or downshifting. For an automated gear shift, the ICE torque is ramped down while the ED torque is increased in the same proportion to avoid any torque interruption. In the next step, the ICE is fully disconnected from the drivetrain by disengaging the gear through the claw units. Gear shift synchronization is realized by the SG, reducing the crankshaft speed by applying a negative torque for an upshift, and respectively increasing it with a positive torque for a downshift. After synchronization and engagement of the target gear, the torque trajectories are applied vice versa between ED and ICE. **Figure 1** shows the torque and speed profiles during a gear upshift and the basic architecture of the powertrain.

2.2. Operation- and driving modes

The powertrain design of the dedicated hybrid transmission prototype vehicle contains three torque sources with different transmission ratios to the wheel. A functional driving strategy has been developed to combine the different torque sources in order to provide the driver torque demand in a repeatable and consistent manner independent of the Operation Mode. The powertrain operation strategy contains both energy management and driveability controls. Given two energy storages, three power sources, and a simplified DHT, a systematic approach is essential to manage all the degrees of freedom within the powertrain and to ensure the driveability requirements. Depending on the driver request, the available energy and the energy flow through the driveline, the various states of the powertrain are defined as either operation or driving modes. In addition, the transitions between various states are defined as discrete and continuous.
An Operation Mode (OPM) is defined as a steady state of the drivetrain, considering the energy transfer between sources and sinks. Depending on the operation mode, driving maneuvers are realized by different combinations of the torque sources (**Figure 2**). The distinguishing criterion between two OPMs is generally a change of the energy source. This refers to both a switching from the fuel tank to the HV battery or vice versa during traction, or the transition to

recuperation of kinetic energy during deceleration.

The main operation modes for acceleration are purely electric and parallel hybrid driving. Electric driving is realized in neutral gear, and only by the ED. ICE load point shifting can be applied either for battery charging, or the ED can support the ICE if the driver torque request exceeds the available ICE torque. Both the ED and the SG can be used for torque boosting. Gear shifting during hybrid driving is a transient phase and therefore not considered as a separate operation mode. Since the DHT does not have any launch element for the ICE, the wheel torque at low speeds must be realized by the ED. To ensure this also when the battery SOC is very low, a serial hybrid operation mode can be applied. Then, during the electric launch in neutral gear, the ICE provides energy to the battery via the starter generator.

Coasting or active deceleration always takes place in neutral gear. Whenever the accelerator pedal is released, the actual gear is disengaged, and the ICE is stopped. This means that there is never a gear shift during fuel cutoff phase. Finally, brake recuperation is always realized by the ED. **Figure 2** shows the energy distribution in the drivetrain during different operation modes.

In addition to operation modes, drive modes can be selected by the driver based on the available state of charge (SoC). The *e-Drive Mode* can be used until the SoC value reaches a defined minimum limit. In the other driving modes, both the ICE and the ED are used for traction, together or separately, depending on different requirements. The intention behind the default *Hybrid Mode*, is the energy efficiency and driving comfort. The torque split is defined depending on various parameters, such as temperatures, speeds, load request, battery SoC or system limitations. This *Hybrid Mode* as *Eco-Mode* is supplemented by a sport option, where the focus lies on fast response and increased acceleration. Here, delayed upshifts and preponed downshifts are applied, and a certain torque reduction is accepted during full load shifting. Furthermore, the side-attached starter generator is used to increase the tractive force during full load acceleration. There is a *Charge Mode*, where the ICE is used to provide the required wheel torque as often as possible. In addition, ICE load point shifting is applied in order to charge the high voltage battery in *Charging Mode*, whenever no high load is requested for acceleration. The *Charge Maintain Mode* aims to keep the battery SoC within a range around the initial value.

Another feature for the driver is the selection between coasting and pedal-off recuperation as a reaction to releasing the accelerator pedal. In the latter case, a light recuperation by the ED simulates the deceleration during fuel cut-off of a conventional vehicle and charges the battery.

The recuperation intensity is increased, when the driver selects the sports mode.

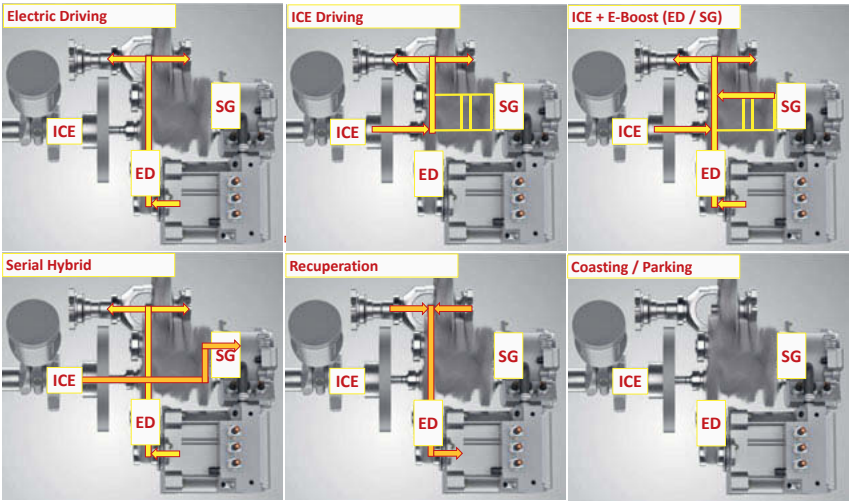

Operation Modes	ICE on		ICE off		
	Parallel Hybrid acceleration	Parallel hybrid + load point shifting	n. A.	n. A	Gear engaged
	Serial Hybrid (ICE+SG) and el. acceleration	Serial hybrid (ICE+SG) and recuperation	Recuperation	coasting / electric acceleration	Gear disengaged
	ED Torque ≥ 0	ED Torque < 0		ED Torque ≥ 0	

Hybrid Driving Modes (Charge Depleting, Charge Sustaining, Charging)

Hybrid Driving Modes + E-Drive Mode

Figure 2 – above: various operation modes of the Cost Efficient PHEV based on DHT and the three torque sources: ICE, electric traction drive (ED) and starter generator (SG) - below: the matrix of available operation modes as combinations of gear, ICE and ED, and the corresponding drive

2.3. Wheel torque request of the driver

In many conventional functional architectures in vehicles with a combustion engine or Hybrid configurations from P0 to P2, the driver demand for acceleration and recuperation is interpreted as an engine crankshaft torque request. This is an appropriate approach if all torque sources of the drivetrain are connected to the same gearbox input shaft with a fixed transmission ratio. In the case of the DHT the gear ratios between wheel and torque sources are changed differently. While the P3 traction drive is connected permanently by fix gear ratio,

the ICE and P1 e-Drive (SG) can be decoupled by variation of different DHT gears. Thus, it is necessary to use an adequate reference for driver request.

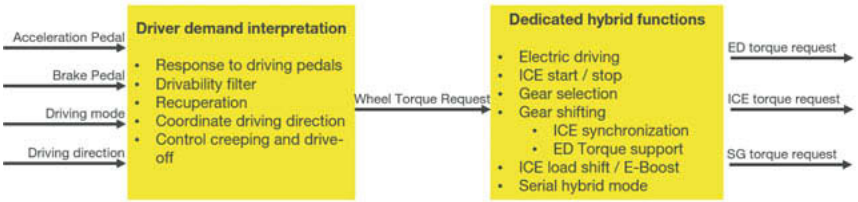

Figure 3 - Function split between wheel torque and drive unit level

In this innovative approach, the driver demand via the brake or accelerator pedals is interpreted as a corresponding torque request at the wheel, which shall be realized independently from the actual operation mode of the drivetrain. Therefore, the driver demand interpretation is performed separately from torque commands to any actuator and power sources. Only the selected driving mode has an impact on the driveability and therefore on the interpretation of the driver demand. To fulfill these requirements, typical driving functions are distributed on separate levels of a wheel torque-based functional architecture (**Figure 3**).

The maximum available wheel torque is an accumulation of the active torque sources in each driving mode. For the *e-Drive* mode, only the maximum available wheel torque of the ED is considered for the driver demand interpretation. In *Hybrid Eco* mode, the available ICE torque is added to this curve. For the highest performance, also the SG torque capability is considered for the *Hybrid Sport* mode as e-Boost. The available torque curves are shown in **Figure 4.**

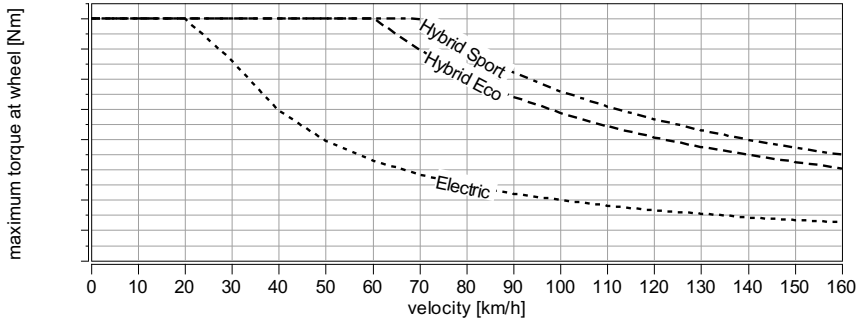

Figure 4 - Maximum available wheel torque for each driving mode

3. Driveability results

In the following section various OPMs and the transitions between them are discussed. The

various degrees of freedom of the presented powertrain enable different possibilities of torque distribution during ordinary driving situations.

In the first driving scenario pedal-off recuperation and brake recuperation are presented. In case of the pushed brake pedal or activated one-pedal driving, the minimum available wheel torque is shifted to negative values. While the one-pedal driving focuses on high driving comfort and smooth continuous torque transitions, the brake recuperation is used for optimal driving efficiency at higher deceleration ratio. **Figure 5** shows an example of seamless transitions between two mentioned operation modes. At the beginning the pedal-off recuperation leads to a reduction of speed increase and finally to steady states. In the second phase, the brake pedal is pushed and active braking is demonstrated by high negative wheel torque as well as speed reduction. In the last step the OPM is changed again to coasting by a ramp up of the wheel torque. During the OPM changes the vehicle speed is permanently changed without any jerk.

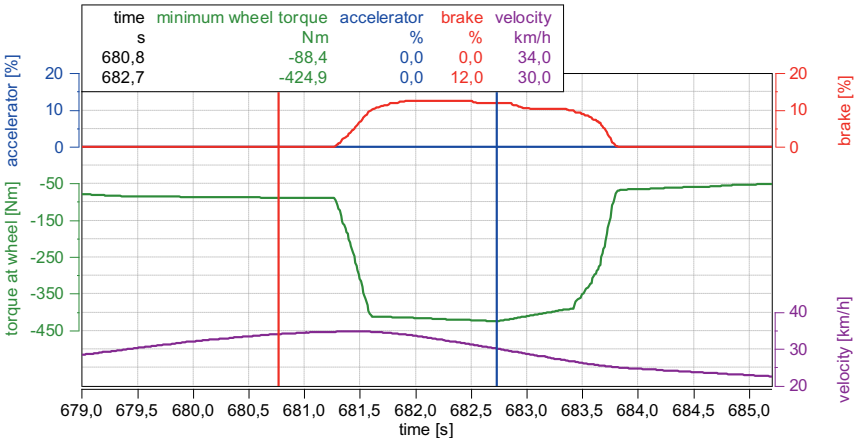

Figure 5 - A seamless transition between pedal-off recuperation and brake recuperation. Pedal-off recuperation shown as low negative value (cursor 1 in red) and brake recuperation with high negative wheel torque to achieve maximum recuperation potential (cursor 2 in blue)

Figure 6 shows an example of starting and adaption of creeping function to keep the creeping speed. Here, at the beginning the vehicle is in the coasting mode, where the speed is reduced without pushing any pedals. Shortly after that, the wheel torque is raised accordingly to achieve the creeping speed of ca. 6 km/h and decreased again to keep a certain velocity at the slope. In the last phase the acceleration pedal is pushed again, and the creeping torque set to zero. The final driver wheel torque request is calculated based on a map with respect to the acceleration pedal value and vehicle velocity. A final torque filter is applied to reduce the pedal

values noises and still meet the expected dynamic response. Consequently, the transition between mentioned OPMs are shown with smooth velocity changes, and no jerk nor shock is noticeable by the driver.

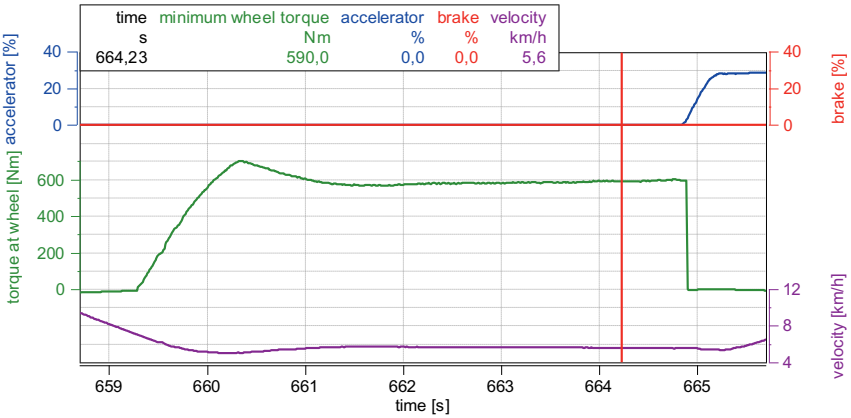

Figure 6 - Minimum available wheel torque for creeping at a slope, where the wheel torque is built up to certain level to keep creeping and avoid vehicle stop and backward rolling

Figure 7 illustrates, how the different torque sources contribute to a drive-off scenario in urban traffic, like an acceleration from 0 – 50 km/h. In section 1, the vehicle accelerates electrically from standstill. Since the vehicle reaches the minimum velocity required for the coupling of the combustion engine, the ICE is started and synchronized in section 2, while the ED still provides total requested wheel torque. Finally, when the correct gear is engaged in section 3, the ICE torque is ramped up while the ED torque is decreased, in order to continue the speeding up with pure combustion propulsion. As a result, a linear increase of vehicle speed is achieved during the whole acceleration phase. The good correlation between requested and measured torque at the chassis dyno, as well as the fast response to driver demands, enable precise execution of the wheel torque request. The signals compare the wheel torque request from the driver against the measured counter torque from a chassis dyno. It must be noted that the response delay at the drive-off, as well as the small raise of the measured torque in section 3, are a result of inaccuracy and inertia in the measurement system which amplifies even minor torque interruptions at the wheel. The delay between measured and driver torque request is due to time delay between chassis dyno control loop. This closed loop control system is only for calibration and not used for any road test. The final drivability validation is shown in the

below section as road test.

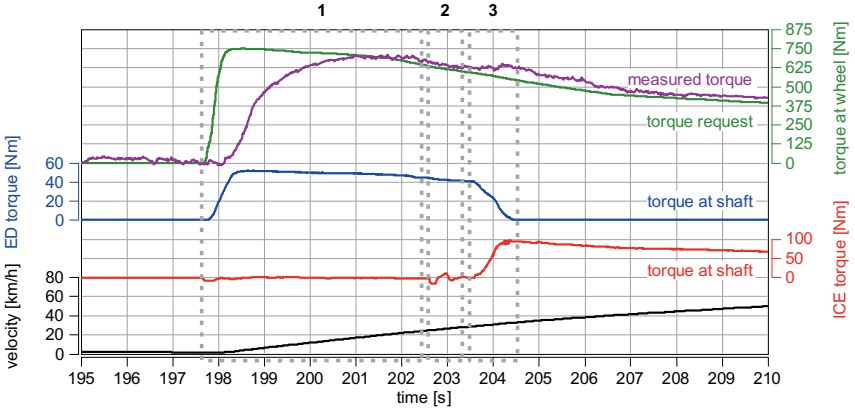

Figure 7 - Example of imperceptible torque transfer between two traction sources: Electrically vehicle launch and take off in first section, followed by ICE start in second phase and a torque fading from ED to ICE in the 3rd step. The effective wheel torque shows excellent correlation to the request, whereby the torque source changes are not noticeable by the driver

Figure 8 presents another common road tip-in scenario, where the vehicle accelerates from 65 to 75 km. Instead of a downshift, the acceleration can be fully handled by the ED. Since the engine operating points at high load and low revolution have higher efficiency, the objective for an environment friendly gear selection is to keep the ICE at these conditions for steady state driving situations. In conventional powertrain architectures this target has to be evaluated based on requirements for acceleration capability and elasticity. In case of spontaneous and short-term acceleration demands, the advantage of the dynamic response of the ED is used. As soon as the driver's wheel torque request is reduced, the ED torque is decreased by still keeping the ICE operation point at the same level. Only after further reduction of driver torque request in section 2, there is a demand to reduce the ICE torque. Subsequently, the phlegmatization of the ICE and the prevention of two transient conditions during gear shift, lead to fuel and emission saving. At the same time, no negative impact on response and

driveability is noticeable.

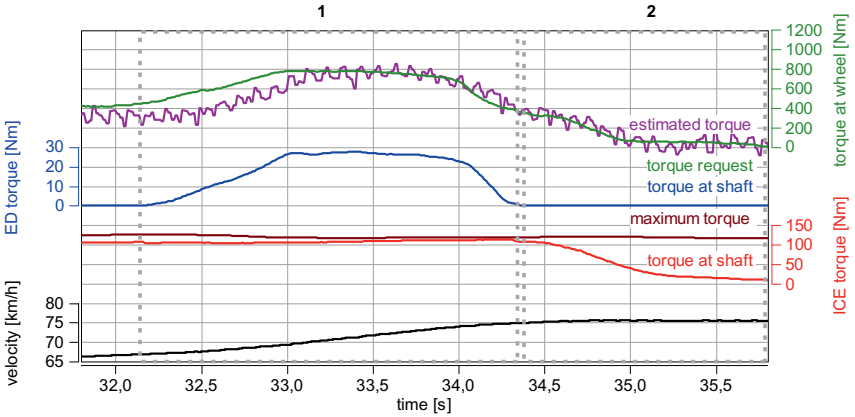

Figure 8 - Boost with ED for spontaneous acceleration: fast response to driver request and continuous linear velocity increase while the ICE operation point is kept at certain level.

The last example (**Figure 9**) demonstrates the torque variation and acceleration during gear shift. In this case, an upshift at partial load at approximately 1m/s² is illustrated. As already discussed in figure 1 the torque blending is started before shifting and is shown as reduced

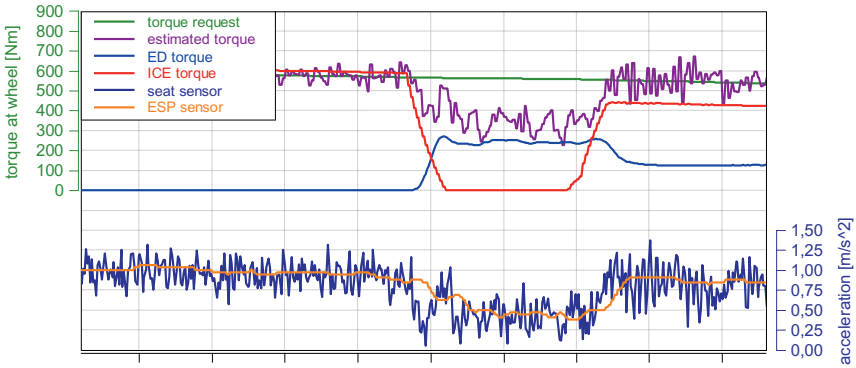

Figure 9 - Example of upshift at partial load from 2nd gear to the 3rd gear: Comfortable gear shift as smooth acceleration changes during the gear shift realized by e-Drive assist for torque fill and shaft synchronization.

ICE respectively increase ED torque. The wheel torque is reduced to ca. 65 % during gear shift and calculated based on acceleration changes. This is shown in the below part of diagram. The acceleration is reduced before and after the gear shift smoothly to the desired value without any shock. As a result, a seamless smooth gear shift is possible. After the upshift the

electric drive performs part of needed wheel torque to fulfill the driver request. This is necessary since the ICE torque at wheel is reduced due to upshift.

Based on the previous outcomes, the main driveability advantages of the presented powertrain approach is summarized as follow:

- The discussed powertrain approach covers all the well-known operation modes, such as hybrid driving, load point shifting, recuperation and serial hybrid
- The torque wheel-based control strategy realizes intelligent torque distribution between all traction components regardless of hybrid topology such as P1, P2 , …
- A unique torque blending between three torque sources enable excellent transitions during different driving scenarios without any jerks and is not noticeable by the driver.
- While the electric drive is used for fast driver request response, the ICE can be driven in the best efficiency range and for very high power requests
- Despite a massive simplification of the transmission, a seamless shifting and good driver response is achieved by using the synergies of electrification for the transmission

4. Powertrain cost analysis

The powertrain approach presented above has shown the capability to meet requirements with respect to comfort, packaging and driving performance. In the last step, the costs for different powertrain approaches are evaluated (**Figure 10**) and compared to the concept proposed in this paper. For this purpose, three solutions available on the market (P2, P4 and power split) as well as two prototype solutions based on DHT are discussed. A “P4 PHEV” uses a gasoline direct injection engine (GDI) with an automatic transmission (AT). In a P4 configuration, the electric traction motor is located on the conventionally non driven axle and runs independently from the ICE. The “P2 PHEV” is typically set up with a dual clutch transmission (DCT), a gasoline direct injected engine and a disc shaped PSM. In addition, the “Powersplit” concept is considered. For this the typical architecture consists of a conventional multi-port injection ICE, a planetary gear set and two electric drives, one as a starter generator attached to the planetary gear, the other electric motor as traction drive directly linked to the output shaft of the transmission. Furthermore, two prototype solutions are considered, based on DHT.
To compare those PHEV solutions, the components for the selected powertrain concepts are adapted to the requirements of Table 1, so that a fair comparison on the same baseline is ensured. The resulting cost comparison is presented in **Figure 10**.

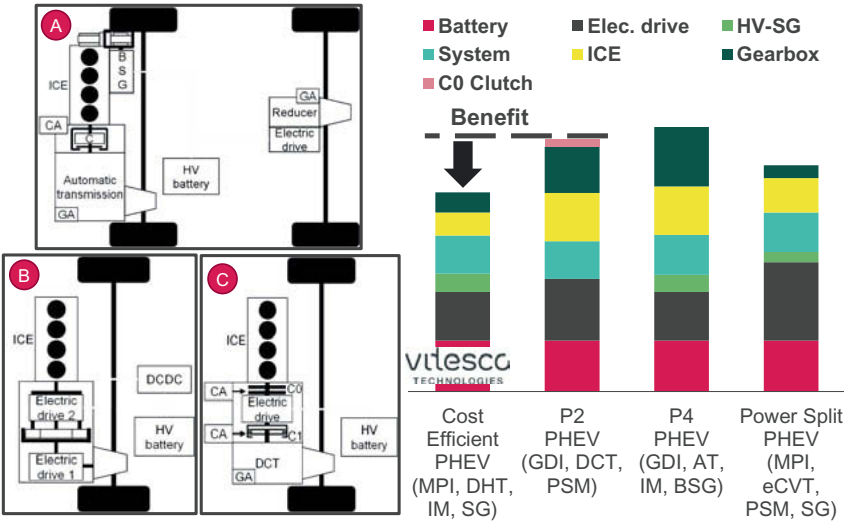

Figure 10 - Powertrain comparison: Left: Three references A: P4-PHEV with automatic transmission (AT) and e-Axle rear drive, B: Powersplit PHEV with two electric drives and planetary gearbox, C: P2-PHEV using double clutch transmission (DCT) and P2 inline machine – Right: a comparison of non-binding market price estimation for mentioned powertrains

It is assumed that all PHEVs use the same battery. The costs of electric machines and power electronics are summarized in section electric drive. The cost benefit of an IM traction drive, which is used for “P4 PHEV” and Vitesco Technologies cost optimized PHEV approach, becomes evident. The bar increment “system” summarizes the cost of components for other systems such as the thermal management components as well as the wiring harnesses etc.

The “P4 PHEV” has the same costs for electric traction drive as the presented Vitesco PHEV. However, using an expensive automatic transmission (AT) and an additional separate gearbox for traction drive diminish this advantage in the overall powertrain cost comparison. The “P2 PHEV” is also driven by expensive PSM, as well as using a DCT. Although transmission costs are significantly reduced for “Powersplit” PHEV approach, this concept is more expensive than the cost optimized PHEV due to higher costs of the electric drive. The presented Vitesco Technologies PHEV approach leads to a remarkable cost reduction and is cost minimal compared to the other PHEV approaches. Here a cost reduction up to 20% is feasible at the same performance level unlocking cost saving plug-in hybrid applications in vehicle A- to C-segment

5. Conclusion

A new and innovative powertrain topology with a simplified transmission concept is proposed, resulting in a significant cost reduction for PHEVs. This is achieved by providing complex mechanical transmission functions, such as launching, synchronizing and reverse driving, by the electric machines, replacing costly synchronization elements by simple dog clutches, and reducing the number of gears. The benefit of the integration with the ICE and electrical motors with decreased mechanical effort in combination with innovative controller functions is the uninterrupted and smooth power delivery to the wheels. The powertrain components are designed to comply with all typical vehicle requirements and use cases. The electric traction drive is realized as an induction machine for optimal benefit-to-cost ratio not compromised by typical PHEV package constraints. Consequently, a cost-efficient ICE with simplified requirements is applied.

This cost efficient PHEV powertrain approach shows convincing performance due the degree of freedom by using two electric machines and an ICE. An elaborated operating strategy was developed in order to demonstrate the driveability potential as well as handle the various combinations of the three torque sources. Consequently, all the typical operation modes such as boosting, recuperation, coasting and hybrid driving can be realized. Indeed, the driver demand interpretation is designed separately from to torque commands to any actuator and power sources. Only the selected driving mode has an impact on the driveability and therefore on the interpretation of the driver demand. A wheel torque based top-level driving strategy ensures fast execution of any driver command and outstanding driveability level. In the hybrid mode the ICE operates mostly in the range of high efficiency, whereas the electric traction drive takes care of minor and fast changes in torque request and therefore avoids downshifting. E-drive assisted gear shifting, makes smooth dog clutch shifting possible while the continuous acceleration is ensured by a secondary electric drive. As a result, the seamless shifting guarantees high comfort by avoiding any torque interruption. Besides that, A unique torque blending between three torque sources enable excellent transitions during any operation mode and driving situation without any jerks and is not noticeable by the driver.

6. References

[1] Sabzewari, K. et al. : Cost efficient powertrain for plug-in hybrid electric vehicle, JSAE Annual Congress Yokohama, 2018

[2] Sarmiento, O. et al.: eDrive Assisted Dedicated Hybrid Transmission Synchronization-Enabling Real-Drive-Emissions, 18th CTI Symposium Berlin, 2019

Rolling into the Future – Bearing Solutions for Electric Mobility

Wälzlagerlösungen für die E-Mobilität

Dr.-Ing. **Franz Völkel**, Dipl.-Ing. (FH) **Manfred Tietz**,
Dipl.-Ing. (FH) **Alexander Schamin**, Dipl.-Ing. (FH) **Sebastian Giehl**,
Schaeffler Technologies AG & Co. KG, Herzogenaurach

Kurzfassung

Lager in E-Antrieben müssen besonderen Anforderungen genügen, welche jenen in konventionellen Getrieben nicht gleichzusetzen sind. Dies trifft zum einen für mechanische Eigenschaften wie z.B. Hochdrehzahlfähigkeit und Laufruhe zu, zum anderen werden im elektrischen und elektronischen Umfeld Zusatzfunktionen benötigt, die das Lager vor Schäden durch Stromdurchgang schützen und einen störungsfreien Betrieb des Aggregats im Fahrzeug hinsichtlich EMV ermöglichen. In der Kombination von Bauelementen wie Sensoren, Stromableitungen und Stromisolationen mit Wälzlagern stecken interessante Lösungen, die eine Erhöhung der Leistungsdichte bei gleichzeitiger Kostenreduktion möglich machen.

Anhand einer E-Achse in Stirnradbauweise werden in diesem Beitrag von SCHAEFFLER entwickelte Lagerinnovationen für die einzelnen Positionen vorgestellt, welche im oben beschriebenen Kontext dem Kunden wesentliche Vorteile bieten.

Abstract

Bearings used in electric drives have to fulfill specific requirements that cannot be compared to those of conventional transmissions. This is true for mechanical properties such as high speed capability and smooth running on the one hand; on the other hand, additional electrical and electronic functions are required that protect the bearing against damage caused by the passage of current and ensure the unit's problem-free operation in the vehicle in terms of EMC. Combining components such as sensors, current shunt elements, and current insulation with rolling bearings provides interesting solutions which allow power density to be increased while reducing costs at the same time.

Using an electric axle with spur gear arrangement as the basis, this paper illustrates bearing innovations developed by SCHAEFFLER for the individual positions that offer significant advantages for the customer in the context described above.

1. Introduction and Overview

To provide an overview, Fig. 1 shows a typical electric axle in lay-shaft design with the bearing positions for the rotor shaft and for the transmission shafts. It is not the bearing arrangement itself, but rather the requirements which have to be fulfilled combined with favorable combination options that open up a range of interesting possibilities for drivetrain engineers.

The first point to mention here is the speed capability of the bearings for the rotor and transmission input shaft. Speeds of up to 20,000 rpm are now the state of the art, with several manufacturers already working on drives with even higher rotational speeds. As a result, both **high-speed ball bearings** and **high-speed roller bearings** are needed, particularly when high loads have to be transferred via the gear and/or a parking lock gear.

A specific problem that additionally occurs on the rotor and transmission input shaft is that of parasitic bearing currents, which must be avoided under all circumstances in order to ensure the unit's safe operation. Separate solutions that allow currents to be grounded between the rotor shaft and the housing are available on the market. The **current shunt bearing** integrates this function in a space-saving manner. If current insulation is additionally needed, hybrid bearings with ceramic balls or coatings are used in accordance with the current state of the art; these, however, have significant commercial disadvantages. SCHAEFFLER's **current insulation bearing** was developed with a significantly more cost-effective plastic overmolding in order to compensate for the additional costs, particularly in the case of large production volumes.

The **sensor bearing** represents another possible combination that is of great interest. For operating synchronous motors, the power electronics must know the rotary position of the rotor shaft and the magnets that are mounted on it. The resolver used here in most cases fulfills this function, but at the same time must be spatially accommodated in the electric motor and controlled accordingly by the power electronics. When this is integrated into the sensor bearing, an increased level of precision and robustness is achieved.

Due to the gear ratio, the intermediate shaft rotates at significantly lower speeds of up to 10,000 rpm, but the forces that must be supported are much higher. The focus here is on bearing types that both save space and generate as little friction as possible at the same time. It is generally well-known that locating/non-locating bearing supports have favorable friction characteristics. When used in high-torque units, however, ball bearings are pushed to their limits. The newly developed **angular roller unit** (ARU) – a derivative of the tapered roller bearing – can be used as a locating bearing and offers the friction-related advantages of comparable ball bearings while requiring a significantly smaller design envelope (refer to source [1]).

In contrast to the intermediate shaft, the highest forces that have to be supported normally occur on the output shaft, so the use of tapered roller bearings is recommended. Lastly, **tapered roller bearings with optimized friction characteristics** have undergone a notable development and now offer the same level of friction-related advantages as ball bearings. Depending on the vehicle parameters and the drivetrain architecture, range extensions in the region of 3 km per 100 km are possible (refer to sources [2] and [3]).

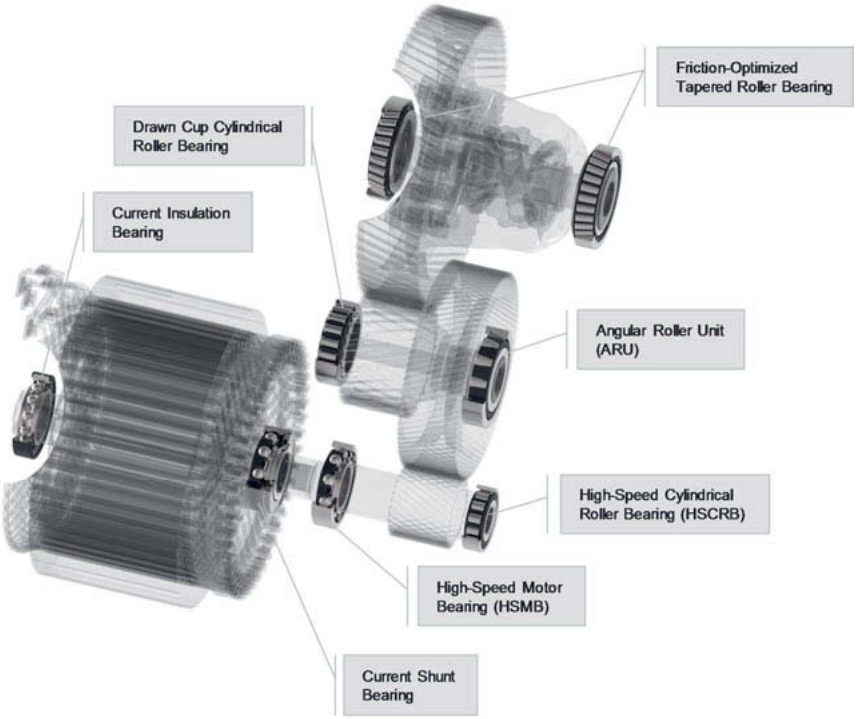

Fig. 1: Overview of different bearing types in an electric axle

The following sections of this paper focus on the innovations for the rotor and transmission input shaft.

2. Rolling Bearings for Fast Rotating Shafts

2.1. The High-Speed Motor Bearing

The **HSMB** (high-speed motor bearing) is a ball bearing with special characteristics as shown in Fig. 2. The speed capability is the required characteristic that must be fulfilled. What is more, the bearing must operate with low levels of noise and friction and be temperature-resistant, compact, and cost-effective. The HSMB can be used in an open or closed design, i.e. with either oil or grease lubrication. In the latter case, special seals and greases are used.

Fig. 2: HSMB 1.3 bearing with characteristics

Typically, the speed parameter of a bearing is the maximum speed multiplied by the pitch circle diameter and stated in units of mm/minute. This value correlates with the cage speed. The HSMB 1.3 series fulfills the requirements described above up to a speed parameter of 1.3 million mm/minute, which for bearing size 6009, for example, corresponds to a speed of over 21,000 rpm. As a point of comparison, a standard bearing can achieve only about half of this value.

If the speed parameter is exceeded as a result of either higher speeds or as a result of the size, the cage is usually the first component to reach its limits in terms of load and/or deformation. Fig. 3 illustrates the impact of the centrifugal force on the cage. When subjected to excessively high centrifugal force, the single-flange HSMB 1.3 cage experiences claw lift, which can lead to contact with the outer ring. To counter this effect, the HSMB 2.0 cage was

developed, which displays virtually no noteworthy deformation thanks to its two-piece, double-flange design. The HSMB 2.0 retains its stable running and temperature behavior up to a speed parameter of 2.0 million mm/minute.

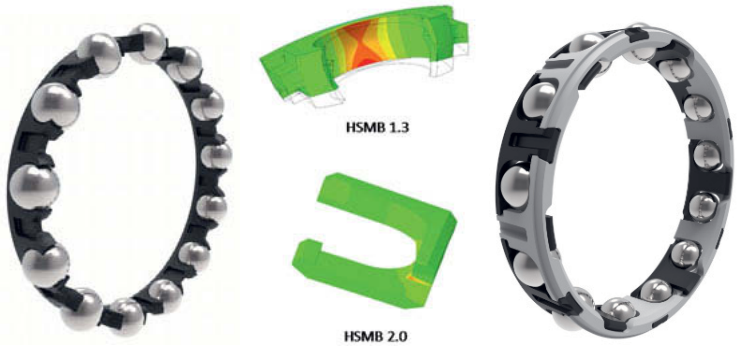

Fig. 3: HSMB 1.3 cage vs. HSMB 2.0 cage

2.2. The High-Speed Cylindrical Roller Bearing

In most cases, the load carrying capacity of the HSMB makes it possible to create a design with an appropriate rating life with regard to the gear forces. Especially in high-torque applications and/or when parking lock gears are used on the transmission input shaft, however, the static load carrying capacity of the ball bearing may be insufficient. In this case, the **HSCRB** (high-speed cylindrical roller bearing) offers a very good compromise between design envelope and load carrying capacity (refer to Fig. 4).

Fig. 4: HSCRB with characteristics

The HSCRB is optimized in terms of its inner profiling, the number of rolling elements and their dimensions, and the guidance and geometry of the cage. The N design, which features a flange-less outer ring and double-rib inner ring, also allows churning losses to be minimized and speed parameters similar to those of the HSMB 1.3 to be achieved.

Fig. 5 shows a comparison of the key parameters. Because the HSCRB would exceed the requirements in terms of rating life using the same design envelope, the average losses in this position can be kept within acceptable limits by downsizing the HSCRB.

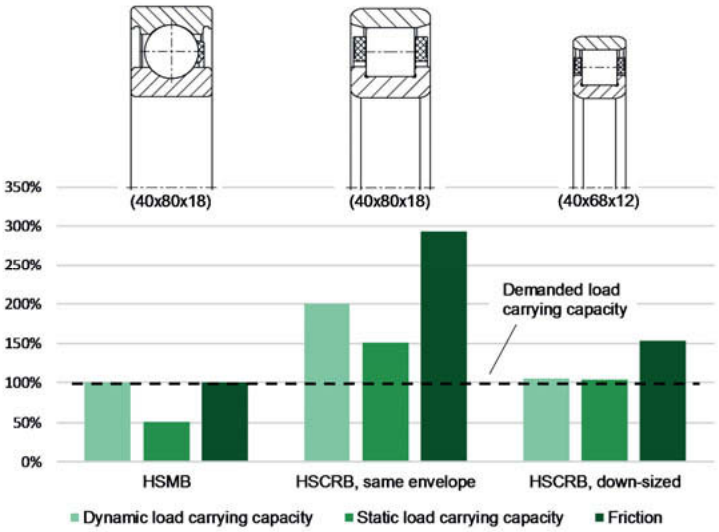

Fig. 5: Comparison of load carrying capacity, friction, and size

3. Rolling Bearings in the Context of Current Passage

Drivetrains with electric traction motors are typically controlled using frequency converters. This type of energy supply has the advantage of variable speeds, which in turn improves the control and energy efficiency of the drive. However, these advantages are accompanied by several negative effects that are rooted in the basic function of intermediate voltage circuit converters and the structure of the drive system. Elements such as insulation, air gaps, and even the lubricant film in the rolling bearing act as parasitic capacities, in other words, a circuit of capacitive resistors is created. High-frequency voltages are coupled into this network of capacitive resistors via steep voltage risings and the so-called common mode voltage of the frequency converter, which can cause the issue of bearing currents. Furthermore, asymmetrical distribution of the magnetic flux in the motor can induce a voltage along the shaft. It

is necessary to specify du/dt, EDM, circulating, and rotor ground currents, although du/dt currents are negligible according to the current state of knowledge [4]. The damage types (refer to Fig. 6) can essentially be limited to frosting and fluting, failures due to WEC (white etching cracks), and accelerated lubricant aging. Even during the frosting stage, significant deteriorations in terms of running noise are discernible.

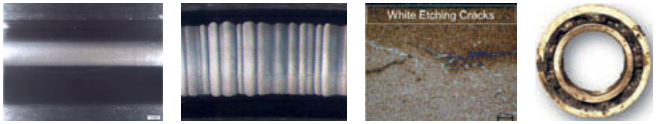

a) Frosting b) Fluting c) WEC d) Lubricant aging

Fig. 6: Typical damage (a-c: SCHAEFFLER damage analysis, d: [4])

The following section describes two countermeasures to prevent damage caused by the passage of current and the occurrence of bearing currents in electric motor bearings: Current shunt elements for reducing voltages and current insulation for interrupting the flow of current. These are “non-electronic” remedial measures, since approaches of this kind (e.g. filtering elements, reduced switching frequencies, etc.) cause a decrease in efficiency as well as higher costs in comparison to the rolling bearing solutions presented here. These solutions are applied depending on the system configuration that is present in the drive unit.

3.1. The Current Shunt Bearing

One remedial measure for the passage of current is to use the so-called **current shunt bearing** (refer to Fig. 7). This bearing comprises an HSMB that additionally features a shunt ring and a coated sleeve. The grounding ring itself consists of a carbon shunt element that is encased in a sheet metal structure and mounted on the bearing’s outer ring. The mating track of the shunt ring comprises a coated sleeve that can also be designed as a flinger shield to protect against the possible ingress of contamination if necessary. The purpose of the coating is to increase the conductivity and reduce the resistance.

The advantages of SCHAEFFLER’s current shunt bearing:

- Significantly reduced potential difference between the bearing’s inner and outer rings
- Low frictional losses of the shunt ring (2 – 7 Ncm at 15,000 rpm)
- No additional mounting processes required for separate shunt elements
- No significant abrasion of the shunt ring
- Cost savings for the entire system
- Compact solution with low design envelope requirements

Fig. 7: Current shunt bearing

The function of the shunt element can be validated using a direct current inspection (or similar). For this purpose, a voltage is applied to the bearing on the test rig using a power supply unit. Contact is made using a sliding contact (refer to Fig. 8). The example shown in the right-hand side of the image illustrates the comparative evaluation of bearings with and without shunt rings. It is clearly visible here that, without a shunt ring, a potential accumulates between the inner and outer ring and is discharged in the form of flashovers in the rolling contact. In the rolling bearing with a functioning shunt element, there is no measurable voltage drop in the bearing at a constantly low voltage. Fig. 9 illustrates the characteristics of the current shunt bearing in terms of ohmic resistance. The voltage increases along with the current. Essentially, the curve shows that a high current flow is made possible even at very low voltages. Typically, the voltages that are required for a flashover to occur on the bearing are significantly higher. Whether and to what extent the potentials can be reduced via the flow of current before a flashover occurs in the rolling contact depends on the interactions in the system. Experience gathered from numerous units has shown that a shunt element reliably prevents the passage of current.

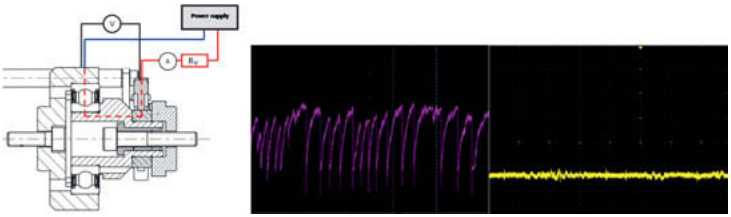

Fig. 8: Principle of test rig (left), drop of voltage without/with shunt element (right)

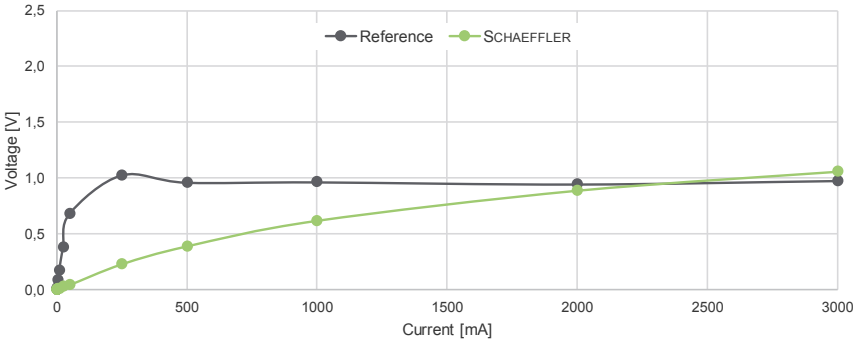

Fig. 9: Characteristic of current shunt bearing reg. continuous current for 15,000 rpm

Another very important electrical parameter, especially when alternating current is applied, is the impedance (alternating current resistance). Fig. 10 shows a comparison between the impedance of the SCHAEFFLER current shunt bearing and that of a reference solution that was also tested over the test period.

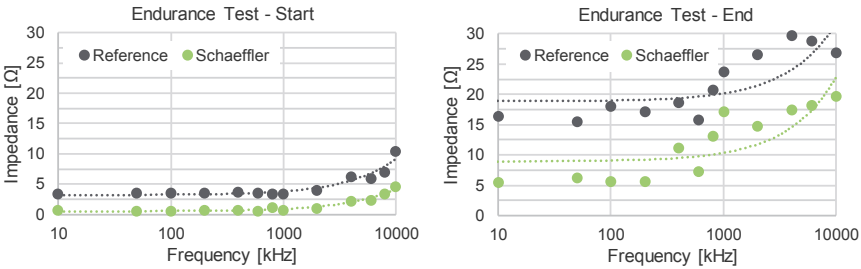

Fig. 10: Characteristic of current shunt bearing reg. impedance for 15,000 rpm

3.2. The Current Insulation Bearing

Depending on the type/cause of the parasitic flow of current, a shunt element or, alternatively, insulation of the affected bearing positions can be helpful. If capacitive discharge currents occur, either the current shunt bearing can be used or all bearing positions located in the current path can be insulated. However, it must be ensured that the current does not and cannot find alternative paths, e.g. via the bearings on the transmission input shaft or the gearing. Insulation of all paths is generally difficult to implement.

If high-frequency circulating currents occur, the use of a current shunt element alone is generally not rational, as the current shunt element encourages this type of parasitic current flow

and leads to damages on other bearings. At least one bearing position in this circuit must be insulated. The current insulation of the bearing on the non-driven side of the rotor shaft represents an effective measure for minimizing these currents in the bearing and can prevent damage caused by the passage of current.

To prevent all current types described above, an overall solution comprising a current shunt bearing on the driving side of the rotor combined with a **current insulation bearing** on the non-driven side of the rotor is recommended. The current insulation is currently implemented by means of hybrid bearings comprising HSMB components made from steel and bearing balls made from ceramic material. An additional solution that is primarily used in the industrial sector is the application of a ceramic coating to the outer ring of the bearing. These solutions display high ohmic resistances and low electrical capacities for a high alternating current resistance in the bearing. They are generally effective, but also costly and, with regard to the oxide ceramic coating, unsuitable for use in high-volume production with the current state of the art. During the search for alternative and, particularly, cost-efficient insulation options, the solution of overmolding the bearing's inner or outer ring using a plastic ring was tested at SCHAEFFLER (refer to Fig. 11).

The following steps were carried out for the purpose of validation:

- Calculations to determine the mechanical stress placed on the plastic ring
- Calculations and tests regarding temperature distribution inside the bearing
- Endurance tests with a rolling contact pressure of up to 3,600 MPa
- Long-term creep tests
- Assembly tests
- Wear tests (for the non-locating bearing design)
- Determination of electrical characteristics (ohmic resistance and impedance)

Fig. 11: Current insulation bearing

The mechanical stress distribution calculation showed that a stress of approximately 50 MPa is to be expected in the plastic ring for the selected material and the radial and axial force specified in the stress test (refer to Fig. 12). In addition to other parameters, the thickness of the steel ring has a decisive influence on this. The insulation on the outer ring can be assessed as more favorable in relation to the stress distribution, since the rolling contact stresses of the inner ring are higher.

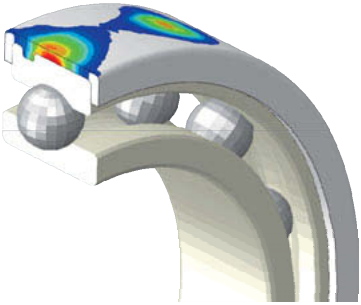

Fig. 12: Mechanical stresses on overmolded layer

The results of the various tests show no deformation of the insulating layer under high radial and axial loads and during the bearing mounting process. In the wear test, the non-locating bearing function of the current insulation bearing was tested. Its fundamental suitability for application (even as a non-locating bearing) was successfully shown. The assembly/disassembly tests also showed no functionally critical deformations in the plastic layer.

In terms of electrical characteristics, it must be noted that both the dielectricity value and the thickness of the insulating material contribute to the capacity of the insulation. The following sequence is thus derived: The capacity of a bearing with ceramic balls is lower than that of plastic insulation and ceramic coatings, and the capacity of plastic insulation is lower than that of the ceramic coating. For instance, the capacitive resistance for a plastic overmolded outer ring is 0,218 MΩ at 10 kHz and 43,6 MΩ at 50 Hz in comparison to an aluminum oxide coating with 0,15 MΩ at 10 kHz and 1,5 MΩ at 50 Hz. However, the impedance (ohmic and capacitive resistance) is mainly influenced by the ohmic resistance as its magnitude shows values in a range of 10 GΩ. In total, the impedance as well as the ohmic resistance are by far sufficient to meet the insulation requirements in automotive applications.

Since the surface area also affects the capacity, it is more favorable for the inner ring rather than the outer ring to be overmolded if a low capacity – and thus a high impedance – is to be

achieved. Which bearing ring is to be insulated is determined based on the mounting position and the expected operating conditions.

The advantages of SCHAEFFLER's current insulation bearing can be summarized as follows:

- Insulation with an ohmic resistance (direct current resistance) of R(DC) > 10 GΩ with a coating thickness of 1 mm on the outer ring (0.1 µA was measured at 1,000 V DC)
- The breakdown voltage is higher than 1,050 V (AC)
- The magnitude of the impedance of the plastic insulation is between that of the ceramic balls and oxide ceramic coating
- The plastic coating has a sufficient level of strength and wear resistance
- The overall system comprises a high-speed motor bearing and insulation layer in one compact unit
- Cost savings in the entire system thanks to cost-effective insulation of the bearing's inner ring or outer ring

4. The Sensor Bearing

Compared to other motor types, the synchronous motor prevails despite the somewhat higher total costs and the greater control effort thanks to the better efficiency and power density. The synchronous motors need angular information from the rotor to the stator in order to inject the right amount of energy into the right winding at the right time. State of the art today is the resolver.

The integration of angle detection function in the rolling bearing minimizes the number of interfaces and reduces the tolerance chain, which makes it possible to shrink the sensors without losing accuracy, compared to the separate sensor concept (see Fig. 13). Besides the reliable angle information for high speeds, the **Sensor Bearing** – which was developed in cooperation with HELLA GmbH & Co. KGaA – is designed to meet the requirements such as low friction, low self-heating, high running accuracy and low noise, high-speed resistance and suitable lubrication.

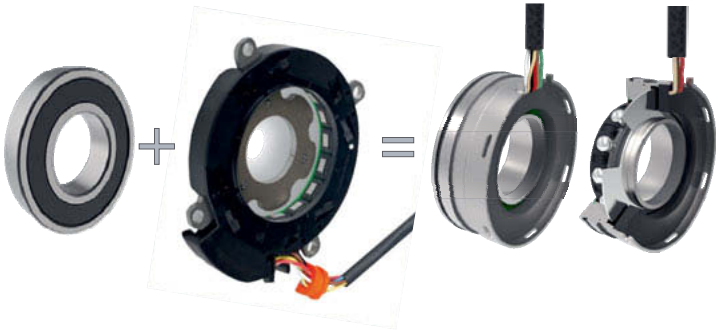

Fig. 13: Bearing with resolver [5] and sensor bearing with its sectional view

For the sensor integration, the bearing rings must be adapted in such a way that no creeping of sensor components occurs in operation. Due to the similar thermal expansion coefficients of the rotor shaft, bearing inner ring and the sensor rotor, an additional locking element can be omitted if the mechanical loads and deflection of the shaft are so low that microscopic movement does not occur. The outer ring must be secured against rotation in the light metal housing due to the different thermal expansion coefficients. Depending on the application, there are various possibilities for realizing the locking of the outer ring. In the version shown in Fig. 11, the locking function is integrated into the sensor sleeve to reduce the number of parts.

The sensor is made up of a scale, or “sensor rotor,” mounted on the inner ring extension in a torsionally stiff manner. The sensor rotor is a stamped part. The actual sensor, also rigidly mounted, sits in the outer ring extension and detects the changes in rotor position. The sensor is designed to be waterproof to meet the strict automotive requirements. It provides the position information to the ECU via a cable in axial or radial direction. The sensor can reliably deliver angle information even at very high speeds. By using inductive technology for angle detection, part of the intelligence is taken over from the ECU into the sensor, which in addition to the smaller sensor leads to a significant reduction in the expensive electrical components that are required for the resolver function (see Fig. 14).

The higher level of integration as well as improvements in design details enable that even proven machine elements such as bearings can be further optimized to create more design freedom for electric vehicles. Leaving old design specifications and using new sensor technologies can lead to cost savings as well as to installation space optimization.

The integration minimizes the number of interfaces and reduces the tolerance chain, which makes it possible to shrink the sensors without losing accuracy. Additionally, the shrinking of the processing areas, offers a system-level downsizing potential. The sensor alignment is unnecessary and the additional sensor receiving surfaces are eliminated, offering, in combination with the easier handling, an enormous advantage for the customer. Simple signal processing on the control side, together with the possible realization of the highest safety standard (ASIL D), speak for a promising future-oriented solution.

The mentioned possibilities allow a cost advantage on the system level in comparison to standalone solutions with the same accuracy of less than ±1° electrical (see Fig. 15). The high accuracy was already validated in tests at component level under the influence of displacements within the bearing clearance, temperature, speed and external magnetic fields in order to simulate the installation conditions of the application [6], in which a separate sensor

shows significant deterioration in accuracy. The next step in the validation of the sensor bearing is a system test.

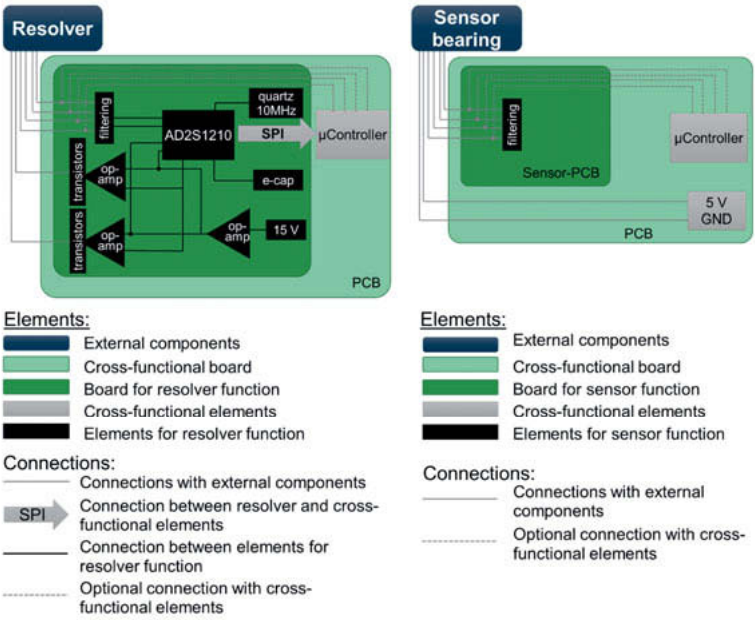

Fig. 14: Comparison of signal post processing between resolver and sensor bearing

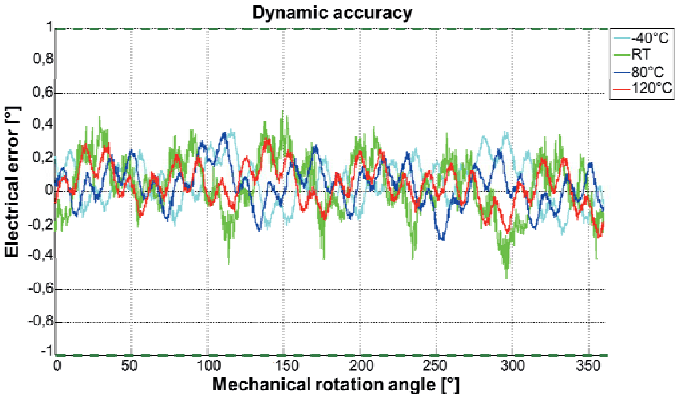

Fig. 15: Dynamic accuracy at 10.000 rpm with temperature influence

5. Summary

Trends in electric axle development such as increasing speeds and power density as well as lowest friction and cost both are challenges and opportunities for bearing manufacturers. Special bearing designs like SCHAEFFLER's HSMB 1.3 and HSCRB combine high-speed capability with high load carrying capacity. Beyond that, the HSMB 2.0 development enables system engineers to design and test next-generation drivetrains today.

To prevent the parasitic passage of current, SCHAEFFLER offers two possible solutions that reliably prevent these currents: The current shunt bearing and the current insulation bearing. Both solutions can be integrated into the electric motor as compact and cost-effective units.

The combination of a rotor position encoder and HSMB in the SCHAEFFLER sensor bearing represents another very favorable option that allows a simplification of mechanical and electronic interfaces as well as savings of cost and design space for future electric drivetrains.

Literature

[1] R. Rumpel, T. Stahl, M. Neumann: "Angular Roller Unit (ARU) – Innovatives Festlager mit hoher Tragzahl und niedriger Reibung", 13th VDI specialist conference on rolling and plain bearing supports, Schweinfurt, 2019

[2] Kim, C.: New next generation eight-speed automatic transmission for FWD vehicles, 19th International VDI Congress Dritev, Bonn, 2019

[3] R. Rumpel, T. Stahl, K. Kavzan: "Application-Optimized Performance – the Way to the UltraLowFriction-Tapered Roller Bearing", ATZ specialist conference on friction in drives and vehicles, Hanau, 2019

[4] H. Tischmacher: "Systemanalysen zur elektrischen Beanspruchung von Wälzlagern bei umrichtergespeisten Elektromotoren" (dissertation), University of Hannover, 2017

[5] TYCO Homepage, https://www.te.com/deu-de/products/sensors/transportation-sensors/transportation-resolvers.html, last accessed 20.09.2019

[6] A. Schamin, F. Utermöhlen, H. Weber: "Sensor Bearing for Automotive Applications", 18th International CTI Symposium, Berlin, 2019

Highly efficient clutch system for multispeed BEV

M.Sc. **H. Gürbüz**, IPEK – Institut für Produktentwicklung, Karlsruhe,
Mubea Tellerfedern GmbH, Daaden;
Dipl. Ing. **S. Ott**, B.Sc. **A. Sutschet**, B.Sc. **J. Kern**,
IPEK – Institut für Produktentwicklung, Karlsruhe

Zusammenfassung

Durch die fortschreitende Elektrifizierung des Antriebsstrangs ergeben sich neue Anforderungen an alle Teilkomponenten wie beispielsweise Kupplungen, Getriebe oder auch dem Differenzial. Insgesamt zeichnet sich ein Trend hin zu schnelldrehenden Traktionsantrieben ab, wodurch die Leistungsdichte bei vergleichsweise geringem Drehmoment deutlich erhöht wird. Um den kompletten Drehzahlbereich des Elektromotors nutzen zu können, bedarf es eines Mehrganggetriebes. Ebenso wird eine lastschaltfähige Kupplung für einen komfortablen Gangwechsel benötigt. Heutige lastschaltfähige Kupplungen sind aufgrund der stark erhöhten Differenzdrehzahlen und den daher eingehenden Gleitgeschwindigkeiten und Fliehkrafteinflüssen nicht geeignet. Um diesen Problemstellungen entgegen zu treten wurden Prototypen eines Kupplungssystems für Hochdrehzahlantriebe mit 30.000 U/min, im Rahmen eines Konsortialprojekts aus den drei Komponentenentwicklern Mubea Tellerfedern GmbH, Miba Frictec GmbH und Kaco GmbH & Co.KG zusammmen mit dem Institut für Produktentwicklung - IPEK, entwickelt.

Das Ergebnis ist ein Kupplungssystem mit Gleitgeschwindigkeiten von maximal 80 m/s die aus den minimal möglichen Durchmessern der rotierenden Teile resultiert. Um dennoch ein hohes Moment übertragen zu können, wird die Anzahl der Reib– und Stahllamellen erhöht. Zur Reduzierung der Axialkraftverluste im Lamellenpaket werden diese im Prototyp beidseitig zusammengepresst. Ferner wurde ein Arretierungsmechanismus konzipiert, der ermöglicht die Kupplung geschlossen zu halten ohne dafür permanent Energie aufzubringen. Durch die Druckbeaufschlagung wird neben der Synchronisierung der Kupplung eine Verriegelung ausgeführt, deren Funktionsweise einem Kugelschreiber nachempfunden ist. Die Funktionsfähigkeit des Arretierungsmechanismus wurde auf einem Prüfstand verifiziert. Die Ergebnisse der Prüfstandsversuche zeigen, dass hierdurch die Betriebsenergie erheblich reduziert werden kann.

Weiterhin erfolgte im Kupplungsbetätigungssystem eine Prinzipvariation, da aus den vorliegenden hohen Belastungen durch Drehzahl und Anpresskraft herkömmliche Ausrücklager nicht geeignet sind. Die Krafteinleitung in die Kupplung wird daher über ein Gleitlager ausge-

führt. In dem vorliegenden Beitrag wird die Funktionsfähigkeit unter den späteren systemischen Wechselwirkungen untersucht. Ebenso werden die Ergebnisse der variierten Parameter wie bspw. Gleitgeschwindigkeiten, Flächenpressungen sowie verschiedenen hochdrehzahlgeeigneten Schmierungsstrategien vorgestellt.

Abstract

The ongoing electrification of the powertrain places new demands on all subcomponents such as clutches, transmissions or even the differential. Overall, there is a trend towards high-speed traction drives, which significantly increases the power density at comparatively low torque. In order to be able to use the full speed range of the electric motor, a multi-speed transmission is required. A powershift clutch is also required for comfortable gear changes. Today's powershifting clutches are not suitable due to the greatly increased differential speeds and the resulting sliding speeds and centrifugal force influences. To address these problems, prototypes of a clutch system for high speed drives with 30,000 rpm were developed in a consortium project consisting of the three component developers Mubea Tellerfedern GmbH, Miba Frictec GmbH and Kaco GmbH & Co.KG together with the Institute of Product Engineering - IPEK.

The result is a clutch system with sliding speeds of up to 80 m/s, which results from the minimum possible diameters of the rotating parts. In order to still be able to transmit a high torque, the number of friction and steel plates is increased. In order to reduce the axial force losses in the clutch pack, the plates are pressed together on both sides in the prototype. In addition, a latching mechanism was designed which makes it possible to keep the clutch closed without permanently applying energy. By applying hydraulic pressure, in addition to synchronizing the clutch, a locking mechanism is implemented, whose function is similar to that of a ballpoint pen. The functionality of the locking mechanism was verified on a test bench. The results of the test bench trials show that the operating energy can be considerably reduced.

Furthermore, a principle variation was carried out in the clutch actuation system, as conventional release bearings are not suitable due to the high loads caused by speed and contact pressure. The force is therefore introduced into the clutch via a plain bearing. In the present paper, the functional capability under the later systemic interactions is examined. The results of the varied parameters such as sliding speeds, surface pressures and various lubrication strategies suitable for high speeds are also presented.

1. Introduction

BEVS such as Tesla models or newly introduced Mercedes-Benz EQC and Audi e-tron represent a real alternative to vehicles with combustion engines and are enjoying increasing customer acceptance. In this vehicle segment, the required range is made possible by a large battery capacity, but this leads to high costs. Furthermore, large and expensive e-machines are used to perform the balancing act between starting torque and maximum speed. However, initial research has shown that a shiftable transmission (2-3 gears) can increase the overall efficiency and power density of the electric drive train in higher vehicle segments. In order to exploit the full potential, the drive speed should be increased to 30.000rpm. At this speed, the costs of the electric machine decrease by reducing the volume and thus the material costs. [1] [2]

Compared to conventional drive trains, an electric drive train with a high-speed electric machine has different requirements and boundary conditions for the clutch. Due to the lower number of gears and higher transmission spread, the maximum differential speed for clutches in electric drive trains is significantly higher than for clutches in vehicles with combustion engines, which leads to high sliding speeds and heat input during the synchronization process [3]. When the clutch is open, the high differential speeds can lead to high resistance losses due to the phenomenon of multi-disc wobble. Further challenges arise in the area of material stress, since with increasing peripheral speed the centrifugal forces reach values which can lead to plastic deformation of the components. The friction clutches used in powershift transmissions of conventional drives have not been developed for high-speed applications with speeds of up to 30.000 rpm according to the state of the art in research and technology. [4] The "High-Speed Clutch" consortium project was launched to demonstrate the innovative components in the field of clutch technology for electric mobility. To increase the development input for e-mobility, the consortium was founded by suppliers who already supply components for conventional friction clutches. The consortium partners Kaco GmbH & Co. KG (Kaco), Miba Frictec GmbH (Miba) and Mubea Tellerfedern GmbH (Mubea) are responsible for the development and implementation of the components. The project partner IPEK - Institute of Product Engineering at the Karlsruhe Institute of Technology (KIT), ensures the system-side validation of the clutch (Fig.1). [5]

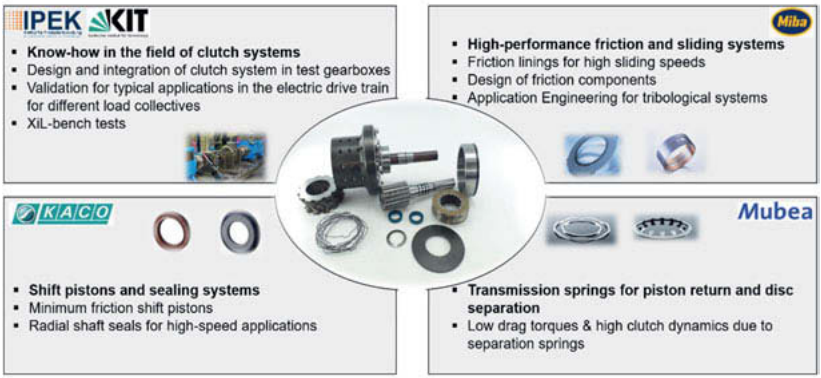

Fig. 1: Consortium Project Highspeed Clutch [5]

2. Clutch design for high speed transmission

Within the consortium project, the clutch concept shown in Fig.2 was developed for multispeed drives in BEVs. For the design of the tribology system with an input speed of 30.000rpm, the permissible differential speed is the decisive design parameter. The result is, for example, the design of mean friction diameters that are significantly below the values known in the automotive sector. For a given engine torque, small friction diameters mean that the number of friction pairs must be increased. A higher number of friction partners can result in higher drag torques in the open state and a higher loss of axial piston force due to toothing friction when the clutch is closed. In the clutch design presented here, the axial force losses are minimised by actuating the disc pack on both sides [6]. This also ensures that the total stroke is divided between two pistons and a high dynamic response is achieved. A further increase in clutch dynamics is achieved by means of separating springs in which the clutch clearance relevant for drag losses is set as low as possible and active coupling of the discs is achieved. Newly developed torsional separating springs are used in this demonstrator, which are designed for speeds of up to 30.000 rpm. In comparison to conventional wave springs or disc springs, the new torsional separating springs lose significantly less spring load under the influence of speed and have a very compact design [7].

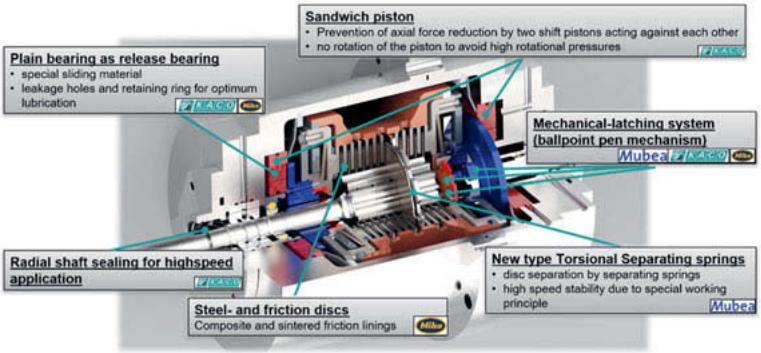

Fig. 2: Highspeed Clutch for multispeed BEV [6]

3. Actuation system of highspeed clutch

The reduction of the energy requirement for the actuation of wet-running multi-disk clutches is one of the main development goals, since a pressure must be maintained for torque transmission. One possibility to reduce the actuation energy is the use of mechanical latching systems, which hold the actuating piston in one position and allow the required pressure to be minimized. Based on the ballpoint pen mechanism, a new latching mechanism was developed within the consortium project. For this purpose, the three essential components latching crown, guidance crown and sliding sleeve are adapted for clutch integration (Fig. 3). [5]

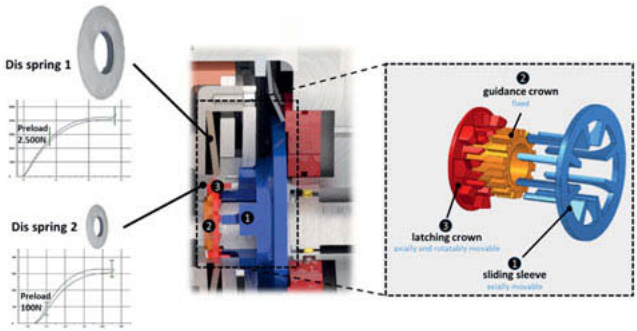

Fig. 3: Mechanical latching system with the essential components

The latching crown can be moved axially and is rotatable relative to the shaft. A fixed guidance crown is used for the axial positioning of the latching crown and the sliding sleeve. Spring

elements are also inserted in the system to maintain the required piston force despite removal of the pressure. Due to their speed stability at low installation space requirements, two disc springs are used. Disc spring 1 is preloaded to the maximum axial force required, so that the force required for synchronization and torque transmission can initially be transmitted. The second disc spring has a lower load in order to minimize the contact stresses on the tooth flanks and to allow independent locking with lower forces than the axial force of the clutch. The pressure increase in the piston chamber moves the shift piston axially and the entire latching unit is moved in the direction of the clutch pack. First of all the clutch clearance is closed and then sppeds are synchronized. Now the pressure is increased further to over-pressurize the pretensioned disc spring 1. The disc spring 2 and the specified tooth geometry of the latching crown, guidance crown and sliding sleeve twist the latching crown and push it into the next tooth gap. When the piston pressure is reduced, the piston moves back through the disc spring 1 and the elements are supported on the output shaft. The axial force required to transmit the torque is now fully applied by the disc spring 1. An additional piston return spring returns the piston so that there is no sliding contact. In order to open the clutch, pressure must be built up and briefly released again. [5]

The functional verification could be verified in initial test bench trials (Fig.4).

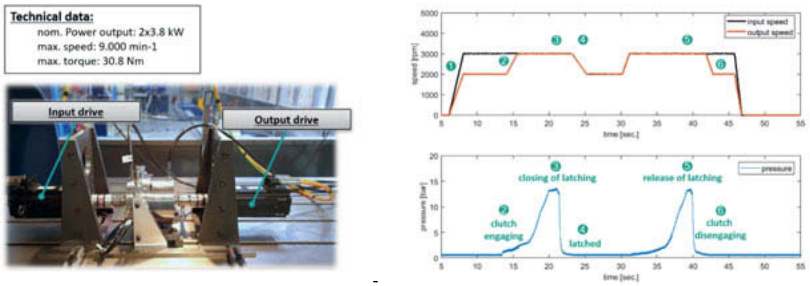

Fig. 4: Test setup and functional verification latching system [6]

4. Clutch release as slide bearing

The rotational pressures generated in the case of rotating pistons require actuation in a high speed clutch by means of release systems. It is clear from the operation of a clutch system that a short (approx. 1 sec.) axial force must be applied to actuate the clutch. Conventional release systems are unsuitable for such a requirement, since clutches usually operate according to the normally open, normally closed or normally stay principle and thus have very different

requirements. Conventional release systems have a ball bearing which absorbs the relative movement between the rotating and stationary side and can transmit axial forces for the frictional connection in the clutch. This is characterized by the fact that high forces and lower speed differences must be realized. In the high speed clutch, however, this shifts to high speed differences and lower forces, which is why an axial plain bearing has the greater potential in terms of function, installation space and costs.

Using the equation for the power loss of axial hydrostatic plain bearings, the factors influencing the system can basically be shown.

$$P_V = \mu * u * F \sqrt{\frac{L}{A}}$$

The coefficient of friction coefficient μ, circumferential speed u and bearing load F have the greatest influence on the system. The lower these variables can be kept, the lower the power loss and the resulting heating of the system. For the validation of the plain bearing, a test configuration was set up on the eDriL (electric Drive in the Loop) test rig. The test stand has a drive unit with a maximum speed of 20.000 rpm. A view of the test setup is shown in Fig.5.

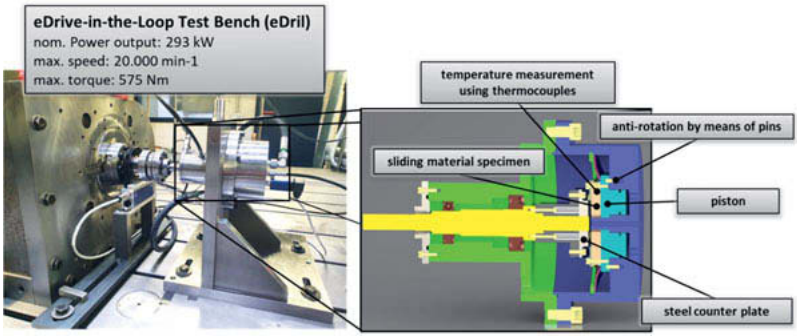

Fig. 5: Validation setup of slide bearing

The shaft is connected to the motor. The non-rotating piston is moved out axially by means of hydraulic pressure. Various test specimens with sliding material to be tested can be screwed to the piston. Bores for thermocouples are provided for temperature measurement near the sliding contact.

From a certain position the piston comes into contact with the rotating counter plate and introduces axial forces into the shaft, which simulates the actuation of a clutch. The piston is returned by a disc spring, which is located in the housing. In order to be able to demonstrate the

dynamics of a clutch with the same test specimen in later tests, the installation space is provided for a clutch pack. It is also possible to simulate the package elasticity by means of springs. The counter plate is made of steel C60.

Different contact partners can be tested on the test set-up and the following design parameters can be set and varied:

i. **Diameter**

Three diameter stages are being investigated in order to be able to set different sliding speeds. The diameters result from the installation space limitations of the locking mechanism. The diameter steps and corresponding average circumferential speeds are listed in table 1.

Table 1: Diameter variants

diameter stage	Inner Ø [mm]	outer Ø [mm]	Average circumferential speed [m/s] @ 30.000rpm
1	20	50	55
2	38.5	60	77
3	38.5	73	88

ii. **Surface pressure in contact**

From the design of the friction system it is specified that an axial load of approx. 2.0 kN is required to transmit the torque. Due to the design of the disc springs used with a horizontal spring characteristic curve and the actuation in a sandwich construction, the additional actuation forces are kept low. Two load stages are introduced which apply a surface pressure of 0.5 MPa (0.7 kN) and 1.3 MPa (2.3 kN).

iii. **Lubrication concept**

Initial investigations have shown that sufficient lubrication is decisive for the function of the slide bearing. Based on these the lubrication concepts provided in the Fig. 6 were developed. Lubrication by means of holes in the shaft is based on today's lubrication concepts for wet-running multi-disc clutches, in which the components are lubricated without pressure by means of rotary feed-through. Lubrication by leakage holes is aimed at active lubrication of the sliding contact surface. The diameter of the leakage hole is set to a minimum.
The retaining ring is used optionally to slow down the immediate release of the lubricant and is included in the test as an optional design element.

A standard ATF with a kinematic viscosity of 20.5mm²/s (40°C) is used for lubrication.

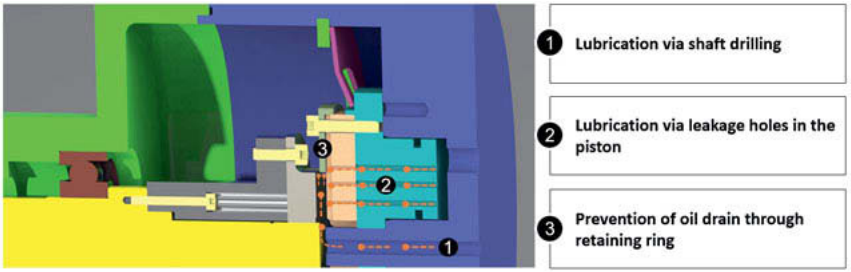

Fig. 6: Lubrication concepts

iv. **Sliding materials and cooling grooves**

As slide material sinter form, sliding coating and an aluminium alloy are used. To ensure the required lubricant film thickness, the test specimens have cooling channels as shown in Fig. 7. This allows a targeted incorporation of the lubricant into the sliding contact.

sliding material		
sintered material	coating	aluminium alloy

Fig. 7: Sliding material and cooling groove design

5. Test results slide bearing

The test run is shown in Fig. 8. During the test the speed was increased in steps starting from 1.000 rpm up to 15.000 rpm. In force level 1 (0.5 MPa) the hydraulics are actuated for 1 s and the piston is extended. This is repeated five times before the speed is increased by 1.000 rpm. The same test run is then carried out with pressure stage 2 (1.3MPa).

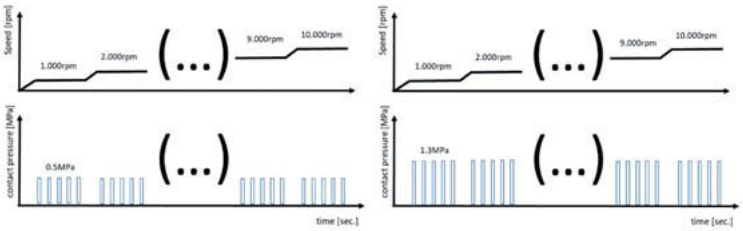

Fig. 8: Test run

The evaluation of the individual test runs is based on three criteria:

Firstly the torque applied to the shaft is measured at all times. Furthermore temperature in the sliding contact is constantly measured through temperature holes on the rear side of the sliding specimen. It should be noted at this point that the temperature is measured by means of resistance thermometers and due to the latency of heat diffusion neither flash temperatures nor the exact temperature in the sliding contact can be determined. However, the temperature measurement is a very good indicator for the comparability of the individual configurations. The lower the heat development, the more robust the contact pairing.

Thirdly after a test run, visual inspection is also used to make an assessment.

In case of high heat development and a torque of more than 10 Nm, the test run is aborted, as it can be assumed that dry or mixed friction conditions in the contact prevail.

In a first test round specimen with sliding coating and aluminium-alloy with diameter stage 2 are tested and a first pre-selection is made to sort out unsuitable configurations. New counter plates are used for each test run.

The Fig.9 on the left side shows the result of the coated material with 10.000 rpm and pressure stage 2. Although an increase in torque can be seen at the moment of actuation, this is due to the increased fluid friction at the moment of switching. In addition to the constant temperature, the visual inspection also shows that the two plates were always separated by an oil film. The plates show no signs of damage (Fig.9 right).

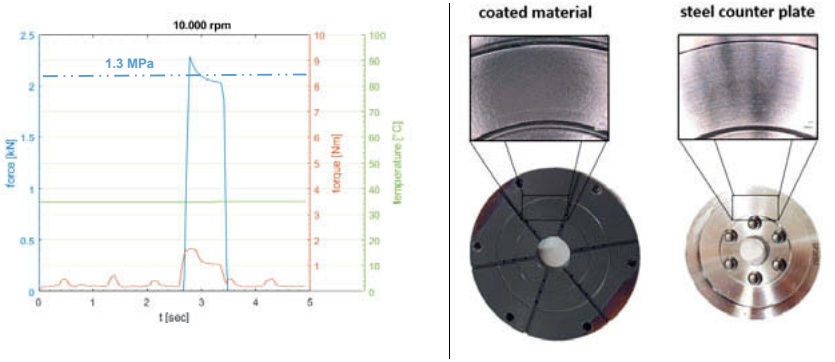

Fig. 9: Test results coated material, diameter stage 2, pressure stage 2, oil temperature 40°C, oil flow 0.5l/min, lubrication via shaft drilling

The test results of aluminium-alloy configuration showed no damage in the first test run, which is why it was extended to 15.000 rpm (Fig. 10 left). Even at these (average) sliding speeds of around 40 m/s, only a non-significant increase in torque and a slight increase in temperature can be determined. The visual inspection also shows that the load from the test run does not cause any noticeable damage (Fig. 10 right).

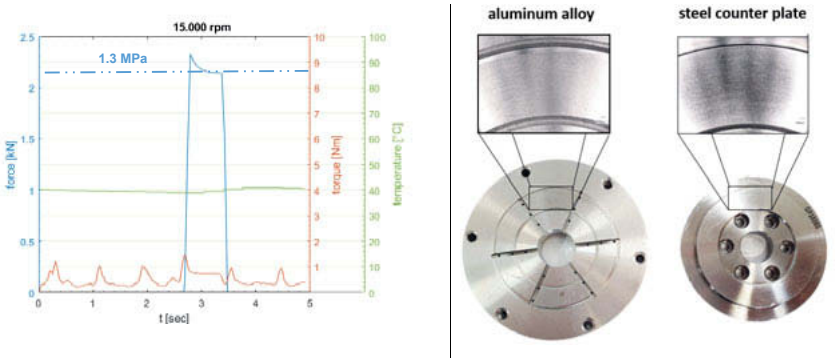

Fig. 10: Test results aluminium alloy, diameter stage 2, pressure stage 2, oil temperature 40°C, oil flow 0.5l/min, lubrication via shaft drilling

6. Conclusion and outlook

This article shows development needs and solution approaches to high speed clutch systems with speeds up to 30,000 rpm. In order to keep the influence of the speeds as low as possible, small diameters were selected, which results in a higher axial installation space requirement due to a high number of discs. An innovative latching mechanism which locks the clutch pack is developed, presented and validated on the test bench. As a result, the clutch system can be kept closed energy-free. The mechanism results in new demands on the actuation system, which was solved by an axial slide bearing system and validated in a suitable test environment. The test results show that the selected design allows high sliding speeds and surface pressure in the samples with sliding material and aluminium alloy.

As a next step, the samples with sintered form are tested and higher sliding speeds and surface pressures are investigated.

In the further progress of the consortium project the two subsystems latching system and release bearing as slide bearing are assembled to form a complete clutch system and validated on the test bench according to the IPEK-XiL-approach. This requires the development of an appropriate powertrain topology as well as driving and shifting strategies.

7. References

[1] Reichert, U. Bause, K. and Ott, S. „Presentation of a multispeed gearbox for a BEV increasing the efficiency and power density," in 16. Internationales CTI Symposium, Berlin, 2017.

[2] Gwinner, P. Stahl, C. Rupp S. and Strube, A. „Innovatives Hochdrehzahl-Antriebsstrangkonzept für hocheffiziente elektrische Fahrzeuge," ATZ – Automobiltechnische Zeitschrift, pp. 72-75, 2017.

[3] Albers, A. Reichert, U. Bause, K. Radimersky, A. und Ott, S. „Entwicklung einer verlustoptimierten Kupplung für ein mehrgängiges Getriebe für ein Elektrofahrzeug," in VDI Kupplungen und Kupplungssysteme in Antrieben, Ettlingen, 2017.

[4] Gürbüz, H. Ott, S. Albers, A. „Entwicklungsansätze für innovative Hochdrehzahlkupplung in E Fahrzeugen" in Forschung im Ingenieurwesen (2019),

[5] Gürbüz, H. Ott, S. Albers, A. „Potentials for improving the system behaviour of high-speed clutches for BEV using optimal transmission springs" in Dritev –Drivetrain for Vehicles, Bonn (2019),

[6] Ott, S. Gürbüz, H. Albers, A. „ Innovative and highly efficient clutch system for multi-speed BEV with highspeed powertrains " in CTI-Symposium, Berlin (2019),

[7] Gürbüz, H. Schulz, J. Kücükay, F. Scheikh Elard, F. Ott, S. „ Significant drag torque reduction and improved clutch dynamics by innovative, very compact separating springs for wet clutches "in CTI-Symposium, Berlin (2019)

Investigation and Potential Analysis of Shiftable Form-locked One-Way Clutches for Hybrid and Electric Vehicles

Friedrich Brezger, **Alexander Moser**,
BorgWarner Drivetrain Engineering GmbH, Ketsch

Zusammenfassung

Die Hybridisierung und Elektrifizierung von Fahrzeugen ermöglicht und erfordert neue Funktionen und Komponenten im Triebstrang zugleich. Einerseits sind mit Elektromotoren effiziente, hochdynamische Antriebselemente vorhanden und andererseits steht die Energieeffizienz - unter anderem wegen der Energiedichten der elektrischen Energiespeicher - mehr im Fokus denn je. Hier ergeben sich Potenziale für neuartige Schaltelemente. BorgWarner hat dazu einen schaltbaren, formschlüssigen Freilauf entwickelt, der den neuen Anforderungen gleichermaßen nachkommt. Da das Schaltelement eine Kupplung mit verschiedenen Modi darstellt (Freilauf links, bzw. rechts, vollständig geöffnet oder gesperrt) wird es im weiteren MMCM für Englisch „Multi Mode Clutch Module“ genannt.

In diesem Paper wird die Funktionsweise des MMCM und ausgewählte Einsatzmöglichkeiten bei verschiedenen Antriebsstrangarchitekturen (von konventionellen, Hybrid- und Elektro-Fahrzeugen) vorgestellt. Daraus abgeleitet ergeben sich eine Vielzahl von Anforderungen. Die erfolgreiche Umsetzung dieser Anforderungen in ein MMCM wird hier sowohl in Simulations- als auch in umfangreichen Testergebnissen an Prototypen vorgestellt. Das sind zum einen Funktionstests, wie Kraftübertragung, Schaltung, Überholtests als auch Dauerlauftests. Aus den Versuchen bestätigen sich die Annahmen zu Schleppmoment und Aktuierungsleistungen am MMCM, was im Nachfolgenden eine genaue Energieeffizienzbetrachtung im Antriebsstrang und Vergleiche zum Status quo ermöglicht. Abschließend werden die Erkenntnisse zusammengefasst und ein Ausblick gegeben.

Abstract

Hybridization or electrification of vehicles propulsion systems enable and demand new functions and components in their respective drive trains. On the one hand, electric engines are highly efficient and highly dynamic drive units, and on the other hand, high energy efficiency is growing in importance because of lower energy density of electrical storages among other

reasons. There are new and growing potentials for new or advanced shift elements. BorgWarner has advanced a shiftable form-locked one-way-clutch which fulfils the new requirements. Because of being a shift element with different modes (one-way-clutch clockwise or counter clockwise, locked and free), it is called Multi Mode Clutch Module (MMCM).
In this paper, the function of the MMCM and selected application possibilities of different propulsion system layouts (conventional, hybrid and electric vehicles) are introduced. Derived from the new layouts, new requirements become obvious. The successful transfer of these requirements in the design of a MMCM is shown in various simulation and test results of prototypes. These are not only pure function tests like force transmission, shift, overrun but also endurance tests. The investigations confirm the assumptions of drag torque and power demands of the MMCM. The energy efficiency of a drive train in comparison to status quo is investigated and discussed. Finally, the conclusions are summarized and an outlook is given.

Introduction & Function

Transmissions not only enable vehicles to use their propulsion system over a wide range of speeds and torques but also contribute to the systems efficiency by trying to run the engine at its most efficient operating point (no matter if utilizing combustion or electric power, including power electronics). Key for market acceptance is also low Noise-Vibration-Harshness (NVH) contribution. Clutch systems have a long tradition in transmissions, starting with brake bands, dog clutches, friction brakes or later on, friction clutches. Brake bands and dog clutches have the advantage of (almost) no drag torque in the disengaged condition. Furthermore, dog clutches can be designed to be bi-stable, so that no power is consumed when in a steady state condition (if the vehicle-FMEA does not require a failsafe or default position). Friction clutches bring the advantage of slip with high controllability in their ultimate usage as start-up clutches of dual clutch transmissions for example. They also allow continuous slip, which can help damp excitations of a combustion engine. However, they need cooling and evoke a small portion of drag torque in disengaged condition with relative speed. In Automatic Transmissions (ATs) or Dedicated Hybrid Transmissions (DHTs) they enable a smooth shift by blending the torque between two clutch elements. There are applications and approaches introducing dog clutches in only a few special cases. With dog clutches, high control effort on adjacent functioning clutches using precise sensors and high-power actuators are required to introduce shifts between gears that are not objectionable. This is necessary in such architectures, since dog clutches cannot handle differential speed easily by themselves.

In order to gain advantages from both clutch types (dog clutch and friction clutch) the Multi Mode Clutch Module (MMCM) is introduced. It is a shiftable pawl clutch, existing of an Outer Race, an Inner Race, Pawls and a Cam. By introducing these Pawls like shown in Fig. 1, it is possible to have a One-Way Clutch (OWC) with its typical passive shift: If relative speed changes it automatically transitions to the opposite mode, either overrun or block. Thinking of automatic gearboxes this transient state does not require any control effort. In addition, a Cam is introduced to control the Pawls' degree of freedom. Doing so, up to 4 modes can be implemented: OWC clockwise, or OWC counter clockwise, block and free, see Table 1. The following Fig. 1 shows an example with three modes and a rotating Cam to switch between modes.

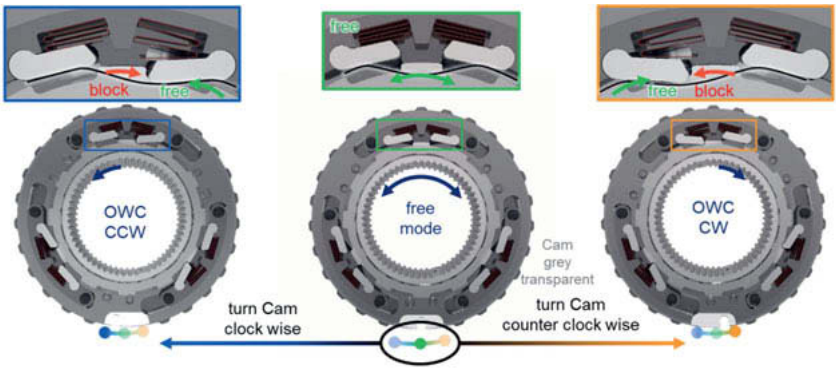

Fig. 1: Example of a Multi Mode Clutch Module with 3 Modes (from left): OWC counter clockwise, free, OWC clockwise

Keeping the basic working principle in mind, the following discussion tries to compare this 3 Mode MMCM with other basic clutch function principles in order to help choose the right device for several transmission applications.

Table 1: All named 4 modes of MMCM, which are possible

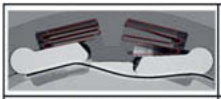	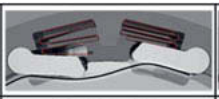	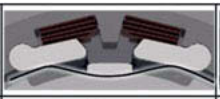	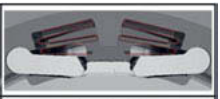
OWC CCW	OWC CW	Free	locked
One-Way Clutch Counter Clockwise	One-Way Clutch Clockwise	Disengaged	Engaged in both directions

Motivation & Comparison of Clutch Types

In regard to the selection of clutch systems, the right answer is that it highly depends on the application which is the best solution to choose. Since it might not be obvious, further basic arguments for pure Friction -, Multi Mode- and Dog Clutches discussed.

It is clear that a smooth torque ramp can be achieved by friction clutches only. By applying a pressure ramp to the friction pack, maybe also in combination with elasticities (springs), it is possible to gain a smooth torque ramp. In Dual Clutch Transmissions (DCTs) this is one of the most important functionalities. However, control effort could be simpler as an on/off friction clutch like in ATs, since the friction clutches need very fine control for creeping in traffic and for vehicle launch at various throttle settings. When friction clutches are compared to the newly introduced MMCM, there is one operation option which is even simpler: overrun mode to engagement or vice versa: simply by changing the relative speed, the clutch passively engages or disengages without any active control event; this is comparable to conventional one-way clutches. However, disengaging under (residual) torque is a similar challenge as for a dog clutch, the actuator needs to overcome friction forces which are usually a function of the applied torque. This feature is rated by “Synchronization Possibility” as half way between a friction and dog clutch in Fig. 2. If one wants to engage the dog clutch in dynamic manoeuvres, there is only a very small timeframe where the relative speed is small enough to engage the dog clutch. The speeds of primary and secondary side also must be observed precisely. Another effect arises from the short time frame: the dog teeth must engage in no-time, which means the masses of dog clutch must be translated axially several millimetres in a very short time. This needs high actuation power to accelerate the components axially fast. Compared to this, the MMCM just gets the command to drop Pawls and whenever a tooth of Inner Race changes relative direction of rotation and hits the Pawl in right direction, it engages itself. This is why the “Low Actuation Power” is rated best in the Fig. 2. On the other side, it is obvious that friction clutches always need higher forces to engage (there is a normally open design or vice versa a normally closed design) because of their friction closure principle. Looking at a steady condition, the friction clutch needs to have continuous force applied in one of the two different states. Of course, there are improvements possible with recently developed products like BorgWarner Latching Clutch Family [Bre18]. But naturally bi-stable versions are achievable with MMCM and dog clutch, only.

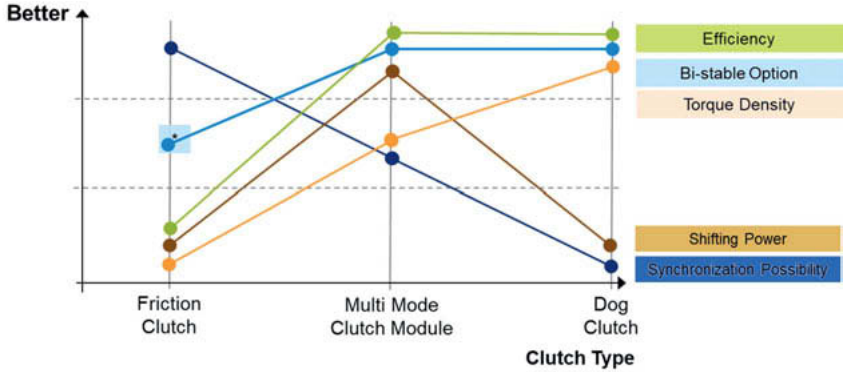

* Bi-stable Option for friction clutches: See BorgWarner's Latching Mechanisms [Bre18]

Fig. 2: Relative Comparison of Clutch Types.

BorgWarner started the development and production of one-way clutches many decades ago and is producing all three technical principles of one-way clutches: sprag clutch, roller clutch and pawl clutch. Some examples are shown in Fig. 3:

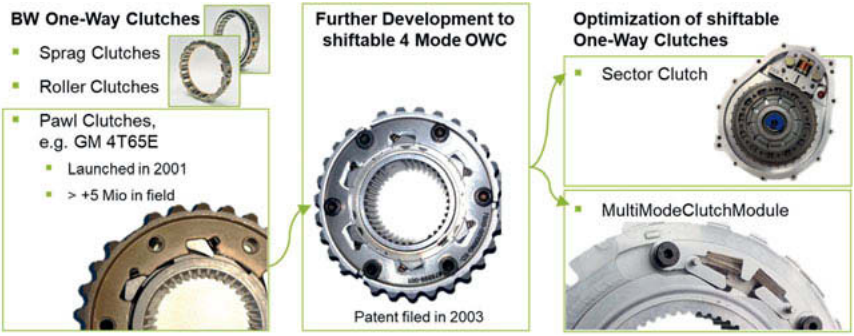

Fig. 3: BorgWarner's history of one-way clutches and further development to MMCM

Starting from a full-functional 4 Mode Pawl Clutch as MMCM (Fig. 3, mid) it turned out that in some cases of brake applications it can be advantageous to use only a small circumferential section of an MMCM that includes the actuator with two Pawls only (top right corner). Each Pawl acts in one direction, resulting in the theoretical availability of four shifting modes; however, in most applications a 2 or 3 Mode Clutch is sufficient. Fig. 3 top right corner shows the Sector Clutch including its Pawls and actuation bar with a solenoid as actuator and additional a position sensor to detect Pawls' position. The biggest advantage is that there is no need for

radial design space around the entire circumference, only a kind of “pocket” for a box in one radial direction is enough. Therefore, the Sector Clutch assembly is egg-shaped to nest electro-mechanical actuator as shown in Fig. 3. Compare this to the optimized MMCM with three modes shown in Fig. 1. Having explained the basic functioning of such a shiftable one-way-clutch with some advantages of dog clutches and friction clutches combined (e. g. it can handle a small relative speed in block direction and an arbitrary profile of overrun speed), some details in applications will be shown in following chapter.

Examples of Possible Transmission Applications

In conventional ATs the MMCM can always be used if shifting to next gear involves a friction clutch. By simply enabling the Overrun Mode, the available friction clutch system defines the operating condition of MMCM. BorgWarner’s demonstrator vehicle uses the MMCM as Low/Rev Clutch. Here, the MMCM is switched in OWC mode when an acceleration is detected and the shift into second gear becomes most likely. As soon as the shift into second gear is executed, the friction clutch overtakes torque until the secondary side of MMCM switches direction and overruns. A smooth transition is easy and only controlled by friction clutch. Moreover, the switch of modes can be conducted before the shift event itself. As a result, the actuation power can be low, since the mode change must not be performed within a very limited time frame like using a dog clutch. Furthermore, MMCM can be a space saver. In this example it replaces a classical OWC and friction brake combination, like demonstrated in [Cam16]. A schematic cross section is shown on the left side of Fig. 4 as well. When shifting into Reverse Gear (Rev) the MMCM is set to block mode. This mode change is also possible while the vehicle is still moving forward without shift shock, if the other clutches and brakes are taken into account of control strategy. There are some applications showing this. One example is Honda’s 10-speed Automatic Transmission [Mur18].

In DHTs the electric motor can play a special role in terms of synchronization manoeuvres. Depending on the propulsion system architecture, the classic synchronization requirements of shifting gears like in ATs can be lowered, since an electric motor can either boost or pre-synchronize. An example of Powersplit (eCVT) was given in [Cam16] where the MMCM is implemented as brake at the sun gear. In this example the MMCM helps to reduce electric power consumption, since the sun gear is locked by brake functionality and not by the holding torque of the motor/generator.

Another example is given by DHT applications with a 6 Speed where brake functions are also needed to support high torques. There are concepts where this brake needs to be disengaged at higher gears. Although, friction clutches can be modified to have low drag tor-

ques, the potential to further improve efficiency can be seen by using MMCM. With classical clutch elements, one might be tempted to favour other layouts, where the torques are lower or the brake can be kept engaged in higher gears. Here, the MMCM can be a game changer since high torques can be supported with almost zero drag torque while in the disengaged mode. See Fig. 4 middle at bottom: three friction clutches and one MMCM at planetary carrier which can support torques greater than several 1.000 Nm.

In the field of electric vehicles, a shiftable transmission is often considered and many arguments are taken into account such as: total system efficiency in certification cycles, range, total cost of ownership and market segment or vocations as well as many others. The MMCM bears a potential to dramatically increase the efficiency of a multi-speed gearbox and therefore the range of a vehicle. Since it is a component with higher torque capacity, synchronization function in one direction, as well as almost zero drag torque like dog clutches, it is an ideal shift element to engage first gear. A first gear allows better accelerations for sportive cars, hill start up with higher loads or other manoeuvres of small vehicles with lower torque of electrical motors, e.g. launch against at the curb. Since an MMCM is disengaged at a respective higher gear and a secondary clutch (e.g. friction clutch) is engaged, there are low parasitic losses in normal driving mode. One possible architecture, implementing an MMCM as a brake, can be seen in the scheme of Fig. 4, right: planetary gearset with two brakes consisting of friction clutch (2nd gear) and MMCM (1st gear).

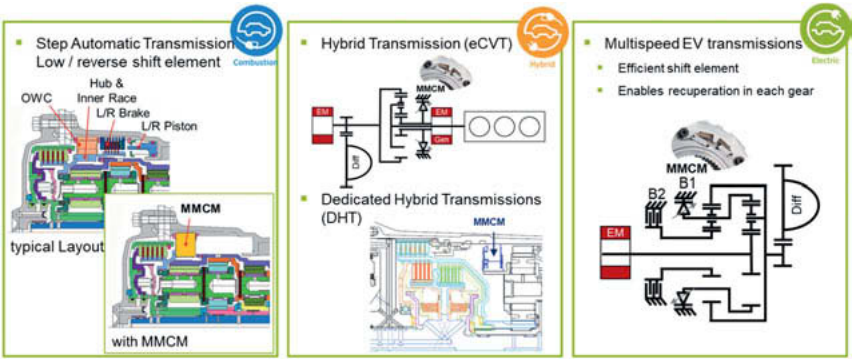

Fig. 4: Propulsion system types and possible MMCM applications: combustion, hybrid, electric driven vehicles; including [Cam16]

For full application flexibility different actuation options can be chosen. So, actuation can be adapted to match the system strategy like the following hydraulic or electric actuators.

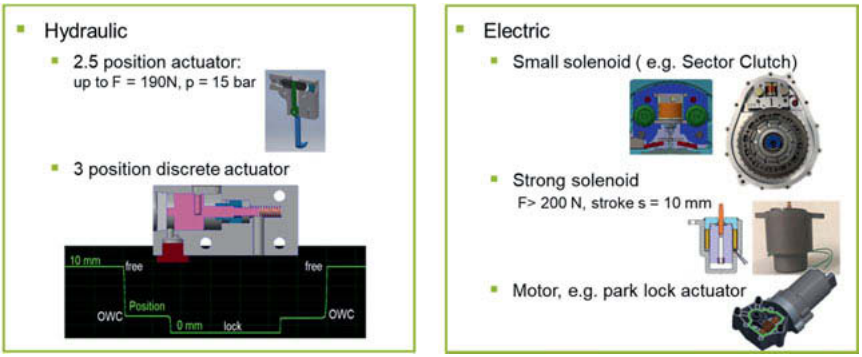

Fig. 5: MMCM actuator possibilities: hydraulic and electric

Some examples of actuators are given in Fig. 5: left – hydraulic actuators, a two position actuator with transient middle position and a discrete three position actuator by using different piston areas; right: two single solenoid solutions and one motor with worm gear. Furthermore, precise force-travel requirements are calculated and verified, see testing & simulation results chapter. Depending on shift strategies and derived requirements, the residual torque and shift speed define the worst-case shift power and therefore the actuator size to choose.

Testing & Simulation Results

As shown in the section application possibilities of different transmissions, various sets of tests were conducted, not only to verify the specifications of MMCM but also to prove the applicability of MMCM in such transmissions. In the following, a large variety of tests and simulations are performed in order to cover future applications, which are in detail:

- Overrun: MMCM is in OWC mode
- Drag torque: MMCM in OWC or free mode
- Stroker test: MMCM actuated in block direction
- Random impact: MMCM is free and shifted in block direction during relative speed
- Disengagement & shift time: MMCM is preloaded in block direction and disengaged, force and time is measured

Overrun, Simulation and Test:

During overrun mode of MMCM the pawl and spring behaviour is important since they are responsible for drag torque and durability of each contacting component. A setup with rotat-

ing Inner Race and transparent Side Plate was chosen in order to observe Pawl and Spring movement with a high-speed camera, see Fig. 6. A visual comparison to simulation results was conducted with one set of parameters in order to determine estimated parameters such as contact damping.

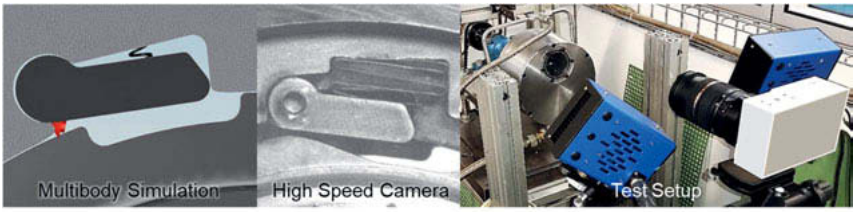

Fig. 6: Image of multibody simulation (left), high-speed camera picture (middle) and test bench setup for overrun mode observations

The simulation model was validated by varying test parameters such as speed, Pawl design, springs in the test setup as well as in simulation setup. The simulation showed good predictability for all combinations.
Afterwards, endurance runs were conducted in order to observe possible wear. After days of different speed ramps representing a specific application and lifetime profile, the parts were inspected with no serious damage found. Of course, using a three mode MMCM allows lifting up the Pawls into free mode by the installed Cam, so this test represents more than a worst-case scenario.

Drag Torque Measurement:

Since efficiency is a big driver of the MMCM, this test is one of the most important. Two different temperature levels were evaluated, as well as the operating conditions: OWC and freewheeling. There is a difference in drag torque of these two modes, since Pawls are frequently pushed or kept in upper position by rotating Inner Race. These forces (including Spring force) influence drag torque. As shown in Fig. 7 the drag torque is always smaller than 0.25 Nm over the whole speed and temperature range. The MMCM, which is introduced here, is also a special variant. It has an inherent friction bearing function by centering Inner Race to Outer Race.

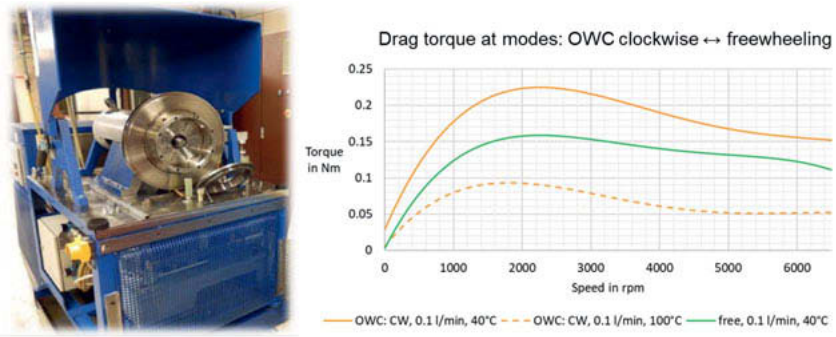

Fig. 7: Drag torque measurement test bench (left) and test result of OWC mode at 40°C and 100°C as well as freewheeling at 40°

Stroker Test:

This investigation is an important durability test: Every cycle, the Pawls get into contact with the same Inner Race tooth and are loaded to the devices maximum torque, which is in this case T = 900 Nm. In Fig. 8 it is shown, that there is an angular movement without torque in order to ensure contact loss before contacting again. As known from Smith-Diagram, this lift-off is important to ensure zero load in-between the cycles because this influences durability.

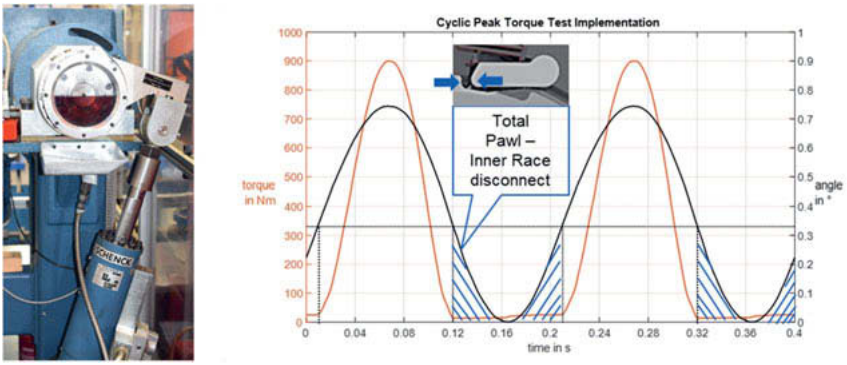

Fig. 8: Cyclic Peak Torque Test setup (right) and example measurement result

Since the introduced MMCM is fatigue endurable for the specified operating condition, it was overloaded to ensure the durability for a certain amount of over-torque cycles.

Random Impact Test:

In drivetrain applications the MMCM needs to shift into block direction with not precisely known or controlled differential speeds. When the relevant inertias and stiffnesses in-between are given, a corresponding torque as function of relative speed can be calculated. However, there are effects which could raise estimated impact such as resonance and effects which can lower the impacts such as joint cushioning. Therefore a specific drivetrain layout was reduced to its relevant parts and implemented in test bench as system. This system includes a friction clutch, shafts and inertias, as well as splines and flanges. The derivation of that setup is shown in following Fig. 9.

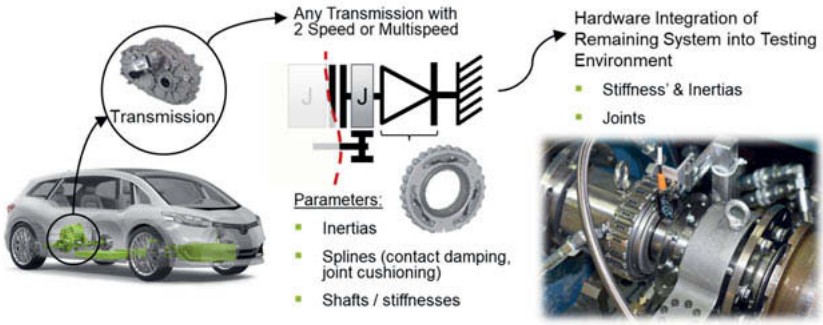

Fig. 9: Derivation of system under test from vehicle to test bench in order to rate shift impacts at MMCM

The scheme of the transmission shown in Fig. 9 (middle), is implemented as test bench layout shown in Fig. 10 (left), with its inputs oil pressure (p), speed (n) and its parameters.

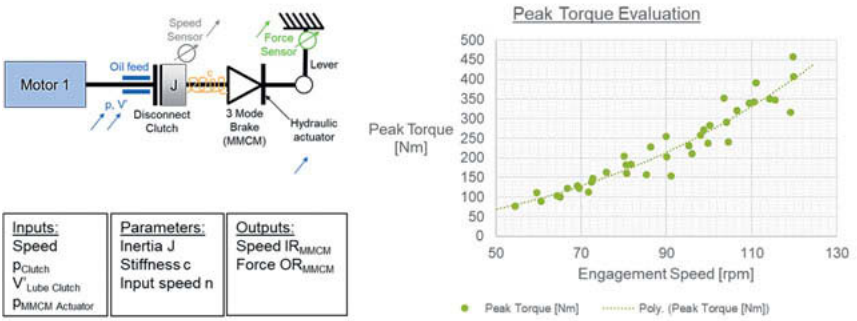

Fig. 10: Test bench implementation of system under test with its inputs and outputs (left) as well as resulting measurement of impact torques at different relative speeds (right)

The relative speed as well as the impact force is measured. As shown in Fig. 10 (right), the resulting peak torques were evaluated for differential speeds in the range of 60 to 120 rpm.

Disengagement at Different Residual Torque Levels

When introducing MMCM to gearboxes, a consideration of residual torques or disengagement under a certain load is important. In many cases, a synchronization by electric engines is possible or the MMCM is automatically overrun. But under some conditions, a residual torque cannot be eliminated even though a shift is required at the same time. Depending on application, different actuator-lever-cam-combinations are possible. For developing the newly introduced MMCM, a residual torque of 5 Nm was considered. To verify calculations, experimental tests were conducted: different torques are applied at Inner Race and the hydraulic actuator has to disengage Pawl-Inner Race contact at the same time. The results are shown in following Fig. 11:

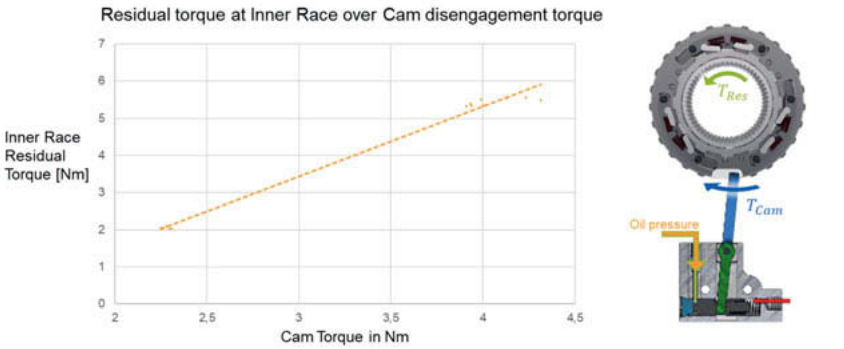

Fig. 11: Measurement example of MMCM disengagement under residual torque, 33°C oil temperature.

The tested MMCM has a hydraulic actuator and a lever which is actuating the cam. Of course, it is possible to change the travel versus force characteristics and also other disengagement parameters, e.g. an axially translating ramp, are available.

Shift time is also important at disengagement. Depending on available line pressure, oil temperature and residual torque, the shift time remains in a finite range. At recommenced actuation pressure of $p_{Actuator}$ = 14 bar and a residual torque of T_{res} = 6 Nm the shift time at 33°C oil temperature is t_{shift} < 10 ms.

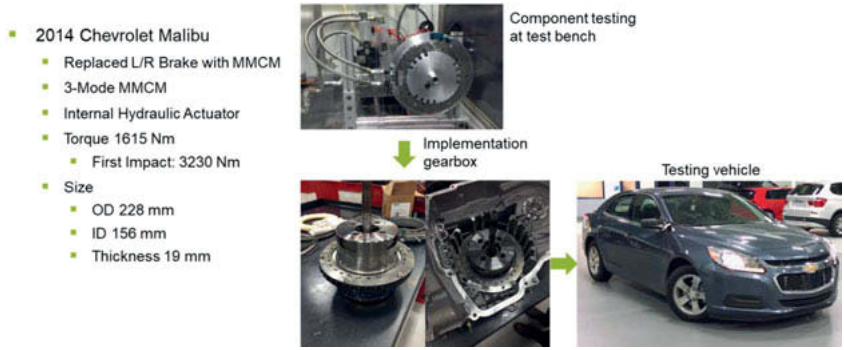

Fig. 12: MMCM vehicle testing

Another variant of the MMCM was successfully tested in a vehicle. The MMCM had a nominal torque capacity of 1615 Nm and an impact torque if 3230 Nm. It was placed in a 2014

Chevrolet Malibu 2014 transmission and replaced a Low/Rev brake. It was actuated with a hydraulic piston; some impressions and geometry values are given in Fig. 12.

Vehicle Efficiency Consideration

In the previous section about testing and simulation results it has been shown that drag torque is always smaller than 0.25 Nm over the given speed range from 0 to 6500 rpm, even though the Outer and Inner Race are designed as a friction bearing.

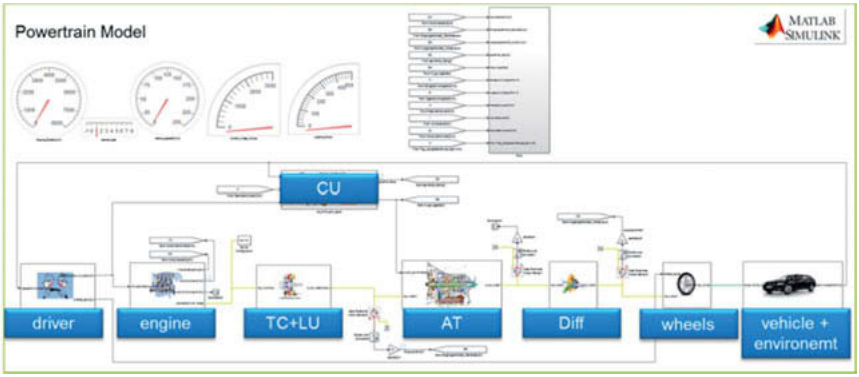

Fig. 13: Scheme of a conventional powertrain model for evaluating efficiency, exchanging friction brake and OWC of Low/Rev gear with MMCM

If replacing Low/Rev clutch in an 8-speed AT of a vehicle in D-/F-Segment, one receives an relative improvement in power loss of 36% by the reduction of drag torque. This value has been calculated by simulating an 1D powertrain model in WLTP. A schematic is shown in Fig. 13. If considering the actuation, a small portion of further efficiency should be observed. For this simple comparison it is neglected since different applications require different actuators like shown in the section “possible transmission applications”.

For another example, even more advantages can be achieved: A small 2-speed electric vehicle (m = 1350 kg, P = 125 kW) with planetary gearsets and two shift elements namely a friction clutch and a MMCM, similar to shown layout in Fig. 4 (right). An improvement of ~ 83% less power loss due to drag torque reduction in WLTP as well as in NEDC is determined by just replacing 1st gear friction brake by an MMCM.

Conclusion & Outlook

First, the Multi Mode Clutch Module is explained as a shiftable form lock clutch with up to 4 different modes (Free, OWC-L, OWC-R, Lock) and a variety of application possibilities in different propulsion systems of vehicles is shown, as well as hydraulic and electric actuation possibilities. The wide range of tests verify and validate functions and requirements of the MMCM: Overrun drag torque and durability, durable engagement testing, random impact engagements as well as shift times below 10 ms with low residual torques. Especially, the energy efficiency of the component shows impressive benefits in a vehicle system consideration due to its drag torque being almost zero. A replacement of a friction clutch as Low/Rev shows improvement of 36% less power loss and in electrical 2 speed vehicle by replacing a 1st gear brake an improvement of 83% in WLTP.

The application as a brake has been verified in many simulations and tests – also including tests in vehicle. The clutch application will also be developed for different examples including alternative actuation possibilities. The latest test results are in que and the MMCM will be available as a verified clutch. Due to the radial arrangement of Pawls, it is simple to achieve specific modes passively using centrifugal forces. So centrifugal disengagement (free mode), centrifugal engagement, or neutral engagement can be designed by simply adding a “backpack” to the Pawl, shifting the center of gravity relatively to its rotation center.

List of References

[Bre18] Brezger, F.; Moser, A.: „Efficiency improvements for wet clutches in DCTs, ATs, and especially for drive trains of hybrids and Electric Vehicles”. CTI Conference & Exhibition, Berlin. 2018.

[Cam16] Campton, C.; Martin, K.: “Multi-Mode Clutch Module – Application and Performance”. CTI Conference & Exhibition, berlin. 2016.

[Mur18] Muramatsu, I.: “Honda’s 10-Speed Automatic Transmission”; Presented at 12th international CTI Symposium, May 2018, USA

High Efficiency Electric Transmission Oil Pump

Transmission hydraulic efficiency improvement through hybridization

Mario Saborío, **Oscar Sarmiento**,
Vitesco Technologies Germany GmbH, Nürnberg;
Christian Böhm,
Vitesco Technologies Germany GmbH, Schwalbach

Abstract

Hydraulic designs are moving away from pure mechanical oil-pumps to give space to flow on-demand pure electrical supply systems i.e. Electrical Oil Pumps (EOP), or hybrid systems that integrate the advantages of a MOP with the flexibility of an EOP i.e. Dual Drive Pumps (DDP). Such hybridized and pure electrical supply concepts show an oil supply system efficiency increase of up to 20 % thanks to a 94 % reduction of the recirculation losses during a WLTC Class 3 test cycle. In terms of CO_2 emissions, reductions of up to 11 g CO_2 per WLTC cycle, or an average of 0,5 g/km less CO_2 compared to a standard, non-optimized oil supply system are observed. This paper shows the benefits in terms of transmission and fuel efficiency for a hybrid DDP solution on a WLTC cycle.

Introduction: transmission oil requirements

Historically speaking, the mechanical oil pump has been a complementary system of the transmission responsible of delivering enough flow to cover the cooling, lubrication and pressure demands of the transmission. Directly geared to the combustion engine, the oil pump had to be dimensioned to be big enough to cope with the demand even at low speeds. Consequently, the resulting pump ends up oversized and, in many cases, delivering far more oil than required. Until a few years back, the energy losses associated with this were not considered. However, newer emission regulations have made it necessary to optimize the different subsystems in the vehicles, the transmission oil supply being one of them.

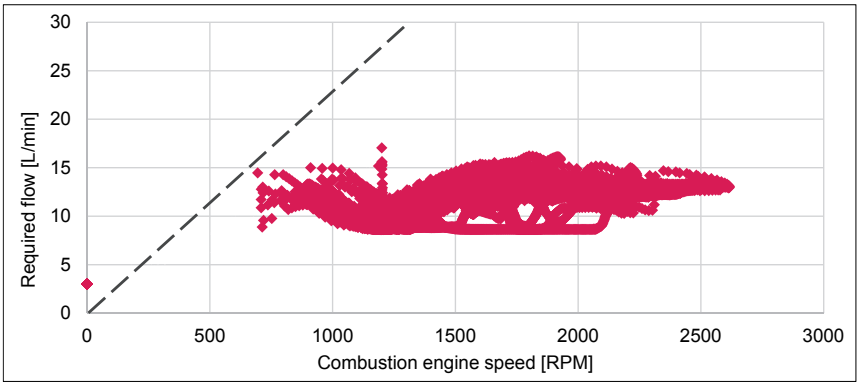

Fig. 1: Transmission flow demand vs engine speed for a generic application

The diagram on Fig. 1 shows an example of a transmission oil demand vs the corresponding internal combustion engine (ICE) speed. The diagram shows that the flow demand and the ICE speed do not correlate. Ideally speaking, volumetric pumps have a flow characteristic which is linearly proportional to the speed, being the proportionality factor the displacement of the pump[1]. With that idea in mind, it might be possible to dimension a pump with a characteristic such that the flow demands of the transmission are covered. The result of such layout is represented with a black dotted line. The resulting pump can cope with the demand at any given ICE speed, but it raises three issues:

1. The application shown on the diagram requires certain amount of flow at zero ICE speed. This is typical for start/stop systems were some oil is required even when the ICE is off. With a purely mechanical oil pump it is not possible to satisfy this requirement.
2. The pump characteristic shown on the diagram corresponds to a high displacement one (22 cm³/rev). At high ICE speeds, the pump flow output will greatly surpass the transmission requirement. A higher pump displacement also increases the required pump torque, which requires a more robust mechanical construction.
3. The surplus oil is brought up to pressure but then recirculated back to the oil sump, and the energy required to do it is dissipated as heat in the pressure control valves used to maintain the supply pressure constant.

The nature of the pump layout and the variability of the transmission needs makes it very difficult to provide flow on-demand and minimize the energy waste due to recirculation using only one mechanical oil pump. Unfortunately, a purely electric solution with a single electric oil pump is not viable for all applications either. The required battery current to operate the pump and cover all the transmission demands are too high, with values easily exceeding 60 A[2]. This issue can be overcome with high voltage solutions, but most of the vehicles nowadays still use 12V systems.

The problem of high oil recirculation can be tackled by the hybridization of the oil pump, whether by complementing the MOP with a high efficiency EOP; or by merging both into one hybrid system as is the case of Vitesco Technologies' Dual Drive Pump.

Achieving flow on demand

In order to optimize the overall efficiency of the oil supply system it is mandatory to reduce or completely cut-off the oil recirculated into the tank. A flexible solution capable of delivering just enough oil while being dynamic enough to react to changes in the transmission demands is necessary. The present paper shows to approaches to minimize the recirculation.

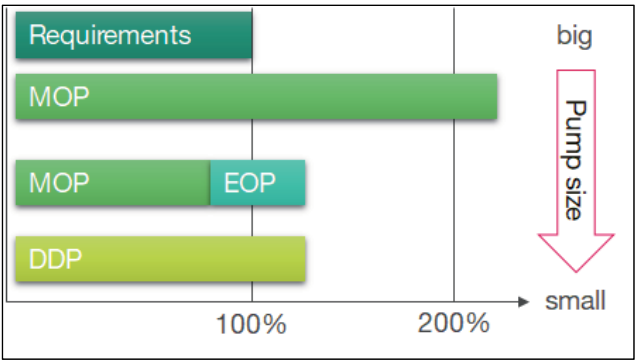

Fig. 2: Energy delivery surplus form a traditional MOP vs flow- on-demand solutions

[1] The discharge flow of a volumetric pump is also affected by the discharge pressure and the temperature. Both effects are reflected in the volumetric efficiency. For the present analysis, an ideal pump is assumed.

[2] Assuming a 12V system and a transmission hydraulic requirement of 450W or more.

Fig. 2 shows the proposed approach to reduce recirculation losses. A classical MOP solution will usually deliver far more energy than required, with the surplus being lost as heat and oil recirculation. By better matching the pump size to the requirements it is possible to decrease this surplus. On this scenario, the energy losses are almost exclusively a consequence of the efficiency of the components (pumps, electric motors, gear trains). The analysis showed also that the optimized solutions resulted in smaller pump sizes, which is to be expected given that the pumps are dimensioned based on hydraulic needs, and not only on the combustion engine speed.

Dual Drive Pump

The Dual Drive Pump (DDP) is an electro-mechanical oil pump simultaneously driven by two rotatory shafts. The pump itself is a double-stroke vane type with the particularity that both the outer ring and the rotor of the pump can rotate independently. The rotor of the pump is driven by the combustion engine, while the outer ring (or housing of the pump) is driven by an electric motor. The pump then works as a power addition/splitting system.

Fig. 3 shows a schematic with the basic principle of the DDP. The outer ring of the pump is driven by an electric motor through a gear set. The ratio between the electric motor and the outer ring is tuned to better match the hydraulic requirements to the size of the electric motor. The rotor is geared to the combustion engine and, in a similar way, the ratio between the ICE and the rotor is selected to better match the pump size to the requirements and make the most of the energy provided by the ICE.

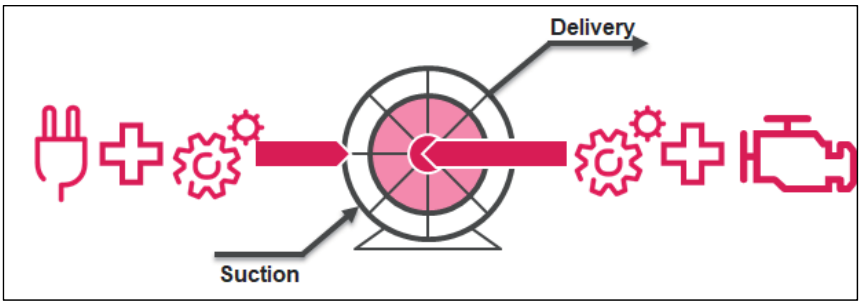

Fig. 3: Schematic layout of the DDP

During operation, the speed of the rotor is driven by the speed of the combustion engine and cannot be influenced in any way. The DDP makes use of the electric motor to modify the

speed and direction of rotation of the outer ring. As a result, the relative speed between the rotor and outer ring can be controlled, and thus, the discharge flow of the pump.

Table 1. DDP operation modes as a function of the rotor/outer ring spring speeds

Rotor speed	Outer ring speed	Operation mode
+	0	MOP mode
0	-	EOP mode
+	-	Dual drive mode: boost
+	+	Dual drive mode: subtract

Depending on the speed combinations between the rotor and outer ring it is possible to derive four operation modes, which are summarized in the Table 1. The four modes are based on the hydraulic requirements of the transmission and the available combustion engine speed:

1. **MOP mode:** the outer ring of the pump does not rotate. The speed of the pump is the speed of the rotor and the hydraulic demand is covered only with the energy input from the ICE.
2. **EOP mode:** the rotor of the pump does not rotate (ICE is turned off). The speed of the pump is the speed of the outer ring and the hydraulic demand is covered entirely with the energy input from the electric motor.
3. **Boost mode:** the energy input of the ICE is not enough to cover the requirements of the transmission. The rotor and outer ring spin in opposite directions increasing the rotor/outer ring relative speed, resulting in an increased delivery flow.
4. **Subtract mode:** the energy input of the ICE is greater than the demands of the transmission. The rotor and outer ring spin in the same direction, decreasing the rotor/outer ring relative speed, resulting in a decreased delivery flow.

One further advantage of a DDP solution is its flexibility. For the layout and dimensioning of a DDP, there are up five degrees of freedom (DoF) to match the design to the requirements of the transmission: the gear ratios for both rotational axes, the pump displacement, the motor size and the operation modes. For a given application, the DDP can make use of all four modes described on Table 1 or just three of them, resulting on a boost-only or a subtract-only solution. The different operation modes are shown on Fig. 4 as a function of the ICE and electric motor speeds. Depending on the energy provided by the ICE and the energetic de-

mands of the transmission, the DDP's electric motor can adjust the speed of the pump's housing to regulate the delivery flow of the pump and alter the direction of the energy flow from the electric motor.

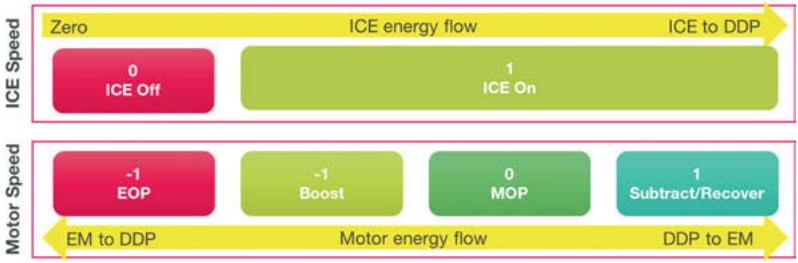

Fig. 4: DDP energy flow for different ICE and electric motor speed combinations

WLTC[3] Energy losses comparison

To determine the impacts of a requirement-oriented layout of the oil supply system, a comparison was made using the hydraulic requirements of a transmission during a WLTC Class 3 cycle. A CVT application with high hydraulic requirements was specifically chosen to better demonstrate the effects of high oil recirculation. The information was populated into a simulation model, and an optimization algorithm was used to select the best possible layouts to optimize the energy usage and minimize the losses for a given pump displacement. The chosen pump sizes were based on existing products of Vitesco Technologies' portfolio.

[3]Worldwide Harmonized Light Vehicle Test Cycle

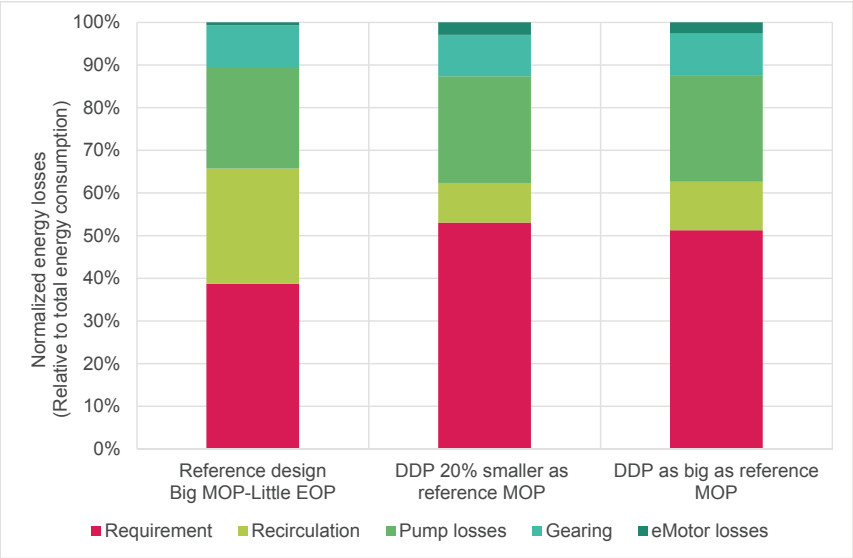

Fig. 5: Normalized energy over a WLTC for different oil supply solutions

Five different topologies were compared. The first one is the reference design currently used on the transmission: A Big MOP/ Little EOP combination with a MOP directly geared to the ICE and a small EOP acting as an auxiliary unit to provide oil mostly during start/stop situations. Next, two DDP solutions with different pump sizes were also ran through the optimization algorithm to find the best combination of pump size and gear ratios. The diagram on Fig. 5 shows the normalized energy losses relative to the total energy consumed by the oil supply system. For all proposed solutions, the total input energy equals the sum of both the mechanical energy provided by the combustion engine and the electric energy provided by the battery to the oil supply system. The different colors represent the energy losses of each topology, normalized relative to the total input energy for that topology:

1. The red bars represent the energy required by the transmission to complete the test cycle and equals the hydraulic energy provided by the pump(s). The raw value is the same for all three topologies, but since it is normalized relative to the total energy consumption of each topology, its percentual contribution changes for each one. Higher values indicate that a higher percentage of the energy consumed by the oil supply system ends up as usable energy for the transmission, meaning also lower system losses.

2. The lime bars represent the energy lost due to oil recirculation, which will be mostly dissipated as heat in the pressure control valves used in the transmission.
3. The green bars represent the energy losses due to the pump's efficiency.
4. The combined efficiency losses due to the gears are shown in light blue.
5. Finally, the dark green bars show the energy losses due to the efficiency of the electric motor.

The first thing to notice is that the reference design has the lowest percentage of usable energy of all concepts. Only 39 % of the energy consumed by both pumps (MOP and EOP) is available to satisfy the needs of the transmission. This is in part due to the 27 % of the energy that is lost as recirculation. This is a direct consequence of the Big/Little layout: The MOP is dimensioned to cover the demand at almost any given ICE speed. The EOP works mostly as an auxiliary system that provides oil during start/stop cycles, where the ICE is shut down. The DDP solutions show a significant improvement with up to 53 % of usable energy. The recirculation losses are brought down to 9 % and 11 % for both solutions, which is considerably lower as the reference design. In addition, there are several potential improvements not considered in the analysis:

1. The DDP makes use of only one pump, meaning that the total weight and space requirements are lower than a two-pump solution. This analysis does not account for possible energy savings due to weight reduction.
2. The topologies shown on Fig. 5 do not make use of the subtraction mode due to specific limitations of the selected application. Enabling it could yield much lower recirculation losses or even bring them down to zero.
3. In order to keep the pump and motor speeds below 4000 RPM and therefore avoid potential high frequency noises, the minimum permitted pump size was limited to only 20 % the size of the reference MOP. Raising the maximum speed to 6000 RPM makes it possible to shrink the pump down to 50 % the size of the reference MOP. The resulting topology is very compact and more efficient, but at the cost of potentially undesired noise.

The results show that a proper matching of the components to the transmission demands can considerably reduce the wasted energy and have a significant impact on the transmission's overall efficiency. Initial estimations on the impact of such efficiency increase points towards an average reduction of up to 0,5 g CO_2/km and a total of 11 g CO_2 for a WLTC cy-

cle[4]. Such reductions are possible without any significant changes to the transmission's topology since a DDP solution can be retrofitted to an MOP-only transmission to better achieve flow on-demand.

Choosing the appropriate solution

The presented analysis showed that a requirement-oriented layout of the oil supply system could yield significant gains in terms of efficiency and lower oil recirculation. However, a hybrid solution is not appropriate for all use cases, being the available electrical power the definitive factor to go for a purely electric solution or a hybrid pump.

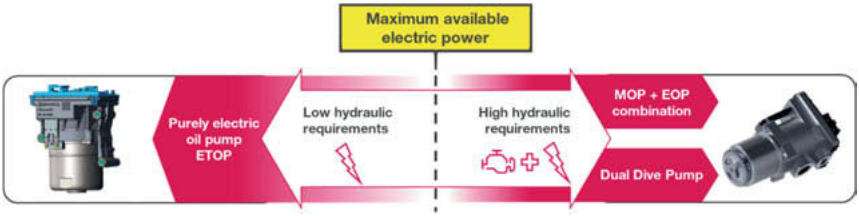

Fig. 6: Oil supply system selection based on available electric power

Assuming a 12V system, three categories can be derived from the diagram on Fig. 6:

1. Applications with hydraulic requirements below 400 W can be classified as low power and can be covered with one single electric oil pump. Examples of such systems are double clutch transmissions where the actuation components require high pressure and low flow, or cooling system which requires the opposite. Vitesco Technologies' ETOP lineup offers different alternatives on this category.
2. Once the maximum available electric power threshold is surpassed, a secondary energy source is required to satisfy the hydraulic demand. Around this limit both an optimized MOP+EOP combination or a small size DDP could be implemented.
3. For hydraulic requirements beyond 1 kW, the DDP becomes the most sensible solution. Thanks to its small footprint (700 cm³) and highly integrated construction, it can better combine the energy inputs from both the ICE and electric motor to efficiently satisfy the transmission demands.

[4] Based on a specific CO2 emission of 69,3 kg/GJ for 95 RON gasoline [2]

Summary

Since 2019, the European Commission had set new targets for the CO_2 emissions for passenger cars, with penalties of 95 € for g/km of exceedance [1]. The solutions proposed on this paper enable significant improvements in terms of efficiency and oil recirculation, which reflects in a CO_2 emissions reduction of up to 0,5 g/km. Such improvements justify the replacement of existing solutions in favor of hybrid ones.

The presented method demonstrates that a requirement-oriented layout of the hydraulic supply system can result in a significant efficiency increase and overall system improvement. For the analyzed application, the oil supply system efficiency can be increased in up to 20 % without significant changes to the transmission topology thanks to its small footprint and weight. Due to its construction, the DDP can be retrofitted to replace traditional MOP-only solutions, enabling significant efficiency improvements without major changes to the transmission topology.

References

[1] European Comission, „Road transport: Reducing CO2 emissions from vehicles,“ Directorate-General for Communication, [Online]. Available: https://ec.europa.eu/clima/policies/transport/vehicles/cars_en#tab-0-0. [Zugriff am 28 02 2020].

[2] V. Quaschning, Regenerative Energiesysteme: Technologie - Berechnung - Simulation, München: Carl Hanser Verlag GmbH & Co., 2011.

Consistently quattro

Ludwig Wittmann, **Michael Wein**, **Maximilian Wolf**,
Audi AG, Ingolstadt

Summary

The foundations for the long and continuing success story of the quattro powertrain were laid in 1976. The concept has been steadily improved through continuous development, and new technology modules have been progressively added. The original quattro that went into production in 1980 featured a manual-locking centre differential. This was followed in 1986 by the variable torque distributing TORSEN differential, which was soon complemented by the asymmetric-distribution crown gear differential. Having mastered longitudinal distribution, the Audi sports differential then extended its scope to lateral distribution. For the first time ever, it became possible to distribute torque beyond the range of the intrinsic locking value to the outer rear wheel on cornering in order to further improve the dynamics, handling and ride based on so-called torque vectoring. The quattro-ultra succeeded in attaining maximum efficiency by decoupling and stopping the rear axle differential as required.

Nowadays, the challenge of lateral and longitudinal dynamics has become less a mechanical and more an application task. Mechanically decoupled electric front and rear axles, as well as rear wheels that also have separate electric motors, meet the challenge very elegantly, as has already been demonstrated with the Audi e-tron S powertrain concept.

But what is the next step? Where will the quattro powertrain's journey take it next? How can ride comfort and customer satisfaction be enhanced further? What will be the technology of the future?

40 years of quattro – evolution of the four-wheel drive

Consistently quattro. That approach has been integral to Audi's DNA since 1980.
Audi has produced some five million cars featuring quattro drive over the past 40 years, meeting customers' wishes for agility, lateral dynamics and safety on even the most difficult surfaces. Today the brand is the world's leading premium-segment manufacturer of cars featuring permanent and selectable four-wheel drive. In 2019 Audi sold more than 316,000 vehicles – once again demonstrating its market-leading position. The current range includes over 100 quattro variants, with a number of models available exclusively with four-wheel drive. Alongside the mass-production vehicles, the dynamic S and RS models are a key element.

The first Audi quattro, produced under the company's then development director Dr. Ferdinand Piëch, debuted at the Geneva Motor Show in March 1980. A five-cylinder 2.1 litre 147 kW (200 hp) turbo engine catapulted the angular-design original quattro coupé into the elite league of fast sports cars at the time.

The original quattro's four-wheel drive design was as efficient as it was elegant. A hollow shaft running through the gearbox made the heavy transfer case, which was previously commonplace, and auxiliary shaft to the front axle superfluous – Audi had developed the first mass-production permanent four-wheel drive for sporty models. A bevel gear differential distributed the forces evenly between the front and rear axle. On slippery surfaces the driver could lock it, and the rear axle differential, manually.

From 1982 onwards, quattro technology was gradually introduced into all the company's model series. In 1984, Audi added to the original with the Sport quattro – a short-wheelbase supersports car developing 225 kW (306 hp). This shortened model, which served as the homologation basis for the competition car in the World Rally Championship, is today a sought-after classic. The long-wheelbase quattro remained in production until 1991 – from 1989 onwards fitted with a four-valve 162 kW (220 hp) engine.

In 1986, Audi put into production a new self-locking centre differential. It still worked mechanically, yet highly intelligently. Its name "Torsen" is made up of the words "torque" and "sensing". Specially meshed worm gears inside the differential were able to instantly redistribute the engine power as and when required, sending as much as 75 percent of the power to the axle and so providing it with improved traction. Thanks to the flexibility of the Torsen differential, the anti-lock braking system remained effective whenever it was needed – another major advance.

The first TDI quattro was launched in 1995, and since 1998 the compact Audi models featuring transverse-mounted engines have also been available with four-wheel drive. They employ a special technology. At the end of the propeller shaft they have an electronically controlled multi-plate clutch, powered by an electric pump. When the plates are pressed together by oil pressure, they seamlessly transfer more torque – up to 100 percent in extreme scenarios – from the front to the rear axle.

2005 saw the debut of another innovation in the classic quattro powertrain – the new self-locking centre differential with asymmetrically dynamic basic distribution. In normal driving, it distributes the forces with a 40:60 ratio between the front and rear axles, sending up to 60 percent of the torque to the front and up to 80 percent to the rear as required. The self-locking centre differential, designed as a planetary gear unit, works entirely mechanically.

Audi launched its first S model in 1990 – the S2 coupé established a successful new line featuring sports power and cultured stylishness. The S models have always been technology leaders. In 2008, the S4 was provided with a new high-end solution: the sports differential, which actively distributes engine torque between the rear wheels depending on the driving situation.

This “torque vectoring” is implemented by two superposition gears on the differential, activated by a control unit via multi-plate clutches. When steering into or accelerating on a bend, most of the torque flows to the outer wheel, pushing the car into the bend. The system thus counteracts any tendency to under- or over-steer.

The RS series, launched in 1994 with the RS 2 Avant, represents the dynamic spearhead of the Audi model range. The RS models, run by Audi Sport GmbH since 2000, have regularly embodied new technologies. One example of this is the Audi RS 6 launched in 2010. Its twin-supercharged V10 engine develops 426 kW (580 hp). The corresponding RS 5 coupé features another update to quattro technology – a crown gear centre differential and wheel-specific selective torque distribution.

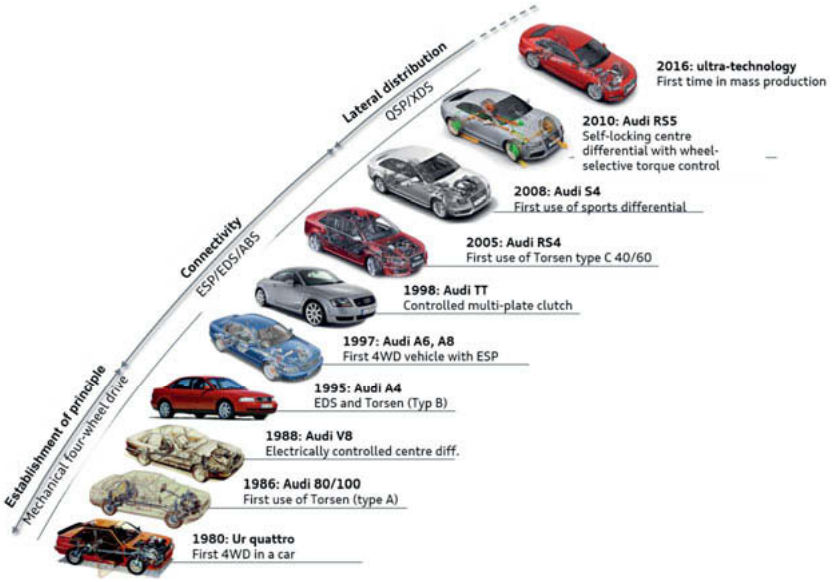

Fig. 1: Evolution of the quattro powertrain [3]

Trend in new vehicle registrations

Sales of four-wheel drive vehicles in Germany continue to show a clear trend according to the new vehicle registration data of the Federal Motor Transport Authority (KBA). Four-wheel drive is on the rise. Fig. 2: Quattro percentage share 2010 to 2019 of the Quattro powertrain shows the trend in four-wheel drive vehicles as a percentage of the total number of vehicles registered in Germany. This rate has more than doubled over the last nine years [1], reflecting the sustained enthusiasm for the 40-year-old powertrain design concept.

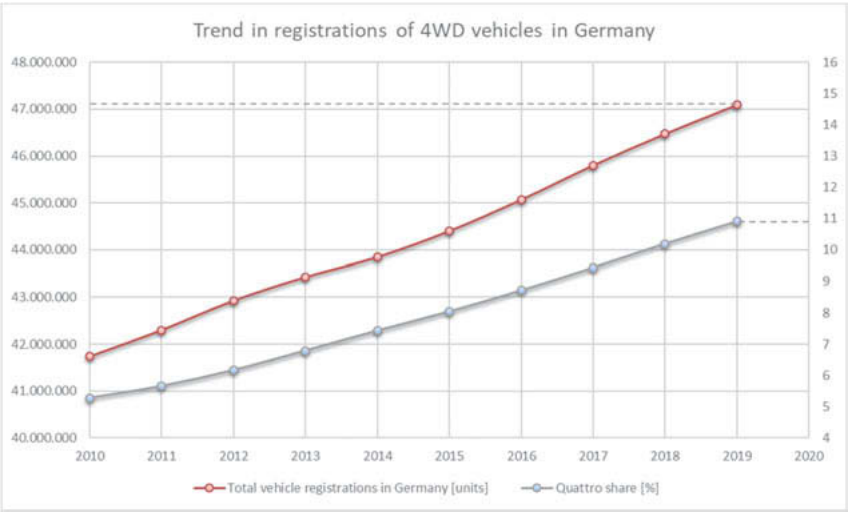

Fig. 2: Quattro percentage share 2010 to 2019 [1]

The range of conventional-drive products is already very extensive, offering the right solution for virtually any application. The range of electric four-wheel drive products is currently undergoing rapid growth. There are, however, fundamental differences in the development of conventional and electric powertrain systems.

Fundamental differences between conventional and electric powertrain concepts

The most fundamental difference between conventional internal combustion engines (ICEs) and all-electric battery electric vehicles (BEVs) is the method of storing the energy carried. This fact has a far-reaching influence on the layout of the individual component units and utilisation of available space in the vehicle, from which in turn different technical component requirements can be derived:

Resulting technical requirements for electric powertrain concepts:

- General crash safety of high-voltage batteries
- Shaft seals in applications featuring varying directions of rotation and higher revs than ICE applications
- Loading on gear components – more frequent overrun resulting from increased braking energy recuperation

- Different centre of gravity and increased total vehicle weight
- More sensitive overall acoustics due to lack of masking noise from the combustion engine
- Less outside audibility because of greatly reduced running noise (pedestrian protection)
- No reverse gear
- Four-wheel drive: No transmission tunnel and centre differential

The ability to meet these new challenges has already been demonstrated. The most basic variation options for manufacturers relate to the number and design of the electric motors (permanently excited, asynchronous, flux-switching, ...). There are currently 57 mass-production all-electric vehicles (BEVs) worldwide [8]. The following looks in detail at example of electric four-wheel drive vehicle designs featuring two and three motors.

Audi e-tron and Audi e-tron S

The next major development step in the advance of the quattro – the Audi e-tron – went on sale back in 2018. The all-electric four-wheel drive systems of the Audi e-tron 50 and Audi e-tron 55 employ asynchronous motors on their front and rear axles. These drive the wheels directly via a non-selectable two-stage transmission. However, it is software that makes these two axle drive systems quattro. That software is distributed across the following control units:

- Drive control unit (ASG)
- Electronic chassis platform (ECP)
- Front and rear axle power electronics (LE VA and LE HA)
- Brake system (BRS)

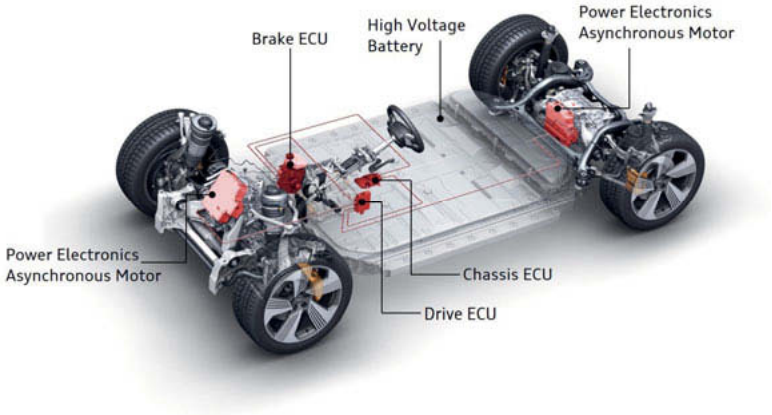

Fig. 3: Distributed software function across multiple control units and actuators in the Audi e-tron [6].

The ASG holds the powertrain functions. They include comfort, efficiency and high-voltage functions. The traction and vehicle dynamics control functions are located on the ECP. The LE VA and LE HA provide a virtual damping function which enhances the controllability of the powertrain. The brake system is controlled by the ECP and used as a hydraulic actuator to enhance handling by means of wheel-specific selective braking. To ensure optimum interaction within the complex network, these software functions are all Audi in-house developments. Only open-source availability of the complete software code enabled rapid, closely targeted development. Black-box software components from outside suppliers are not integrated into the action chain due to lack of transparency.

The traction and vehicle dynamics control on the ECP can influence the torque distribution between the axles, limit the torque individually on each axle, and set wheel-specific selective braking torques on the wheels. To this end, the ASG and ECP domain control units communicate with each other and with the power electronics and brake system actuators through a FlexRay data bus. To ensure fast signal transmission, they communicate at 5 to 10 millisecond intervals. For detailed information on the design of the network architecture and controller functionality see [5] and [6].

In the four-wheel drive systems of the Audi e-tron 50 and Audi e-tron 55 the mechanical connection between the two driven axles has been replaced by software, as has the rear axle

differential on the new Audi e-tron S. Each of the two rear wheels is driven by its own electric motor. The mechanical connection and the differential between the wheels on the rear axle have been entirely eliminated [7]. This opens up new possibilities for traction and vehicle dynamics control, but also poses new challenges in terms of the transition from mechanics to software. Audi is the first manufacturer to put such a drive system into electric vehicle mass production. In this respect, too, implementation of such a complex system with the high precision required was only possible based on full and transparent knowledge of the action chain. It begins with the Audi-built electric motor and ends with the software functions of the control system.

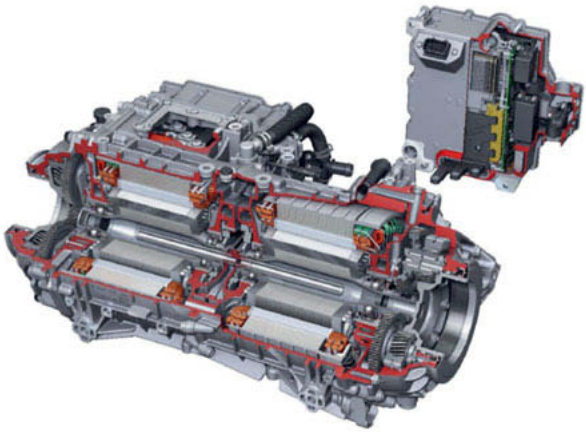

Fig. 4: Twin-motor rear axle drive of the Audi e-tron S [7].

The functional architecture for longitudinal distribution of drive torque from the Audi e-tron 50 and Audi e-tron 55 was applied for the lateral distribution of drive torque in the Audi e-tron S. The twin-drive control functions are again distributed via the ASG, the ECP and the two rear axle drive power electronics units. The ECP calculates the electric differential, limited-slip differential and torque vectoring functions. These utilise the potential of the two electric motors to improve traction and vehicle dynamics. The drive torque between the two wheels on the rear axle is adjusted every five milliseconds for this purpose. For instant control these functions must be intermeshed with the functions on the ASG and the power electronics. When cornering, the electric motors on the inside and outside of the bend run at different speeds. This means that the power demand – and so the required current in the overall system – changes

during torque redistribution when the power is distributed from the slower inner wheel to the faster outer one. The control in the high-voltage vehicle electrical system is extremely complex in such situations, and has repercussions extending as far as the battery management system.

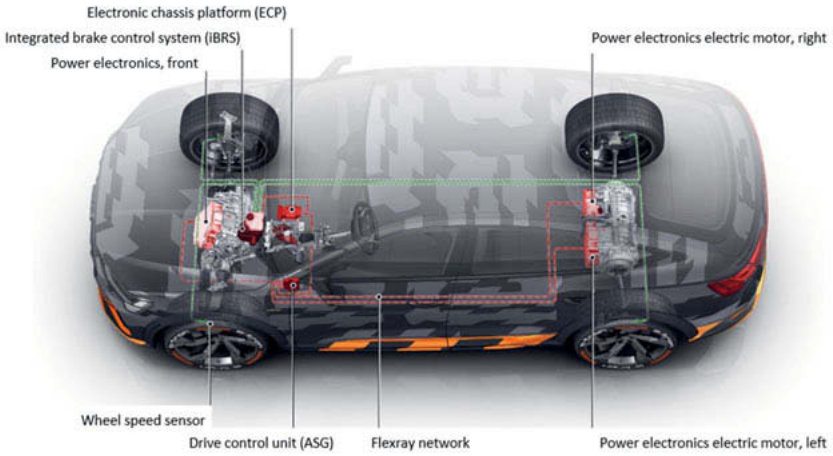

Fig. 5: Network architecture of the Audi e-tron S drive control functions [7].

The electric torque vectoring of the Audi e-tron S can create a torque difference of as much as 220 Nm at the motor level between the two rear axle drives. With the gear ratios, there are torque differences of as much as 2100 Nm between the two rear wheels. Additionally, as in the other two Audi e-tron powertrain variants, the brakes also apply torque vectoring. In the Audi e-tron S, however, this is only necessary on the front axle. On the rear axle the function can be implemented by electric torque vectoring. The Audi e-tron S marks 40 years of the Audi quattro, and sets a new benchmark for vehicle dynamics.

The key to the rapid and successful development of such complex drive systems is consistent transparency in the hardware and software action chain. This makes it possible to manage the integration of new technologies into the tightly timed product creation process of a mass-production vehicle.

Q4 e-tron concept

The Audi Q4 e-tron concept is a foretaste of the Audi models based on the modular electrification kit (MEB). This combines different types of electric motor to improve the dynamics and efficiency of the powertrain. The permanently excited 150 kW synchronous motor on the rear axle is characterised by great dynamism, thermal stability and high efficiency. It is therefore the main drive motor. A 75 kW asynchronous motor provides support on the front axle. It is characterised by a high overload capacity and low loss in no-current mode. This type of motor is therefore ideally suited to a permanently available four-wheel drive system capable of delivering the necessary drive torque very rapidly as and when required. No mechanical coupling and decoupling is required for this.

Fig. 6: Powertrain of the Audi Q4 e-tron concept with asynchronous motor on the front axle and permanently excited synchronous motor on the rear axle [8].

e-tron GT concept

The e-tron GT concept is Audi's interpretation of an electric Gran Turismo model. As the technical basis Audi has used the J1 performance platform developed by Porsche [9]. In the show car, permanently excited synchronous motors work on the front and rear axle. The two drives featuring 800V technology have a combined output of 434 kW, and deliver 830 Nm of system torque [10].

The J1 platform offers a range of drive technologies that can be deployed in vehicles on this basis. They include a two-speed gear unit on the rear axle which permits extremely fast acceleration from 0-100 km/h using the Launch Control function, combined with high top speeds and high-speed efficiency. The functional architecture of the four-wheel drive control system is similar to that of the Audi e-tron, also implementing intelligent interaction between the suspension and drive domain control units with the two power electronics units on the front and rear axles. The J1 platform also includes a controlled differential lock on the rear axle which improves traction and vehicle dynamics, and optimally supports the rear-end-heavy set-up of the four-wheel drive system typical of sports cars. Intelligent mechatronics and conventional gear technology complement the state-of-the-art electric drive system.

Electric four-wheel drive systems of the future

Electric four-wheel drive systems are complex, integrated systems combining electronic control units and actuators. Vehicle manufacturers have recognised that software expertise is key to the rapid and successful development of complex systems, and thus of vehicle models. In this regard Volkswagen has initiated a transformation process to become a “software enabled car company” [3]. Electric four-wheel drive systems are predominantly driven by software, and as such are in the midst of this transformation process.

In concrete terms, future domain architectures featuring highly integrated control units for electric four-wheel drive systems will pose a challenge with regard to their action chains. On the one hand, the system requires a high degree of intermeshing with the drive and suspension functions on the overall vehicle level, while on the other hand actuator-linked functionality enables short latency times and fast control functions.

Sporty. Safe. Systematic. – Outlook

The technical maturity and finesse that have already made it possible to maximise performance and efficiency in the conventional powertrain now need to be applied to electric drive systems. One measure targeting greater efficiency is to stop unnecessary rotating masses in a given situation in order to minimise friction and other losses.

This form of efficiency enhancement has already been successfully put into mass production in the quattro-ultra system for the conventional segment. In those applications, the propeller shaft and most of the gearing components in the rear axle drive are shut down by opening a multi-plate clutch and simultaneously decoupling a rear axle flanged shaft. The differential no longer rotates in its entirety when decoupled, and only the differential gears are in motion. This

leads to a reduction in splash and bearing losses, and so increases the range by as much as 0.3 litres per 100 km.
As range will be one of the key issues for future electric vehicles, this form of efficiency enhancement must now also be applied to electronic drive systems.
The fact that there is no mechanical coupling between the front and rear axles in electric powertrains means that additional components such as a multi-plate clutch for stopping the propeller shaft can be dispensed with. All that is needed is an opening mechanism for decoupling the power transmission to the wheel. A further challenge is the bearing of the differential gears because, in the decoupled state, they are subject to continuous road-speed-dependent variations in rotational speed. In the best-case scenario, such decoupling would be integrated into existing systems by modular means, and could be optionally conFig.d for the customer. The reduction in consumption is estimated at 2.4-4.1% (WLTP-High) [3].

Torque vectoring technology can also be applied to future drive systems. It has already been optimised in the quattro-sport rear axle differential for conventional powertrains. The basic approach in this is to achieve a more dynamic driving style by shifting the drive torque towards the outer wheel on the bend. In the case of the electric axle drive, this is conceivable by means of a separate superposition motor or by the infrastructural arrangement of two separate electric motor/gear unit combinations on one axle.
Comparing the torque distribution of an open differential with a weigh-beam system, an additional superposition motor allows the system to be detuned towards one side. The additional superposition motor improves system performance and enables torque superimposition even at maximum speed. A twin-motor system design must allow for a power reserve, though this can be available as a boost reserve when driving straight-ahead. Both variants offer advantages, though the higher-performance version of the twin-axle drive is already in use in the Audi e-tron S.

Comparing electric torque vectoring with clutch-based superposition variants, the following benefits can be expected [4]:

- Higher efficiency in the non-actuated operating state, comparable to that of a current standard differential.
- Much less power loss in the actuated operating state. For a mid-class car, the loss is estimated at a maximum of 1 kW. This enables the gearbox to generate high differential torques continuously whilst avoiding thermal problems or efficiency disadvantages.

- Very high actuating dynamics.
- Easy controllability of the differential torque due to the proportional correlation with the torque of the electric motor.
- Differential torque between the wheels is not kinematically limited, even in very small bend radii.
- Differential lock function, allowing 100% locking while balancing the wheel speeds.
- Compared to standard axle drives, axle drive designs featuring an active differential can be virtually neutral in terms of installation space requirement.
- Build-up of differential torque with neutral effect on power flow: Whereas in clutch-based systems the clutch losses generate braking torque on the driven axle, the power flow balance of both driven wheels is constant with an active differential.
- The low power demand with active control, together with the high actuating dynamics, enable additional functions that are permanently required. For example, the vehicle's sensitivity to ruts and cross-winds could be mitigated, with the resultant transmission power loss being just a few 100 watts.

In conclusion, the question as to the powertrain of the future cannot be answered unambiguously. What is certain, however, is that "electrification" will represent a new chapter in the success story of the quattro. The potential options are wide-ranging, and offer scope for innovative and exciting solutions.

Sources:

[1] Kraftfahrtbundesamt (German Federal Motor Transport Authority); https://www.kba.de/DE/Statistik/Fahrzeuge/Neuzulassungen/Zulassungsbezirke/zulassungsbezirke_node.html

[2] Andreas Füßel: “Technische Potenzialanalyse der Elektromobilität” [Technical Analysis of the Potential of Electric Mobility]; Springer Vieweg; 2017; chapter 2, p.10

[3] Audi internal

[4] Prof. Dr.-Ing. B.-R. Höhn, Dr.-Ing. Ch. Wirth, Dipl.-Ing. F. Kurth: “Aktives Differential mit Torque-Vectoring-Funktion” [Active Differential with Torque Vectoring Function]; 2. Automobiltechnisches Kolloquium; 2011

[5] Dr.-Ing. Ch. Graf, Dr.-Ing. M. Wein, B.Sc. Marc Baur, Dr.-Ing. S. Strasser, Dr.-Ing. R. Schwarz: quattro with e-tron Technology – Electric All-Wheel Drive System with Wheel Selective Torque Control; 27th Aachen Colloquium Automobile and Engine Technology; 2018

[6] Dr.-Ing. Ch. Graf, Dr.-Ing. M. Wein, Dr.-Ing. S. Strasser, Dr.-Ing. S. Poltersdorf: Der elektrische Allradantrieb des Audi e-tron; ATZ; Juni 2019

[7] Press release – Dynamisch, agil und elektrisch: Audi stellt Antriebskonzept für e-tron S-Modelle vor; Audi AG; 2020

[8] Press release – Audi Q4 e-tron concept; Audi AG; 2019

[9] Press release – Vier Plattformen für die E-Autos von Audi; Audi AG; 2019

[10] Press release – Audi e-tron GT concept; Audi AG; 2019

Evolution of the drivetrain and high voltage system in the new Corsa-e

Dr. **Peter Ramminger**, Dr. **Ralf Jäger**,
Opel Automobile GmbH, Rüsselsheim

1 Zusammenfassung

Der verstärkte Einsatz von Elektrofahrzeugen trägt wesentlich zur Dekarbonisierung des Verkehrssektors bei. Da Elektrofahrzeuge immer mit Energie aus erneuerbaren, CO2 neutralen Quellen geladen werden sollten, gibt es dadurch auch eine Verschiebung in der Nutzung erneuerbarer Energien - mit Ausnahme der zunehmenden Zeiten von Überschuss in der Elektrizitätsproduktion aus erneuerbaren Quellen. Je stärker BEV und PHEV Fahrzeuge im aktiven Fahrzeugbestand repräsentiert sind, umso größer wird der Beitrag der Dekarbonisierung im somit energetisch gekoppelten Verkehrssektor durch zeitlich noch folgenden Ausbau erneuerbarer Quellen für die Elektrizitätsproduktion insgesamt.

Der neue Corsa-e stellt einen weiteren Meilenstein für Elektrofahrzeuge im Opel Portfolio dar. Anders als der geräumigere Ampera-e ist der Corsa-e in der Mitte des B-segments positioniert. Durch dieses Fahrzeug wird Elektromobilität für einen größeren Kundenkreis erschwinglich. Außer einem begeisternden Design des Exterieurs und des Innenraums waren sehr gute Fahrbarkeit und beste Schnelladefähigkeit in der B- Klasse wesentliche Entwicklungsziele.

Dieser Aufsatz beschreibt die Fortentwicklung der EV Funktionalität, aufbauend auf dem Ampera-e. Vereinfachungen in der Hochvolt - Achitektur wurden entwickelt. Die starke Gleichteilenutzung mit dem konventionell angetriebenen Corsa und ein stärkerer Produktionsanteil des Fahrzeugherstellers gegenüber Zulieferteilen wurden als Strategien eingesetzt, um die Erschwinglichkeit für einen größeren Kundenkreis zu realisieren.

Mit 337 km elektrischer Reichweite gemäß WLTP Testzyklus, einer Verbesserung an den Fahrwiderständen für den Autobahnbetrieb und mit einer DC Ladeakzeptanz von max. 100 kW bietet das Fahrzeug eine perfekte Balance von Batteriegröße und Fahrleistung, auch für längere Fahrten.

Im Aufsatz werden die wesentlichen Hochvolt Antriebskomponenten mit denjenigen des Ampera-e verglichen. Schlüsselfunktionen für das elektrische Fahren und Laden werden erläutert und quantifiziert. Ladeoptionen werden verglichen und Ladepräferenzen für die verschiedenen Bauarten von Elektrofahrzeugen dargestellt.

2 Abstract

Electric vehicle usage contributes to the target of decarbonizing the traffic sector. While EVs should always be charged from renewable, CO2 neutral sources and operated CO2 neutral, there is of course a shift of renewable energy from other usages towards EV charging - except for increasing phases of excess in renewable energy. Once BEV and PHEV cars are stronger represented in passenger car fleets, societies will take further benefit from progress in decarbonization of the energy sector through this growing, coupled lever in the traffic sector.

The new Corsa-e marks another milestone of EV's in the Opel product lineup. Other than the well-known, roomier Ampera-e, the Corsa-e is more clearly placed in the B-segment. It will make electric mobility more affordable for a wider customer range. Besides an enthusing exterior and interior design, great driveability and class-leading charging capability were key development targets.

This paper describes how EV functionality was maintained and improved subsequent to the Ampera-e. High Voltage (HV) architecture design simplifications were brought in place. Commonality leverage with the "Corsa" sister model as well as manufacturing insourcing within the corporation were employed to widen the affordability of this car to a broader customer area.

With 337 km electric range in WLTP, further optimized road-load for motorway driving and DCFC charging up to 100 kW peak, the car provides a perfect balance of battery size even for longer distance usage.

Details on the major HV Powertrain components are compared to the Ampera-e as reference. Key functions related to electrical driving and charging are explained, supplemented by performance data.

The paper also compares charging options and delivers charge recommendations for different types of EVs, including BEV vehicles, like the Corsa-e.

3 CO2 emissions attributed to EV operation

Many societies on the globe are moving towards a sustainable energy management. This movement is not uniform, neither in speed nor in the individual strategy. Different countries or societies are moving with different speeds, leveraging their individual prerequisites, powered by capability to invest financially for the change, lead time to implement new infrastructure - partially against the interest of individuals or groups - and progress in research and technical development, e.g. regarding generation of energy from renewable sources, distribution, storage and power-to-x coupling.

The agreement on CO2 emission reduction achieved in 2015 under the authority of the UN marks an important milestone on the way to a future where mankind will continue to employ energy for many purposes, but will strive towards the ideal of complete usage of renewable energy sources. As a part of the UN agreement, European Union and its member states have set tough targets for de-carbonization of road traffic. Electric driving in all forms is a contribution to this CO2 reduction, starting with mild and strong hybrids, over Plugin Hybrid cars with efficient combustion engine on board all the way to either pure rechargeable Battery Electric Vehicles or to Fuel Cell Vehicles which may or may not offer a plug to externally charge the battery. To take maximum benefit for CO2 avoidance with BEV cars, these need to be charged with CO2-neutral, or even better renewable energy. Otherwise, the CO2 avoidance benefit for the environment will be lower at begin of operation and will rise every year with the progress in CO2-reduction for electrical energy production.

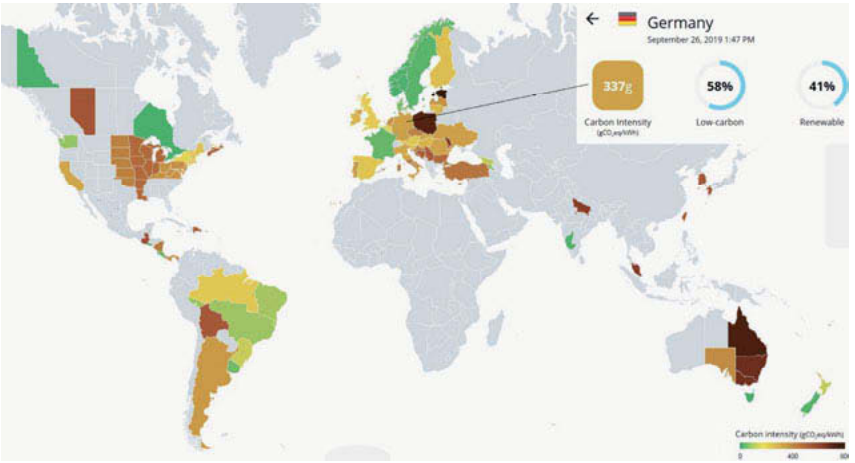

Fig. 1: Carbon intensity related to electricity production: www.electricitymap.org

Taking the arbitrary example of average electricity production in Germany on a cloudy autumn day (26th Sep 2019 13:47), one kWh electrical energy creates 337g CO2 [1]. Assuming 20% distribution and charge losses source until arrival in a BEV's energy storage system, and further assuming a BEV car with 15 kWh per 100 km, the operation consumption from the Battery results in ~60 g CO2 per km attributed to electricity production ("well to energy storage"), if the

car is charged with electricity from this energy mix. This figure compares to a 2020 fleet average requirement of 95g CO2 per km, equalling 4 litre gasoline per 100km (“energy storage to wheel”). If the very same BEV car is charged from renewable sources, e.g. own photovoltaics or dedicated “green energy” contract, the emission in operation is zero grams CO2 per km. Similar beneficial figures are valid for countries with almost 100% of electricity production from renewables (as e.g. observed at same time in Western part of Norway with 34 g CO2 per kWh, translating into 6,4g remaining CO2 per km).

The sustainable conversion of the electricity sector to carbon-free operation remains a challenge for at least one entire generation. Multiple complex levers must be identified and employed to arrive at the zero-carbon target [2]. Fig. 2 shows an analysis related to offshore wind used for electricity production. The resulting cost of energy (LCOE) for the investigated locations is displayed in ct/kWh.

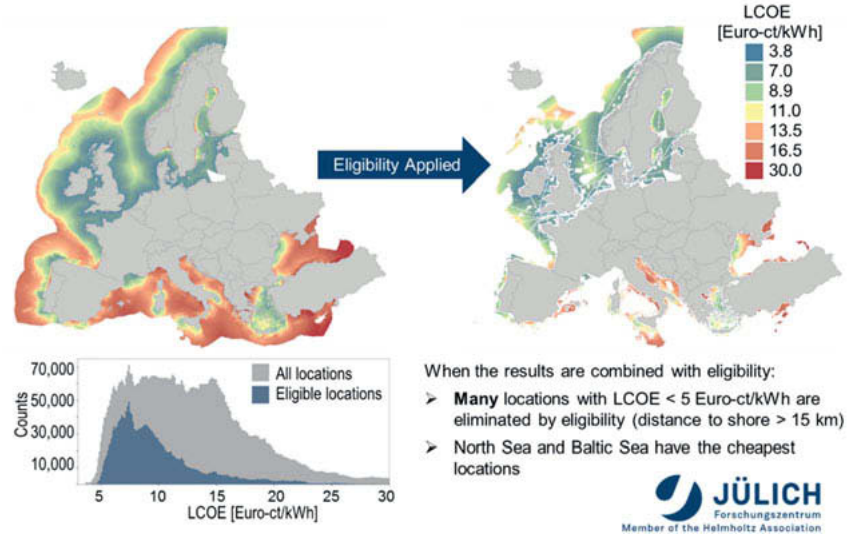

Fig. 2: Offshore Wind Analysis Europe [2]

Principally, enough regenerative energy is available worldwide in different forms to support a sustainable energy approach, but the suitable harvesting, conduction between source and sink areas, mid-term storage, power buffer capability to maintain reliable electricity grids and the

final distribution including intelligent load managements are subject to technical and scientific progress.

4 Electric Vehicle Experience at Opel

Opel has built, operated and sold a variety of Electric car series, being it Battery Electric Vehicles (BEV), Fuel Cell Electric Vehicles (FCEV) or Extended Range Electric Vehicle (EREV). Some of the products were operated in test fleet including for public funded projects.
Especially EVs that went into mass production and were sold to the public generated a lot of learnings for the development teams, the manufacturing processes, for service operations and finally generated a broad knowledge about how these vehicles are used in a “real world” environment.

4.1 Ampera (EREV vehicle)

The Ampera is an EREV, hitting the market very early and setting metrics. It offers full Electric Drive Performance (max 150 kW), but the pure electric range is limited to 80 to 40 km (summer/winter). Public charge infrastructure for AC mode 3 charging was not well covered over all places at the time of launch, of course with different progress per sales country. Mode 4 (DC Fast Charging) was not applicable and not necessary, since a combustion engine with more than 70 kW power was onboard for power generation in range extension mode. Many users primarily relied on 220 V household sockets for EREV charging. This mode2 charging was overly used and limitations for the installations became apparent. Most important learnings from the Ampera operation were:

- Charging should occur through dedicated and orderly installed mode 3 equipment.
- Majority of customers could manage their daily distance within limited EV range, but autonomy range was substantially influenced in winter and to some extent in summer.

4.2 Ampera-e (BEV vehicle)

The Ampera-e [3] did not hit the European market as the first BEV, but its performance was outstanding in the comparable class when it arrived. When it was developed, time to market was an imperative. The product was and still is working as catalyst to expose more customers to long distance EV driving and DC Fast Charging (DCFC). It was preparing the market, and defending the Opel position as an EV pioneer brand. The Ampera-e was launched with an overall manageable ratio of public charge points to EV cars in use, but still today there are many blank areas left on the landscape regarding public charge, especially in rural areas. The number of DCFC points was substantially increased in Germany in the last two years (after

Ampera-e launch), supporting longer distance traffic with BEV cars in general. Most important learnings from the Ampera-e operation were:

- Especially for pure BEV operation, balancing interior roominess versus aero efficiency may lead to reduced autonomy range at higher speeds. This emphasizes the general importance of aero-optimized surfaces and optimized wheels / tires.
- Regarding charging, new BEV users tend to hold the car fully charged, just for the case they might spontaneously decide to take a longer trip. More experienced users hold the average charge level around 50%, charging once or twice per week, better factoring in the distance they would really expect to drive instead of preparing for drives they might exceptionally make.
- Range autonomy is negatively impacted in winter season due to cabin heating and entire HV system conditioning as well as some other friction and aero effects, especially for consecutive short distance drives, where energy used to heat-up will dissipate when the car is parked.
- Even if a BEV battery has good DCFC capability, average outside temperatures and thermal mass of the Battery may frequently limit fast charging to lower than peak power, impeding a quick charge-up on travel.
- Reviewing the company's test fleet data, we recognize the usage of installed 150kW peak power and related torque, same as driving at the max velocity of 154 km/h, were reserved for short to medium distances only. For mid to longer distances, customers learned how to drive efficiently and did not use installed power.
- A common experience for long distance driving with EV's is, that going slower can mean: arriving faster! This effect is not known from ICE propulsion, where fuel-filling takes minutes only. While the gap between fuel-filling time (ICE) to charge up time (BEV) is being reduced by progress in quick-charge capability, higher power charge connections and automated authentication and payment, the effect mentioned remains generally valid, as illustrated in Fig. 4:
  a. The propulsion power needed to maintain constant speed (also called road load) includes a dependency from 3rd order of velocity. In a given example, when travelling with 120 km/h compared to 40 km/h, the required power rises by a factor of 10.5, requiring 3.5 times more energy to travel the same distance (blue curve).
  b. With ICE propelled vehicles, this effect is partially compensated by the basic drivetrain not having reached its maximum efficiency at part-load low speeds (red curve, dashed).

c. Electric Propulsion systems typically have very good efficiency already at low speeds, approaching its maximum at comparably low speed (red curve, solid). The example curve is idealized, while with higher power (and for higher speeds) losses in the entire system rise in all parts of the high voltage system, which add to the road load effect.
d. As a result, the driver of a BEV may achieve record ranges beyond the advertised range (WLTP based) when going constantly slow, while same driver would observe a further declining range with constant higher speeds e.g. on motorway (black curve, solid). In contrast, a driver of conventional propulsion is used to higher energy consumption at low speed (like in cities), an optimum point between 60 and 80 km/h on rural roads, and again rising consumption with higher speed (black curve, dashed).
e. To avoid an additional DCFC stop, driving slower may be a suitable method for arriving faster.

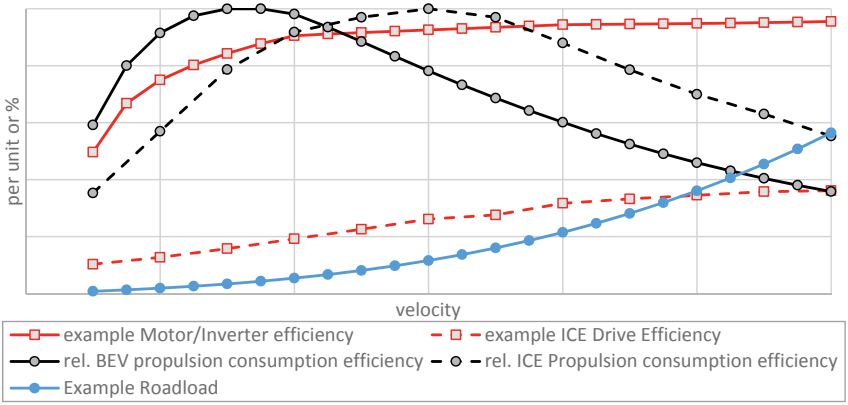

Fig. 3: Driving slower and arriving faster with a BEV

4.3 Grandland PHEV (Plugin-HV)

This PHEV was launched at fall 2019 and therefore only briefly covered. It features an electrically (or hybrid) driven front axle and an electrically propelled rear axle as AWD option. The AWD version, equipped with a 13,2 kWh Battery, has less energy onboard for the pure electrical drive, when compared to the Ampera EREV, but the PHEV offers better drive performance in the hybrid operation combined with more interior flexibility.

5 Marketing targets Corsa-e (compared to Ampera-e)

The experience gathered with electric vehicles at Opel contributed to the marketing targets for the new Corsa-e. First of all, a compelling and enthusing exterior and interior design remain some of the main purchase criteria for vehicle customers. This aspect includes the expectation not only to have the “EV specifics” embedded into a car but as well to benefit from other leading-edge product characteristics, as e.g. exterior lighting, modern seat technology.

In order to increase the percentage of BEV sales of our group, the product must be affordable for a higher share of our customer base. Still EV technology as such is expensive, but a huge step has been made with the current product as will be explained below. The public subsidies for EV purchases as well expected penalties for CO2 generation in operation of vehicles factor into the equation for overall cost of ownership. But apart from a pure financial consideration, industry should expect customers with pronounced interest for sustainability to constitute a substantial part of the BEV sales.

The range autonomy for a given car is one of the major product characteristics for a BEV, it may become more important then what used to be the power figure of a combustion engine. A lighter car with better aero and drag behavior can afford a smaller capacity (and thereby lighter) battery. Rising fast charge capabilities for eventual long distance travel will balance against the requested initial autonomy range.

The Corsa-e and Grandland PHEV mark new milestones in the effort to provide a wide portfolio of electrically propelled vehicles in our lineup. Technologies and strategies used are supposed to take effect on future products, contributing to the wide EV lineup mentioned before.

6 Design & Manufacturing difference Corsa-e vs Ampera-e

6.1 Evolution in Manufacturing

The Corsa-e is built on PSA’s “Common Modular Platform (CMP)”. This decision was taken in order to balance production volumes between conventional and EV powertrains and to maintain, where possible, identical parts (besides the drivetrain, HV and Battery system.) This main imperative also took effect on the Battery design as explained later on.

To some extent, also the logistics and production process make use of this synergy: The powertrain plant produces an e-Powertrain assembly consisting of Reduction gear, e-Motor w/ Inverter, On Board Charger with DC/DC and eVCU plus internal connections and ships this “Electric” Powertrain to the vehicle assembly plant.

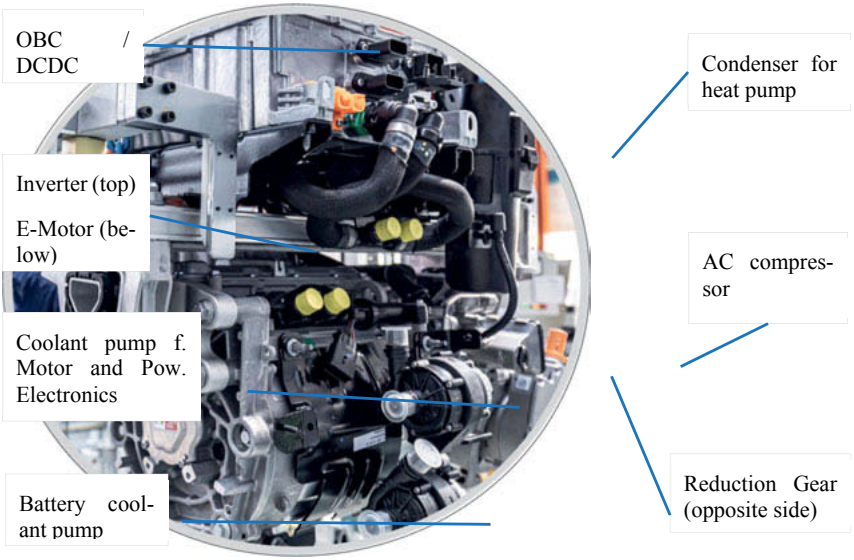

Fig. 4. PSA e-Propulsion assembly delivered to the vehicle plant

Table 1: Main differences regarding components make or buy

	Corsa-e	Ampera-e
Battery	Make assembly (e.g. from purchased modules)	Buy
Reduction gear (RG)	Make. Design with side e-Motor, parts partially from MT machinery , c/o differential & housing strategy	Buy. Design with integrated e-Motor, hollow shaft, premium parts, oil pump on demand, Park Lock
e-Motor	Buy	Buy
Inverter	Buy with Motor (interconnected)	Buy (separate)
On Board Charger	Buy, 1 ph & 3 ph option	Buy, 1 phase
DC/DC	Integrated in OBC	Separate, buy
HPDM	Up- integrated in OBC	Separate, buy
PLCM	Up- integrated in OBC	Separate, buy
Connection points / Connectors	Less (integrated)	More (split)

6.2 High Voltage Architecture Design

The HV Architecture for the Ampera-e was designed for a quick- to – market approach. Most of the suppliers were challenged to concentrate on developing dedicated modules with dedicated functionality, as e.g. a standalone DC/DC converter, a standalone On Board Charger (OBC), an external battery heater or the dedicated connection module (HPDM) itself. Clearly defined interfaces helped to reduce interdependency and thereby the engineering complexity of every individual component.

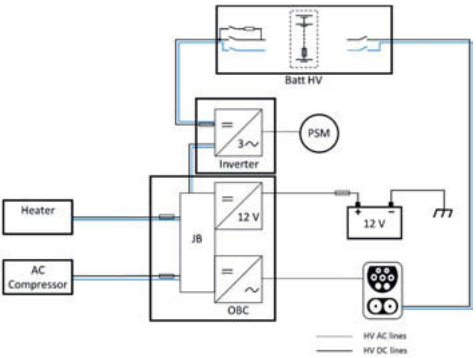

Fig. 5: High Voltage Architecture of the Corsa-e

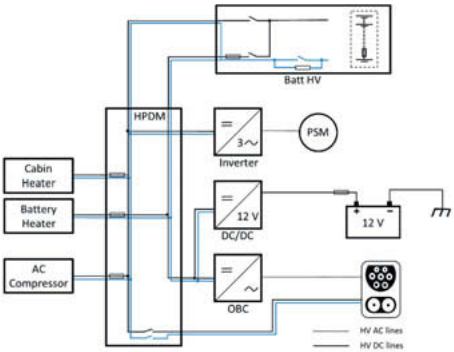

Fig. 6: High Voltage Architecture of the Ampera-e

The HV architecture of the Corsa-e design features multiple steps of up-integration, which deliver package, weight and cost advantage. As a tribute to this up-integration, the complexity of interdependent functionality concentrated in one device was risen. The most compelling example is the combined OBC and DCDC module, also providing a junction box function “”HPDM”) plus that it delivers the Powerline communication (“PLC”) for DC Fast charging, according to the fast charge limits governed by the Battery Control System.

Also, the Battery heater is included in the Battery Housing. With every module not showing up separately, the Corsa-e saves a housing, mounting provisions, housing-side HV connectors, cable-side HV connectors and the entire associated assembly time.

7 High Voltage Battery Design

Groupe PSA is producing the HV Battery system assembly in its own facilities. Due to a larger rollout of BEV vehicles in the group, PSA decided for the use of pre-manufactured modules. Same or similar modules like the ones used for the Corsa-e can be used in other Battery assemblies as energy storage for cars with other package requirements. The mentioned modules include 12 cells (2 in parallel, 6 pairs in series) with approximate dimensions 390 mm* 150 mm * 110 mm.

Table 2: Comparison of High Voltage Battery properties

	Corsa-e	Ampera-e
Battery Chemistry	Lithium Ion	Lithium Ion
Battery nom. Energy	50 kWh	60 kWh
Battery Mass	350 kg	430 kg
Peak Battery Power	163 kW	160 kW
Battery nom. Voltage	394.2 V	350 V
Peak Power / Energy	3,3	2,67
Cells, configuration	216 (2P, 108S)	288 (3P, 96S)
Sub-Modules	18 identical modules (12 cells each)	5 module assemblies (3 * 60, 2 * 54 cells)

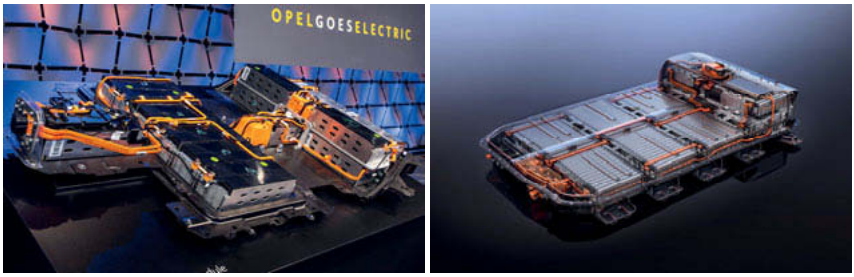

Fig. 7: High Voltage Battery of Corsa-e (left) versus Ampera-e (right)

8 The e-Motor (propulsion motor)

In the Corsa-e, the electric motor is side-mounted to the reduction gear (RG) and therefore has an own water cooling system. Also, the motor comes pre-assembled with the inverter power electronic on top including an internal controller, receiving the propulsion command from a vehicle Controller (eVCU).

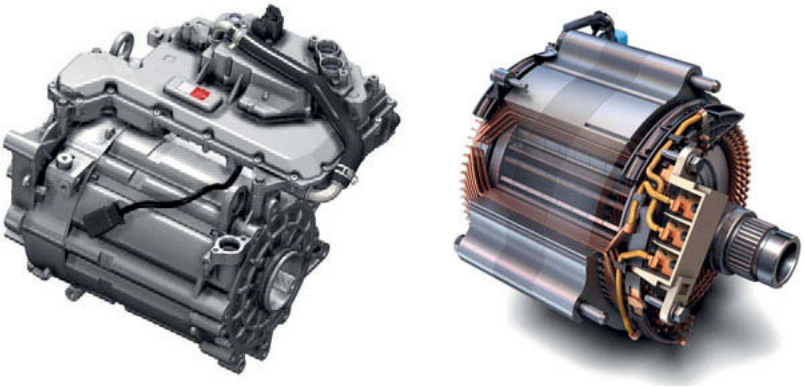

Fig. 8: Propulsion Motor of Corsa-e (left, incl. Inverter) and of Ampera-e (right, Motor only)

Table 3: Comparison of e-Motors

	Corsa-e	Ampera-e
Type	Permanent Magnet Synchronous, PMSM	Permanent Magnet Synchronous, PMSM
Peak Torque	265 Nm	360 Nm
Peak Power	100 kW	150 kW
Continuous Power	57 kW	55 kW
Max motor speed	14565 rpm	8810 rpm
Stack length	175 mm	125 mm
Outer Ø	190 mm	204 mm
Pole pairs	4	4
Cooling	Water jacket	Oil. Dissipation within drive unit

9 The reduction and differential gear

The respective reduction gears of Ampera-e and Corsa-e both are equipped with fixed ratio, include the differential drive and include a park lock system.

To support the cost target and to leverage existing production facilities for manual transmissions, the reduction gear for Corsa-e is manufactured in-house PSA and uses, where possible, carry-over parts from the manual transmission, e.g. the Differential drive with its ring gear. Same as for some manual transmissions, the housing is a 2-piece design and the gears are lubricated by splash. The motor is side-mounted to the RG. To realize the park-lock function, an intelligent actor is installed in the RG.

In the case of Ampera-e, the e-Motor is an integrated part of the Transmission assembly. Here, the stator of the e-motor leverages the thermal mass of the Transmission and is also cooled by the transmission oil, when necessary. In contrast, the e-Motor in the Corsa-e is side-mounted and therefore needs a separate cooling, in this case a water circuit shared with the power electronic components.

The reduction gear in the Corsa-e is adequately designed for the given power, torque and speed characteristics of the e-Motor, while it still maintains synergy with one of the group's manual transmissions.

On a propulsion system base, the overall weight made up from for reduction gear, e-motor and inverter is almost identical in the two cases.

Table 4: Comparison of Reductions gears

	Corsa-e	Ampera-e
Peak Axle Torque	2525 Nm	2500 Nm
Gear ratio	9.71	7.05
Mass	25 kg (excl. Motor/Inv)	76 kg (incl. Motor)
Total Oil Volume	1,2 lit.	2,9 lit.

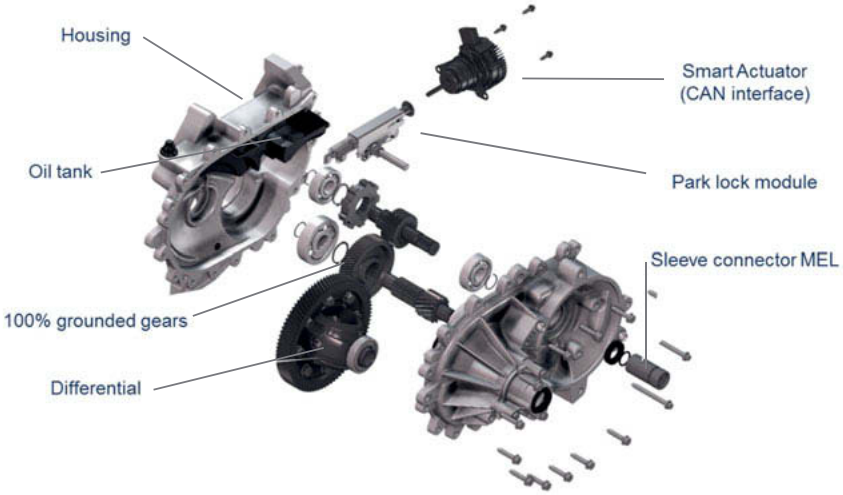

Fig. 9: Reduction gear of Corsa-e

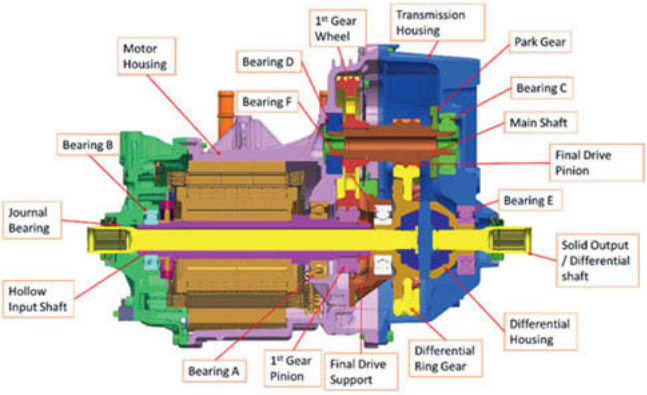

Fig. 10: Drive unit of Ampera-e

10 On Board Charger (OBC) and DC/DC Converter

The Corsa-e comes with a standard OBC designed for 1-phase 32 A charging, resulting in a maximum power intake of 7,4kW. A similar 1Ph charger functionality but with different design can be found in the Ampera-e.

As an option, the Corsa-e will offer a 3 phase Charger for max. 11 kW Power Intake. This option is getting increasingly important due to widespread public charging opportunities (3 phase AC) and imbalance restrictions for the case of 1-phase charging, differing from country to country. The 3Ph charger of the Corsa-e will automatically reconfigure to a 1Ph 32A charger if paired with a 1Ph supply.

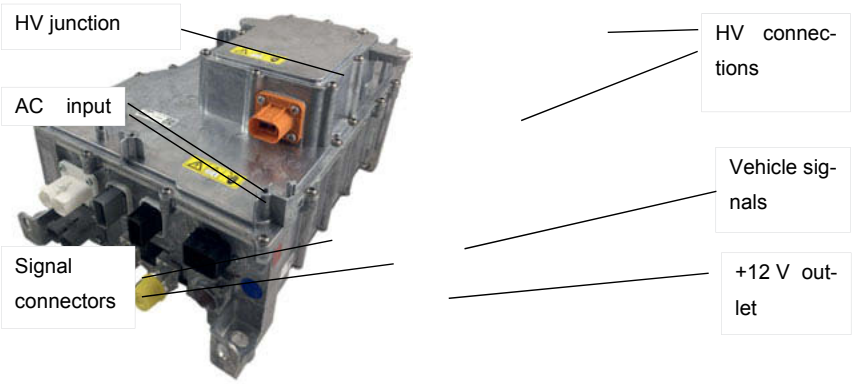

Fig 11: On Board Charger, DC/DC converter and Junction box integrated in one part

11 System functions comparison (related to EV drive & EV charge)

Table 4: System functions comparison related to drive and charge

	Corsa-e	Ampera-e
Dynamic modes	Eco, Normal, Sport	Normal, Sport
Drive modes, recuperative braking	D and B (max ~ 50 kW)	D (max 40 kW), L (max 70 kW)
Charge modes	mode 4 with max 100 kW mode 3 AC 1 ph 7,2 kW mode 3 AC ph 11kW	mode 4 with max 53 kW mode 3 AC 1 ph max 7,2 kW
	Mode 2, 8 A (1,8 kW) to 12 A (2,7 kW)	Mode 2 , 6 A (1,3 kW) or 10 A (2,3 kW)
Charge point find & navigate	Onboard data base & Over the air service	Find on Android phone Navigate: Android Auto
Climate control	Remote	Remote

12 Drive, recuperation and charge performance data of the new Corsa-e

The maximum speed for the Corsa-e is limited to 150 km/h. With respect to the basic dependency of range and travel speed as explained in section 4.2, this is a very appropriate limitation. The Corsa-e is certified with 337 km electric autonomy range in WLTP. It accelerates very sporty from 0 to 50 km/h in 2,8sec and from 0 to 100 km/h in 8,1 sec.

Beyond those figures, there are plenty of other performance criteria, important for the daily use of EV customers. For example is the recuperation performance and efficiency important for customers whose daily routes include a lot of up- and downhill or who like to apply a rather short sighted driving with very much different speeds.

The graph in Fig 12 correlates to a route with almost 1000 m difference in height, a real excitement for any newcomer to electric driving. While the range prediction dramatically goes down with climbing up in altitude, the driver can really experience the “value” of potential (height) energy which pays off on the way down. The grey curve in the graph displays the altitude and with that the relative potential energy attributed to height over sea level, as found on the selected route up to the Schauinsland Hill in Baden-Württemberg. The bar graphs, correlating to

section 2 and 3 show the drive energy consumed uphill in green. It is made up from the incremental potential energy as well as the drive energy to overcome the non-altitude drive resistances and a nonlinearity effect: While the grey bars for the way up respectively down have the same magnitude since they simply represent the incremental potential energy uphill or downhill, the incremental drive energy needed to climb up (green minus grey bars) is higher compared to the returned energy (grey minus blue bars). This is due to the efficiency of the propulsion system under very high load (uphill, resulting power flow out of the battery) which is lower compared to the propulsion efficiency under low downhill load (resulting power flow into the battery).

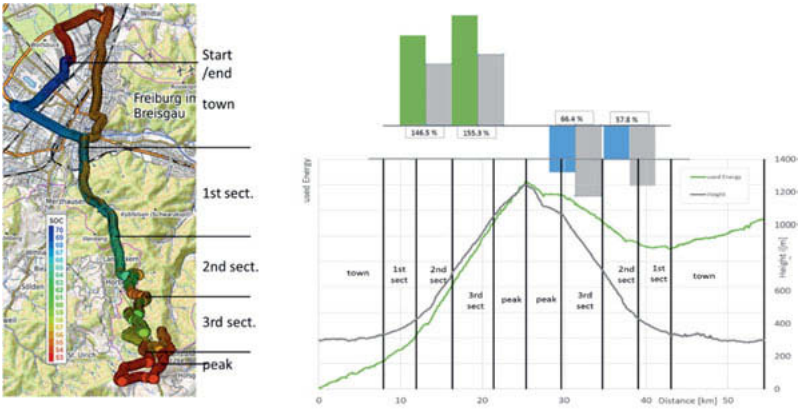

Fig 12: Drive energy on a route with almost 1000 m difference in height over sea level

Mass data acquired with the Opel EV's as mentioned in paragraph 4: "Electric Vehicle Experience at Opel" suggest up to 20% of drive energy being recuperated into the battery during drives of e.g. company car drivers, mostly acquired around Rüsselsheim (with very moderate differences in sea height). If same data would have been acquired in hill areas, this percentage would have been higher and with that, the importance of recuperation performance and efficiency. Vice versa, long-distance drives on motorway by experienced EV drivers show anticipated driving behaviour and avoidance of unnecessary energy flow.

13 Using an Electric Vehicle: The importance of charging!

The following paragraph is dedicated to the importance of charging but also the different needs for EV charging, depending on EV type and charging modes. It is a generic statement not exclusively related to the Corsa-e.

Any recharge should occur with electricity from renewable energy sources. The recommended charging method is mode3 charging, i.e. from a dedicated wallbox or public charge point, while mode 2 charging, connected to a household socket should be an exception on travel for BEV's.

*13.1 Hybrid (HEV) and mild Hybrid Electric Vehicles **(mHEV)***

Those are not designed for external charging. Hybrid batteries are installed to recuperate all or most of the energy during deceleration phases (or downhill phases) and to insert this energy again in the next applicable propulsion phase. With Hybrid vehicles, there is no need for the customer to change his/her fuel filling behavior, just the overall energy consumption is lower. Batteries in Hybrid Electric Vehicles are relatively small, typically < 2 kWh usable Energy and partially even < 0,5 kWh in cases of mild hybrids. (Also, those FCEV's which do not offer a charge plug cannot be electrically recharged.)

13.2 PHEV, EREV and FCEV-plugin cars

This class of "plug-in cars" today come with typical Battery Energy of up to ~ 20 kWh (e.g. 16 kWh for Ampera). Most common in this vehicle group are 1Phase AC charge interfaces for mode 3 and mode 2 charging 16 A / 240 V maximum. The resulting charge power input of 3.7 kW would fill up a completely depleted 12 kWh Battery in less than 4 hours, a duration which constitutes a common requirement e.g. for half-day parking. For the reason of reduced CO_2 emissions, it is important that PHEV drivers recharge their car regularly whenever they can. A full charge in shorter time then e.g. 4 hours, is desirable to facilitate a multiple use of the installed electrical energy per day. Therefore, newer PHEV designs sometimes offer optional 1 ph / 32 A or 3 ph /16 A charge interfaces. Regarding future developments we should expect to see wireless charging first in upper-segment PHEV, to make multiple and frequent recharging more convenient and thereby more likely to occur.

13.3 BEV vehicles

Current BEV vehicles today are sold in capacity ranges between ~ 20 kWh (small) and over 100 kWh. For these vehicles, a closer look into charging options is needed. Any mode 2 charging should be regarded a rare exception, due to the duration and the low power level. These BEV vehicles are appropriately charged through a dedicated wallbox installation (mode3).

Private AC charging for owners of parking slots (shared garage / own house).

In a part of Europe, the electricity supply to private houses is implemented in 1-phase technology, high current connection. Depending on the location, up to 32 A / 230 V Power intake (7,4 kW, 1-Phase) for EV charging is permitted for installation at households. A related power output will provide a 50 kWh Energy “refill” in ~ 7,5 hours (a typical overnight charge requirement for 50 kWh Battery). In another part of Europe, private houses are supplied with 3Phase systems, and therefore offer 3 phase supply for EV charging (11kW, 3 phase), resulting in delivery of 50 kWh Energy in 5 hours if a BEV is equipped with such a 3 phase charger. In those counties where 3 phase supplies are common, phase imbalance limits do exist. A vehicle equipped with 1-phase On Board Charger will only be allowed to draw e.g. 3,7 kW of power since throttled down to the permitted imbalance limit, resulting in 15 hours to deliver 50 kWh energy.

Public AC charging. The growing majority of public 3ph charge posts in Europe provide 3 ph 22 kW power. Older installations provide 3 ph 11 kW only. In about half of the European countries, newly installed charge posts will be throttled down to 16A or 20A imbalance limit in case of a vehicle with a 1 ph charger is connected to the charge post. The corresponding charge up time for a full 50kWh charge are the values mentioned in previous paragraph. More intelligent installations, as charge farms may level out the imbalances imposed by cars of multiple cars are charging on 1Phase each.

AC charging (general). In order to best cope with the different charge power needs for the different customers and in order to provide maximum versatility regarding the public charging installation, the Opel Corsa-e offers two OBC charger options. First, a standard OBC charger for 1Phase and 7,4 kW intake and second, a option of automatically reconfiguring OBC charger for 3 phase and power up to 11 kW intake which can fully use both, a 16 A 3 ph supply and a 32 A 1 ph supply.

DC Fast Charging, High Power charging. The power flow for this charging method bypasses the OBC. Instead the voltage conversion occurs at the (bigger and more expensive) public charging station. The power directly flows into the battery through the high-current connector. This method is suitable for charge-up on travel, especially along the motorways. Limited by battery protection, the Corsa-e is designed to accept peak charging power of about 100 kW (up to 270 A) resulting in a best recharge time of 30 min to reach 80% (a state of charge where usual Battery technologies require substantial derating). This duration changes depending on e.g. outside temperature and battery temperature [4].
HPC Charging stations for > 100 kW are still the exception and will primarily be needed for Sport/Lux cars with very high Battery capacity (e.g. > 80 kWh) and which target to provide fast-driving (e.g. 180 km/h and more) where high driving power is needed.

14 Summary

With the new Corsa-e, Opel launches an all-new BEV in the B-segment. A strongly improved DCFC capability and an optional 3phase charger will make it an ideal fit for many customers, while the mixed energy platform approach which it is built on, an up-integrated HV architecture and an increased amount of OEM make parts make it affordable for a wide customer base.

15 References

[1.] Ramminger, Dr. P, Schade, G.: The propulsion, energy storage and charging system of the new Opel Corsa-e, 18th International CTI Symposium Automotive Transmissions, HEV and EV Drives, Berlin (2019)

[2.] Electricitymap homepage, www.electricitymap.org, accessed 2019/09/26

[3.] Stolten, D., (FZ Jülich, IEK-3: Institute of Electrochemical Process Engineering)

[4.] Ramminger, Dr. P.: The propulsion system of the new Opel Ampera-e, 15th International CTI Symposium Automotive Transmissions, HEV and EV Drives, Berlin (2016)

[5.] Matthé, R.: EV battery technology and charging strategies, 16th International CTI Symposium Automotive Transmissions, HEV and EV Drives, Berlin (2017)

[6.] Jäger, Dr. R.: The electric propulsion system in the new Opel Ampera-e, VDI Kongress Getriebe in Fahrzeugen, Bonn (2017)

Development of a Transmission Control for an Innovative High-speed Powertrain using Motor-related Control

Simulative approach to develop an angular position controlled engagement of dog clutches in a two drive transmission

Daniel Schöneberger, M.Sc., Prof. Dr.-Ing. **Stephan Rinderknecht**,
Institute for Mechatronic Systems in Mechanical Engineering (IMS),
Technical University of Darmstadt;
Dominik Reitmeier, M.Sc., Prof. Dr.-Ing. **Axel Mertens**
Institute for Drive Systems and Power Electronics,
Leibnitz University Hannover

Zusammenfassung

Der Speed4E-Antriebsstrang wurde basierend auf den Erkenntnissen aus dem Speed2E-Projekt entwickelt und ist ebenfalls ein mehrmotoriger, mehrgängiger elektrischer Antriebsstrang. Diese Eigenschaften tragen in Verbindung mit einer geeigneten Betriebsstrategie zur Erhöhung der Reichweite und zur Verbesserung der Fahrleistungen gegenüber konventionellen elektrischen Antrieben bei [1]. Als Schaltelemente kommen bei den entwickelten Konzepten Klauenkupplungen zum Einsatz. Sowohl für Speed2E als auch den Hybridantriebsstrang DEREX wurden am IMS bereits Schaltablaufsteuerungen entwickelt [2,3,4]. In diesen Projekten stand das Gangeinlegen unter Differenzdrehzahl im Fokus. Aus [4] geht jedoch hervor, dass für Schaltvorgänge mit Klauenkupplungen mit Hilfe einer Differenzwinkelregelung eine Verbesserung des Komforts und der Dynamik des Schaltvorgangs erreicht werden kann. Darüber hinaus wird darin empfohlen, die Regelung nah am Motor auszuführen, um Totzeiten durch z.B. eine CAN-Kommunikation zu vermeiden und somit die Regelgüte zu verbessern.
Um das Potential eines Schaltvorgangs mit Differenzwinkelregelung voll ausschöpfen zu können, sind alle Komponenten des Speed4E-Antriebsstrangs von Beginn an hierfür entwickelt worden. Hierzu zählen die Klauenkupplung, der Schaltaktor und insbesondere auch die Steuergerätearchitektur, auf die in diesem Beitrag detailliert eingegangen wird. Hierbei dient die zentrale Antriebssystemsteuerung als Koordinator des Schaltablaufs. Die Drehzahl- und Differenzwinkelregelung wird jedoch motornah auf der Leistungselektronik durchgeführt, um das

notwendige Maß an Dynamik und Regelgüte zu erzielen. Auf Systemebene wird mit Hilfe geeigneter Simulationsmodelle die Schaltablaufsteuerung entwickelt und es werden die entsprechenden Regler ausgelegt. Besondere Herausforderung liegt hier in den hohen absoluten Drehzahlen der E-Maschinen, die eine schnelle AD-Wandlung und eine hohe Regelkreisfrequenz erfordern. Ausblickend sollen diese Verfahren in einem Antriebssystemprüfstand appliziert und im Fahrzeug erprobt werden.

Abstract

The Speed4E powertrain is based on the knowledge from the Speed2E project and is also a multiple motor, multiple speed electric powertrain. In combination with a suitable operating strategy, this architecture will increase the vehicle range and improve the driving performance compared to conventional electric powertrains [1]. Dog clutches are used as shift elements in the developed concepts. Transmission controls have already been developed at the IMS for both, the electric powertrain Speed2E and the hybrid powertrain DE-REX [2,3,4]. In these projects the gear engagement under differential speed was examined in detail. It emerges from [4] that an improvement in the comfort and dynamics could be achieved for gear changes with dog clutches with the aid of an angular position control. In addition, it is recommended to locate the control close to the motor to avoid dead times for example from CAN communication and thus to improve the control quality. In order to be able to fully exploit the potential of a gear change with angular position control, most components of the Speed4E powertrain were developed for this purpose right from the start. This includes the dog clutch, the shift actuator and in particular the control unit architecture, which is discussed in detail in this article. The central powertrain control unit serves as the coordinator of the gear change. However, the speed and differential angle control is performed close to the motor on the power electronics in order to achieve the necessary level of dynamics and control quality. At the system level, the transmission control is developed using suitable simulation models and the corresponding controllers are designed in the simulation. A particular challenge in Speed4E are the high absolute speeds of the electric motors, which require fast AD conversion and a high control frequency. Looking ahead, these operations are to be applied at a powertrain test bench and tested in a demonstrator vehicle.

1. Introduction

Speed4E is a joint project of German universities and industry partners in which an innovative electric powertrain is been developed. Progressive optimization approaches in different areas of the powertrain aim for a higher overall powertrain efficiency compared to state-of-the-art

electric powertrains. The main approaches are high-speed electric motors to decrease the powertrain weight, SIC power electronics, an innovative cooling and lubrication system and the multiple motor, multiple speed concept combined with an innovative operation strategy. As shown in [1] a multiple motor and multiple speed powertrain can lead to a significant reduction of electric energy consumption with comparable maximum wheel torque and maximum wheel speed compared to a conventional electric powertrain.

To exploit the benefits of this so called Two Drive Transmission (TDT), while keeping a high driving comfort and low transmission costs, a dedicated shifting system is developed in Speed4E consisting of an actuator, the dog clutches and a shift control. Strong interdependencies between these three topics require a close co-development. Beside an optimized dog clutch and actuator, the shift control is crucial for fast and comfortable gear changes. The main innovation to other shifting controls with dog clutches is the angular position control, already mentioned in [4,5]. To achieve a precise angular position control even at high rotational speeds of the electric motors an actuator-related-control is necessary. Hence the synchronization of the dog clutch is implemented directly at the power electronics. A powertrain control unit however is used to initiate the shifting process and coordinate torques to guarantee a comfortable shifting process.

This paper will show how the shift control is developed with a simulative approach. This approach will be tested and improved both at powertrain test benches and in a demonstrator vehicle.

2. Speed4E powertrain

The Speed4E powertrain shown in Fig. 1 consists of two electric motors, each coupled to one sub transmission (STM). Electric motor 1 (EM1) is an asynchronous motor (ASM) which drives sub transmission 1 (STM1). EM2 is a permanent-magnet synchronous motor (PSM) driving the two speed sub transmission 2 (STM2). Both motors are high-speed motors with up to 50.000 rpm maximum speed, powered by power electronics using SIC semiconductors to achieve low losses at a switching frequency of 48 kHz. Both, power electronics and motors, are developed by universities and industry partners in the Speed4E project. In the following chapters the layout of the transmission, the actuator and the dog clutches will be described briefly.

Fig. 1: Speed4E powertrain [6]

2.1 Layout and Drive Modes

As shown in Fig. 2, EM1 drives the sun of a planetary gear stage with a fixed ring gear. The planetary carrier drives the output shaft of STM1. STM1 has a fixed gear ratio and is not decouplable. Decoupling is however not necessary because EM1 is an ASM with very small drag losses when inactive. This permanent coupling is also beneficial for the angular position control because the resolver of EM1 can be used to determine the speed and angular position of the dog clutch when no gear is engaged in STM2. Furthermore, EM1 is used to guarantee seamless gear changes by applying a support torque.

The speed of EM2 is reduced with a first set of spur gears to the countershaft. The dog clutch is located at the output shaft

The final drives of STM1 and STM2 meet the same spur gear of a differential where the torques are aggregated.

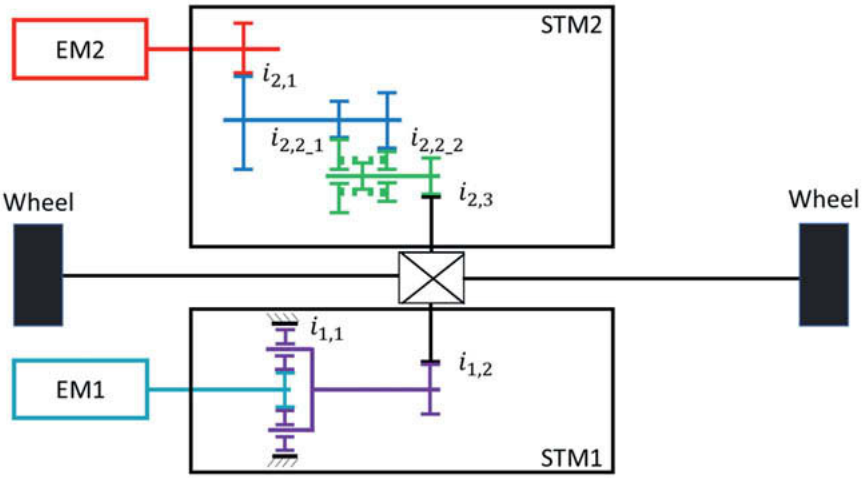

Fig. 2: Layout of the Speed4E powertrain

This layout leads to five possible drive modes shown in Fig. 3. An operation strategy (OS) decides which mode and with that, which gear should be used to achieve the best overall powertrain efficiency. As EM1 is an asynchronous motor no mechanical decoupling is necessary. Therefore, a mode change between E11 and E01 only requires a torque transfer from STM1 to STM2. This is done seamlessly by the OS on its own by emphasizing the so-called split factor, describing the ratio of the wheel torque covered by EM1 to EM2. Hence the transmission control is only necessary for gear changes.

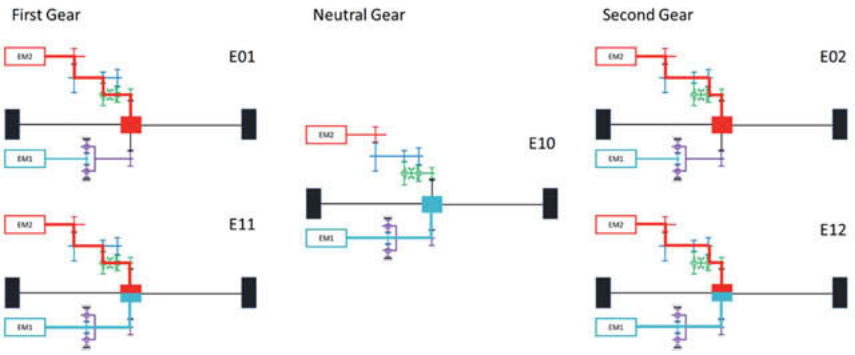

Fig. 3: Drive modes of Speed4E

2.2 Actuator

In the Speed2E project a carryover actuator was used not specifically designed for shifting an electric powertrain with dog clutches. In Speed4E an actuator will be used which is optimized for this powertrain. In conventional automated transmissions, as dual clutch transmissions (DCTs) or automated manual transmissions (AMTs), the actuators are able to apply over 1000 N axial force at the shift sleeve. This is for example necessary to achieve fast mechanical synchronizations. In the Speed4E project however, dog clutches are used. Hence the actuator does not need to be as strong as in conventional transmissions. As recommended in [4] and confirmed in [5] linear direct drive actuators are well-suited for this purpose. In Speed4E a dual coil permanent excited shift actuator is been developed and optimized, detailly described in [7]. The actuator is designed for a maximum axial force of 250 N. As shown in [7] the actuator volume and thus the mass is nearly proportional to its maximum force, if all other boundaries are the same. Hence one of the objectives of Speed4E is to identify which actuator force is really necessary for a robust shifting under various circumstances in a TDT. The necessary actuator force is dependent on the dog clutch design, mainly its back angle, and the control strategy. It is assumed that the angular position control of the dog clutches will significantly reduce the necessary actuator force, also mentioned in [5].

The Speed4E actuator is designed to be a smart actuator. The disengaging and engaging process is a closed loop position control performed by the smart actuator itself. This leads to high control frequencies and with that to very fast, position-controlled gear engagement and disengagement [7]. The communication between the transmission control and actuator is realized via high speed CAN and will be described more detailed in Section 2.4.

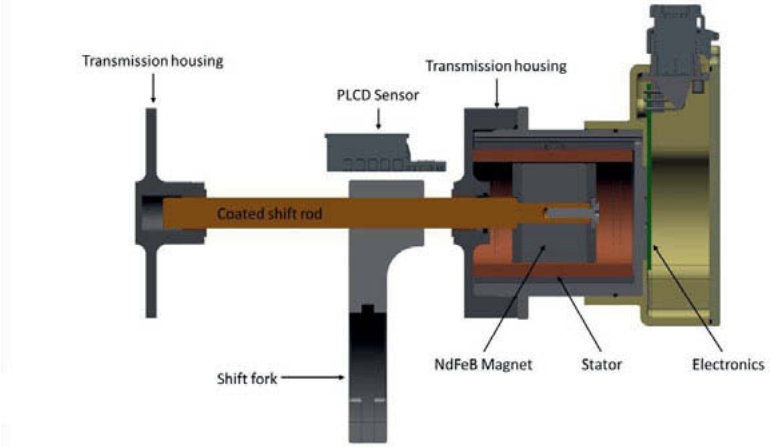

Fig. 4: Speed4E smart actuator [7]

It can be seen in Fig. 4 that the actuator and its electronics are not fully integrated into the transmission. This leads to a slightly increased space demand but simplifies the transmission assembly and increases flexibility. Hence it is possible to test a smaller, less powerful actuator without disassembling the whole transmission. Furthermore, a potential mass production of the transmission would not have to differ from the production of a conventional transmission. The actuator will be mounted afterwards.

2.3 Dog Clutch

Even though the Speed2E Powertrain was also equipped with dog clutches, they have been significantly redesigned in Speed4E to suite the actuator and control concept as good as possible. As written in Section 2.2 a reduction of the necessary actuator force is beneficial to reduce its size. Hence a small mass of all moving parts is beneficial at highly dynamic shifting processes. The mass of the dog-ring was reduced significantly by increasing the inner diameter.

As it can be appreciated in Fig. 5 at the right side, the tooth geometry of the dog clutch is specifically designed for the Speed4E powertrain and angular position controlled shifting. To keep the backlash of the dog clutch as small as possible some assumptions for the reachable precision of the angular position control were made and the backlashes of the transmission have been considered. Even the locking forces were reduced to a necessary minimum to acquire precise but effortless engaging and disengaging but still keep the gear safely engaged when the actuator is passive.

Fig. 5: Dog clutches of Speed2E (dark grey [2]) and Speed4E (light grey)

2.4 Control System Architecture

As shown in Fig. 6 the powertrain control unit (PCU) will be the link between the vehicle/driver and the Speed4E powertrain. Its main task is to fulfil the torque-request of the driver as good as possible. Therefore, beside various safety related hard- and software functions, it mainly consists of the operation strategy (OS) and the transmission control (TC). It communicates via the vehicle CANs with the vehicle/driver and with a separate CAN with the Speed4E powertrain.

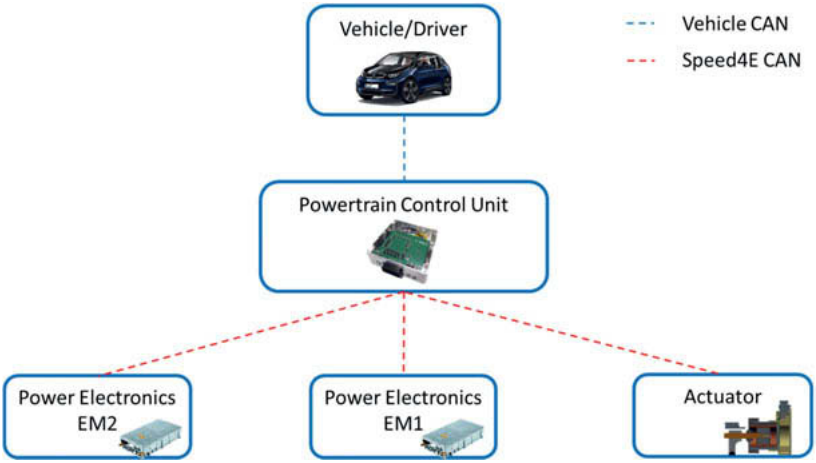

Fig. 6: Control system architecture

The position control of the shift actuator and the angular position control of the dog clutch require very high control frequencies. To achieve this, these control algorithms are implemented actuator/motor-related to avoid additional dead times e.g. through CAN cycle times. None the less the transmission control needs to coordinate the shifting process, especially to guarantee seamless and comfortable gear changes. Therefor shift flags are sent via CAN to the sub-control-systems and vice versa which will be described more detailed in Section 3.2.

3. Simulation and Control

Even before the hardware of the powertrain is available at a testbench, the transmission control and the angular position control should be developed and tested in various scenarios. Therefore, a detailed simulation model of the powertrain and a simplified model of the vehicle is exploited. An overview over the simulation model will be given. Afterwards the transmission control and motor control will be explained with the help of simulation results.

3.1 Simulation model

Fig. 7 shows the utilized simulation model and its main sub models. A feed forward driving simulation is used to obtain a more realistic simulation not only from simple scenarios as constant acceleration and deceleration, but also from more complex scenarios as harmonization driving cycles. This can be used to examine the robustness of the control strategies.
The “Driver” is a simple speed controller which calculates the target wheel torque depending on the target speed from the “Scenario” and the actual speed of the vehicle. The “Powertrain Control System” contains the operation strategy and the transmission control. Its main outputs are the target torques for both electric motors and various shift flags for the shifting process described more detailed in Section 3.2. The “Driveshaft” is the link between the “Powertrain” model and the “Vehicle” and is modelled as a torsional spring and damper model. The “Powertrain” consists of the electric motors, their power electronics and the transmission. The Simulink extension PLECS was used to simulate the electric motor and the transmission. Beside the different gear stages, the moments of inertia of the gears and shafts were modelled. The vehicle model is a simplified longitudinal one degree of freedom model (1DOF). It mainly consists of the vehicle mass and driving resistances.
The following sections will describe how a seamless angular position controlled gear change will be performed in the Speed4E powertrain. Therefore, firstly the gear change from the powertrain control unit’s point of view will be described in Section 3.2 as it is the coordinator of the shifting process.

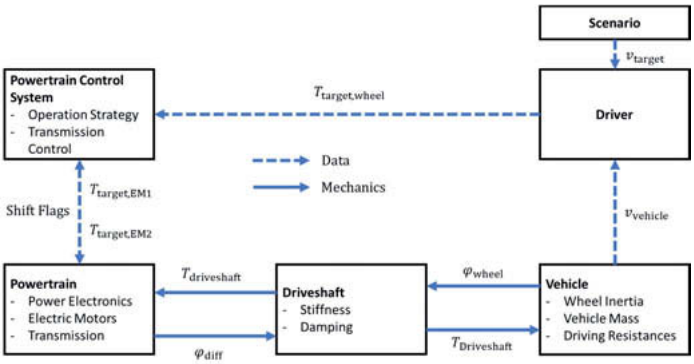

Fig. 7: Overall simulation model

3.2 Powertrain Control System (PCU)

The PCU shown in Fig. 8 is a rapid prototyping control system developed in a strong collaboration between the Leibnitz University Hannover and the Technical University of Darmstadt in terms of hard- and software within the Speed4E project. Beside its main task (operation strategy and transmission control) it will be used for various additional tasks as communication with the vehicle and hard- and software safety functions.

Fig. 8: Hardware of the Powertrain Control System

As shown in Fig. 9 the software of the PCU mainly consists of the operation strategy (OS) and the transmission control (TC). The OS tries to increase the powertrain efficiency and durability by splitting the torque requested by the driver between both electric motors and by choosing an appropriate gear of STM2.

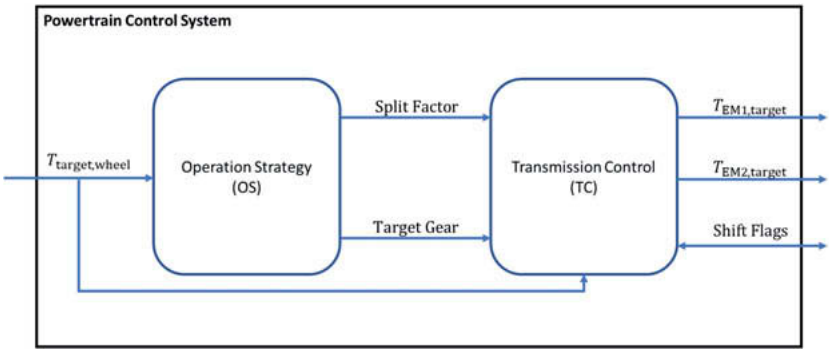

Fig. 9: Main functions of the powertrain control system

Because of its complexity, the OS-Algorithm cannot be computed with high frequency in real time with the used hardware. Hence the target wheel torque is transferred directly to the TC as shown in Fig. 9. The TC tries to transpose the commands of the OS as fast and comfortable as possible. Fig. 10 shows an exemplary upshift from first to second gear with a required wheel torque of 2500 Nm at an initial vehicle speed of 50 km/h. Initially both motors are driving the vehicle with a defined split factor. Similar to the shifting explained in [3] a gear change can be divided in different phases. In the first phase, here called “Balance”, the TC shifts the torque from EM2 to EM1. In this phase the torque at the wheels does not change, so the driver will not recognize this balancing and the torque gradient can be high. Because the required 2500 Nm wheel torque cannot be provided solely from EM1 even for this short time, EM1 reaches its maximum possible torque and a further reduction of the torque of EM2 leads to a reduction of wheel torque. This will lead to a decrease of acceleration and thus will be noticeable by the driver. To guarantee a comfortable shifting the torque gradient is reduced in the “Decrease” phase. In this phase a high torque gradient would lead to a high vehicle jerk and the eigenfrequencies of the drivetrain would be excited more. As soon as the torque of EM2 is reduced completely the dog clutches should be released completely to guarantee a fast and precise disengagement with the shift actuator. Afterwards the gear can be disengaged with ease by the actuator. Fully disengaged, the new, in this scenario the second gear, will be synchronized. In this phase, not only the differential speed will be synchronized, but also the angular positions of the dog clutch, further described in Section 3.3.

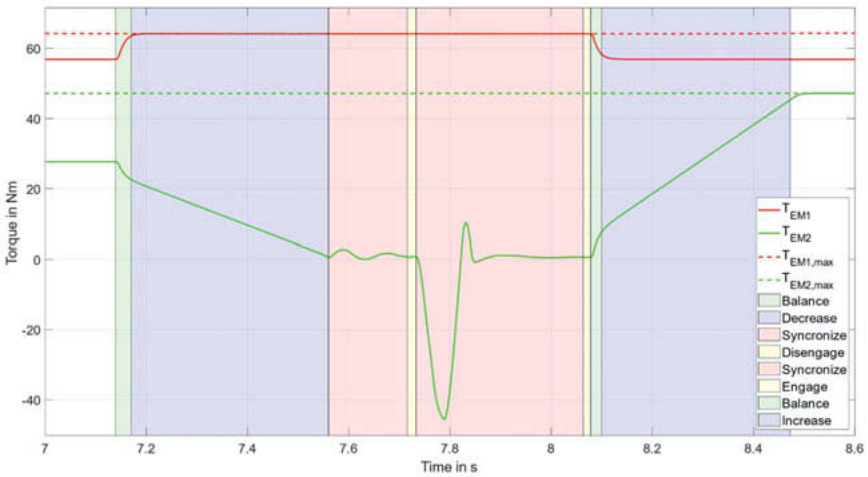

Fig. 10: Shifting phases

After the synchronization the second gear can be engaged and the torque of EM2 can be increased again.

In the phases “Balance”, “Decrease” and “Increase” both EMs are in torque-mode and the transmission control sends the target torque and the allowed torque gradient via CAN to the motor controller. In the “Synchronization”, “Engaging” and “Disengaging” phases however EM2 is in shift-mode. Synchronizations will be asked by the TC via CAN and will be confirmed by the motor controller. The angular position control will stay active until the next gear is securely engaged. As described in [3] this is not possible with a differential speed engagement. As soon as the required gear is engaged the TC will bring the EM2 back to torque-mode and again send the target torque and gradient to the motor controller of EM2.

As shown in Fig. 11 the actual disengagement and engagement of the dog clutch has no effect on the acceleration of the vehicle. Compared to the former engaging process, the differential speed is zero when the gear is engaged and with that the rotational impulse.

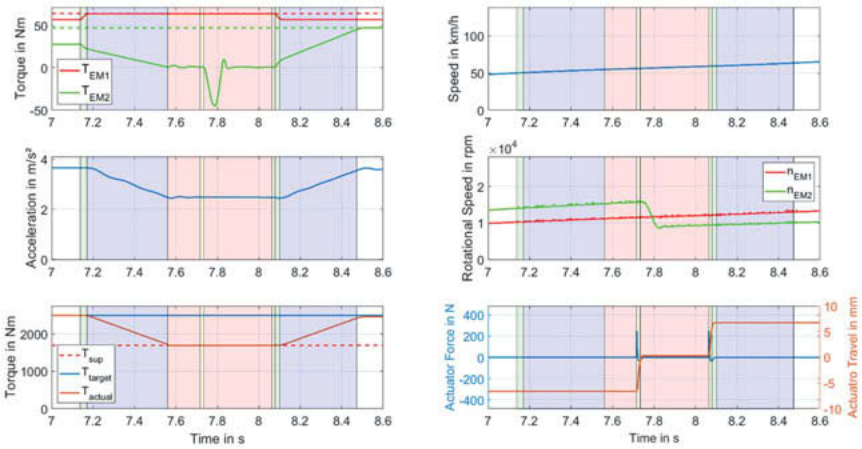

Fig. 11: Shifting process with 2500 Nm target wheel torque

In Fig. 12 an upshift from first to second gear with only 1700 Nm target wheel torque can be appreciated. This wheel torque can be covered solely by STM1 which means that no drive torque reduction is necessary. The gear change will not lead to a reduction of the vehicle acceleration and will hardly be noticeable by the driver. Without the comfort related decreasing and increasing of the wheel torque the gear change will be significantly faster.

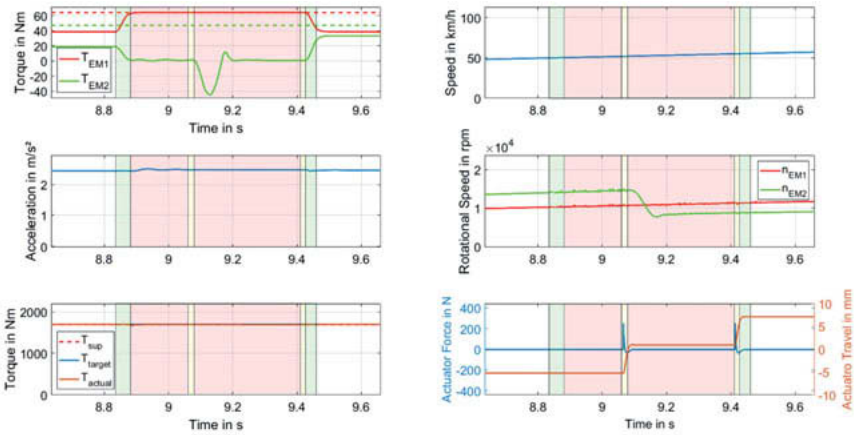

Fig. 12: Shifting process with 1700 Nm target wheel torque

3.3 Motor Control System

The structure of the powertrain including the electric motor and the 3-phase-inverter is shown in Fig. 13. The actual torque control of the asynchronous and the permanent-magnet synchronous motor is designed as field-oriented control, whereby the reference values of the current are generated by a Maximum Torque Per Ampere (MTPA) process. The evaluation of the current sensors, the resolver signal as well as the current controllers are executed for each motor in a separate Field Programmable Gate Array (FPGA). The high-level functions such as the generation of the reference values and communication with the powertrain control are executed in the processor.

In addition to the torque control for driving operation (torque-mode), the processor of EM2 has a control for synchronizing the dog clutch (shift-mode). This control is used during the shifting process. The speed and position of the EM2 can be used to adjust the speed and position differences on the dog clutch. For this reason, a synchronization process takes place at the dog clutch via the control of the EM2 already described in Section 3.2.

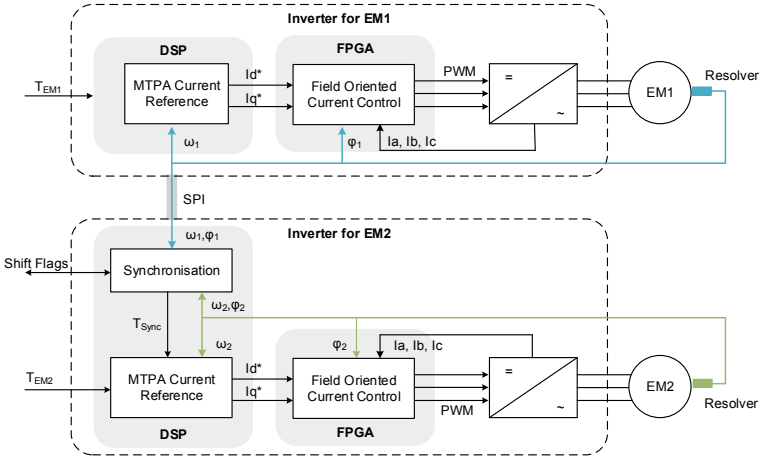

Fig. 13: Structure of the general drive control

The structure of the control for the synchronization process is shown in Fig. 14. It consists of a cascaded speed and position control loop and superposes the already implemented torque control. In addition, the reference values for the speed and position of the EM2 are calculated in the *Reference Calculation* block.

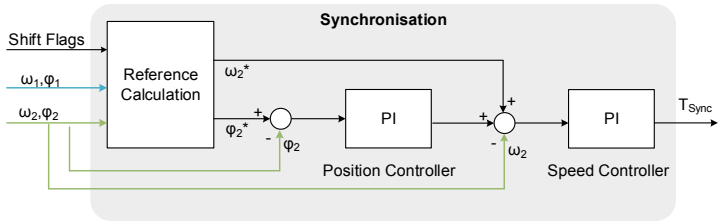

Fig. 14 Structure of the control for the synchronization of the dog clutch

In addition to the rotor position and speed of EM2, the position and speed of EM1 is required to calculate the angle difference at the dog clutch. This signal is evaluated in the FPGA of the EM1 and transmitted via an Serial Peripheral Interface (SPI) to the motor control of EM2. The whole communication takes place within one PWM period (~20 µs).

The speed reference value for EM2 is derived from the condition that the speed of the dog ring and the gear that should be engaged should be the same before engaging. The speeds of the

dog ring and the gears are not measured directly and need to be determined indirectly via the speed of the two electric machines measured by resolvers. Using the gear ratios shown in Fig. 2, the speed of the dog ring can be calculated as follows:

$$n_{\mathrm{Dog\_Ring}} = \frac{n_{\mathrm{EM1}} \cdot i_{2,3}}{i_{1,1} \cdot i_{1,2}} \qquad (1)$$

The speeds of the gear wheels can be calculated as follows:

$$n_{\mathrm{Gear1}} = \frac{n_{\mathrm{EM2}}}{i_{2,1} \cdot i_{2,2\_1}} \qquad (2)$$

$$n_{\mathrm{Gear2}} = \frac{n_{\mathrm{EM2}}}{i_{2,1} \cdot i_{2,2\_2}} \qquad (3)$$

In the first part of the synchronization these reference values are first transferred to the speed controller. The position controller is not active at this time. As soon as the speed difference drops below a defined value, the position controller is switched on. This now sends an additional setpoint component to the speed controller. The setpoint position for the speed controller is also calculated via the transmission ratio. However, the phase jump of the position has also to be considered. Due to the symmetrical design of the dog clutch, the position can also be synchronized to the nearest tooth-to-gap pairing. As soon as the difference in speed and position stays in a defined window for a defined time the synchronization process is finished. This condition is then sent to the powertrain control unit via a shift flag and the gear will be engaged. Afterwards the motor controller will be switched back to toque mode.

Results

Fig. 15 shows the simulation results of a synchronization process similar to Fig. 11. At roughly 7.2 seconds EM2 is switched into shift-mode and is asked to release gear one. Afterwards the gear can be disengaged. From 7.4 seconds on the next gear will be synchronized. It can be appreciated in Fig. 15 that firstly the speed is synchronized. When the speed difference is small enough, the angular position control will be activated. At roughly 7.6 seconds the synchronization is finished and the shift flag will be send to the PCU which will then initiate the engagement of the second gear by the actuator. The angular difference shown in the lower diagrams are referred to the mechanical angle at the EM2. The mechanical angle at the dog clutch are the same for both gears. Hence the difference from gear 1 ($\Delta\varphi_1$) to gear 2 ($\Delta\varphi_2$) is reasoned in different transmission ratios. In general, the time of synchronization depends on the speed

difference to be bridged. When the synchronization is finished, the shift flag “synchronized” will switch from zero to one.

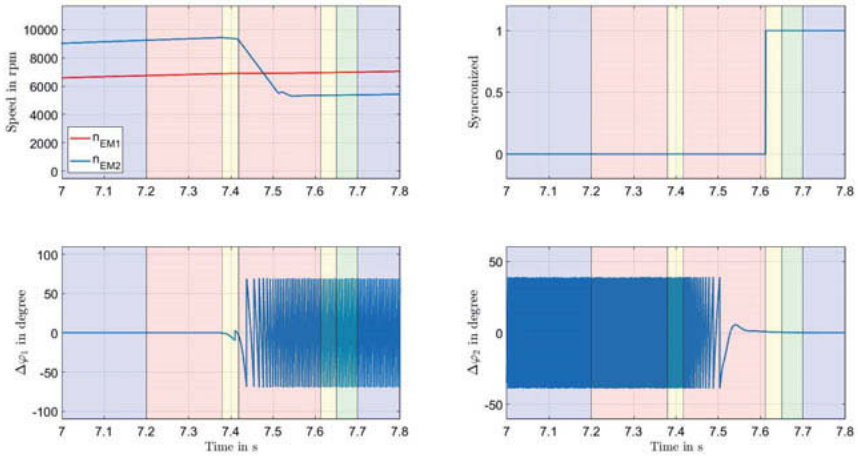

Fig. 15: Simulation results of the synchronization process

4. Summary and Outlook

This paper shows how a comfortable and fast gear change can be realized in an innovative two drive transmission with dog clutches. It further shows how a simulative approach was used to develop a transmission control and an angular position control and how all components of the Speed4E powertrain are designed to guarantee comfortable and highly efficient driving. On defined gear changes the transmission control and the angular position control is explained in detail.

The next step will be to validate these strategies on a powertrain testbench. Control parameters have to be tuned to guarantee successful gear changes in various driving scenarios. With a robust setup the actually necessary actuator force will be determined.

Finally, a demonstrator vehicle will be used to validate the concept in real driving scenarios. It will also be used to find a suitable torque gradient for the phases “decrease” and “increase” which are subjective parameters. It is assumed that they will differ for different driving modes e.g. sport vs. comfort.

5. References

[1] Viehmann, A.; Schleiffer, J.-E.; Rinderknecht, S.: Evaluation of the Dedicated Range-Extender Transmission Powertrain Concept DE-REX regarding Efficiency, Costs and Complexity. 19th International VDI Congress, “Drivetrain for Vehicles 2019“. Bonn 2019

[2] König, R.; Reul, A.; Rinderknecht, S.: Abschlussbericht des Projekts Speed2E, Teilvorhaben, Getriebesteuerung und Fahrstrategie. Darmstadt 2017

[3] Viehmann, A.; König, R.; Rinderknecht, S.: Investigation of Gear Shifts in a Parallel-Series Hybrid Powertrain with Dog Clutches in a Demonstrator Vehicle (Two-Drive-Transmission with Range-Extender, DE-REX). 18th International VDI Congress, “Drivetrain for Vehicles 2018“. Bonn 2018

[4] König, R.: „Gang- und Moduswechsel in elektrischen und hybrid-elektrischen Antriebssträngen mit aktiv synchronisierten Klauenkupplungen“. Darmstadt (2018)

[5] Taylor, R.; Fracchia, M.: Integrated Multispeed 48V EV Powertrain. 16th International CTI Symposium Automotive Transmission. Berlin 2017

[6] Mileti, M.; Schweigert, D.; Pflaum, H.; Stahl, K.: Speed4E: Hyper-High-Speed Driveline and Gearbox for BEVs. CTI Symposium USA. Novi 2019

[7] Schöneberger, D.; Mileti, M.; Stahl, K.; Rinderknecht, S.: Development of an Innovative Shift Actuator for Electrified Multispeed Transmissions. International Conference on Advanced Vehicle Powertrains. Hefei (China) 2019

48V eDRIVE Modularity: An answer to eMobility complexity

Dipl.-Ing. **Pierre Cholvy**, Valeo Transmission Systems,
Dipl.-Ing. **Paul Armiroli**, Valeo Engine & Electrical Systems,
Amiens Cedex, France

Abstract

As electrification is a key enabler to reduce emission of transport solutions, multiple architectures are emerging to answer e-mobility. Two wheelers, three wheelers and passenger cars are leading to a large diversity of powertrain specifications. In order to tackle this complexity while keeping optimal trade-off between cost, time to market and performance, development of a technological platform is a strategic lever.

The paper will describe the complexity of e-powertrain requirements and associated specifications. From those requirements, modularity between solutions will be discussed defining the drivers for the technological platform development. Finally, example of applied solutions and associated vehicle benefits will be demonstrated.

eMobility: new opportunities and complexity

Electric powertrains have to answer an increasing demand not only in volume but also in the number and types of mobility solutions. Passenger car sales forecast show that by 2025, 43% of vehicles will be electrified, combining all possible architectures including one or more electrical motors contributing to vehicle propulsion. Electric passenger car (BEV) sales forecast shows an increase of market share from 3% in 2020 to as much as 28% in 2030 [1].

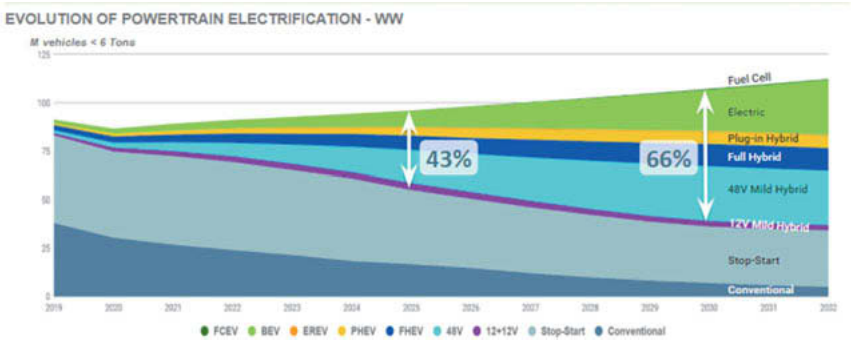

Fig 1: Electrification of passenger car market (source internal Valeo prior Covid 19 crisis)

However the electrification revolution is not only limited to passenger cars, emerging mobility solutions like autonomous shuttle or pods and light city cars, are increasing the demand for efficient and cost effective electric powertrains. One example of those latest developments being PSA O2C launched with a Valeo 48V powertrain.

Fig 2: PSA O2C

System specification per segment

Vehicles electrification leads to a variety of powertrain definitions both in performance, functions and cost targets. Peak Performance requirements of BEV powertrain are very similar to ICE passenger vehicles in order to meet driving dynamics. HEV and PHEV applications are following two paths. The first one, for already existing PHEV applications, EV mode range extension drives the

increase of max power requirement. The second one shows the downscaling of hybridization to A & B segments.

New urban vehicles are exhibiting high torque at wheel requirements and limited maximum speed both being driven by urban driving cycle.

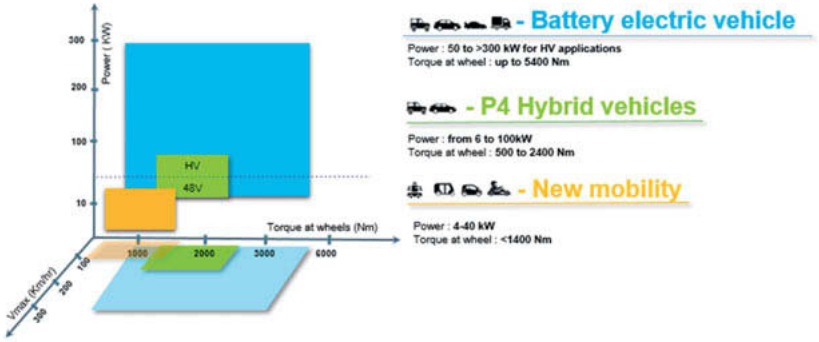

Fig 3: ePowertrain performance requirements per vehicle segments

Large range of power and torque, various vehicle dynamics, NVH requirements and cost targets translates into a wide array of powertrain diversity.

Industrial context

Above-mentioned complexity of ePowertrain requirements combines with a challenging landscape. Established OEMs and Tier1's are competing with each other. Many new companies are entering ePowertrain production. Product complexity is rising with smaller volumes per type. The time for high volume applications is probably over. This translates into strong pressure on Innovation, simulation and prototyping capacity, design change flexibility and enhanced product / process development. Above all, cost performance will remain the main driver [2].

Fig 4: ePowertrain market drivers

Key question for ePowertrain suppliers is therefore: how to succeed in such a challenging context?

Modularity through Technical Platforms

In order to take this challenge, Valeo has implemented 48V product platforms. Platform is based on defined architectures (functional, physical) and a set of standard Building Blocks (Fixed, Variable & Specific) from which products can be efficiently developed, manufactured and maintained.

Platforms teams are focusing on innovation and competitiveness of the product throughout the complete product life cycle. The key foundation is the definition of optimized and re-usable building blocks for the product platform.

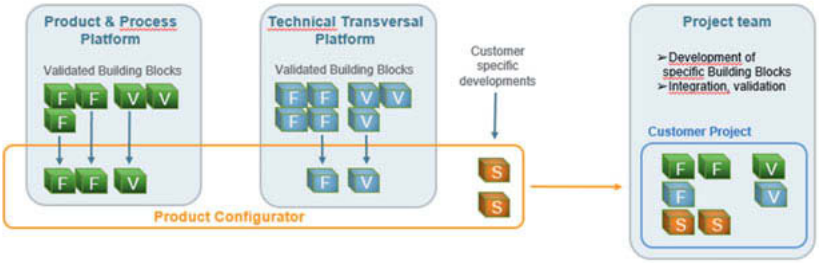

Fig 5: Illustration of building blocks used in customer projects

In case of customer projects, a product configurator tool enables efficient and robust association of product and process building blocks with transversal platform (SW for example) building blocks. Specific parts are developed and managed by the application team. Integration and validation plans are defined with the platform team.

48V Product platform: applications and benefits

48V systems are today well suited to address peak output power in the range of 20 to 30kW with significant benefits in terms of integration and maintenance costs.

Simulation and prototype testing are confirming the potential CO2 savings offered by 48V systems for P0P2/P3/P4 HEV vehicles.

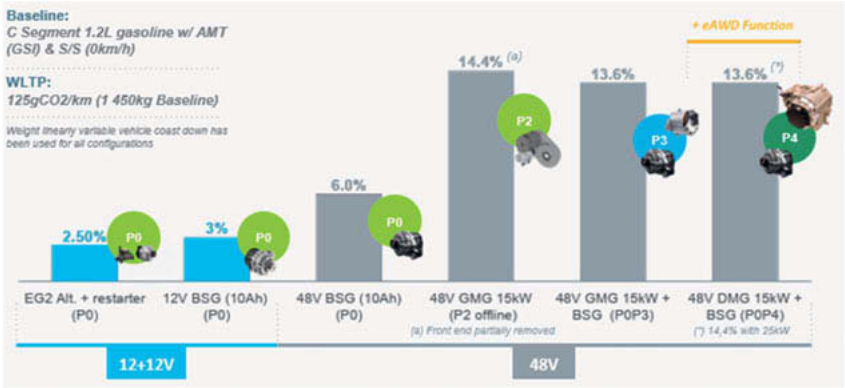

Fig 6: CO2 benefit for different 48V topologies

In order to address a maximum of application this study has been extended to higher segment vehicles. Kinetic energy recovery from C-SUV to E-Segment requires close to 25kW electrical power.

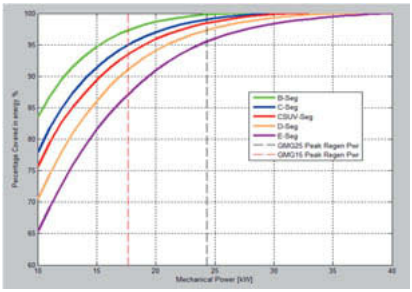

Fig 7: Kinetic energy recovery power requirement per vehicle segment over WLTC

Valeo has developed a 25kW XMG eMachine according to platform methodology. High level of peak and continuous torque is achieved in a compact package. Specific machine control is applied above 4500rpm to reach higher performance operating points and to improve efficiency. Loss reduction reaches up to -50% from mid to high loads compared to standard control. Long lasting performance associated with high efficiency level are key levers to address P2, P3 and P4 applications.

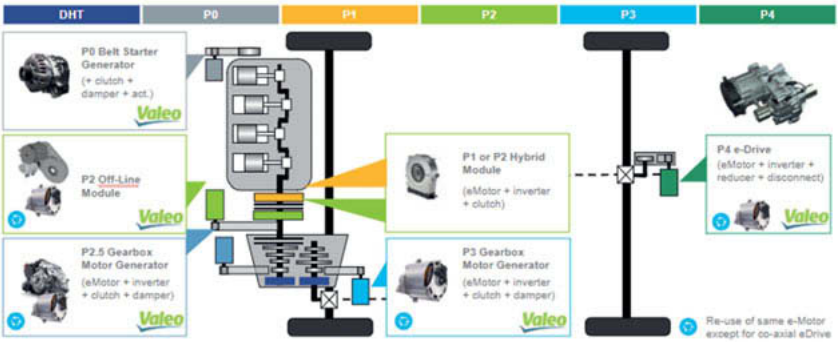

Fig 8: Re-use of eMachine on different topologies

CO2 is considered as the main driver for 48V adoption. Valeo has demonstrated 48V P0P4 CO2 benefits through multiple 48V P0P4 prototypes using 15kW XMG machines. In order to extend vehicle segment coverage and demonstrate eAWD capacity, Valeo has developed in partnership with DANA a unique 48V P4 25kW eDRIVE system. This product has been optimized for package, NVH, efficiency and cost.

eAxle specifications	
Overall ratio	18.31 : 1
Peak output torque	1 460 Nm
Max connected speed	~ 130 kph
eMotor specifications	
Torque	85 Nm peak
Power generator mode	25 kW peak
Max speed	> 18 000 rpm

Fig 9: 48V 25kW eDRIVE specification

In order to prove out the eAWD capacity the system has been implemented in a C segment prototype vehicle and extensively tested in Arjeplog, Sweden in the toughest conditions. Extension of vehicle traction capacity, stability and dynamics are confirmed to be similar to mechanical variants in most use cases for such vehicles.

Fig 10: Picture of 48V P4 25kW eDRIVE Demo Car.

Conclusion

Electrification of vehicles shows a high level of requirements diversity leading to a unique ePowertrain complexity. 48V Platform products are key levers to tackle this complexity and achieve CO2 targets. On top of fuel economy, the 48V P4 System is also bringing significant enhancement of vehicle dynamics and fun to drive to the end customer. New mobility market is an ideal candidate to benefit from already developed 48V solutions in order to speed up development at affordable cost as already proven by recent vehicle launches.

Reference:

[1] Bloomberg NEF EVO 2020

[2] Requirements for E-motors from production point of view, Dr.J.Hyvonen, 8th International Conference Advanced E-Motor Technology 2020, Berlin

Borg Warner's P1 and P2 Hybrid Drive Modules

Modular Kit for P1 and P2 Hybrids

Christopher A. Spangler,
BorgWarner Drivetrain Engineering, Ketsch

Abstract

P2i: A Family of Modular, Scalable, and Integrated Hybrid Drive Modules

Among the many hybrid architecture configurations, the P2 layout is a cost-effective solution that provides one of the best combinations to achieve CO2 reduction especially within a given ICE vehicle architecture. The P2 layout allows the engine to be disconnected from the driveline, and the electric motor leverages the ratios of the gearbox to drive the wheels. However, packaging of the motor and disconnect clutch without increasing the overall length of the powertrain is very challenging and needs detailed knowledge in electric motor and clutch module development and integration. By leveraging a unique method for winding the stator in the drive motor with scalable length for MHEV up to PHEV applications and years of experience designing compact clutch systems BorgWarner has developed a family of new drive modules including scalable and modular custom engineered hydraulic actuation systems.

P2 On-Axis modules for Dual Clutch Transmissions and Automatic Transmissions are in various stages of development within BorgWarner. For the DCT, the disconnect clutch and dual launch clutches are integrated inside the rotor and stator. Currently in pre-production phase at multiple customers, this P2 Triple Clutch Module has a very compact design that minimizes the impact to overall powertrain length. For planetary automatic transmissions and CVTs, modules are being developed that are compatible with both torque converter and launch clutch configurations.

This presentation describes the breadth of the BorgWarner Modular Kit to enable rapid development of P1 and P2 systems to support multiple transmission architectures and OEM installation needs.

Introduction

The upcoming limits for fleet CO2 emissions, especially in Europe and China, are significantly pushing electrification of vehicles. To achieve a balance between powertrain costs and reduction in CO_2 emissions, different levels of hybridization are being developed and will exist in parallel in the market for a certain time. Besides very low electrification of an entry level of 12V dual storage hybrids (also called micro hybrid vehicles), which already allow a small amount of brake energy recuperation and engine off coasting, mild hybrids with 48V electrical systems will occupy a significant portion of the market and are expected to replace conventional vehicles as a new baseline in some segments.

The standard architecture for the first mild hybrid vehicles is the P0 architecture with maximum power during recuperation of up to 12 kW (mainly limited by the belt) and usually less power for electric boosting on the crankshaft. P0 applications are simple to install, however, the losses on the recuperation path from the wheels to the motor generator unit (MGU) are relatively high, which limits the CO_2 benefits of this approach. On the other hand, the P0 allows a quick engine restart, which enables extended start-stop and engine off coasting.

As the need to reduce CO_2 emissions increases so does the need to recuperate a higher share of the available kinetic energy. An alternative to achieve this is to move to a different hybrid architecture which allows for higher electric power and a closer recuperation path to the wheels. In this context, a P1 or P2 architecture represents a good compromise between added functionality, cost and potential for CO_2 reduction. One of the biggest benefits of a P2 hybrid architecture is its potential for scalability both in terms of both power and voltage, which makes it a suitable solution for a variety of electrification needs.

Due to these advantages regarding scalability and packaging, as well as the potential to reduce the CO_2 emissions, the market for P1 and P2 hybrids is expected to grow in the upcoming years. In this context, Figure 1 presents the market outlook for 2024 which shows that the combined P1 and P2 hybrids will reach a market share of about 20%. Moreover, it is projected that the dominant layout will be on-axis with a fairly even split between 48V and high voltage systems.

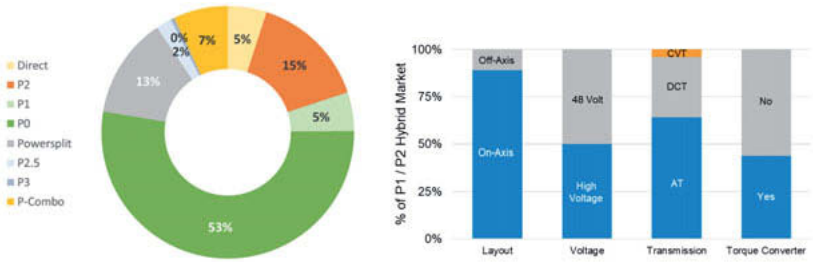

Fig. 1: 2024 Hybrid Architectures Market Outlook

P1 and P2 Hybrid Architecture Characteristics

In general, the CO_2 benefit of a hybrid powertrain is mainly influenced by the level of brake energy recuperation that is possible and the opportunity to operate the combustion engine as close to the efficiency sweet spot as possible. From a system perspective, the energy portion which can be harvested in the battery is influenced by the losses in the recuperation path from the wheel to the battery and the maximum power of the generator. For most vehicles, 48 V system power levels allow the recuperation of a high portion of the brake energy available in the standard fuel consumption test cycles. However, the exact amount depends on the architecture and the power of the electric motor. For example, the common P0 architectures electric power level is limited by the torque transfer capabilities of the belt and the overall recuperation path including the engine and belt losses also significantly reduce the overall efficiency in recuperation.

A P1 hybrid architecture offers some advantages compared to the P0 mainly due to the higher EM capability of the P1 due to not having the belt limitation of the P0 system. This allows for a greater boost capability in hybrid driving and the potential for some low speed electric only vehicle driving (eCreeping). The P2 hybrid architecture offers even further advantages compared to the P0. As a result of the addition of the clutch to allow the combustion engine to be decoupled from the drivetrain the losses in the recuperation path are significantly reduced allowing the EM to recapture a higher portion of the kinetic energy available in the drive cycle. The increased EM power along with the disconnecting from the engine enables P2 hybrids to provide electric driving to the vehicle and the benefit of the P2 architecture continues to in-

crease as the vehicle voltage level, EM power and battery size are increased. Figure 2 provides a comparison of the relative functionality of the P0, P1 and P2 architectures along with approximate WLTP cycle CO_2 benefits.

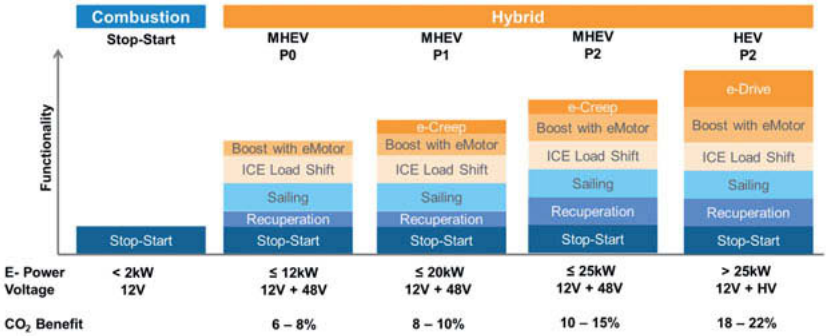

Fig. 2: Comparison of P0, P1 and P2 Hybrid System Functionality

Modular Kit for P1 and P2 Hybrid Architectures

In response to the growing market demand for P1 and P2 hybrids, BorgWarner has developed a comprehensive module kit of both components and full systems to support the needs of the various transmission manufacturers. Included in this kit are:

- Traction Motors
- Power Electronics
- Control Software
- Wet Friction Clutch Systems
- Hydraulic Control Systems
- Chain Drive Transfer Systems
- Permanently Engaged Starter One-Way Clutch
- Driveline Dampers

Traction Motors

The traction motor is the core building block for a hybrid drive module. BorgWarner has developed a variety of traction motors for both on and off-axis drive system utilizing our innovative S-Wind stator technology. These motors provide the customer with a motor with an application

optimized axial length, a high maximum continuous performance and low levels of both NVH and torque ripple to provide the driver with a seamless driving experience.

On-axis motors are available for both 48V and high voltage systems and provide up to 130 kW of power and 440 Nm of torque depending on the application. The off-axis motor is optimized for 48V systems and provides up to 25 kW of power and 70 Nm to torque. In addition, the off-axis motor has the advantage of being used across other hybrid architectures such as P3 and P4 applications to maximize its economies of scale and minimize the development time for any one specific application.

Fig. 3: On and Off-Axis Traction Motor Solutions

.

Power Electronics

In addition, BorgWarner has also developed a family of 48V inverters that are optimized for usage with the traction motors. The co-development of both the motor and the inverter allows for the optimization of the hybrid system. The 48V inverter options include both a stand-alone inverter (Fig. 4) or an integrated inverter as part of both the on and the off-axis traction motor systems. Depending on the specific OEM solution the stand-alone inverter can be integrated into the transmission housing itself while providing the following optimizations:

- Compact Design (<1 Liter internal volume)
- Body integrated WEG cooling system to maximize heat rejection
- 20kW continuous performance / 25kW peak performance

- Optional auxiliary controls hardware for ePumps and Solenoids for disconnect clutch actuation and cooling

Fig. 4: Stand Alone 48V Inverter

Control Software

BorgWarner has developed modular motor control software that can be used across multiple different Px module applications ranging from P1 and P2 to P3 and P4 drive units. This reuse of software enables faster development of new motor control features and expanded reuse to minimize the overall development time while fulfilling AUTOSAR, ISO26262 and Cyber-security requirements.

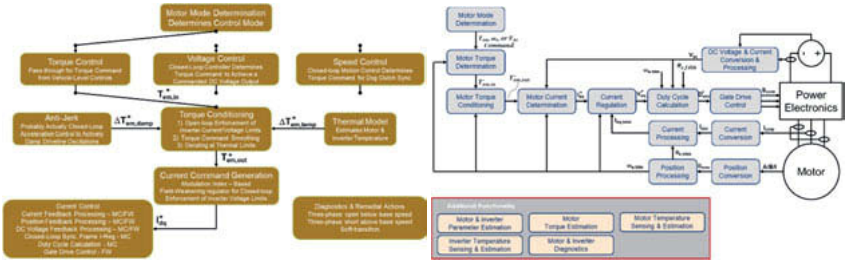

Fig. 5: Traction Motor Control Algorithms and Software

Wet Friction Clutch Systems

Building on BorgWarner's long history with one-way clutches and wet friction clutches the modular kit includes a number of different solutions for the engine disconnect clutch and starting devices.

- For applications where the P2 module does not need to start the combustion engine the disconnect clutch can be simplified to a mechanical one-way clutch;
- Various wet friction clutch system solutions ranging from one to three clutch packs for engine disconnect and vehicle launch depending on the application requirements;
- For applications with higher maximum launch weights a torque converter is available.

Fig. 6: Engine Disconnect and Launch Device Options

Hydraulic Control Systems

Also building on BorgWarner's long history with hydraulic control systems a variety of solutions are available in the modular kit to meet all variety of customer needs.

- For stand-alone P2 systems where it is not possible to exchange oil with the main transmission a direct acting pressure pump is utilized;
- For systems where oil exchange is possible with the main transmission but additional control solenoids are required there small local control hydraulic modules available to add the necessary clutch pressure and lubrication flow control components;
- For cases where the P2 module hydraulic controls are integrated into the main transmission hydraulic control system BorgWarner has solutions for both conventional 20-bar and high-pressure 40-bar clutch systems including the necessary clutch pressure

control solenoids, gear actuation control pressure and flow solenoids and flow control cooling and lubrication systems.

Fig. 7: Breadth of Hydraulic Control Solutions

Mechanical Systems

In addition the electric drive system items for P1 and P2 modules BorgWarner can also leverage other traditional mechanical systems to further optimize the overall integration of the driveline.

- A Permanently Engaged Starter one-way clutch in combination with an enhanced tradition starter from the OEM can serve as an alternative to using a P0 starter system with a 48V P2 module. This system allows the maximum usage of the 48V P2 module for electric vehicle driving by removing the necessary torque reserve for starting the combustion engine.
- A Dual Mass Flywheel (DMF), a wet Torsion Vibration Damper (TVD) or the Variable Spring Absorber (VSA) to minimize the torque pulsations from the combustion engine.

Fig 8: Permanently Engaged Starter and Driveline Damping Solutions

Modular Toolkit Case Studies

While working with OEMs from across the global BorgWarner has developed a large number of different integration examples from the Modular Toolkit.

Example 1: Off-Axis P2 Module

The OEM requirements for this case were to develop a sealed, self-contained P2 system that could be added between the existing engine and transmission in the vehicle with no increase in overall axial length of the system. Based on these constraints an off-axis system was developed utilizing a number of components from the Modular Toolkit:

- A 48V off-axis motor with integrated inverter;
- A direct acting hydraulic pump for the engine disconnect clutch;
- A wet clutch applied via a concentric apply piston and bearing;
- A WEG based cooling system for the traction motor and inverter;
- A chain drive transfer system to connect the eMotor to the transmission input shaft.

Fig. 9: Self-Contained Off-Axis P2 Module

Example 2: On-Axis P2 Module

The OEM requirements for this case were to develop a triple clutch module integrated along with a high voltage traction motor for a new high efficiency dual clutch transmission design. Based on these constraints an on-axis motor and clutch cartridge design was developed utilizing a number of components from the Modular Toolkit:

- Provisions for either a 45mm or a 60mm traction motor depending on the vehicle application requirements;
- A high pressure clutch actuation system using concentric apply pistons with apply bearings;
- A combined water and oil cooling system to maximize the continuous torque operation for the motor;
- Three wet friction clutches to provide the engine disconnect and odd and even shaft input clutches for the transmission.

Fig. 10: High Pressure Triple Clutch DCT Module

Example 3: Add-On On-Axis P2 Module

The OEM requirements for this last case were to upgrade an existing planetary automatic transmission by adding a P2 module with torque converter onto the front of the existing OEM transmission. Based on these constraints an on-axis system was developed utilizing a number of components from the Modular Toolkit:

- A 48V 30mm traction motor;
- A single wet friction clutch for engine disconnect and starting;
- A stand-alone hydraulic control system to actuate the disconnect clutch;
- A reduced volume torque converter to minimize the overall length;
- A integrated damper to address the combustion engine NVH torque oscillations.

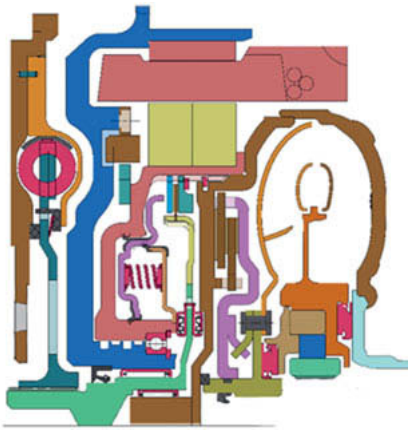

Fig. 11: Add-on Planetary Transmission P2 Module

Summary

As shown in this paper, BorgWarner has developed a comprehensive modular kit of both components and systems for P1 and P2 hybrid vehicle applications (Figure 12). This modular kit includes components and solutions for:

- On and Off-Axis P1 and P2 modules;
- 48V and High Voltage vehicle electrical systems;
- Compatible with A/T, DCT, CVT and DHT;
- Providing full hybridization potential with the minimum investment

Fig. 12: BorgWarner Modular P1 and P2 Module Toolkit

References

[1] Eichler, F.; Bennewith, K.; Helbing, C.; Philipp, K.; Lück, P.; Weiß, N. Felsch, C.: Volkswagen Electrifies the New Golf.; 38th Int. Vienna Motor Symposium, 2017.

[2] Bondards, A., Mohon, S., Semenov, D., Wenzel, W.: Comparing 48 V Mild Hybrid Concepts using a Hybrid Simulation Toolkit; Stuttgart Symposium 2019.

[3] Blumenröder, K.; Bennewitz, K.; Zillmer, M.; Mann, A.; Voeltz, T.; Dick, V.: Das 48V Mild-Hybrid Antriebssystem des Volkswagen Golf: Auslegung und Steuerung; 40th Int. Vienna Motor Symposium, 2019.

[4] Eglinger, M.; Hengst, J.; Kücükay, F.; Li, M.; Sieg, C.; Wenzel, W.: Next Generation 48V MHEV, Int. VDI Congress Dritev - Drivetrain for Vehicles; Bonn; 2019.

[5] Bongards, Anita, et al. "Comparing 48V mild hybrid concepts using a hybrid-simulation-toolkit." 19. Internationales Stuttgarter Symposium. Springer Vieweg, Wiesbaden, 2019.

[6] Eckenfels, T.; Kolb, F; Lehmann, S.; Neugebauer, W.; Calero, M.: Eine intelligente Aufwertung des Antriebsstrangs; 18. Schaeffler Colloquium; 2018.

[7] Timmann, M.; Inderka, R.; Eder, T.: Development of 48V powertrain systems at Mercedes-Benz, Int. Stuttgart Engine Symposium 2018.

[8] Bäumler, R.; Moser, A.; Schäfer, M.: Dry running, Permanently Engaged Starter System (PES) for a comfortable start of combustion engines providing further potential to reduce fuel consumption, Motortechnische Zeitschrift, 12/2014.

[9] Yausel, H.; Wenzel, W.: P2i: A Family of Modular, Scaleable and Integrated Hybrid Drive Modules; CTI Sympoisum Berlin; 2019.

E-Drive and Hybrid-Drive with 2 High-Speed E-Motors and a 2-Speed Gearbox

Prof. Dr.-Ing. **Peter Tenberge**, **Ahmad Alnahlaui**, M.Sc.
Ruhr-University Bochum

Abstract

New drivetrains for cars should be designed around the electric motors (EM) and other electrical components with a minimum of gearsets and shift elements and other energy consuming subsystems. In future hybrid drives the internal combustion engine (ICE) should be the assistant drive with the main task of providing sufficient driving range.

This paper presents the layout of a traction gearset which allows the E-motors to operate at very high speeds. Two of such motors can cooperate through a planetary gears system in a first driving mode with constant speed ratio and in a second driving mode with variable speed ratios. The shifting is controlled by torque and speed control of the e-motors. The necessary shifting-brake consists of 2 ratchet freewheels which can be disengaged by a small electro-mechanical device.

An internal combustion engine can easily be linked to this e-drive only via a small clutch with an integrated damper.

Market Situation für Electric Vehicles and Hybrid Vehicles

Over the past more than 100 years, the internal combustion engine has been the dominant vehicle drive. In a small and light tank fits enough fuel for long driving ranges. Today, the energy conversion with an ICE is very efficient, quiet and has low emissions. With widely spread gearboxes with stepped or continuously variable ratios, the ICE can often be operated along its optimal characteristic line. Launch operations and ratio changes are done comfortably and efficiently. For a long time, electric motors have been integrated into the powertrain in order to regenerate potential and kinetic energies which had been charged into the vehicle masses during acceleration and uphill driving. But the whole drive system was subordinated to the internal combustion engine.

In the future, the electric motor will be the main drive of many vehicles. It does not need a launch system like the ICE. From a standstill it can accelerate the vehicle with maximum torque forward or backwards. Due to its torque-speed characteristics it only needs a gearbox with a fixed ratio between rotor shaft and wheels in vehicles with reduced traction requirements and reduced maximum speed. Expensive shifting systems can be omitted. This also reduces the need for auxiliary energy. Electric vehicles can be extremely comfortable and quiet on the road. Supercars with electric drives will soon be far superior to their predecessors with ICEs.

Electric vehicles need batteries with environmentally friendly generated electrical energy. All the necessary technologies for energy conversion as well as the production and recycling of batteries and also some charging infrastructures already exist and they are getting better and better every day. More and more people and governments want this technology change and support it with great effort and big investments.
Hybrid drives enable a smooth transition from ICE technology to EM technology. In the case of new developments, however, the electric motor should now be put into the foreground in hybrid drives.

This article is firstly about very compact and with high speeds rotating electric motors with a down-speeding traction gearset with an integrated damper function. Thereafter, an arrangement of two such electric drive units is presented in a drive system with two torque ratios and an infinitely variable speed overlaying. The shiftings in this drive system are made with 2 switchable one-way clutches, which consume almost no switching energy and form a very compact shifting unit. The shifting process is only controlled by the two e-motors and a small electric actuator with an effective actuation power of less than 30 W. Such a purely electric drive system can drive a vehicle alone, but it needs a large battery. Instead of a large battery, the vehicle can also have a smaller battery pack plus a tank and an internal combustion engine for a sufficient driving range, whereby the ICE is only connected via an additional clutch- and damper-unit to the e-drive.

High speed electrical motor plus a damping traction drive

The characteristics of electric synchronous motors fit much better than those of internal combustion engines to the demand characteristics of vehicles. Most electric vehicles use

only a gearbox with one fixed ratio or with only two ratios. A basic drive unit consisting of electric motor and gearbox with one ratio needs only very small space and can be connected to its energy source (battery) much easier than an internal combustion engine which needs a lot of fresh air for the burning process. An electric motor also does not require an elaborate exhaust system.

That is the reason why in several electric vehicles already more than one drive unit drive the vehicle. But then it also makes a lot of sense to combine different identical basic units for different vehicle classes depending on the power requirement. This increases the number of units and reduces the cost per drive unit.
For small cars up to small distribution vehicles a drivetrain with only one basic unit is sufficient. Slightly larger and heavier vehicles with higher top speeds have a basic unit with a conventional 2-speed gearbox, or even 2 electric motors with an innovative 2-speed e-gearbox. For sports cars and heavy SUVs, such systems with 2 EM plus e-gearboxes can be installed on both axles.

The maximum speeds of internal combustion engines in most vehicles range from 5,000 rpm to 10,000 rpm. Often mass effects in the accessory drives of the cam shafts for the intake- and exhaust valve-systems limit this rotational capacity. But electric motors can easily rotate much faster. E-motors have already been used in several development projects with top speeds above 25,000 rpm. Electric drives with peak speeds of >150,000 rpm are already installed in spindles of textile machines.

Fig. 1 shows an electric motor with 100 kW peak power, 130 Nm peak torque and 25,000 rpm peak speed in a drive unit. As the maximum speeds increase, the peak torques decrease. With the same transferable tangential force in the air gap per air gap surface, these electric motors become very small. However, their heat capacity decreases. Thus, the requirements for the cooling systems increase so that also these small motors can provide big constant output power. To achieve this, the stators of these motors are cooled from the outside and possibly in the slots of the windings or in another grooves. The end windings are also cooled. And, furthermore, the rotor can dissipate heat via an internal cooling. For these technical targets there are worldwide already good cooling concepts investigated and plenty prototypes have been tested.

In order to reduce a maximum speed of an electric motor from e.g. 25,000 rpm to a wheel speed of 780 rpm (1000 rpm) at a vehicle speed of approx. 100 kph (128 kph), a multi-stage gearbox with total ratios of 32 (25) are needed. If such a gearbox would have gear wheels with e.g. 24 teeth on the fast-running shaft in the first gear stage, the tooth mesh frequency would be 10,000 Hz. The excitations from this first gear stage lie in a wide speed range within the very audible range for human ears.

In gearsets the noise excitations arise from the mesh impacts of the elastically deformed teeth under load and the principle-related stiffness steps between single, double or even triple tooth contacts depending on the gear design. Due to optimized gear designs with integer profile overlaps and integer helical overlaps, the noise behavior can be improved very much.

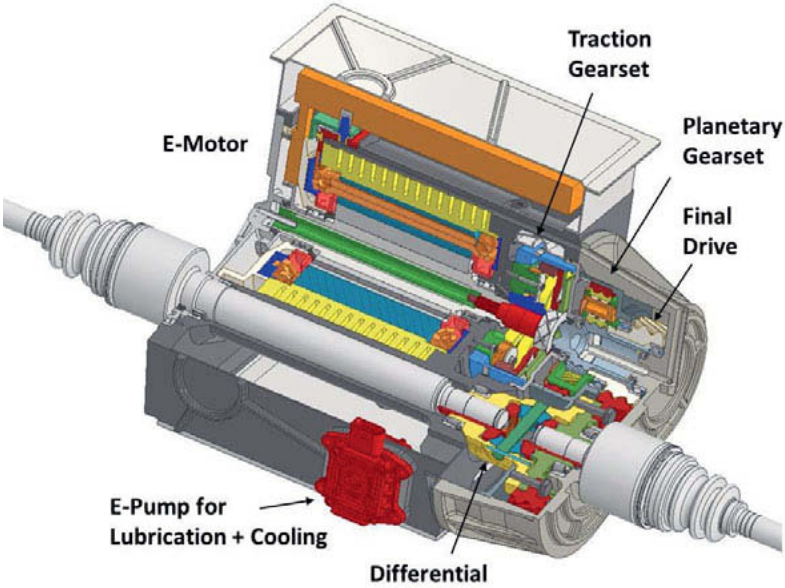

Fig. 1: Drive unit with high speed e-motor, damping traction gearset, final drive and differential

But for such small input torques, also completely different transmission principles are possible, which at the same time offer further big advantages.

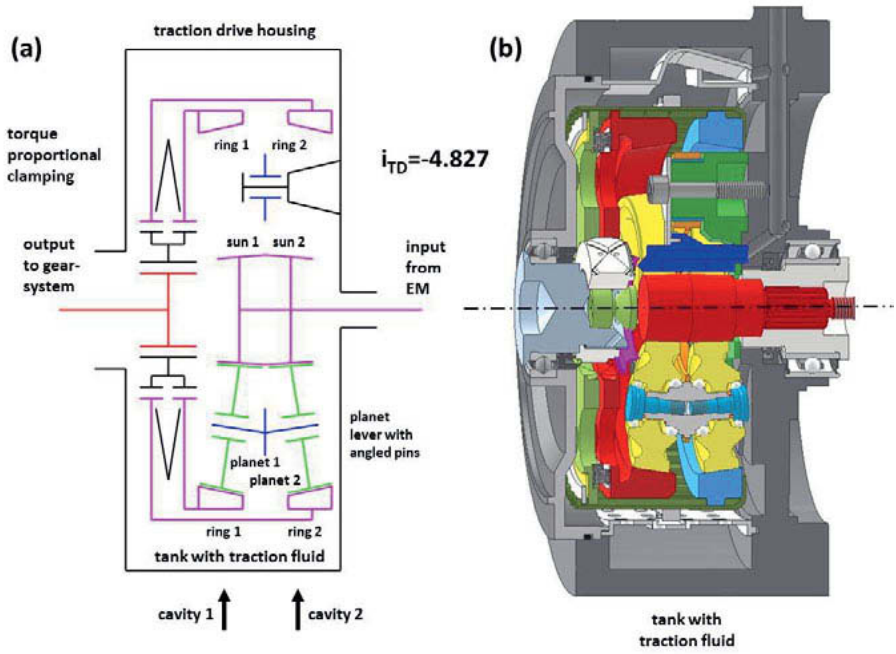

Fig. 2: Traction planetary gear set for the high-speed reduction

The first small and fast-rotating planetary gear stage can also be designed as a planetary gearset with traction bodies instead of gearwheels. Fig. 2 shows such a planetary traction gearset with a planet carrier which is fixed to the housing. This gearset has a stationary ratio of i_{TD} = -4,827 (TD = Traction Drive).

For a simple preload of the traction contacts, this gearbox consists of two mirror-image-like partial gears in cavity 1 and cavity 2, which are braced against each other in axial direction. Each of these partial gears has a sun body, a ring body and three planet bodies, whose planet bolts in this design do not sit perpendicular to a forehead section plane through the planet carrier, but which are inclined at a small angle.

All traction bodies have conical traction surfaces. All traction cones of a partial gearsets meet in one point, so that no spinning slip is created in the sliding rolling contacts. In taper roller bearings, this is done in the same way to avoid spin losses completely. As in any friction clutch, the efficiency of the spinning-free traction gearbox then results from the slip between

the driving and the driven elements as well as from the low hydrodynamic losses in the lubricated contacts.

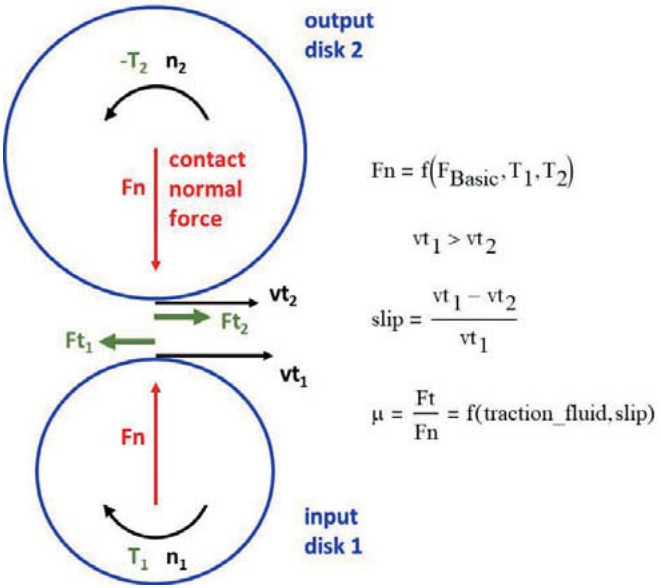

Fig. 3: Basic functions of a damping traction gearset

In traction drives with case hardened, grinded and honed traction bodies, the power transmission happens in lubricated traction contacts. In the sliding rolling contacts of the traction bodies, a traction fluid is compressed and sheared under locally high contact loads, which reach up to 1600 MPa in the contacts of the ring bodies to the planets and up to 3300 MPa in the contacts between the planets and the sun bodies.

Traction fluids from the Japanese oil and additive supplier Idemitsu Kosan Co. Ltd. can create traction values of e.g. 0.06 at these contact loads at a slip of only 0.15% and circumferential speeds up to 40 m/s. Up to these low slip values and thus high transmission efficiency levels, the coefficient of traction increases quite linearly with the differential speed in the lubrication gap. At a circumferential speed of max. 40m/s at the very high speeds, but small radii on the sun bodies, 0.15% slip means a speed difference of 60 mm/s or 60 μm/ms. These relative velocities in circumferential direction in the traction contact of a traction drive

are at least one order of magnitude bigger than the relative contact movements in contact normal direction of the tooth flanks in gearsets, which produce there a small damping effect. With two traction contacts in line, a planetary traction gearset then runs with a slip of approx. 0.3%. A geometric ratio of 4.8 is thus increased only slightly.

The traction force and thus the transferable torque in a traction drive increases with the sliding speed. Then a big torque vibration effects only a strongly variating slip but not a collision of tooth flanks within very small clearances in the tooth flank contacts. A torque which increases proportional to a speed difference has the physical properties of a damping torque. Therefore, a traction drive is physically a speed- and torque-converting damper without form-fitting contacts with periodically changing stiffnesses. Thus, such a traction drive combines two physically important functions in one subunit.

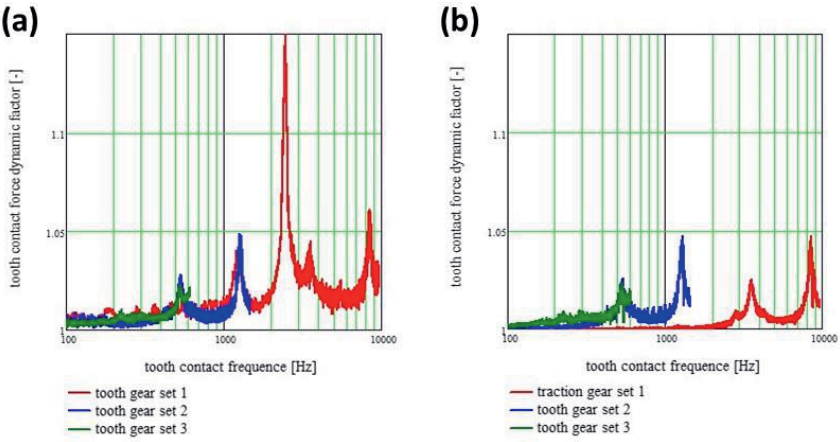

Fig. 4: Dynamic tooth contact forces and traction forces in a transmission (a) with three helical gearset and in a transmission (b) with one traction gearset and two helical gearsets

Fig. 4 clarifies the dynamic tooth contact forces and the traction forces in the gearbox with three gearsets and a total ratio of 31 at an acceleration from zero speed to a maximum rotational speed of 25,000 rpm at the input of gear stage one.

In a first layout (a) the first stage is designed as a helical gearset with gearwheels and in a second layout (b) the first stage is a traction gearset. The second and third stages are always

designed as helical gearsets. It can be clearly seen that the transmission (b) with the traction drive as first stage shows significant lower amplitudes of the torque-forming tangential forces than in transmission (b). The dynamic tooth forces in the second and third stages are nearly the same in both drive variants and uncritical at dynamic factors well below 1.05.

To preload the traction contacts, the two output torques from the ring bodies are transferred via a helically splined connection to the output shaft. In this spline connection, the resulting axial forces are balanced. Their axial reaction forces on the ring bodies act through the planets onto the connected sun bodies and are balanced there. The relatively small axial forces generate large contact normal forces via the cone angles at the traction bodies. The contact normal forces create tractions forces if slip an according to the slip a traction coefficient occurs.

An additional low spring preload in the axial direction ensures that all traction bodies always remain in contact even under a minimum load. A traction drive of this type with constant ratio does not require any further control unit and control power for efficient power transmission. Without spin slip and a need for auxiliary energy, the efficiency of such traction drives is above 99%. It is comparable to that of good gearsets with gearwheels, whereby as well in their sliding rolling contacts quite high sliding movements occur under high contact loads.

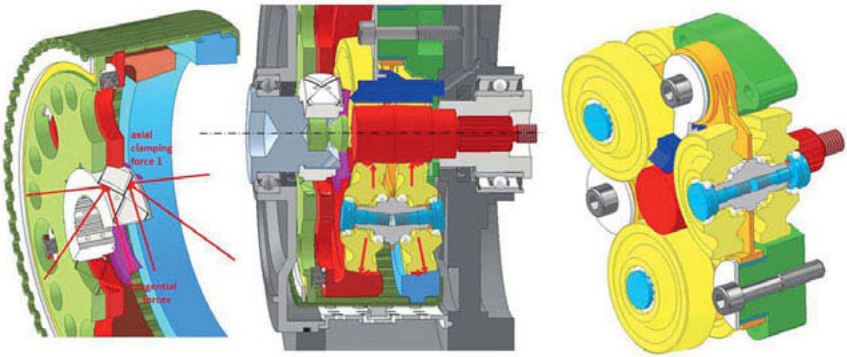

Fig. 5: Preload system and planet suspension of the planetary traction gearset

The big contact normal forces lead to elastic deformations of the traction bodies, especially on the relatively soft ring bodies. To keep the bodies in contact at all times, these rings can

be moved up to 3 mm in axial direction. And it is also necessary to design the connection between the planets and their carrier in a way that they can easily be moved in radial direction in the space between the rings and the sun bodies. For that purpose, the planet bolts (yellow) are connected to the planet carrier (green) via swivel levers (orange).

An electric motor with a top speed of 25.000/min plus such a traction gearset with a ratio of 4.8 is smaller and lighter than a slow-rotating motor with a peak speed of only 5200 rpm. From this speed level, it is possible to reduce the speeds further to the wheel speeds with well-known helical gearsets and to increase a torque from 620 Nm to 3200 Nm up to over 4000 Nm.

Drive system with 2 electric motors and innovative 2-speed / 2-mode transmission

With such a compact high-speed motor unit with 100 kW peak power and in combinations with further gear stages and a differential, city cars with limited maximum speed and limited traction forces can be driven. Such a system is also sufficient for taxis, other smaller passenger vans and as well for distribution vehicles on the last mile. For higher traction requirements or higher top-speeds the vehicles need more torque and other gear ratios or a 2-speed transmission between the electric motor and the wheels.
But multi-speed transmissions require a shifting system. Today, hydraulically or electrically driven actuators can synchronize gear elements precise and sensitive and they can actuate dog clutches or tooth clutches for shiftings with torque interruption or they can control the clutch forces in friction clutches for shiftings without torque interruption. Such quite complex control and switching systems require installation space and they require auxiliary energy, which reduces the system efficiency.
The ratio step of usually $\varphi 12>2$, which must be realized in such a 2-speed transmission for electric vehicles, leads to a loss of comfort due to the short-term high dynamic mass effects at the rotary masses to be accelerated or delayed. Such shiftings do not meet customer expectations for a pure electric drive.

With two of these small electric motors, however, an electric drive system with 2 speeds or 2 driving modes and load shiftings can be realized by means of a speed overlaying gearsystem almost without additional energy demand for the shifting process. Then the shifting system then has only two one-way clutches whose locking function can be activated or deactivated

nearly load-free with a very small electric-mechanical shifter. The mass effects on the output shaft remain minimal.

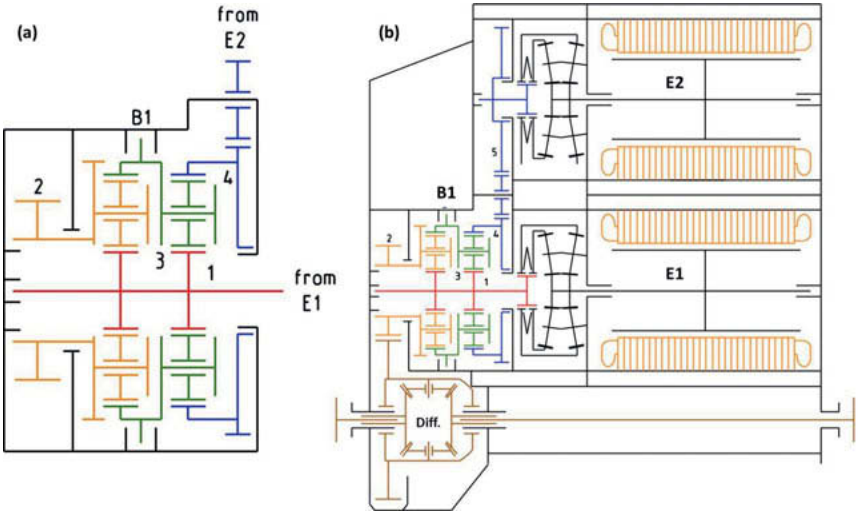

Fig. 6: Drive system with 2 e-motors and a new 2-speed respectively 2-mode gearbox

Fig. 6 shows such a drive system in a structural graphic (b) and more in detail its speed overlaying and shifting system (a). 2 small, fast-rotating electric motors lie parallel here and each of them drives via an already explained damping traction gearset into a transmission system in which the two power outputs of the electric motors flow together.
The first electric motor E1 drives the shaft 1 of the transmission system. The second electric motor E2 drives the shaft 4 of the transmission system via an intermediate gear. Via the shaft 2 of the transmission system, the total output power flows to a differential and from there to the driven wheels. A third shaft 3 of the transmission system can be connected to the gearbox housing via brake B1. This brake B1 consists of the two switchable one-way clutches, of which a first freewheel A can block the forward movement of shaft 3 and a second freewheel B can block the reverse movement of shaft 3.

Fig. 7 shows a very compact 3D-layout to this drive system. The speed-overlaying system and the shifting system are hardly viseable in this design, because of their small sizes. They

sit between the electric motors, the final drive to the differential and a small electrically driven oil pump for lubrication and cooling.

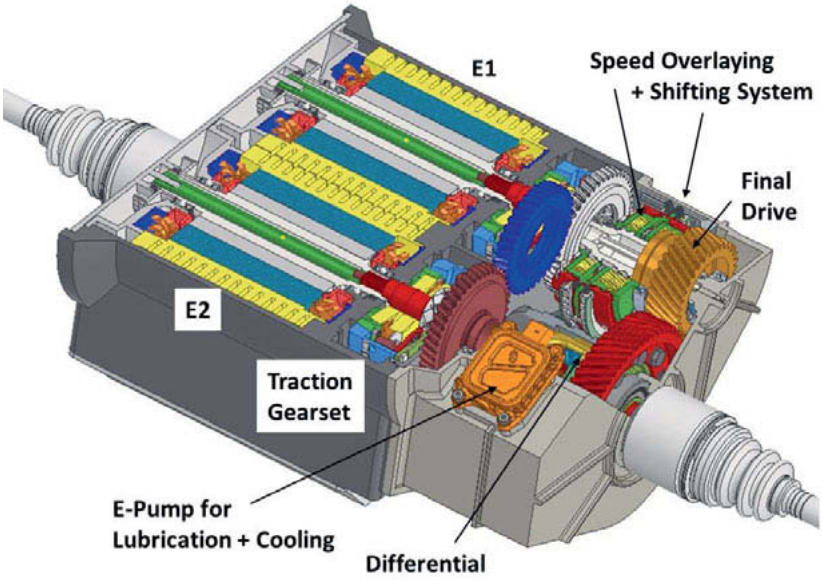

Fig. 7: 3D-Layout of the electrical drive-unit with 2 E-motors and 2 driving modes according to Fig. 6

The four shafts 1 to 4 of the speed overlaying gearset define a 4-shaft planetary gearset, which can be designed e.g. as a Ravigneaux planetary gearset or can be composed of two simple planetary gearsets each with three shafts.
In this example, the 4-shaft system consists of two simple planetary gear sets with identical stationary ratio. The two sun gears are both located on shaft 1. Shaft 4 drives a ring gear of the first overlay-stage. Its planet carrier is connected via shaft 3 to the ring gear of the second gearset. The planet carrier of this second gearset sits on shaft 2, i.e. the output shaft of the speed-overlay system.

In order to understand quickly the functions of the speed-overlaying gearbox and the freewheels A and B in the brake B1, it is helpful to clarify the speed relations and the torque ratios in this gearbox in some speed ladder diagrams. This is done in Fig.8.

In such speed ladder diagrams, the linear speed relationships in such a speed-overlaying gearbox can be displayed very easily. The positive speeds of each of the 4 shafts are applied upwards on a speed arrow or speed ladder. The distances between the speed ladders are chosen in such a way that the speeds of the 4 shafts can be connected by a straight line in each operating point. These distances also result from the stationary ratios and the fixed gearwheel-connections in this gear structure.
In addition to the speeds also the torque relations can be visualized in such a diagram. The torques in such a speed-overlaying gear system act as forces on a lever that lies above the straight connecting line of the speeds.

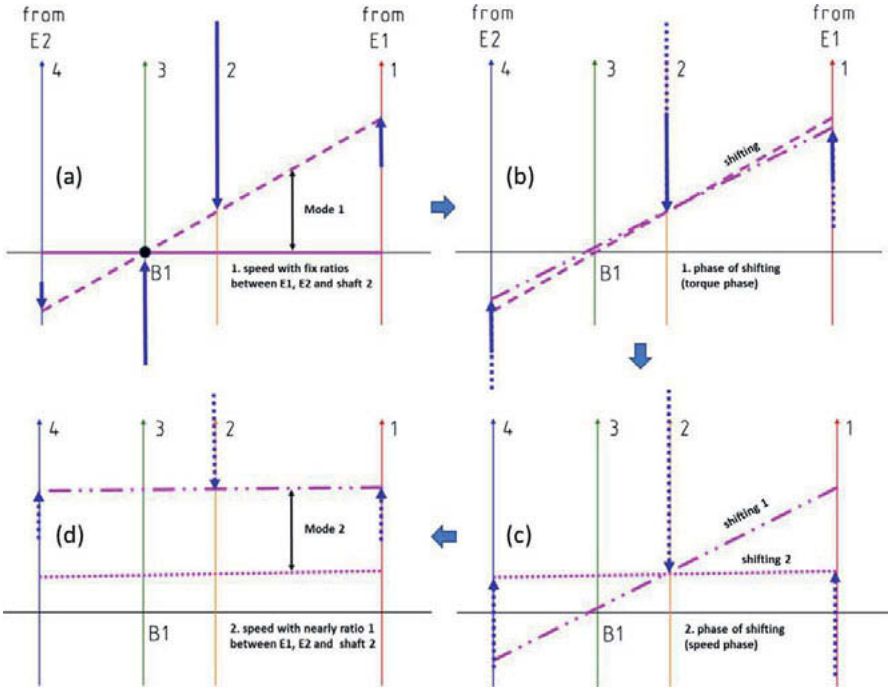

Fig. 8: Acceleration with this 2 EM-System and shifting between 2 driving modes

The starting point of the consideration is the standstill of the vehicle. All speeds in the speed overlaying gearbox are zero. To this state belongs the solid pink line in Fig. 8a. In order to

accelerate the vehicle in a 1st mode forward with large ratio, the reverse movement of the shaft 3 is blocked in the brake B1 via the freewheel B. The freewheel A, which only has to be closed for a reverse drive, is still closed or already opened. Both would be possible. This means that in this situation shaft 3 is connected to the housing, but only in a positive torque direction from the housing to shaft 3. E-motor E1 drives shaft 1 with a positive torque (blue torque arrow upwards).
In the second gearset a fixed speed ratio and a large increase in torque to shaft 2 results. The large negative output torque at shaft 2 requires a positive support torque on shaft 3 from the gearbox housing.
In addition to E1 and independent of E1, the e-motor E2 can drive at a negative speed of shaft 4 at this operating point and increases the output torque further.
This means that both electric motors, together with a high increase in torque, drive the vehicle in a 1st mode until reaching a shifting speed, at which E1 has already reached a high motor speed. This operating point relates to the dotted pink line in the Fig. 8a and 8b.

Not later than just before shifting to the 2nd mode, the unloaded freewheel A, which would prevent a forward movement of the shaft 3, was opened in a load-free way. In order to move the shaft 3 forward for shifting into the 2nd mode, the torque in motor E2 is reversed and increased until the freewheel B is load-free (Fig. 8b).
Both electric motors now drive the output with almost the same torque, without reaction torques to the housing. This torque-shift needs only a few milliseconds and happens therefore at almost constant speeds. Thus, the torque change from mode 1 to mode 2 as phase 1 of the shifting has already been completed.

The output torque at shaft 2 has decreased by the ratio step. However, this can also be compensated in milliseconds if motor E1 still has some torque reserves up to the full load characteristic or can be temporarily overloaded. This state corresponds to the dotted pink line in the Fig. 8b and 8c.

In phase 2 of the shifting, the speed change is now made by the two electric motors. The torque on E2 is increased and the torque on E1 is reduced. This accelerates E2 and decelerates E1. The output torque and the vehicles acceleration remain high.
This speed phase of the shifting last between 0.8s and 1.4s. At the end of this speed phase, both electric motors have approximately the same speeds and torques and drive together the vehicle in the 2nd mode. Then all shafts in the overlaying gearbox rotate fast with the same

speed and with minimal gear losses. This state corresponds to the dotted pink line in the Fig. 8c and 8d.

If the shifting starts at a speed of motor E1 close to its maximum and if it ends at a speed of E1 in the range of the maximum power hyperbole, then the vehicle can have the same acceleration before and after the shifting.

With a further acceleration from there in mode 2 up to high speeds, the output torque is naturally reduced with constant drive power. The condition at a very high speed is illustrated by the dotted pink line in Fig. 8d.

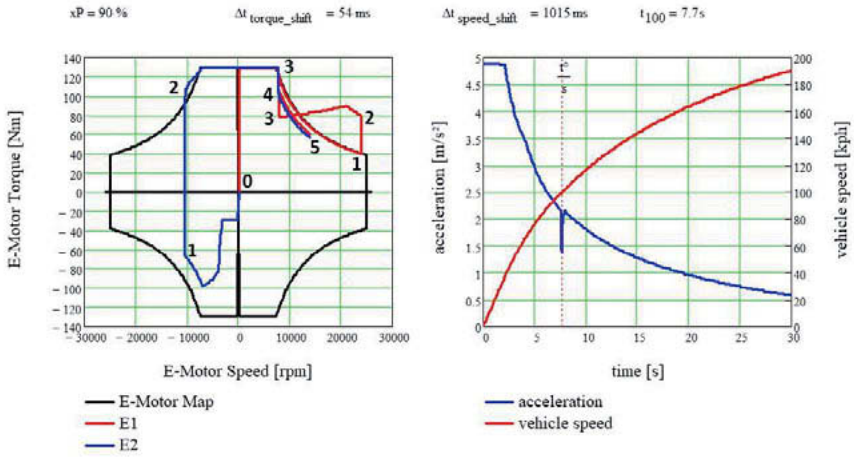

Fig. 9: Operating Points of the 2 EM during a 90% full power acceleration of a bigger car with a total mass of 2350 kg

Fig. 9 shows the operating points of both identical electric motors at such an acceleration with 90% power in one common motor-diagram. The acceleration starts for both e-motors at zero speed at point 0 in Fig. 1. In mode 1 between states 0 and 1 (0 => 1), at first the torques are increased and then the speeds are increased up to switching speeds. The torque phase of the shifting happens very fast (1 => 2). This is followed by the speed phase of the shifting (2 => 3). In mode 2, the torques of the EM are then adjusted for further acceleration (3 => 4), which then continues at almost the same motor speeds (4 => 5). In this example, in the torque phase there is a small reduction in acceleration, but only for 54 ms. This happens in this case because the short-term overload of E1 is limited to 200%. After that, the

acceleration continues with constant power. With such a 2-motor drive unit and a total drive power of 200 kW, a vehicle with a total mass of 2350 kg accelerates from 0 to 100 kph in 7.15 s.

Fig. 10 shows the shift system with the two freewheels A and B between and around the two planetary gearsets of the speed overlaying system. But the elements of the shift system are so small that its functions cannot be explained only with this figure.

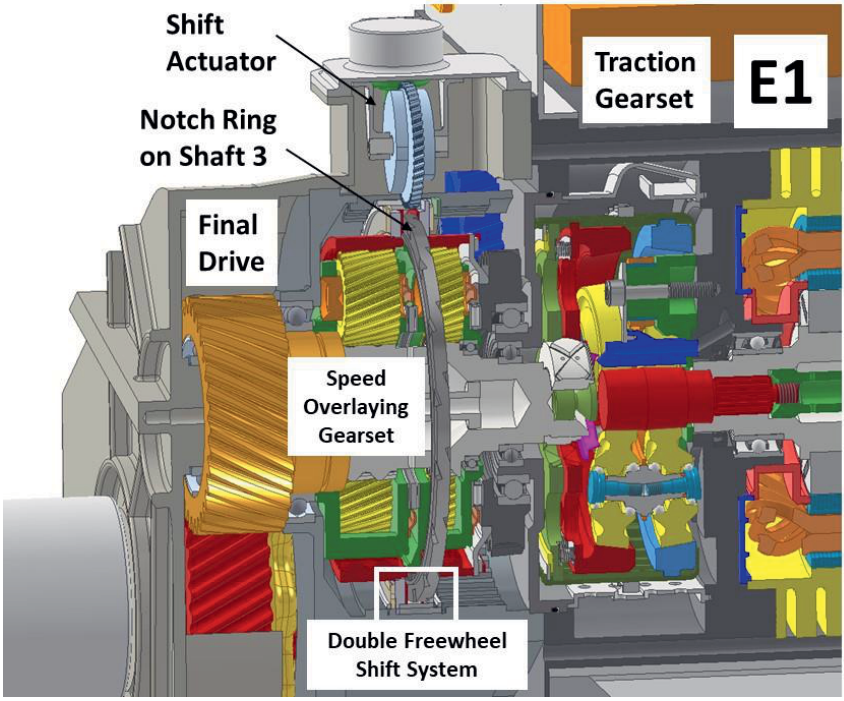

Fig. 10: Speed overlaying gearset and Double freewheel shift system of the drive unit

More details of the shift-system are shown in Fig. 11 and Fig 12. The shift system consists of the two identical and mirror-image-arranged pawl freewheels A and B, which are very similar to switchable freewheels of Means Industries Inc., which are used in several automatic transmissions in mass production. Because Means Industries call the pawls struts and with

the reason to show the similarity of these freewheels with already existing components also in this paper the same names of the elements are used.

The two freewheels are pre-assembled in a common brake pocket and fixed by circlips. Between them a notch ring is located, which has a spline at its inner radius, through which it can be connected to shaft 3 of the speed-overlaying gearbox. A distance ring keeps the freewheels at a distance, so that the notch ring cannot be clamped.
The rotatable notch ring has on one side several notches for the locking of one direction of rotation and on the other side the notches for the locking of the other direction of rotation. The struts can engage into these notches. For each locking direction, these struts sit between a strut ring and a very thin selector plate and are preloaded by strut-springs against the selector plate, which then prevents the engagement of the struts into the notches of the notch rings. The strut-springs for each locking direction are designed as bending springs and are punched and bent from only one piece of sheet metal.

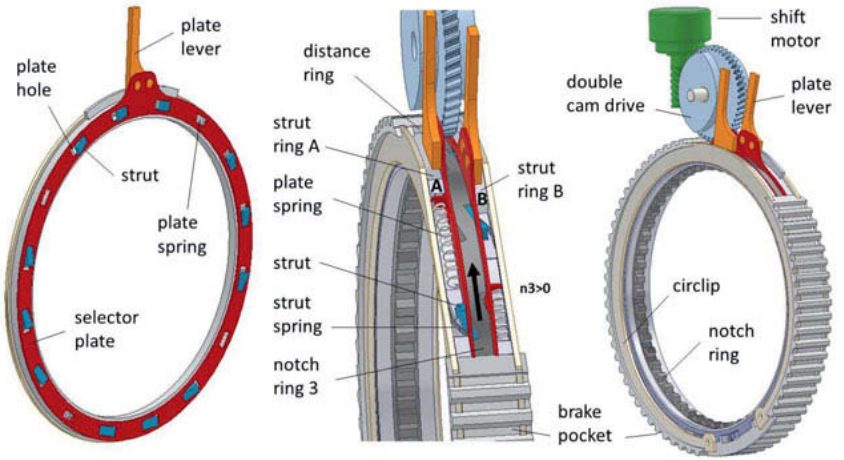

Fig. 11: Shift system with 2 one-way-clutches and electro-mechanical actuator

In order to let the struts engage into the notches of the notch ring, the selector plates have some holes or gaps. The selector plates can be twisted in circumferencial direction relative to the strut-rings, so that the struts can engage through the holes in the selector plates into the notches of the notch rings.

The movement of the two selector plates is carried out by a double cam system, which is driven by a small actuator via a screw gear. The two cams of the double cam system act via contact levers on the selector plates, which are kept in contact with the cams by plate springs.

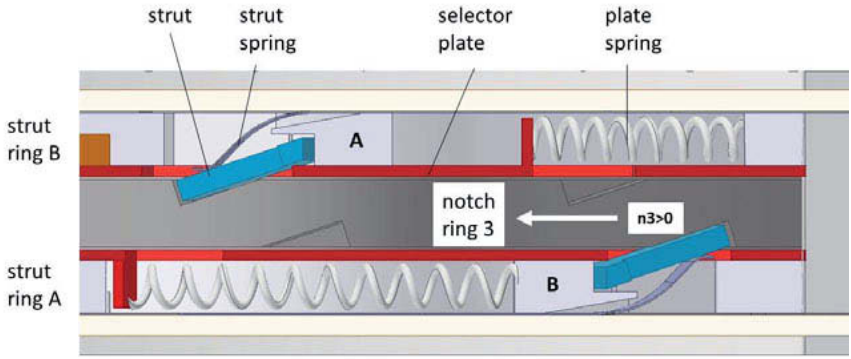

Fig. 12 Strut springs between housing and struts and plate springs between housing and selector plate

Fig. 13 illustrates the shifting positions in the actuator of brake B1. In the starting position (13a) in both freewheels A and B the struts are locked through holes in the selector plates in the notches of the notch rings. In this switching position, the vehicle can be moved forward and backward with the big transmission ratio in mode 1. Shaft 3 is locked to the housing in both directions.

After the start of driving forward, the cam system is twisted by 120° (13b). The freewheel A, which has prevented the forward rotation of the shaft 3, is opened by twisting its selector plate, which moves the struts out of the notch ring. This is particularly easy if the freewheel B exerts a positive torque from the housing on the notch ring. Due to the component tolerances, the freewheel A then is load-free and can be switched easily.

During the shifting from mode 1 to mode 2, freewheel B is also relieved in the torque phase. As soon as the notch ring moves in a positive direction, the notch ring moves relative to the spring-loaded struts, which want to snap in here again and again. Therefore, the cam system is then rotated again by another 120° to in total 240° (13c). The selector plate of freewheel B is then twisted in the other direction against the contour of the cam B, whereby the struts are taken out of engagement to the notch ring. After that, the notch ring can rotate freely within the brake.

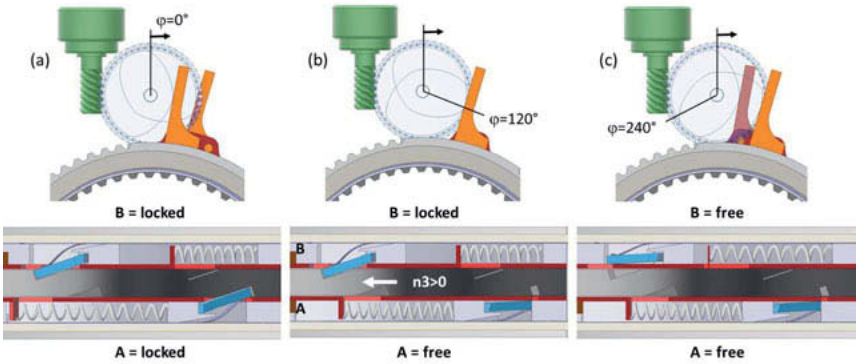

Fig. 13: Shiftpositions in the shiftsystem with the two one-way-clutches A and B

The cams of the actuator system are designed in such a way that in the rotating positions 0°, 120° and 240° the contact normal force on the cam does not create a torques around the camshaft. Thus, the electrically driven actuator is torque-free in these positions and does not require a permanent holding current.

For a reverse drive, both freewheels A and B are closed and locked in brake B1. The shaft 3 is then blocked in both directions of rotation. This is the switching state in brake B1 after the start of the system. As soon as the driver selects the forward movement at the drive switch, a forward movement of shaft 3 is allowed in the brake B1. The corresponding freewheel A is unlocked. Immediately after completion of the torque phase of the shifting according to mode 2, freewheel B is also switched in a release position, so that the struts of the clutch do not snap into the grooves of the counterpart at high frequency. Thus, in mode 2, all freewheels are unlocked.

Hybrid Drive based on this 2-motor and 2-mode transmission

A hybrid drive can easily be derived from such an electric drive with 2 E-motors. The shaft 1 of the speed-overlaying gearbox already has a rotational speed suitable for the coupling of an internal combustion engine. Here, the ICE can be connected via a well-known friction

clutch C1 with an integrated rotary vibration damper. Figure 14 shows such an extended drive structure for hybrid drives.

Conceptually, this is an electrically power-split hybrid drive with E1 on the drive shaft 1 and E2 on a control shaft 4 and the brake B1 on shaft 3t and the common power-output on shaft 2. This drive is related to the hybrid drives with 2 e-motors from Toyota, GM, BMW, Geely and others, but in this case the system is designed for two equally sized electric motors.

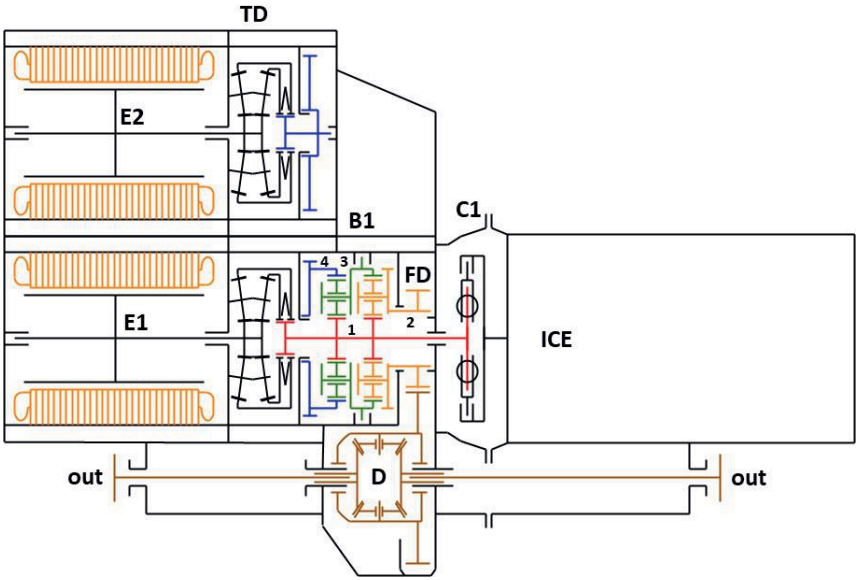

Fig. 14: Hybrid Drive with ICE and E-Drive with 2-EMs and 2-driving modes

Because the internal combustion engine is only switched onto the drivetrain if the vehicle is already in motion and at rotational speeds of the ICE where it is already running smoothly, the vibration damper may be smaller. If the ICE has its own starter, its launch process has no retroactive effect on the output shaft. Instead of a friction clutch C1, whose heat capacity allows a fast ICE-start through this clutch, a clutch-system could be used, which connects the ICE to the drivetrain after a synchronization by the ICE-controller. This would greatly simplify also this coupling device.

Conclusions

Two E-Motors can drive a car and can control the necessary shiftings in a 2-speed / 2-mode transmission system. Further energy consuming accessory drives like actuators and oil pumps for hydraulic systems can be minimised.
With a damping traction planetary gearset as a first speed-reducing subunit the e-motors can run at high rotational speeds.
In a hybrid environment the internal combustion engine assists the electrical propulsion system via a small clutch and damping device.
Because the e-drive with 2 e-motors and 2-modes can also operate as a powersplit transmission with a wide ratio range no further gearbox is necessary for such a hybrid drive.
A wide range of drivetrains for EVs and HEVs can be designed based on these concepts.

References

[1] T. Yaegashi: Toyota Hybrid System THS, Toyota Motor Corporation, 1997

[2] Dong, P.: Modelling and Simulation for Optimized Control of the Shifting Process in Automatic Transmissions with respect to Spontaneity, Comfort, and Shift Loads. Dissertation, Ruhr-Universität Bochum, 2015

[3] Tenberge, P.: Powersplit Plug-in Hybrid with very compact mechanics. 5th International CTI Symposium, Shanghai 2016

[4] Jordan, M., Tenberge, P.: Optimized Start-Stop-Control of a P2-Hybrid. 16th International VDI Congress Drivetrains for Vehicles 2016, VDI-Berichte 2276, S.421-434

[5] Jordan, M., Kupka, D., Tenberge, P.: Control of e-motor-assisted shiftings in dedicated hybrid transmissions, 17th International VDI Congress Drivetrains for Vehicles 2017, VDI-Berichte 2313, digital published

[6] Danzer, C.: Systematische Synthese, Variation, Simulation und Bewertung von Mehrgang- und Mehrantrieb-Systemen rein elektrischer und hybrider Fahrzeugantriebsstränge, Dissertation, TU Chemnitz, 2017

Dedicated Hybrid Transmissions (DHT) by PUNCH Powerglide

Innovative concepts for optimized DHT in terms of efficiency, cost and packaging

Philippe Ramet,
PUNCH Powerglide Strasbourg SAS, Strasbourg Cedex, France

The Automotive industry is currently looking for efficient hybrid transmission concepts suitable for various electrified vehicle architectures. The aim is to find a cost effective alternative to current parallel and power-split hybrid concepts and thus increase affordability and market penetration.

To meet this challenge, PUNCH Powerglide is introducing two novel hybrid concepts that deliver electric and mechanical states using a limited number of gears and dog clutches to maximize efficiency.

DHT CONCEPT AS COST REDUCTION OPPORTUNITY

Car manufacturers around the globe have to hybridize or electrify their vehicle range to meet increasingly challenging CO_2 and emission standards. We all acknowledge that CO_2, emissions and energy transition will be prevalent for the years to come. This is one reason why a holistic approach is required. Unavoidably, this challenge results in additional development effort and costs for all organizations involved in powertrain development.

Hybrid P0 and P1 versions are attractive solutions from a cost perspective. However, they provide limited potential to achieving future emission standards. Other approaches, such as P2, P3 and P4 hybrid solutions, have shown that significant vehicle alterations to integrate an electric motor and power electronics onto the front or rear drivetrain are required.

The main driver for DHT and DHE (Dedicated Hybrid Engines) drivetrains is to facilitate cost reductions for specific sub-systems. The benefits afforded by the electric motor to reduced emissions while maintaining the same vehicle performance, can also support a de-contenting

of the combustion engine and transmission. This is one logical step to compensate for the on-cost of these electrified drivetrain solutions. Cost reduction will be instrumental in facilitating DHT's market penetration.

DHT is a radical transformation of the conventional transmission, bringing new philosophies that need, per definition, permanent electric power management. DHTs driven by an internal combustion engine and an electric machine, offer multiple running modes where the e-machine is used either as a generator or as a motor.

Given the high cost of batteries, amongst other items, further improvements in efficiency (reduction of losses) of the DHT is one of the key success factors.

AMBITIOUS GOALS FOR OEM REQUIREMENTS

Having identified the technical issues, PUNCH Powerglide has developed the following requirements in order to identify suitable dedicated hybrid transmission concepts.

A key objective is to identify technical solutions to optimize gearbox efficiency, while assuring a similar level of comfort and performance as today's solutions. Under such efficiency perspective a weakness of current power-shift transmissions on the market is the use of multiple friction plates for the shifting system. It is generally recognized that dog clutches represents the most efficient solution for this type of connection. However, in today's transmission market, only few have implemented dog clutches and expertise is still limited (ZF 9HP and Renault e-Tech).

In order to limit vehicle electrification cost, a de-contenting approach has been considered for the DHT definition. A solution with four mechanical gear states (ICE) and one electric gear state is sufficient to meet the emission targets. Apart from the significant reduction in the number of components, a considerable benefit is realized in the required installation space.

The project target is to use high-speed IM (induction machine) fully integrated into the DHT where torque, speed and packaging is adapted to suit various hybrid vehicles (modularity). The number of gears and ratios are to be flexible to cater for various vehicle requirements such as gradeability and top speed. Pending on vehicle electric architecture, DHT concepts require one or two electrical machines to achieve all the standard hybrid functions, including the combustion engine restart.

Concepts with two low-power electric machines, with similar or even identical power level, extend the business opportunity to the 48V electric vehicle market, and provide a significant opportunity for further system cost reduction.

From a technical standpoint, even if the concept must utilize dog clutches, the DHT has to be a power-shift transmission – knowing that torque interruption is typically not well perceived by customers – and has to fulfill standard hybrid functions such as regeneration / recuperation, boost mode, and serial mode.

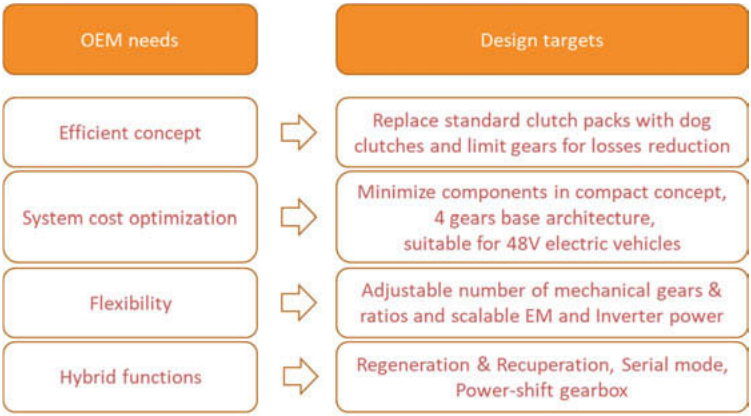

Fig. 1: PUNCH Powerglide's Integrated Hybrid Design Targets

An additional challenge for the DHT concept is to be able to handle different architectures of hybrid vehicles, either with a stand-alone hybrid configuration as shown in Fig. 2, or with an electrified axle as shown in Fig. 3.

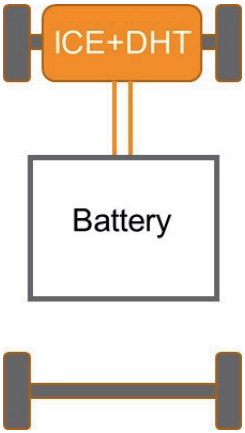

Fig. 2: Stand-alone hybrid vehicle

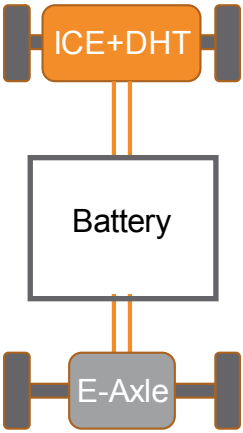

Fig. 3: Hybrid vehicle equipped with an electrified axle

PUNCH POWERGLIDE CONCEPTS: DHT WITH DOG CLUTCHES

PUNCH Powerglide's research outcome has resulted in two DHT with modular powerflow: a first one with a single electric machine (called XT20), and a second one with two electric machines (called XT22).

1. XT20 CONCEPT INTRODUCTION

Equipped with a single electric machine, the XT20 DHT is dedicated to vehicles equipped with an electrified axle (fig. 3).

The core element of the powerflow is a single planetary gear set where the carrier is directly connected to the output shaft, the ring gear to the electrical machine, and the sun to the combustion engine through a C0 connection. This is the key element to enable an EVT mode in which the relative speed of the connection elements is controlled.

This powerflow provides 8 different modes comprising: 1 electric gear, 4 mechanical gears (ICE), 1 EVT mode, and 2 serial modes. Only 5 connection elements are needed to provide these states. In hybrid mode, the torque at the wheel is a combination of the combustion engine and electrical machine torques. In this mode, the electric machine is used either as a generator or as a motor, allowing for boost, regeneration (also at standstill) and recuperation functions.

The primary and intermediate shafts contain all the connection elements and gears. The advantage of this configuration is to limit the number of transmission components, i.e. main shafts, bearings and casings. This arrangement is significant in minimizing the transmission length and helps facilitating the transmission integration into what is typically a limited workspace in hybrid variants. Naturally, lowering the component count also results in cost reduction.

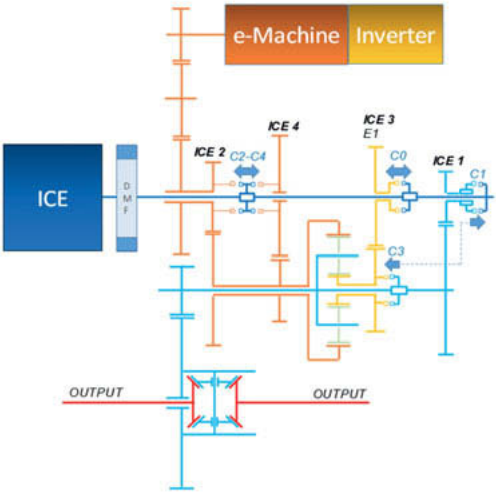

Fig. 4: PUNCH Powerglide's XT20 DHT powerflow

Activation of various connection elements enable the various mode and gear states. These are described in the table depicted in Fig. 5. The ratios shown in this table are only one example and are modifiable through different gear designs, i.e. number of teeth.

In hybrid mode, upshifts and downshifts are performed with the release of one connection element (dog clutch) and the application of another one. However, during this state change, C0 remains engaged putting the transmission into EVT mode. This mode is used to control the speed of the connection elements for shifting into the various states.

Mode	ICE ratio	EM ratio	C0	C1	C2	C3	C4
Hybrid drive 1	8.72	5.61	X	X			
Hybrid drive 2	6.07	8.55	X		X		
Hybrid drive 3	4.16	10.66	X			X	
Hybrid drive 4	2.90	12.06	X				X
E1	/	10.66				X	
EVT	13.79	15.26	X				
Serial mode 2	0.71				X		
Serial mode 4	0.24						X

Fig. 5: XT20 DHT actuation table – 8 modes

1.1. DOG CLUTCH MANAGEMENT TRHOUGH EVT MODE

The advantage of dog clutches is the negligible losses when closed, but especially when open. However, their use brings new constraints on transmission concepts. Engagement and disengagement of a dog clutch is possible only if the relative speed of elements as well as the torque are close to zero. The challenge is even more complex considering that synchronization of dog clutches should take place without wheel torque disruption, to maintain an acceptable shift comfort.

Strategy for dog clutch disengagement in hybrid mode:

In hybrid mode, the reduction of torque required for tooth disengagement of the dog clutch is managed by adjusting the torque distribution between the combustion engine and electrical machine. The kinematics of this transmission has engaged dog clutches physically linked to the combustion engine and electrical machine. Therefore, there is always a torque state where the dog clutch transmitted torque becomes null, allowing the disengagement of the element.

Strategy for dog clutch synchronization before engagement:

The synchronization engagement speed of the dog clutch is achieved again via the EVT mode. In this mode (C0 remains closed), the carrier is connected to the wheel while the electrical machine is connected to the ring gear, and the combustion engine to the sun gear. For a simple planetary gearset arrangement, there are infinite possibilities of motor speeds for a given output speed. Based on this relationship the combustion engine and the electrical speed are controlled until the dog clutch teeth speeds reach the design threshold for engagement. The benefit of the EVT mode is that constant speed at the wheels is maintained while synchronizing the connection elements.

Optimized shift comfort:

The introduction of an EVT mode supports perfectly the dog clutch implementation. The result is a powershifting transmission (refer to Fig. 6 for gear 1 to gear 2 change). However, this specific mode requires precise control of speed and torque of both motors to prevent misengagement and to limit output torque disturbance affecting shift quality. There are tooth design and the actuation selections that improve this concept's implementation success.

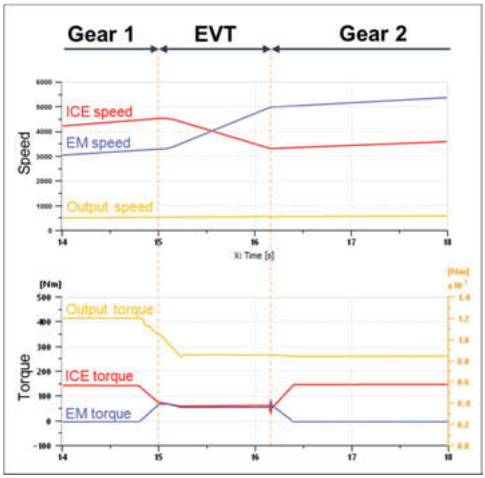

Fig. 6: XT20 DHT Hybrid mode - Gear 1 to gear 2 change

Additional benefit from EVT mode: for vehicle launch

In standard driving conditions, the vehicle launch occurs in pure electric mode. However, in case of low Battery State of Charge (Low SOC), the EVT mode will be used during vehicle launch. While pure electric mode consumes energy from the High Voltage battery, in EVT mode and low speed condition, the electric machine is acting as a reaction element, and therefore as a generator.

As the torque ratio in EVT mode is higher than in first gear, this mode can act as an additional gear to the transmission. Although this DHT concept has four mechanical gears, it can behave as a five-gear transmission if desired.

Combustion engine restart

During transitions from electric to hybrid mode, the combustion engine is restarted using the connection to the electrical machine. However, as the transmission has only dog clutches, the ICE restart is only possible when the vehicle is stopped. While driving, to avoid loss of vehicle traction, the electrified rear axle supersedes the front powertrain during engine restart.

1.2. XT20 DHT PERFORMANCE AND FLEXIBILITY

Fig. 7 shows the traction force in each modes of PUNCH's XT20 DHT. Traction torque depends on ICE (Internal Combustion Engine) and EM (Electric Machine) characteristics, and values shown are only one application example. Here, the maximum available traction force is similar for EVT mode, 1st gear with EM boost, or 2nd gear with EM boost.

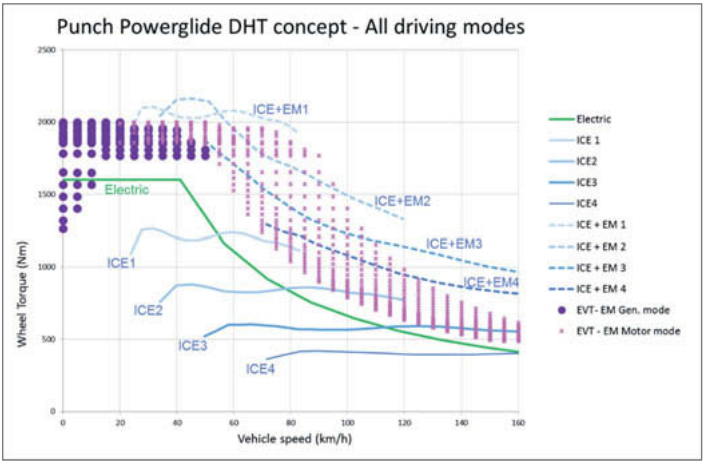

Fig. 7: XT20 DHT performance and traction diagram

The base kinematic variant has been developed to propose four mechanical speeds, which allow a good compromise between functionality and system cost. By applying slight changes within the modular design, the proposed concept can be adapted to a 2-gear transmission with EVT mode or even a single gear transmission. These may be advantageous in supporting a lowest transmission family cost due to common parts on the same manufacturing line.

For example, C1 and C4 (refer table in Fig. 5) could be optional connecting elements which are removed for cost optimization without compromising DHT functionalities.

1.3. XT20 DHT DETAILED DESIGN

A 3D model (Fig. 8) has been developed for a powertrain configuration of 50 kW [150 Nm peak] for the electric motor and 70 kW / 150 Nm for the ICE.

The transmission is designed for a transversal installation using four axes. The ICE is on the primary shaft while the planetary gear set on the intermediate shaft, the differential on the

output shaft and the EM on an offset axis. For integration simplicity, reliability improvement and cost reasons, a common housing is used for the gearbox, the electrical machine and the inverter. As a result, the total length of the transmission does not exceed 350 mm.

Fig. 8: XT20 DHT 3D Model with a 50 kW EM

2. XT22 CONCEPT INTRODUCTION

Equipped with two electric machines (same power), the XT22 DHT is suitable for standard hybrid vehicle configuration (fig. 2) or for hybrid vehicles equipped with an electrified axle (fig. 3).

Kinematic concept:

The powerflow consists of two electric machines, EM1 and EM2, 6 reduction ratios (GS1 to GS6) and 5 dog clutches (A to E).

EM1 is connected to the output via the GS1 and GS3 reductions, the D dog clutch and the GS5 reduction. EM2 is connected to the output via the GS2 and GS4 reductions, the dog clutch E and the GS6 reduction. The dog C connects one path to another at the upstream sides of D and E.

The ICE engine connects to the path from EM1 via the dog clutch A and to the path from EM2 via the dog clutch B.

These connections are depicted in Fig. 9.

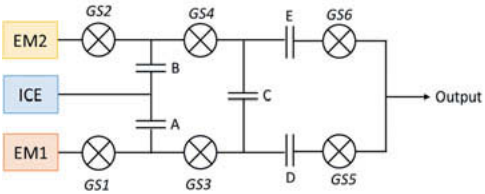

Fig. 9: XT22 DHT kinematic diagram

The powerflow provides 4 mechanical ratios (refer to Fig. 10), 2 electric ratios for EM1 and 2 electric ratios for EM2. The combination of these ratios allows the achievement of 5 electric modes, 10 parallel hybrid modes, 2 serial hybrid modes and 5 serial modes.

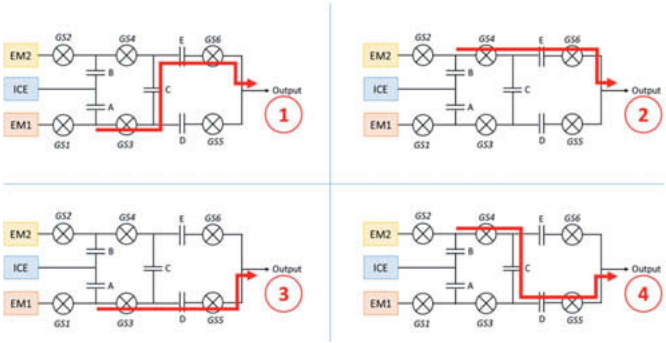

Fig. 10: XT22 DHT mechanical ratios

Only 5 connection elements are needed to provide these different states.

In parallel hybrid modes, the torque at the wheel is a combination of the combustion engine and electric machines torques. In this mode, the electric machines are used either as generators or as motors, allowing boost and recuperation functions.

In serial hybrid modes, a single electric machine transmits power to the wheels, while the other charges the battery with power supplied by the combustion engine.

DHT arrangement:

EM1 and EM2 have their own specific axes. By using chain transfer in EM2 reduction, both electric machines can be installed in the same plane. The primary and intermediate shafts contain all the connection elements and gears. The advantage of this configuration is to limit the number of transmission components, i.e. main shafts, bearings and casings. This arrangement is significant in minimizing the transmission length and helps facilitating the transmission integration into what is typically a limited space in hybrid variants.

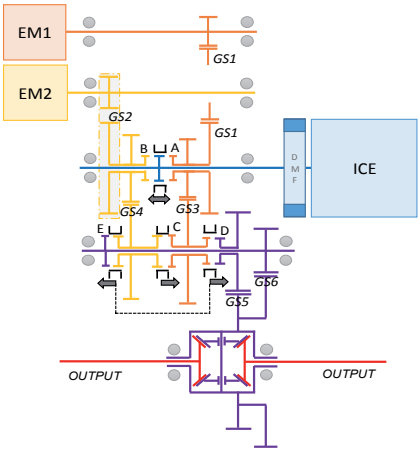

Fig. 11: XT22 DHT powerflow

Activation of different connection elements enable the various mode and gear states. These are described in the table depicted in Fig. 12. The ratios shown in this table are only one example and are modifiable through different gear designs, i.e. number of teeth.

Drive mode				Ratios					Connection state				
MODE	GEAR	Associated EM gear		ICE / ouput	EM1 / ouput	EM2 / ouput	EM1 / ICE	EM2 / ICE	A	B	C	D	E
		EM1	EM2										
Electric mode	Elect 1	/	2	0	0.0	11.9	0	0					X
	Elect 2	1	2	0	22.0	11.9	0	0			X		X
	Elect 3	3	2	0	10.8	11.9	0	0				X	X
	Elect 4	3	4	0	10.8	5.8	0	0			X	X	
	Elect 5	3	/	0	10.8	0.0	0	0				X	
Parallel hybrid mode	ICE1	1	2	8.7	22.0	11.9	0.4	0.7	X		X		X
	ICE2	1	2	6.0	22.0	11.9	0.3	0.5		X	X		X
		2	2	6.0	15.1	11.9	0.4	0.5	X	X			X
		3	2	6.0	10.8	11.9	0.6	0.5		X		X	X
		/	2	6.0	0	11.9	0	0.5		X			X
	ICE3	3	/	4.3	10.8	0	0.4	0.0	X			X	
		3	2	4.3	10.8	11.9	0.4	0.4	X			X	X
		3	3	4.3	10.8	8.5	0.4	0.5	X	X		X	
		3	4	4.3	10.8	5.8	0.4	0.7	X		X	X	
	ICE4	3	4	2.9	10.8	5.8	0.3	0.5		X	X	X	
Serial hybrid mode	Serial Hyb 1	/	2	0	0	11.9	0.4	0	X				X
	Serial Hyb 2	3	/	0	10.8	0	0	0.5		X		X	
Serial mode	Serial 1	/	2	0	0	0	0.4	0	X				
	Serial 2	1	2	0	0	0	0.4	0.7	X		X		
	Serial 3	2	3	0	0	0	0.4	0.5	X	X			
	Serial 4	3	4	0	0	0	0.3	0.5		X	X		
	Serial 5	3	/	0	0	0	0	0.5		X			

Fig. 12: XT22 DHT actuation table

2.1. XT22 POWER-SHIFT CONCEPT

The main strategy to achieve a power-shift with the XT22 concept is to transfer the ICE torque to one or two electrical machines during gear selection. As the electric machines have to maintain a constant output torque, the number of involved machines is depending on ICE torque level at shift initialization.

Therefore, the shift strategy will be selected as followed:

- Through Serial Hybrid mode, using one single machine, for part load conditions
- Through Parallel Hybrid mode, using both machines, for full load conditions

Through Serial Hybrid mode:

An example of such a part load 1-2 power-shift is shown in Fig. 13.

The benefit of this strategy is to shorten the synchronization phase as the electric machine controls the ICE speed during Serial mode transient state. However, this solution is limited by the electric power from one electric machine to the wheels. The gear change through parallel hybrid mode must be preferred in case of a full load shift.

Through Parallel Hybrid mode:

An example of such full load 1-2 power-shift is shown in Fig. 14.

The actuation table shows that two consecutive mechanical ratios have a parallel hybrid mode operating with the associated electric ratio: ICE1 and ICE2 with E12, ICE2 and ICE3 with E32, ICE3 and ICE4 with E34. This feature allows the torque to be transferred from ICE to both electric machines.

Once the torque transfer is complete, the gearbox connection to the combustion engine has to be swapped, from connection A to connection B (or vice versa). While connection A disengages, the available electric mode maintains the requested torque to the wheels. The connection B is engaged when the ICE speed reaches the synchronization speed using its brake torque. The shift is then completed and ICE torque substitutes electric torque.

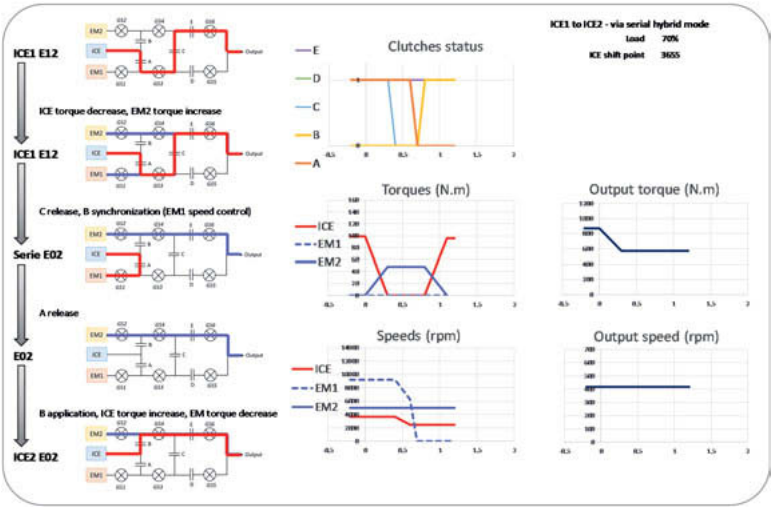

Fig. 13: example of a part load 1-2 power-shift via a serial hybrid mode

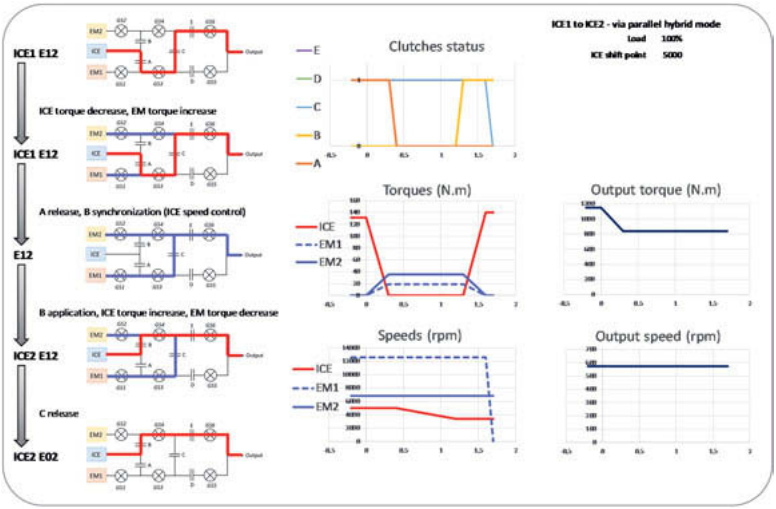

Fig. 14: example of a full load 1-2 power-shift via a parallel hybrid mode

2.2. Vehicle launch

In standard driving conditions, vehicle launch is performed in electric mode. In case of insufficient battery state of charge, the serial hybrid mode is selected: one electric machines powers the wheels and the other one charges the battery (refer to Fig. 15)

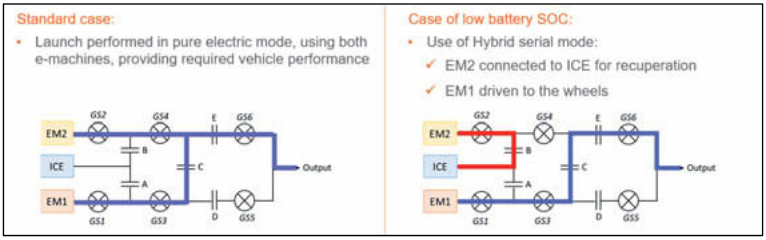

Fig. 15: Vehicle launches

2.3. Combustion engine restart

When the vehicle is moving, any parallel or serial hybrid mode allows the restart of the combustion engine. During engine restart, one electric machine supplies the needed cranking torque while the other one is powering the wheels. In contrast to the XT20 the engine starter motor can thus be suppressed.

Note that Serial mode can also be used in standstill condition to charge the battery, before vehicle launch in electric mode.

2.4. XT22 vehicle performance

The high reduction ratios applied to the electric machines reduces the peak torque requirement to a level suitable for 48-voltage architecture and provides high enough vehicle performance.

Compared to the XT20 concept, for the same electric power at the wheels, EM1 and EM2 power can be halved, which is an additional argument to use a 48V system.

Fig. 16 shows the vehicle performance reached with a XT22 DHT combining ICE at 70 kW (150 Nm) and EM1 ad well as EM2 at 25 kW (60 Nm) peak.

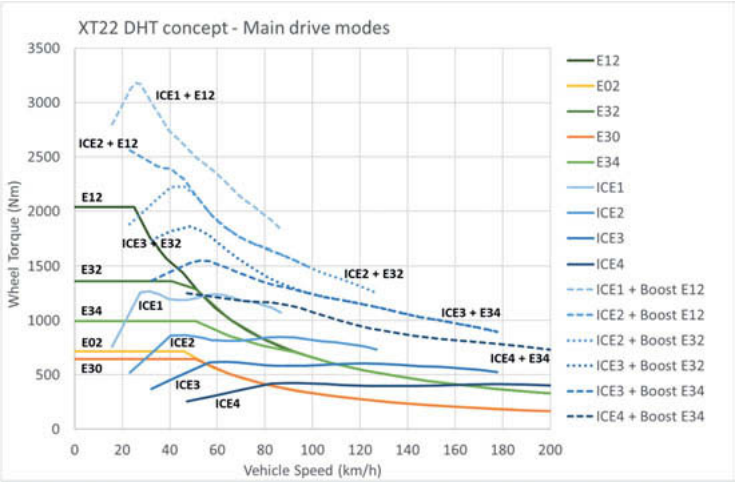

Fig. 16: XT22 DHT performance and traction diagram

OUTLOOK

In the past years, OEMs have introduced HEV/PHEV vehicles using to a large extent existing transmissions and adding electrification concepts such as P0, P1, P2, P3 or P4. The market trend is clearly to develop electric drivetrain solution with increased electrification content and power.

Consequently, more affordable, dedicated solutions with combustion engines are needed. DHTs that are cleverly de-contented are attractive concepts in delivering efficient, compact solutions with comparable performance and comfort compared to currently available solutions at reduced cost. The increasing market share of hybrids will provide the needed volumes for such dedicated drivetrains and thereby help to reduce the overall fleet consumption. It is clearly the logical next step!

New high efficiency CVT for middle class FWD vehicle

Senior Research engineer, **Kwanghun, Kim**,
Hyundai Transys Inc., Korea

Abstract

Many kinds of transmissions have been developing and recently electrification is processing rapidly to reduce fuel consumption. Automatic transmission has been developing in multi-stages to improve fuel economy and power performance. CVT, kinds of transmissions, also need to increase the ratio spread to improve the two performances. Thus CVT has better fuel economy performance through the engine's optimal operating. So, CVT would be a good solution for fuel economy among the conventional transmissions.

The newly developed CVT for FWD vehicles has wider pulley ratio spread than any other competitors. And in spite of wide ratio coverage, CF28 has good competitiveness in the overall length by minimizing the length increase. In spite of reducing transmission length, we had achieved maximum torque capacity, minimum length, highest efficiency, and largest pulley ratio coverage compared to competitors' middle-class CVTs.

Introduction

Recently many kinds of transmissions have been continuously developing to increase driving performance and reduce fuel consumption, And to achieve vehicle mount-ability, it necessary to miniaturize the transmission, because the room for transmission gets smaller and smaller.

The newly Continuous Variable Transmission(CF28) for the front-wheel-drive vehicle which was recently developed, substantially enlarge the torque capacity based on the current Small-CVT(CF18). Nevertheless, the driving performance has greatly improved through the expansion of ratio span, the competiveness of efficiency, weight and overall length is the best in the same class CVT.

The planetary gear was newly designed to reduce the overall length of the transmission and the clutch, hydraulic system, torque converter and oil pump were optimized to improve the efficiency. And the belt & pulley also had been newly designed for the wider ratio span, fewer components, and shorter overall length, lower the weight.

In this paper, the new planetary gear, new belt & pulley system, and newly optimized systems for marketability would be described.

<Specification Comparison>

	CF18 (Existing Model)	CF28 (New Model)
Torque Capacity [kgf.m]	18.3	28
Overall Length [mm]	351	359
Gear Span [UD/OD]	7.0	7.5
Weight [Wet, kg]	73	88

TORQUE-UP, MINIMIZING AND WEIGHT REDUCTION

Figure 1 below shows that the CVT for front-wheel (CF18), which is currently in production, has one planetary gear set, one clutch set and one brake set.

The newly developed CF28 has been increased only 8mm in overall length despite the fact that the torque capacity was increased by 53% compared to the current mass production CF18.

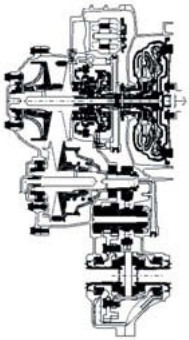

Fig. 1: Cross section of CF18

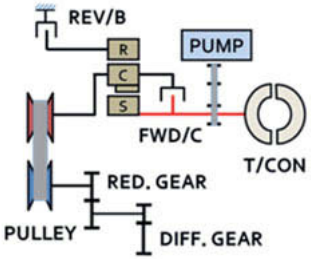

Fig. 2: schematic of CF18

The following is a description of how we were able to minimize the increase of the overall length and weight.

1. Structure of Planetary gear and Brake

To reduce the overall length, it was necessary to change the structure of planetary gear and brake system. Regarding this changes, there are also changes in power flow. The hub of the brake was changed to integrate with carrier rather than the annulus gear. Therefore it was

possible to remove the connecting plate of annulus gear and one thrust bearing, and the overall length could be reduced by 6.1mm. The input of power flow was changed from sun-gear to annulus-gear, and output of power flow was changed from carrier to sun gear.

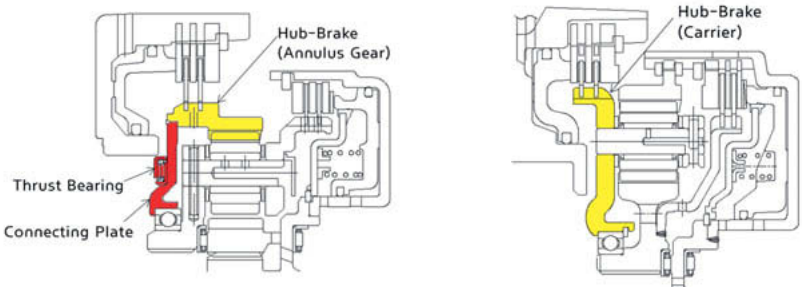

CF18 CF28

Fig. 3: Planetary Gear & Brake

2. Structure of Sheave Connection

To reduce the overall length, it was necessary to change the structure of the pulley system. Fixed sheave and movable sheave of CF18 were connected by rollers so that movable sheave can rotate together with fixed sheave and can move through the fixed shave's axis. But fixed sheave and movable sheave of CF28 were changed to be connected by spline without rollers. Therefore the pulley length could be reduced by 4.2mm. In addition to the overall shortening effect, this change also has an effect on reducing the number of parts and simplification of the assembly process.

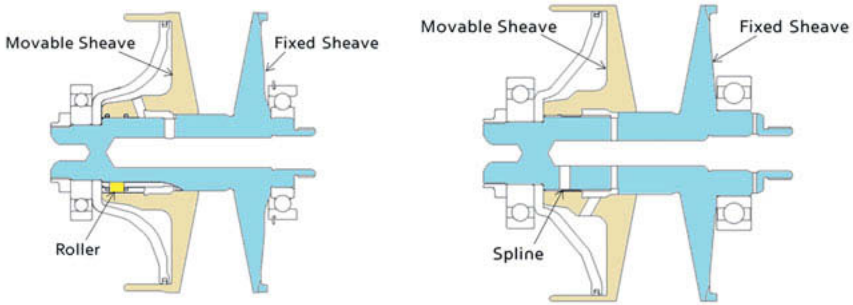

CF18 CF28

Fig. 4: Fixed Sheave & Movable Sheave

3. Optimize the Packaging Condition

To improve the packaging condition on vehicle, packaging analysis had been completed with various vehicles. So, it was necessary for CF28 to optimize external designs of transmission. Design of Housing parts and external devices had been more optimized to improve the mount ability on middle class vehicles. As a result CF28 has a good competitiveness compared to competitors' middle class CVT.(Fig. 5) According to In-Diff. distance, CF28 has two option to satisfy the mount-ability on various vehicles(189mm/204mm). Especially 189mm of In-Diff. distance is difficult condition for constructing internal parts in middle class CVT. This is about 8mm smaller than the competitor's middle class CVT.

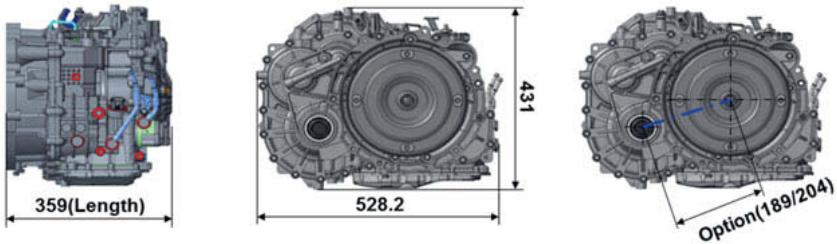

Fig. 5: Package Layout

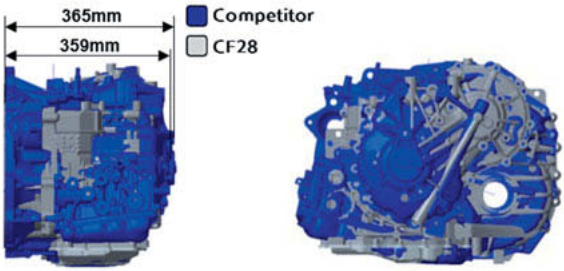

Fig. 6: Comparison of Packaging Condition

EFFICIENCY IMPROVEMENT

Needless to say, the transmission efficiency is more important than ever in accordance with the recent fuel efficiency regulations.

The front-wheel CVT(CF18), which is currently in production, boasts the world's highest level of CVT efficiency. Likewise CF28 has significantly improved efficiency compared to competitor's middle-class CVT.

1. Oil Pump

Oil pump was one of the biggest losses in the transmissions using hydraulic control and We could improve transmission efficiency through optimization of capacity and minimized drive losses. The oil pump of CF28 is vane type, which is able to reduce drive torque loss by maximum 9% in comparison to gear-type pump. It allowed an improvement of 0.4% in CVT efficiency.

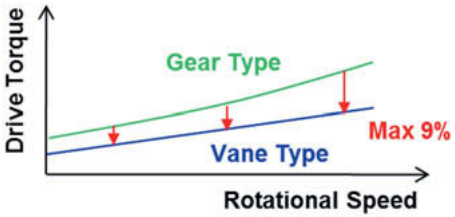

Fig. 7: Comparison of Drive Torque

2. Chain Belt

Chain belt is also important item to improve the efficiency dramatically. The chain was also applied to the CF18 and had been proved to be very efficient compared to the push belt. Chain belt of CF28 has better efficiency of 5% in under-drive area, 3% in over-drive area than push belt of CF28 in same CVT assembly. As a result, chain belt has better efficiency of 1.9% than push belt, It also appeared with a fuel economy difference of 1.2% on vehicle test. It is due to the fact that the chain has less friction loss than the belt.

Chain Belt Push Belt

Fig. 8: Variator of CVT Pulley

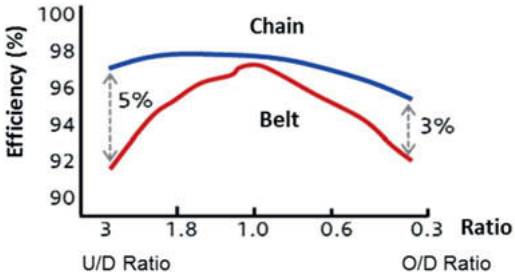

Fig. 9: Efficiency Test in CVT Assembly

3. Separating Spring

Separating springs were applied to reverse brake system to improve the efficiency while driving forward. Because when CVT operates driving forward, the drag torque must be occurred on disk set of reverse brake. Forward clutch does not need separating spring because forward clutch is engaged in step “D” position and drag torque is not generated.

These springs are assembled between the disk set, and help the brake’s each disk to maintain same clearance. This prevents the drag torque loss from increasing because the disk is positioned to one side.

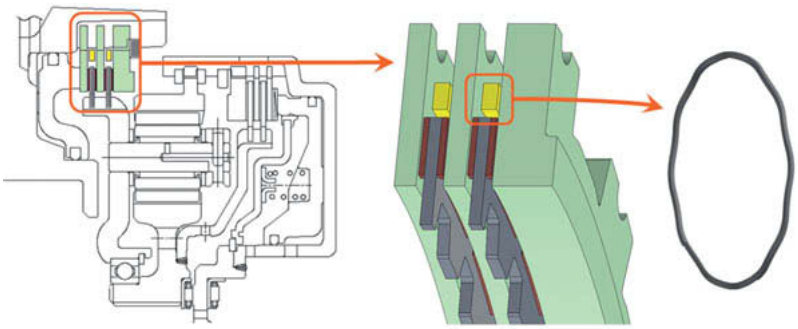

Reverse Brake Disk set Separating Spring

Fig. 10: Separating Spring in Brake

4. Wider Pulley Ratio Span

Ratio span is one of the important performance indicators of transmission. Wider ratio coverage improves fuel economy in the high ratio region and acceleration in the low ratio region. In the high ratio region, the engine speed is lowered to improve fuel efficiency. In the low ratio region, the engine torque is multiplied to improve the acceleration performance.

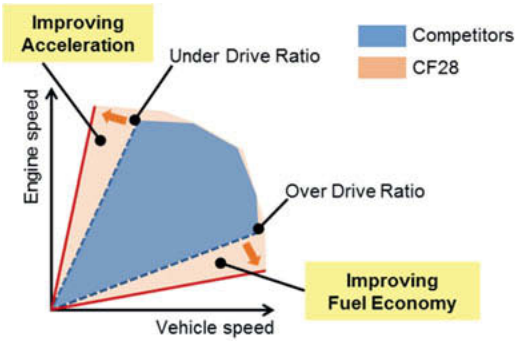

Fig. 11: Wider Pulley Ratio

To increase the pulley ratio width, the distance between two pulleys‘ axes was also increased by 5%. And system analysis had been done to secure stiffness under the worst use conditions, to optimize sheaves in terms of weight reduction.

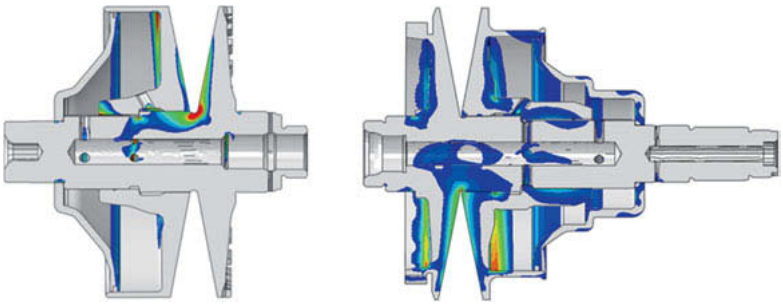

Primary Pulley Secondary Pulley

Fig. 12: Pulley Strength by CAE Analysis

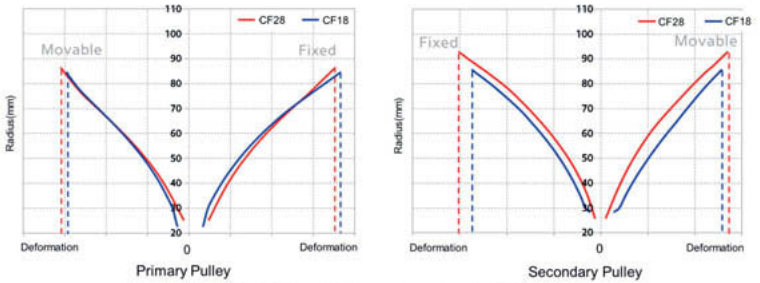

Fig. 13: Pulley Deformation by CAE Analysis

COST REDUCTION

In modern rimes, the competition of the transmissions on the price and efficiency is getting overheated. The cost reduction technologies had also been applied to lower the material cost, and then to improve the marketability of CF28. The price competitiveness of CF28 also reached the world's highest level in the middle class vehicles' CVTs which is currently in production.

1. Single Pinion Planetary Gear

In the case of two-step CVT, simple compound planetary gear set is required, which increases the burden of material cost. But CF28 can shift only by Belt & Pulley; CF28 only needs one planetary gear set for step "forward" and "backward".

To save the material cost and weight, single pinion planetary gear has been applied. The material cost of single pinion type could be reduced by about 27% compared to double pinion type, and also could be reduced by about 50% compared to simple compound type.

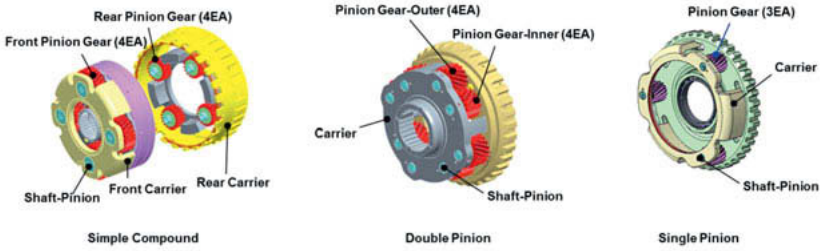

Fig. 14: Carrier Assembly of Planetary Gear

NVH

The CF28 has some noise sources. Planetary gear noise, transfer gear noise, differential gear noise, and chain belt noise are present. First of all, the local stiffness of the case was secured.

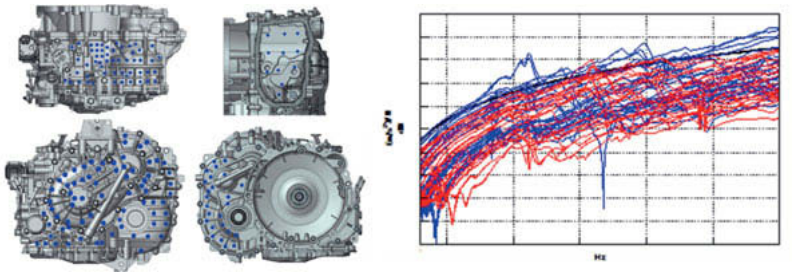

Fig. 15: Housing Local Stiffness

1. Noise improvement of Planetary Gear

In the NVH development, planetary gear‘s noise and transfer gear‘s noise were improved. In the case of planetary gears, the number of teeth was reduced and the bite rate was increased to improve the noise of the planetary gears when driving backward.

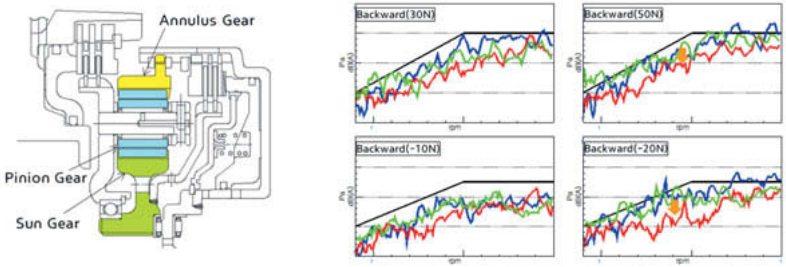

Fig. 16: Noise Improvement of Planetary Gear

2. Noise improvement of Transfer Gear

For improving of transfer Gear’s noise, the internal clearance of the roller bearing supporting the secondary pulley was opimized. As a result, there was a dramatic noise reduction effect than 5dB(A).

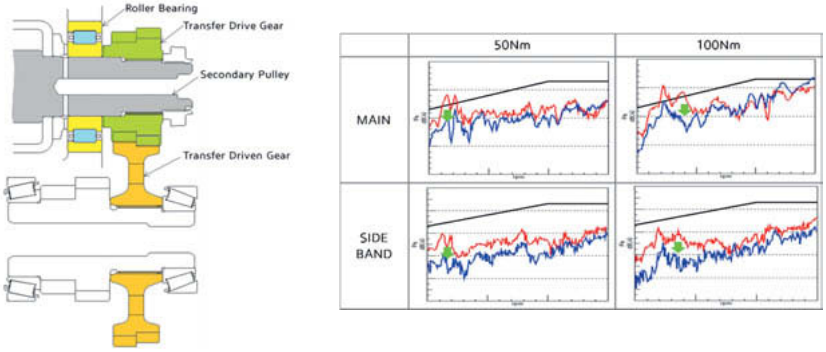

Fig. 17: Noise Improvement of Transfer Gear

3. Noise improvement of Chain belt

In the development, two noises of chain belt were present. The one is impact noise between pulley and chain belt, the other is string vibration noise of chain belt. As string noise is due to the impact noise, the first improving sequence is to lower the impact noise.

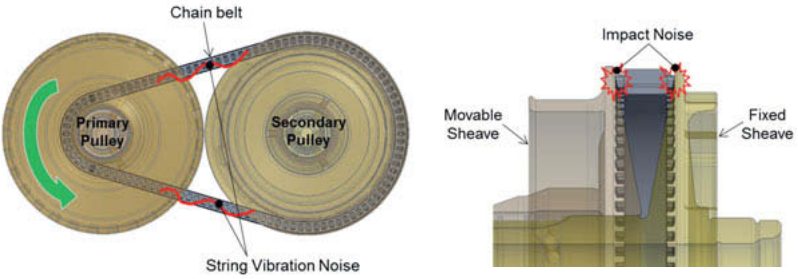

Fig. 18: Noises of Chain belt

The one method for lowering impact noise is to change the sequence arrangement of the chain's two kinds of link plates. Chain has two kinds of link plate(long, short), which is able to avoid the concentration of vibrations at specific frequencies. The other methhod for lowering impact noise is to shorten the pitch(distance between prior pin and next pin) for lowering

impact energy. By reducing the pitch by 15% and optimizing the arrangement of the link plate, it was possible to find the optimal conditions for reducing the impact noise.

The second improving sequence is to lower the chain‘s vibration noise. To lower the chain’s vibration noise, usually two guide-rail sets are added. CF28 also has two guide-rail sets. The shape of the parts was optimized for further noise improvement. In this process, it was also possible to derive the design parameters of the guide rail to reduce the vibration noise of the chain.

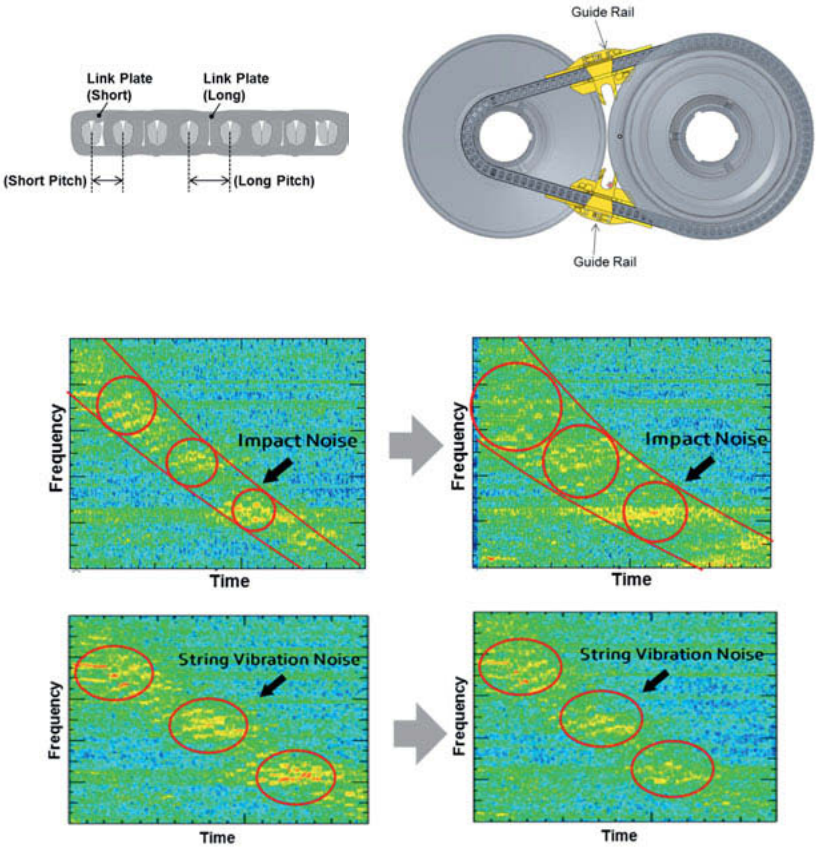

Fig. 19: Improving Noise of Chain belt

OPTIONAL DEVICES

The CF28 is available for various requirements of carmakers by applying various options.

1. ISG (Attached EOP)

ISG (Idle Stop & Go) is an inverter-integrated type that supports vehicle sailing and creep operation and is mounted outside the transmission. It is not necessary to make additional space for the motor controller and wiring between the motor and the controller.

2. Attached TCU

If the customer wants attached type, TCU can be equipped to side part of converter housing of transmission.

3. ATF Cooler/Warmer (Attached)

ATF cooler is equipped to outside the transmission. At low temperature when starting the engine, the ATF temperature of the automatic transmission is increased by using cooling fluid from engine, which can contribute to the improvement of fuel economy by reducing the friction loss due to viscosity reduction.

Fig. 20: Optional Devices

CONCLUSION

In order to reduce the overall length, the hub of brake is integrated with carrier, and the input of power flow was changed from sun-gear to annulus-gear, and output of power flow was changed from carrier to sun gear. The existing connecting plate and thrust bearing were eliminated by this change.

And connecting structure between fixed sheave and movable sheave were changed from roller type to spline type which is integrated with sheaves. In addition to the overall shortening effect, this change also has an effect on reducing the number of parts and simplification of the assembly process. As a result, the CF28 simultaneously achieved torque capacity of 28kgf.m and over length of 359 mm.

In terms of weight, CF28 had achieved 88kg, which is an amazing value of 3.14kg/kgf.m in terms of weight versus torque.

For efficiency of CVT, the pulley ratio span was extended, which was also advantage in acceleration performance. And in addition to, chain belt, vane type oil pump, separating spring had been applied. As a result, the newly developed CVT achieved efficiency of world highest level in the middle class CVT. CF28 achieved more than 2% efficiency compared to competitors' mid-sized cvt.

The new CVT has been designed to give the driver a feeling of shift quality similar to the automatic transmission under certain condition. But this function requires higher durability performance of the transmission. The CF28 meets this high level of durability.

The CF28 has various options available. It is possible to use the ISG integrated with the inverter and extended function to support the sailing and creep operation of the vehicle, the ATF cooler(warmer), and the attached type of TCU.

The newly developed CF28 has been introduced above. The CF28 not only improves marketability by increasing torque capacity of the transmission, but also improves the mount ability by minimizing the increase in the overall length due to the reinforcement torque capacity. And world’s highest level is achieved in terms of torque capacity, efficiency, weight, mount ability. It is considered as the world's best mid-sized CVT in every aspect.

REFERENCE

[1] Yohei Shimokawa, ‘‘Technical Development to Improve Jatco CVT8 Efficiency“ SAE International Paper, 2013-01-0364.

[2] Daisuke Niii, Hiroki Kondo, Taichi Washio, Shinya Kuwabara, and Masanori Shimizu. Toyota Motor Corporation. ‘‘Development of New Continuously Varible Transmission for 2.0-Liter Class Vehicles“, SAE International Paper, 2018-01-1062.

10R80 MHT

Cost Efficient Modular Hybrid Transmission (MHT)

Greg Gardner, Ford Motor Company, Livonia, MI

Abstract

Increasing focus on fuel economy has driven the need for hybridization across multiple vehicle platforms at Ford. While powersplit hybrid architectures are well suited to front wheel drive applications, the lack of a mechanically connected reverse gear is an inhibitor to using these architectures in larger rear wheel drive vehicles that have significant towing capability. Ford needed a rear wheel drive hybrid architecture that could deliver improved fuel economy, provide a mechanical reverse gear for towing applications, and package into existing rear wheel drive architectures. In order to accomplish this a modular hybrid architecture that was an add on to the existing 10R80 transmission was adopted. This paper explores the development goals of the 10R80 MHT architecture and discusses the advantages achieved with this approach to rear wheel drive hybridization.

Introduction

Ford introduced its first-generation Ford Escape Hybrid in 2005. In the 15 years since this introduction Ford has grown to be the second in the industry in terms of Hybrid's produced with 780,000+ in global sales. In addition, in the last three years Ford has received over 1300 patents for hybrid technologies. The company has plants to invest an additional 11 billion US dollars in electrifications by 2022 and has also made a half billion US dollar investment in a strategic partnership with Rivian.

Hybrid Portfolio

Figure 1 illustrates Ford's hybrid portfolio. Lighter vehicles are built around a front wheel drive platform that utilize power split eCVT technology to deliver hybridization. Larger vehicles that require higher payload and towing capability utilize the new rear wheel drive modular hybrid architecture to deliver hybridization without compromising on high payload/towing requirements.

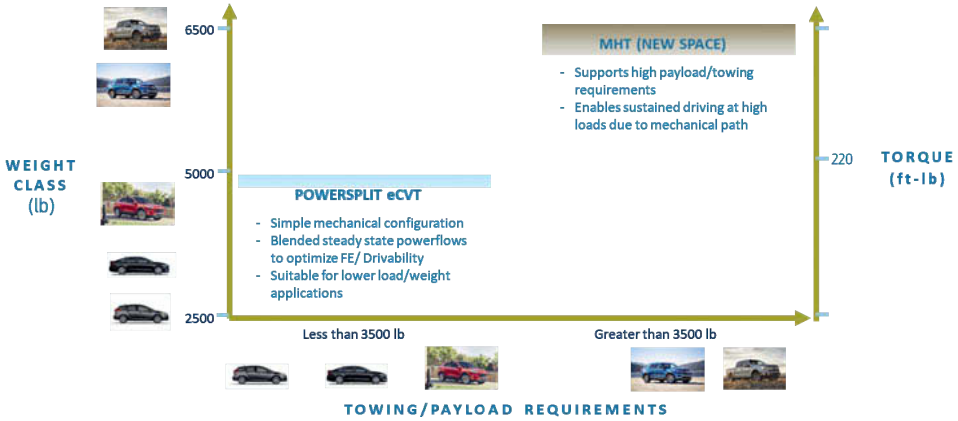

Fig. 1: Ford's Hybrid Portfolio

Program Goals

The goals of the MHT program were to deliver a no compromise rear wheel drive hybrid powertrain that delivers improved efficiency, increased range, equivalent interior space to a conventional internal combustion engine (ICE) powertrain while delivering equivalent towing and off-road performance and durability equivalent to ICE powertrains. In addition the program needed to $_{\text{utilize}}$ the existing rear wheel drive footprint in place at the Livonia Transmission Plan.

The resulting transmission was integrated and assembled by Ford in conjunction with our supplier partners. Hitachi manufactures the motor and inverters which are integrated with an MHT module engineered and manufactured by Schaeffler. The MHT transmission combined with a liquid cooled battery pack that is totally hidden from the customers delivers enhanced powertrain efficiency, delivering lower CO_2 and evaporative emissions while at the same time providing improved performance capabilities without compromising 5,000 pound towing capability. Key specifications are detailed in Table 1.

Table 1: MHT Performance Characteristics

Power (KW)		Torque (NM)
213 @ 6500 RPM	Engine (Regular Fuel)	353 @ 4000 RPM
33 @ 3500 RPM	eMotor (Adjusted for Losses)	300 @ 5000 RPM
237 @ 6500 RPM	TotaL System	437 @ 2500 RPM

Manufacturing Footprint

A key goal of the MHT program was to utilize an existing manufacturing footprint at the Ford Livonia Transmission Plant. As a result a bolt on module developed by our supplier partner Scaheffler was utilized. The base 10R80 transmission architecture changes were kept to a minimum by utilizing motor cooling and clutch feeds/controls integrated into a stand alone e-pump module. This allowed the transmission to be assembled on the existing 10R80 assembly line allowing for quick adaptation to changes in hybrid demand.

MHT Design Features

The MHT hybrid application has 90% common parts with the 10R80 transmission. The differences include a modified oil pan with hydraulic feeds to the bolt on MHT module and a unique e-pump that incorporates controls for the MHT K0 clutch. Figure 2 provides a cross-section of the 10R80 MHT Transmission

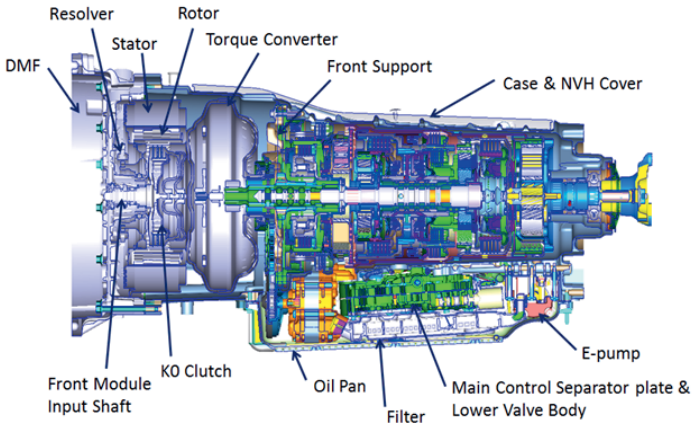

Fig. 2: 10R80 MHT Transmission

Conclusions

The MHT transmission enables Ford to deliver a no compromise rear wheel drive hybrid architecture while maximizing the existing 10R80 manufacturing footprint. This engineering efficient design is enabled by close cooperation with Hitachi on e-machines and Schaeffler on module development.

The High-Efficiency Fully Electric Drivetrain of the New Porsche Taycan

Dr.-Ing. **Thomas Casper**,
Dipl.-Ing. **Gerhard Spengler**,
Dipl.-Ing. (FH) **Matthias Bromberger**,

Dr. Ing. h.c. F. Porsche AG, Weissach

Zusammenfassung

Mit dem neuen Taycan hat Porsche eine neue Ära eröffnet. Nach den erfolgreichen Hybrid- und Plug-in-Hybrid-Modellen im Cayenne und Panamera sowie dem Supersportwagen 918 Spyder ist der vollelektrische Taycan die konsequente Weiterentwicklung der Porsche Elektrifizierungsstrategie. Dabei stand bei der Elektrifizierung immer auch der Zugewinn an Fahrspaß und Performance im Blickpunkt.

Im vorliegenden Bericht wird das Allrad-Antriebskonzept des Porsche Taycan vorgestellt und im Detail auf die Vorder- und Hinterachsgetriebe eingegangen. Insbesondere das Zweigang-Hinterachsgetriebe stellt dabei ein Highlight dar. Es ist seit mehr als 25 Jahren das erste von Porsche wieder selbst entwickelte Getriebe. Konsequente Optimierungen der Effizienz und konstruktive Gewichts-Reduzierungsmaßnahmen werden aufgezeigt. Die daraus ent-standenen Getriebe prädestinieren sich für den Einsatz im Porsche Taycan.

Abstract

With the new Taycan, Porsche has opened a new era. Following the successful hybrid and plug-in hybrid models in the Cayenne and Panamera, as well as the 918 Spyder super sports car, the fully electric Taycan is the logical further development of Porsche's electrification strategy. The focus of electrification has always been on increasing driving pleasure and performance.

This report presents the all-wheel drive concept of the Porsche Taycan and goes into detail about the front and rear axle transmissions. The two-speed rear axle transmission is a particular highlight. It is the first transmission developed by Porsche in-house in more than 25 years. Consistent optimizations of efficiency and constructive weight reduction measures are shown. The resulting transmissions are predestined for use in the Porsche Taycan.

1. Introduction and Targets

As early as 2010, the Cayenne S Hybrid became the first Porsche to rely on a powertrain with integrated electric drive. For Porsche, this was the cornerstone of a well-though-out strategy. Even then, the potential of powertrain electrification was recognized, not only from the efficiency but also, and above all, from the performance aspect. In the years that followed, Porsche consistently developed the technology further with great market success (Fig. 1).

The 918 Spyder showed that electrification can further enhance the performance of even super sports cars. In the Panamera and Cayenne models, plug-in hybrid models mark the top of the range, for example the Panamera Turbo S E-Hybrid. As a consistent further development of the adopted strategy, and to complete the successful product portfolio, the introduction of a purely electrically powered sports car was the logical next step.

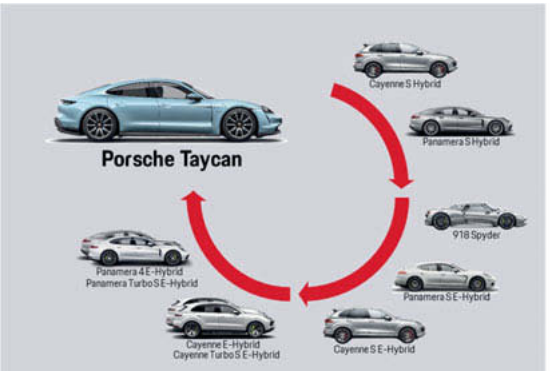

Fig. 1: Chronological development of electrification at Porsche

A New Era

The Taycan combines values such as innovation and tradition in an absolutely unique way - typical Porsche. With its 800-volt technology, it points the way to the future of e-mobility. At the same time, in the best Porsche tradition, it stands for pure emotion and particularly high driving pleasure. This makes the Taycan the sports car in the electric vehicle segment. To live up to its claim of being the leading supplier of exclusive, sporty mobility, Porsche is presenting the Taycan, a sports car with up to 560 kW of overboost power when using Launch Control.

The First of its Kind

The Taycan was designed from the ground up as a purely electrically powered sports car (Fig. 2). The resulting degrees of freedom were used to get the most out of the vehicle concept in terms of technology. The low and central installation position of the performance battery contributes to a very low vehicle center of gravity and an optimum balance between front and rear axle. In combination with Porsche's highly developed suspension systems, this results in lateral dynamic capabilities of a kind never before seen in a four-door sports sedan.

Fig. 2: Targets of the Porsche Taycan

In combination with electric drive units, the special battery management system ensures breathtaking longitudinal dynamics, coupled with exceptional continuous performance and reproducible driving performance at a new level for electric vehicles. The Taycan accelerates from 0 to 100 km/h in a fantastic 2.8 seconds and covers a distance of 28 meters in 2.5 seconds - surpassing the 918 Spyder. The Taycan thus offers exactly what is expected of the sports car in this segment: an amazing, sporty driving experience that only a genuine Porsche can offer (Fig. 3)

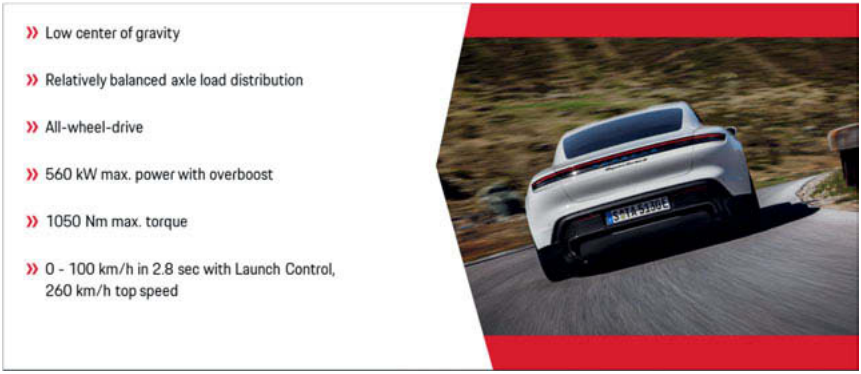

Fig. 3: Requirements for the Porsche Taycan Turbo S

2. Electric Drive Units of the Porsche Taycan

Electrical Machines

In the Porsche Taycan, a permanent magnet synchronous machine is used on the front and rear axle respectively (Fig. 4).

The rotor of the permanent magnet synchronous machine consists of high-quality permanent magnets, which generate their own magnetic field. Their speed is generated by the 120° phase-shifted electromagnetic rotary field in the stator coils. The synchronous motor has a high efficiency and a high power density, which leads to the following effects in the Taycan:

- high reproducibility
- high continuous output
- longer range
- high power density and thus lower weight.

In the Porsche Taycan, the e-drives are particularly powerful and also enable several acceleration runs in succession without any problems.

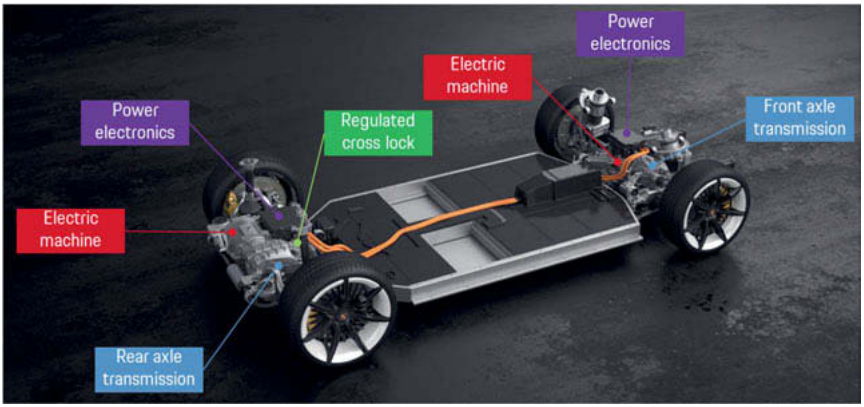

Fig. 4: Arrangement of the drive units of the Porsche Taycan Turbo S

The permanently excited synchronous machine on the front axle has an active length of 160 mm and a diameter of 190 mm. The one on the rear axle has an active length of 210 mm and a diameter of 245 mm. While the machine on the rear axle is mounted parallel to the output shaft, the machine on the front axle is mounted coaxially. This made it possible to make much better use of the installation space in the front of the vehicle.

Transmission Concepts

In the concept phase, initial investigations showed that high drive and recuperation torques can also be applied to the front axle due to the low center of gravity and the almost even axle load distribution. This means that the installation space for a drive unit on the front axle had to be optimally utilized in the tight package of the front end of the vehicle. For this reason, the original parallel-axis solution was rejected and converted to a coaxial solution with the lowest weight and installation space requirements (440 Nm and 16 kg dry weight of the transmission) (Fig. 5). The detailed design of the front axle gearbox is shown in chapter 3.

The rear axle drive unit in particular had to solve the conflict between a very high acceleration capacity and a simultaneously high final speed. After determining the electrical power, calculations showed that this conflict could only be resolved with a two-speed transmission without making major compromises in performance. Due to the corresponding demands on installation space for the electric machine with the power electronics and the two-speed transmission, the rear drive unit could only be designed as an parallel-axis structure (Fig. 5). The detailed design of the rear axle transmission is shown in chapter 4.

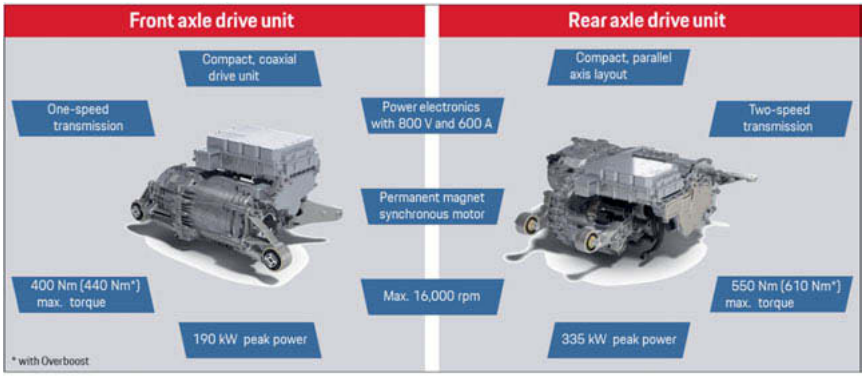

Fig. 5: Drive units of the front and rear axle

Tangential Force Diagram

Nowadays, modern simulation tools make it possible to represent driving performance very reliably and to predict it already in the concept phase. However, it is very helpful for the development engineers in the design department to be able to perform rough design calculations with sufficient accuracy using simple calculation tools. A very helpful method is given by the tangential force diagram, which is explained in more detail below.

The tangential force distribution diagram (Fig. 6) was developed in the early seventies of the last century to graphically determine the brake force distribution of a motor vehicle when driving straight ahead. Later it was further developed and also used to depict an optimum drive force distribution. In order to be able to show different quantities in a diagram, they were made dimensionless by dividing them by a corresponding quantity (e.g. wheel contact force divided by the longitudinal force on the wheel, which corresponds to the coefficient of friction μ between the tire and the road).

The following quantities are included in the tangential force diagram:

- Vehicle weight
- Center of gravity position in relation to the front axle
- Center of gravity height to the road
- Wheelbase
- Normal forces on front and rear axle
- Tangential forces on front and rear axle
- Air resistance

- Rolling resistance
- Gradient of the road
- Vehicle speed

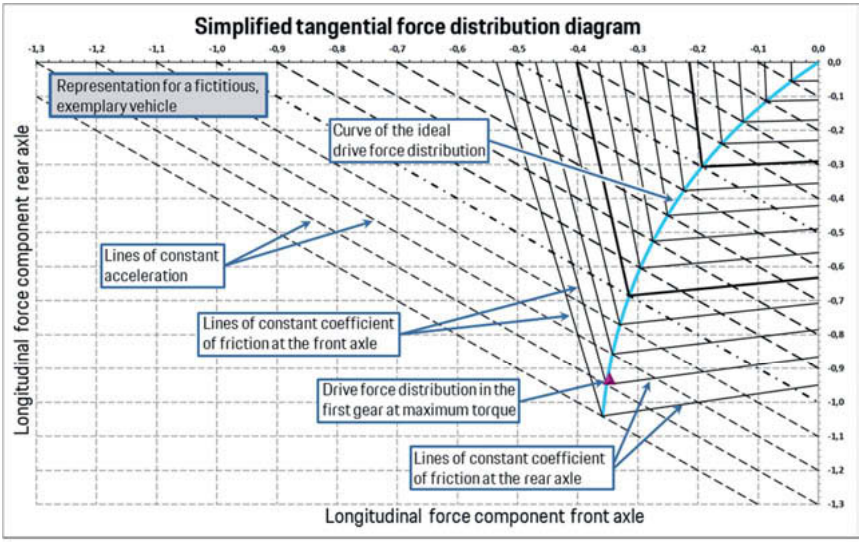

Fig. 6: Tangential force diagram, exemplary for a fictitious vehicle

The blue curve in Fig. 6 is a parabola and represents the ideal drive force distribution, i.e. it is generated from the points of intersection where the drive force (tangential force) on the front and rear axles has the same coefficient of friction between tire and road.

The drive force distribution of the vehicle is marked with a red triangle (Fig. 6). It results from the calculated longitudinal force on the front and rear axle in relation to the vehicle weight, depending on torques, rotating masses, efficiency, transmission ratios and wheel radii.

If this point lies exactly on the parabola, the same coefficient of friction is used on the front and rear axle at maximum acceleration. This means the acceleration of the vehicle is ideal. If the point lies to the right of the blue curve, the rear axle starts slipping first. If the point is above the curve, the front axle slips before the rear axle. In both cases, acceleration performance would have been lost.

Composition of Tractive Force and Wheel Torque

After the performance data of the electric machines and the transmission ratios of the two gears have been determined, the torques on the front and rear wheels can be shown. The interaction between tractive force and wheel torques is shown in Fig. 7.

Depending on the determined gear ratio, the torque applied to the electric machine results in a total wheel torque per axle. The diagram shows for the Taycan Turbo S which total wheel torque per axle and gear (without overboost) is possible and which total wheel torque can be achieved with the vehicle.

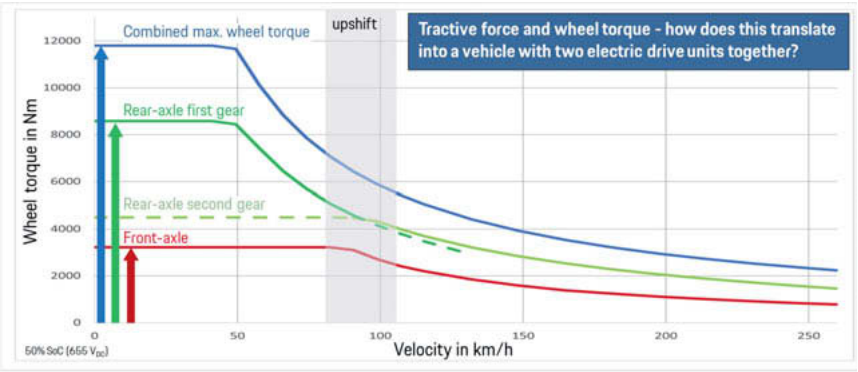

Fig. 7: Tractive force and wheel torque of the Taycan Turbo S (without overboost)

3. Front Axle Transmission Design

The front axle transmission, which was developed in a development partnership with Schaeffler on behalf of Porsche AG, consists of two planetary gear sets with a narrow spur gear differential (Fig. 8).

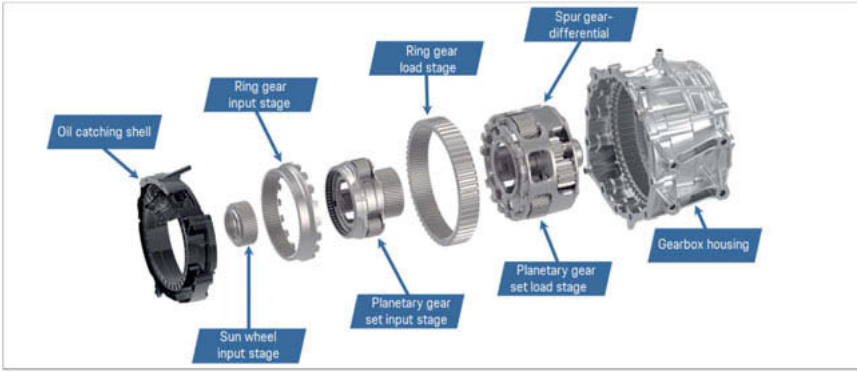

Fig. 8: Components of the front axle transmission

The sun of the first planetary gear set (input gear set) sits on the rotor shaft of the electric machine, the ring gear is attached to the planet carrier of the second set. The planet carrier of the input gear set carries the sun of the second planet gear set (load stage). The ring gear of the load stage is non-rotatably mounted in the housing, the planet carrier serves as output and also houses the planets of the spur gear differential.

Between the input sun gear and an intermediate shaft, which forms the connection to the drive shaft at the end of the electric motor, there is a radial shaft seal ring, which seals the oil chamber of the gearbox towards the electric motor. The design of this seal poses its own challenges, as the rotary shaft seal is not fixed to the housing as usual, but rotates at a maximum of 16,000 revolutions per minute.

Here are a few general points about the front axle transmission:

- The lubrication of the torque-conducting components is passive (no oil pump), the oil quantity of 0.73 litres is due to the compact design (Fig. 9).
- The breather of the gearbox compartment had to fit into a very tight package. Cavities and clever oil routing were used accordingly.
- The gearbox is cooled via the flange to the electric machine. Therefore, a carrier frame gasket made of aluminum sheet was provided here to ensure an unhindered heat transfer from the gearbox housing to the stator housing of the electric machine.

Fig. 9: Front axle transmission assembly

4. Rear Axle Transmission Design

The two-speed transmission installed on the rear axle of the Taycan is a completely in-house Porsche design that was made for the specific requirements of the Taycan. With its transmission ratio design and overall concept, it makes a significant contribution to very high acceleration and high maximum speed at the same time (Fig. 10).

The gearbox is based on three shafts. In addition to the two spur gear stages, which technically represent the transmission ratio of the second gear, a shiftable planetary gear set is also used, which enables a corresponding reduction for the first gear. This is designed to be very short with a ratio of approx. 15:1. In first gear, Launch Control provides a total wheel torque of over 12,000 Nm in the Turbo S (total of front and rear axle drive unit). The result is an impressive starting acceleration.

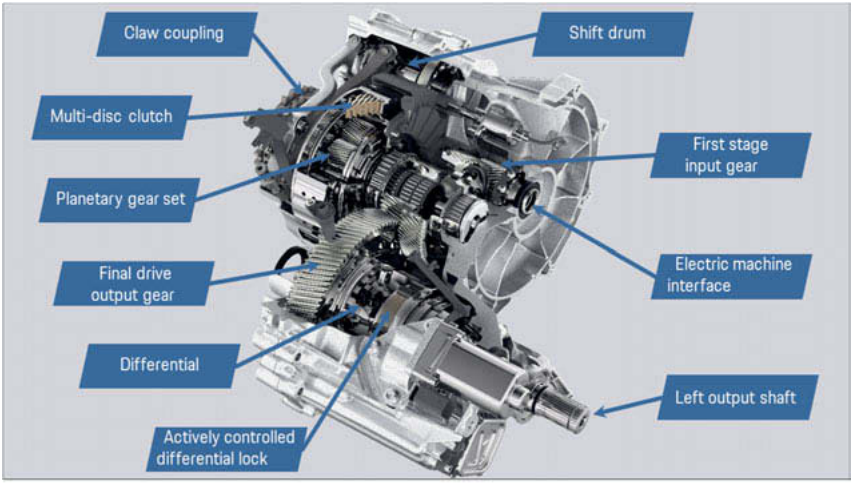

Fig. 10: Rear axle transmission of the Porsche Taycan

The second gear is considerably longer, with a ratio of 8:1. This allows for typical sports car acceleration reserves at high speeds and a top speed of up to 260 km/h. Also from an efficiency point of view, the Taycan with its two-speed transmission offers optimum efficiency at higher speeds. In second gear, the friction clutch is closed and the planetary gear set rotates as a block. In order to increase the efficiency of the multi-plate clutch, it is designed as a "normally-closed-clutch" with a membrane spring.

The two speeds are achieved with the aid of a freewheel, a claw clutch and a multi-disc clutch. This allows for shifts with uninterrupted tractive force as well as using the impulse from the rotating mass to improve acceleration.

The first gear is not needed in the range mode designed for maximum efficiency, as the high starting torque is sufficient to start in second gear. The second gear is also preferred in the comfort-oriented normal mode. In the dynamically designed Sport and Sport Plus modes, on the other hand, first gear is used more frequently, especially for starting and accelerating. Launch Control is also available in these modes. In this mode, the transmission remains in first gear for a relatively long time before shifting into second gear in combination with an impulse-aided shift.

The function of the parking lock was realized by using a dog clutch and a friction clutch by engaging the two gears simultaneously. This eliminates the need for a (classic) parking lock with its associated actuation, further reducing the transmission weight.

5. Efficiency Optimizations

As with conventional vehicles, a development goal for purely electric vehicles is to optimize the efficiency of the individual components as far as possible. In order to achieve a long range under normal conditions, the efficiency of all components in the powertrain must be brought to the highest possible level so that as much electrical energy as possible is converted into propulsion.

The goal to be achieved was to implement the Porsche philosophy of "Intelligent Performance" in hardware. As already mentioned, the development goal in the Taycan Turbo S was a top speed of 260 km/h and acceleration capability at the edge of the rear wheel slip limit. These two requirements could only be achieved with a two-speed transmission at the given drive torque of the electric machine. The additional losses of the more complex design had to be compensated by a higher overall efficiency of the transmission.

The following measures for a very good efficiency were implemented in the rear axle transmission (Fig. 12):

- Low-viscosity lubricating oil with optimized power loss for lubrication systems.
- Electric oil pump with lubrication as required.
- Encapsulated final drive gear with targeted oil flow (Fig. 11)
- Guided recirculation of slung oil into a settling chamber to reduce splash losses
- Multiple use of oil streams through cascade lubrication.
- Single-actuator solution for shifting with lowest possible energy consumption (energy consumption only during shift).
- Multi-plate clutch in "normally closed" design.
- Planetary gear set rotates as a block in main gear (second gear), eliminating gear and bearing losses from the planetary gear set.

Fig. 11: Encapsulation output wheel

- Use of efficiency-optimized bearings (for example optimized taper roller bearings).

The oil supply of the gearbox is designed in such a way that excess oil is avoided to reduce splash losses and bearings, gear teeth and other lubrication points are lubricated as accurately as possible (Fig. 12).

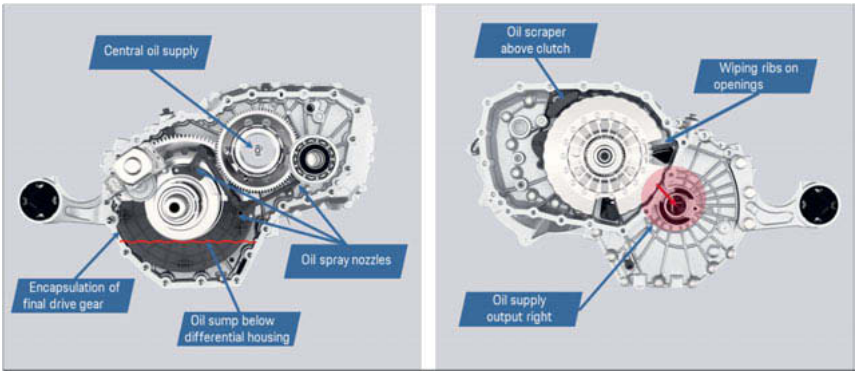

Fig. 12: Rear axle transmission oil supply

As an example, the effect of the oil scraper on the outer plate carrier of the multi-plate clutch is shown below. The oil scraper ensures that the splashing oil from the multi-plate clutch is collected and directed to the other lubrication points. If this were not the case, too much oil would accumulate in the clutch area and lead to considerable drag torque losses. By this measure alone, the drag torques, especially in first gear, could be significantly reduced even at low, but especially at relatively high speeds (Fig. 13).

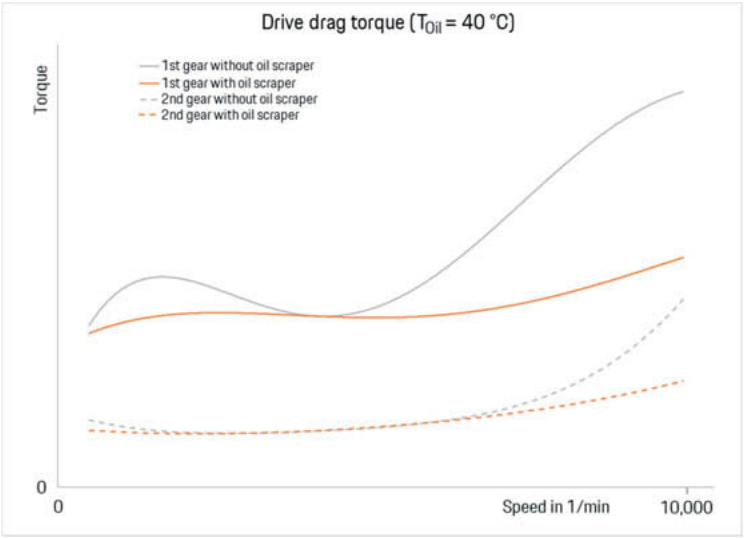

Fig. 13: Reduction of drag torque through use of oil scraper

6. Weight Optimization

The drives do not contain any materials that are "exotic" or unusually expensive (e.g. titanium, magnesium or high-strength plastics). All components were optimized at Porsche itself in terms of design and weight. Simulation tools were developed for gear load patterns, also for the gear-rolling simulation of the gears in the finite element calculation. The wheel bodies and the webs were optimized in terms of weight and load-bearing behavior of the gearing. All components, including those of the actuators, were improved and further developed with regard to minimum material usage. For example, all large gears have holes, as does the freewheel carrier. The webs of the gear wheels are very narrow. All levers, the freewheel, and claw components are weight-optimized forged parts. The housings were made lighter with each stage of construction and continuously adapted to the loads and necessary installation space.

Here are some concrete examples of weight reduction measures:

- In the assembly of the planetary gear set and the multi-plate clutch, screw connections were replaced by caulking and rolling of components. By saving on individual components, it was possible to achieve weight reductions while at the same time reducing assembly complexity. (Fig. 14)

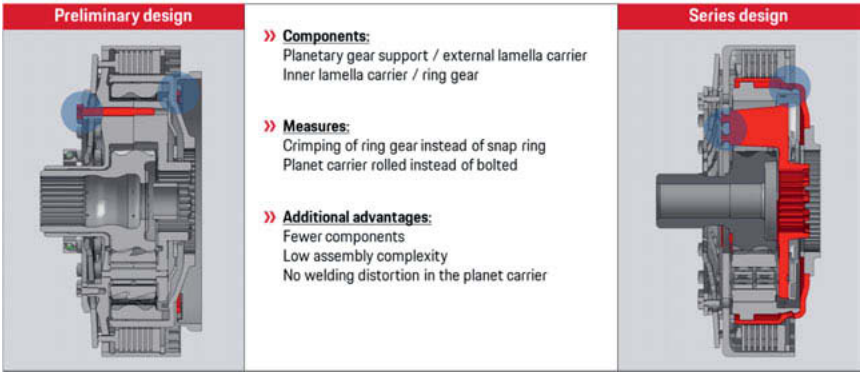

Fig. 14: Weight optimization – planetary gear stage

- For the first construction stage the final drive gear was screwed to the differential cage. This solution was replaced by welding in later development stages. This redesign provided additional possibilities for the weight-optimized design of the gearwheel web from an "I" to a "Z" shape. This "Z" shape, which was also applied to a further spur gear stage by means of the finite element displacement calculation, made it possible to implement a uniform, weight-optimized force transmission into the components. (Fig. 15)

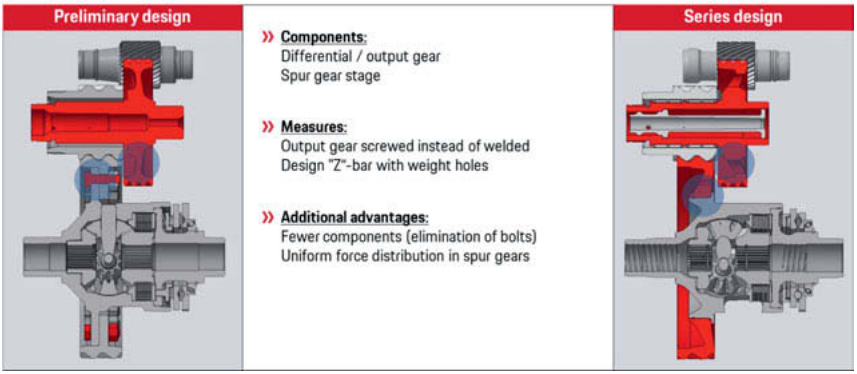

Fig. 15: Weight optimization – output wheel to differential

- Standard bearings were initially used for the bearings of the spur gear stages. After further analyses and calculations, the double-row angular contact shoulder bearing was replaced by two axial and one radial needle roller bearing; a needle roller sleeve replaced the relatively bulky cylindrical roller bearing. Although the design of the radial needle roller bearing without bearing inner ring increased the strength requirements on the shaft surface in the area of the bearing raceway, the overall advantages clearly outweigh the disadvantages. In addition to the weight reduction, the load carrying capacity was increased, the efficiency improved and the shaft deflection reduced due to the increased diameter. (Fig. 16)

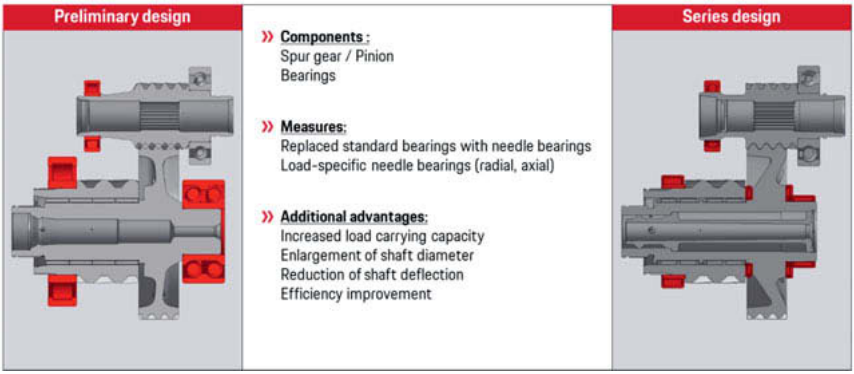

Fig. 16: Weight optimization – bearing selection

The weight optimization measures implemented during the course of development from the first design to series production design reduced the weight of the rear axle transmission by a total of 9.8 kg.

7. Summary

This article showed that Porsche has succeeded in opening the new era of all-electric sports cars with the new Taycan model. The consequent layout and design of the front and rear axle drives, the combination of powerful electric machines with the input transmission on the front axle and the two-speed transmission on the rear axle contribute significantly to the Taycan's high driving pleasure. The breathtaking acceleration and high top speed are just two examples. The transmission development engineers at Porsche are particularly proud to have developed a transmission themselves again for the first time in more than 25 years and to have set new standards in terms of efficiency and weight.

Automotive industry in Europe: delivering on the Green Deal

Sigrid de Vries, CLEPA – European Association of Automotive Suppliers, Brussels, Belgium

Abstract

This document contains a summary of the presentation “Automotive industry in Europe: delivering on the Green Deal” post COVID-19.

Executive summary

The automotive industry is undergoing the biggest transformation in over a hundred years, with mobility becoming increasingly electric, connected, automated and shared. Automotive suppliers embrace actions towards the industry transformation while striving for sustainable economic growth that secures jobs in Europe and contributes to environmental goals. The Covid-19 crisis has added a highly challenging dimension to this goal. The European Green Deal requires a wide variety of actors to work closely together for Europe to emerge world leader in environmental and digital technology. The automotive industry wants to offer the best range of options for people and businesses to move around and needs the right framework conditions to let companies manufacture and employ in Europe.

Impact on Industry: facts and figures[1]

- 13.8 million Europeans work in automotive, accounting for 6.1% of all EU jobs.
- 11.4% of EU manufacturing jobs – some 3.5 million – are in the automotive sector.
- Motor vehicle taxation brings in €440.4 billion for governments in major European markets
- The automobile industry generates a trade surplus of €84.4 billion for the EU.
- The turnover generated by the automotive industry represents over 7% of EU GDP.
- Investing €57.4 billion in R&D annually, the automotive sector is Europe's largest private contributor to innovation, accounting for 28% of total EU spending.

[1] https://clepa.eu/who-and-what-we-represent/business-leader/

- The EU motor vehicle fleet is getting older year-on-year. Passenger cars are now on average 11.1 years old, vans
- 11 years and heavy commercial vehicles 12 years

COVID-19 is having a major impact on the economy, with an unprecedented halt in retail and manufacturing activity in Q3 and concerns mounting on sustained pressure on consumer sentiment. This is the dramatic backdrop against which the European automotive industry is trying to recover and find back to its previous strength.

Sentiment among suppliers is worrying. Three out of four businesses fear that it will take more than a year to recuperate, a CLEPA survey found[2]. One third of respondents foresee a timeframe of two to three years. To cope with the crisis, a large share of businesses plan to cut investment and reduce their workforce and half of businesses intend to adjust investment and workforce already in the short-term. The remainder foresees such measures being taken in the next 6-12 months. Revision of manufacturing footprint is also considered.

For many decades, the European automotive sector has been one of the key pillars of the economic and social welfare of Europe. Indirectly, the sector provides employment to 13,8 million workers. The European assembly plants still produce 1 in every 4 cars worldwide. The sector is highly innovative and accounts for 20% of industrial research funding in Europe. Europe's automotive sector has become a global leader with a strong export orientation. It is a stronghold of European industry and a driver for jobs and economic growth across Europe. As a result of the substantial economic interlinkages with other sectors along the value chain, its importance for employment and growth for the whole economy is clear.

CLEPA has urged EU and national governments to launch EU-coordinated vehicle renewal schemes to kickstart economic recovery and support the relaunch of the sector. Demand stimulus will help to increase the utilisation of manufacturing capacity and therefore safeguard jobs and investment capacity. The automotive sector will act as an engine of overall economic recovery thanks to the sector's vast and interconnected ecosystem, significant employment impact and immediate knock-on effect on other sectors of the economy.

[2] https://clepa.eu/mediaroom/outlook-automotive-suppliers-worsens-considerably-latest-survey-shows/

A bold industrial recovery plan should be based on two objectives. First of all, bringing the industry back on track by stimulating sales and reviving production, and secondly, supporting the industry in its journey towards a carbon-neutral future, based on the Green Deal and Europe's climate objectives. To date, the sector has been substantially investing in its transition towards the new paradigm of a carbon-neutral and digitalised economy: including, alternative powertrains, batteries, connected cars, mobility services, and automated driving. The industry can make a real contribution to the Green Deal and mitigating the climate emergency. But due to COVID-19, strong support from the national governments and the Commission is needed in order to help the sector to make the necessary investments in transitioning to decarbonisation while supporting European jobs and keeping its contribution to EU exports and the social welfare of European citizens.

The crisis is accelerating the transformation of the sector, and industry and policy makers must work together to sustain employment and make the workforce future proof. To underpin Europe's long-term competitiveness, the EU should also leverage all instruments at its disposal to support research and innovation. This includes the EU budgets for Horizon Europe, public procurement and financing tools from the EIB. Almost 40% of respondents in the CLEPA survey have already taken steps to cut R&D budgets, with 32% undecided and 30% at this stage having decided against. Supporting the innovative capacity of the sector will be crucial to relaunch from the crisis in a sustainable way. Automotive suppliers are among the largest private investors in R&D, contributing significantly to the competitiveness of the automotive sector in Europe.

The sector wants to contribute to a policy response to COVID-19 that ensures public health, minimises the impact on the economy and maintains focus on the overarching objectives of our time: the digital and carbon-neutral society. Europe needs a strong automotive ecosystem to push ahead with ambitious environmental, digital and road safety targets. Investment in people and R&D remain essential, and yet is under immediate pressure.

Real-Driving-Based Comparison of the Eco-Impact of Powertrain Concepts using a Data-Driven Optimization Environment

Arved Esser, **Tobias Eichenlaub**, **Stephan Rinderknecht**,
Technical University of Darmstadt

Abstract

In order to limit the effects of man-made climate change, the assessment of the ecological impact of different powertrain concepts is of increasing relevance and intensely studied. In this contribution we present a data-driven optimization environment that enables to identify the ecological potential of different concepts for different scenarios. The parametrization of each powertrain concept is dedicatedly optimized to minimize the ecological impact, which allows for an unbiased and reliable comparison on an uniform evaluation basis. To exploit the potential of each single powertrain parametrization, the operating strategy of the powertrain is adapted. Naturalistic driving profiles, including the speed, acceleration and road-slope information are depicted by multidimensional and representative driving cycles, allowing for an efficient search of the real-driving-optimal powertrain parametrizations within the optimization. In this study, we investigate long-range capable vehicles for a scenario in the reference year 2030 in Germany. Conventional vehicles, battery electric vehicles, fuel cell electric vehicles and plug-in hybrid electric vehicles are examined. Finally, the results are compared to an evaluation of the CO2 emissions according to the Worldwide harmonized Light vehicles Test Procedure (WLTP).

1 Introduction and Motivation

The increasingly visible effects of man-made climate change and its consequences [1] require to maximize the efforts of reducing the global greenhouse gas (GHG) emissions. Regarding the automotive sector, various studies have investigated the total GHG emissions of different powertrain concepts over the entire life cycle of the vehicle and this topic is prominently discussed in public debate. In most existent studies, typical representative vehicles are defined for each powertrain concept, based on available market vehicles. These representative vehicles are defined to depict typical parametrizations of the powertrain concepts regarding their components such as the electric machine and the battery.

The comparison of these representative vehicles is suited to compare state-of-the-art vehicles. However, these representative market vehicles are designed with various different objectives.

The vehicle's performance, the respective brand image or monetary costs are exemplary objectives that are considered in the development. Due to the differing development objectives, it remains unclear how the powertrain concepts would have performed in the comparison of GHG emissions if they had been specifically designed to minimize the ecological impact instead.

In [2], an optimization environment for the comparative analysis of the ecological potential of different powertrain concepts has been introduced for this purpose. For given scenarios and required design constraints of the vehicles, the powertrain parametrization is optimized towards minimal total GHG emissions over the life cycle of the vehicle (including production and End-of-Life), resulting in the ecological potential of a powertrain concept. By identifying this achievable minimum in the GHG emissions for each powertrain concept, a reliable and unbiased comparison of the different powertrain technologies is possible on a uniform evaluation basis.

The comparison of the GHG emissions of different powertrain concepts becomes increasingly complex due to various new developments such as the synthesis of fuels from electric energy (Power-to-X), that can potentially be supplied by renewable energy power plants. Furthermore, manufacturers are starting to take compensatory measures, such as planting trees, to argue that a certain vehicle is produced with an even GHG emissions balance. In future scenarios, all powertrain concepts could therefore potentially become nearly GHG-neutral if all the production and operation supply is based on renewable energies or if compensatory measures are taken. For this reason, it is meaningful to consider further quality measures, besides the GHG emissions, for the ecological assessment of powertrain concepts. Within this study, we additionally consider the total energy demand (TED). The TED quantifies the total electric energy, taken from the electric grid, to produce, operate and dispose a vehicle. For the operational phase, it is assumed that all fuels are synthesized via Power-to-X considering corresponding synthesis efficiencies. Especially for future scenarios that assume near 100 % renewable energies, the TED is suited to assess the eco-impact of different powertrain concepts.

Consensus in various different studies is that short-range battery electric vehicles (BEV) with a relatively small battery capacity perform very well in the comparison of the ecological impact of different powertrain concepts. On the other side, regarding long-range capable vehicles, different studies have been conducted. While [3] quantifies that BEV concepts outperform internal combustion engine vehicle (ICEV) concepts until very high ranges of 800 km for the reference year of 2019, [4] finds that fuel cell electric vehicles (FCEV) achieve smaller GHG emissions than BEV for ranges higher than 250 km. In [2], our team predicted that plug-in hybrid electric vehicles (PHEV) can lead to the lowest GHG emissions in 2030 for an exemplary

range of 350 km, if the vehicles are optimally used and regularly charged electrically. From the presented studies, no general consensus about the most suitable powertrain concepts for long-range capable vehicles can be concluded. Therefore, we further investigate long-range capable vehicles in this work.

An additional limitation in available studies on the ecological impact of different powertrain concepts is the absence of studies that investigate all currently relevant powertrain concepts on a uniform evaluation basis, which might be part of the reason for the lack of consensus about long-range capable vehicles. PHEV or ICEV, driven by the combustion of compressed natural gas (CNG), and FCEV are often excluded from available studies. Furthermore, FCEV are mostly considered without external charging (plug-in) functionality. Within the present work, we incorporate all previously mentioned concepts into the optimization framework to provide a comprehensive comparison of the ecological potential of the presented concepts on a uniform evaluation basis.

Additionally, a significant impact factor on the resulting GHG emissions and TED are the considered driving profiles, that are used for the evaluation. As pointed out in various studies, the consideration of real-driving profiles resulting from the naturalistic driving of the relevant application is essential. To address this point, we perform our analysis for two given naturalistic driving profiles measured on public roads in the area of Darmstadt in Germany, that are characterized by the occurrence frequency of operating states concerning speed, longitudinal acceleration and road-slope. Further, the results of these real-driving profiles are compared to the method of the “Worldwide harmonized Light vehicles Test Procedure” (WLTP) for the quantification of GHG emissions.

In Section 2 of this work, the optimization framework for the comparative analysis of the eco-impact is presented. Section 3 provides details about the naturalistic driving data sets and the derivation of driving cycles applied in this study. Thereafter, the vehicle simulation model for the simulative evaluation of fuel (including hydrogen (H2) and CNG) and electricity demands is introduced. The results of the ecological potential concerning the GHG emissions and the TED are presented in Section 5 for the different driving profiles. Finally, we summarize the presented work and draw conclusions in Section 6.

2 Optimization Framework to enable an unbiased Comparison

As stated above, the assessment criteria for the vehicles to be compared in this work are the TED and the GHG emissions. Both measures are affected by various different factors in different phases of the vehicle life cycle. The GHG emissions are considered for the complete

life cycle including emissions during the operational phase, production and End-of-Life ('Cradle-to-Grave').

Concerning the TED, the energy chain from the grid to the demand for driving, i.e. 'Grid-to-Wheel' energy demand, is considered. This also incorporates the energy demand for the production of synthesized fuels. For the TED, it is assumed, that all fuels are synthesized via Power-to-X. Due to the current lack of detailed data for the energy demands in the production and End-of-Life phases for most powertrain components, only the production of the battery, as a main contributing component, based on [5], is considered.

The energy demand during the operational phase is further dependent on the powertrain type and the parametrization of the powertrain components like the energy converters, but also on the specific usage of the vehicle. A specific parametrization of a powertrain might be advantageous for a specific usage of the vehicle. For example, a higher peak power of the electric motor affects the vehicle's consumption due to a higher vehicle weight and because it may be operated in less efficient operating points of the motor. This in turn requires a larger battery capacity to meet a specific range, which again leads to higher emissions during production of the battery. Therefore, an unbiased comparison of different powertrain concepts can only be ensured when the parametrization is optimized for the specific usage and for the respective assessment criterion.

To ensure an uniform evaluation basis for the different powertrain concepts, the consumption of the vehicles is determined on the same driving profiles and with the same minimal range requirements. To analyze the influence of the driving profile on the results, two different naturalistic driving profiles are examined in this work. Representative driving cycles are derived from the naturalistic driving profiles by a cycle synthesis method based on [6] that can be used to efficiently determine realistic consumptions of the vehicles. A detailed description of the naturalistic driving profiles and the derivation of representative driving cycles is given in Section 3. In addition to meeting the traction demand imposed by the driving cycle, technology neutral design constraints are defined for all powertrain concepts to ensure the general drivability of the vehicles. All vehicles must be able to meet multiple acceleration characteristics (0-60 km/h in 4,2 s, 0-100 km/h in 8,6 s, 80-120 km/h in 6 s). Additionally, a maximum speed of 180 km/h and a launch acceleration of 2,5 m/s² on a slope of 30 % are demanded.

As mentioned above, the optimization of the powertrain sizing and parametrization has the objective to minimize either the GHG emissions or the TED in order to create an unbiased basis for the comparison of the powertrain concepts' potentials. For this purpose, a set of main design parameters d is defined that enable the encoding of a specific powertrain parametriza-

tion, shown in Table 1. Amongst others, they comprise of the peak powers of the energy converters (Internal Combustion Engine (ICE), Electric Machine (EM) and Fuel Cell (FC)) and the capacity of the battery C_{Batt}. More detailed information about the powertrain modelling based on these parameters is given in Section 4.

Table 1: Summary of the design parameters d that are optimized for every powertrain concept and for every driving profile both towards minimal GHG emissions and minimal Total Energy Demand.

N_{ICE}	Index of the internal combustion engine in the database
$P_{EM,max}$	Peak power of the electric machine
$P_{FC,max}$	Peak power of the fuel cell
C_{Batt}	Capacity of the battery
n_{Transm}	Number of speeds in the transmission system
i_n	Gear ratio of the transmission speeds i_1 to i_N
$i_{EM,Hybrid}$	Relative ratio of the connection of the electric machine for Parallel-Hybrid-Electric-Powertrains to the gearbox inlet

These design parameters are optimized with a genetic algorithm [7] using the presented assessment criteria as objective functions. The algorithm creates populations of encoded powertrain parametrizations, evaluates their respective fitness, i.e. the GHG emissions or TED, and iteratively creates new generations through selection, mutation and recombination methods. In every evaluation of the fitness function, an efficiency-oriented operating strategy of the vehicle is applied for each parametrization that is based on a locally optimal control approach. The operating strategy is adapted for every individual parametrization of the population to ensure the comparability of different parametrizations in the framework. Since the optimal encodings of the powertrains might differ for both objective functions as well as the considered driving profiles, all powertrain concepts are optimized separately for both objective functions and both driving profiles. The whole optimization framework described here is illustrated in Fig. 1.

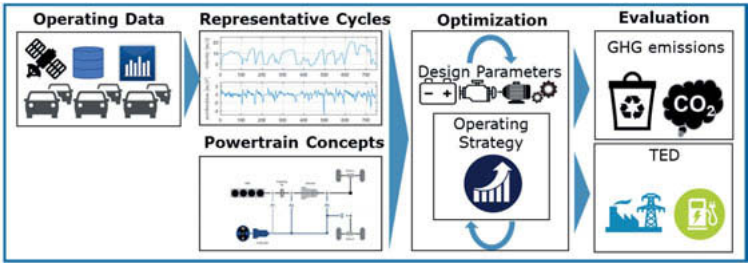

Fig. 1: Data-driven optimization framework for the comparison of the eco-impact of different powertrain concepts.

3 Naturalistic Driving Profiles

It has been shown that driving profiles differ significantly [8] and strongly influence a vehicles consumption [9]. Therefore, the considered driving profiles are of fundamental relevance in the simulative assessment of the eco-impact.

To enable an unbiased estimation of the ecological impact of the powertrain concepts, the real driving data from the relevant application must be considered. Since the chosen driving profiles have a significant impact on the resulting consumptions and powertrain parametrizations, we investigate two different naturalistic driving profiles, which allows us to analyze the differences with respect to the driving characteristics. The two driving profiles result from the naturalistic use of two vehicles that have been equipped with vehicle data loggers. The first driving profile comprises of tracks recorded with a pool-vehicle at TU Darmstadt (pool-vehicle profile), which is operated by various different drivers for business purposes. The second driving profile was recorded with the private vehicle of a single employee of TU Darmstadt (employee profile) which is only driven by this person. However, the here presented method could be repeated with any given driving profile, from a certain application field (certain drivers, regions, vehicles classes etc.) enabling to quantify the potential of different powertrain concepts for the specific driving profile.

For the two real-driving profiles, the vehicle's speed and longitudinal acceleration as well as the GPS positions are recorded for this study. From the GPS position, the elevation is interpolated with the free topology data from the "Radio Shuttle Topology Mission" (RSTM) [10]. The road-slope is estimated based on the elevation and speed information. In summary, the driving profiles can be regarded as three-dimensional matrices that contain the occurrence frequency of operating states in the speed, acceleration and road-slope dimension. In Fig. 2, two-dimensional representations of the three-dimensional pool-vehicle profile are shown by adding all

occurrence frequencies in the respective missing third dimension. The pool-vehicle profile is characterized by rather dynamic driving with high top speeds and accelerations at higher speeds. Furthermore, the different drivers frequently use adaptive cruise control (ACC) with commonly selected desired speeds resulting in various visible peaks in the pool-vehicle profile on the zero acceleration axis.

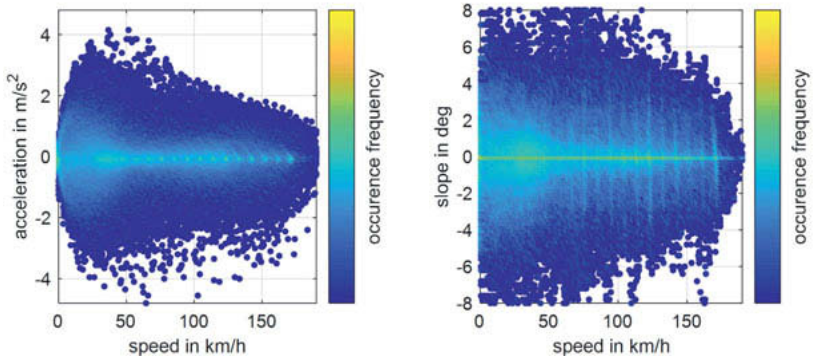

(a) (b)

Fig. 2: Illustration of the pool-vehicle profile. 9077 km of operating data have been recorded. SubFig. (a) shows the occurrence frequency of operating states in the speed-acceleration plane from the three-dimensional driving profile. SubFig. (b) shows the occurrence frequency in the speed-slope plane.

In the following, we present, how the driving profile is considered in the optimization framework in detail for the pool-vehicle profile. The same approach is applied for the employee profile.
Within the previously presented optimization framework, representative driving cycles are used to depict the entirety of the driving profiles data in a compressed manner. As mentioned before, the use of the representative driving cycles allows to evaluate the characteristics of a high number of powertrain parametrizations very efficiently within the optimization, compared to the consideration of all the data for each powertrain parametrization. We apply the driving cycle synthesis method presented in [6] to generate multidimensional and representative driving cycles, including the road-slope in addition to the vehicle speed and acceleration. The synthesis procedure is able to maintain the physical dependencies between the speed, acceleration and road-slope signal from the original data within the generated cycles [6].
For vehicle powertrain concepts with only one energy source, like ICEV and BEV, we could compress the entire driving data of a driving profile into a single cycle since the consumption

only depends on the occurring operating states. However, in the case of plug-in hybrid concepts with two energy sources, such as PHEV and fuel cell plug-in hybrid electric vehicles (FCPHEV), the consumption also depends on the distance of the tracks. Shorter tracks allow for an increased percentage of electric driving compared to longer tracks. The PHEV might drive a short track completely electrically, but needs to use the combustion engine for longer tracks (even if the tracks have equal operating points) to achieve the desired range. Therefore, the distribution of trip distances, shown in Fig. 3 for the pool-vehicle profile, has to be considered for each driving profile. On the left, the number of trips for different distances are illustrated showing that most trips are rather short. On the right, the cumulative proportion of driven kilometers from the total mileage of the driving profile is shown. A significant share of nearly 50 % of the driven kilometers is performed on tracks with a distance between 120 and 170 km despite the relatively small number of these trips.

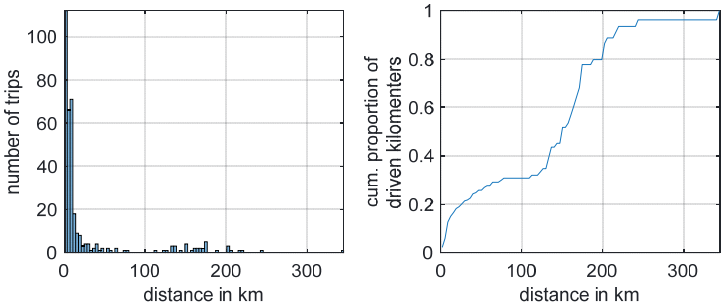

Fig. 3: Distribution of trips and driven kilometers over the trip distance. A total of 9077 km has been recorded for the pool-vehicle profile.

To consider the distance distribution within our model, we assign the available driving data to multiple distance clusters, using the 'k-means' algorithm. Each distance cluster contains all tracks from a certain distance range. Each cluster represents a driving subprofile for which a representative driving cycle is synthesized. The driving cycles are then used in the vehicle simulation model of the optimization framework with distances of the corresponding cluster centers.

The number of distance clusters is a trade-off between a low variance of distances inside a cluster, to avoid that tracks are assigned to cluster centers far from their original distance, and a sufficiently large number of tracks inside a cluster to enable a meaningful compression of the data through the cycle synthesis. Further, each distance cluster requires a driving cycle simu-

lation for each parametrization of a powertrain concept within the optimization leading to increased computational effort. To identify an adequate number of distance clusters, we repeat the k-means clustering with multiple cluster numbers and analyze the distribution of the distance deviation of the tracks from their assigned cluster centers using boxplots as shown in Fig. 4. The boxplots show the maximum deviation, the 2-sigma interval, the 25 % and 75 % quantiles as well as the median deviation. Until a number of 5 clusters, the maximum distance difference of the tracks decreases significantly. The 2-sigma interval, the 75 % quantile and the median distance stay nearly constant from two to four clusters, but there is a significant improvement for five clusters. From five to eight clusters, these values stagnate again. Therefore, we use a cluster number of five for the pool-vehicle profile as a good compromise of computational effort and modelling accuracy.

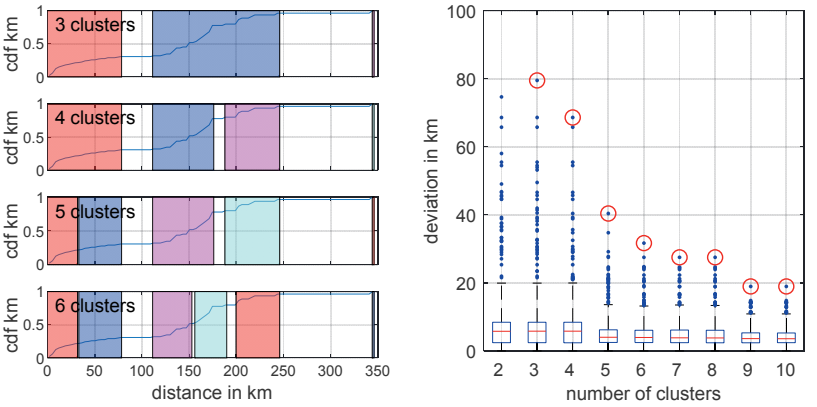

(a) (b)

Fig. 4: Results from the cluster analysis of tracks in the pool-vehicle profile. SubFig. (a) shows the results of the clustering for three to six clusters with the cumulative density function (cdf) of the driven kilometers. SubFig. (b) shows the boxplots of the deviations of all track distances to their assigned cluster centers in kilometers. The maximum deviation is marked with a red circle. Tracks with a deviation above the 2-sigma interval are marked with blue dots. The 2-sigma interval is shown with a black line. The 25 % and 75 % quantile are shown with blue boxes. The median is indicated by the red line.

For each of the five chosen distance clusters, we synthesize 10,000 representative driving cycles using the method presented in [6]. From the multitude of cycles of every cluster, we

chose the cycle with the lowest error in the speed-acceleration-slope frequency distribution (SASFD) e_{SASFD}.

$$e_{\mathrm{SASFD}} = \frac{1}{2} * \sum_{n} \left| \frac{t_{\mathrm{ref},n}}{t_{\mathrm{ref,tot}}} - \frac{t_{\mathrm{syn},n}}{t_{\mathrm{syn,tot}}} \right| \quad (1)$$

The e_{SASFD} sums up the relative difference of times t spent in state *n* between the cluster profiles and the synthesized cycles. The states *n* consist of the combinations of speed, acceleration and road-slope that occurred in the driving profile. Additionally, cycles with a difference in elevation from start to end are omitted to maintain balanced recuperation potentials.

Fig. 5 shows the subprofiles of the five distance clusters in the speed-acceleration plane and the chosen cycles with minimal SASFD error that fulfil the elevation constraint. As expected, the driving cycles of the clusters for higher distances contain a larger amount of high-speed driving and less frequent acceleration or deceleration manoeuvres than the cycles of short distance clusters.

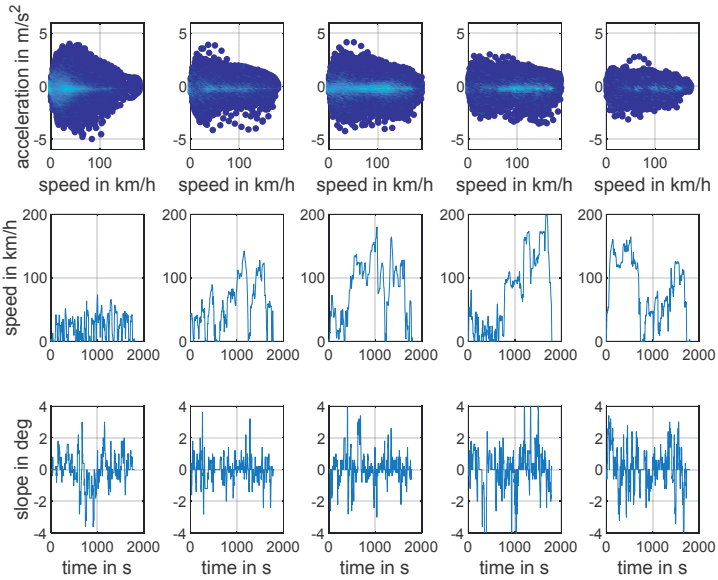

Cluster 1	Cluster 2	Cluster 3	Cluster 4	Cluster 5
Center = 12 km	Center = 53 km	Center = 155 km	Center = 211 km	Center = 345 km
Mileage weight	Mileage weight	Mileage weight	Mileage weight	Mileage weight
20 %	9 %	48 %	19 %	4 %

Fig. 5: Sub driving profiles from the five distance clusters of the pool-vehicle profile together with the synthesized driving cycles for each of the five clusters. Furthermore, the cluster center distances and the mileage-weights of the cycles are denoted.

For each cluster and corresponding driving cycle, the distance of the cluster center and the driven percentage of the total mileage within the cluster are summarized in Fig. 5. The mileage-percentage is used to weight the consumption values, identified by the vehicle simulation model on the different driving cycles to a total mean consumption.

The two-dimensional projections of the employee driving profile are shown in Fig. 6. The employee profile is characterized by more efficiency-oriented driving at moderate speeds and accelerations, compared to the pool-vehicle profile. During highway driving, the ACC system was applied frequently with a set speed of 120 km/h, visible in the profile 120 km/h and zero acceleration.

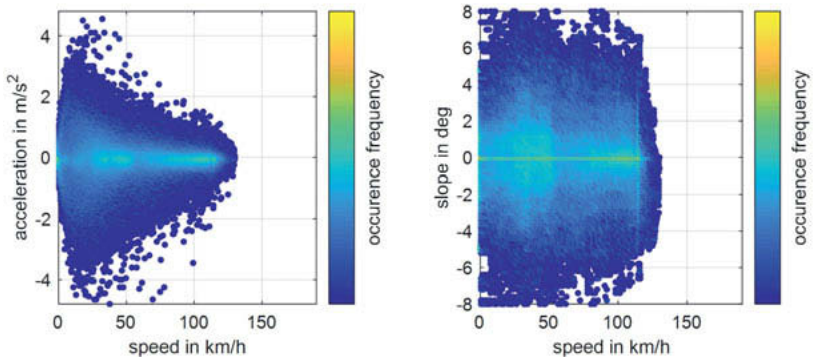

(a) (b)

Fig. 6: Illustration of the employee profile. 8193 km of operating data have been recorded. SubFig. (a) shows the occurrence frequency of operating states in the speed-acceleration plane from the three-dimensional driving profile. SubFig. (b) shows the occurrence frequency in the speed-slope plane.

From the cluster analysis, we derive a number of four clusters for the employee profile, which results in similar key values (max deviation, 75 % quantile and median) in the distance deviation of the tracks from their assigned cluster centers compared to the pool-vehicle profile. The information about the clusters is summarized in Fig. 7.

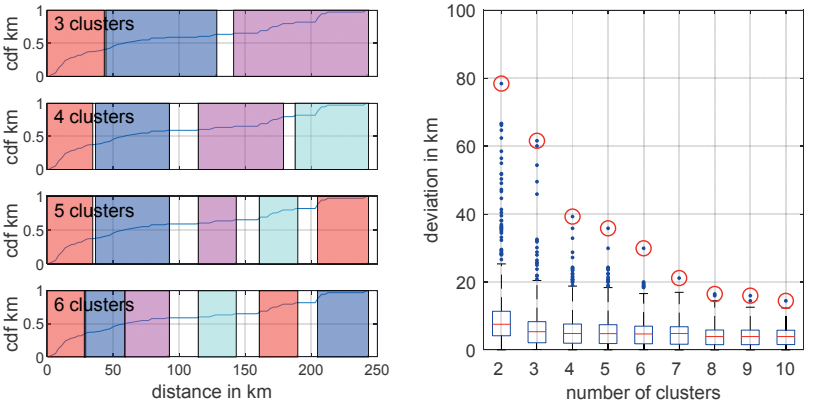

Fig. 7: Results from the cluster analysis of tracks in the employee profile. SubFig. (a) shows the results of the clustering for three to six clusters with the cumulative density function (cdf) of the driven kilometers. SubFig. (b) shows the boxplots of the deviations of all track distances to their assigned cluster centers in kilometers. The maximum deviation is marked with a red circle. Tracks with a deviation above the 2-sigma interval are marked with blue dots. The 2-sigma interval is shown with a black line. The 25% and 75% quantile are shown with blue boxes. The median value is shown with a red line.

As can be seen from the Fig., the longest track of the employee profile is around 250 km, compared to a maximum track length of 345 km in case of the pool-vehicle profile. In order to achieve a better comparison between the two naturalistic driving profiles, we use an equal minimum range requirement for both profiles. Therefore, we will simulate the driving cycle from the last distance cluster of both driving profiles twice. At first, with the respective center distance and mileage weight. Secondly, with a range requirement of 380 km, which corresponds to the longest track of the pool-vehicle profile and a 10 % 'buffer', and a mileage weight of zero. This represents an equal long-range requirement for both profiles, but will not directly affect the consumption values of the profiles, since the mileage weight is set to zero.

The best synthesized driving cycles for each distance cluster of the employee profile are shown in Fig. 8. The cycles for higher distance clusters are characterized by fewer stops and fewer acceleration and deceleration manoeuvres.

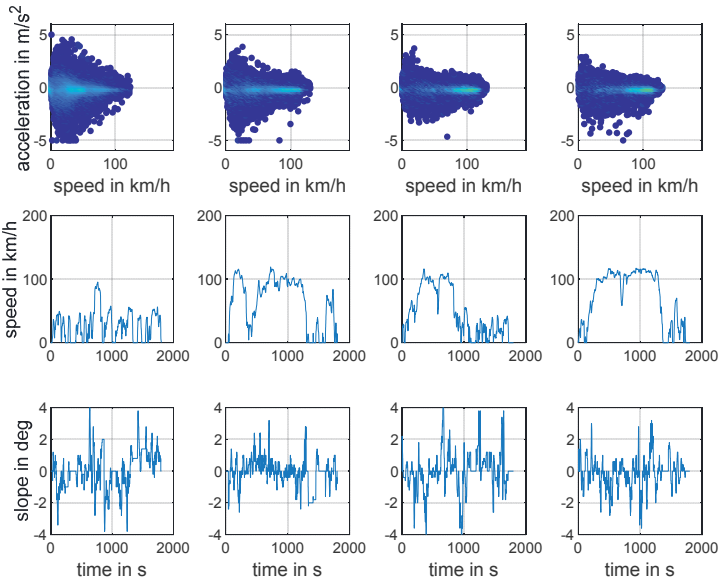

Fig. 8: Sub driving profiles from the four distance clusters of the employee profile together with the synthesized driving cycles for each of the clusters. Furthermore, the cluster center distances and the mileage weights of the cycles are denoted.

In this work, we also compare our approach to the evaluation of GHG emissions using the WLTP. The use of the presented optimization framework for the WLTP would not deliver plausible powertrain parametrizations due to the missing consideration of GHG emissions in the production, in the electricity and fuel supply and in the End-of-Life. Therefore, we consider the powertrain parametrizations from the optimization towards the GHG emissions for the pool-vehicle profile and compare the results of the WLTP and total GHG emissions evaluation. To depict the method of the WLTP, we simulate the Worldwide harmonized Light Duty Test Cycle (WLTC) two times using a charge-depleting and a charge-sustaining strategy. The fuel and electric consumptions of the two simulations are then weighted by the utility factor for the estimated electric range on the WLTC. The estimated GHG emissions of the WLTP evaluation result exclusively from the tailpipe emissions. The WLTC and the range dependent utility factor

are shown in Fig. 9. Road-slopes and secondary demands, for example for the climatization of the cabin, are not considered for the WLTP evaluation.

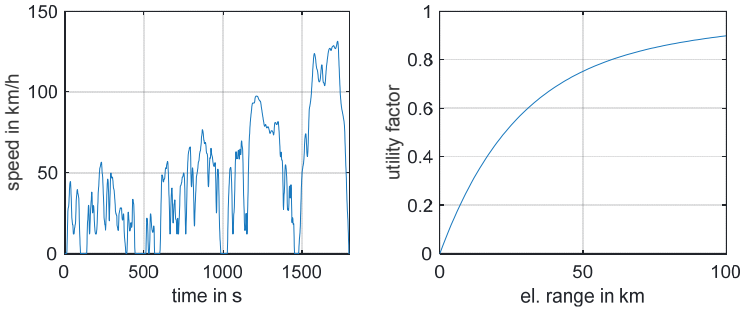

(a) (b)

Fig. 9: SubFig. (a) shows the speed over time for the WLTC. In (b), the utility factor dependent of the electric range on the WLTC is illustrated.

4 Vehicle Simulation Model

To calculate the consumption of the powertrain concepts, a vehicle simulation model is integrated into the optimization framework. Inputs to the model are the design parameter set d, which is chosen by the optimizer and determines the parametrization of a single powertrain variant, and the driving cycles derived from the driving profile. The consumption of different powertrain concepts that is calculated in the vehicle model is then used to calculate the TED or to calculate the emissions in the operational phase as one part of the total GHG emissions of the vehicle. In addition to the primary consumption for moving the vehicle, a secondary energy demand is considered in the model that represents the energy demand of auxiliary systems like Heating, Ventilation and Air Conditioning. For a more detailed description of the secondary energy model, we refer to [11].

To differentiate between multiple powertrain concepts, a generic powertrain model is defined that consists of energy converters, a battery and three sub-transmissions TM1-TM3. The resulting tractive force is transmitted to one of the wheel axles. A specific powertrain concept can thus be built up by employing or omitting parts of the total powertrain model. The model and the connections of the different parts are shown in Fig. 10.

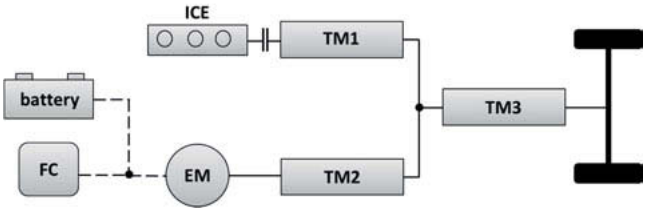

Fig. 10: Generic powertrain model used in this work. All of the analyzed powertrain concepts are derived from this model.

In this work, we examine conventional internal combustion engine vehicles (ICEV) with petrol and CNG engine, two battery electric vehicles, one with a fixed gear ratio (BEV-1) and one with a 2-speed transmission (BEV-2), fuel cell electric vehicles with and without plug-in functionality (FCPHEV and FCHEV) and plug-in hybrid electric vehicles (PHEV) with internal combustion engines (petrol E10 and CNG). The relevant parts of the generic powertrain model that are used for every powertrain concept are given by a binary encoding of the powertrain and is summarized in Table 2.

Table 2: Overview of the powertrain concepts analyzed in this work. The powertrain of a specific concept is built from the generic powertrain through the binary encoding (1 means existing, 0 means non-existing).

Class	Concept	Description	Binary encoding (ICE,EM,FC,TM1, TM2,TM3,battery)
ICEV	ICEV-E10	Conventional vehicle with petrol engine	(1,0,0,1,0,0,0)
	ICEV-CNG	Conventional vehicle with CNG engine	(1,0,0,1,0,0,0)
BEV	BEV-1	Battery electric vehicle with fixed gear ratio transmission	(0,1,0,0,1,0,1)
	BEV-2	Battery electric vehicle with two-speed transmission	(0,1,0,0,1,0,1)
FCEV	FCHEV	Fuel cell hybrid electric vehicle	(0,1,1,0,1,0,1)
	FCPHEV	Fuel cell plug-in hybrid electric vehicle	(0,1,1,0,1,0,1)
PHEV	PHEV-E10	Plug-in hybrid (P2 configuration) with petrol engine	(1,1,0,0,1,1,1)
	PHEV-CNG	Plug-in hybrid (P2-configuration) with CNG engine	(1,1,0,0,1,1,1)

The vehicle model used is a backward-facing implementation of the longitudinal dynamics. Lateral and vertical vehicle dynamics are assumed to have an insignificant effect on the consumption. Also, no driver model is hence required for following the speed defined in the driving cycle. In a driving resistances equation, the tractive demand at the wheels is calculated as a function of vehicle speed, longitudinal acceleration, road-slope and the assumed vehicle parameters, summarized in Table 3. The vehicle masses, shown for each parametrization in Section 5, is calculated from the base mass of 1150 kg and the parametrization dependent mass of the powertrains.

Table 3: Vehicle parameters for the calculation of traction forces in the driving resistances equation.

Frontal area	Air drag coeff.	Roll res. coeff.	Base mass	Powertrain mass
2,2 m²	0.3	0.008	1150 kg	$f(d)$

As mentioned in Section 2, an efficiency-oriented operating strategy, the Equivalent Consumption Minimization Strategy (ECMS) [12], is applied which decides on gear shifting and the distribution of the tractive demand on ICE and EM, represented by the gear mode gm and the torque split ts. The idea of the ECMS is to define a cost function J comprising an equivalent fuel mass flow of chemical and electric energy that is weighted by the balancing cost factor s. The cost function is minimized in every time step t_i, yielding a locally optimal gear mode gm^* and torque split ts^* in every time step of the simulation.

$$J(gm, ts, t_i) = b_e(gm, ts, t_i) T_{ICE}(gm, ts, t_i) n_{ICE}(gm, t_i) + s \frac{1}{LHV} \frac{1}{\eta_{EM}(gm, ts, t_i) \eta_{batt}} T_{EM}(gm, ts, t_i) n_{EM}(gm, t_i) \quad (2)$$

$$ts^*(t_i), gm^*(t_i) = \arg\min_{ts,gm} J(gm, ts, t_i) \quad (3)$$

Here, b_e denotes the brake specific fuel consumption, T the torque, n the rotational speed, LHV the lower heating value and η the efficiency. With this operating strategy, hybrid operating modes like load point shifting can be chosen if they are identified to be optimal in the current operating point. The energy management of the operating strategy depends on the balancing cost factor s. For vehicles with plug-in functionality, the value of s is determined in a separate iteration loop assuring that the battery is fully depleted at the end of the trip distance[1]. Hybrid vehicles without plug-in functionality, on the other hand, are operated in charge-sustaining

[1] If the trip-distance does not exceed the purely electric range of the vehicle, the battery is not depleted.

mode. The exemplary operating behavior of a PHEV in P2-configuration, that results from the described operating strategy, is shown in Fig. 11.

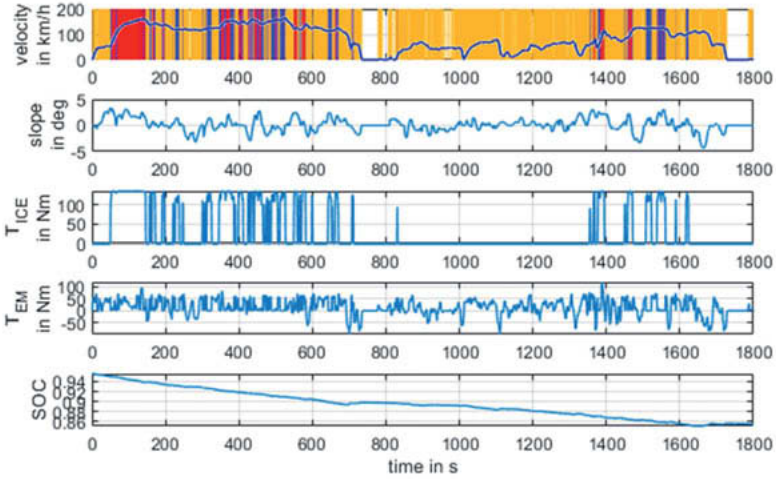

(a)

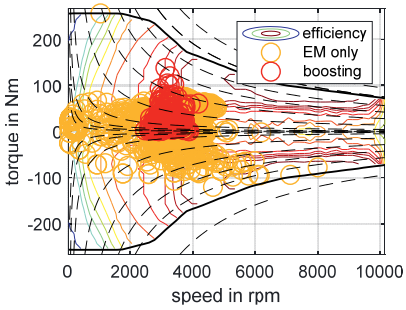

(b)

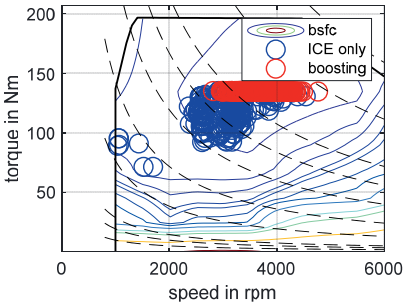

(c)

Fig. 11: Exemplary simulation results of the vehicle model for a PHEV-E10 parametrization. SubFig. a) shows the driving cycle, the road-slope and the time-dependent motor torques and state of charge of the battery. The colors indicate operating modes like purely electric driving, combustion engine driving or hybrid modes like boosting for the highest traction power demands. SubFig. b) shows the corresponding operating points of the EM. SubFig. c) shows the operating points of the ICE in the map of brake specific fuel consumption (bsfc).

Concerning the individual powertrain components, we use efficiency maps for the ICE and the EM as functions of torque T and rotational speed n. To differentiate between powertrain parametrizations based on the design parameter set d, multiple scaling approaches are applied to the components. For the EM, a reference efficiency map η_{ref} is defined and a torque-based scaling approach, as in [13], is used to scale the efficiency map as a function of the peak power of the EM $P_{\mathrm{EM,max}}$.

$$\eta_{\mathrm{EM}}(T_{\mathrm{EM}}, n_{\mathrm{EM}}) = \eta_{\mathrm{ref}}(T_{\mathrm{EM}} \frac{P_{\mathrm{ref,max}}}{P_{\mathrm{EM,max}}}, n_{\mathrm{EM}})$$

The efficiency of the FC in our model depends on the momentary power of the FC. The power-dependent efficiency characteristics of a reference FC η_{ref} are scaled to other FC with different peak powers $P_{\mathrm{FC,max}}$ for the simulation of different powertrain parametrizations.

$$\eta_{\mathrm{FC}}(\mathrm{P_{FC}}) = \eta_{\mathrm{ref}}\left(P_{\mathrm{FC}} \frac{P_{\mathrm{FC,ref,max}}}{P_{\mathrm{FC,max}}}\right)$$

Since similar scaling approaches applied to a reference internal combustion engine are assumed to induce larger uncertainties, the ICE is not scaled, but a database of various ICE with different rated powers and efficiency maps is built up. During optimization of a powertrain concept, one of the engines can be selected and its respective power and efficiency characteristics are considered in the vehicle model. The efficiency of the transmission is dependent on the momentary output power and on the powertrain concept, the battery is assumed to have a constant efficiency.

Alongside the efficiency characteristics of the powertrain components, the emissions of the components during production and End-of-Life phases have a considerable effect on the overall GHG emissions. The GHG emissions G_j of component j are therefore calculated based on the constant emission coefficient c_j and the mass of the component m_j, which is a function of the parameter set d.

$$G_j(\boldsymbol{d}) = c_j m_j(\boldsymbol{d})$$

For example, the mass of the EM is made dependent on its peak power $P_{\mathrm{EM,max}}$ and the mass of the battery is dependent on its capacity C_{batt}. Various nonlinear regression curves are derived based on data of existing components to model these characteristics. In Table 4, a summary of the most relevant parameters of the investigated scenario is given, which are relevant to evaluate the GHG emissions and the TED for the different powertrain concepts. The parameters are meant to describe the scenario of Germany in the reference year 2030 and are applied for all results, presented in Section V.

Table 4: Scenario parameters for the estimation of the GHG emissions and the TED.

Description	Value
Fuel supply E10 (GHG)	0,71 kgCO2-eq/kg [2]
Fuel supply CNG (GHG)	0,77 kgCO2-eq/kg [3]
Fuel supply H2 (GHG)	9,83 kgCO2-eq/kg [4]
Power-to-X synthesis efficiency petrol	44,6 %
Power-to-X synthesis efficiency CNG	62 % [5]
Power-to-X synthesis efficiency H2	65,5 % [6]
Production of battery (GHG)	10,17 kgCO2-eq/kg [7]
Production of battery (TED)	Electricity: 9 kWh/kg & Heat: 5,55 kWh/kg [8]
Production of fuel cell (GHG)	17 kgCO2-eq/kW [9]
Production of H2-tank (GHG)	340 kgCO2-eq/kgH2 [10]
Energy density of the Battery	126-170 Wh/kg [11]
Depth of discharge for the Battery	90-95 % dependent on battery size [12]
Specific emissions in the electricity supply	400 gCO2/kWh [13]
Total vehicle mileage	250 000 km [14]

5 Ecological Potential of Different Powertrain Concepts

Within this section, we present the results of the comparative evaluation of the eco-impact of different powertrain concepts in terms of the GHG emissions and the TED. For the first naturalistic driving profile, the pool-vehicle profile, a detailed discussion of the results is given. In

[2] Based on [14].

[3] Based on [14].

[4] Based on [4] with an assumption of 20% H2 via Power-to-X with renewable energies.

[5] Based on [15].

[6] Based on [15, 16].

[7] Based on [4].

[8] Based on [5].

[9] Based on [4].

[10] Based on [4].

[11] Scaling with battery size. Lower limit from [17].

[12] Further improvements for 2030 from study of [5].

[13] Chosen value between [18] and [3].

[14] Annual mileage of diesel vehicles within Germany [19] combined with the mean lifetime of passenger vehicles in Germany [20].

case of the second driving profile, the overall results and differences from the first profile are presented and discussed.

All results were obtained using the presented boundary conditions for the reference year of 2030. As described in Section III, a minimum range of 380 km is imposed to all vehicles. Smaller minimum ranges would lead to different results, as it was studied in previous publications [2]. Especially for BEV class vehicles, the minimum range requirement is a main influencing parameter. For this reason, we additionally investigate the sensitivity of different range requirements for the BEV-2 on the pool-vehicle profile. A comparison to the results from the WLTP is presented in an additional section at the end.

Pool-vehicle profile

The optimized powertrain parametrizations of the different concepts, identified by the optimization framework, are summarized in Table 5. For the concepts with a single energy source (ICEV, BEV, FCHEV), the optimizations towards GHG emissions and TED lead to identical optimal parametrizations. For the plug-in hybrid concepts (FCPHEV & PHEVs) however, the optimal parametrizations differ.

Table 5: Parametrizations of the powertrain concepts, identified by the optimization framework, for the pool-vehicle profile.

concept	objective function	power ICE in kW	power EM in kW	power FC in kW	Battery capacity in kWh	total mass in kg	Max. torque req. in Nm	transmission ratios
ICEV-E10	GHG & TED	140	0	0	0	1278	1911	[7.1 5 3.6 2.7 2.1 1.6 1.3]
ICEV-CNG	GHG & TED	140	0	0	0	1278	1911	[7.1 5 3.6 2.7 2.1 1.6 1.3]
BEV-1	GHG & TED	0	168	0	91,7	1763	2636	4.8
BEV-2	GHG & TED	0	157	0	90,8	1764	2637	[6.1 3.1]
FCHEV	GHG & TED	0	134	91	10	1464	2189	[5.4 2.8]
FCPHEV	GHG	0	140	28	35,6	1576	2357	[6.9 3.1]
PHEV-E10	GHG	96	80	0	35,7	1604	2398	i_{ICE}:[13.5 8.8 5.9 4.2 3.1 2.4 1.9] i_{EM}:1.08*i_{ICE}
PHEV-CNG	GHG	96	78	0	35,6	1598	2389	i_{ICE}:[13.5 9.4 6.7 4.9 3.7 2.9 2.4] i_{EM}:0.88*i_{ICE}
FCPHEV	TED	0	152	21	56,8	1681	2513	[6.4 3.2]
PHEV-E10	TED	71	165	0	85,1	1873	2801	i_{ICE}:[21.4 13.4 8.8 6.0 4.2 3.1 2.4] i_{EM}:0.48*i_{ICE}
PHEV-CNG	TED	96	154	0	59,6	1758	2628	i_{ICE}:[14.8 10.4 7.4 5.4 4.1 3.1 2.4] i_{EM}:0.58*i_{ICE}

Regarding the class of BEV concepts, the BEV-2 normally allows for a significant reduction of the required traction power [2]. This is due to the shiftable transmission, so the launch torque can be achieved with the first transmission speed and the maximum vehicle speed with the second transmission speed. For the BEV-1 on the other hand, the maximum vehicle speed and the launch torque must be achieved with the same transmission ratio. Therefore, to

achieve the launch torque for a given transmission ratio, the EM power has to be raised. However, the downsizing potential here is rather small since the pool-vehicle profile is quite dynamic and requires a very high power output irrespective of the design constraints, leading to EM-powers of 168 kW and 157 kW for the BEV-1 and BEV-2. Due to the slightly downsized EM and the shiftable transmission, the BEV-2 allows for a reduction of electric consumption in the usage phase (see Fig. 12), which additionally enables to reduce the installed battery capacity. On the other hand, the two-speed transmission is heavier than the fixed-speed transmission of the BEV-1, hence the total vehicle masses of both vehicles are almost identical.
The vehicles of the FCEV class were equipped with a two-speed electric drive since this is beneficial for the GHG emissions and the TED, as previously discussed for the BEV vehicles. For the FCEV class, the plug-in variant requires a larger EM power due to a higher total vehicle mass mainly caused by a larger battery capacity. The power of the fuel cell is significantly lower for the plug-in variant, since enough energy and power support can be provided by the larger battery capacity for longer high traction power phases. The battery capacity of 10 kWh for the FCHEV, which is operated in charge sustaining mode, is necessary to provide enough combined electric power of fuel cell and battery to boost in high traction demands and for recuperation. For the FCPHEV, a battery capacity of ~35 kWh for the GHG optimization and ~57 kWh for the TED optimization are calculated. Both allow for a very high electric range to limit the use of H2. However, to minimize the TED, a higher battery capacity is even more beneficial than to minimize the GHG emissions.

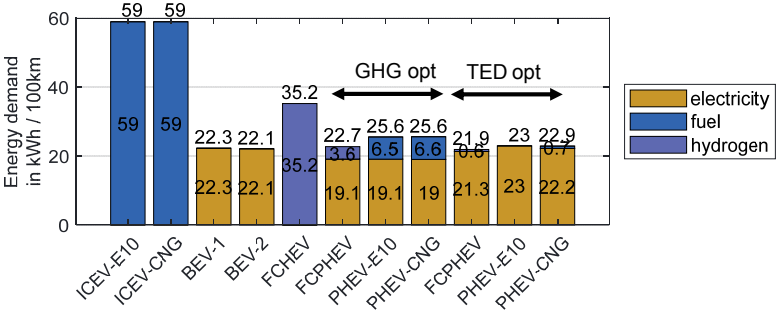

Fig. 12: Energy demands of the different powertrain concepts in the usage phase (1 liter petrol-E10 corresponds to 8.95 kWh, 1 kg H2 corresponds to 33.42 kWh, 1 kg CNG corresponds to 12.83 kWh).

The parametrization of the two PHEV concepts optimized towards the GHG emissions are pretty similar. Both have EM powers of around 80 kW and battery capacities of around 35 kWh,

which allow to achieve a high electric driving percentage up to the driving cycle of the third distance cluster with a distance of 155 km (see Section III for details). For higher distances, it is preferable to use the combustion engine instead of further increasing the battery capacity in order to minimize the GHG emissions. For the TED optimization of the PHEV concepts on the other side, higher battery capacities are chosen to limit the energy demand in the Power-to-X fuel synthesis resulting in a parametrization that can drive almost purely electric for the E10-variant. The PHEV-E10, optimized towards the TED, is the heaviest vehicle since it is equipped with a high battery capacity (~85 kWh) and the combined components of the hybrid powertrain. The synthesis of CNG via Power-to-X is less energy intensive than the synthesis of petrol, which is why the battery capacity is set to ~60 kWh for the PHEV-CNG, relying on a minor use of CNG on the highest distance tracks.

The results concerning the GHG emissions of the different concepts are summarized in Fig. 13. The different parametrizations of the same concept resulting from the two objective functions have a noticeable effect on the GHG emissions. As a first general conclusion, it can be seen that the electrification of the powertrains is essential, since the conventional powertrain concepts lead to the highest GHG emissions. Concerning the BEV class concepts, the BEV-2 shows slightly better results than the BEV-1. In the FCEV class, a plug-in option is very beneficial, since it allows to make use of the efficient electric path from the charging station trough the battery to the EM. Using H2, on the other hand, is less efficient and also causes high GHG emissions in the fuel supply as shown in Table 4. The FCPHEV concept achieves the lowest GHG emissions for this scenario.

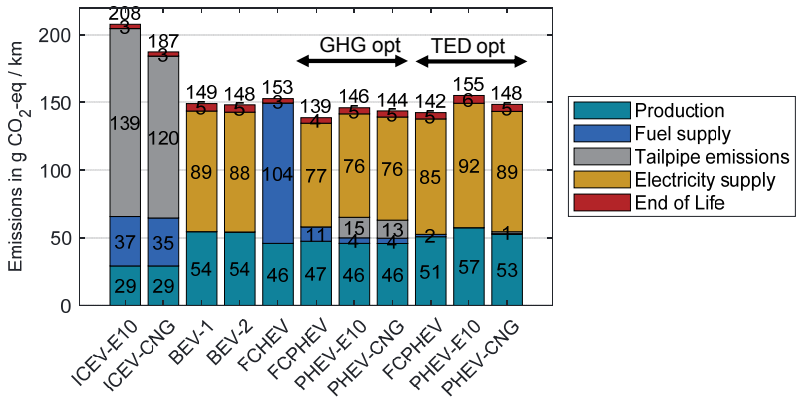

Fig. 13: GHG emissions of the powertrain concepts identified by the optimization framework for the pool-vehicle profile with GHG emissions and TED as objective functions. For the ICEV and BEV class concepts and the FCHEV, the powertrain parametrizations are identical for both objective functions and are therefore displayed with one bar respectively.

The PHEV concepts which were optimized towards the GHG emissions show, by a small margin, worse results concerning the GHG emissions than the FCPHEV. The reduced battery capacity compared to the BEV concepts still allows for a high percentage of electric driving, but reduces the emissions in the production phase significantly. It is beneficial for the PHEV to drive long distances with the help of the combustion engine, which results in 15 and 13 g CO2/km of tailpipe emissions for E10 and CNG, respectively. Due to the lower emissions in the supply of CNG compared to petrol, the PHEV-CNG achieves lower emissions than the PHEV-E10.

If the use of Power-to-X with renewable energies would be partly assumed for CNG in the year 2030, as it was done for H2 within this study, the GHG emissions of the PHEV-CNG would further improve. Another fundamental difference between the PHEV and the FCPHEV is the use of the ICE and the EM in parallel mode for traction, which is not possible for the fuel cell. Therefore, the parametrizations of the PHEV offer greater acceleration reserves and could be especially suited for premium class vehicles.

The resulting TED of the optimized powertrain parametrizations is shown in Fig. 14. Since the fuel supply via power-to-X is very energy intensive, the conventional concepts lead by far to the highest TED. The FCHEV without plug-in option suffers from the same problem and leads to a relatively high TED. All concepts with a direct plug-in option achieve significantly better

TED values since they profit from the high efficiency of the electric path. The BEV concepts achieve values very close to their mean electric consumption. The difference between the TED and the mean electric consumption results from battery production. For the plug-in hybrid concepts (FCPHEV and PHEV), the TED values differ dependent on the objective function of the optimization. The plug-in hybrid concepts, optimized to reduce GHG emissions, lead to higher TED values, since they still partly rely on the use of H2, petrol or CNG. To achieve a minimum TED, it is better to increase the battery capacity to further limit the necessary amount of fuel synthesis via Power-to-X.

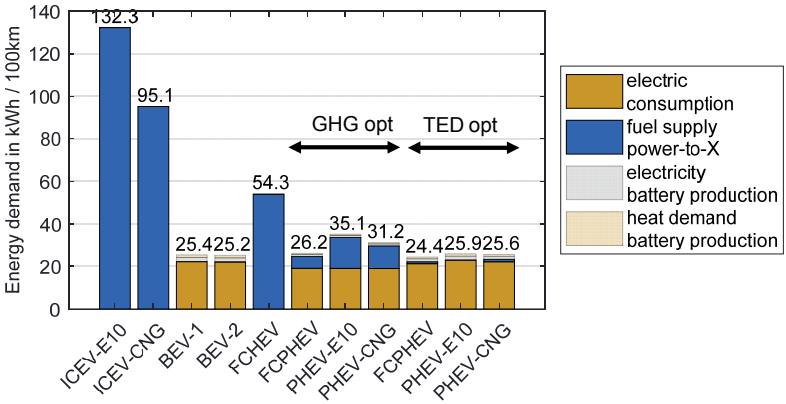

Fig. 14: TED of the powertrain concepts identified by the optimization framework for the pool-vehicle profile with GHG emissions and TED as objective functions.

The FCPHEV shows a very good performance for both optimization criteria. Firstly, the synthesis efficiency for H2 is higher than for petrol or methane. Therefore, even the GHG-optimized FCPHEV achieves a relatively good TED of 26.2 kWh/100 km. Secondly, the mean efficiency of the FC is higher compared to the ICE. Thirdly, the vehicle weight of the FCPHEV is slightly smaller compared to the PHEV concepts. The combined weight of the fuel cell and the H2-tank in our model are less than the weight of the combustion engine, the more complex transmission and the exhaust gas treatment.

As mentioned before, the GHG emissions of the BEV are highly dependent on the minimum range requirement in contrast to all other powertrain concepts which would only need a larger fuel tank.

The GHG emissions of the BEV-2 based on the pool-vehicle profile for different range requirements are summarized in Table 6. When compared to the nearly constant values of 144 and

139 g CO2/km for the PHEV-CNG and FCPHEV, respectively, the BEV class proves to be suitable only for smaller range requirements.

Table 6: GHG emissions of the BEV-2 concept for the pool-vehicle profile with different maximum range requirements. For each range, a separate optimization of the powertrain parameters has been performed. The base scenario corresponds to the longest track of the profile with a 10% buffer.

BEV-2	Values			
Range in km	250	300	380	450
GHG in gCO2/km	142	145	148	155
Battery capacity in kWh	68	81.9	90.8	109.8
El. Consumption in kWh/100km	21.6	21.9	22.1	22.6
Vehicle weight in kg	1665	1726	1764	1879

Employee profile

The parametrization of the optimized powertrain concepts for the employee profile are summarized in Table 7. Again, the parametrizations of the concepts with a single energy source are identical for both objective functions. For the plug-in hybrid concepts, on the other hand, the resulting optimal parametrizations deviate for both objective functions.

Due to the more efficiency-oriented and calm driving of this profile compared to the pool-vehicle, a significant reduction in installed power is possible for all concepts. Further, this leads to a reduction of the energy demands during operation, as shown in Fig. 15, and a smaller battery capacity for the BEV concepts, compared to the pool-vehicle profile.

Table 7: Parametrizations of the powertrain concepts identified by the optimization framework for the employee profile.

concept	objective function	power ICE in kW	power EM in kW	power FC in kW	Battery capacity in kWh	total mass in kg	Max. torque req. in Nm	transmission ratios
ICEV-E10	GHG & TED	96	0	0	0	1261	1885	[11.4 7.6 5.2 3.6 2.6 1.9 1.4]
ICEV-CNG	GHG & TED	96	0	0	0	1261	1885	[11.4 7.4 5 3.4 2.4 1.8 1.3]
BEV-1	GHG & TED	0	124	0	63,1	1630	2437	6.4
BEV-2	GHG & TED	0	118	0	62,4	1633	2442	[8.5 4.2]
FCHEV	GHG & TED	0	100	40	6,2	1380	2062	[7.3 3.7]
FCPHEV	GHG	0	102	41	9,4	1407	2103	[8.4 4.3]
PHEV-E10	GHG	71	50	0	27,6	1528	2284	i_{ICE}:[17.5 10.7 6.9 4.6 3.3 2.4 1.9] i_{EM}:1.14*i_{ICE}
PHEV-CNG	GHG	96	43	0	10,3	1398	2090	i_{ICE}:[11.8 7.1 4.6 3.2 2.3 1.9 1.6] i_{EM}:1.37*i_{ICE}
FCPHEV	TED	0	113	42	27,4	1538	2300	[8.9 3.9]
PHEV-E10	TED	71	63	0	34,9	1579	2360	i_{ICE}:[18.1 11.7 7.7 5.2 3.6 2.5 1.8] i_{EM}:0.82*i_{ICE}
PHEV-CNG	TED	71	64	0	34,8	1579	2360	i_{ICE}:[18.1 11.9 7.9 5.4 3.7 2.6 1.9] i_{EM}:0.81*i_{ICE}

In the case of the plug-in hybrid concepts, the battery capacity is also reduced in comparison to the previous profile. The reason for this lies in the distance distribution of driven kilometers shown in Fig. 7. As can be seen, a higher percentage of the kilometers are driven on trips bellow a distance of 100 km, compared to the pool-vehicle profile. Therefore, a smaller battery capacity is sufficient to achieve a high electric driving percentage for the hybrid vehicles, which is beneficial for the GHG emissions and the TED.

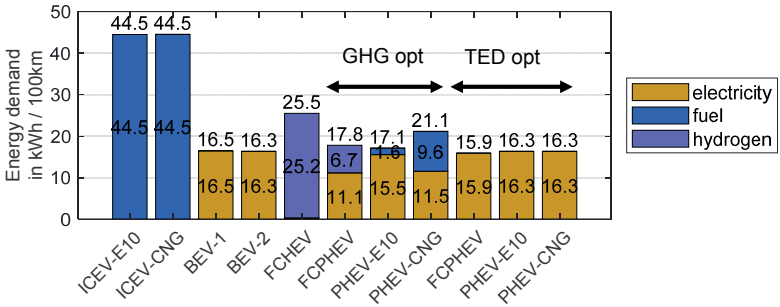

Fig. 15: Energy demands of the different powertrain concepts in the usage phase for the employee profile (1 liter petrol-E10 corresponds to 8.95 kWh, 1 kg H2 corresponds to 33.42 kWh, 1 kg CNG corresponds to 12.83 kWh).

The resulting minimal GHG emissions are presented in Fig. 16. As mentioned before, the more efficiency-oriented driving results in lower GHG values for all concepts compared to the pool-vehicle profile. However, the relative ranking of the concepts stays similar and previously drawn conclusions are confirmed.

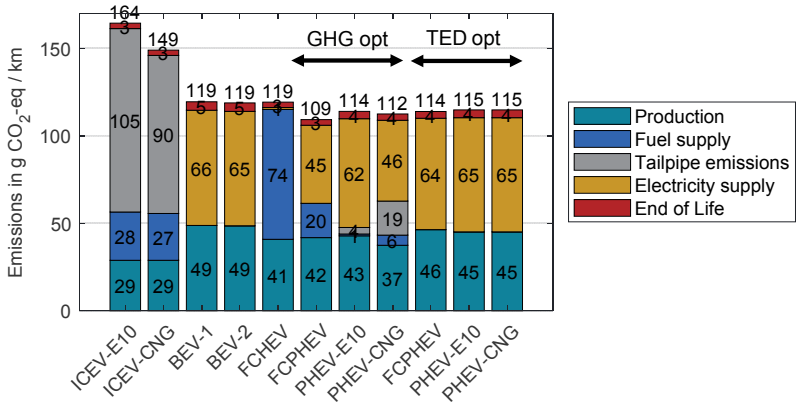

Fig. 16: GHG emissions of the powertrain concepts identified by the optimization framework for the employee profile with GHG emissions and TED as objective functions.

An electrification of the powertrain concepts is essential. For the FCEV class, a plug-in option is beneficial to reduce the GHG emissions and the TED. The FCPHEV and the PHEV-CNG can achieve the best GHG emission values, when they are parametrized to specifically minimize the GHG. For the employee profile, the plug-in hybrid concepts show a larger percentage benefit over the BEV concepts, which is due to the higher occurrence of shorter trips in this profile, that can be driven mostly electrically with a smaller battery by the plug-in hybrid concepts. For the PHEV-CNG concept, it is beneficial to rely on a significant use of the combustion engine in case of the GHG optimization instead of increasing the battery capacity. For the petrol-E10 counterpart, the fuel consumption is limited by an increased battery capacity and more electric driving.

Regarding the TED, the results are shown in Fig. 17. According to the results for the GHG emissions, the minimum achievable TED values are also reduced, compared to the pool-vehicle profile, due to the calmer driving profile. The plug-in hybrid concepts, optimized towards the TED, allow for a smaller TED than the BEV concepts. Their battery capacity of around 30 kWh is sufficient to complete the representative driving cycle of the highest distance cluster with 210 km almost purely electrically. At the same time, the reduced power of the EM allows for the operation of the EM with higher efficiencies in electric driving situations, due to higher specific power utilization, compared to the BEV concepts. Additionally, the higher number of gear modes of the transmission can be used during purely electric driving, further increasing the efficiency.

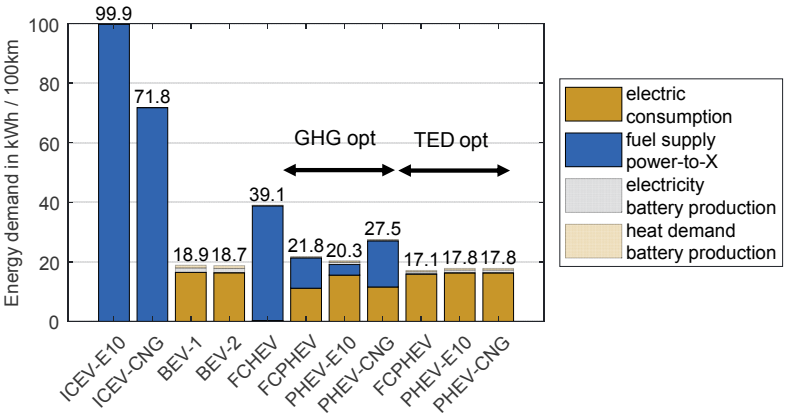

Fig. 17: TED of the powertrain concepts identified by the optimization framework for the employee profile with GHG emissions and TED as objective functions.

Worldwide harmonized Light vehicles Test Procedure

As described at the end of Section III, we evaluate the previously presented powertrain parametrizations on the WLTP and compare the results to the determined GHG emissions. The relevant values are summarized in Table 8. The vehicles from the optimization towards the GHG emissions for the employee profile are considered for the comparison, which means that all values result from the vehicle simulation with the parametrizations presented for the employee profile. Additionally, the CO2 emissions resulting from the WLTP evaluation, which only consider the tailpipe emissions, the previously determined total GHG emissions and the TED are compared.

Table 8: Evaluation of the CO2 emissions of the vehicle parametrizations from the employee profile according to the WLTP. The results from the consideration of the total GHG emissions and the TED are denoted for the comparison from the GHG-optimal powertrains.

	units	ICEV-E10	ICEV-CNG	BEV-1	BEV-2	FCHEV	FCPHEV	PHEV-E10	PHEV-CNG
WLTP									
utility factor	~	0	0	1	1	0	0,92	0,97	0,90
petrol	l/100km	4,7						0,1	
CNG	kg/100km		3,2						0,6
H2	kg/100km					0,6	0,3		
elecricity	kWh/100km			12,9	12,8		6,8	12,1	8,6
tailpipe emissions	gCO2/km	96	83	0	0	0	0	2	17
Ecological impact on employee profile									
GHG	gCO2/km	164	149	119	119	119	109	114	112
TED	kWh/100km	100	72	19	19	39	22	20	28

From the comparison, it is clear that the evaluation according to the WLTP is not suited to measure the eco-impact considering the complete GHG emissions. This is plausible since the WLTP does only consider direct tailpipe emissions. The GHG emissions of all powertrain concepts are underestimated. Especially the emissions of 0 gCO2/km for BEV and FCEV vehicles are misleading. Furthermore, regarding the eco-impact according to the TED, the WLTP leads to wrong conclusions. For example, the benefit of the plug-in option for FCEV concepts shown in this work is not getting transparent. Also, the previously determined low GHG emissions and TED values of the PHEV-CNG cannot be concluded by the evaluation according to the WLTP. Despite these issues, the evaluation according to the WLTP is the established process, used by policy makers to induce changes to the vehicle market. For example, the average fleet emissions of manufacturers, limited to 95 gCO2/km for 2020 by the European Commission, are determined using the WLTP. The authors believe that the current homologation process leads to distorted incentives in the reduction of the ecological impact and that the introduction of a more suited evaluation procedure would improve the effectiveness in achieving the goal of a more ecological mobility.

6 Conclusions

In this contribution, we present a data-driven optimization framework for the comparative evaluation of the eco-impact of different powertrain concepts. Naturalistic driving profiles, containing the occurrence frequency of operating states in the speed, acceleration and road-slope dimension are the basis for the evaluation. Representative and multidimensional driving cycles are generated to depict the driving profiles in a compressed manner within the optimization framework. The representative cycles allow for an efficient search of the optimal powertrain

parametrizations in the optimization. Since the ecological potential of all powertrain concepts is identified with this framework, an equal and unbiased evaluation basis is generated to compare different powertrain concepts. We investigate the GHG emissions and the Total Energy Demand (TED) of vehicles with long-range capability for the reference year of 2030 in Germany. In our study, most of the currently discussed powertrain classes (BEV, FCEV, PHEV) are included to provide a comprehensive comparison of the ecological potential of the presented concepts on a uniform evaluation basis.

Important conclusions can be drawn from our study of two exemplary naturalistic driving profiles:

The driving profile itself has a significant impact on the GHG emissions and the TED. For example, the calm and efficiency-oriented driving style of the employee profile leads to a reduction of 19,6-22,2 % of the GHG emissions, for the concepts that were optimized towards the GHG emissions, compared to the pool-vehicle profile. This shows that the use of real-driving profiles from the relevant application should be used to ensure that the real ecological impact of the vehicles is estimated.

The results of both driving profiles show that the electrification of powertrain concepts is essential to reduce the GHG emissions and the TED. Conventional vehicles have the lowest potential of the studied powertrain concepts to reduce the eco-impact by 2030.

The class of BEV leads to improvements compared to the ICEV class. Within the BEV class, a shiftable transmission, enables to reduce the power of the EM, the electric consumption, the battery size and therefore both the GHG emissions and the TED.

For the plug-in hybrid concepts (FCPHEV and PHEV), the parametrization of the concepts differs dependent on the objective function of the optimization. To minimize the GHG emissions, a smaller battery capacity compared to the BEV concepts already allows for a high electric driving percentage. The use of fuels to manage high distance tracks is preferred instead of further increasing the battery capacity, which would lead to higher vehicle weights and relevant emissions in the production phase. To minimize the TED on the other hand, higher battery capacities are advantageous to limit the use of fuels, which have to be synthesized via Power-to-X with a relatively low efficiency.

The suitability of plug-in hybrid concepts for a reduction of the eco-impact is highly dependent on the distance distribution of tracks in the driving profile. For profiles with a significant share of shorter distance trips, the battery capacities of the plug-in hybrid concepts can be relatively small without diminishing the electric driving percentage. Therefore, on such profiles the benefit of the plug-in hybrid concepts over the BEV increases. Conversely, if most tracks are of a high distance, the battery of the plug-in hybrid concepts and BEV will be dimensioned similarly

and the benefits become smaller. However, in our model, we assume a fully charged battery before each trip for the plug-in hybrid concepts. Therefore, this ecological potential of the hybrid vehicles can only be achieved with a suited user behaviour and regular charging. Unregular charging, on the other hand, would increase the GHG emissions and the TED of the plug-in hybrid concepts significantly.

In the class of FCEV, a plug-in option is identified to be very beneficial for the eco-impact of these concepts. The plug-in option enables to make use of the higher efficiency electric path and enables to reduce the required H2-tank size.

The PHEV concepts achieve reduced GHG emissions compared to the BEV concepts for both investigated profiles. The high electric driving percentage with a reduced battery capacity and vehicle weight is one of the main reasons for this. At the same time, the power of the EM of the GHG-optimized PHEV is smaller compared to BEV vehicles, since the ICE allows to fulfil the highest traction demands by boosting. In the less demanding driving situations, which occur much more frequently, the lower EM power allows for a higher specific power utilization of the EM and therefore the operation in generally more efficient operating points.

Within our contribution, monetary costs have not been considered. Certainly, the ecological return on monetary invest is relevant for the comprehensive comparison of different powertrain concepts and should be further studied. Additional expenses regarding necessary infrastructure could also be included in the investigation. Certainly, the PHEV concepts demand the least adaptions of currently available infrastructure despite the conventional ICEV concepts.

Generally, the three concepts BEV-2, FCPHEV and PHEV-CNG were identified to have the best ecological potential. The plug-in hybrid concepts are especially suited when the distance-distribution is characterized by a high percentage of driven kilometers in the lower distance range while maintaining the requirement of long-range capability.

As additional investigation, we compared the GHG emissions resulting from the evaluation according to the WLTP to the presented comprehensive evaluation. We showed that the obvious discrepancies in the assessment between our holistic approach and the WLTP lead to non-optimal incentives in the design of powertrain concepts. In order to support the development of real-world efficient eco-friendly vehicles, the certification process should be further adapted.

Literature

[1] IPCC, “Climate change 2014 - Synthesis report: Contribution of Working Groups I, II and III to the Fifth Assessment Report of the Intergovernmental Panel on Climate Change [Core Writing Team, R.K. Pachauri and L.A. Meyer (eds.)]. IPCC, Geneva, Switzerland, 151 pp.,” 2014.

[2] A. Esser, J.-E. Schleiffer, T. Eichenlaub, and S. Rinderknecht, “Development of an Optimization Framework for the Comparative Evaluation of the Ecoimpact of Powertrain Concepts,” In: 19. Internationaler VDI-Kongress "Dritev - Getriebe in Fahrzeugen", Bonn, 10.-11. Juli 2019, In: VDI-Berichte, 2354, ISBN 978-3-18-092354-3, 2019.

[3] M. Wietschel, M. Kühnbach, and D. Rüdiger, “Die aktuelle Treibhausgas- emissionsbilanz von Elektrofahrzeugen in Deutschland: Working Paper Sustainability and Innovation No. S 02/2019,” 2019.

[4] F. ISE, “Treibhausgas-Emissionen für Batterie- und Brennstoffzellenfahrzeuge mit Reichweiten über 300 km,” 2019.

[5] J. F. Peters and M. Weil, “Providing a common base for life cycle assessments of Li-Ion batteries,” *Journal of Cleaner Production*, vol. 171, pp. 704–713, 2018, doi: 10.1016/j.jclepro.2017.10.016.

[6] A. Esser, M. Zeller, S. Foulard, and S. Rinderknecht, “Stochastic Synthesis of Representative and Multidimensional Driving Cycles,” *SAE Int. J. Alt. Power.*, vol. 7, no. 3, pp. 263–272, 2018, doi: 10.4271/2018-01-0095.

[7] MathWorks, *Genetic Algorithm.* [Online]. Available: https://www.mathworks.com/help/gads/ga.html (accessed: Sep. 9 2019).

[8] J. Lin and D. A. Niemeier, “Regional driving characteristics, regional driving cycles,” *Transportation Research Part D: Transport and Environment*, vol. 8, no. 5, pp. 361–381, 2003, doi: 10.1016/S1361-9209(03)00022-1.

[9] J.-M. Zaccardi and F. Le Berr, “Analysis and choice of representative drive cycles for light duty vehicles – case study for electric vehicles,” *Proceedings of the IMechE*, vol. 227, no. 4, pp. 605–616, 2013, doi: 10.1177/0954407012454964.

[10] T. G. Farr *et al.,* “The Shuttle Radar Topography Mission,” *Reviews of Geophysics*, vol. 45, no. 2, 2007, doi: 10.1029/2005RG000183.

[11] P. Jardin, A. Esser, S. Givone, T. Eichenlaub, J.-E. Schleiffer, and S. Rinderknecht, “The Sensitivity in Consumption of Different Vehicle Drivetrain Concepts Under Varying Operating Conditions: A Simulative Data Driven Approach,” *Vehicles*, vol. 1, no. 1, pp. 69–87, 2019, doi: 10.3390/vehicles1010005.

[12] G. Paganelli, S. Delprat, T. M. Guerra, J. Rimaux, and J. J. Santin, “Equivalent consumption minimization strategy for parallel hybrid powertrains,” in *IEEE 55th Vehicular Technology Conference*, Birmingham, AL, USA, 2002, pp. 2076–2081.

[13] A. Balazs, *Optimierte Auslegung von Hybridantriebsträngen unter realen Fahrbedingungen*. Fakultät für Maschinenwesen, RWTH Aachen, Dissertation, 2015.

[14] B. Belmonte, Esser, Weyand, Franke, Schebek, and Rinderknecht, “Identification of the Optimal Passenger Car Vehicle Fleet Transition for Mitigating the Cumulative LifeCycle Greenhouse Gas Emissions until 2050,” *Vehicles*, vol. 2, no. 1, pp. 75–99, 2020, doi: 10.3390/vehicles2010005.

[15] FVV, Ed., “Defossilisierung des Transportsektors,” 2018. [Online]. Available: https://www.fvv-net.de/fileadmin/user_upload/medien/materialien/FVV__Kraftstoffe__Studie_Defossilisierung__R586_final_v.3_2019-06-14__DE.pdf

[16] FVV, Ed., “Energiepfade für den Straßenverkehr der Zukunft: Optionen für eine klimaneutrale Mobilität im Jahr 2050,” 2018. [Online]. Available: https://www.fvv-net.de/fileadmin/user_upload/medien/materialien/FVV__Kraftstoffe__Studie_Energiepfade__final_v.3_2018-10-01__DE.pdf

[17] A. Thielmann, A. Sauer, R. Isenmann, and M. Wietschel, *Technology roadmap energy storage for electric mobility 2030.* [Online]. Available: https://www.isi.fraunhofer.de/content/dam/isi/dokumente/cct/lib/TRM-ESEM-2030_en.pdf (accessed: Sep. 19 2018).

[18] H. Helms, Julius Jöhrens, Jan Hanusch, Ulrich Höpfner, Udo Lambrecht, and Martin Pehnt, *UMBRELA: Wissenschaftlicher Grundlagenbericht gefördert durch das Bundesministerium für Umwelt, Naturschutz und Reaktorsicherheit (BMU)* (accessed: May 16 2018).

[19] statista, *Fahrleistung der Pkw in Deutschland im Jahr 2018 (in Kilometern).* [Online]. Available: https://de.statista.com/statistik/daten/studie/246069/umfrage/laufleistung-privater-pkw-in-deutschland/ (accessed: Sep. 25 2019).

[20] Plötz, Gnann, Kühn, and Wietschel, “Markthochlaufszenarien für Elektrofahrzeuge,” 2013.

Virtual RDE: Ensuring RDE conformity of hybridized powertrains in the early stage of the development process

Dr.-Ing. **Michael Grill**, Dr.-Ing. **Mahir-Tim Keskin**, FKFS, Stuttgart;
Prof. Dr.-Ing. **Michael Bargende**, Universität Stuttgart

Zusammenfassung

Die RDE-Gesetzgebung stellt inzwischen strenge Anforderungen an die Schadstoffemissionen hybridisierter Antriebsstränge im Realfahrverhalten. Wichtig hierbei: Es gibt keinen „typischen“ RDE-Testzyklus, vielmehr bedeutet „Realfahrverhalten“ immer eine Absicherung gegenüber unterschiedlichen Worst-Case-Szenarien.

Kritische Phasen eines hybridisierten Antriebsstrangs sind Kaltstarts, insbesondere bei höherer Last, Auskühlphasen der Abgasnachbehandlung in Stausituationen sowie grundsätzlich alle sehr dynamischen Belastungen des Verbrennungsmotors. Wird im Rahmen einer Antriebsstrangsimulation der Verbrennungsmotor als Kennfeldmodell integriert, können diese Effekte oft nicht hinreichend genau abgebildet werden. Dies kann dazu führen, dass Mängel in der RDE-Konformität erst sehr spät im Entwicklungsprozess erkannt werden. Wenn diese erst spät im Entwicklungsprozess über Eingriffe in die Applikation behoben werden, ist dies durch „Heizmaßnahmen“ meist mit deutlichen Verlusten im Wirkungsgrad des Gesamtsystems verbunden.

Für einen maximalen Wirkungsgrad des gesamten, hybridisierten Antriebsstrangs ist es daher sehr vorteilhaft, bereits sehr früh im Entwicklungsprozess die RDE-Konformität absichern und den Antriebsstrang unter deren Einhaltung optimieren zu können.

Zusammen mit der Robert Bosch GmbH hat das FKFS hierfür einen neuen Ansatz entwickelt. Kern davon ist eine kombinierte, physik- und datenbasierte Modellierung des Verbrennungsmotors einschließlich der Abgasnachbehandlung als Quelle der Emissionen. Physikbasiert werden dabei insbesondere die Bauteile modelliert, die bzgl. RDE-Konformität von besonderer Relevanz sind. Als Beispiele können die Trägheiten von Luftpfad, AGR-Pfad und Aufladesystem genannt werden oder die thermische Trägheit der Abgasnachbehandlungsanlage. Der Brennraum als Quelle der Emissionsbildung wird hierbei mit dem neuen RapidCylinder-Ansatz als Kombination einer physikbasierten Beschreibung des Ladungswechsels und einer datenbasierten Modellierung der „heißen“ Hochdruckphase beschrieben.

Im Betrag wird die Motivation erläutert, die Methodik vorgestellt und ein einfaches Anwendungsbeispiel präsentiert.

Abstract

With the introduction of "Real Driving Emissions" (RDE) powertrain simulation has become indispensable to identify critical operating conditions for the exhaust aftertreatment system at an early stage in the development process and to analyze possible corrective actions. Therefore a rudimentary virtual RDE calibration is also necessary in the early concept phase. For doing so, it makes a lot of sense to use 1D flow simulation to model effects such as boost pressure built-up, high/low pressure EGR travel times or thermal inertia. There are two challenges regarding 1D simulation of RDE:

- Combustion system development is usually done at single cylinder engines. It is necessary to integrate the results of the single cylinder engine in an effective way into a virtual full engine for RDE investigations and first virtual calibration
- Moreover, it is typically necessary to investigate a vast number of RDE driving patterns, taking up much more computational time than it was the case previously with a single type-approval driving cycle. Consequently, "Fast Running Models" (FRM) that reduce the computational effort needed for flow simulation have been used to counteract this increase. However, it is inevitable that such an approach reduces the accuracy of the boundary conditions at intake valve closing (IVC), e.g. EGR rate, temperature and pressure, and crucially, the predictive power of quasi-dimensional burn rate, emission or knock models is very sensitive to these parameters. Such an approach thus yields results of questionable reliability, with the risk of overlooking critical conditions that have to be addressed later on at much higher costs.

Existing data-based approaches avoid these challenges, but fail to depict relevant physical processes in the flow path predictively (boost pressure built-up etc.), making it hardly possible to assess technologies such as variable valve trains.

Therefore Robert Bosch GmbH and FKFS developed a new simulation approach. The new tool presented in this paper thus combines a physics-based model for the gas exchange (intake and exhaust system) with a data-based model for the high pressure-part, using mean effective pressure and emission values derived from the test bench or detailed 1D flow simulation. This solves the aforementioned dilemma and provides at the same time an easy way to use test bench data for RDE simulations and powertrain analysis.

The implementation of such an approach will be presented in this paper, along with some exemplary results showing how the new tool can be used to generate accurate and reliable results for RDE investigations at minimal computational cost.

RDE Challenge and Existing SimulationTools

From 2017 on new passenger cars in the EU have to fulfil exhaust gas emission limits also under RDE conditions. While the emission limits will tighten from current Euro 6d-TEMP to Euro 6d in 2020 and Euro 7 beyond the RDE regulation includes many drive requests that go beyond the current pre-defined driving cycles. E.g. on the one hand vehicle speeds up to 160 km/h and severe accelerations on inclining roads can cause high raw emissions that have to be converted reliably by exhaust gas aftertreatment (EAT). On the other hand low ambient temperatures (down to -7°C), long single stop durations (up to 5 minutes) and downhill drives can lead to an underrun of the lower operational temperature limits of the EAT components. In the near future the latter issue might be even strengthened by two striven efficiency-enhancing measures – hybridization with longer ICE standstill periods and reduction of fuel demanding cold start heating strategies.

A series of the RDE requests as well as the emission calculation itself are related to extensive drive sections or even the full RDE drive. As a consequence the substitution of RDE drives by a small number of representative powertrain operation sequences is only possible to a very limited extent. The consideration of RDE performance within powertrain and EAT concept evaluation causes thereby a high testing effort which might even be complicated by missing hardware during early concept phase. 0D/1D powertrain simulation including the prediction of the thermal behaviour of ICE and EAT as well as EAT conversion rates could help to virtualize RDE tests in order to save time and costs of powertrain development.

Additionally simulation can be used for synthetic RDE driving profile generation to create “worst-case” drives, either by combining a variety of cut up measured real driving sequences or by utilizing stochastic driving parameter distributions derived from them. Fundamental condition for harnessing the potentials of virtual RDE tests is a simulation tool that constitutes an optimal compromise between predictability, flexibility and simulation time.

Assessing existing simulation approaches shows that all of them have severe drawbacks regarding this demand profile (see Fig. 1):

1. Detailed 1D flow simulation model coupled with quasi-dimensional models

Physical modeling has proven itself to be a valuable tool in the development of engine technologies: especially 1D-CFD allows the modeling of the whole combustion engine with great flexibility and moderate effort. Air system dynamics, EGR-mixing and the gas exchange can be simulated accurately. Combustion models are available in a broad variety - from measured burn rates over simple Vibe approximations up to phenomenological approaches that allow the prediction of the rate of heat release ([1]-[3]). The application ranges from very ear-

ly stages in the development where the engine hardware is not necessarily defined or available until the support of function development and software calibration in the final development stages. Virtual hardware components like turbochargers can be matched to the respective requirements or EGR control strategies can be evaluated. All in all it represents a very powerful tool, albeit with a crucial drawback with regard to RDE boundary conditions: computational times (real time factor 50…200, [4]), although rather low compared to 3D-CFD simulations, are still quite high – too high for the high amount of different operating conditions that has to be tested for RDE development. To a limited degree, this can be mitigated by using smart features like master/slave modes for the cylinder objects in full engine models, allowing to reduce the computational effort for the high pressure part distinctly (e. g. almost 75% in a four-cylinder engine). However, as the main part of the computational time is consumed by the flow simulation, the overall reduction is insufficient for RDE demands.

2. Fast-running 1D flow simulation model coupled with quasi-dimensional models

This approach addresses exactly the already mentioned, high computational effort for 1D CFD flow simulation. The basic idea is to lump various flow volumes together, reducing thus the number of required calculations per time step while enabling a larger time step size at the same time. A considerable reduction in simulation time can be reached in this way, coming close to real time capability depending on the level of simplification (a factor of two compared to real time can be considered as a typical value), which is definitively enough to qualify for the "fast" tag. However, this approach inevitably changes the model's ability to predict pressure waves in the flow part – actually one of the most important benefits of 1D simulation compared to a pure 0D approach – leading to significant changes in the boundary conditions at IVC for the high pressure part. By nature quasidimensional models are very sensitive to these starting conditions (not unlike the real engine), so they should only be used with flow models that can deliver accurate boundary conditions for the combustion.

3. Data-based models/mean value models

Data-based approaches are the tools of choice when it is required to quantify characterize existing systems accurately. Here, former map-based interpolations are increasingly replaced by statistical models that are able to describe the desired result value in dependence of more than just one to three input parameters, which are typical for maps. This can either be necessary to describe results depending on the degrees of freedom of operation that modern engines provide or to represent the deviations from stationary operation an engine faces while operated under highly transient conditions. Besides the proven fulfillment of ac-

curacy demands, trained data models can be evaluated with nearly no computational effort. Here the limitation is the extrapolation capability – data based models can only provide trustful information where training data was available. In particular this means that changes in the intake or exhaust system compared to the original configuration cannot be taken into account in the simulation model, making it highly inflexible and unsuitable for tasks like function development and calibration.

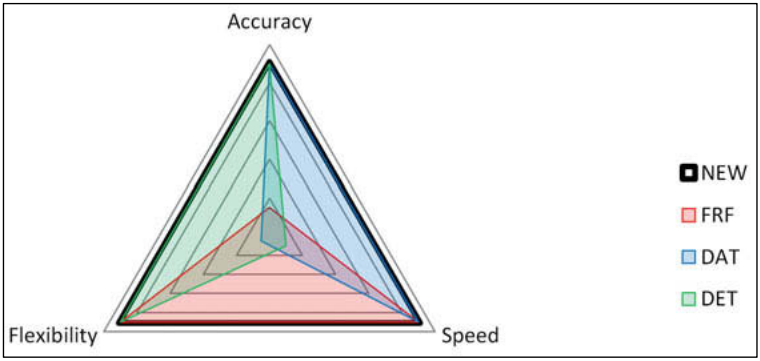

Fig. 1: Positioning of different simulation set-ups along the three basic requirements for RDE simulations (DET: detailed 1D flow simulation model coupled with quasidimensional models; FRF: Fast-running 1D flow simulation model coupled with quasidimensional models, DAT: data-based models/mean value models)

Basic Idea for New Tool

To get a fast, accurate and flexible simulation tool, a combination of data-based and physics-based modelling was chosen, an approach that has already been successfully applied with regards to emission models (see [5]):

- Data-based representation of combustion characteristics and emissions to increase computational speed and to reduce the sensitivity of the high pressure part to inaccuracies from fast-running gas exchange calculations
- Physics-based representation of gas exchange, air system dynamics and EGR-mixing to maintain full flexibility

To link both parts, the pressure at EVO is the most important quantity that has to be modelled. A dedicated interface was developed (dubbed “RapidCylinder®”) that calculates the

pressure trace based on characteristic combustion values (such as the pressure at EVO) and sets the engine-out emissions to the desired values. This basic idea is depicted in Fig. 2.

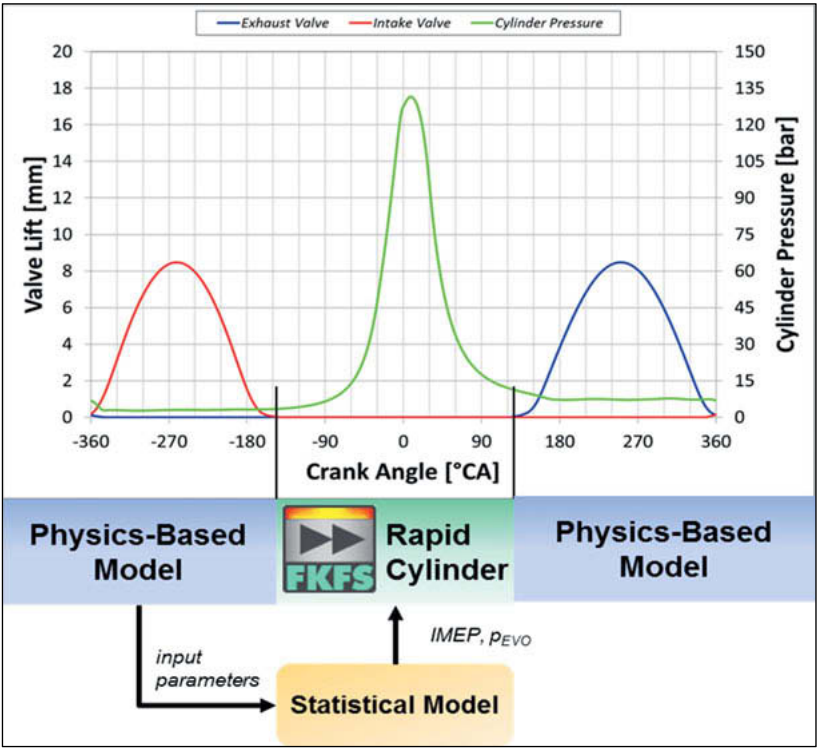

Fig. 2: Basic approach of new simulation tool

While the physics-based model is basically the same as in existing simulation tools – the use of a Fast Running Model is recommended – the data-based part requires some preparatory work to be done. The process can be described as a three-steps-approach, which is detailed in the following sections:

- "Data Sampling": Generating input data for the data-based model (engine measurement campaigns or detailed 0D/1D simulations)
- "Training": Generating of statistical models that derive the desired characteristic values from input parameters of the intake path

- "Calculating": The characteristic combustion values as well as emission values are fed to the "RapidCylinder®" that links the physics-based flow model to the data-based in-cylinder model.

Data Sampling

The necessary database for the data-based model can be either generated by means of detailed 1D flow simulation or on the test bench (typically one cylinder engines are used). In both cases, the first step is the design of experiments.

Users should start with the question which control parameters are to be used as input parameters for the statistical model. The answer will obviously depend on the type of engine (i.e. gasoline or Diesel), but also other factors will decide which set of parameters represents a sensible choice. For instance, if a simulation model is used for data generation, the residual gas content at IVC can be easily and directly determined, whereas other quantities such as valve overlap would have to be used when data sampling is test-bench-based. Table 1 shows an exemplary –by no means exhaustive – list of parameters that could be varied to generate the necessary database.

Table 1: Example of possible variation parameters for data generation

variation parameters Diesel engine	variation parameters gasoline engine
engine speed	engine speed
amount of injected fuel	manifold pressure
rail pressure	air/fuel ratio
EGR rate	residual gas content
boost pressure	inlet valve closing (IVC)
start of injection (main injection)	ignition timing
amount of fuel (pilot injection)	temperature at IVC
[…]	[…]

The number of variation parameters as well as the individually set sensible variation range will determine the number of required operating points. Generally speaking, a one-digit number of variation parameters and some hundred resulting operating points will represent an adequate database. Depending on the desired accuracy of the statistical model and the number of output parameters that are of interest for the user, the number of operating points

may increase. For instance, if a prediction of soot emissions with high accuracy is desired, a higher number of variation parameters will be needed typically.

Training

The output parameters that have to be determined based in the generated database are already fixed within the RapidCylinder®. There are both mandatory and optional quantities as described in Table 2.

Table 2: Output parameters of the statistical model that are fed to the RapidCylinder®

mandatory parameters	optional parameters
indicated mean effective pressure of high-pressure part (Shelby definition) cylinder pressure at exhaust valve opening (EVO) […]	peak pressure prank angle of peak pressure emission values […]

Finally, a statistical model is needed to connect the input parameters (as listed in Table 1) with the output parameters (as listed in Table 2). The statistical model then uses the generated database for training.

For the simplest cases, i.e. when a very low number of input parameters is chosen, the statistical model could be as straightforward as a 2D or 3D table that can be directly stored in the flow simulation program. However, for more complicated cases, other tools will be more useful. Neuronal networks (for instance MATLAB-based) or Gaussian Process Modelling (for instance with ASCMO® by ETAS GmbH) could then be used for the statistical model. In any case, the user only has to make sure that based on the boundary conditions from the flow simulation, the statistical model calculates the parameters described in Table 2 and feeds them forward to the RapidCylinder®.

Calculating

The RapidCylinder®, which is fed with the data from the statistical model, finally has to create a synthetic pressure trace that meets the desired target values (i.e. indicated mean effective pressure and pressure at EVO plus optional parameters if specified). By doing so, the gap

between intake and exhaust path in the flow simulation model is closed and the model can run like any conventional 1D CFD flow simulation.

Fig. 3 illustrates how a pressure trace algorithm is used to generate the pressure trace from the target values. This is done automatically within the RapidCylinder® source code and does not require any user input. Additionally, the temperature and heat transfer rate for every time step are estimated, as these could be useful quantities for the design of the engines cooling system or the dimensioning of components. Furthermore, if emission values are specified by the statistical model, the RapidCylinder® will make sure that the exhaust gas has exactly the desired composition in the flow simulation, which can be in turn useful for modelling the exhaust aftertreatment.

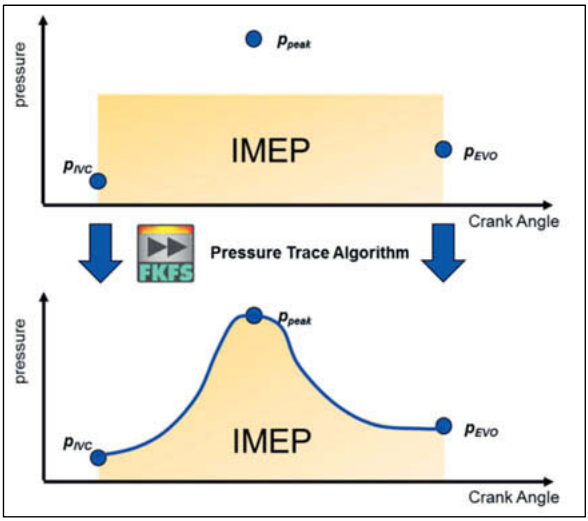

Fig. 3: Generation of pressure trace

Application and Exemplary Results

In Fig. 4, a section of a RDE drive cycle calculated with the RapidCylinder®-approach is compared with the results using the UserCylinder®, both running in the same fast running 1D flow model. For the comparison, a RDE-ready 4-cylinder Diesel engine with 2l of displacement volume and a start-stop system was used. For a gasoline engine, the same quality of results can be expected. The RDE section includes the longest allowed single stop duration of five minutes. It can be seen that both calculation methods can follow the target vehicle

speed reasonably well, thus proving the quality of the transient controllers. In this example, the computation time when using the RapidCylinder® is reduced by a factor of 0.5 to 200 min compared to the UserCylinder® calculation.

At the first part of the cycle, including the standstill phase, the SCR catalyst wall temperatures of both approaches are almost identical. After the fast acceleration following the standstill phase of the cycle, the maximum difference of only 14 K is reached. For the rest of the drive cycle, the temperature difference is close to zero.

These results clearly illustrate the benefit of the RapidCylinder® in drive cycle calculations: While producing almost the same results as the detailed calculation of combustion processes, only half of the computational time is needed. Still, transient effects like the boost pressure built-up are accounted for in simulation. Especially when comparing different set-ups of engine periphery (like turbochargers) or different car configurations, the RapidCylinder® allows an investigation of more variants in a shorter time, while simultaneously maintaining the high level of reliability of simulation results.

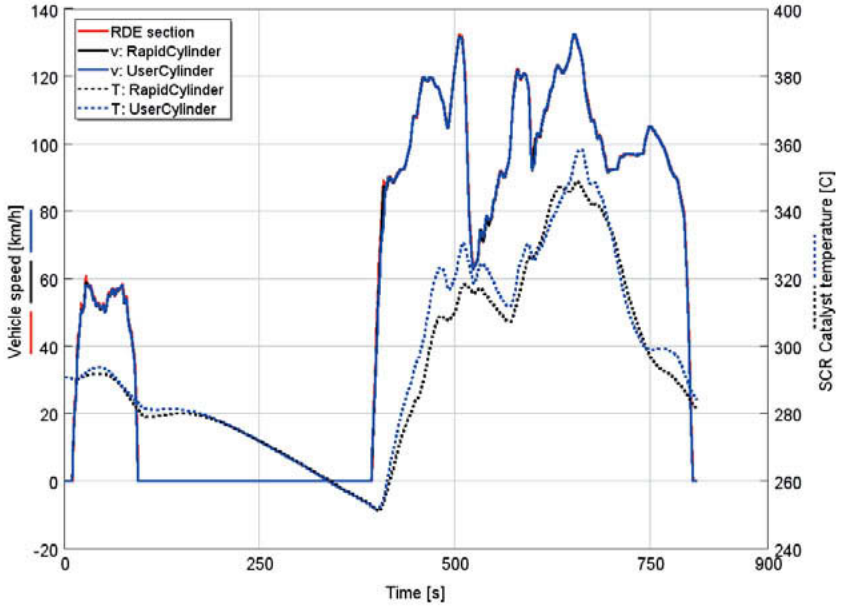

Fig. 4: RDE-application of RapidCylinder® vs. UserCylinder®: comparison of catalyst temperature

Literature

[1] Fandakov, A.; Grill, M.; Bargende, M.; Kulzer, A.: Two-Stage Ignition Occurrence in the End Gas and Modeling Its Influence on Engine Knock. SAE paper 2017-24-0001, 2017.
[2] Kaal, B.; Grill, M.; Bargende, M.: Transient Simulation of Nitrogen Oxide Emissions. SAE paper 2016-01-1002, 2016.
[3] Grill, M.; Kaal, B.; Rether, D.; Keskin, M.: Strömungsmodelle zur Analyse und Optimierung von komplexen Systemen in transienten Zuständen. 17th Conference VPC – Simulation and Test, Hanau, 2015.
[4] Mirfendreski, A.: Entwicklung eines echtzeitfähigen Motorströmungs- und Stickoxidmodells zur Kopplung an einen HiL-Simulator. Dissertation, Stuttgart, Universität, 2017.
[5] Cornetti, G.; Kruse, T.; Huber, T.: Simulation of diesel engine emissions by coupling 1-D with data-based models. 14th Stuttgart International Symposium – Automotive and Engine Technology, Stuttgart, 2014.
[6] Grill, M.; Keskin, M. T.; Bargende, M.; Bloch, P.; Cornetti, G.; Naber, D.: A new, Model-Based Tool to Evaluate RDE Compliance during the Early Stage of Development. In International Conference on Calibration Methods and Automotive Data Analytics (p. 188), expert verlag, 2019.
[7] Bloch, P.; Cornetti, G.; Naber, D.; Keskin, M.-T.; Grill, M.; Bargende, M.: A Combined Approach of Physical and Data Based Modeling to Simulate the Combustion Engine. In: Power-train Diagnostic Symposium, Baden-Baden, 2018.

Generic optimization environment and knowledge-based guided evolutionary algorithms for automated transmission calibration

Method to generate a knowledge base through impact analysis of parameters and using it to reduce unnecessary iterations using GA

Thomas Korb, Dr.-Ing. **Markus Nussbaumer**, BMW Group, München;
Prof. Dr.-Ing. **Stephan Rinderknecht**, Institute for Mechatronic Systems in Mechanical Engineering (IMS), Technical University Darmstadt

Zusammenfassung

Der Aufwand hinsichtlich der Kalibrierung von Funktionsparameter in einem Getriebesteuergerät zur Steuerung und Regelung der Schaltstrategie, der Schaltabläufe bzw. der Zustandsübergänge, hat in den letzten Jahren automobiler Entwicklung erheblich zugenommen. Dies ist auf diverse und vielfältige Gründe zurückzuführen, beispielsweise auf die immer weiter zunehmende Anzahl von Antriebsstrangvarianten, die Hybridisierung, oder auf die unaufhaltsame Erweiterung des Funktionsspektrums. Um sich dieser Herausforderung anzunehmen und sie zu bewältigen, existieren diverse Ansätze, dem steigenden Kalibrierungsaufwand und den damit steigenden Kosten durch die Automatisierung des erforderlichen Abstimmungsprozesses zu begegnen. Für gewöhnlich werden dazu konventionelle Optimierungsalgorithmen verwendet, um definierte Bewertungsgrößen zu maximieren oder Kostenfunktionale zu minimieren. Die Metaheuristik dieser Algorithmen, in Kombination mit der Skalarisierung von Fehlerkriterien, sorgt für eine nicht immer zielgerichtete Vorgehensweise der Optimierung, wodurch unnötige Iterationen gerechnet werden müssen, welche die Optimierungszeit in die Höhe treiben.

Ein in diesem Artikel vorgestellter neuartiger Ansatz adressiert diese Thematik durch ein anderes Verfahren. In diesem werden alle Informationen, die ein zeitbasierter Verlauf beinhaltet, verwendet und nicht nur skalare Bewertungsgrößen berechnet. Dies dient der Extraktion von Informationen bzgl. der Parametereinflüsse auf das Systemverhalten, wodurch eine Wissensbasis generiert werden soll. Der zugehörige Prozess startet mit dem Aufteilen eines Zeitverlaufs nach einer Parametervariation in charakteristische Segmente. Diese werden anschließend den Abschnitten innerhalb einer Referenzkurve zugeordnet, wodurch phasenweise analysiert werden kann, welche Unterschiede erzeugt wurden. Das dadurch gewonnene Wissen enthält folglich den Zusammenhang zwischen den Funktionsparametern und dem Systemver-

halten, welches darauffolgend innerhalb einer Metaheuristik eines konventionellen Optimierungsalgorithmus verwendet werden soll, um die Optimierung zu lenken und so die Konvergenz zu verbessern. Das Ziel dabei ist es, Rechenzeit einzusparen, was ganzheitlichere Ansätze und Betrachtungen ermöglicht.

Abstract

The effort for calibration tasks regarding the transmission control unit and especially the functional parameters for the shifting strategy, shifting processes or mode changes, has increased dramatically. This is due to various reasons, e.g. the increasing number of powertrain variants or the unstoppable expansion of the functional spectrum. To overcome this, there were many attempts to cope with the rising calibration efforts and costs, by automating the necessary calibration processes. Commonly used are conventional optimization algorithms, whose metaheuristics, combined with the scalarisation of error criteria are not always target-oriented, thus causing unnecessary iterations and increasing computation time. An approach presented in this paper proposes a different procedure. It uses all the information within the time-based signals and not only scalars to extract information about the functional parameter's influences on the system behaviour. This is done through splitting up an obtained signal after a parameter variation. The segments are subsequently matched into the reference curve, whereby analyses concerning the differences are made possible. The knowledge, generated about the connection between the functional parameters and the system output, is intended to be used within a metaheuristic of a conventional algorithm to guide the optimization and improve convergence, thus potentially saving simulation time.

1 Introduction

The effort an OEM has to put into calibration tasks regarding the transmission control unit and its functional parameters for the shifting strategy, shifting processes or mode changes has considerably increased over the last few years. This is due to numerous influences out of various categories of boundary conditions. The following listing and the order of those items does not imply their importance nor claims completeness. The first group of influences causing calibration work load runs under the term of "variety": In the last decade many new vehicle derivatives were introduced [1,2]. This, combined with the increased number of powertrain variants [3], resulting of different power classes of the engines, engine types, degrees of electrification, transmission types or the powertrain topology - to name some attributes - lead to more and more calibration effort [4]. That is because every variant has to be calibrated to fulfil the highest quality standards of customers, including the longitudinal behaviour as one core element. The

latter leads to the second group, the driving functions and the functional spectrum. This group contains the driving modes, like comfort, eco or sport on the one hand and automated driving functions (e.g. ACC, LKAS) or customer functions like the parking or the reversing assistant on the other hand. In addition, by using DHTs, there is possibly a larger amount of possible operating modes (e.g. serial or eCVT) and mode changes. Also, relatively new topics such as Highly Automated Driving or Fully Automated Driving enlarge the functional spectrum even further, because manual driving is still a major application. When driving on one's own, there are influences on the vehicle by the environment, such as slopes with different gradients or curves, which leads to the third group of influences on the calibration effort. The vehicle has to behave sovereignly in every driving scenario, also including the influence by the ambient temperature and other weather conditions, as well as the temperature of the possibly used hydraulic oil used for actuators to control e.g. the transmission. The latter leads to the fourth group, which contains effects that are inherent in the used system, like nonlinearities due to temperature dependency (oil viscosity, friction, leakage) or wear occurring over lifetime. Those influences on the calibration effort strongly depend on the installed components in the vehicle. The fifth and last group that should be mentioned at this point are the different markets, where many different legal requirements exist, concerning the fuel consumption and resulting emissions, for instance, that have to be fulfilled. All those aspects result in a huge amount of calibration effort, that causes high personnel costs for application engineers or application contracts, high costs due to a lot of prototypes for testing – also in different climate regions – as well as high and expensive test bench times in return. Besides to the high costs, the application process as a whole and achieving the desired quality of the system behaviour is very time consuming, which stands in contrast to continuously shortened development times [5]. Also, the responsiveness on market developments and customer needs is thereby sluggish. The mentioned aspects and qualitatively and exemplarily indicated impacts by the automation are illustrated in figure 1.

To reduce the costs is an omnipresent task in the automotive industry, particularly in these times of changing market requirements and uncertainty [6]. Therefore, there has been many attempts to cope with the rising calibration efforts and costs, by automating the necessary calibration processes [7,8,9,10,11].

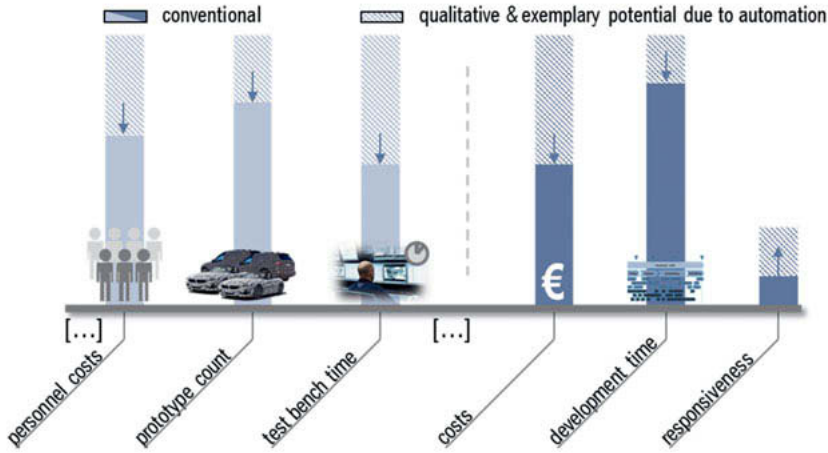

Fig. 1: Overview on affected aspects through the automated calibration

The conventional procedure during the transmission calibration is done in a vehicle and on the road, by a test driver that typically adjusts functional parameters of the control unit software and evaluates the system behaviour. This is an iterative procedure until the shift quality satisfies the quality standards or set requirements, which are often subjective to the test driver's experience. In addition the use cases are difficult to reproduce on the road or test track.

To simplify this procedure it is possible to use software to evaluate the shift quality [12]. Originating from the conventional process, different approaches were made in the field of simplifying the calibration process, starting with ways to make the scenarios more reproducible, using a trailer while still calibrating on the road or test track [13] for instance. Approaches that tend more into the direction of automation use a chassis dynamometer and a corresponding software interface [14], or only some hardware of the vehicle in so-called hardware-in-the-loop test benches. Starting from this point of configuration the so-called model-based calibration is feasible. More recent approaches are based on software-in-the-loop (SiL) [15] or model-in-the-loop environments [16], where virtual simulation models substitute expensive vehicle components [9].

Most works in this research field resemble each other considering the rough structure of the used methodologies: To represent the system behaviour – in this case the transmission and the TCU – simulation models are built up, mostly resulting in a total vehicle simulation. Those models, which are later used in model-in-the-loop environments need to precisely represent

the influence of the functional parameters, characteristic curves and characteristic maps on the system output characteristics. However, there is always a conflict between model quality – meaning precision – and simulation time [17].

To evaluate the quality of the simulation model behaviour, for example the longitudinal acceleration or its characteristic, some kind of rating system is needed, that substitutes the subjective assessment grades or rating, done by application engineers or test drivers within the conventional process. The rating system, or rather objectification, transfers physical quantities and their time response over one or more use-cases into scalars that can be interpreted more easily. Some commercial tools including such a method exist that also offer the possibility to use the evaluation system in the vehicle, on the road or test track (online) during real driving manoeuvres [18,19]. In general the evaluation is based on the influence of the vehicle acceleration or movement and the occurring vibrations on the human body. Therefore the arising frequencies are sometimes filtered to obtain the most relevant frequency range, which is the range defined by the resonance frequencies of human organs (e.g. stomach) [8]. After using mathematical evaluations like VDV or P2P, reference values are needed, to classify the obtained scalars. This is possible through expert knowledge or proband tests and threshold values to span an evaluation grid. VDV means ‘Vibration Dose Value’ and is an assessment value for oscillations, which is explained later. P2P means ‘peak-to-peak’ value and describes the value difference between a peak value and the adjacent (local) minimum.

A different approach is to use the subjective assessment grades or mathematical scalars and match them with a meta-model to an objective grade system [8]. Summarizing, the general approach is to transfer time-based behaviour into scalars and transfer the latter into interpretable objective grades, thus losing the time-based characteristics and shapes of the physical quantities. A cost function evaluates one or more use cases or driving scenarios within a simulation and puts out the combined costs, based on the objectification.

Based on the previously described objectification and the cost function output, mostly stochastic and evolutionary optimization algorithms are used to minimize the cost criteria, using built-in metaheuristics. For detailed explanations about popular optimization algorithms, such as (MO)PSO or NSGA-II, see further appropriate literature [20,21,22]. The quality of the optimization results depends heavily on the made settings, the initialization of the individuals or particles within the value space, which is spanned by the allowed parameter values and especially for nonlinear effects, on the exploration behaviour of the algorithms. Exploration simplified means to obtain new solutions that are not derived from existing ones through multi-point or arithmetic crossing, for instance [23].

While exploration can be decisive, it also deteriorates the convergence behaviour [24,25] and thus increases unnecessary iterations and consequently optimization time.
The simplification of many values into scalars by calculating simple error criteria and the unguided behaviour of the used algorithms in a wide spread value space of the parameters and thus high optimization time for holistic approaches are possible causes, why no holistic method has yet been established.
To contribute to this cause, this work presents a different approach for automated calibration: The weak point of undirected exploration and possibly unnecessary iterations of conventional optimization algorithms is addressed in this work, as well as it focuses on the mentioned loss of time-based characteristics and the shape of the physical quantities through objectification. Therefore, in contrast to scalar error values, the present work focuses on generating a knowledge base through analysing the changes in the system behaviour depending on a specific parameter variation and using the total shape of physical quantities, instead of scalar error values. The motivation for the latter is explained in the following section.

2 Scalar rating and scalar error criteria

As mentioned in the introduction, scalar rating values are often easy to interpret and contain the essential ‘absolute’ information. How the number was calculated is neglected, although there could be many variants to obtain the same value through different time-based signals, regarding the calculation of the VDV rating, for instance. Its formula is taken from [26], simplified and shown in equation (2.1).

$$B_{VDV} = \sqrt[4]{\int a(t)^4 \, dt} \tag{2.1}$$

For the following explanation why this is a possible problem, a fictive and abstract example is illustrated and shown in figure 2. The x-axis represents a functional parameter value, the y-axis the scalar rating value, calculated based on the current setting of the fictive parameter. The graph and its extremes are presumed to be unknown and require a lot of simulation time to be acquired. The circles (C1, C2 and M1) represent individuals of the current iteration of a stochastic evolutionary algorithm. The population size in this example is three (npop = 3) and M1 was obtained through mutation and is a perfect example for exploration, because it ‘jumps’ near the extreme E3 through this metaheuristic procedure. The solutions C1 and C2 were selected for a crossing procedure – an arithmetic one in this case. The RNG-value (random

number generator) determines the new functional parameter value (p12) for the ‘descendant’, represented by a red X in figure 2.

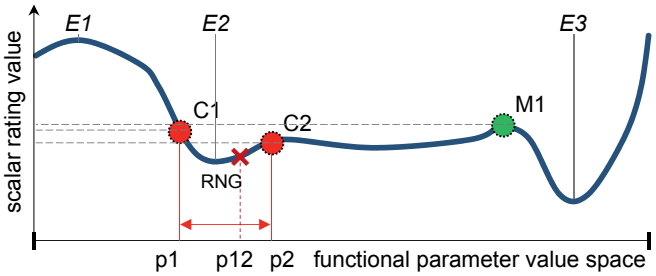

Fig. 2: Example for an algorithm temporarily getting stuck due to focus on local optima and unfortunate settings

Given the fact that the scalar rating values of C1, C2 and their descendant – through crossing – are below M1’s rating value, they are objectively performing better. Because there can only be a specific number of individuals per generation (npop) considering computer power and the defined settings, a selection of the individuals qualifying for the next iteration is made. One selection type is the so-called plus-selection $(\mu/\rho+\lambda)$ [25] and is commonly used. This selection method considers every parent individual and every descendant through crossing or mutation while evaluating and sorting them by rank – descending from the best and non-dominated rank one (R=1). Because of crossings and mutations the number of individuals for the current generation (including parents) is higher than the defined number (npop). Therefore only the first npop elements qualify for the next iteration. In the present case this means that C1, C2 and their descendant (npop = 3) are considered for the next iteration while M1 is lost. This shows – continuing from here – that it is only possible to identify and reach the global minimum (E3) through mutation, which will take a lot of unnecessary iterations, depending on the random number generation, the system nonlinearities and crowding distance techniques.
The described inherent characteristics of scalar criteria and the information loss is transferrable to common error criteria.

2.1 Weak points of conventional error criteria

Returning to the automated calibration and given the fact an ideal longitudinal acceleration time sequence exists and is known, a target/actual comparison is needed. The time sequence can originate from literature [9], test group studies, the desired and defined characteristics of

a vehicle derivative or from measurements of a calibrated derivative which serves as a template for other derivatives. This is analogue for regarding drive mode changes in DHTs or similar procedures. For the target/actual value comparison there are many error criteria like MAE, MSE, RMSE, MAPE and other [27]. When reducing a lot of samples or data points of a time sequence into a scalar (or two: STD), every conventional error criteria has the information loss in common, which could mislead optimization algorithms. Derived from the fictive example shown in figure 2, figure 3 serves as an example for the mentioned weak point and shows idealized and exemplary longitudinal acceleration time sequences for fictive traction upshifts.

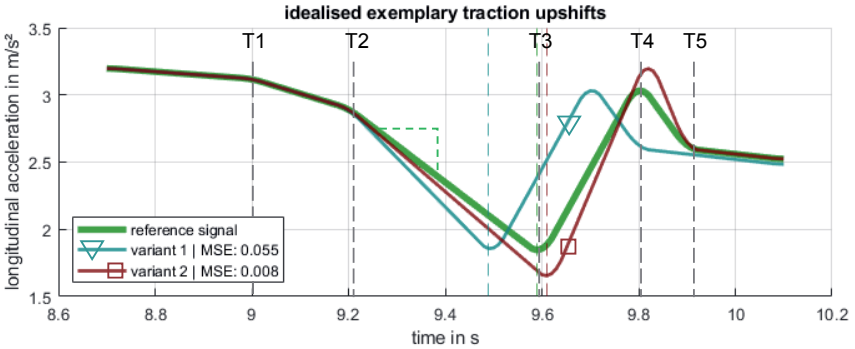

Fig. 3: Example for a misleading scalar error criteria value on the base of idealised exemplary traction upshifts

The thick green graph is the reference signal representing the ideal behaviour of the system, taken from fictive test person studies, for instance. The turquoise (triangle) and dark red (square) graphs are the result of current functional parameter values within two different individuals of an optimization. The optimization algorithm's goal is to minimize the error criterion – in this case the MSE between the reference signal and each variant. As shown in the legend the second variant achieves a mean error of 0.008, which is about a seventh of the mean error of variant 1. Therefore the algorithm prefers solutions such as variant 2 because it is interpreted that this curve fits the reference better due to the smaller error value. If the variant 1 is regarded more detailed concerning its shape, it becomes apparent, that only the phase between T2 and T3 of the reference signal and between T2 and the minimum of the turquoise graph are different, because of the gradient in this phase. The minima and maxima of both mentioned graphs have the same values, also the acceleration values after the minima are exactly the same. That means if there is the possibility to change the gradient by a parameter

that does not affect the other phases, the reference signal will be met with very little effort, despite the mean squared error suggests a different approach.
The described phenomenon is the motivation for a different consideration of deviations between target and current solution.

2.2 Phase-wise analysis

To evaluate the differences between reference signal and the current signal in a more suitable way, the analysis needs to occur in a sequential manner. For the example shown in figure 3 this means that the “variant 1” graph has to be divided into phases or characteristic sections. In this case a segmentation is already suggested for the reference signal. The needed segmentation for variant 1 is done analogous. After splitting up the graph, each obtained phase needs to be assigned to the corresponding phase within the reference signal, allowing it to analyse the phase-wise differences. If this procedure is repeated after a functional parameter variation numerous times, it appears feasible to extract the influence of functional parameters on the system behaviour and their properties against the background to use this knowledge for a faster optimization. As the latter, the following attributes are plausible to be extracted: affected phase, intensity of the influence, interaction with other parameters through non-linearity, characteristic change on the graph (stretching/compression, gradient change, oscillation, offset).

3 Method

The present work shows an approach to extract the mentioned influences due to functional parameters by dividing a signal into characteristic segments, matching them into a parent curve and analyse the differences, caused by the parameter variation. The long-term objective is to use the generated knowledge base to guide the exploration behaviour of an optimization algorithm and prevent unnecessary iterations in order obtain a better convergence behaviour and a more intelligent optimization. Furthermore the method could lay the foundation for an intelligent optimization.

3.1 Phase dividing

Before time-based signals are divided into characteristic segments, a pre-processing is performed, including a signal check, filtering and smoothing, based on the inherent curve properties. Thereby, also measurements are a valid input for the method, not only simulation outputs without natural measurement noise. For signals including noise a related amplitude estimation

is done and used as an input for the dividing procedure. The latter is based on finding geometrical shapes within a signal to define a section, which is not as simple as just using regression calculation, because there are many unknowns such as the time-resolution or rather relation of step width to signal length and how many sections there may be, the remaining noise, outliers and more. In addition the method needs to be efficient in terms of computation, because it will be used repeatedly. The following list outlines the steps roughly:

1. linear regression calculation to determine a breakpoint for a phase
2. quadratic regression calculation to determine a breakpoint for a phase
3. evaluation of the breakpoints using a multi-criteria decision including a last check through an artificial neural network designed for recognizing geometrical shapes

3.1.1 Linear regression analysis

The linear regression analysis starts using a horizontal initial value corridor, that uses the mean of the first few values, if feasible (depending on step width), else the first y-value. This is due to the fact, that there could be a fuzziness of the previous split or an offset through noise, which would bias the evaluation. To span the corridor the doubled estimated noise amplitude is added per side, to prevent outliers to extremely shorten the first attempt and to counteract strong gradients at the start of a phase. The initial breakpoint is the index of the data vector which value exceeds the corridor in any directions minus one. Afterwards the first linear regression attempt using the determined initial breakpoint is calculated. To span a corridor the estimated noise amplitude is added to the calculated regression line - once per side. To evaluate the next breakpoint, also the last index within the corridor is taken. Starting from there an iterative process is followed up: Analogue to the first non-horizontal corridor, a regression and a new corridor are calculated, updating the break index with two considerations. The first one is to find a defined number (n_{out}) of consecutive outliers. An alternating signal that returns into the corridor every few (n_{out}-1) steps due to – e.g. oscillations – is not split correctly by this approach. The second variant counts outliers until the maximum allowed number is reached, which is configurable and should depend on the time step width. In addition an option to also regard the percentage of overshooting the corridor is available. The two mentioned approaches both return an index, from which the minimum serves as the next break index. This iterative process of updating the breakpoint is continued until a certain number of iterations is exceeded or until two iterations deliver the same index. Another option before the final step of returning the breakpoint (C), is to follow the signal back to the centreline (A) or to the middle of centreline and the boundary of the corridor (B), which increases the sharpness of the separation for the

current phase, but could make the divide more difficult for the next phase. See figure 4 for the illustration of the mentioned sharpness variants.

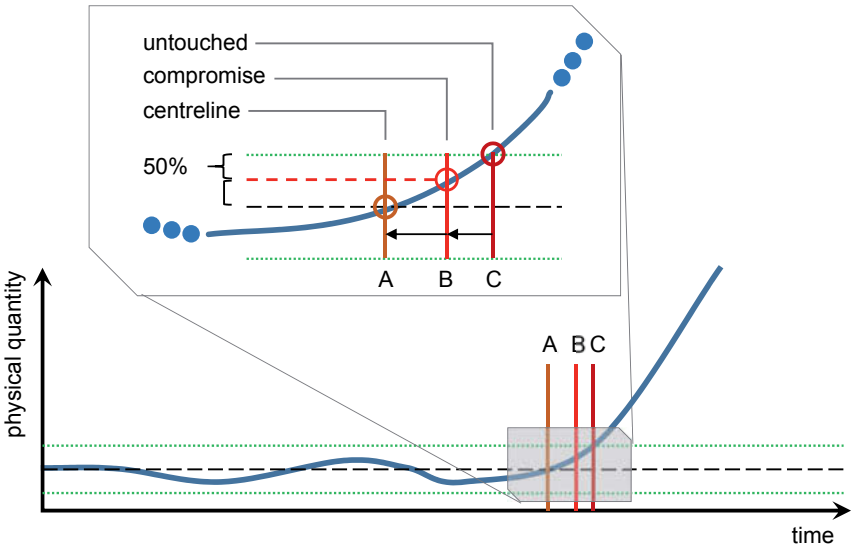

Fig. 4: Variants of sharpness of splitting up a curve

Diverse checks and error analyses concerning the detected noise amplitude value, break index, etcetera, were omitted in the explanation but are existent. The result of the explained linear regression-based evaluation is a breakpoint that is evaluated in section 3.1.3.

3.1.2 Quadratic regression analysis

The quadratic regression analysis to take shapes with curvatures into account, uses the same framework as the linear approach, with some differences. As the name already suggests, there is no linear regression but a quadratic polynomial is fit into the data points within the iterations. Nevertheless there is an exceptional case, which requires an additional feature. It is possible that the regression is faulty due to a relatively short current data segment and bad approximation as illustrated in figure 5.

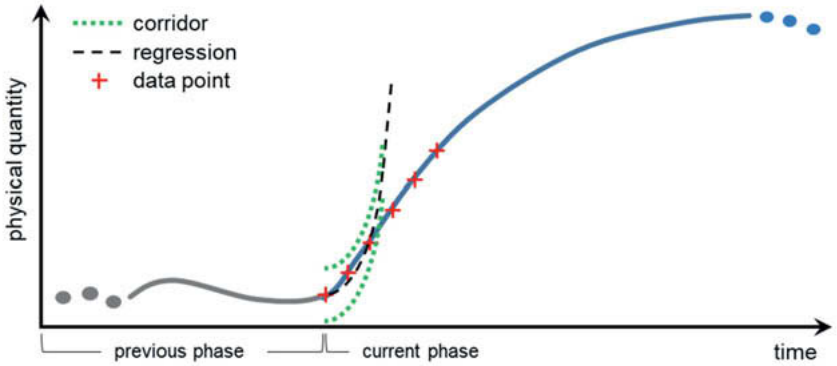

Fig. 5: Possible quadratic regression problem due to the unknown shape of the current segment and thus preventing progress

In that case the iterative process is not capable of continuing and will fail, because the faulty regression approach will not deliver any further indices. Due to that case, reaching the half of allowed iterations, there will be an anticipation into a further area of the signal, to potentially improve the regression quality. Empirical studies on that behaviour revealed the function's necessity. Also, differing from the linear process, the breakpoint does not advance further monotonous, so a logging is necessary. After repetitive results or the maximum number of iterations, the best result is taken as an output of this analysis.

3.1.3 Multi-criteria decision and ANN-based verification

After identifying two possible breakpoints, one needs to be selected to divide a phase from the remaining time-based signal. For this purpose there are several considerations within a multi-criteria selection logic: The usage of the corridor spanned through the noise estimation, the mean error between the data points and the regression's centreline as well as the resulting phase length through the found breakpoints.

The meaning of noise corridor usage is illustrated in figure 6 by two examples. In example a) there will be about 50% estimated noise usage while in b) about 100% are achieved. For b) this is an indication for the inappropriate regression method. It should also be mentioned, that this criterion is extremely vulnerable to outliers, however through the filtering in the pre-processing there should not be any of these left. The mean error is used as an indication for the correct regression as well. The longer phase length is rated better, because the regression method then matches the shape presumably better. The mentioned criteria are evaluated and

result in handicaps for the two methods that are multiplicatively combined to serve the selection of the index.

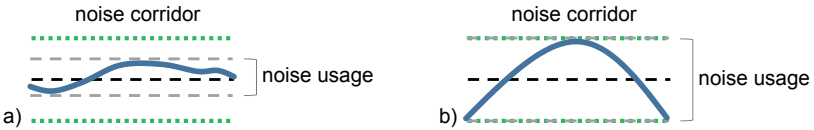

Fig. 6: Noise corridor usage as selection criterion

Empirical reflections have shown that in particular cases the multi-criteria selection logic fails and the index with worse progress or fit is selected. To overcome those scenarios and to improve robustness, an artificial neural network for the purpose of geometrical shape recognition was built-up and implemented (see 3.1.4). The ANN is able to override decisions, made by the conventional selection logic, if the classification is confident. The outcome of the ANN-based multi-criteria selection is an index at which the time-based signal is split, whereby a phase is created. The remaining curve undergoes the explained process until the whole signal was divided into phases.

3.1.4 ANN for shape recognition

As mentioned in the previous section, the ANN serves the purpose of shape recognition to split up the signal with higher robustness. The trained net is saved as network class file in MATLAB, so it can be evaluated very fast. To obtain such an ANN, training data, target data, a net design, training process and validation is needed. In this case the training data and target data were generated in an automatic process of shape generation. Therefore several geometrical shapes that are valid to appear in the time-based signal of a physical quantity are considered, which means straight lines and parabolas in general and modified shapes based on them. To modify the basic shapes different gradients, lengths, coefficients, oscillations with different frequencies and phase shifts as well as noise with different noise amplitudes are used, determined by a random number generator. By this, also incomplete curves are generated and every obtained shape is also flipped vertically and horizontally to enhance the training data amount. Concerning the target data, the origin of each shape is stored to train the ANN and to evaluate the training success afterwards. Figure 7 shows the entirety of training data for an example with reduced samples for better visibility. The left coordinate system shows the multitude of straight lines and the angle variation, without any manipulations. The middle one represents the used

parabolas, already including partial curves, but also without any manipulation. The right picture illustrates every used shape representing the training data.

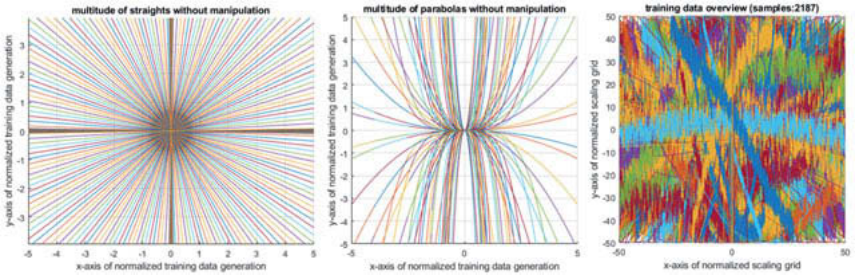

Fig. 7: Multitudes of straights and parabolas being manipulated to represent the training data used for training the artificial neural network for shape recognition

To prevent the ANN from getting too large and resulting calculations from being too computationally intensive, a pre-processing is performed. In doing so, the shapes are fitted and scaled into a normalized area without any loss of details. Now, depending on the desired settings, some loss of details is possible because the normalized area is discretised into grid elements to enable an occupation or pixel analysis. Within the latter, every grid element is checked concerning the signal crossing it, or not. The result is a matrix with Zeros and Ones, describing which ‘pixel’ was touched by the signal. To reduce the input information to the ANN, the matrix is reduced to a column vector by parsing through the matrix in horizontal direction and by averaging the occupied pixels into one. The resulting column vector is later used as a direct input on the input layer neurons of the ANN. The explained procedure is shown in figure 8, in which the shape within the normalized area is shown, together with the resulting pixel analysis and the generated column vector for the neuron input layer on the right. The pixel analysis looks a bit different concerning the shape, because the axes are not scaled equally. It is also noticeable that the y-axis is inverted, which is due to the matrix notation in MATLAB, beginning at 1 at the top line. This is not corrected, because it does not affect the learning process of the ANN. The same applies on the illustrated column vector in the right sub-figure of figure 8. There, the y-axis describes the indices of the vector, while the horizontal bars represent the values within the indexed slot of the vector.

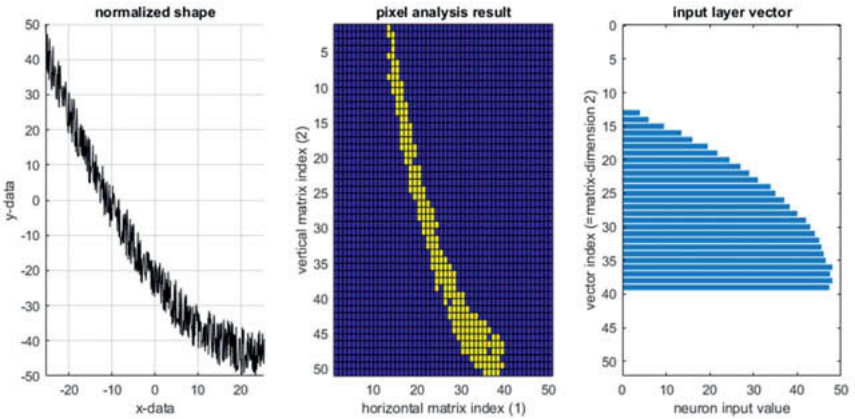

Fig. 8: Multitudes of straights and parabolas being manipulated to represent the training data used for training the artificial neural network for shape recognition. Here, a grid discretisation of 2% is used.

The used net is based on a MLP [28] (feed forward net) but with a classification element before the output, which defines it as a pattern recognition network [29]. The chosen net design is depending on the pre-processing and chosen grid discretization. As mentioned before the number of elements of the input column vector and within the input layer need to be equal. The chosen net design is shown in figure 9, whereas different discretisation levels are also feasible, resulting in a different pixel analysis and net design.

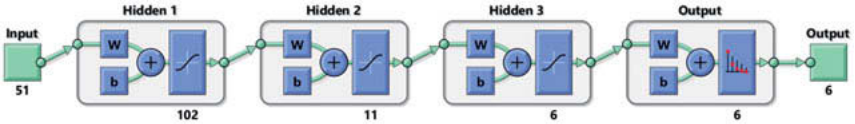

Fig. 9: Structure of the used pattern recognition neural network with the input neuron count depending on the discretisation

The ANN is trained using the neural network toolbox from MATLAB with respect to all effects that could deteriorate the training success, like overfitting. The trained network classifies even unused sets out of the training data very good, which shows its generalisation capabilities. The training success is displayed in figure 10 for an exemplary and reduced data set. The target data is sorted and represented with the thick green curve, which means the ANN has to calculate these target values after evaluating the mentioned column vectors including the shape

information. The red curve is the result of the ANN evaluation, showing a few outliers, representing theoretical misclassifications. Within the misclassifications there are also false positives. This means that the basic shape was manipulated heavily and the ANN classifies the generated shape differently as stored within the target data, but the shape does really resemble the made classification more, rather than the old target class.

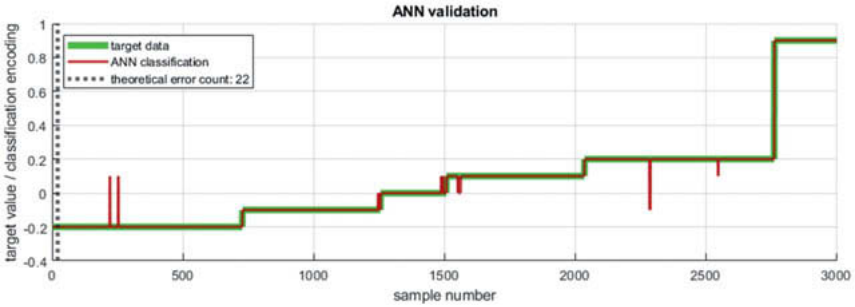

Fig. 10: Validation of the used ANN with every sample of the training data, also unused samples to evaluate the generalisation capability of the net

As mentioned for some errors it is permissible to speak of false positives, because although the target data is not matched, the ANN is still classifying correctly, if compared with the human eye. This is shown in figure 11 b). There, the ANN classifies the shape as ascending straight line, although the target data contains the class of a parabola. Figure 11 a) on the contrary, shows a real error index, because the net also outputs “ascending straight line”, but the target data is more correct and stored the shape to be a flipped (upside down) parabola.
For further explanations concerning artificial neural networks, please refer to relevant literature, such as [30,31].

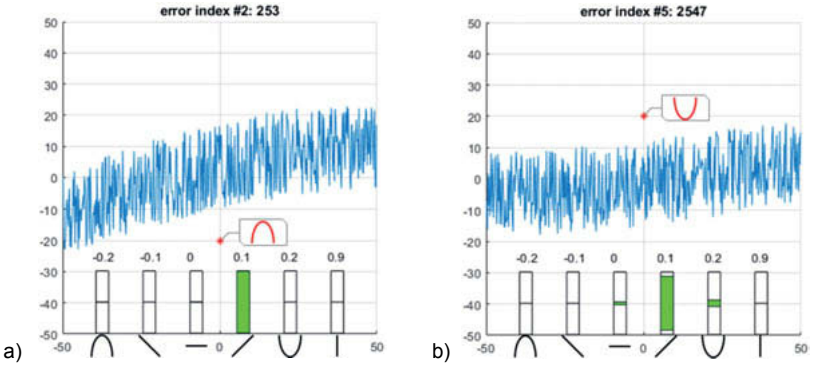

a) b)

Fig. 11: Real error index (a) and false positive (b) as results of the trained artificial neural network

3.2 Phase matching

In the previous subsection the phase dividing was explained, which delivers the input for the phase matching. The latter serves the purpose to match possible altered phases, originating out of a functional parameter variation, into a parent graph. The phase matching is generally based on shape evaluation, which is done via normalized cross-correlation analyses (NCC). The NCC is a method often used in template matching algorithms like facial recognition or motion-tracking use cases [32,33]. The quality of the match is described with the calculated NCC-coefficient (NCCC) γ, which outputs a floating-point number between -1 and 1. In the equation (3.1) [30] to calculate the NCCC, f is concerning to the parent or original graph, $\bar{t}$ is the mean of the template, $\bar{f}_{u,v}$ is the mean of $f(x,y)$in the region under the template.

$$\gamma(u,v) = \frac{\sum_{x,y}\left[f(x,y) - \bar{f}_{u,v}\right]\left[t(x-u,y-v) - \bar{t}\right]}{\sqrt{\left\{\sum_{x,y}\left[f(x,y) - \bar{f}_{u,v}\right]^2 \sum_{x,y}\left[t(x-u,y-v) - \bar{t}\right]^2\right\}}} \tag{3.1}$$

While parsing the template (phase) through the parent, the NCC-coefficient is calculated and documented. Its curve is later on analysed, concerning existing peak values that point out good matches with the parent graph. Ideally there is one peak within the NCC-coefficient curve, so it is clear into which position the current phase has to be matched. This is generally the case when the template is rather long and the parent graph does not resemble a stringing together of template lookalikes. An example for this is shown in the left example of figure 12, where

there is an unambiguous maximum in the NCCC curve. Owed to the processing and parsing through the parent, the added padding has to be subtracted from the found peak value index for finding the starting position, which is illustrated with the horizontal arrow.

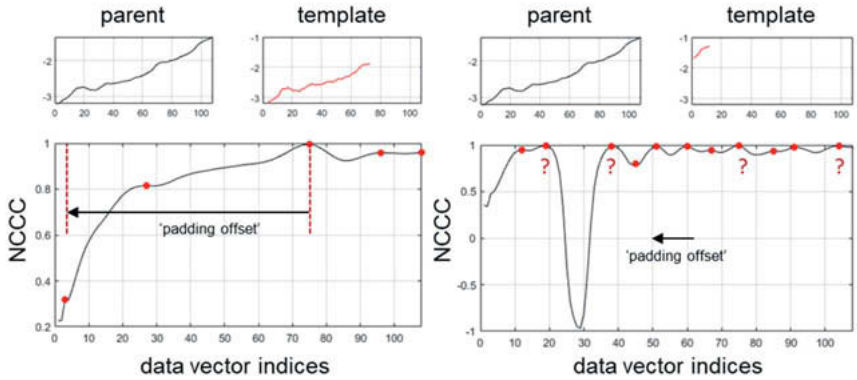

Fig. 12: Exemplary NCC-analyses showing an easy and unambiguous case on the left and a more complex case on the right. The red dots are automatically identified peak values of the NCCC curve

Short templates and long parent graphs complicate the matching process, because many and inconclusive peak values may exist in the NCCC graph, as shown in the right part of figure 12. In that case, making a choice which peak value index is the correct one, is much harder than in the example before, if not unmanageable. In particular, due to the fact that a parameter variation occurred in between the calculation of the curves.

Obviously just picking the highest NCCC value is not expedient. Consequently, an approach taking more available information into account and evaluating defined performance indicators was built-up. Basically the mentioned approach consists of a shape rating, based on the NCCC and a position rating, regarding the estimated position of the current phase. In addition this first matching approach is only working sequentially and will be referred to as ‘sequential matching’ further on.

To influence the performance and needed processing power of the sequential matching, there are some options available: One is the minimum phase length that is accepted for the matching. Because assigning very short phases is hardly possible, phases with phase lengths lesser than a defined threshold value are attached to adjacent phases. The second option enables

or disables temporary attachment or adjacent data points in both directions on the x-axis. This means the current phase is extended using e.g. 10 data points left and right, which simplifies the matching process. The third option restricts the search area for the template and thus the parsing through the parent graph, which is only reasonable if there is existing knowledge about the curves, but can increase performance or the matching quality. The latter is especially the case, if long signals are present. The forth option is a threshold value for the maximum used NCCC peak values that are found while parsing the template through the parent. An overview on the explained options is shown in figure 13.

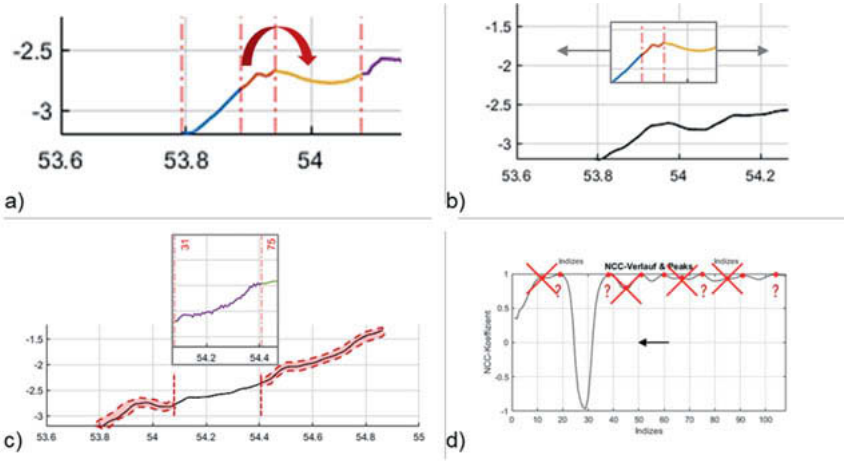

Fig. 13: Options for the phase matching procedure. a) minimal handled phase length; b) temporary attachment (parts of blue and yellow to orange); c) restricted search are within the parent curve; d) limited usage of peak values of the NCCC

3.2.1 Sequential phase matching

After the settings are defined the sequential matching starts, as the name suggests, with the first phase. For each phase the NCC-analysis is executed to obtain possible starting indices of the phase (template) within the parent. The same procedure is carried out after flipping the parent and template curves to determine possible end indices. The flipped NCC analysis basically returns the same peak values, but depending on the options the results differ, especially in edge regions. Also the index back calculation considering the padding added by the NCC is done differently, to acquire the end indices.

All calculated NCC-coefficients are, by subtracting them from one, transferred into a cost value treatment. As noted in the equations (3.2) and (3.3), the subscripts ‘NCC’ and ‘BNCC’ refer to the NCC or backwards executed NCC and ‘B’ is the rating value vector:

$$\boldsymbol{B}_{NCC} = 1 - \boldsymbol{\gamma}_{NCC} \tag{3.2}$$

$$\boldsymbol{B}_{BNCC} = 1 - \boldsymbol{\gamma}_{BNCC} \tag{3.3}$$

As mentioned previously the second part of the assessment of the obtained NCCCs is a rating using the estimated starting position $\hat{P}$. For the first phase that position is 1 (based on data array indexing in MATLAB). For following phases the estimated position is calculated though the chosen starting index of the previous phase and the length of the previous phase, which underlines the sequential character of this matching approach. With $\hat{P}$ the starting positions of the NCCC values are rated, using the symbolic function $I(\boldsymbol{\gamma})$ to obtain the belonging starting indices as described in the equations (3.4) and (3.5).

$$\boldsymbol{B}_{p,S,cu} = \frac{\left|I\left(\boldsymbol{\gamma}_{NCC,cu}\right) - \hat{P}\right| + 1}{L_{cu}} \tag{3.4}$$

$$\boldsymbol{B}_{p,E,pr} = \frac{\left|I\left(\boldsymbol{\gamma}_{BNCC,pr}\right) - \hat{P}\right| + 1}{L_{cu}} \tag{3.5}$$

While the ‘B’ stands for the cost-oriented rating (lesser equals better) the subscripts describe that it is a position rating (‘p’) for starting indices (‘S’) or ending indices (‘E’) for the current (‘cu’) or previous (‘pr’) phase. The phase length is ‘L’ and $\boldsymbol{\gamma}_{NCC,cu}$ as well as $\boldsymbol{\gamma}_{BNCC,pr}$ are column vectors of NCCC values, whose index values are extracted, using the function $I(\boldsymbol{\gamma})$. With the two position rating vectors $\boldsymbol{B}_{p,S,cu}$ and $\boldsymbol{B}_{p,E,pr}$, there are two possible decisions for defining the starting value of the current phase later on: Either the start indices of the current phase are rated better or the end indices of the previous phase, also defining the start index for the current phase. Both rating formulas include an additional increase in the numerator, preventing the position comparison between estimated position and NCCC-defined position from becoming zero. That is because the position rating is later used for a multiplicative selection evaluation and would override other criteria, if zero. The current phase length L_{cu} in the denominator provides more tolerance for longer phases, because for longer phases the NCCC is better and more certain, as already explained, while the estimated position remains an approximation.

The ratings concerning shape $\boldsymbol{B}_{NCC}$ & $\boldsymbol{B}_{BNCC}$ and position $\boldsymbol{B}_{p,S,cu}$ & $\boldsymbol{B}_{p,E,pr}$ are combined multiplicatively, motivated through different value dimensions, into scalars as stated in the equations (3.6) and (3.7).

$$\boldsymbol{B}_S = \boldsymbol{B}_{NCC} \cdot \boldsymbol{B}_{p,S,cu} \tag{3.6}$$

$$\boldsymbol{B}_E = \boldsymbol{B}_{BNCC} \cdot \boldsymbol{B}_{p,e,pr} \tag{3.7}$$

It is possible to grant duplicate indices (originating from NCC,cu and BNCC,pr) a bonus, because they were found independently. After this evaluation the best total rating is selected as well as its index, used to set the start of the current phase, while the evaluation values are stored for later use. For the selection, two variants are possible in principle: defining the start index by the start index ratings ($\boldsymbol{B}_S$) or the end index ratings ($\boldsymbol{B}_E$) from the previous phase. The sequential matching continues until the last existing template is matched into the parent graph.

3.2.2 Overlap correction

Although the estimated position $\hat{P}$ partly takes a target position into account, there is no interception to prevent overlapping from happening. This means it is possible that a selected starting index is lower than already chosen indices. The detection of this scenario is very simple through checking start and end indices. If detected a recursion is started by going back a defined number of phases, starting from the faulty assignment. This is due to the uncertainty when the error was made exactly. Starting from a previous matching, going towards the current matching where the error was detected, every position rating is checked. If the position rating is above a threshold value, it is regarded as unsatisfactory and the column vector of starting positions is re-evaluated in search of a better position rating. If there is no satisfying position rating, the current phase length is used to define the start index for the following phase. Through iteratively calculating towards the phase, where the error was detected, the overlap is corrected. This was proven in empirical studies. If an overlap is still detected after the matching and corrections, it is at least known, so the following analysis can respond to this by skipping some phase interpretations, for instance.

3.2.3 Exemplary matching results

The matching approach was tested using measurements from conventional torque-converter automatic transmissions. To recreate parameter changes, a manipulation environment for the signals was created, which randomly alters signals and their characteristics through stretching, compressing, adding noise or oscillations, shortening or lengthening the phases. Therefore the

variations and matching could be tested without having the exact TCU software and needing a lot of computation power. The examples in figure 14 prove that the matching is working fine under the made prerequisites for the sequential matching.

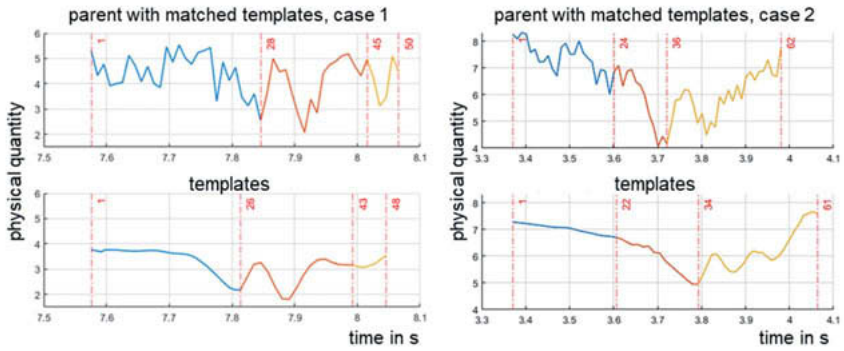

Fig. 14: Exemplary results of the sequential matching process

The sequential matching mentions its disadvantage already within the name and has problems when phases are not existent or interchanged. For this purpose there is already a different work in progress about non-sequential matching or a more robust hybrid form of matching.

3.3 Feature extraction and impact analysis

Through the presented methods of phase divide and phase matching it is feasible to implement an iterative procedure to vary parameters, interpret and understand impacts on the system behaviour by functional parameter changes and save the gathered information. To prevent interdependencies between functional parameters to happen or misinterpretations a one-step-at-a-time-method seems the most viable approach. Therefore and because a parameter sensitivity analysis is usually done before optimizing parameters, the feature extraction and impact analysis could go hand in hand with the Morris Method [34]. There, multiple trajectories through the value space of functional parameters are planned, executed and elementary effects of the changes are calculated. Yet, there is no framework to automatically run the presented method, because no notation of the identified effects was developed until now, but is a work in progress. The feature extraction is already feasible, as stated, and one exemplary impact analysis is shown in table 1.

Tab. 1: Result of the phase-wise analysis considering features like NCCC, data point differences, time and data offsets, stretch or compression percentages, additional frequencies with their corresponding amplitudes and the estimation of noise

	phase_index	NCCC	delta_data_p	time_offset	data_offset	x_stretch	y_stretch	
	1	2	3	4	5	6	7	
1	65	0.8502	0	0.1219	-2.1925e-04	0.0621	0.9437	
2	111	0.0028	0	0.5618	0.0115	0.0442	0.4265	
3	59	0.8837	0	0.2093	-2.8415e-05	0.2244	0.0816	
4	21	0.3434	2	-0.2322	-6.2099e-04	0.4013	1.3228	[...]
5	2	0.8360	0	-0.1188	-0.0045	0.2282	0.1404	
6	63	0.8113	0	0.0694	0.0039	0.1666	0.1763	
7	80	0.9268	0	0.3977	0.0038	0.1061	0.5493	
8	87	0.7365	-2	0.6629	0.0071	-0.1370	0.8169	

Also, based on calculated ratings and correlation coefficients, it is possible to filter the generation of the knowledge base, by only including interpretations that are based on high certainties. The latter is easily feasible using a threshold value.

3.4 Knowledge-based guidance of algorithms

Based on the knowledge base and extracted influences of the parameters the defined aim was to use this knowledge to influence optimization algorithms in the first run. By that unnecessary iterations or unguided mutations could be reduced. An exemplary closed loop optimization using the knowledge base is shown in figure 15.

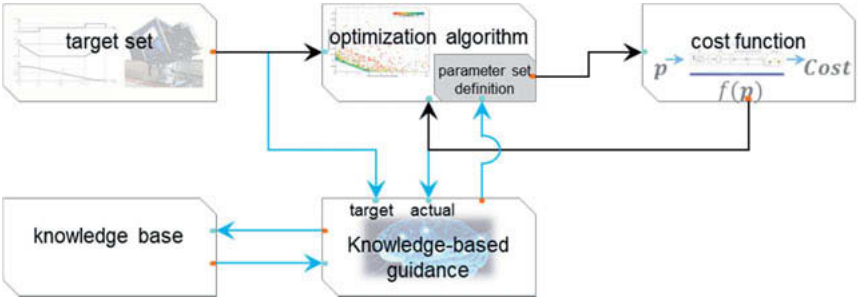

Fig. 15: Closed loop of an optimization algorithm with additional knowledge-based guidance through target-actual comparison and influence on the parameter set definition

In the illustration of the closed loop optimization the black arrows symbolize the conventional optimization progress. Depending on the target set, the metaheuristics of the algorithm define a parameter set that is evaluated within a cost function. The individuals or particles are equipped with their performance rating, on which the further procedure through the metaheuristics is based (selection, mutation, crossing, …). Whereas the blue arrows and the modules in the second row are new. Through intercepting individuals and comparing the achieved system behaviour and target behaviour it is possible to evaluate the deviations in detail, in contrast to scalar error criteria. Based on consulting the knowledge base it is possible to identify necessary changes in the parameter set of the individual. This information is passed on to the parameter set definition module within the optimization algorithm, together with the concerned individual. Now it is possible to influence the mutation metaheuristic to a desired extent.

4 Optimization environment

Every explained approach or method within this paper is implemented within a generic optimization environment, which aims on being easily applied on optimization problems. Therefore the structure is simple: For an optimization or sensitivity analysis there are three key elements needed: configuration, object, cost function. The configuration contains the settings for every used module such as the parameter sensitivity analysis, the chosen optimization algorithm and its parameters, the environment interface as well as many more possible modifications. One of the most important and obligatory elements is the environment interface, which contains the parameters, their type, value space, resolution and if it is a discrete parameter, also the possible values. Possible parameter types are workspace variables, constant block's values in MATLAB Simulink, parameters in an s-function interface from Dymola (Dassault Systèmes) or Excel-based parameters. The mentioned object is a simulation model, mathematical problem or an Excel sheet. It is also possible to use more than one object at a time for an optimization. The last thing needed, is the cost function, which evaluates the performance of the current iteration or the system behaviour, if a sensitivity analysis is executed. Through only three key elements, easy templates and standard settings, it is very simple to start an optimization or analysis within the built-up framework. A heavily discrete optimization problem was already tested, optimizing the shifting matrix of a novel DHT concept, defining which gears to choose, depending on the initial and desired gear.

5 Results

As seen in the corresponding sections, the phase divide works and enables the phase matching, which is also functional within the boundary conditions of signals being of sequential nature. Thus, mathematical analyses between the matched phases and parent segments are feasible. Characteristic changes, such as differing data points, offsets in y-direction or delays, distortions such as an extension or compression in each coordinate direction, additional oscillations and their amplitudes or different noise assessments can already be detected. For rather constant segments the gradient change and thus the angle difference is evaluated. All calculated and found features are stored with a reference to the underling functional parameter variation, causing the differences. Based on the parameter set dimensions, changed to enforce a different behaviour, a notation is necessary to describe the parameter's influence in an understandable way.

6 Conclusions and future work

This paper presents an approach to improve the procedure of common optimization algorithms, through the implementation aiming on generating a knowledge base to describe the influence of functional parameters on the system behaviour. This is leaned on and comparable to the human way of working. Therefore the phase divide is a first step to extract characteristic segments out of the considered signal. Although the results are mostly satisfactory, there is still need for improvement. Sometimes the found breakpoint is only a bit off, which could be addressed by snapping to extremes, found through a pre-analysis or an auxiliary signal analysis. There are already some concepts and work concerning this is in progress.

The found segments are matched using the sequential matching approach presented in subsection 3.2.1 with the mentioned disadvantages. The latter are the inability to handle interchanged phases or if a phase is masked out. To address this weak point a non-sequential matching procedure is currently in work, stronger depending on the shape of the segments, rather than their estimated position. The principle is to match non-sequentially, starting from the segments with the highest matching certainty and optionally blocking the assigned time area. However, first attempts show a larger sensitivity to overlapping. Therefore a combined matching method could be a solution to overcome the mentioned weaknesses. Nevertheless, the results of the matching procedure are satisfactory to a great extent and used for the impact analysis, which extracts the differences between matched segments. There, a notation for the characteristic changes is still pending. This is also possible to be a piecewise definition, depending on the section of the parameter value space. Or, possibly with more sophisticated

methods such as an automatic feature extraction with AI or based on big data and statistical approaches, because a lot of data is collected while generating the knowledge-base.
With this notation, the closed loop shown in figure 15 is realisable and first holistic experiments are viable, which will answer many questions concerning the efficiency or feasibility for more complex systems or complex parameter relationships. Although every function within the presented approach was programmed efficiently and with the commonly huge number of iterations in mind, statements about efficiency are not possible yet. However, analysing one traction upshift takes less than 2-3 seconds with an older program status of the presented functions and should be more efficient in the current version. Considering that a total vehicle simulation model is used, the additional time should be of no weight.
Another question is how the approach treats highly non-linear systems where it turns out really difficult if not impossible to clearly state the influence of a functional parameter. Anyway, it should still be possible to rate the intensity of the influence on the corresponding phases.
The handling of parameter characteristic curves or maps or a even a dedicated framework for an intelligent optimization are long-term objectives to further contribute to the automation of parameter calibration.

Acknowledgements
The authors want to thank Michael Johannes Sangl for his contribution to the optimization framework and Ishwor Koirala for his support within feasibility studies.

Abbreviations

ACC	**A**daptive **C**ruise **C**ontrol (also known as dynamic cruise control)
ANN	**A**rtificial **N**eural **N**etwork
BNCC	'**B**ackwards' **NCC** (using flipped curves)
DHT	**D**edicated **H**ybrid **T**ransmission
eCVT	**e**lectrical **C**ontinuously **V**ariable **T**ransmission
GA	**G**enetic **A**lgorithm(s)
HiL	**H**ardware-**i**n-the-**l**oop
LKAS	**L**ane **K**eep(ing) **A**ssist **S**ystem
MAE	**M**ean **A**verage Error
MAPE	**M**ean **A**bsolute **P**ercentage **E**rror
MLP	**M**ulti**l**ayer **p**erceptron
(MO)PSO	(**M**ultiple **O**bjective) **P**article **S**warm **O**ptimization
MSE	**M**ean **S**quared **E**rror

NCC	**N**ormalized **C**ross-**C**orrelation
NCCC	**NCC-C**oefficient
npop	**n**umber of individuals in a **pop**ulation
NSGA-II	**N**on-dominated **S**orting **G**enetic **A**lgorithm
OEM	**O**riginal **E**quipment **M**anufacturer
P2P	**P**eak-**to**-**P**eak (value difference between minimum and maximum)
RMSE	**R**oot-**M**ean-**S**quare **E**rror
SiL	**S**oftware-**i**n-the-**l**oop
STD	**St**andard **D**eviation
TCU	**T**ransmission **C**ontrol **U**nit
VDV	**V**ibration **D**ose **V**alue

References

[1] BMW Group (2019). The first-ever BMW 2 Series Gran Coupe. [online] 16.10.2019 [accessed: 04.03.2020]. <https://www.press.bmwgroup.com/global/article/detail/T0301580EN/the-first-ever-bmw-2-series-gran-coupe>

[2] BMW Group (2019). The new BMW M8 Gran Coupe and BMW M8 Competition Gran Coupe. [online] 09.10.2019 [accessed: 04.03.2020]. <https://www.press.bmwgroup.com/global/article/detail/T0301406EN/the-new-bmw-m8-gran-coupe-and-bmw-m8-competition-gran-coupe>

[3] Schlott, S. (2018). Konzeptwildwuchs in der Getriebetechnik. [online] 04.01.2018 [accessed: 04.03.2020]. <https://www.springerprofessional.de/getriebe/schaltgetriebe/ konzept-wildwuchs-in-der-getriebetechnik/15275986>. Springer.

[4] Reichenbach, M. (2019). Schaltstrategie und Hybridisierung. ATZ-Automobiltechnische Zeitschrift, 121(12), 20-21.

[5] Hoesli, S., Klomp, M., & Bleicher, H. (2018). Virtuelle Absicherung von Pkw-Lenksystemen. ATZ-Automobiltechnische Zeitschrift, 120(12), 46-51.

[6] Wirth, G. (2019). Bayerischer Rundfunk Homepage. Analyse: Bayerns Autoindustrie im Wandel. [online] 04.04.2019 [accessed: 04.03.2020]. <https://www.br.de/nachrichten/wirtschaft/bayerns-autoindustrie-im-wandel,RMaSE7E>

[7] Rot, I. (2017). Methode zur modellbasierten Kalibrierung der Schaltablaufsteuerung von Getriebesteuergeräten in virtueller Umgebung. Shaker.

[8] Alvermann, G. (2009). Virtuelle Getriebeabstimmung. Shaker.

[9] Kahlbau, S. (2013). Mehrkriterielle Optimierung des Schaltablaufs von Automatikgetrieben.

[10] Ranogajec, V., Deur, J., Ivanović, V., & Tseng, H. E. (2019). Multi-objective parameter optimization of control profiles for automatic transmission double-transition shifts. Control Engineering Practice, 93, 104183.

[11] Ranogajec, V., Coric, M., Deur, J., & Ivanovic, V. (2018). Multi-objective parameter optimization of automatic transmission shift control profiles (No. 2018-01-1164). SAE Technical Paper.

[12] Reddy, R., Matthies, F., & Heyder, U. (2019). Mess-und Bewertungssystem für das Fahrverhalten. ATZ-Automobiltechnische Zeitschrift, 121(4), 42-47.

[13] Binnenbruck, R., & Petzold, G. (2011). Bremsanhänger als Werkzeug für die ortsunabhängige Fahrzeugerprobung. ATZextra, 16(5), 64-67.

[14] Küçükay, F., Kassel, T., Alvermann, G., & Gartung, T. (2009). Effiziente Abstimmung von automatisch schaltenden Getrieben auf dem Rollenprüfstand. ATZ-Automobiltechnische Zeitschrift, 111(3), 216-223.

[15] Gläßgen, P., & Menold, S. (2018). Virtual Transmission-in-the-Loop. Ein vielversprechender Entwicklungsansatz. ATZextra, 23(2), 22-26.

[16] Lampe, A., Mettin, U., & Serway, R. (2017). Generische Getriebesteuerung mit virtueller Doppelkupplung. ATZ-Automobiltechnische Zeitschrift, 119(12), 28-33.

[17] Matthies, F. & Lindemann, M. (2008). Untersuchung der Modelltiefe für Fahrbarkeitsaussagen. Simulation und Test in der Funktions- und Softwareentwicklung für die Automobilelektronik II. expert Verlag GmbH, Renningen.

[18] Ortner, M., Kerschbaumer, A., Resel, M., & Schörghuber, C. (2019). Antriebsstrangprüfstände für die Getriebekalibrierung von Nutzfahrzeugen. ATZ-Automobiltechnische Zeitschrift, 121(12), 22-29.

[19] Krause, M., Haverkort, G., & Beck, R. (2011). Werkzeuge und Methoden zur effizienten Getriebeapplikation. ATZextra, 16(5), 58-63.

[20] Coello, C. C., & Lechuga, M. S. (2002, May). MOPSO: A proposal for multiple objective particle swarm optimization. In Proceedings of the 2002 Congress on Evolutionary Computation. CEC'02 (Cat. No. 02TH8600) (Vol. 2, pp. 1051-1056). IEEE.

[21] Deb, K., Pratap, A., Agarwal, S., & Meyarivan, T. A. M. T. (2002). A fast and elitist multiobjective genetic algorithm: NSGA-II. IEEE transactions on evolutionary computation, 6(2), 182-197.

[22] Zitzler, E. (1999). Evolutionary algorithms for multiobjective optimization: Methods and applications (Vol. 63). Ithaca: Shaker.

[23] Kaya, Y., & Uyar, M. (2011). A novel crossover operator for genetic algorithms: ring crossover. arXiv preprint arXiv:1105.0355.

[24] Weiß, F. (2018). Optimale Konzeptauslegung elektrifizierter Fahrzeugantriebsstränge. Eine computergestützte Methodik zur Beschleunigung des Auslegungsprozesses (Vol. 122). Springer-Verlag.

[25] Sittig, A. (2014). Optimierung und Applikation von Betriebsstrategien in Hybridfahrzeugen (Doctoral dissertation, Technische Universität München).

[26] Verein Deutscher Ingenieure (2002). VDI-Richtlinie 2057. Part 1: Human exposure to mechanical vibrations – whole-body vibration. Düsseldorf.

[27] Grover, P. (2018). 5 Regression Loss Functions All Machine Learners Should Know. Choosing the right loss function for fitting a model. [online] 05.06.2018 [accessed: 03.03.2020]. <https://heartbeat.fritz.ai/5-regression-loss-functions-all-machine-learners-should-know-4fb140e9d4b0>

[28] Pal, S. K., & Mitra, S. (1992). Multilayer perceptron, fuzzy sets, classification.

[29] Beale, M. (2008). Pattern recognition neural network – MATLAB function, MATLAB Documentation. The MathWorks, Inc.

[30] Zurada, J. M. (1992). Introduction to artificial neural systems (Vol. 8). St. Paul: West Publishing Company.

[31] Gurney, K. (2014). An introduction to neural networks. CRC press.

[32] Lewis, J. P. (2001). Fast Normalized Cross-Correlation. Industrial Light and Magic. 10.

[33] Kaso, A. (2018). Computation of the normalized cross-correlation by fast Fourier transform. PloS one, 13(9).

[34] Morris, M. D. (1991). Factorial sampling plans for preliminary computational experiments. Technometrics, 33(2), 161-174.

The systematic way to your sustainable powertrain platform – holistic and customizable

Systematical methods to investigate mobility scenarios of tomorrow

Dr. **Christoph Danzer**, **Tobias Voigt**, **Alexander Forell**, **Marc Sens**, **Erik Schreiterer**, **René Kockisch**, Dr. **Jörg Müller**, **Erik Schneider**, IAV GmbH, Berlin and Chemnitz / Stollberg

Zusammenfassung

Um die globalen CO2- und Emissionsziele zu erreichen, muss die Mobilität ganzheitlich und unter Einbeziehung von Nachhaltigkeitskriterien bewertet werden. Durch verschiedene Mobilitätsszenarien wird eine Vielzahl an hybriden und elektrischen Antriebssystemen erzeugt, welche systematisch hinsichtlich CO2-Tank-to-Wheel, Well-to-Wheel, Cradle-to-Grave sowie Primärenergie und Produktionskosten optimiert werden. Darüber hinaus werden die verschiedenen Parameter der Antriebsstrangdefinition auf Flottenebene optimiert, um Plattformsysteme für Hybrid- und Elektrofahrzeuge mit einem Maximum an Übernahmeteilen zu generieren und die Gesamtkosten zu reduzieren. Diese innovative Werkzeugkette zeigt den systematischen Arbeitsablauf von der Definition der Anforderungen an zukünftige Mobilitätslösungen hin zu nachhaltigen Antriebsstranglösungen.

Abstract

To reach the global CO2- and emission-targets the mobility needs to be assessed holistically also including sustainability criteria. With different mobility scenarios a variety of hybrid and electric powertrain systems will be generated which are systematically optimized in regard of CO2 Tank-to-Wheel, Well-to-Wheel, Cradle-to-Grave, primary energy and production costs. Furthermore the powertrain settings will be optimized on the fleet level to generate platform systems for hybrids and electric vehicles with a maximum of carry over parts and reduce the overall costs. This innovative tool chain shows the systematical workflow from mobility demands to sustainable powertrain solutions.

Introduction

CO2 fleet targets in Europe through to 2030 are defined essentially by legislation [1], with target values ranging from 50 to 70 g CO2/km, depending on fleet composition. These targets

can only be achieved with considerable electrification measures, which reduce the consumption level in the currently tank-to-wheel balancing (TtW). But carbon-neutral mobility can only be achieved by 2050 if most of the necessary primary energy comes from renewable energy sources. Consequently, carbon balancing should be extended from the wheel at least to the fuel or energy source (chemical/electrical), known as well-to-wheel (WtW). An honest comparison of the powertrain concepts needs to consider cradle-to-grave balancing (CtG), due to the fact that the various powertrain forms differ in terms of their global warming potential (GWP - ecological footprint for manufacturing, production and recycling) in addition to emissions from their operation.

Another challenge encountered the route to carbon-neutral mobility is that for certain vehicle segments, complete electrification cannot be realized in competitive terms, neither from an economic nor from a technical point of view. Combustion engines are still the expedient solution for vehicles that demand continuously high power like airplanes, heavy commercial vehicles or construction machinery. This kind of mobility needs synthetic fuels (e-fuels) synthesized from ambient CO2 and renewable hydrogen. The demand for renewable primary energy is increased considerably by the relatively low efficiency of these power-to-gas/liquid generation paths of between 45% and 65% (WtT) [2]. Besides CO2 and emission legislation, manufacturing costs and customer acceptance will define which powertrain types are offered in which vehicle segments. This is accompanied by the challenge of defining cost-efficient platforms with modular components so that a wide range of vehicles can be offered with different levels of electrification. Modular powertrain systems must also be highly flexible to withstand possible changes in legislation (WtW, CtG), unclear establishment of renewable energies (renewables) and a volatile purchaser behavior.

Systematic Concept Development

Optimizing these powertrain components, topologies and functions requires a development process on the system level for powertrain and vehicle, as well as a long-term product strategy for the whole vehicle fleet. IAV offers unique methods and tools for proceeding systematically the whole development process, from the end user requirement through to the system release recommendation.

The systematic process (Fig. 1) starts by recording all the requirements made by the end user, legislation, the target markets, the vehicle manufacturer, suppliers and energy providers. IAV then uses mobility synthesis to describe the influence of market and environmental conditions

on the user behavior, thus developing future mobility scenarios that can be described in terms of their technical requirements and customer acceptance. Based on these mobility scenarios, IAV systematically ascertains and optimizes powertrain concepts that are expedient solutions for the specific vehicle and primary energy source in order to achieve carbon-neutral mobility.

Powertrain synthesis systematically collates the large number of all possible powertrain components to obtain powertrain variants that are optimized in terms of cost, efficiency and driving performance. The main powertrain parameters are thus defined as the basis for then developing the structures of the respective components, using the proven synthesis methods among others for transmission, electric motor and actuation. The final result consists in a powertrain concept with specific individual components. At the same time, the vehicle-specific powertrain variants form the basis for optimization on fleet level. Platform synthesis collates the vehicle-specific optimized powertrain variants in modular systems for systematic minimization of diversity, emissions and costs on fleet level (Fig. 1). This extensive approach thus permits a dedicated and sustainable development of the future mobility.

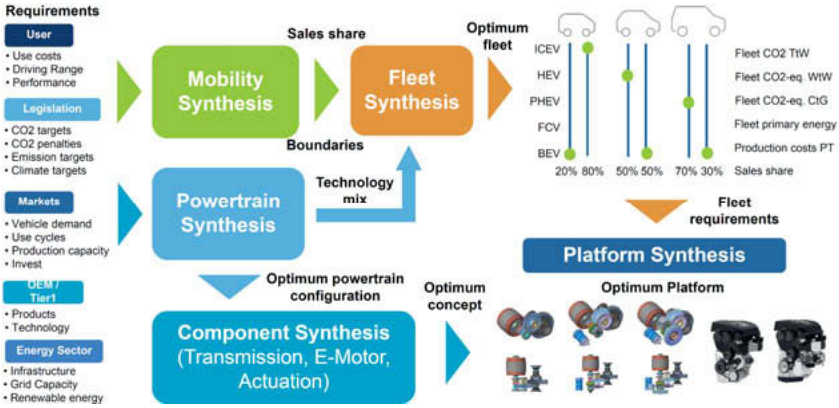

Fig. 1: IAV Methods for advanced development

For an objective comparison of powertrain concepts regarding their impact on the greenhouse gas effects a focus on the vehicle operation is not sufficient. Life cycle assessment (LCA) is one way of extending the scope. Here WtW balancing also considers synthetic fuels with various energy paths. Furthermore, a CO2 assessment of the manufacturing and production process (CtG) is necessary for a neutral comparison of the concepts behind various powertrain

types. This paper extends the traditional TtW view by adding the CO2 influences for the WtW and CtG system limits. In particular, this takes account of the CO2-intensive manufacturing process for the battery systems and magnet materials used in electrified powertrains. The LCA properties can be generated for every single powertrain variant in the overall system, with downstream fleet synthesis (Fig. 1) permitting an overall assessment of all powertrain types in all vehicle segments including CO2-TtW, -WtW and -CtG, primary energy demand and manufacturing costs.

Variation Study for Powertrain Mix 2030

For the following variation study the five key powertrain types - combustion engine, hybrid, plug-in hybrid and pure electric with fuel cells or battery - are assigned to the three main vehicle segments (B, C, D/E segment). The TtW-CO2-emissions for every vehicle/powertrain combination are calculated according to the WLTP, together with the CO2-equivalent for WtT-, WtW- and CtG-balancing. Furthermore, the primary energy demand is ascertained for manufacturing and producing the fuel/electrical energy, the vehicle and the powertrain. The primary energy demand and the manufacturing costs for the powertrain components including the energy storage system are added to the dataset.

The variation study (boundary conditions in Fig. 2) includes a maximum of three powertrains for each vehicle segment. The combination of powertrain types is open and subjected to a fully combinational analysis. It is thus possible to assess how many powertrain types are expedient for which vehicle segments in terms of CO2 fleet targets and manufacturing costs.
At the moment, it is not known how the purchasing acceptance of end users will develop for the new powertrain types. This unknown purchaser acceptance has been quantified by considering all combinations of sales distributions, in order to take account of the production prediction for 2030 and also to view 100 % or mixed scenarios.

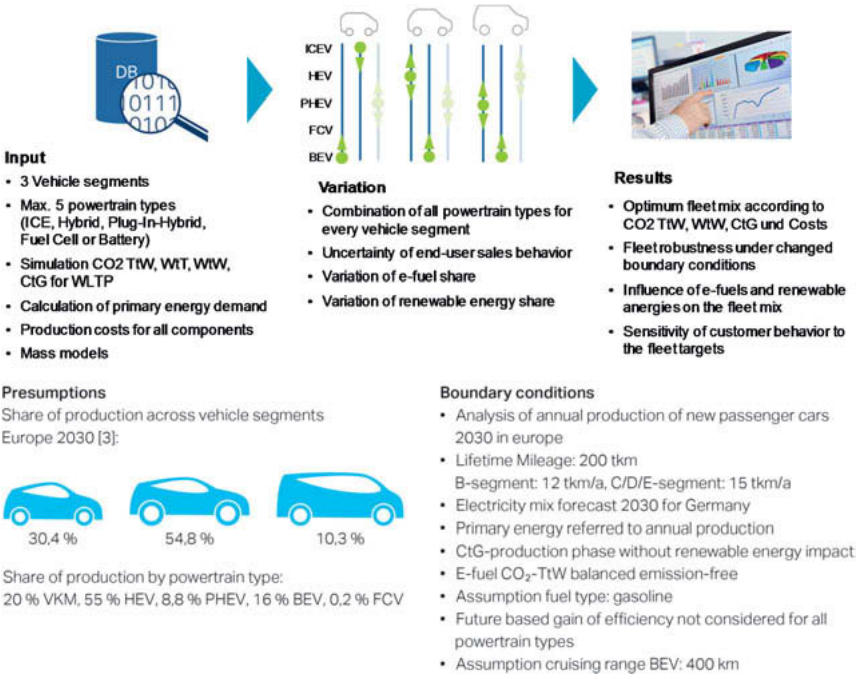

Fig. 2: Boundary conditions of the variation study

Influence of CO2 Legislation

Fig. 3 shows the individual fleet scenarios in the total solution set of approx. 9 million powertrain and fleet variants, thus giving an overview of limits and sensitivities for the key fleet characteristic numbers. It shows the two 100% scenarios ICEV and BEV as well as the predicted fleet forecast for 2030. Color-coding is used to show the share of battery electric vehicles. The third area of the parameter area is marked by a theoretically possible 100% scenario for fuel cell vehicles.

Under current TtW-legislation, average OEM CO2-fleet emissions are reduced primarily by zero-emission vehicles, with an almost linear increase in manufacturing costs on the fleet level. Expanding the CO2-balancing limits, for example to WtW, would result in an absolute increase in emissions as well as greater potential for optimizing costs. Fig. 3 (on the right) also shows a high cost gradient as soon as WtW-emissions are reduced to values below approx. 120 g CO2eq./km with the predicted 2030 electricity mix. It is not possible to bring the WtW-value

below approx. 80 g CO2eq./km, even with 100% battery electric vehicles. CO2-neutrality can only be achieved by further increasing the share of renewable energy compared to the 2030 electricity mix.

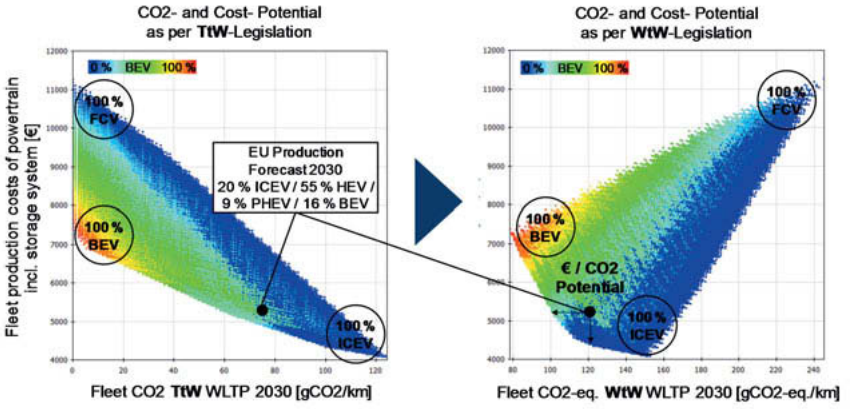

Fig. 3: CO2 and cost potential due to changes in legislation

Influence of Powertrain Types on CO2-Potential

Another challenge consists in the systematic generation of modular powertrain systems to take account of the complete combination of maximum three out of five possible powertrain types (ICEV, HEV, PHEV, FCV, BEV) for every vehicle segment. It is thus possible to ascertain the powertrain types needed for the fleet objectives, and to minimize their quantity. Fig. 4 on the left shows the impact of number of powertrains on TtW-CO2-emissions. There are considerable differences between all the noted scenarios for optimum costs, optimum TtW and optimum WtW, in terms of both CO2-potential and the composition of the power-train types. All three optimization targets exhibit seven different powertrain types for the fleet that achieve the lowest TtW-CO2-emissions overall. Every single fleet configuration (point in the data cloud) includes a segment-specific distribution of the powertrain types with all information about CO2, primary energy and cost values. Furthermore, the powertrain types needed for the WtW-optimum scenario shown in Fig. 4 as well as the vehicle-specific distribution.

The results show that the pure ICE powertrain has a very high share for the B-segment with 40%, due above all to the lower consumption advantage compared to HEV with far lower costs. HEV technology dominates the C-segment with an 80% share. Here the high sales figures make a significant contribution to the CO2-fleet target.

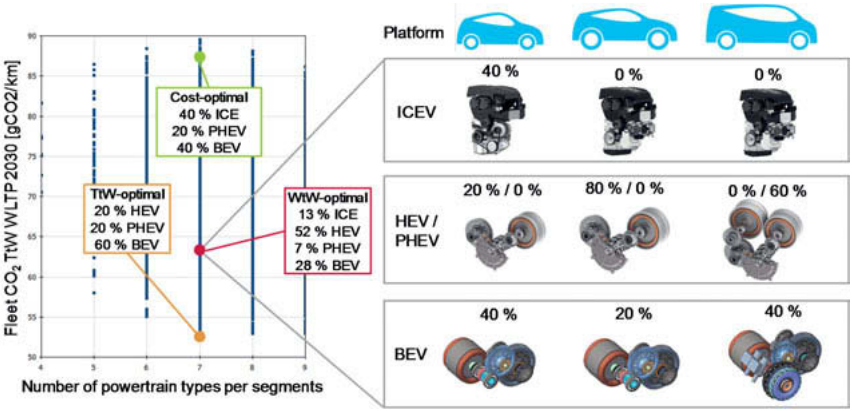

Fig. 4: Powertrain types optimized in terms of WtW-CO2, TtW-CO2 and costs

The use of plug-in hybrids is expedient for the D-segment even after WtW-balancing, as consumption can be clearly reduced by electric driving particularly in urban traffic. The BEV powertrain type accounts for a relatively high share in the B- and D-segment with 40%. The results also show that only in the B-segment a pure combustion engine powertrain is seen as expedient for the fleet targets. All other vehicle segments have combustion engines combined with either HEV or PHEV technology. Summarized this leads to a demand of a wide-spread applicable powertrain platform for HEV-system in B- and C- segments and for PHEV-application in D- and E-segments. Additionally a BEV-powertrain platform with single- and multispeed transmissions are needed to cover effectively a wide spectrum of vehicle applications.

Dedicated Hybrid Transmission Platform

How can one modular DHT system cover the divergent boundary conditions of a whole vehicle platform? This is the main question when it comes to the requirements definition of a future hybrid system for a front-transverse vehicle platform. Between a subcompact car, which is mainly used for urban driving, and a full-size SUV, which needs to provide a high load and towing capacity, the main development targets like system costs, package, driving performance and comfort as well as functional aspects can differ in a wide range, even if all these vehicles are based on the same platform. The breakdown of these requirements from the vehicle level to the hybrid system leads to different demands for output torque and power, range of hybrid functions and the level of driving comfort. A reasonable approach is to define a basic

DHT layout for the demands of the smaller vehicle classes, where low system costs, advantageous low fuel consumption, small system package and a decent drivability are important. The enhanced requirements of mid-size passenger cars and full-size SUV can be covered by the smart integration of a second e-motor into the drive train (see Fig. 5).

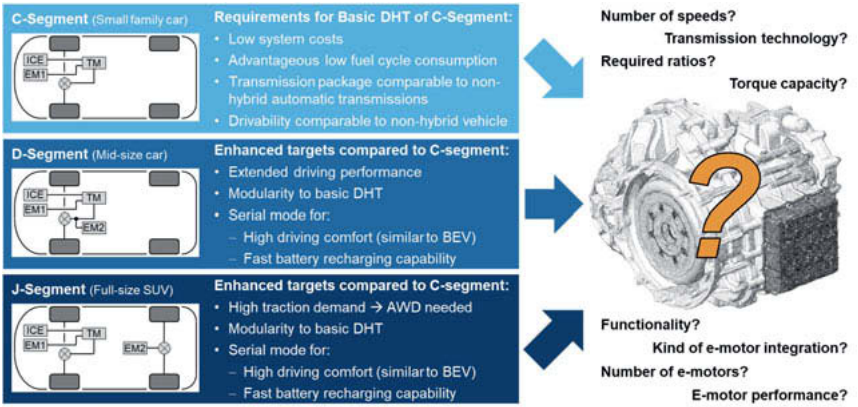

Fig. 5: Modular approach for the DHT platform

In case of the D-segment vehicle, the additional e-motor is installed in the DHT in order to increase the driving performance in electric and hybrid drive and to offer a serial driving mode for very good driving comfort at low and medium vehicle speed, which is on the level of battery-electric vehicles. In addition, the serial driving mode enables a fast battery recharging. The high traction demand of a full-size SUV and the needs for a good off-road capability requires an all-wheel-drive system. Here the second e-motor is mounted at the rear axle. The advantages of a serial driving mode can also be captured with this powertrain con-figuration.

The next question in the development process of the modular DHT platform is to find the right setup for the basic hybrid system with one e-motor. The pre-mentioned IAV Powertrain Synthesis offers the right methodology for answering this question by varying the general hybrid topology as well as the main parameters of the hybrid system like number of speeds, ratio configuration, performance parameters of the e-motor as well as the kind of the e-motor integration. (see Fig. 6)

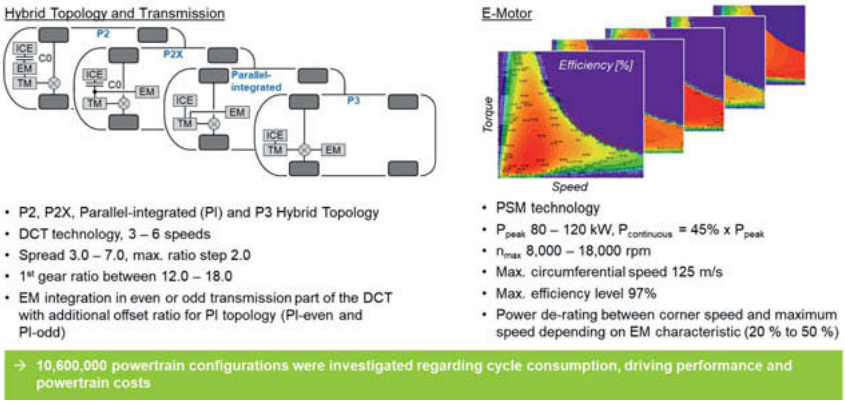

Fig. 6: Investigation of the basic DHT system with IAV Powertrain Synthesis – variation parameters

The variation study of the hybrid systems, which are all based on a DCT technology, shows a clear tendency towards systems with three or four speeds, since they offer a good compromise between fuel consumption and system costs. A higher number of speeds does not lead to a reduction of the fuel consumption, but the costs increase due to the higher mechanical effort. A comparison of the different hybrid topologies - P2(X), parallel-integrated and P3 - does not show an obvious trend towards one specific system layout. With an optimized parameter set all investigated topologies can achieve a very good overall compromise in regard to efficiency, performance and powertrain costs. From this reason, an investigation of the rough package situation is added to the system investigation. At this point the P2 configurations show a noticeable disadvantage, because the additional C0 clutch and the arrangement of the e-motor at the input shaft lead to an increased overall transmission length. Furthermore, the shift of the differential position towards the left front wheel can be critical for the length of the left side shaft, especially in smaller vehicle segments. In conclusion, a DCT with a parallel integrated e-motor, which is connected to the hollow input shaft, offers a very good compromise between the properties from the powertrain variation study and the package investigation and was therefore selected for a further detailing of the modular DHT platform.

An investigation of a suitable gear structure with the IAV Transmission Synthesis methodology ended up with a very compact 4-speed DCT structure, which uses a winding power flow in the first speed for a low mechanical effort and a short gear set with only 3 gear set levels (Fig. 7).

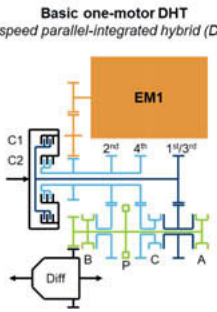

Gear			Clutch		Shift Element			Overall ratio (ICE)	Ratio Step (ICE)	Ratio EM1-Out	Ratio ICE-EM1
	Engaged	Preselected	C1	C2	A	B	C				
Parallel HEV	1	2	X			X	X	13.92	1.68		1.25
	2	1		X		X	X	8.28		11.18	0.74
		-		X		X			1.69		
		3		X	X	X					0.44
	3	2	X		X	X		4.90	1.68	3.93	1.25
		4	X		X		X				0.74
	4	3		X	X		X	2.91	(4.78)		
EV	1	-				X		-	-	11.18	
	2	-			X		X	-	-	3.93	

EM1 ratio change

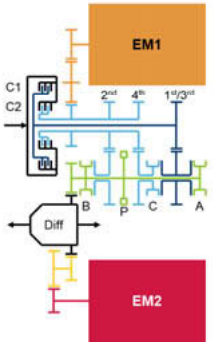

Gear			Clutch		Shift Element			Overall ratio (ICE)	Ratio Step (ICE)	Ratio EM1-Out	Ratio EM2-Out	Ratio ICE-EM1
	Engaged	Preselected	C1	C2	A	B	C					
Parallel HEV	1	2	X			X	X	13.92	1.68			1.25
	2	1		X		X	X	8.28		11.18		0.74
		-		X		X			1.69			
		3		X	X	X						0.44
	3	2	X		X	X		4.90	1.68	3.93	10.65	1.25
		4	X		X		X					0.74
	4	3		X	X		X	2.91	(4.78)			
Serial HEV	-	-		X				-	-	-		0.74
EV	1	-				X		-	-	11.18		
	2	-			X		X	-	-	3.93		

EM1 ratio change

Fig. 7: Transmission structure and functionality of the basic and the extended DHT system

The first e-motor (EM1) is used in both system configurations and is connected to the hollow input shaft with the second and fourth gear on it. The overall spread of the ICE and HEV speeds is 4.8, as this was identified as the favourable transmission spread in the Powertrain Synthesis. A change of the ratio between the e-motor and the output happens in the third HEV mode by changing the preselection from second to fourth speed. During this shift process, an active torque support from the ICE provides enough output torque to prevent a noticeable vehicle jerk. With this adjustable e-motor ratio, the rotational speed can be lowered at high vehicle velocities, which helps to achieve better operating points of the e-motor and lowers the speed dependent losses. For a good drivability in the EV mode, the first speed with a ratio of 11.18 is optimized for both a sufficient pure electric output torque and a maximum e-drive velocity of 130 kph. A shifting of the e-motor ratio is therefore not mandatory in a typical EV mode velocity range. However, a second pure electric gear (EV2) is available. The decision of using this

optional speed depends on the driving comfort requirements and can differ across the vehicle fleet. For the extension of the basic DHT to a combined hybrid system, a second e-motor (EM2) drives the differential gear over an independent intermediate shaft. The overall ratio of EM2 is comparable to the first speed ratio of EM1 as the output torque demands are on a comparable level. A limitation of the rotational speed of EM2 is possible with an optional disconnection device at the intermediate shaft (not shown in Fig. 7).

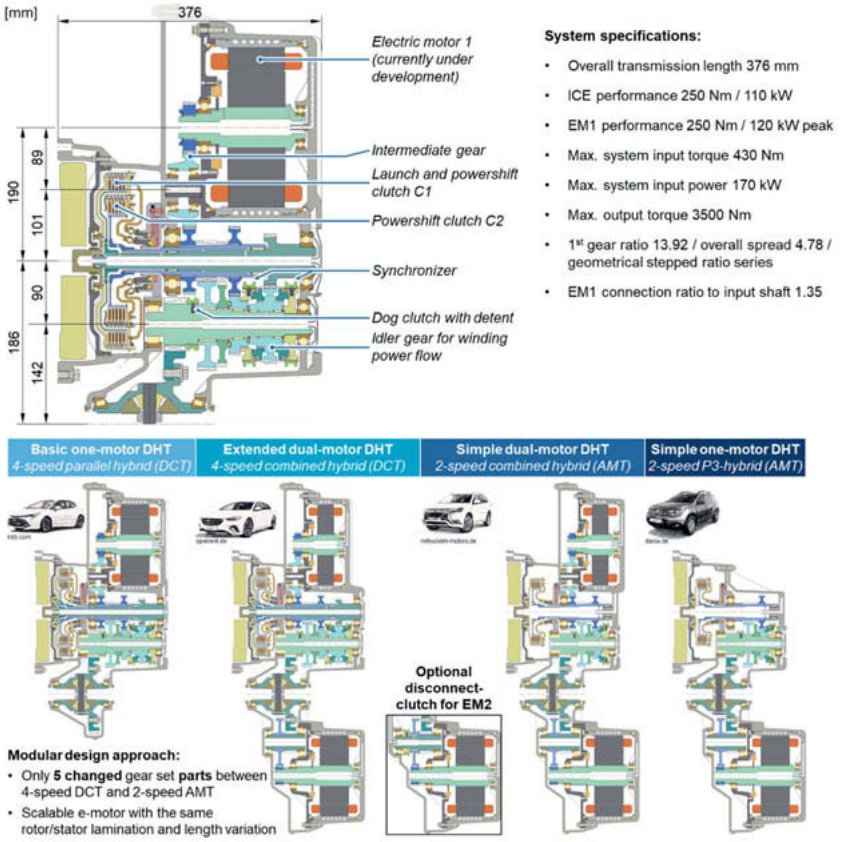

Fig. 8: Main specifications of the 4-speed basic transmission and introduction of the DHT platform design

In order to demonstrate the potential of the DHT system and to investigate the feasibility of the design with the given boundary conditions, a design study is implemented. As a result, Fig. 8 shows the cross section of the basic DHT system with its main specifications as well as different derivates of the modular platform for several vehicle applications. The layout of the components is focused on a high modularity. Besides the 4-speed DCT, an additional, simplified 2-speed AMT version is derived for powertrain configurations with a high level of electrification and a focus on pure electric and serial hybrid driving. The design study for the 4-speed basic DCT ended up with a detailed 2D cross section, which shows a promising transmission length of 376 mm, based on an input torque limitation to 430 Nm at a maximum system input power of 170 kW.

Dedicated E-Drive Platform

Due to current and future regulations, car manufacturers are working to reduce the CO2 emissions of their vehicle fleets. For this reason, the focus of manufacturers is shifting from combustion engine driven vehicles to purely electric vehicles. As in the past, the requirements for pure electric vehicles are very different. The manufacturers must develop small compact vehicles for pure urban traffic, have the full-size SUV in their portfolio, which needs to provide a high load and towing capacity, and provide sporty vehicles with a high dynamic driving feeling for their customers. These different requirements in terms of efficiency, performance, sportiness and costs are often difficult to harmonize.

For these reasons, a modular electrified powertrain platform development makes sense for the entire vehicle fleet to reduce system complexity, use common parts, have a smaller variety of design solutions, save development costs and effort, reduce production costs and still have the optimal powertrain configuration for each application.

Fig. 9: Creation of a modular drivetrain platform for electrified passenger cars

Starting point of the development is a fleet study with the tool IAV Powertrain Synthesis (see Fig. 10). With this unique methodology the modular electric drive unit can be adjusted to the requirements of an exemplary fleet in terms of consumption, performance, range and costs. In this first step, the boundary conditions for the platform are set. The IAV Powertrain Synthesis tool delivers proposals for the key data of the drive unit, amongst others the number of gears and their ratios depending on the vehicle segment. In the following detailing phase the IAV tools e-motor synthesis and IAV Actuation Synthesis are used to support the engineers during the detailed dimensioning of the drive unit.

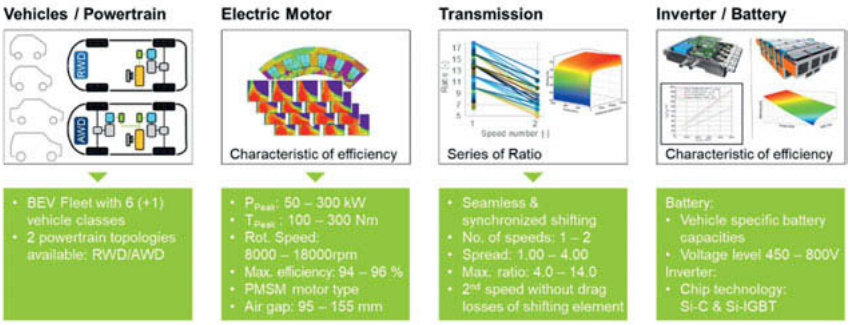

Fig. 10: Boundary conditions and components of the IAV Powertrain Synthesis

In order to limit the amount of different powertrain configurations for each vehicle class, the search area is limited by defined boundary conditions such as maximum number of gears, gear spread, maximum ratio of the gears, different types and power classes of EM and inverter,

battery voltage level and technologies. Various modular scenarios can be defined then. The focus can be on minimum costs for the entire fleet, a high number of identical parts across the different vehicle classes, maximum efficiency or maximum performance for the respective vehicle class. The IAV modular electrified powertrain platform (see Fig. 11) offers a good balance of efficiency, a high degree of common parts, low costs across the entire vehicle fleet and an attractive performance for the customer, especially in the higher vehicle classes.

Vehicle classification	A	C-Class	C-Class SUV	D-Class sedan mid	D-Class sedan high	D-Class SUV
Curb weight [kg]	1,200	1,555	1,770	1,694	1,694	1,997
Powered Axle	FWD	RWD	RWD	RWD	RWD	RWD
Powertrain Requirements						
Acceleration time 0-100 km/h [s]	8.6	8.92	7.8	7.3	6.9	8.9
Max. Velocities [km/h]	180	180	180	198	215	190
Gradeability			> 30 % (all topologies)			
EV cruising range [km]	250	350	350	400	400	400
Energy consumption WLTP [kWh/100km]	11.5	11.7	16.5	13.3	13.0	18.1
Powertrain Configuration						
EM peak torque [Nm]	250	250	250	250	250	300
EM peak power [kW]	100	100	150	150	150	150
Number of speeds	1	1	1	1	2	2
Ratio 1. speed/ 2. speed	8.5	9.2	11.5	11.0	13.3 / 6.6	13.8 / 7.6
Vehicle Sale Shares (Germany)						
Specific Sale Share [%] ∑ = 100 %	24.9	25.5	21.2	12.6	5.5	5.1

Fig. 11: Modular electrified powertrain platform – key figures

The results of the synthesis are used as a starting point for the further development of the platform. It is important to provide the right configuration for every customer and market requirement. For this reason, in addition to a 1-speed solution, various 2-speed solutions are investigated and developed (Fig 12). The benefit for the end-customer is that the efficiency of a 2-speed solution, especially in full-size SUV and sporty vehicles based on a fundamentally consistent gear set. The special feature of the introduced platform is that it can be offered with fully power shiftable, partially power shiftable or in a 2-speed configuration without seamless shifting.

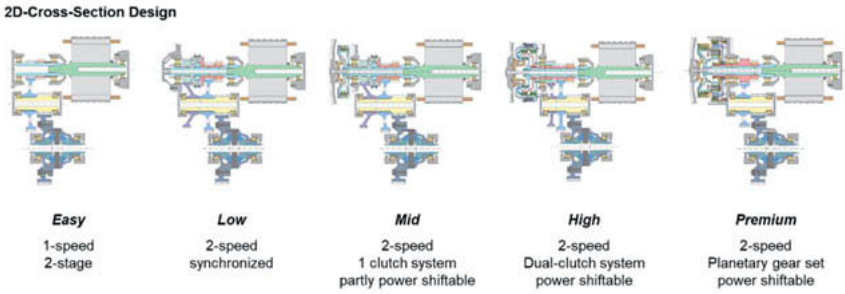

Fig. 12: 2D design IAV modular electrified powertrain platform

The complete power shiftable 2-speed solution is designed with a dual-clutch system, which leads to a very sporty driving feeling. Due to its higher costs, however, this variant is also more likely to be used in the high-price segment. In order to be able to offer low-cost 2–speed solutions for the mass market, IAV has developed a partially power shifting system (see Fig. 13). This variant combines a sporty feeling of acceleration with a high degree of efficiency and a cost-effective approach to the components in order to keep the costs for the drive unit as low as possible.

The scalable electric machine is classified as permanent magnet synchronous machine. With respect to conventional electric machines, it distinguishes in terms of its rotor and stator design. The stator is operated by five current phases, which lowers the system cost and leads to improved fail-operational behavior. On the other side, the rotor is trimmed for a maximum reluctance, balancing out the trade-off between high performance and small drive cycle losses. The electric components run at a system voltage of up to 800 VDC. In order to meet package restrictions, the inverter is integrated in a very compact way next to the active parts of the electric machine.

Fig. 13: IAV 2-speed solution partly power shiftable topology

Conclusion

The future powertrain mix will be derived above all from the stipulations for a CO2- and emission-optimized vehicle fleet. IAV Fleet Synthesis can be used to allocate the five main powertrain types – internal combustion engine, hybrid (incl. plug-in) and electric with fuel cells or battery – to the main vehicle segments. The TtW-CO2 emissions for every vehicle/powertrain combination are generated according to the WLTP, together with the CO2 equivalent for WtT, WtW and CtG balancing. Furthermore, the sales distribution is varied for every segment. The results of the variation study show that a scenario with high HEV share in the fleet is robust with regard to the external boundary conditions, particularly the electricity mix and the share of renewables. The high share of combustion engines also makes it easy to reduce CO2 emissions using e-fuels. The low share of PHEV, BEV and FCV also results in reduced manufacturing costs on the powertrain level. Furthermore, the analysis also looked at which powertrain mix would be expedient for WtW-CO2-legislation. The results also show that only in the B-segment a pure combustion engine powertrain is seen as expedient for the fleet targets. All

other vehicle segments have combustion engines combined with either HEV or PHEV technology. The BEV powertrain type accounts for a relatively high share in the B- and D-segment with 40%, while the plug-in hybrid share is particularly prominent in the D-segment with 60%. Finally, modular powertrain systems were allocated to the three vehicle segments to allow for a combination of combustion engines with dedicated hybrid transmissions with one or two electric motors and various electric axle configurations from single-speed to seamless-shifting multi-speed transmissions.

References

[1] EU Regulation 2019/631

[2] Kratzsch, M.; Wukisiewitsch, W.; Sens M.; Brauer M.: The path to CO2-neutral mobility in 2050, Vienna Engine Symposium 2019

[3] IHS Market Data Vehicle Production, as of 05/2019

Method for a cloud based Remaining-Service-Life-Prediction for Vehicle-Gearboxes based on Big-Data-Analysis and Machine Learning

Daniel Vietze, M.Sc., Dr.-Ing. **Michael Hein**,
Prof. Dr.-Ing. **Karsten Stahl**,
FZG – Gear Research Centre, Technical University of Munich

0. Zusammenfassung

Die meisten heutzutage eingesetzten Fahrzeuggetriebe sind für eine endliche Betriebsdauer ausgelegt. Dies eröffnet erhebliches Potential für Gewichts- und Kostenreduktion sowie Verbesserung der CO_2-Bilanz. Jedoch ist der langfristige Betrieb mit zunehmender Wahrscheinlichkeit eines Schadens verbunden. Insbesondere, wenn der Ausfall einen hohen wirtschaftlichen Schaden verursacht, entsteht hierdurch ein Zielkonflikt aus steigendem Ausfallrisiko und frühzeitiger Außerbetriebsetzung bzw. überhöhten Instandhaltungskosten. Um diesen Konflikt aufzulösen, ist eine Methodik wünschenswert, die es ermöglicht, mit möglichst geringem Aufwand die verbleibende Lebensdauer und den aktuellen Gesundheitszustand eines Fahrzeuggetriebes laufend abzuschätzen.
Die Kernkomponenten von Fahrzeuggetrieben sind die Zahnräder, deren Schaden meist zum Ausfall des gesamten Getriebes führt. Die Betriebsfestigkeitsrechnung befasst sich seit Langem mit der Dimensionierung von Zahnrädern entsprechend der zu erwartenden Belastungen und der geforderten Lebensdauer. Während des Betriebs ist es aber bisher kaum möglich, die hierzu erforderlichen Annahmen zu überprüfen. Im Rahmen dieser Veröffentlichung wird eine Methode präsentiert, die es ermöglicht, die Restlebensdauer und den Gesundheitszustand von Verzahnungen laufend während des Betriebs zu prognostizieren. Hierbei werden Big-Data-Ansätze und Methoden der künstlichen Intelligenz verwendet. Das grundlegende Konzept ist hierbei so ausgestaltet, dass eine Übertragung der Methode auf andere Maschinenelemente und Maschinenarten gut möglich ist.

1. Abstract

Most vehicle-gearboxes operating today are designed for a limited service-life. On the one hand, this creates significant potential for decreasing cost and mass as well as reduction of the carbon-footprint. On the other hand, this causes a rising risk of failure with increasing operating time of the machine. Especially if a failure can result in a high economic loss, this fact

creates a conflict of goals. On the one hand, the machine should only be maintained or replaced when necessary and, on the other hand, the probability of a failure increases with longer operating times. Therefore, a method is desirable, making it possible to predict the remaining service-life and state of health with as little effort as possible.

Centerpiece of gearboxes are the gears. A failure of these components usually causes the whole gearbox to fail. The fatigue life analysis deals with the dimensioning of gears according to the expected loads and the required service-life. Unfortunately, there is very little possibility to validate the technical design during operation, today. Hence, the goal of this paper is to present a method, enabling the prediction of the remaining-service-life and state-of-health of gears during operation. Within this method big-data and machine-learning approaches are used. The method is designed in a way, enabling an easy transfer to other machine elements and kinds of machinery.

2. Motivation

Transmissions are a key component of vehicle drive trains. Cars, powered both, by electric and internal combustion engine, trucks, trains and constructional and agricultural machinery would not work the usual way without gearboxes in their drive trains. Over the last decades these components have become more and more sophisticated and capable of transferring more and more power, while at the same time becoming even lighter and more compact. At the heart of nearly every gearbox are the gears, realizing the transmission of the engine torque and reducing or increasing the rotational speed of the engine.

Research institutions and development departments all over the world are working on increasing the load carrying capacity and the reliability of high performance gears. Nevertheless, failures occur and can lead to a total loss of drive. With increasing lifetime and millage this becomes more and more likely, creating a conflict of goals especially for owners of commercially used vehicles. On the one hand the vehicle should only be maintained or replaced when necessary and, on the other hand the increasing probability of a failure, causing expensive downtime, creates a serious economic risk. Additionally the ecological footprint of a vehicle is increased unnecessarily if maintenance or replacement takes place earlier than necessary. Therefore, a method is desirable making it possible to constantly predict the remaining service-life of the gearbox considering the actual operating conditions without taking the gearbox apart or installing a lot of expensive equipment.

Usually gears used in vehicle transmissions are dimensioned in a way that they only can withstand the operational load for a certain amount of load cycles. This approach enables a reduction of weight, size and cost of the transmission. To safely reach the calculated end of service-

life the occurring loads have to be within the predicted load spectrum and the strength of the gears has to be within the allowed tolerance margin. Especially unconsidered overloads and their effects are a large source of uncertainty.

Over the last couple of years more and more sensors have been included in machinery of every kind. Utilizing the data created by these sensors is a major part of the megatrend Industry 4.0. Because of the increasing availability of modern mobile networks, like 5G, it is possible to create a data connection nearly everywhere. Today predictive maintenance is using this data and connectivity to predict whether a machine needs to be maintained. Sometimes these methods also make predictions about the remaining service-life, but the high potential of the knowledge and methods of fatigue life analysis is not utilized.

Modern vehicles, especially electric cars, are able to provide a lot of data regarding their drive train. For example, an electric motor is able to deliver a signal of the output torque at any given moment. Goal of this paper is to present a method, which uses such data to estimate the state of health and predict the remaining service-life of a vehicle transmission, while utilizing the knowledge of fatigue life analysis and including the potential of machine-learning and big data. This paper presents the whole concept in an easy understandable and accessible way and does not specify the method and its calculation in every detail. At the beginning, the required knowledge about fatigue life analysis is presented in a compact summary. Afterwards the method is presented in four steps, where every of these steps expands the concept up to the full remaining-service-life-prediction.

3. State of the art

4. Fatigue life calculation of gears

Gears can fail due to numerous kinds of damage. Not all of these damages can be analyzed with the methods of the fatigue life analysis. Some damages like scuffing can occur after just one load cycle under critical conditions. Other damages like pitting and tooth root breakage are typical fatigue failure mechanism and are usually caused by a high number of load cycles and can be analyzed using the methods of the fatigue life analysis [1].

Usually gears in vehicle transmissions can only withstand the load occurring in operation for a limited amount of load cycles. Especially the highest loads cannot be tolerated many times. To describe this load carrying capacity the “Woehler” curve / S/N-curve is often used [2].

To dimension gears according to the rules of fatigue life analysis a load spectrum is required additionally to the “Woehler” curve / S/N-curve. Load spectra deliver the information about the loads occurring during operation. These usually divide up the whole range of occurring loads

into a certain amount of discrete levels. The load spectrum delivers the information how often a load of a certain level will occur during the operation.

Damage accumulation hypotheses are used to connect the load carrying capacity and the load spectrum [2]. These predict how likely a damage is, when a certain load spectrum is applied to a gear. Linear damage accumulation hypotheses are most common for the herein considered use case. These are based on the assumption, that every load cycle of one load level is causing the same amount of damage regardless of when it occurs. The linear hypotheses calculate a partial damage sum for every load level and add all these partial damage sums up to the damage sum. If this damage sum exceeds a threshold a failure is likely to occur for the considered probability of failure.

The simplest and most widely used linear damage accumulation hypotheses is the “Miner-rule” [3]. This hypotheses exist in the original, elementary and modified form according to Miner-Haibach [2, 3]. The three variants differ by the consideration of loads below the endurance limit.

A weak spot of linear damage accumulation hypotheses is the fact, that they do not take the chronology of the loads into account. Experimental investigation have shown that the sequence of loads can have influence on the life time. Hein [1] has shown that a pitting damage will occur at a significantly higher damage sum if the loads where applied with a more frequent mix of high and low loads. Such effects cannot be taken into account by linear damage accumulation hypotheses and therefor the accuracy of the service-life-prediction based on those is limited.

There are different approaches in the fatigue life analysis which address these issues, for example the methods of the fracture mechanics [4] or nonlinear damage accumulation hypotheses [5]. But these methods are linked to a significantly higher effort and often need a lot of very precise input data. Therefor these methods are not common to be used for the fatigue life analysis of gears.

5. Condition monitoring and predictive maintenance

The preceding section shortly summarized the basics of the fatigue life analysis. Due to the increasing spread of sensors in machinery more and more operation data is recorded and approaches to monitor the condition of machine elements were developed. The analysis of this recorded data can supply valuable information for the further operation. Predictive maintenance utilizes this data to predict if a machine needs to be maintained in the nearby future. The goal of this approach is to reduce downtime and decrease operating costs. Main emphasis

of this methods is to analysis the present data delivered by the sensors. At the moment the evaluation of vibrations is widely used in this field [6 bis 8].
Vibration based monitoring of machinery is only able to recognize damage if the damage already is causing a change of the vibration. Especially for the monitoring of fatigue damages this can be a challenge, because the damage can grow without significant impact on the vibrations. To predict the remaining service-life of a gearbox with special regard to fatigue failure modes, it is not sufficient to analyze the current status. The history has also to be taken into account. At the moment only very few publications address a constant prediction of the remaining service-life of gearboxes.
Publications by Foulard et al. [9 bis 12] presented a method using a signal of the input torque of a vehicle gearbox to constantly estimate its state of damage. The remaining service-life is also predicted with this approach. Linear damage accumulation hypotheses are utilized for this prediction. Therefor it is not possible to incorporate the chronology of the loads. If a very high load or overload is occurring its possible effects on the resulting endurance limit of the gears cannot be taken into account. The whole presented approach only focuses on one gearbox and does not analyze a whole fleet of identical gearboxes, like within a fleet of electric cars.
The following chapters will present a method for a remaining-service-life-prediction utilizing as much potential of big-data, machine-learning and fatigue life analysis as possible, while remaining as simple and cost efficient as possible. The whole concept is meant to be a cloud-based service. All calculations and analysis shall not take place on the onboard systems of the vehicles. The vehicles only send recorded sensor-data to a server farm and receive the results of the calculation.

6. “Woehler” curve / S/N-curve, remaining life line and state of health

In an electric car the wheels are driven by an electric motor. The output torque of this motor is usually transferred through a gearbox before being delivered to the wheels. The gearbox normally reduces the rotational speed and increases the torque. This approach enables the use of a smaller motor operating at a higher rotational speed. Usually the gearbox uses spur gears to convert the torque and rotational speed. This type of gears is known for its high efficiency, little space requirement and economic production cost [13].
As presented in chapter 3 these gears are usually designed for a limited service-life. The “Woehler” curve / S/N-curve is often used to describe this limited load carrying capacity. With every load cycle the remaining load carrying capacity is reduced. This happens during the operation up to the moment when the gear fails. To visualize this change of load carrying capacity the remaining life line is introduced in this paper. This line starts out identical to the

“Woehler” curve / S/N-curve and describes the remaining load carrying capacity over time. Fig. 1 shows a “Woehler” curve / S/N-curve and a remaining life line after a certain operation-time. Because of the already occurred loads the load carrying capacity described by the re-maining life line is lower than the one described by the “Woehler” curve / S/N-curve.

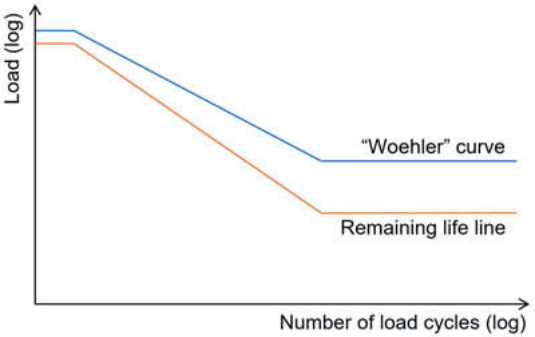

Fig. 1: “Woehler” curve / S/N-curve and remaining life line

The remaining load carrying capacity of the gears will reduce during the operation until the moment when one of the gears fails. The failure occurs when a higher load is applied than the highest load that can be tolerated at the given moment. The gap between the “Woehler” curve / S/N-curve and the remaining life line can be interpreted as the state of health of the gears. For a new gear both curves are identical and the state of health is at 100 %. During the oper-ation this gap will increase and the state of health will decrease.

The remaining life line can be calculated using the “Woehler” curve / S/N-curve as a starting point. Furthermore a signal is needed, which is characteristic for the load of the gears. A pos-sible signal is the input torque of the gearbox. In an electric car this torque usually is equal to the output torque of the electric motor, because no clutches or torque-converters are used between the two. Through continuous analysis of the signal with a damage accumulation hy-pothesis the remaining load carrying capacity can be calculated and expressed as the remain-ing life line. This calculation can also be done by machine learning methods. To train methods like deep learning training data is required. This data shall exist of the whole load-time-record and the moment of failure. It is possible to generate this data with experimental investigations or by using the data recorded by a fleet of vehicles. The high potential of this approach is the ability of deep learning to discover connections between the failure and the occurring loads, which would not have been considered by classic damage accumulation hypotheses.

The order of the single steps and the according data-flow of the presented method is shown in Fig. 2. As example an electric car is chosen. This example will be expanded over the course of the following chapters up to the whole concept of the remaining-service-life-prediction.

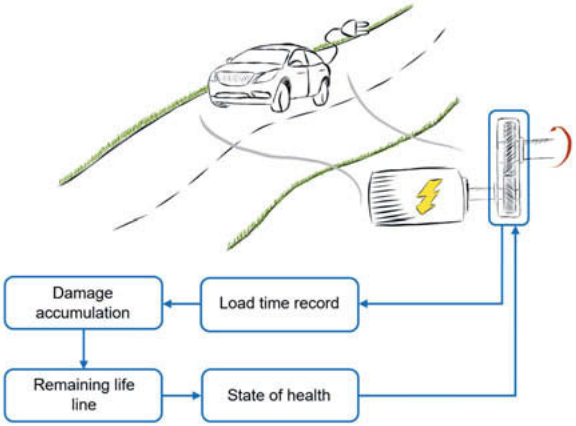

Fig. 2: Dataflow for the state of health estimation

7. Adaptive “Woehler” curve / S/N-curve utilizing Big-Data-Analysis and Machine Learning

“Woehler” curves / S/N-curves are usually the basis of service-life calculations in the field of fatigue life analysis and are created through experimental investigations. Usually experimental investigations for the load carrying capacity (Woehler-Tests) are carried out during the design process of the gearbox for the used materials. The “Woehler” curve / S/N-curve used for the service-life-calculation is based on those investigations [14]. During the manufacturing process of the gears a lot of parameters will be within a certain margin of tolerance and will change over the different produced batches, for example the hardness of the surface. This can have effects on the load carrying capacity [15]. These effects will not be considered within the “Woehler” curve / S/N-curve and therefore not within the service-life-calculation. Another uncertainty are the operational conditions the gears will be used with. For example the temperature, humidity or local characteristics, like sea salt, may have an influence on the service-life of the gears.

To account for all these factors within the design phase of the gears is nearly impossible and would require a vast amount of experimental investigations. Hence, a different approach to consider these factors within a service-life-prediction has to be utilized.

A lot of gears are not custom-made and therefor used in a big amount of machinery. For example the gears used in cars are a mass product and operating all over the world. All these machines can be utilized as test racks for the gears, if data about the occurring loads can be recorded and it is possible to transfer this data to a central database. The optimum solution would be a cloud computing based approach. Today nearly every modern car has the ability to connect to a mobile data network and to receive or send data.

The load-record of the gears can be used to constantly calculate the expected damage. The results of this can be used to validate the “Woehler” curve / S/N-curve, as long as a statistically relevant number of gears is monitored.

The damage can be calculated using a damage accumulation hypothesis or a machine learning based approach (see chapter 4). In order to calculate the damage, the load record sent by the vehicle has to be classified in load levels and divided into load cycles. This data can then be used to calculate the damage sum at any given moment. Additionally to this damage sum the actual status of the gear has to be known. The simplest case is to separate the gears into those already failed and those still operating. With this information it is possible to validate the “Woehler” curve / S/N-curve or the permissible damage sum and eventually make adjustments to it. The “Woehler” curve / S/N-curve describes the load carrying capacity of the gears. A damage accumulation hypothesis predicts the failure of the gears after a certain amount of damage occurred. This prediction is based on the “Woehler” curve / S/N-curve and the occurring loads. The failures will be distributed over a certain spread of the damage sum. If the distribution of failures occurring in reality dose not match with the distribution predicted by the damage accumulation hypothesis, the load carrying capacity is not represented correctly by the “Woehler” curve / S/N-curve. For example, if failures are occurring at damage sums at which the prediction is not expecting any failures yet, the load carrying capacity is overestimated. This system also works if the statistics of the prediction is already expecting failures but the gears are still operating without issue, then the load carrying capacity is underestimated. In a final step the “Woehler” curve / S/N-curve can be adjusted to fit better to the actual load carrying capacity of the gears.

This system can be used in a way evaluating the load carrying capacity of all monitored gears together. A more powerful approach is to use big-data-methods and machine learning to cluster the gears into groups and monitor these groups separately. Big-data-tools are able to analyze a lot of data and find similarities, which would have remained hidden to the human eye. For example, it can be useful to separate the gears according to the height gradient of the roads they are operating on, according to the climate or by their production batches. These groups can be monitored separately and the “Woehler” curve / S/N-curve can be adjusted to

represent the load carrying capacity as accurate as possible. In this presented manner an adaptive “Woehler” curve / S/N-curve can be created, which enables to predict the service-life of gears more accurate. The data-flow for this adaptive “Woehler” curve / S/N-curve is shown in Fig. 3. Within this Fig. the example of the electric car used in chapter 4 is taken up again and expanded by the adaptive “Woehler” curve / S/N-curve.

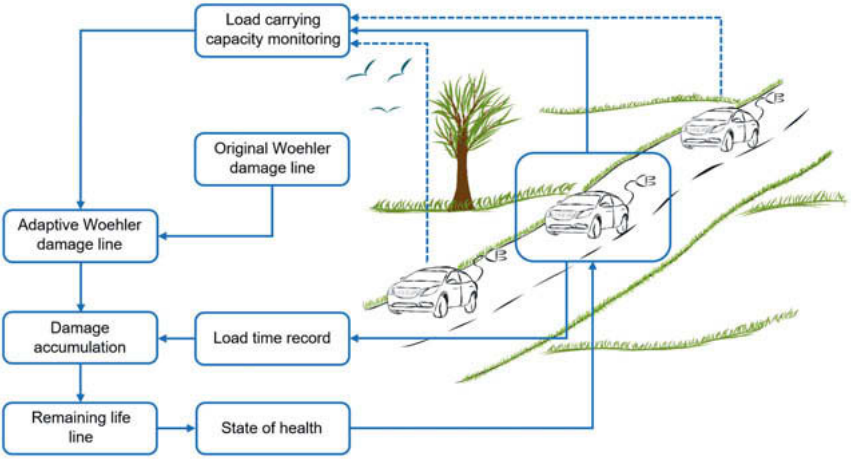

Fig. 3: Dataflow expanded by the adaptive “Woehler” curve / S/N-curve

8. Using Big-Data-Analysis to increase the validity of load spectra

The preceding chapters dealt with the load carrying capacity and a way to increase the validity of the “Woehler” curve / S/N-curve, the used damage accumulation hypothesis and the permissible damage sum. Additionally to the load carrying capacity the operational loads have to be known or predicted for a dimensioning according to the fatigue life analysis and are required for a remaining-service-life-prediction.

The loads are usually characterized via load spectra. To generate load spectra accurately representing the actual operation of the gears can be challenging. Using records of the actual loads occurring in operation is common practice. Such a load spectrum can be used for the dimensioning of the gears.

How a customer is going to use a vehicle cannot be predicted with high reliability. Therefor it is not optimal to use the original load spectrum to predict the remaining service-life of a gear in operation. The recorded load-data used in chapter 5 to validate the “Woehler” curve / S/N-curve can also be utilized to increase the accuracy of the load spectrum applied for the service-

life prediction of the gears. Big-data-methods can be used in a similar manner to chapter 5. Clustering the gears into groups with similar load characteristics can be useful to predict the service-life more accurate. This clustering can also be used for future developments. For example it is conceivable to adjust the load carrying capacity of a gearbox according to the costumer. This approach can be useful for commercial customers and save money and reduce expensive downtime.

The presented method can be used to create an adaptive load spectrum or many load spectra depending on the use case. In some cases, it can be considered optimal to adapt the original load spectrum for every gearbox separately and in other case it may be optimal to separate the gearboxes into groups with one common load spectrum according to their operational characteristics.

Fig. 4 shows the data flow for the adaptive load spectrum. The spectrum uses the original load spectrum as a starting point and adjusts accordantly to the occurring loads. The adaptive load spectrum will be put to use in the following chapter, when the whole concept is shown.

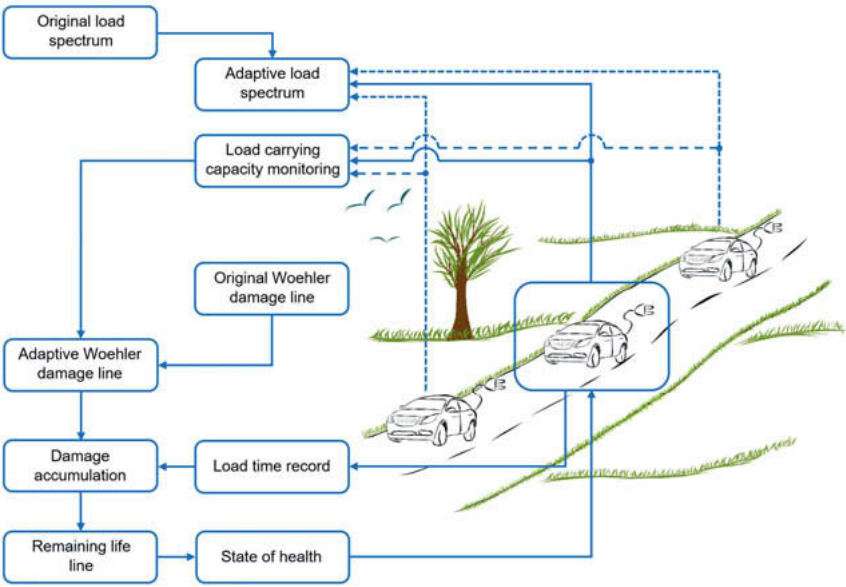

Fig. 4: Dataflow expended by the adaptive load spectrum

9. Method for an online remaining-service-life-prediction

The three preceding chapters presented elements of the concept for a remaining-service-life-prediction. This chapter unites all these steps to the whole concept. The prediction of the remaining-service-life uses a damage accumulation to calculate how much longer the gear will withstand the loads occurring in operation. The data-flow for the whole concept is shown in Fig. 5.

The remaining life line was introduced to describe the load carrying capacity of the gear at any given moment of its operational life. Therefor this line will be used in the calculation of the remaining service-life. The adaptive load spectrum was implemented to deliver more accurate information about the loads occurring in operation, compared to the load spectrum used for the dimensioning of the gear. The adaptive load spectrum will be used within the remaining-service-life-prediction for an accurate prediction of the loads occurring in the further operation.

The calculation can be done with a classic damage accumulation hypothesis or based on a machine-learning approach similar to the one presented in chapter 4. The output of this calculation will be the number of load cycles tolerable until the gear will fail. This number can be converted into remaining service-time.

Uniform for this whole method is the fact, that it has always to be considered, that all of these predictions are connected to a certain probability of failure. This probability usually is one, ten or 50 percent in the field of fatigue life analysis depending on the application and the type of failure. For the remaining-service-life-prediction the user has to decide which probability of failure is the right one for his use case. For example, if a failure has severe consequences a lower probability has to be chosen as if the failure has nearly no direct consequences.

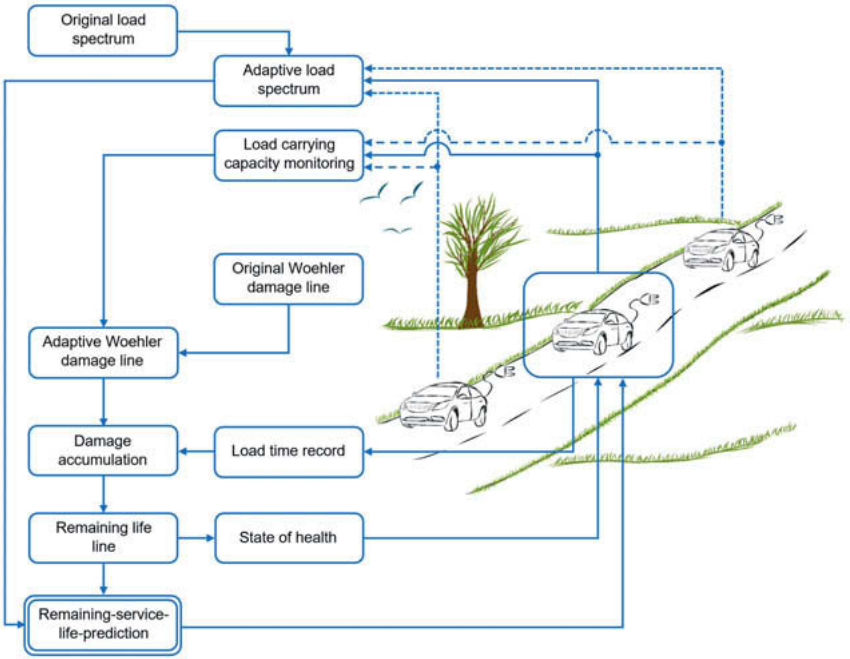

Fig. 5: Data-flow for the remaining-service-life-prediction

10. Conclusion and outlook

This paper roughly presents a method for a remaining-service-life-prediction for the gears of a vehicle-transmission, but the method can similarly be applied to different machine elements and other machines, like a wind turbine for example. The concept utilizes the relatively new potential and opportunities created by machine-learning and big data analysis. Also does the method not only focus on one single machine, but analysis a whole fleet together and uses knowledge only accessible through this holistic approach.

In the coming steps of the author's research the single elements of the calculation have to be specified and implemented in detail. Especially the use of machine learning requires the construction of a database with a lot of operational data of gears. For this, already existing research data can be used as well as experimental investigations can be conducted to create datasets.

11. References

[1] Hein, M.: Zur ganzheitlichen betriebsfesten Auslegung und Prüfung von Getriebezahnrädern, TU München Dissertation. München 2018

[2] Haibach, E.: Betriebsfestigkeit. Verfahren und Daten zur Bauteilberechnung. VDI-Buch. Berlin: Springer 2006

[3] Miner, M. A.: Cumulative Damage in Fatigue. Journal of Applied Mechanics 12 (1945) 3, S. 159–164

[4] Edel, K.-O.: Einführung in die bruchmechanische Schadensbeurteilung. DOI: 10.1007/978-3-662-44264-7. Berlin, Heidelberg: Springer Berlin Heidelberg 2015

[5] Sander, M.: Sicherheit und Betriebsfestigkeit von Maschinen und Anlagen. DOI: 10.1007/978-3-662-54443-3. Berlin, Heidelberg: Springer 2018

[6] Barszcz, T.: Vibration-Based Condition Monitoring of Wind Turbines. DOI: 10.1007/978-3-030-05971-2, Bd. 14. Cham: Springer International Publishing 2019

[7] Fromberger, M., Weinberger, U., Kohn, B., Utakapan, T., Otto, M. u. Stahl, K.: Condition Monitoring by position encoders. Conference Paper. 45th International Congress and Exposition on Noise Control Engineering (INTER-NOISE 2016), Hamburg, Germany (2016)

[8] Fromberger, M., Weinberger, U., Kohn, B., Utakapan, T., Otto, M. u. Stahl, K.: Evaluating signal processing methods for use in gearbox condition monitoring. Conference Paper. 24th International Congress on Sound and Vibration (ICSV 2017), London, United Kingdom (2017)

[9] Foulard, S., Rinderknecht, S. u. Fietzek, R.: Leichtbau von Fahrzeuggetrieben durch Online- und Echtzeit-Lebensdauerüberwachung. ATZ 118 (2016) 3, S. 74–79

[10] Foulard, S., Rinderknecht, S., Ichchou, M. u. Perret-Liaudet, J.: Real-time and online lifetime monitoring of automotive transmissions. Determining of the remaining lifetime of transmission components with the aid of torque measure. International Conference on Gears. VDI-Berichte 2199. 2013

[11] Foulard, S., Rinderknecht, S., Perret-Liaudet, J. u. Ichchou, M.: Online and real-time damage calculation in automotive transmissions Application to remaining service life estimation. International Gear Conference 2014. Conference proceedings Volume II. 2014, S. 933–949

[12] Foulard, S.: Online and real-time load monitoring for remaining service life prediction of automotive transmissions. Damage level estimation of transmission components based on a torque acquisition, TU Darmstadt Dissertation 2015

[13] Niemann, G. u. Winter, H.: Maschinenelemente Band 2. Getriebe allgemein, Zahnradgetriebe - Grundlagen, Stirnradgetriebe. Berlin: Springer 2003

[14] Hein, M., Tobie, T. u. Stahl, K.: Test method for time-scaled fatigue tests of gear transmission systems. Forschung im Ingenieurwesen 81 (2017) 2-3, S. 291–297

[15] Hein, M., Tobie, T. u. Stahl, K.: Calculation of Tooth Flank Fracture Load Capacity – Practical Applicability and Main Influence Parameters. American Gear Manufacturers Association Fall Technical Meeting 2017 (2017), S. 346–366

Package-optimized configuration of transmission elements for automated design concepts

Design concept generation based on results of transmission synthesis

M.Sc. **David Evenschor**, BMW Group, Munich;
Prof. Dr.-Ing. **Peter Tenberge**, Ruhr-University, Bochum;
Dr. techn. **Martin Wolkerstorfer**, PfeifferControl, Taufkirchen

Zusammenfassung

Im Rahmen der Getriebeentwicklung ist es oftmals notwendig, in kurzer Zeit den benötigten Bauraum eines Getriebekonzepts abzuschätzen. Hierbei kann eine Vorgabe von definierten Übersetzungen von Verzahnungen, Belastungen von Getriebeelementen und eines verfügbaren Bauraums in eine Vielzahl von Konstruktionsentwürfen münden. Die manuelle Erstellung dieser Konstruktionsentwürfe ist ressourcenintensiv und unvollständig.

Daher wird in dieser Arbeit ein automatisierter Ansatz zur belastungsgerechten Dimensionierung und bauraumoptimalen Anordnung von Getriebeelementen präsentiert. Dieser fußt auf der Generierung von logischen Anordnungen von Getriebeelementen. Zu diesem Zwecke wird die Ausgangstopologie durch Einfügen von Schaltelementen und Gehäuseknoten variiert, Lagerungskonzepte auf Basis von Zentralwellenbeziehungsmöglichkeiten abgeleitet und danach Kombinationen von Lagerungsarten, -positionen, und -partnern erzeugt. Zur Validierung der automatisch erzeugten Axiallagerungskonzepte wurde eine effiziente graphenbasierte Methode entwickelt. Des Weiteren wird ein neuartiger Algorithmus zur optimalen axialen Anordnung von Getriebeelementen vorgestellt und die gesamte Methodik anhand eines durchgängigen Beispiels veranschaulicht.

Abstract

For transmission development it is necessary to evaluate transmission concepts with respect to their assembly space requirements in a short time. A single specification of gear element ratios, transmission element load, and an available assembly space may lead to numerous design concepts. The manual creation of these concepts is resource-intensive and incomplete. In this work an automatized approach for load-dependent dimensioning and optimal placement

of gear box elements is presented. Its foundation is the generation of the logical order of elements. It includes the variation of the base-topology by insertion of shifting elements and additional knots representing the housing. This is followed by the definition of bearing concepts based on central shaft relations, as well as the combination of types, positions, and partners of bearings. For validation of the generated axial support concepts an efficient graph-based mechanism is proposed. Furthermore, a novel algorithm for the optimal axial placement of gear box elements is presented. Throughout, the various steps of the methodology are demonstrated by means of a continuous example.

1. Introduction

The aim of transmission development is not only to find the optimal number of gears and to define their specific gear ratios, but also to meet the requirement of an optimal utilization of the existing assembly space. The optimal number of gears and their specific gear ratios can be found for different types of transmissions by known algorithms for transmission topology synthesis, as shown in [1], [2] or [3]. Optimal utilization of a given assembly space critically hinges on the load-dependent design of the used transmission elements and their arrangement. There are several computer-aided engineering (CAE) software tools available which determine the load-dependent design of transmission elements such as spur gears, planetary gear sets, bearings, shafts, or shifting elements. Some of them are specialized in calculating a specific transmission element and some support several of the listed transmission elements in a specific arrangement. In every case, the arrangement of the transmission elements and the selection of their geometry must be performed manually. Furthermore, most of these CAE-tools can only be controlled from within the software application.

In this paper a novel methodology for the automated design concept generation of transmissions is proposed. It starts with a solution of transmission topology synthesis, including a topology draft as exemplified in Fig. 1. These can be calculated automatically [4]. They provide information about the order of gear elements and the route and type (fix or shifting) of connections between them. Shifting elements may be located in different possible positions inside and outside of the original shifting connection route. This multiplies the number of possible theoretical topologies. In the next step, central shafts and their support-relation to the neighboring central shaft are defined. This leads to a variety of possible relations between the central shafts and therefore to a further multiplication of the number of possible theoretical solutions. Next, different bearing arrangements for each central shaft arrangement are defined and their potential for axial and radial load transfer to the housing is validated. As this is done for any central shaft arrangement, the number of possible theoretical solutions increases even more.

After this step, any theoretically possible arrangement of transmission elements is generated respecting a single solution of transmission topology synthesis and a corresponding topology draft [5].

The second part of automated design concept generation is the load-dependent calculation of all possible geometries of the transmission elements. The size of shifting elements depends on the number of lamellae which leads to a width-diameter dependence. As the design of shifting elements is mainly dependent on torque and rotational speed load, which is an output of transmission topology synthesis, the position of shifting elements is assumed not to be influenced by their geometry. Also, the size of gear elements is primarily dependent on torque load and an assumed operation time. The overall operation time of the transmission in every gear is either given by the user or the result of a predictive assumption. Similarly to shifting elements, the design of gear elements is width-diameter dependent and their position is assumed not to be influenced by their geometry. The independence of the design of the transmission element from its position does not hold for bearings and shafts [5].

In addition to varying the bearing concept and transmit ratios per stage, all 2^S tooth-angle sign combinations are generated for the S stages. However, before starting the optimization of a specific simulation-case, the axial bearing forces in the MIN-case are calculated for all sign combinations, and the one combination which results in the minimum sum-absolute-total-axial-force value is selected.

The topology draft of a continuous example used to illustrate the key concepts of the proposed methodology is shown in Fig. 1.

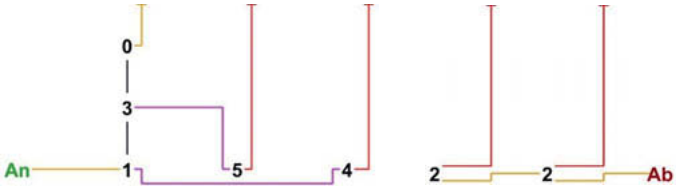

a) Shaft-level 1 b) Shaft-level 2

Fig. 1: Exemplary topology draft

In Fig. 1, red lines (“2”, “4”, “5”) represent spur gears, pink lines (“1-4”, “3-5”) shifting connections, and yellow lines (“0”, “An/1”, “2/2”, “2/Ab”) fixed shafts.

In this work we focus on two aspects of the proposed methodology: 1) The generation of a

logical order among elements based on topology modification, and 2) the dimensioning and positioning of gear box elements.

2. Logical Order Generation

The transmission topology contains information about logical connections between gear box elements (stages, shifting elements and input-/output-shafts). First, central knots, such as gear elements (sun gear, spur gear) or in- and output shafts, are detected in the transmission topology draft. These central elements define central shafts which route exclusively through the center of the considered shaft level. Connections which run below central shafts are central shafts as well. In addition to central shafts, central elements define sections (before/after/between elements), which determine together with the element positions the possible logical axial positions usable in bearing concepts. In the example shown in Fig. 1, there are 3 central gear elements on shaft level 1 (1 sun gear “1”, 2 spur gear wheels (“5”, “4”), 1 input shaft “An” and 1 output shaft “Ab”). Both, the input shaft (“1”/”An”) and the output shaft (“2”/”Ab”) each lead to a single central shaft. The route and number of resulting central shafts from the shifting connections between “3” and “5” and between “1“ and “4“ are dependent on the defined positions of the respective shifting elements. Possible exemplary positions can be seen in Fig. 2 as rectangles.

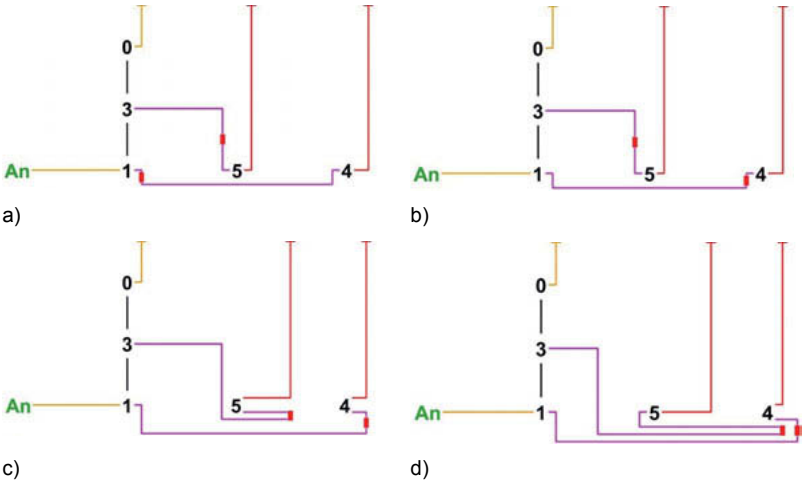

Fig. 2: Exemplary topologies generated from the topology draft in Fig. 1 with determined positions of the shifting elements

Fig. 2a and Fig. 2b show exemplary topologies which are based on the topology draft in Fig. 1 by specifying the position of the shifting elements on shifting connections (pink lines).
In Fig. 2c and Fig. 2d two further possibilities of shifting element positioning are exemplified. The positions were generated by bending shifting connections without crisscrossing lines.
The housing can be taken into consideration as additional central knots with a fixed connection to the housing. Thereby, additional bearing concepts can be taken into consideration, especially but not exclusively for radial outermost shafts. Such a knot may be inserted in a section between central elements if it has access to both, the housing and the central space below one or both of the neighboring elements.

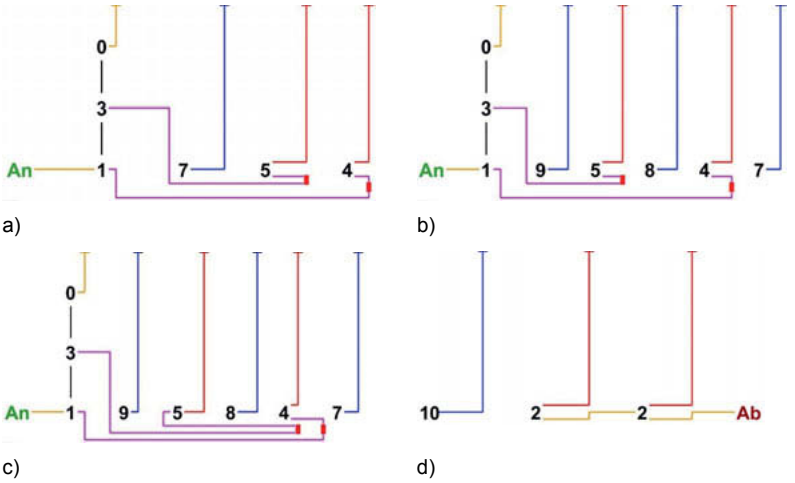

Fig. 3: Exemplary topologies generated from topologies in Fig. 2 by inserting combinations of feasible “housing-knots” as new central elements.

Fig. 3 shows possible extensions of the topologies in Fig. 2 with blue / red / pink lines represent housing connections / spur gears / shifting connections. Note that a topology results in multiple modified topologies by considering all combinations of knot insertions, cf. Fig. 3a and Fig. 3b which originate from the same topology / shifting element position combination in Fig. 2c.
In summary, positions of central gear elements as well as input and output define sections. The definition of central shafts and their start and end depend on these central elements and the shifting element arrangement. Bearings can be positioned under elements or in sections

when feasible with respect to bearing partners (e.g., access to the housing). In this way, a (partial) logical order among all gear box elements is generated and can be combined with the calculated range of geometrical dimensions of the considered transmission element (e.g., gear- and shifting elements in Fig. 7). In the given example, the iteration of different shifting element positions and combinations of inserted housing knots results in 44 modified topologies on shaft level 1 and 2 topologies on shaft level 2, respectively. The combination of topologies per shaft level therefore results in 88 base topologies.

Note that also the selection of a specific central shaft relation (cf. Section 1) can be interpreted as a topology modification. To see this, Fig. 4 shows two such modifications.

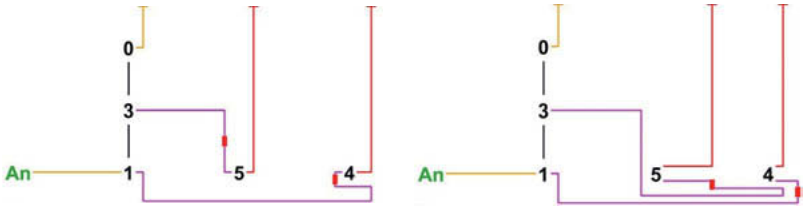

Fig. 4: Modified topologies resulting from a specific central shaft relation/topology.

The Fig. shows how an exemplary central shaft relation among shafts “1” and “4” dictates that shaft “1” tunnels through shaft “4” and supports it.

3. Validation of the Axial Support

After the logical order generation in Section 2, central shafts and feasible support-relations among central shafts are identified for each (modified) topology [5]. Any central shaft arrangement leads to several possibilities of theoretical bearing concepts, such as, e.g., fixed bearings or a combination of axial- and floating bearings. Also, the supporting partner, and, by implication, the supporting direction, of fixed bearings and axial bearings need to be considered in order to calculate the route of axial forces and their possible support in the housing. More formally, a matrix capturing the axial bearing partners of each shaft is created, with a logical “1” at row i / column j indicating that shaft i is axially supported by shaft j. This matrix is created for both axial directions and can be converted into a directed graph, with nodes representing shafts and edges representing a support relation. An axial support concept is said to be valid if every shaft has a unique path to the housing.

A possible axial support concept for our example on shaft level 1 can be seen in Fig. 5 and Fig. 6.

	“1”	“3”	“4”	“5”	“0”
“1”	0	0	0	0	1
“3”	1	0	0	0	0
“4”	0	0	0	0	1
“5”	0	0	1	0	0
“0”	0	0	0	0	0

Fig. 5: Binary axial support matrix

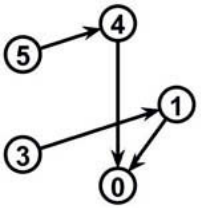

Fig. 6: Directed axial support graph

It corresponds to the topology in Fig. 2a, with the central shafts given by shafts “1“, “4“ and “5“. Shafts “1“ and “4“ are independent, while shaft “5“ is “carried” by shaft “4“. A possible bearing concept in this case is to support both, shafts “1“ and “4“, by a fixed and a floating bearing in the housing, to support shaft “5“ by a combination of two axial and one floating bearing on shaft “4“, and to support non-central shaft “3“ by a fixed bearing on shaft “1“. As can be seen in Fig. 6, there exists a unique path between each node and the housing-node “0”, and the exemplary axial support concept is therefore valid.

The number of axial support graphs that need to be checked for validity is equal the sum of all unique bearing concepts per shaft level. This number is significantly smaller than the number of bearing concepts, which result from a combination of bearing concepts over shaft levels.

After detection of central shafts and checking all possible central shaft relations and resulting axial/radial support (bearing selection and axial support partner combination) per shaft, one obtains over 4.8 million bearing concepts. Among those, approximately 3 million bearing concepts are found valid after the described axial support graph check.

4. Dimensioning and Positioning of Gear Box Elements

The problem of dimensioning the gear-box elements and positioning them in the constraint space is divided into three nested optimization problems: a) The “Axial Gear-box Element Positioning” (AGEP) problem of axially shifting the elements in order to avoid conflicts on the same (and optionally on other) shaft levels while obeying the logical bearing concept introduced in Section 2; b) the gear-box positioning (GBP) problem of shifting the gear-box and its elements and rotating the axes such that the gear-box fits inside the specified constraint space; and c) the element dimensioning (ED) problem of linearly combining the sizes of the stages,

bearings, and clutches with respect to their height and width under minimal radial extension and maximal radial extension, respectively, while minimizing the axial gear-box length (as obtained by the AGEP subproblem) and obeying feasibility of positioning the gear-box inside the constraint space (as determined by the GBP subproblem). The hierarchical structure of the proposed optimization approach is shown in Fig. 8a. The implementation which led to the simulation results in the following sections deviates slightly from this scheme as the GBP problem only shifts the gear-box in one piece and rotates the gear-box around its input axis, while keeping a previously calculated solution of the AGEP problem, cf. Fig. 8b. Thereby one avoids solving the AGEP problem for each position/rotation during our search, leading to a complexity reduction. However, this modification prohibits solutions where gear-box elements are individually axially shifted in order to fit the constraint space, e.g., in order to position the elements around an obstacle inside the constraint space. An intuitive advantage of the modified scheme is the closer similarity to the original MIN-case and MAX-case calculations, which has an impact on whether the linear combination approximation for bearing dimensions holds in the combined case.

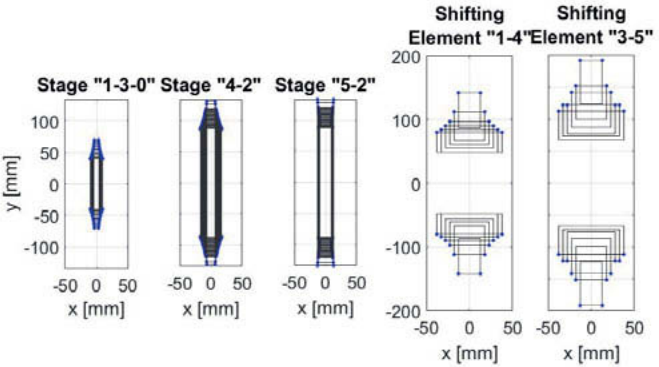

Fig. 7: Sampled tradeoff curves for stage dimensions and shifting-element dimensions

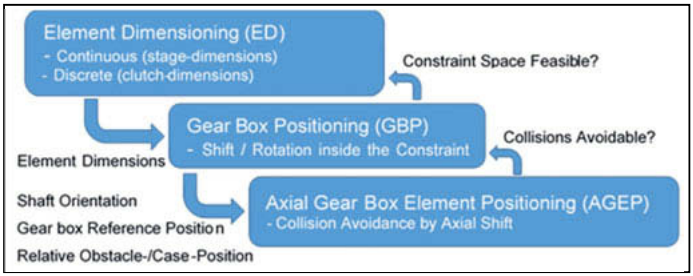

General Positioning: Move Gear box Elements Individually

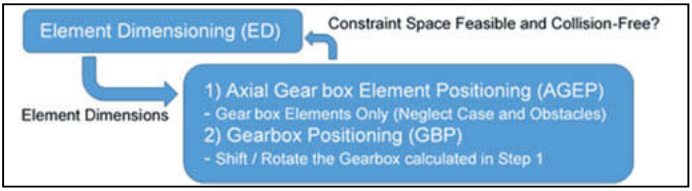

Modified Positioning: Move Gear box Elements Collectively

Fig. 8: Gear box element dimensioning and positioning

In the following the ED and GBP problems are described, while the AGEP problem is discussed in Section 5. The description applies to both schemes in Fig. 8. Also, it is evident that the combinatorial ES problem, the global GBP problem, as well as the AGEP constraint satisfaction problem may be solved by various other optimization algorithms in the respective fields, and that the proposed algorithms bear potential for future research, cf. our suggestions for future work in Section 0.

Element Dimensioning (ED)

The ED problem is to select continuous variables $\chi_s \in [0,1]$ for each stage indexed $s \in S$ and discrete variables $\phi_c \in \{1,2,\dots,N_c\}$ for all clutches indexed $c \in C$ such that the GBP subproblem finds a feasible placement of the resulting gear box inside the constraint space, and the gear box length is minimized. An exhaustive grid search is performed in order to select the stage sizes, where the continuous variables are discretized according to a specified grid-size and all combinations of variables are tested. Local searches can be performed on a finer grid, using the points on the larger grid as starting points. The dimensions of stages are calculated by linear combination of their dimensions in the minimum shaft-distance (“MIN”) case and maximum shaft-distance (“MAX”) case, respectively. The dimensions of clutches are obtained by

discrete selection of specific width/inner-radius/outer-radius values (generated by varying the number of friction discs). Fig. 7 shows the sampled tradeoff curves between the elements' width and height. Note that the selection of the MIN and MAX dimensions depends not only on the load, but also on the base topology and central shaft relations through the resulting diameters of the carrying shaft.

Differently to the sizes of stages and clutches, the dimensions of the bearings depend on their position on the shaft. Hence, in order to obtain two reference instances that allow to form a linear combination when performing the gear box/element positioning, the gear box is calculated under minimal radial dimension of all stages/clutches (MIN-case) and maximal radial dimension of all stages/clutches (MAX-case) prior to the dimension optimization. After a combinatorial search for bearings which sustain the calculated forces one obtains two sets of bearing dimensions, one for each case. During the ED problem an average over all factors χ_s on a specific shaft is calculated, which is used to calculate the linear combination for the bearings on the shaft.

Gear Box Positioning (GBP)

The goal of the GBP problem is to shift and rotate the gear box (or its elements) in order to find a feasible positioning inside the constraint space. An exhaustive search of a reference position vector (x/y/z coordinates) and rotation of the gear box around its input shaft is performed. Under the scheme in Fig. 8a the AGEP problem would be solved to axially position the elements on one side of the reference position (taking the constraint space/obstacles into account). Under the scheme in Fig. 8b the AGEP problem would be solved only once (without taking the constraint space/obstacles into account) and the result shifted/rotated as one piece in an effort to fit the gear box into the constraint space. The search halts once a feasible positioning has been found. The output is a binary value meaning the positioning inside the constraint space is feasible or not.

5. The Axial Gear-box Element Positioning (AGEP) Problem

The axial gear-box element positioning (AGEP) problem consists of deciding on the axial shift variables $\boldsymbol{x} = [x_1, x_2, \dots, x_N]$ for all elements indexed $i \in I$ (i.e., gears, bearings, clutch-elements, etc.) such that no conflict exists among those elements and such that the total axial gear box length is minimized. Importantly, the geometry of the elements (cylindric objects with inner-/outer radius r_i / R_i, width W_i, and axial direction) is known and fixed at this point.

The first set of constraints that are considered are "disjunctive binary differences" (DBD) of the form

$$a_1 \leq (x_i - x_j) \leq b_1 \vee \cdots \vee a_n \leq (x_i - x_j) \leq b_n, \quad (1)$$

where $a_1, b_1, \ldots, a_n, b_n$ are real numbers such that the n possible intervals for the difference $(x_i - x_j)$ are disjoint. These numbers originate from the following requirements:

- **Couplings** among element positions x_i and x_j (e.g., the position of two centered floating bearings below the supported central gear element, or the gears belonging to a single spur-gear-stage) -> $(x_j - x_i) \in \{[E_{ij}, E_{ij}]\}$, where E_{ij} depends on the elements' widths, the bearing concept, and the targeted inter-element space.
- **Special variables** x_L, x_U, measuring the lowest and highest occupied axial positions, implying 2 inequalities per shaft (with the "first" and "last" positioned element according to element order, respectively) -> $(x_L - x_i) \in \{(-\infty, -W_i/2]\}$, $(x_U - x_i) \in \{[W_i/2, \infty)\}$
- **Logical sequence** - Inequalities based on the positions of elements in logical sections and on shafts according to the topology and bearing concept, possibly including a maximal axial overlap -> $(x_i - x_j) \in \{(-\infty, S_{ij}]\}$, where S_{ij} is the required gap between the elements' center positions
- **Radial conflict** between two otherwise unordered elements, resulting in two inequalities (including margins) per conflict (e.g., taking also the actuator positions of clutches in the same logical section into account) -> $(x_i - x_j) \in \{(-\infty, L_{ij}], [L_{ji}, \infty)\}$, where L_{ij} and L_{ji} are the required gaps among the elements for the two possible conflict-free element orders
- **Unary position limitations** - Variable x_0 can be regarded a reference position (fixed to an arbitrary value) which can be used to turn any unary constraint on the position x_i of an element (e.g., due to external fixed-position obstacles, a given enforced position, or the assembly space in which the elements must lie) into binary constraints (i.e., constraints involving at most 2 variables) -> $(x_i - x_0) \in \{[\check{E}_i^1, \hat{E}_i^1], \ldots, [\check{E}_i^{e_i}, \hat{E}_i^{e_i}]\}$, where $\check{E}_i^k$ and $\check{E}_i^k$ are the lower-/upper ends of interval k in which variable i may reside

Note that the relation of the "reference position" x_0 and the position of the gear box inside the assembly space is subject of the GBP problem. Furthermore, the radial dimensions of a bearing considered for conflict detection are not only determined by the actual dimensions, but also by the bearing-partner (e.g., the shaft on which a bearing is mounted, or the gear-case). When applying multiple criteria then interval intersections must be applied appropriately.

Besides these binary constraints, nonbinary "central-shaft constraints" are considered as well. More specifically, the positions of elements on a central shaft result in a certain range in which the shaft is central with given shaft radius. Elements on the same or on other shaft levels may

collide with that shaft. Hence, a possibly colliding element must be to the left of the first element on the shaft, or to the right of the last element on the shaft.

Mathematical Model for the AGEP Problem

The problem of finding a solution $\boldsymbol{x}$, where each variable lies in its domain, $x_i \in D_i$, and $\boldsymbol{x}$ satisfies all constraints in the constraint set is in general referred to as a "Constraint Satisfaction Problem" (CSP). If such a solution exists, the CSP is called "consistent". In a "temporal" CSP (TCSP) variables represent time points or intervals (or more generally, totally ordered continuous variables) and the constraints represent temporal relations. A specific type of TCSP is obtained when all variables are real ($D_i \doteq \mathbb{R}$) and all constraints are in the form of DBDs [6]. Detecting consistency of these "Binary TCSPs" (B-TCSP) is NP-complete [7].

One observes that the problem of selecting axial shifts $\boldsymbol{x}$ falls into this subclass when the non-binary constraints and our objective function are neglected. These problems can be represented as a DBD network (directed constraint graph) with the nodes and edges representing the variables and binary constraints, respectively. Selecting a single disjunction per edge ("labelling" the TCSP) results in a "Simple B-TCSP" (SB-TCSP) which may be converted into a weighted/directed "distance graph" with the nodes representing again the variables, and a directed edge from x_i to x_j labelled a_m represents the constraint $(x_j - x_i) \leq a_m$, while an edge from x_j to x_i labeled b_m represents the constraint $(x_j - x_i) \leq b_m$. Deciding consistency of an SB-TCSP can be accomplished in $O(nE)$ time using a single-source shortest paths algorithm by deciding whether the graph has negative cycles, where n is the number of nodes and E is the number of edges in the distance graph (i.e., the number of binary constraints) [6], [7]. Constraints are "minimal" if any instantiation of 2 variables satisfying all constraints involving those two variables only, can be extended to a solution of the CSP. The "minimal network" for the SB-TCSP can be calculated using an all-pairs shortest paths algorithm in $O(n^3)$ time [6].

AGEP Algorithm

In the following the algorithm solving the AGEP problem to optimality is described. More precisely, it is based on the described B-TCSP model and comprises various previously proposed methods and improvements for solving B-TCSP problems in [7], [8], [9], [10]. **The key additions of Algorithm 1 to these methods are the following:** 1) The constraints are split into those which have DBD form and consequently are treated under the B-TCSP framework using backtracking [8] and incremental consistency checking [9], and non-DBD central-shaft constraints which are evaluated once a leaf node of the backtracking-search tree is reached in order to evaluate consistency of the original TCSP; 2) The objective of minimizing the axial

gear-box length leads to an optimization problem. The objective is nondecreasing when descending the search tree (i.e., selecting disjuncts and thereby further constraining the SB-TCSP), and therefore one can use the axial length of a partial solution (possibly not obeying all constraints) to prune the search tree. This is implemented by updating the distance graph (the weight on the edge between variables x_L and x_U) every time a new incumbent solution is found. 3) Consistent solutions found on leaf nodes are further refined by minimizing shaft-lengths (for fixed gear box length) and maximizing inter-bearing distances (for fixed shaft lengths and gear box length). This means that 3 objectives are optimized hierarchically, with the gear box length being the one with the highest priority. The empirical motivation behind is that the elements shall be positioned compactly, and that larger inter-bearing distances may result in less bearing-stress. The three objectives are hierarchical and serve to rank solutions.

In Line 1 of Algorithm 1 all possible actuator-position combinations over all clutch elements are generated. The actuator position (to the left or to the right of a clutch element) influences the extent to which another element may be shifted inside the clutch element. Also, the logical bearing concept, the transmission topology (logical sections), and the element dimensions (possible collisions) are mapped into DBDs, cf. Equation (1), resulting in an individual B-TCSP model for each actuator-position combination. In Line 3 “Upper-Lower Tightening” is performed, which has a complexity $O(n^3 \cdot e \cdot E + (e \cdot E)^2)$, where e is the maximum number of disjunctions per constraint, and E is the number of DBD constraints [8]. The algorithm iteratively applies the Floyd-Warshall all-pairs shortest path algorithm with complexity $O(n^3)$ on the distance graph of a relaxed SB-TCSP to tighten the formulation. This step also serves to exclude inconsistent B-TCSP’s at an early stage. In Line 4 a SB-TCSP is initialized using the lowest and highest interval borders per DBD. In Line 5 the order in which the disjunctions are selected is chosen (e.g., using the sum-length of the infeasible intervals between the disjuncts), which determines the search space. In Line 6 a backtracking algorithm is run in order to search for the optimal labelling of the disjunctive constraints. This backtracking runs on a “meta-CSP” with variables representing disjunctions and values corresponding to binary-difference disjuncts [10]. The complexity, assuming the Bellman-Ford algorithm is used for consistency checking, is therefore $O(n \cdot E \cdot e^{\check{E}})$, where $\check{E}$ is the number of constraints with more than one disjuncts. When branching, the labelling decision is checked for consistency by incrementally updating the distance graph and its shortest paths from x_L to all other nodes using the queued Bellman-Ford algorithm in [9]. When a leaf node is reached, the consistency of the corresponding SB-TCSP (which includes all binary DBD constraints) and the nonbinary central-shaft constraints are tested. If a solution of the B-TCSP has been found, the following

objectives are optimized hierarchically: 1) the gear-box length; 2) the shaft lengths; and 3) the inter-bearing space. Note that all three optimization problems can be solved using the queued Bellman-Ford algorithm [9], or alternatively using any linear program solver. After the evaluation of a solution to the original B-TCSP, the incumbent gear box length can be used by updating the weight on the directed edge between variables x_L and x_U. This way, all following consistency checks (e.g., during branching) take the latest incumbent gear box length into account. This means that not only inconsistent partial solutions are pruned, but also suboptimal partial solutions. As mentioned above, this is possible since the gear box length is monotonously increasing when selecting specific disjuncts for the disjunctive constraints during backtracking.

Algorithm 1: Axial gear-box element positioning (AGEP)

1: Setup the B-TCSP data for each clutch-actuator-combination
2: For each B-TCSP:
3: Run “Upper-Lower Tightening” [8]
4: Initialize the SB-TCSP (i.e., its distance graph)
5: Select the order in which disjunctions are selected (i.e., constraints are labelled)
6: Run a backtracking algorithm if constraints with disjunctions exist [10]

a) Branching/Pruning: Update the distance graph, and incrementally check consistency using the algorithm in [9]

b) Leaf-node Evaluation: Check consistency [9]; check nonbinary central-shaft constraints; minimize the gear-box length; minimize the shaft-lengths (for fixed gear box length); maximize the inter-bearing space (for fixed shaft lengths and gear box length)

6. Simulation Results

In order to demonstrate the impact of the discussed logical order generation for gear box elements, two constructions based on different base topologies are compared in the following, cf. Fig. 9. Both subFig.s show a) the intermediate construction “MIN” based on the minimal shaft-distance per stage, b) the corresponding design with maximal radial size per stage and shifting element (“MAX”), and c) a feasible construction obtained by linear MIN-MAX-combination and reevaluation. The latter step includes the positioning of the gear box in the housing represented

by the light-green cylinders. Shifting elements are shown in brown, gear-stages in blue, shafts in red, and bearings in yellow/black. The construction in Fig. 9a uses a bearing concept based on the central-shaft relation and topology / shifting-element positions shown in Fig. 4a (based on the topology in Fig. 2b), i.e., shaft “1” extends through all of shaft level 1 and thereby supports both spur gear stages. Differently, the construction in Fig. 9b uses a bearing concept based on the topology / shifting-element positioning in Fig. 2a, where shaft “4” supports shaft “5” as well as shaft “1”. The position of the right-most shifting element in Fig. 9a leads to a limitation of its radial size due to the presence of the output shaft “2”, while in Fig. 9b the corresponding shifting element can be assigned its axially shortest dimension option, cf. also Fig. 7. The difference in axial length between the two constructions in Fig. 9 is approximately 34 mm (or 22 % referred to the axially shortest construction).

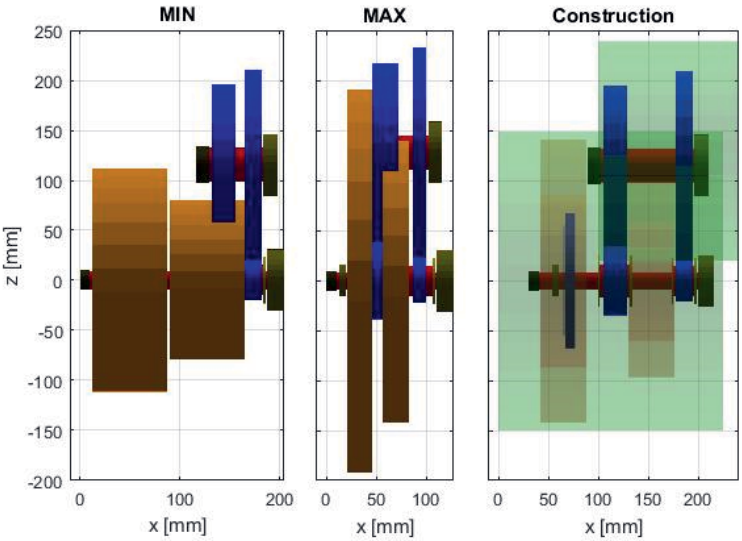

Fig. 9a) Exemplary intermediate “MIN”-, “MAX”-, and final construction using a bearing concept based on the topology/central-shaft relation shown in Fig. 4a.

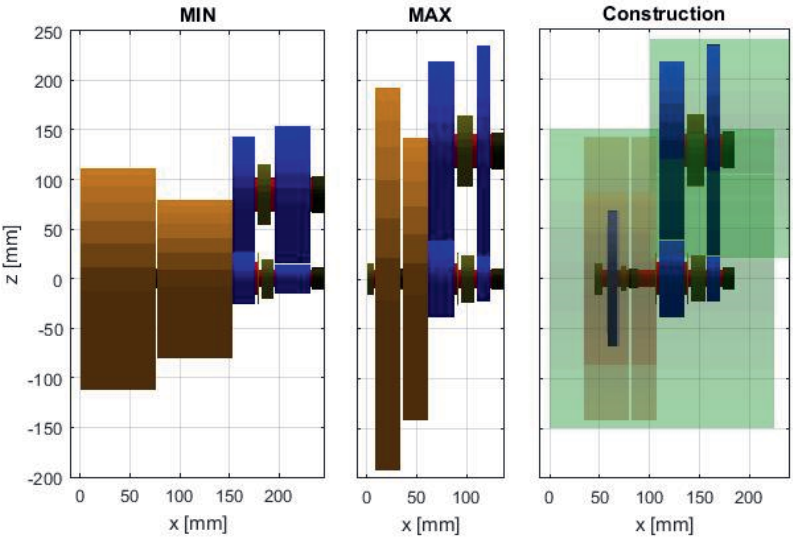

Fig. 9b) Exemplary intermediate “MIN”-, “MAX”-, and final construction using a bearing concept based on the topology shown in Fig. 2a.

In Fig. 9a) is a clash of a gear element and a shifting element visible. This is the first step, when the geometry data meets the logical order generation. These overlaps appear in transmission topologies with more than one shaft level because the logical order only is dependent on the respective shaft level and the order and position of gear elements. In a further step, clashes are detected and the construction is overlap-free after all.

7. Conclusion

Automated generation of transmission design concepts results in a large number of feasible design concepts starting with a single transmission topology, a single transmission topology draft (cf. Fig. 1), and an assembly space specification. The addition of case knots (cf. Fig. 3), and variation of the positions of shifting elements (cf. Fig. 2) multiplies the number of feasible topologies. Each such topology in turn leads to various central shaft definitions and support relations among them (cf. Fig. 4), which are verified following a set of general rules.

For each central shaft arrangement, numerous bearing concepts are generated by varying types, logical positions (below/between elements), and partner-shafts of bearings. An axial support graph model is proposed to confirm the validity of each bearing concept (cf. Fig. 6).

The construction of each bearing concept requires solving several further, inter-related optimization problems, including bearing force calculation, bearing selection, axial element positioning, gear box positioning (inside the assembly space) and element dimensioning. Several general problem statements and selected algorithms are discussed. Exemplary feasible constructions of the topology draft shown in Fig. 1 can be seen in Fig. 9.
Future research will target the reduction of the tool's computation time (e.g., by preselection of bearing concepts), the routing of non-central shafts, and the improvement of the tool's applicability. To that end it is planned to extend the work to allow for multiple input shafts and further transmission elements like other clutch types.

8. Literature

[1] Gumpoltsberger, G.: Systematische Synthese und Bewertung von mehrgängigen Planetengetrieben. Technische Universität Chemnitz Dissertation. 2007

[2] Leesch, M.: Beitrag zur systematischen Synthese und Bewertung von Doppelkupplungsgetrieben. Technische Universität Chemnitz Dissertation. 2012

[3] Müller, J.: Beitrag zur systematischen, rechnergestützten Synthese und Bewertung mehrgängiger konventioneller und hybrider Planetenautomatikgetriebe. Technische Universität Chemnitz Dissertation. 2012

[4] Kupka, D. u. Tenberge, P.: Automated concept design for the evaluation of favourable AT structures. VDI-Berichte, 2276 (2016) S. 193–206

[5] Evenschor, D., Dennin, D. u. Tenberge, P.: Automated design concept generation of automatic transmissions. VDI-Berichte, 2328 (2018) S. 181–196

[6] Rossi, F., van Beek, P. u. Walsh, T.: Handbook of Constraint Programming. Amsterdam: Elsevier. 2006

[7] Dechter, R.: Constraint processing. San Francisco: Morgan Kaufmann Publishers. 2011

[8] Schwalb, E. u. Dechter, R.: Processing disjunctions in temporal constraint networks, Artificial Intelligence, 93 1-2 (1997) S. 29–61

[9] Cesta, A. u. Oddi, A.: Gaining efficiency and flexibility in the simple temporal problem. Proceedings Third International Workshop on Temporal Representation and Reasoning (TIME '96) (1996) S. 45–50

[10] Dechter, R., Meiri, I. u. Pearl, J.: Temporal constraint networks, Artificial Intelligence, 49 1-3 (1991) S. 61–95

Transferability of economic electrification concepts in heavy goods traffic to mobile machinery

Prof. Dr.-Ing. **A. Riegauf**, RWTH Aachen University

PEM at RWTH Aachen University
Chair of Production Engineering of E-Mobility Components

PEM | RWTH AACHEN UNIVERSITY

Production Engineering of E-Mobility Components

Prof. Dr.-Ing. Achim Kampker

- First Part Right
- Next Gen Technologies
- One-Click Production
- Scale Up Process Technologies

Powertrain: Manufacturing-oriented design		Powertrain: Production technology and organization		Fuel Cell
Battery Components	Battery Engineering	Battery Production	Electric Drive Production	Production technology and organization

PEM of RWTH Aachen University develops different solution for the sustainable and emission-free road freight transport

LiVe

Lifecycle cost reduction in electrical distribution transport by means of an adaptable drivetrain

- **Application scenario:** Distribution transport
- **Vehicle weight:** 7,5t – 18t
- **Project start:** September 2017

LiVePLuS

Life cycle cost reduction in electrical distribution traffic through catenary trolley based electrification systems for tractor units

Image source: Siemens

- **Application scenario:** Long haul goods traffic
- **Vehicle weight:** 40t
- **Project start:** February 2020

To achieve climate targets and legal requirements, there is a high demand for the electrification of heavy trucks

Growing freight traffic[1]

Fright traffic is expected to grow by 32% by 2030 compared to 2014 while almost 80% is conducted by trucks

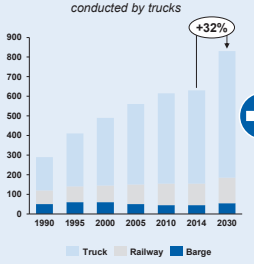

Share of CO_2 emissions[2,3]

Although heavy-duty trucks make up only 1% of overall vehicles, they are responsible for about a quarter of the CO_2 traffic emissions

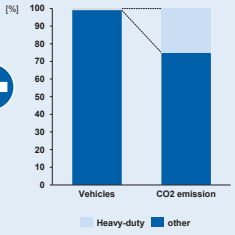

State of the art[4]

Alternative powered tractor units only have a share of less than 0,1%

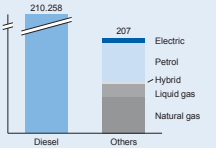

- Target: Reduction of truck based CO2 emissions of 15% till 2025 and 30% till 2030
- Fines to be paid from 2025 if CO2 limits are exceeded

Sources: (1) VDA, Dekra, BMVI (2) IW Köln; (3) KBA; (4) KBA

High costs for the components of the electric drive train prevents an unified and economic vehicle configuration for different use cases as for convention combustion based drive trains

Set of possible energy sources for an electrified powertrain

- Fuel cell & H2-storage
- Traction battery
- Pantographsystem

Cost-intensive

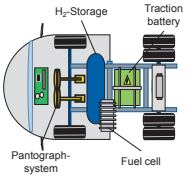

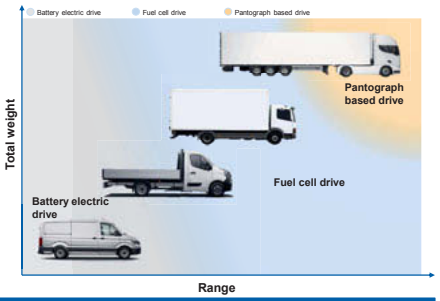

To ensure the competitive electrification of trucks a use case specific and economic vehicle configuration is required.

Especially the sector of high energy demand continues to be a major challenge for the economic drive train electrification

Set of possible energy sources for an electrified powertrain

- Fuel cell & H2-storage
- Traction battery
- Pantographsystem

Cost-intensive

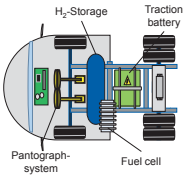

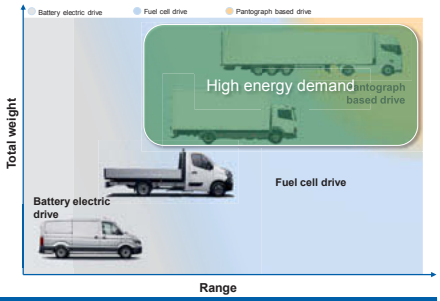

To ensure the competitive electrification of trucks a use case specific and economic vehicle configuration is required.

There is a significant number of mobile machines which, like heavy trucks, have a high energy demand

One solution is the modular, adaptable powertrain construction kit that enables competitive powertrain configurations through scalability at component level

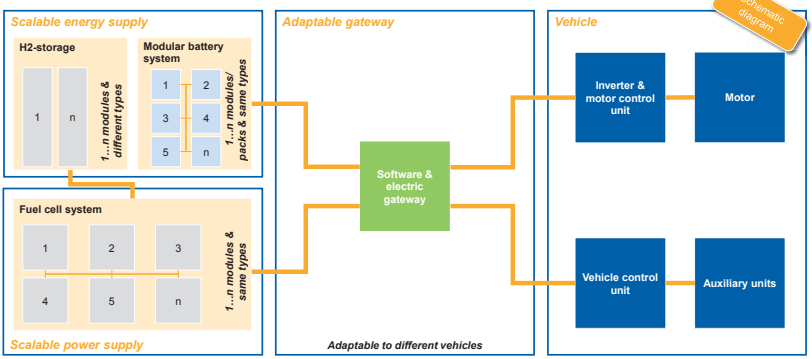

Scalability and thus cost reduction for the fuel cell system can be accomplished by different strategies

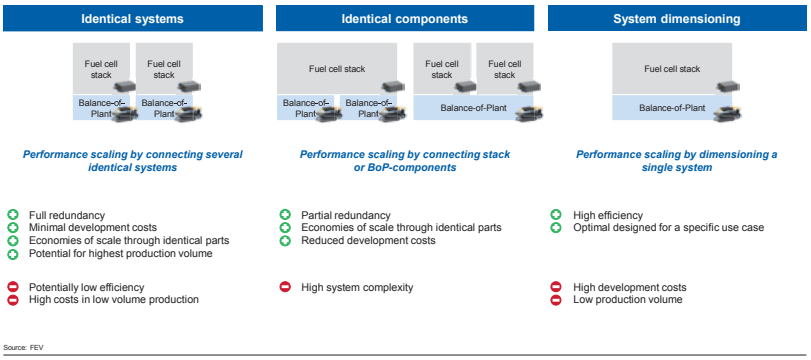

Source: FEV

Scalability and thus cost reduction for the fuel cell system can be accomplished by different strategies

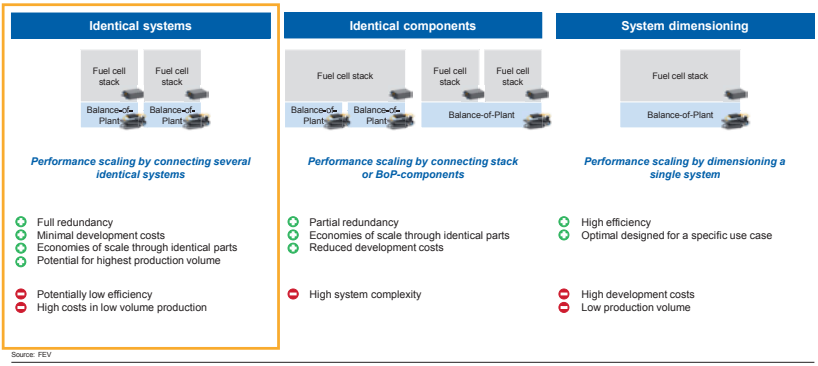

Source: FEV

The highest economies of scale can be achieved by using the highest possible number of identical parts in the fuel cell system

Example fuel cell System

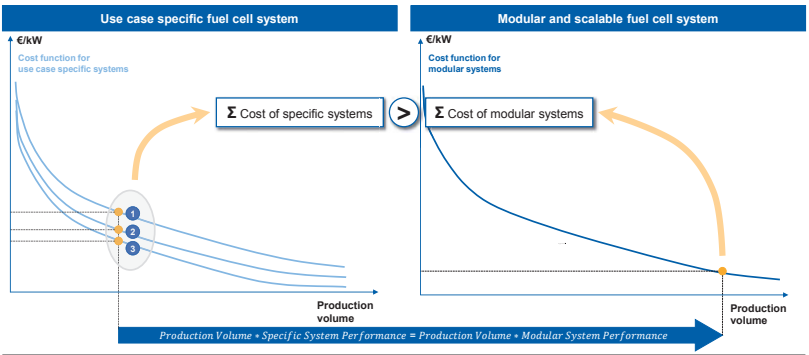

The performance scaling is realized by connecting and integrating several identical systems as range extender

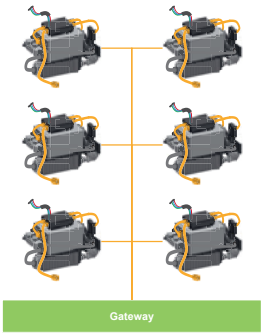

System specifications

- Modular fuel cell system including stack and balance of plant
- Design of the system as range extender and provision of the dynamic by the traction battery
- Scaling of the overall performance by series or parallel connection of the systems
- Single performance of 12-24kW for each fuel cell system
- Three operating modes (off, optimum load operation, standby)
- Low operation pressure of the fuel cell system
- Extension of the life cycle through retrofit capabilities

Powered by our partner

ALTERNATIVE ENERGY DRIVEN SOLUTIONS

System potential

- Cost reduction by increasing the production volume and realization of economies of scale
- Low power loss of the entire system
- Use of proprietary technologies available on the market
- Long durability through operation at the optimal operation point
- Flexible integration into different vehicles and vehicle platforms possible

A modular battery system can be enabled on the level of the battery module or on the level of the battery pack

Battery module

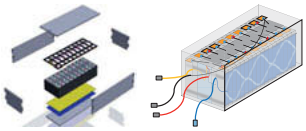

Modularization potential

- Scaling of power or capacity by a different number of serial or parallel connected cells
- Despite variation in module size there is a high number of identical parts for different module sizes
- Design adaption of the cell contacting system is needed
- Cheaper components due to lower currents

Battery pack

Modularization potential

- Variation of capacity by parallel connection of various battery packs via PDU
- Realization of different vehicle ranges
- High complexity in the interconnection of several packs
- High currents lead to high component costs

A modular battery system can be enabled on the level of the battery module or on the level of the battery pack

Battery module

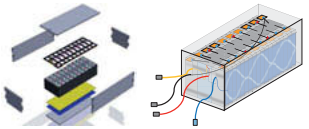

Modularization potential

- Scaling of power or capacity by a different number of serial or parallel connected cells
- Despite variation in module size there is a high number of identical parts for different module sizes
- Design adaption of the cell contacting system is needed
- Cheaper components due to lower currents

Battery pack

Modularization potential

- Variation of capacity by parallel connection of various battery packs via PDU
- Realization of different vehicle ranges
- High complexity in the interconnection of several packs
- High currents lead to high component costs

With innovations in the thermal management and the cell contacting potentials for modularization strategies can be tapped

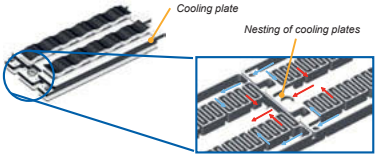

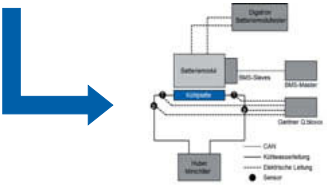

Modular thermal management

- Transfer of the cooling plate from the battery tray into the battery modules to remove restrictions for the number of modules
- Implementation of a cooling plate for each module
- Connection of the module cooling plates to enable the overall thermal management of the battery systems
- The scaling of the thermal management is coupled with the number of modules and therefore with the vehicle range

Detachable cell contacting system

- Design of a cell contacting system which can be removed non-destructive
- Targeted replacement of single, damaged cells instead of the whole module
- Reduction of vehicle costs by extending the battery life and enabling an economical after-life use

VDI Wissensforum

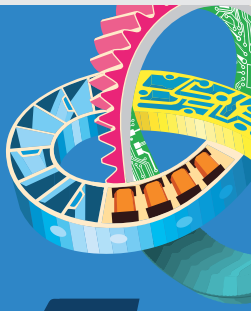

Dritev

20th International VDI Congress

Dritev – Drivetrain for Vehicles

ISBN 978-3-18-092373-4

VDI Wissensforum

VDI-Berichte 2373

International Conference
EDrive

June 24 and 25, 2020

Main topics:

- Electrified powertrains in series
- Electric motor design and integrated battery design
- Switching concepts for electric drives
- Challenges in system integration
- Next-Gen E-Drive

VDI-BERICHTE
Herausgeber:
VDI Wissensforum GmbH

Bibliographische Information der Deutschen Nationalbibliothek
Die Deutsche Nationalbibliothek verzeichnet diese Publikation in der Deutschen Nationalbibliographie; detaillierte bibliographische Daten sind im Internet unter www.dnb.de abrufbar.

Bibliographic information published by the Deutsche Nationalbibliothek (German National Library)
The Deutsche Nationalbibliothek lists this publication in the Deutsche Nationalbibliographie (German National Bibliography); detailed bibliographic data is available via Internet at www.dnb.de.

Der VDI-Bericht, der die Vorträge der Tagung enthält, erscheint als nichtredigierter Manuskriptdruck.
Die einzelnen Beiträge geben die auf persönlichen Erkenntnissen beruhenden Ansichten und Erfahrungen der jeweiligen Vortragenden bzw. Autoren wieder. Printed in Germany.

ISSN 0083-5560
ISBN 978-3-18-092373-4

Content

E-motor Design

Next Generation E-Drive

Energy storage systems

Ingenieure wollen immer alles ganz genau wissen. Wie wär‘s mit einem E-Paper- oder Zeitungs-Abo?

Mehr Meinung. Mehr Orientierung. Mehr Wissen.
Wesentliche Informationen zu neuen Technologien und Märkten.
Das bietet VDI nachrichten, Deutschlands meinungsbildende Wochenzeitung zu Technik, Wirtschaft und Gesellschaft, den Ingenieuren. Sofort abonnieren und lesen.
Donnerstagabends als E-Paper oder freitags als Zeitung.

Jetzt abonnieren: Leser-Service VDI nachrichten, 65341 Eltville
Telefon: +49 6123 9238-201, Telefax: +49 6123 9238-244, vdi-nachrichten@vuservice.de

www.vdi-nachrichten.com/abo

VDI nachrichten
Die journalistische Heimat der Ingenieure.

Many thanks to the Gold-Sponsors of the Congress:

www.zf.com

www.castrol.com/de

Market-driven electric motor designs from Schaeffler

Optimized electric motor design process via technology and production kits

Peter Schwanemann, **Thomas Pfund**,
Schaeffler Automotive Buehl GmbH & Co. KG, Bühl (Baden)

Zusammenfassung

Die Hybridisierung und Elektrifizierung konfrontieren uns mit einer Vielzahl teils konträrer Anforderungen. Meist liegen sehr individuelle Kundenwünsche zu Bauraum, Leistung, Drehmoment, etc. vor. Haupttreiber sind jedoch in fast allen Projekten die Kosten.

Um die optimale E-Maschinen-Lösung zu finden, müssen diese Anforderungen daher priorisiert werden.

Hieraus ergeben sich selbstredend kundenspezifische Produktlösungen. Um die Produktkosten dennoch niedrig zu halten, ist es erforderlich in projektübergreifende Technologie- und Produktionsbaukästen zu investieren. Ein komponentenbasierter Baukasten ist hingegen meist nicht zielführend.

Bei der Lösungsfindung sind deshalb holistische Werkzeuge von Nöten, die alle Faktoren von Beginn an berücksichtigen. Agile, iterative Kommunikation mit dem Kunden ist hierbei ein weiterer Schlüsselfaktor.

In diesem Vortrag wird diese Herangehensweise beleuchtet und beispielhaft diskutiert.

Abstract

Hybridization and electrification confront us with a multitude of requirements of which some are directly contrary to each other. There are usually very individual customer requests for installation space, power, torque, etc. However, in almost all projects cost is the most important requirement. Therefore, in order to find the optimal e-machine solution these requirements must be prioritized.

This naturally results in customer-specific product solutions. In order to keep the product cost down nevertheless, it is necessary to invest in cross-project technology and production kits. Contrary to that a component-based kit does not seem to be generally useful.

Therefore, when finding a solution, holistic tools that take all these factors into account are required. Agile, iterative communication with the customer is another key factor.
In this talk this approach is highlighted and discussed based on examples.

Market situation

In the past few years, many concepts for hybrid and electric drivetrains have been developed. The main driving force behind this is CO_2 legislation and type authorization in automotive industry, which mandate compliance with limiting values for pollutant emissions.
Since September 2019, it is necessary for all new vehicles sold to demonstrate compliance with the pollutant limiting values on the road (Euro 6d TEMP, RDE). Defining the right fleet mix, while at the same time living up to customer demands for price and performance is a hard task for the OEMs. This is even more true as customer preferences vary greatly around the world. [1]
The task for suppliers on the other side is by no means less complex. The situation described above combined with the vast possibilities to combine electric drive systems, transmissions, combustion engines and several energy sources like gasoline, diesel, alternative fuels, fuel cells (hydrogen) and batteries lead to a massive development diversity. This again is done in parallel for all segments of passenger cars, commercial and heavy-duty vehicles.

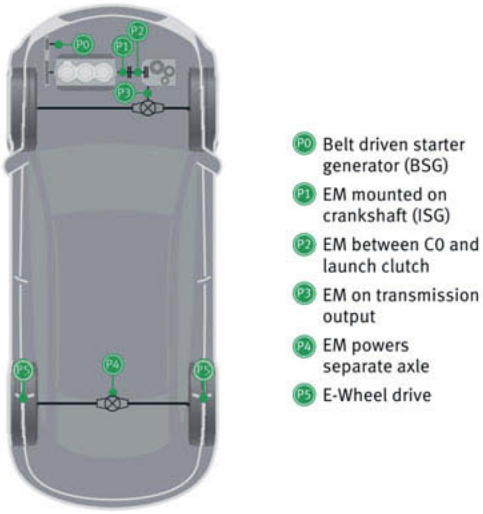

Fig. 1: Installation position of the electric drive in vehicles [1]

On a top level view the possibilities to integrate electric drive systems in a powertrain seem to be limited (Fig. 1). However, adding some further parameters like vehicle specific power requirements, battery voltage levels and different transmission arrangements already lead to a massively increased solution space (Fig. 2). This again still does not show the full big picture as each solution can be combined with one or more of the others to generate a system that further improves the overall powertrain according to the most relevant parameters like efficiency, performance or driving comfort.

Although a big part of all possible combinations is not technically constructive, the actual number of electric drive system variants requested on the market is still huge. Specific optimized electric drive systems and therefore e-motors are needed for each of these solutions.

As a consequence, e-motor suppliers are forced to adapt their strategy to these boundary conditions. Taking the current volatility of the market into account, focusing on one specific technology comprises a relevant risk. Therefore, to compete in the current e-motor market environment, suppliers like Schaeffler need to position themselves as flexible as possible.

However, looking at the positive side of the situation, the need of flexibility in terms of available e-motor technology is especially a chance to improve the product cost structure as well as for the elaboration for new unique selling points.

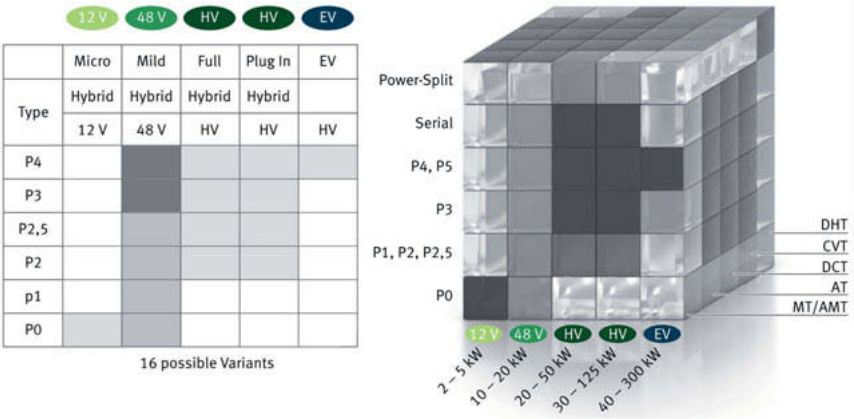

Fig. 2: Variants of electric drive systems based on different parameters [1]

Technology and Production kits: The cost benefit

As a rule of thumb for mass-produced electric motors, the proportion of the production process is roughly 20% of costs, while the proportion of materials accounts for around 80%. However, e-motor designs for specific requirements and boundary conditions might look completely different depending on the e-motor and production technology considered (IM, PSM, ESM, SRM, HSM, different winding technologies, etc.). Since these different designs have a direct influence on the required materials and thus on cost, different e-motor technologies must be considered in parallel to find the best cost solution while keeping the best possible requirement compliance for each new project – and of course all this needs to be done in no time. Consequently e-motor suppliers must define and invest in a technology and production kit, which provides the backbone for the parallel e-motor concept development. By defining and using that technology and production kit, optimization of the 80% cost share of materials already can be considered in early design processes.

The difficulty is to define the technology and production kit in such a way that it provides the needed maximum flexibility in the variety of variants of the electric motor design, while considering synergies in the production technology to keep the necessary investments as low as possible. If later goal is reached as well, optimization of most of the 20% cost share of processes is taken account of as well.

In other words, the task is to develop manufacturing and assembly processes with a maximum overlap to all e-motor technologies preferred by the research and development department to reduce the number of needed tools and machineries for the value chain to be.

Once that happened the next step is to check which other e-motor technologies as well as variants of already considered e-motor technologies can be produced with the very same manufacturing and assembly processes in order to further increase the variety of e-motor technologies available in the design kit. (Fig. 3).

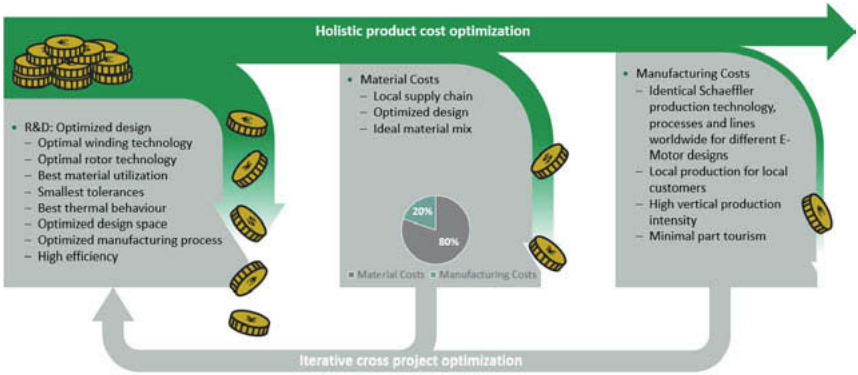

Fig. 3: influence on cost share of R&D, material and manufacturing

Finally, it should be considered that “part tourism” (transportation of parts between different production facilities or suppliers during production) is a relevant leverage on overall production cost as well. Schaeffler’s solution to this part is a high vertical production intensity inside localized value streams leading to a reduction of transportation, packaging and handling cost (Fig. 4).

Fig. 4: Localized high vertical production intensity

Technology and Production kits: The technical benefit

The outcomes of the technology and production kit are not limited to cross-project cost down measures. As pointed out above, the combinations of the defined technologies and processes with each other lead to new opportunities and to possible unique selling points. To name just one out of many examples at Schaeffler: Wave winding (radially inserted bar wound continuous hair pin winding) has a relevant advantage in terms of heat dissipation due to small tolerances between the copper wire and the stator teeth surface, leading to a reduced distance filled with air / impregnation and thus to reduced thermal resistance between cooper and iron in comparison to classical (axially inserted) hair pin winding.[2]

But as classical hairpin winding designs still have their justification in some specific boundary conditions, taking the technology and process know how from one to the other seems like a good idea and indeed leads to smaller wire-to-teeth tolerances and therefore to a better thermal performance than the one from classical state of the art hair pin stators.

The holistic approach – Step 1: Using the design kit to find the best solution

To be successful on the E-mobility supplier market additional flexibility to the previously mentioned one in e-motor technology is useful. Ideally a holistic approach is applied to the project acquisition process as well as to the available production scope. Key aspect is a strong system understanding and iterative technical discussions with the customer to get a good view on the big picture and to consult the customer in regard of specific technical features and advantages in their design if desired by the customer.

The technology and production kit discussed in previous chapter provides the needed backbone for this holistic design, while the corresponding generic value streams should provide the flexibility to cover different scopes of supply. E.g. with Schaeffler's highly vertical production intensity, different scopes of supply can easily be offered, from production machinery to complete electric drive systems (comp. Fig. 4).

In order to illustrate this theoretical implementation, the holistic approach is considered in the following exemplary request for two electric motors for a dedicated hybrid transmission (DHT) application.

The request includes a P1 e-machine, which is mainly used as a generator / range extender, and a P3 traction e-machine being used as main drive for the target vehicle. The rough specifications of these two electric machines are summarized in Table 1.

Table 1: Specification of both E-Machines

	E-Machine P1	**E-Machine P3**
Application	DHT integrated range extender Main drive	DHT integrated traction Main drive
E-Machine arrangement	Internal rotor	Internal rotor
Max. design voltage	300 V_amplitude	300 V_amplitude
Max. design current	350 Arms	475 Arms
Max. outer diameter Stator	275 mm	275 mm
Min. inner diameter Rotor	182 mm	182 mm
Max. axial length without 3~ terminals	60 mm	90 mm
Peak torque	200 Nm	400 Nm
Peak power	80 kW	130 kW
Continuous torque	100 Nm	200 Nm
Continuous power	40 kW	65 kW
Max active speed	7000 rpm	
Cooling system	Active oil cooling	

Intuitively the very first step is to check, whether any existing product of the portfolio is fulfilling exactly these requirements without any deviation. But in almost all cases that will not be the case. So, the actual first step is to open the technology kit on a high level, fill in the customer requirements and check which e-motor design parameters it returns. This step is not about looking at actual designs, but about finding the right base technology based upon an early estimation on available production technology.

Starting with the rotor technology, based on the applications of both e-machines as integrated main drives running on combustion engine speed, a solution with permanent magnet rotor is considered in the initial design. This is no final decision, but the best guess to start with. In the later design progress alternative concepts should always be considered in parallel anyhow to compare strength and weaknesses of the solution. E.g. separately excited e-machine rotors might be a solution for these requirements as well, whereas induction machine rotors

are less likely to be rewarding as a main drive (but would have been an option for auxiliary drives). However, as we will see in the following stator technology selection, due to the very narrow design space separately excited e-machines would be out of consideration as well (see exemplary Figure 5).

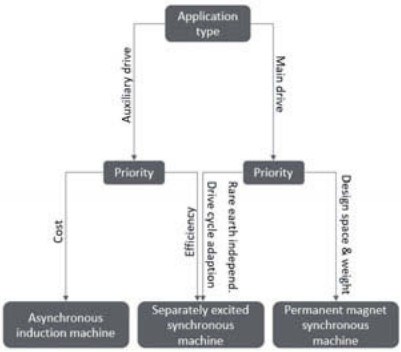

Fig. 5: Example of a high-level rotor technology selection

Based on the defined rotor technology, the stator technology can be selected via a high-level comparison as well. An exemplary result for the requirements for the P1 machine is shown in Figure 6. The highlighted area in the lower right corner of Figure 6 shows the results which advices to build the initial E-machine design on concentrated winding technology. However, taking a closer look at the details, the picture is not that black or white. A distributed bar wound e-machine might lead to a better NVH behavior, and cooling a bar wound stator with oil is more effective than cooling a concentrated windings stator due to the shorter active length and the bigger end winding surface.

At this point prioritization of different aspects is needed. Understanding the customer's needs and the overall system design of the customer's product is essential to bring the prioritization to life. In this very example the result is based upon the assumption that efficiency, design space and cost are higher prioritized than NVH and the cooling concept (as seen in Figure 6). Base for this assumption is that

- The E-machine (as P1) is directly connected to the combustion engine which as a unit needs to be damped due to the vibrations of the combustion engine anyhow.
- A sufficient amount of oil for cooling the e-motor is provided via the rotor integrated clutches reducing the need for an additional oil cooling design.

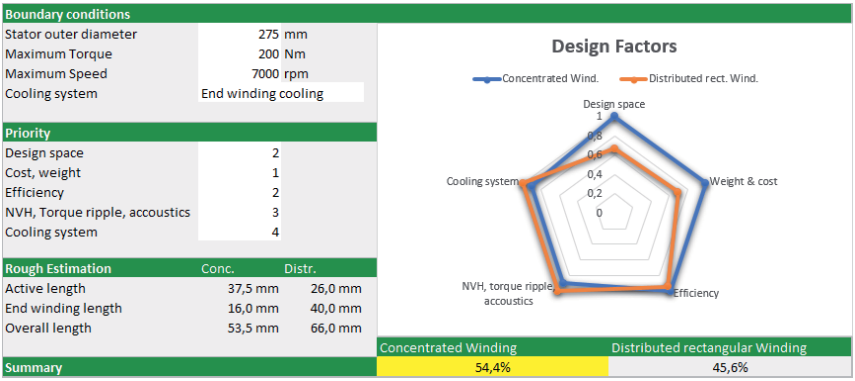

Fig. 6: Example of a high-level stator technology selection (P1 EM – DHT Generator)

But let us take a look at the second requested e-machine. Figure 7 shows the exemplary result of the high-level stator technology check for the requirements of the P3 machine.

In contrast to the results of the P1 E-machine, the picture is clearly advising to design the P3 E-machine based on distributed bar wound winding technology. Using that technology seems advantageous in each considered aspect. But still the picture is not as black or white as Figure 7 might suggest. Our exemplary high-level check does not consider, that our P1 E-machine has the exact same outer and inner diameter as well as maximum speed.

This is where scaleable component-based design kits are (re-)invented. To avoid the need of double investments for two e-motor production lines, scaling the P1 E-machine in axial direction appears tempting. Using such a component-based design kit will work out as long as the piece price (including the invest share per e-machine) and the technical solution of the axially scaled version is competitive (or better) than an e-machine developed without any scaling from existing designs.

However, experience shows that these cases are rare and further more the share of the additional invest needed for an optimized design decreases with the ever increasing production volumes of electric & hybrid cars.

Checking our rough design space estimation, the competitiveness of a scaled e-machine seems very unlikely. Although the amount of copper in the distributed winding e-machine will be higher than the one from the concentrated this cost effect is no proportion to the 23mm additional steel sheet and magnet length of the concentrated winding e-machine.

So, the logical decision is to offer two different technologies for these two e-machines to ensure the best cost and best technological solution.

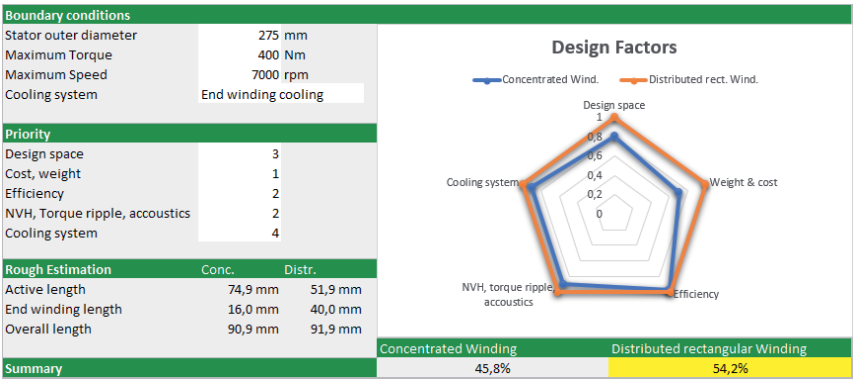

Fig. 7: Example of a high-level stator technology selection (P3 EM – DHT Traction motor)

The holistic approach – Step 2: Using design kit flexibility for USPs

The electromagnetic and CAD design process can begin once the basic technology concepts of the E-machines are defined. The specific design process depends on the workflows, processes and tools used, and is a complex topic on its own that shall not be discussed in this talk. However, the previously introduced technology and production kit has direct influences on the design process. These influences will be explained continuing the previous example.

The requirements of the P3 E-machine can be reached with different pole-pair, number of slot and wires per slot combinations. Which of these combinations is leading to the best fit solution relative to the full set of requirements is depending on the specific available winding and magnet arrangement technologies. Of course, different technologies lead to different advantages in the specific design. Consequently, one might think, that it would be beneficial to have as many different technologies available as possible. However, the actual number of technologies is not as important as the percentage of reachable designs based on the technology & production kit in comparison to the entirety of possible design solutions.

If several unique technologies are available that cover more or less the exact same design solution space, each of these technologies might have their own slight advantage either in price, efficiency or any other parameter for a certain specific application. But each of these technologies need to be maintained even if these specific applications are not requested and

thus these technologies are not used in any project. Consequently, being competitive in terms of available technology does not equal having many technologies in the portfolio but having just the right mix in the portfolio.

To illustrate this issue, Figure 8 shows an excerpt with three out of many possible distributed bar wound stator technologies. Each one of these three technologies could be used as a basis for our P3 E-Machine design.

Comparing the three technologies in Figure 8 to each other shows no relevant advantage in having Ipin technology in the portfolio when Hairpin technology is already available. This is because Hairpin technology includes some parts of Ipin technology for special wires. However e.g. we at Schaeffler have both Hairpin and Wave winding technology in our portfolio, as comparing Wave winding and Hairpin shows, that Wave winding provides the best cost solution under normal conditions whereas Hairpin has a slightly higher flexibility in design and therefore could be used as a fallback solution in case the resulting winding scheme would lead to a too complex wave winding design.

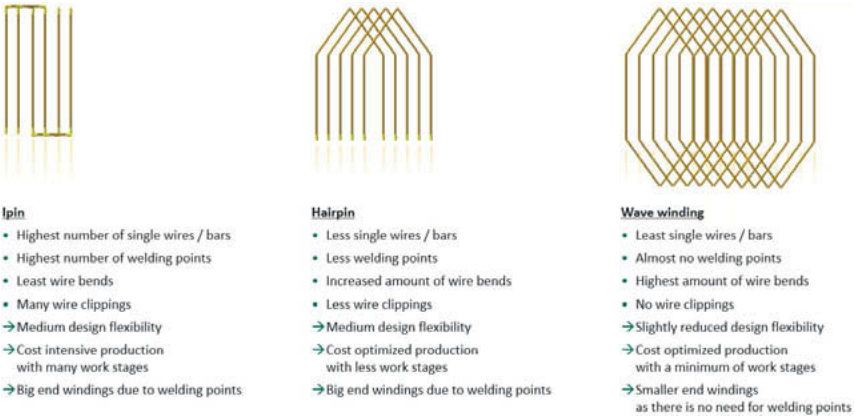

Fig. 8: Excerpt of possible stator bar wound winding technologies

Furthermore, the reachable solution space for wave winding stators and Hairpin stators is only partly overlapping. Figure 9 shows the strongly simplified overlapping solution spaces of Hairpin and Wave Winding Technology on a chart of Stator slots vs. stator outer diameter respectively Maximum available output power vs. stator outer diameter.

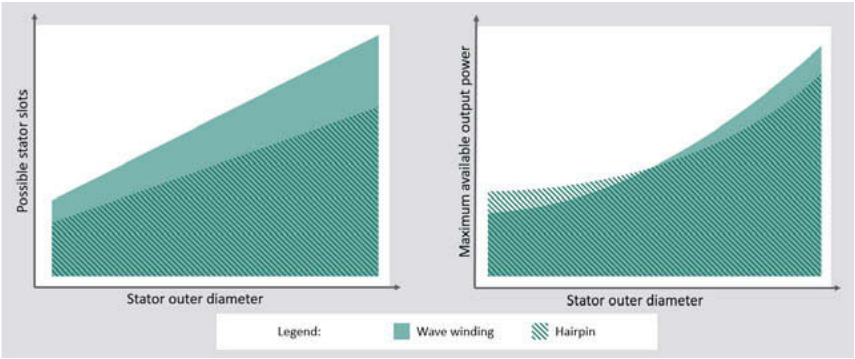

Fig. 9: Solution spaces of Hairpin and Wave winding over stator outer diameter

As seen in the map on the left of Figure 9, Wave winding technology opens up the possibility to design e-machine topologies with higher slot numbers than with Hairpin technology. This is due to the high number of needed welding points in Hairpin designs. To ensure the weldability of the ends of the Hairpins, a certain space between each welded pin is needed to have room for insertion of the welding tool. Therefore, when keeping a certain stator outer diameter, the maximum number of slots useable for a Hairpin stator design is limited, whereas stators designed with Wave winding technology does not have the same limit. Furthermore, each welding point is one additional work step in production and has a direct influence on the cost of the e-machine, increasing the wish to only design Hairpin stators with a small number of slots.

Anyhow, the chance to increase the number of slots in Wave winding stator designs enables to improve the wave form of the magnetic flux in the airgap and therefore to reduce additional loss produced by harmonics, as well as to reduce noise and vibration generated by the e-machine. Aside of these advantages, having the current density split to a higher number of slots leads to a higher surface area from copper to the iron lamination and therefore to a better heat dissipation, which again has a direct influence on the reachable power density of a Wave winding e-machine (see [2] as well).

The later effect explains as well, why the map on the right of Figure 9 shows a higher maximum power density of Wave winding designs at bigger stator outer diameters in comparison to Hairpin. In contrast to that, the map on the right shows as well, that Hairpin is (currently) at an advantage at lower stator outer diameters. This is due to the fact, that the output power of an electric machine is (via current and voltage) directly connected to the amount of copper

used in the stator windings. As the state of art Wave winding is inserted radially from the inside of the stator into the stator slots and the insertion of the winding needs a certain space for the windings itself as well as the insertion tool, the size of wire and therefore the maximum available output power is limited at a certain value. Hairpins in contrast are inserted in axial direction and do not have this constraint in the same strength. Thus said, this constraint is only relevant for small stator outer diameters as the power limit at higher diameters is not the space inside the stator, but the physical borders of iron saturation, magnet flux, copper current density and heat dissipation. Further the constraint is only based on the state of art wave winding technology.

Anyhow this constraint again shows the advantage of having both technologies, Hairpin and Wave winding in the technology and production design kit. Based on the very reasons above e.g. Schaeffler has both technologies in their portfolio.

Keeping the current technology perspective of Figure 8 and 9 and bringing it into line with our initial stator technology estimation for our P3 E-Machine in Figure 7 as well as with the customer requirements for that machine, the target should be to design the stator based on Wave winding technology.

The available design space with a possible stator outer diameter of up to 275mm is far above the size of those stators where the previously explained constraints regarding the needed size for radial wire insertion could occur. Therefore, using a Wave winding design enables us to not only reduce the size of the end windings (which is indeed needed to reach the customer design space requirements), but as well to improve in regard of heat dissipation in a oil cooling design and to reduce possible noise and vibration influences.

As stated above, this talk is not meant to dig deeper regarding the specific electromagnetic and CAD design processes. However, Schaeffler made very good experience in discussing the interim results with the customer in an agile and iterative, transparent manner during the design process. The more and regularly the customer is involved in the process, the better the possible advantages resulting from the emerging e-machine design can be incorporated into the system design and thus considered in the customer's development. From our perspective this is the best if not the only way to develop the perfect electric machine and thus the electrical powertrain.

The holistic approach – Step 3: Cost down via process selection & harmonization

The influence of the manufacturing processes should be considered in every development step.

Figure 10 shows a simplified overview of an e-machine value stream setup. Each of these steps shown has an influence on the e-machines price, both by the actual process cost as well as by the share on needed investments for the machinery and tooling. However, a not so obvious additional cost leverage results from the technical influences of the specific process on the mechanical, thermal or electromagnetic properties of the electric machine.
Looking at our E-machine designs, the selection of the lamination stamping process as well as stacking process for the stator and rotor of our e-machine has a direct influence on the magnetic properties of the iron sheet metal and therefore, on the e-machine's efficiency and then again on the heat that needs to be dissipated.
Consequently, it is not enough to choose a cheap production process to reduce production costs on this basis. Instead the various process results have to be iteratively transferred to our e-machine design process in order to achieve the most affordable overall design. This again is a vital part of the holistic design process.

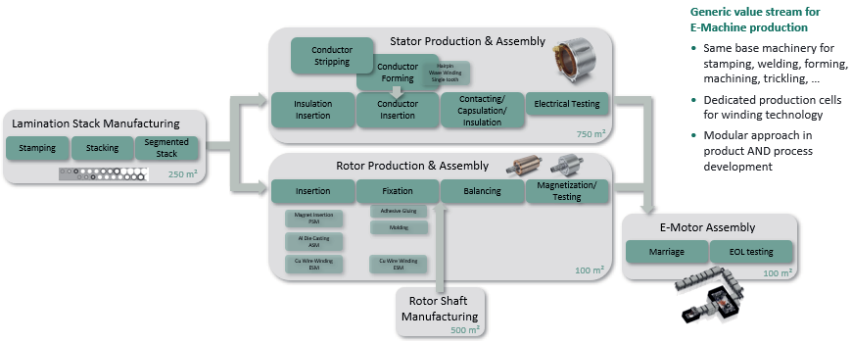

Fig. 10: Simplified overview of an e-machine value stream setup

As an example, if we assume, that we try to reduce the iron core losses in our P3 E-machine design and we assume that the initially considered lamination is a 0.3mm interlock stamped, one option would be to change the lamination material to a thinner one (e.g. 0.25mm). The effect will be that the eddy currents inside the lamination are reduced and therefore the overall e-machine's efficiency increased. However once looking at the actual lamination production, several aspects need to be considered. First of all, the lamination stacking factor (percentage of iron inside a stack) is reduced, as the resulting lamination stack has roughly 20% more transitions between the thinner sheets, which leads to a slightly reduced effect of the

thinner material. Second, the influence of stacking processes like interlock stamping or welding are bigger in a percentage comparison to the influence on the thicker material. Therefore, the advantage of the thinner and more expensive material will again be slightly reduced when using one of these processes. Consequently, a stacking process like baked enamel or glue lock could be used to avoid the effects of interlock or welding. However, of course this again comes with an additional cost. And once these processes are considered, it would be wise to double check the initial 0.3mm design with baked enamel / glue lock.

Please keep in mind this is just one aspect as there are several different types of 0.3mm or 0.25mm materials. And in the end the truth might still be in the middle, e.g. leading to a 0.27mm thick sheet metal.

Coming pack to the holistic approach, the target should not be to minimize the cost of the E-machine in the boundaries of the given requirements, but to find the best cost solution in the overall system of the customer. Customer contact is vital especially if specific features of the design lead to a simplification or requirement reduction, which might have an influence on the customer's design.

As a final example in this talk, fixing the magnets of our P1 e-machine with a small amount of glue is a cost optimized assembly process. The downside of this process is, that the heat generated by the magnet losses cannot be ideally dissipated. If this leads to a performance reduction in the overall system design, one option would be to optimize the active oil cooling system to ensure wetting of the axial surfaces of the rotor with oil, whereas another option would be to use transfer molding as process for fixing the magnets. Using this process will lead to an improved heat dissipation from the magnets to the lamination and finally to the shaft.

This issue is more relevant for the P1 E-Machine, as the air gap flux of concentrated windings typically lead to higher eddy currents inside the magnets than in designs with distributed windings. However, as our example project comprises both e-machines, if transfer molding is selected for the P3 E-Machine, it should be explicitly considered to use it for the P3 E-Machine as well. Depending on the actual production volume per year and volume over lifetime, the additional process and material cost for transfer molding might be smaller than the additional investment for a magnet glue assembly. And speaking of the holistic design, if other projects are planned or already running at the same location, the processes used there should be considered as well and wise versa.

Summary

In this talk the advantages of a holistic design process based on a technology and production tool kit for E-Machines with a positive influence on fast concept decisions, design flexibility, and interdisciplinary as well as interproject connections has been discussed.

As stated, the technology and production tool kit offers higher flexibility in contrast to classical component based e-machine design kits and leads to a better cost performance in most cases. This applies even more with increasing production volumes of battery electric as well as hybrid vehicles and therefore with increasing e-machine production volumes.

Bibliography

[1] Englisch, A., Pfund, T.: Schaeffler E-Mobility - With Creativity and System Competence in the Field of Endless Opportunities, Schaeffler Symposium 2018 Documentation, Schaeffler Technologies AG & Co. KG, Herzogenaurach 2018

[2] Müller, B., Angrick, C., Fritz, M.: New concepts for electrical drive trains for high power density, Dritev, International VDI Congress EDrive, 2 - VDI-Berichte / 2019, Bonn 2019

Performance study of a PMSM with molded stator and composite housing

With internal slot cooling – resulting in high continuous power

M. Sc. **S. Reuter**, Fraunhofer ICT, Karlsruhe;
H. De Keyser, SBHPP, Vyncolit NV, Gent;
Prof. **M. Doppelbauer**, KIT, Karlsruhe

Zusammenfassung

Vorgestellt wird ein neuartiger Ansatz einer permanent erregten Synchronmaschine mit konzentrierter, hochkant-Flachdrahtwicklung. Durch Umspritzen mit einem hochwärmeleitfähigen, gefülltem Expoidharz werden Kühlkanäle in den Statornuten erzeugt. Dadurch muss kein wärmeleitfähiges Material für das Gehäuse zur Kühlung verwendet werden, sondern es kann ein Gehäuse aus Faserverstärktem Phenolharz verwendet werden. Simulationen und Messungen auf dem Prüfstand zeigen die Leistungsfähigkeit des Konzepts.

Abstract

Introduction of a permanent magnet synchronous machine (PMSM) with concentrated, upright flat wire windings. During over molding with a filled, high thermal conductive epoxy compound, cooling channels are created in the stator slots. This enables the use of a fiber filled phenolic resin for the housing, instead of a thermal conductive metallic housing, necessary for a cooling sleeve. Simulations and experiments on the testbench proof the performance of the concept.

1. Design of the internal slot cooled motor

The motor was developed in the project “DEmiL”, a cooperate research project between the Fraunhofer Institute for Chemical Technology (ICT) and the Karlsruhe Institute of Technology (KIT), founded by the Vector Stiftung. The concept is based on the work of Dr. M. Schiefer [1]. A machine design with single teeth and concentrated windings that can have the same slot

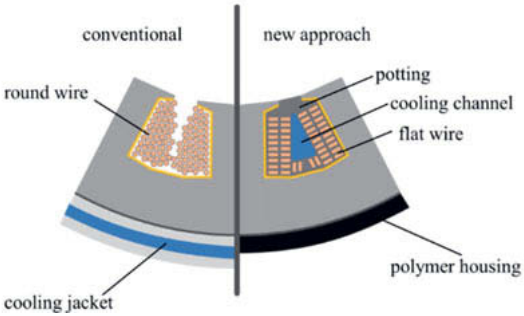

Fig. 1: Comparison - conventional and DEmiL approach

fill ratio as round wire, but with additional space for a cooling channel, as seen in Fig. 1. The aim in the DEmiL project was to use mainly manufacturing processes that are high volume capable and to adopt the 2D cooling idea into a 3D feasible concept. The key manufacturing process for the use of high thermal conductive materials from Sumitomo Bakelite Co.,Ltd. (SB) is transfer molding.

Transfer molding is typically used for thermoset materials. It is a further development of compression molding allowing more complex shapes to mold and is easier to automate and very well suited for high volume production of automotive EV/HEV powertrain applications. It is comparable with an injection molding process.

The composite material, preformed as a pellet and preheated, is placed in the transfer cylinder and then pressure is applied to the ram(piston), causing the composite material to flow through the transfer gate to the mold cavity. Excess charge (typical name is “cull”) is used to allow a hold pressure to be applied to the mold cavity and to accommodate sample shrinkage during cure. The pressure is maintained during cure and released when material is solidified.

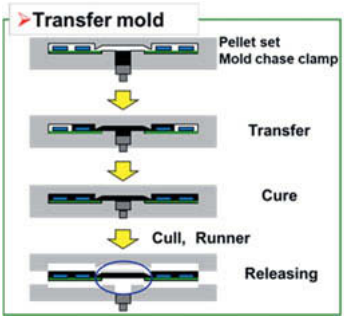

Fig. 2: Transfer molding of chip packaging systems

Typical SB composite materials are epoxy molding encapsulation (EME) compounds used in integrated chip packaging (bare die), ECU & TCU encapsulation and magnet fixation for IPM eMotors. Other SB Thermoset composite materials like SB Phenolic molding compounds for structural applications are used for transfer molding. This process is well described by Fig. 2.


Fig. 3: Screw pre-plastification unit [2]

Transfer molding requires four key equipment: a preheater, a press, the die mold, and a postcure oven. The preheater is used for preheating the preform or pellet to a defined temperature. This to allow a smooth flow of the composite material and to reduce the cycle time. Preheating can be done by high frequency (HF) or by pre-plastification, seen in Fig. 3. Screw pre-plastification is very well suited for automated high-volume production and gives flexibility in changing the pellet size.

The transfer molding press is hydraulically operated and equipped with an auxiliary ram (piston) that is tightly controlled in pressure, speed, course and time. This allows for smooth and controlled (pressure, speed, dosing) filling of the mold cavities with sensitive electronic inserts (PCB, chips, capacitors, ect..).

The mold has a built-in transfer pot separate from the mold cavities as shown in Fig. 4. The mold can either be equipped with multiple small transfer pots (A) or with one single transfer pot (B).

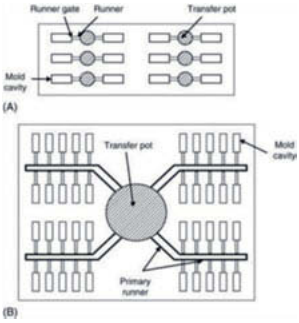

Fig. 4: Different types of transfer pots

The Stator consists of 12 single teeth with concentrated, upright, flat wire. A phase connector ring, with the three phases and the neutral connector ring is attached on top of the teeth. The windings are welded to the connector rings. For the prototype phase this can be done via a TIG-welding machine. For serial production laser welding could be suitable. Fig. 5 shows the assembled stator held together with a hose clamp. The assembled stator is over molded at the SB Openlab facility, Fig. 6, with Sumikon A730E. This is a filled epoxy with up to 91% of spherical silicon oxide. This material has a very low viscosity during injection to fill very small gaps even with low mold pressure. To avoid filtration of the fillers, the silicon oxide spheres have a maximum diameter of 75 micrometer.


Fig. 5: Assembled stator


Fig. 6: SB Openlab facility

Fig. 7 shows the over molded stator. Only the phase connections and three connectors for temperature sensors are not over molded. The polished tool surface is transferred onto the part, with no cavities visible. This allows for O-rings to directly seal to this surface. On the outside, the grooves for the torque transfer are visible.

Fig. 7: Over molded stator

To form the cooling channels no additional parts are needed. In the mold are twelve cores that directly form the cooling channels in the material. These cores must be able to demold in a single direction so no undercuts are possible. To distribute the cooling fluid a simple loop flow pattern was chosen and can be seen in Fig. 8. The fluid travels in six channels through the stator to the other side, is redirected and travels in the other six cooling channels back again, so that the in- and outlet of the cooling fluid is on the same side of the motor. The distribution to the cooling channels is done with two ring channels. To get an equal flow in all cooling channels, the connections are formed slightly different. Fig. 9 shows the minimum and maximum cross section. To decrease the overall pressure drop the cross sections of the ring tubes are increased by making them oval, expanding them more axial than the radial space would allow for a round channel.

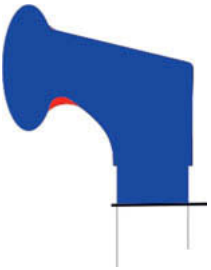

Fig. 9: Cross section and difference of the inlets

Fig. 8: Cooling medium

The housing is manufactured via injection molding with Vyncolit® X7530 / Vyncolit ®X7700. The material needs to be water/glycol resistant and has to withstand high temperatures for long durations. Via sandblasting the part gets deburred and the bearing seats are directly machined out of the material. The finished housing can be seen in Fig. 10.

Fig. 10: Injection molded and machined housing

Stator and housing are then assembled by simply sliding them into each other. The ribs on the inside of the housing, slide into the corresponding grooves on the outside of the over molded stator and create a positive locking feature for the torque transfer. The assembly is seen in the cutaway Fig. 11. The centering of the housing to the stator is created on the inner diameter of the over molded stator. Both surfaces do not need machining due to the low shrinkage of the material and the relatively low young's module compared to aluminum, which leads to much lower stress in the material for a given deformation. The bearing seat is directly machined into the housing. This is possible, because high performance thermoset materials have a high resistance to creep, thus the bearing seat does not relax over time. The bearing seat is connected to the centering surface with a massive ring of material, to create the stiffest bearing seat possible.

To help demold the stator a demolding incline on the outside of the stator of 1° was created. To further more help with demolding the housing, a demolding incline of 2° was created. This leads to an increase in wall thickness towards the bearing shield and helps with the stresses introduced by the stators torque.

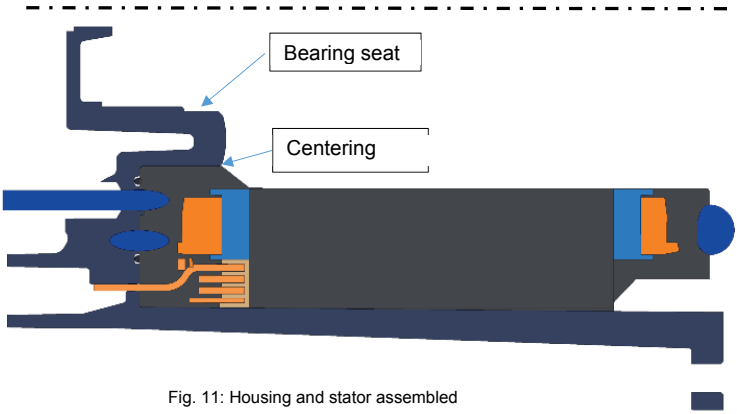

Fig. 11: Housing and stator assembled

The ring-channels for the cooling fluid are sealed via an O-ring to the inner diameter as well as to the outer diameter. This guarantees a proven and reliable seal to the phase connectors as well as to the rotor gap. To seal the two ring-channels against each other only a small step is used. Leakage that occurs between the ring-channels only decreases the effectiveness of the cooling, but does not leak into the environment. Fig. 12 shows the cross section on the real prototype, no O-rings are installed yet.

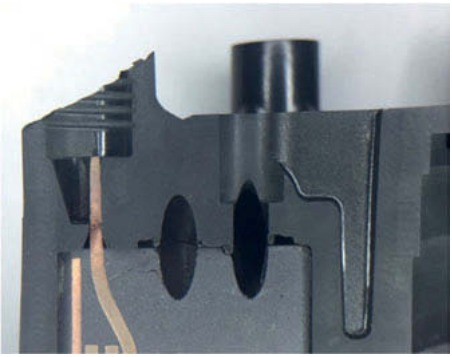

Fig. 12: Sealing of the cooling channels and between

The rotor cooling is shown in Fig. 13. A water lance is bonded to the housing. The cooling fluid is pumped into the hollow lance with the encoder at the end. At the end of the lance are small radial holes where the cooling fluid exits into the hollow rotor shaft. The fluid travels back inside the hollow rotor shaft until it exits at the end and leaves the motor in an outlet, not visible in this cross section. To seal the rotor gap, a single Turcon Varilip radial shaft seal is used. The sealing lip is made from filled PTFE and capable to seal up to 40 m/s surface speed. The surface speed of the sealing surface is at 17 000 rpm just under 30 m/s.

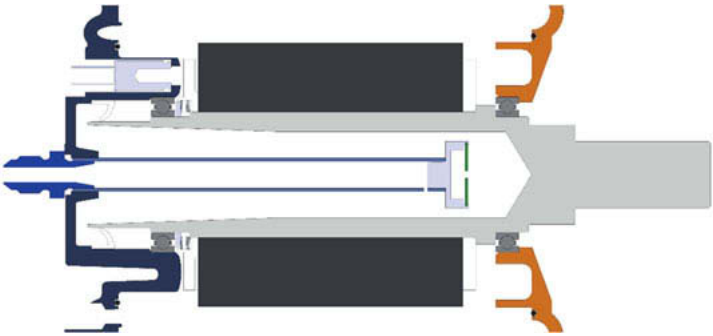

Fig. 13: Rotor cooling

To measure the rotor temperature directly a pyrometer is directed at the balancing disk. The rotor is supported by two ball bearings, one axial preloaded with a wave spring to increase running precision and allow high thermal expansion of the shaft.

The magnets are dived axial in 10 pieces to reduce losses. For the prototype production, they can simply be glued into place. However for a serial production, a different approach would be sutiable.

A recent transfer molding application is rotor magnet fixation for IPM e-Machines. Transfer molding with SB EME material is used in fully automated high-volume production for single stack and multi-stack magnet fixation.

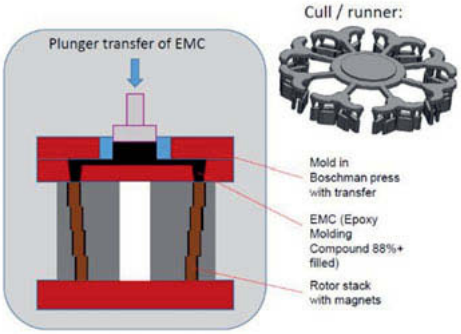

Fig. 14: Magnet fixation for serial production [3]

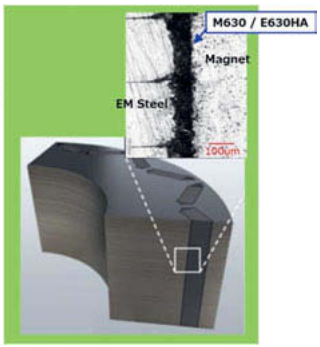

Fig. 15: Magnet fixation [3]

This application is already in serial production in Asia for several years. In Europe first start of productions are planned for beginning of 2021.

One OEM has studied all current technologies for magnet fixation and concluded that the SB Material technology with transfer molding is outperforming all existing magnet fixation technologies both in functional performances as economically.

2. *Benefits and challenges of the slot cooling*

The distribution of the losses of the designed machine at peak power are plotted in Fig. 16. The vast majority of losses occur in the windings. With the new concept the thermal path from the windings to the cooling fluid is shorter than a state-of-the-art cooling sleeve.

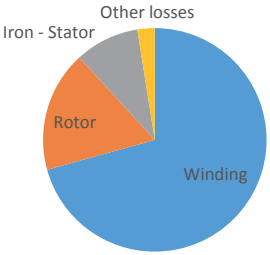

Fig. 16: Simulated losses at peak power

To better understand how much the concept improves cooling, the cross section of the motor is analyzed with a FEM tool. The model used for the simulation is shown in Fig. 17 and the thermal material properties in Table 1. The losses were simulated in a different electromagnetic simulation [4] and serve as input values for the thermal simulation. Due to the current displacement the distribution for every wire is very inhomogeneous, with the highest losses in the layer 1 and layer 2, wire 10. This is also represented in the results, Fig. 18, that show the temperature distribution for a working point outside the continuous operational area. The heat distribution in the coil is very inhomogeneous. This is due to the low thermal conductivity between the copper wires. [5]

Table 1: Thermal conductivity

Material	λ W m^{-1}K^{-1}
Isolation paper	0.115
Molding material	3.0
Copper isolation	0.22
Bonding varnish	0.5
Laminated iron	21.56
Copper	358

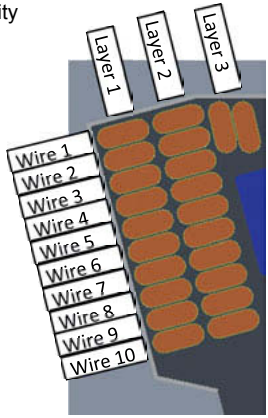

Fig. 17: Cross section of the simulated model

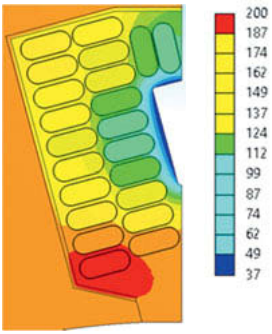

Fig. 18: Temperature distribution [°C]

To determine the effectiveness of the slot cooling and the high thermal conductive material, a simple parameter variation was set up. This simulates 50 Nm of torque for given speeds and outputs the highest occurring winding temperature delta to cooling fluid. The results are illustrated in Fig. 19. With higher speed of the machine the current deflection increases, which causes additional losses in the windings. Remarkable is the small difference between the slot cooling and a cooling sleeve with a low thermal conductive molding compound of 0.69 W $m^{-1}K^{-1}$. The small cooling channel area is not capable to detract enough thermal energy to benefit from the shorter thermal path. Comparing the cooling sleeve with the low thermal conductive molding compound to Sumikon A730E with a higher one of 3 W $m^{-1}K^{-1}$ the cooling performance is significantly better. The slot cooling with the high thermal conductive material is the best simulated concept, this is the concept used for this motor. [5]

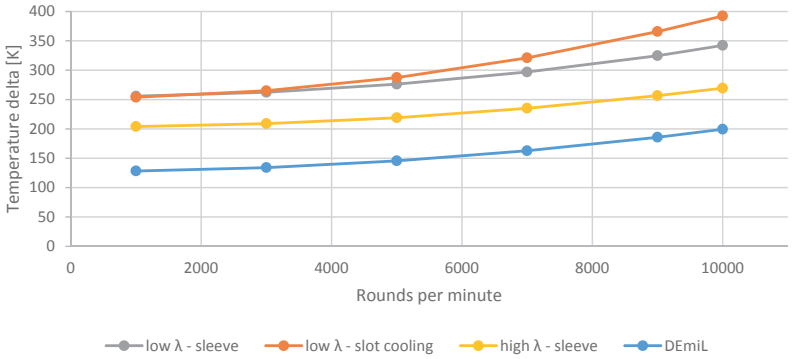

Fig. 19: Cooling performance for different concepts

3. *Prototype production and test setup*

To measure the critical winding temperature three PT100 (DIN EN 60751) sensors are used. The position can be seen in Fig. 20, they are fixated with Loctite EA 9497, a structural heat conductive epoxy glue, to keep them in position during over molding. The adhesive has a thermal conductivity of 1.4 W $m^{-1}K^{-1}$. One sensor is attached close to the winding head on the layer 1, wire 10, that makes the transition to layer 2, wire 1(L1W10/L2W1), please refer also to Fig. 17. The second sensor is attached to the wire closest to the rotor gap also on layer 1, wire 10 (L1W10). This is the hottest wire corresponding to the simulation. The third sensor is attached to the winding close to the phase connection ring, it is attached between

the two layer 3 wires (L3W1/L3W2). This area is possibly critical due to the long distance to a cooling channel.

Fig. 20: Placement of the temperature sensors prior to gluing

The rotor temperature is measured via an infrared MLX90616 temperature sensor from Melexis. This sensor is pointing directly towards the balancing plate of the rotor.

4. Design verification

To validate the motor, the first one of the built prototypes was carefully examined. The coils are semi-automated handmade and show a corresponding tolerance distribution. In Fig. 21 three illustrative cases are shown. On the left the worst case, with a bigger than designed distance between the layers is shown. In the middle the designed case is shown. The wires are very close to each other. On the last picture the best case is shown in respective to package size. The examined motors mostly had the designed case windings, however for the exact test specimen there is no data available, because this can only be examined by cutting the stator open. Noticeable is how every gap is filled with the Sumikon A730E material, with no pores or cavities visible. Even small gaps between the windings are filled, as can be seen in the worst case, Fig. 21 on the left. The cross section was also measured under the microscope, revealing the thickness of the copper isolation of 0.04 mm, for the used rectangular wire of 2.5 mm by 1.0 mm.

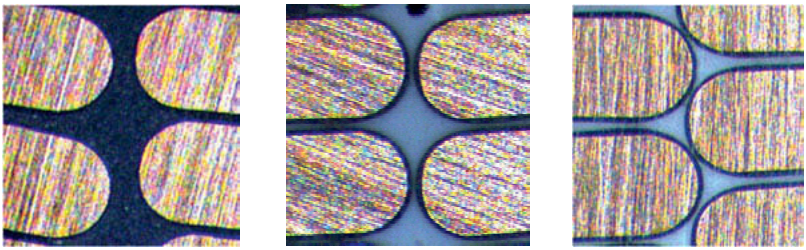

Fig. 21: Cross section of the windings

To validate the fluid distribution in the six parallel cooling channels, a special bearing shield is used, see Fig. 22. The flow of each of the channels is directed out of the motor, measured by a total of six IFM vortex sv3050 sensors and then redirected into the motor again, flowing through the remaining six channels to the motor outlet.

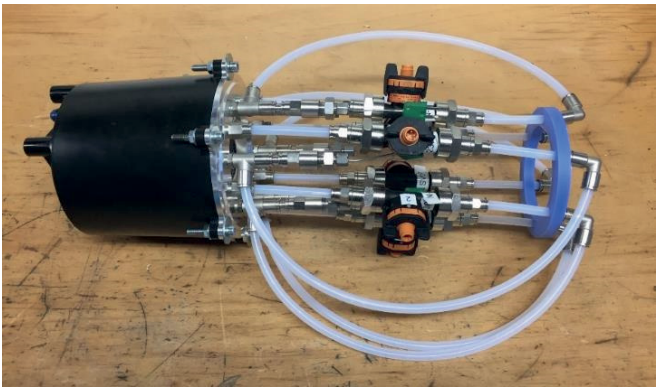

Fig. 22: Motor with measuring bearing shield

In Fig. 23 are the measured results for the flow through every of the six cooling channels in parallel. The volume flow appears to be consistent even with variations of the total fluid flow.

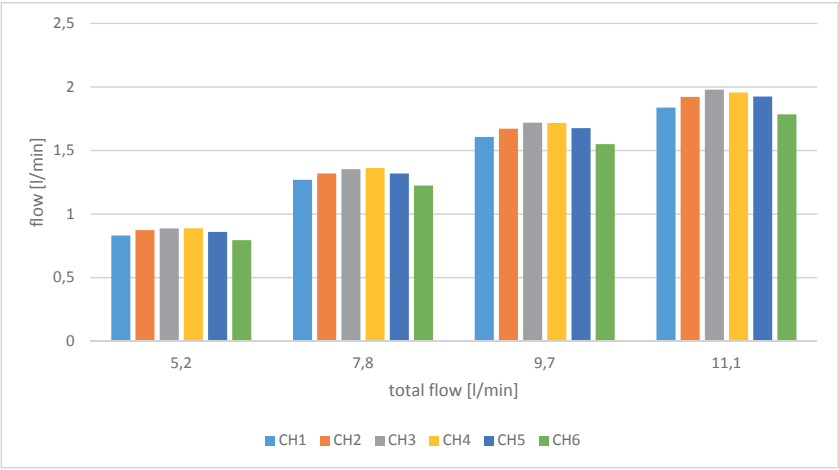

Fig. 23: Flow distribution

5. Testbench

In Fig. 24 the testbench setup can be seen, the motor is not yet connected to the cooling system. The unit under test and the load machine are coupled via a torque measuring shaft to calculate the transmitted mechanical power.

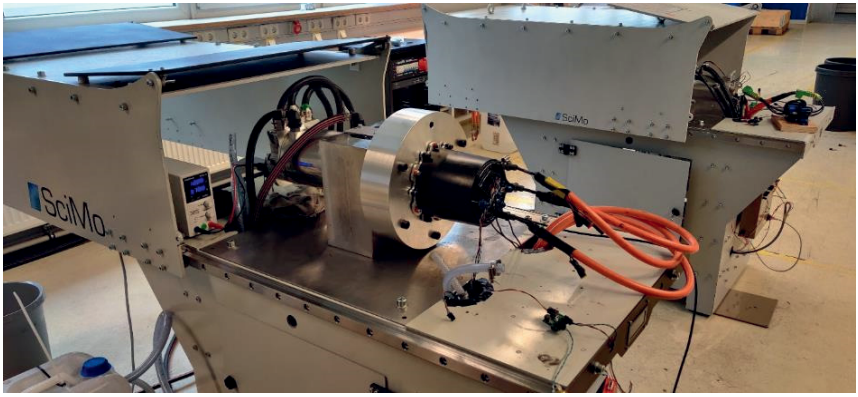

Fig. 24: Testbench

The cooling system is split into two circuits, with a common compensation tank. Each circuit has its own adjustable pump. The stator cooling circuit contains a plate heat exchanger to dissipate the waste heat into a big stationary cooling system.

The flowrate of the stator cooling circuit was set to 6.5 liters per minute, the rotor cooling circuit was set to 1.3 liters per minute. The pressure drop of the stator circuit was measured with a digital pressure gauge at 210 mbar. For the test, only plain tap water was used. This will result in slightly better cooling measurements due to the higher thermal capacity of plain water, compared to water glycol mixtures that are commonly used to avoid oxidation.

In Fig. 25 the measured efficiency map of the motor can be seen. The blue line shows the maximum continuous load measured. Noticeable is the high continuous power compared to the peak power of the motor at 9 000 rpm and 60 Nm, resulting in 56 kW of power. The peak power limit is the inverter with a rating of 310 amperes maximum. Continuous Power is at 9 000 rpm and 50 Nm, resulting in 48 kW of mechanical power. With the complete motor weighing 10.5 kg this makes a continous power density of 4.5 kW kg^{-1}. The temperature of the L1W10/L2W1 sensor did not exceed 115 °C, with a cooling fluid temperature between 30 °C and 35 °C over the 30 minute test routine.

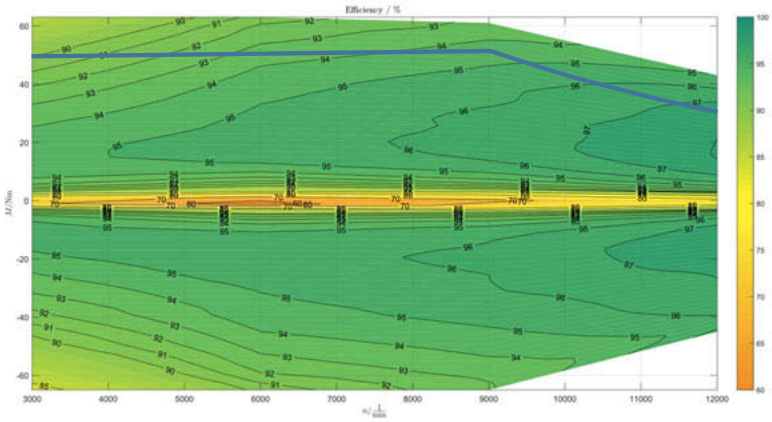

Fig. 25: Measured efficiency map

In Fig. 26 the temperature for the stator during a step in the output power is plotted. The motor rotates at 9 000 rpm. The temperature of the L1W10 sensor increases with the steepest temperature curve, resulting in the highest temperature of the three sensors. The sensor on the L1W10/L2W1 measures a similar increase in temperature. This spot does not get as hot, because of the much lower losses in the winding head and because the wire scheme is that the next position after layer 1, wire 10 is layer 2, wire 1. This is a wire much further away from the

rotor gap, thus exposed to less current deflection that leads to fewer losses. The coolest temperature sensor is the L3W1/L3W2. This shows that the most critical area for overheating is in the stator slots, not the winding head.

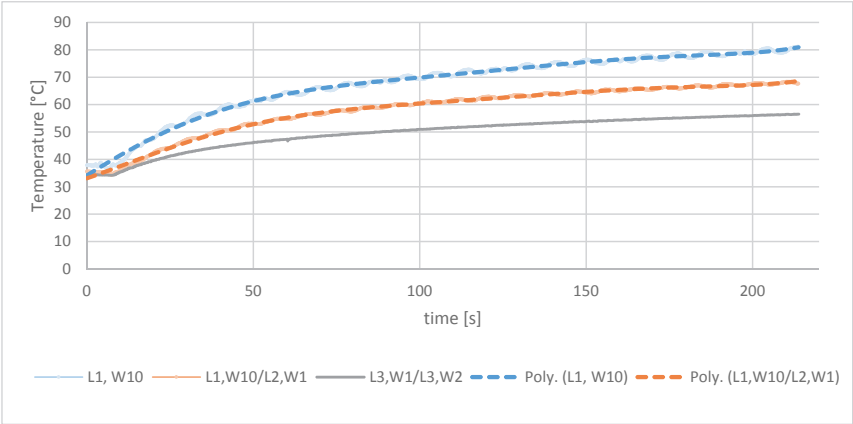

Fig. 26: Temperature evolving during step up in output power

The temperature sensors on L1W10 and L1W10/L2W1 are directly connected to the inverter and measured with a frequency of 25k Hz. Because the signal is quite noisy, a polynomial fit was added to better visualize the measured effect. The temperature sensor L3W1/L3W2 is read with a separate board and with a much lower frequency transmitted to the data recorder via CAN bus.

6. Conclusion

The application of an internal slot cooling together with molding technology demands design changes in every aspect of an electric motor. The simple substitution of plastic materials for the housing and a completely over molded stator generate a lot of disadvantages over metallic materials and tool free impregnation. But a purpose designed motor is superior in function integration, assembly complexity and continuous power output. The internal slot cooling improves the continuous power output to nearly the peak power output. The ability to use injection moldable material makes complex parts with low per part prices possible and enables new possibilities of function integration to save weight, assembly complexity and part counts. The high continuous power density means that compared to a more traditional motor with the same output power, the new motor is lighter and smaller and thus needs less copper, less iron and less magnets.

[1] M. Schiefer: Indirekte Wicklungskühlung von hochausgenutzter permanenterregter Synchronmaschinen mit Zahnspulenwicklung. Dissertation. Karlsruhe 2017

[2] Screw pre-plastification unit, Relase, boyke-tec.de, Germany

[3] Magnet fixation, Relase, Boschman.nl, Netherlands

[4] A. Langheck, S.Reuter, O. Saburow, R. Maertens, F. Wittemann, L-F. Berg, M. Doppelbauer: Evaluation of an Integral Injection Molded Housing for High Power Density Synchronous Machines with Concentrated Single-Tooth Winding. Paper, EDPC 2018

[5] S. Suppanz: Designverifikation eines hochausgenutzten Elektromotors mit innenliegender Kühlung und duroplastischem Leichtbaugehäuse. Master thesis. Karlsruhe 2019

CeDrive – Electric Drive Technology for a new era

Advanced Cooling and control of high-speed eDrive

Sean Worrall, **John Foulsham**, **Ian Stone**,
GKN Innovation Centre, Abingdon, UK;
Theodor Gassmann, GKN Automotive, R&D Centre Lohmar

Zusammenfassung

Das Projekt **ACeDrive** steht für “Advanced Cooling and control of high-speed eDrive” und wird von der Englischen Regierung gefördert. GKN Automotive leitet das Projekt, mit DSD und der University of Nottingham als Partner.

Ziel des Entwicklungsprojektes ist es, ein fortschrittlichen Technologiebaukasten für zukünftige Elektroantriebe zu entwickeln um deren Dauerleistung und den Wirkungsgrad deutlich zu verbessern. Durch den Einsatz von SiC-MOSFETS in Verbindung mit variable Schaltfrequenz und anspruchsvoller Ansteuerung des hochdrehenden Motors sowie ausgeklügelter Technologie zur verbesserten Kühlung sowohl des Elektromotors als auch der MOSFET-Leistungsschalter kann die Leistungsdichte im Dauerbetrieb gegenüber existieren Elektroantrieben nahezu verdoppelt werden. Gleichzeitig wird durch ACeDrive-Technolgie einen um 10% besseren Systemwirkungsgrad im WLTP Fahrzyklus ermöglichen. Der Artikel beschreibt den Zwischenstand des Projektes, das Ende 2018 begonnen hat und Mitte nächsten Jahres mit einem Fahrzeugdemonstrator abgeschlossen wird.

Abstract

ACeDrive stands for “Advanced Cooling and control of high-speed eDrive”. It is a UK funded project led by GKN with DSD and the University of Nottingham as partners. ACeDrive will develop and prove the technology building blocks that will enable cost effective, ground-breaking power density and cycle efficiency of future electric drive units. The project started in April 2018 with the results to be demonstrated in a vehicle in summer 2021. Key features to achieve

the cutting-edge power density and efficiency are the advanced cooling of the high-speed motor and the SiC power modules combined with variable switching frequency and sophisticated control software. Advanced simulation tools and extensive experimental testing have been used to design and validate EDU component design and system layout.

This paper gives an overview of the project and interim results.

Motivation

Electrification has taken off, sales numbers of EVs are increasing and all major OEM are bringing electric vehicles to the market. With the increasing volume requirements for electric drive units (E.D.U.) it is getting tougher to deliver more power and better cycle efficiency at lower cost. Volume forecast are indicating that the largest EDU. segment will be in the 100-200kW power range. Whilst 1st generation of E.D.U.s have been developed for peak power and best sweet spot efficiency, now the focus has moved more to continuous power and system efficiency in the driving cycle. This comes with the desire for smaller, more compact designs (increased power density) and to reduce the use of the expensive material (copper/rare earth materials) to keep cost under control. A more enhanced EM characteristic is desired to match vehicle launch performance and max vehicle speed requirement without use of complex multi speed transmissions.

To address all these new challenges GKN started the project ACeDrive, presented in this paper, with the goal to develop advanced technology building blocks for easy use in future applications and prove system performance on bench and in a demonstrator vehicle.

ACeDrive is a UK funded project led by GKN with Drive System Design (D.S.D.) and the University of Nottingham (UoN) as partners. It started end 2018 and will be finished summer 2021.

Overall project target for the complete EDU. system has been set as:

- 25% reduction in size and weight
- 10% increase in WLTP cycle efficiency

with no cost penalty compared to a state-of-the-art EDU. with same output torque and continuous power. With the set project goals for continuous power density and cycle efficiency ACeDrive is supposed to deliver APC. UK road map targets for 2030 years in advance.

To address the biggest market segment for future XEV the EDU. system is supposed to deliver the vehicle acceleration and max speed of C-segment cars fitted with a 2 l TDi I.C.E.

Concept Definition

1st step of the project was to define the specific system performance requirements and to derive the basic components requirements and layouts. This work-package has been led by D.S.D., who have enhanced and applied their “System optimisation process” (Fig. 1) to define in a wholistic approach the:

- Gearbox type and layout, number of gears & transmission ratio
- Motor type and layout, peak and nominal torque, max speed
- Inverter requirements

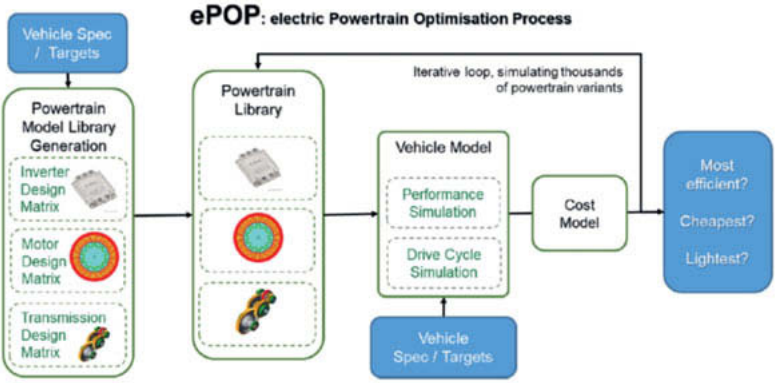

Fig. 1: DSD Electric Drive system optimisation process

Considering the given project, vehicle performance and cost targets following basic component specifications have been defined:

- Permanent Magnet assisted Synchronous Reluctance Machine (PMaSRM)
- Inverter 800V, SiC MOSFETS; variable switching frequency
- Enhanced gearbox lubrication and EM cooling
- Gearbox: Single ratio (R 14:1), 2-step, helical gears, offset design

A more detailed description of the DSD ePOP tool and process can be found in [1].

Electric Motor Design

Vehicle simulation has been used to define the Electric Motor (E.M.) basic specification as:

- Maximum speed: 21.000 rpm
- Peak Torque 280 Nm @ 5.000rpm
- Peak Power 140kW
- Continuous Power 100 kW
- Torque ripple: < 4% @ max torque
- kVA: < 200

Number of poles (Tab.1), type of winding and key dimensions of the e-machine have been defined using GKN and UoN inhouse optimisation tools and state of the art simulation. Models and tools have been verified using comprehensive benchmark testing of production motors.

Tab. 1: Comparison of various number of poles

	4-pole	**6-pole**	**8-pole**
J_{slot} [A/mm^2]	22,8	18,6	21,4
kVA	179	176	250
Iron weight	102%	100%	103%
Copper weight	105%	100%	85%
Magnet weight	97%	100%	71%
Overall Rating	J_{slot} high	Selected	kVA too high

A common approach for initial motor designs is to use the tip speed of the rotor to limit the rotor stress. But this is not accurate enough for more sophisticated lamination designs and magnet arrangements of such a high-speed motor.

Key challenge for the lamination design of high-speed motors is to manage stress and flux at the same time. Bigger ribs reduce the stress but allow more flux leakage reducing torque and affecting torque ripple.

Hyperstudy in combination with SimLab and Optistruct has been applied to run an automated optimisation of the lamination design. The max principal stress for the 3 load cases ½ max speed, 1x max speed, 1.2x max speed has been used as criteria to define the best lamination and magnet design (see Fig.2 left).

Flux- SW has then been applied to simulate the EM performance in terms of torque and torque ripple at max torque at base (5krpm) and top (21krpm) speed (see Fig. 2 right).

A unique fatigue calculator has been developed inhouse to calculate, based on the estimated stress values, the damage to the rotor through a real -world drive cycle reflecting 240.000 km.

As a result of the advanced optimisation process the final design provides a much better stress distribution, with the ribs sharing the load more equally and each individual rib loaded mostly in tension avoiding unnecessary bending and stress concentrations in the rib corners. This was achieved whilst keeping the peak stress within limits and still maintaining the torque and torque ripple.

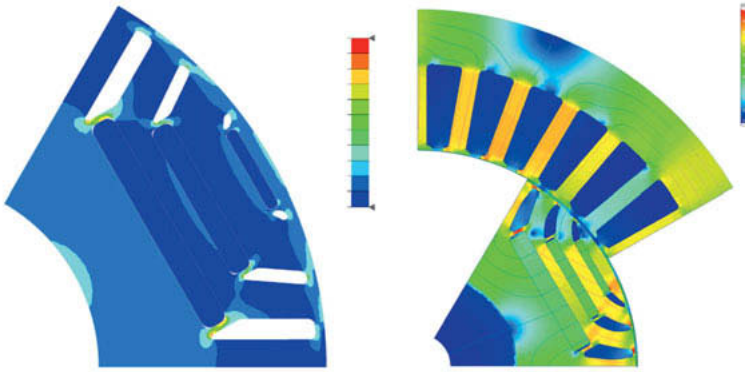

Fig. 2: Examples of stress (left) and flux (right) simulation to optimise the Rotor design

Alongside the Hyperstudy tool for flux and stress optimisation MotorCAD has been applied to define the optimum winding patterns, phase advance and skew-angle for best torque and lowest ripple. Significant reduction of the torque ripple has been achieved through an optimised short pitched winding pattern.

Electric Motor Cooling

The continuous power of an EM is strongly related to the efficiency of the cooling system.

Continuous power of state-of-the-art EM with water jacket cooling is often less than half of the rated peak power.

Target for ACeDrive was to be able to deliver 100kW continuously which is 70% of the peak power, and this even at lowest battery voltage. This can only be achieved with enhanced cooling techniques for stator and rotor. Advanced Thermal Modelling has been used to define cooling requirements represented by the Heat Transfer Coefficient (H.T.C.) in the critical areas of the motor. Comprehensive tests have been performed on an experimental motor (cross section shown in Fig. 3) to verify the thermal model and confirm the results.

The experimental motor provides various cooling features to be tested individually or in combinations such as:

- Water jacket
- Oil lance in the rotor
- Oil jet impingement outside of winding head
- Oil spray cooling facing winding head

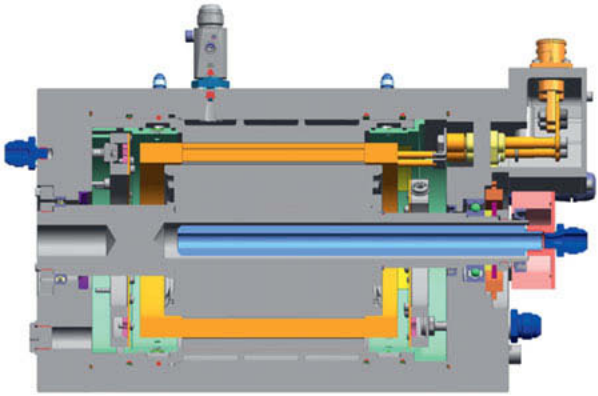

Fig. 3: experimental Motor for cooling concept investigation and model verification

Fig. 4 shows the measured continuous power for various cooling configurations.

Cooling the stator with a water jacket is used in most of the electric motors on the market today. A slight improvement in continuous power can be achieved by cooling the rotor with oil (oil lance).

Jet impingement cooling of the winding heads provides a significant step up, but the tests confirmed that spray cooling is required to achieve the 100kW target.

Both, jet and spray cooling show a strong effect of the used hydraulic power (oil pressure and flow rate) reflected by the 10 W and 80 W column.

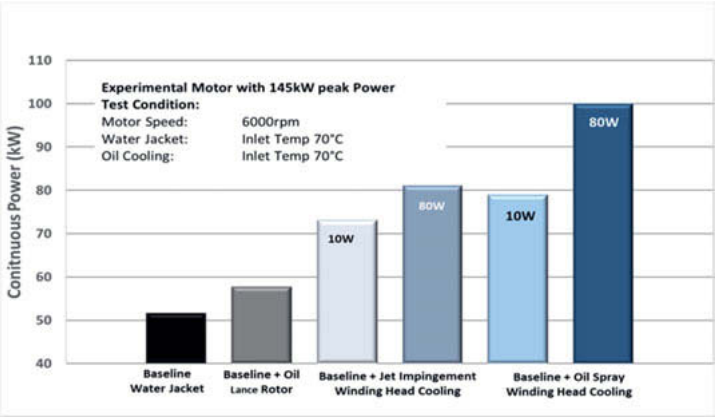

Fig. 4: Effect of tested cooling concepts on achieved continuous power

Tests have confirmed what was indicated by the simulation: Spray cooling with roughly 80W hydraulic power is required to meet the 100kW continuous power target.

Spray nozzles are readily available on the market, however none provided the cooling effect we required. The challenge was to achieve a spray cooling system design that achieved the required cooling with minimal hydraulic power whilst being robust, mass production feasible and low-cost.

Fig. 5 shows on the right the basic concept of a spray nozzle and on the left a snap shot of a spray test in the experimental single nozzle spray test set up used for nozzle design optimisation.

Fig. 5: Experimental setup for Nozzle Tests and basic nozzle concept

Various nozzle features like swirl chamber design, orifice diameter and orifice shape have an effect on the cooling pattern and the HTC for a given oil pressure and flow rate.

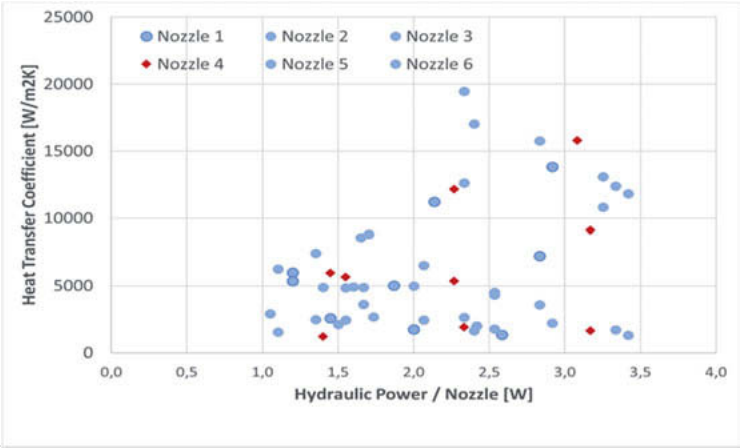

Fig. 6: Nozzle design optimisation results (selected examples)

A multi-dimensional nozzle design optimisation process has been applied to identify the best nozzle design. Fig. 6 shows results for a selection of nozzles. Nozzle design #4 provided the best compromise of achievable cooling effect (H.T.C.) and lowest overall power consumption across all operating conditions and has been selected for the final spray cooling system.

Inverter Layout

The inverter is required to operate over a DC bus voltage of 520 to 750V and motor simulations indicate that the inverter needs to provide a current of $350A_{rms}$ continuous and a peak of $500A_{rms}$ for 60 seconds. The use of a high-speed motor operating at up to 21.000 rpm results in a high fundamental frequency underlining the need for high switching frequency.

The inverter is designed as a platform to enable evaluation of various Motor Control Strategies in order to identify potential strategies that are more efficient. The strategies that could be evaluated are:

- Fixed Switching Frequency in the range 10kHz to 30kHz
- Variable Switching Frequency
- Pattern Switching

Switching losses of Si-IGBTs are a significant part of the overall system losses and increase massively at higher frequency. To be able to provide high speed operation and meet the overall system efficiency targets SiC-MOSFETS had to be considered for ACeDrive (Fig. 7).

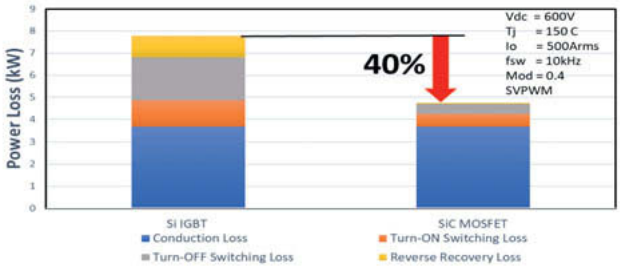

Fig. 7: Comparison of switching losses of IGBTs and SiC MOSFETS

SiC power modules will provide significant inverter efficiency improvement, but to get to the 10% system target, variable switching frequency and ability to change switching patterns had to be considered. Switching patterns will provide further benefits in minimising inverter losses but needs to be balanced carefully with potential NVH effects.

The Silicon Mobility T222 processor will be used to allow variable switching frequency algorithms to be implemented (Fig. 8).

The T222 FPCU does support:

- High switching frequency, FOC hosted in FPGA (>200kHz capable)
- Variable switching frequency for switching loss reduction
- Optimise switching patterns for iron and copper losses reduction
- ISO26262, ASIL-D
- Autosar

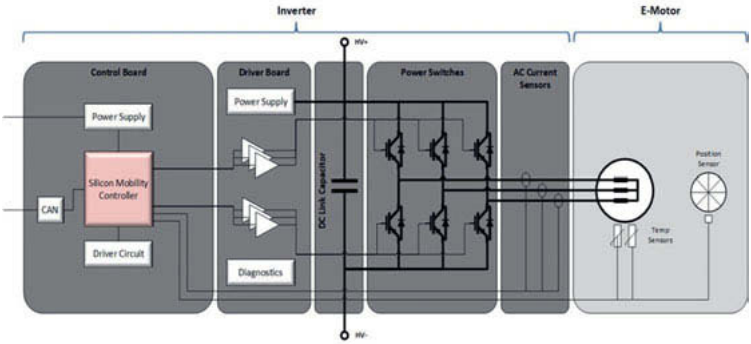

Fig. 8: Inverter basic layout with T222 SiMobility controller

The T222 FPCU has the ability to switch operating modes as a function of conditions between:

- Space Vector Pulse Width Modulation (SVPWM) – time-based switching
- Selective Harmonic Elimination Modulation (SHEPWM) – angle-based switching

This feature allows the execution of custom switching patterns for each operating point of the motor power curve to minimise the predominant losses or improve NVH, e.g. close control of phase current at low motor speeds, or using angle-based switching at high speeds and power.

The features and libraries of the T222 processor have helped to implement the required functions and sophisticated control, but significant modifications or additional SW features, highlighted in red in Fig. 9, had to be implemented to meet our specific needs.

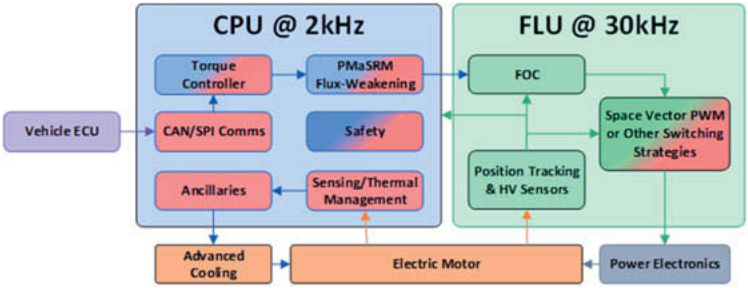

Fig. 9: Inverter basic SW structure

Functional safety, F.T.A., SFMEA has been undertaken using the ISO-26262 procedures as guidelines. The ACeDrive EDU has been analysed as a Safety Element Out-of-Context (independent from its vehicle integration). The FTA and Functional Safety have been studied for the primary function (torque delivery) and its safety mechanisms mainly applied in the rotor position sensing (resolver and related devices).

Advanced Cooling of the Power Modules

Although SiC MOSFETS work with significantly lower switching losses, another project goal was to maximise the power density of the Power Module. SiC dies are expensive, better cooling will allow the use of fewer or smaller dies to reduce costs.

Simulation of various cooling strategies undertaken by UoN has indicated that the application of a vapour chamber between the substrate and water cooled pinfin arrangement can significantly reduce junction temperature (Fig. 10).

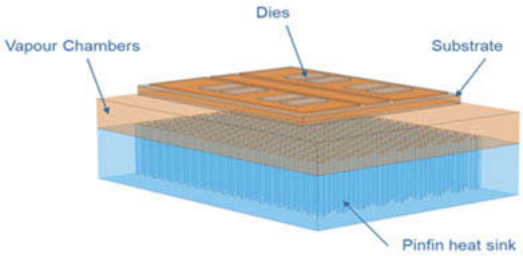

Fig. 10: Basic Vapor Chamber arrangement

The vapour chamber as a passive element reduces thermal resistance of baseplate and improves heat dissipation across the surface of the baseplate, thereby giving the pinfin arrangement a greater effective area to work on (Fig. 11).

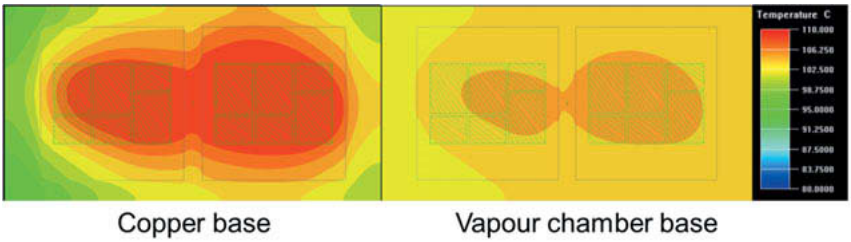

Fig. 11: Base plate temperature distribution with (right) and w/o (left) vapor chamber

This lowers significantly the peak temperature in the dies allowing either higher continuous current or smaller/less dies.

Transmission

The basic transmission layout with 2 step helical gear offset- design and a fixed ratio of 14 has been chosen as best compromise between packaging, weight, efficiency and cost (Fig.12).

Gear macro geometry has been defined and bearings have been selected considering the conflicting NVH, weight and efficiency targets.

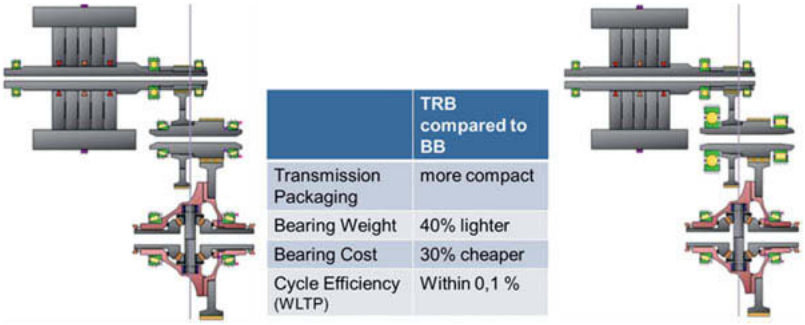

Fig. 12: Basic transmission layout and comparison bearing concepts

Although ball bearing would have provided a slightly better efficiency and hence are often used in existing E.D.U.s, TRB bearings have eventually been selected due to their significant packaging, weight and cost benefit. Simulation indicated that in such a high torque application friction-optimized TRB in combination with a smart preload concept will bring the cycle efficiency very close to best in class ball bearings. The combination of active and passive lubrication will further help to minimise churning losses at high speed.

Estimated system performance

Key components like motor, inverter and transmission are defined, modelling and performance as well as efficiency simulation have been performed on component level.

An EDU. system model and a vehicle model have been created and verified with measured vehicle efficiency data in WLTP driving cycle. A first comparison of the vehicle with production EDU. (measured) and the same vehicle with the ACeDrive EDU. (simulated) indicate a reduction of the used energy in WLTP cycle of 9 % (Fig. 13).

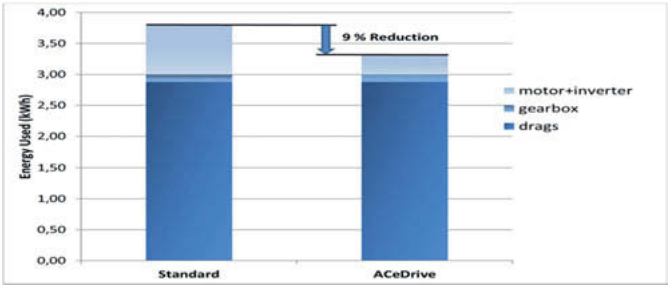

Fig. 13: Comparison of Vehicle power consumption in the WLTP cycle of production system (measured) and ACeDrive system (predicted)

This is already very close to the 10% target. We are positive that we will be able to deliver the 10% target, considering the conservative approach for the simulation and some further already identified optimisation potentials. After building and bench-testing of the hardware, we will finally confirm the system performance and efficiency in an iPace demonstrator vehicle in 2nd quarter next year.

Conclusion

There is a strong trend to more powerful EDU systems for performance Hybrids as well as long-range BEV. Along with this trend, weight, packaging, and the use of expensive material must be reduced, driving the need for a massive increase in power/torque density of EM and inverter.

Continuous torque and max speed of future electric motors need to be improved at the same time as delivering the desired performance without expensive multi speed gearboxes. Focus has moved from peak efficiency to best system efficiency in the driving cycle to maximise vehicle range.

A wholistic system approach using advanced analysis of the EDU. components individually and as part of the complete system is required to achieve such stretched performance and efficiency targets.

Experimental tests and component and system level simulation confirmed that cycle efficiency can be improved by 10 % and continuous power density can be almost doubled by minimising

losses in motor, inverter and transmission in combination with the use of sophisticated cooling concepts, SiC power modules and enhanced control.

[1] 32nd Electric Vehicle Symposium (EVS32), Lyon, France, May 2019 (D.S.D.)

High Speed Electric Drive System

A Solution for the Next Generation E-Cars

Dipl. Ing. (FH) **Mathias Deiml**, AVL Software & Functions, Regensburg

Zusammenfassung

Elektrische Fahrzeuge werden in immer größeren Volumina produziert und genießen vermehrt Kundenakzeptanz. Um in höheren Volumina mit konventioneller Technik konkurrieren zu können ist Kostenreduktion das Ziel vieler Entwicklungsteams.
Der Ansatz in diesem Artikel ist, den Materialeinsatz in der elektrischen Maschine durch Drehzahlerhöhung und so eine Reduzierung des Volumens zu verringern.
Die neuentwickelte E-Achse ist für DC Spannungen von 800 V ausgelegt und besteht aus einem SiC Doppelinverter, zwei E-Maschinen mit Nmax= 30000 Upm und zwei unabhängigen Getrieben in einem Gehäuse. Der Doppelinverter verwendet eine variable Schaltfrequenz und eine Interleaving Strategie, was eine kleine Zwischenkreiskapazität ermöglicht. Die Leistungdichte erreicht 3,5 kW/kg auf dem Gesamtsystem.

Abstract

The electric vehicle is on its way to greater production volumes and enjoys more and more customer acceptance. To be able to compete with combustion technology cost reduction is a target for the next generation.
In this work it is proposed to increase speed of the e-motor and so reduce weight and material effort and cost. The new e-axle works with 800Volts constists of two 30000 rpm-e-motors, a dual-SiC inverter and two single speed transmissions in one housing. The dual inverter uses an interleaving switching strategy to reduce the DC link capacitor size. The power density reaches 3,5 kW/kg on e-axle-system.

Introduction

The electric vehicle is on its way to greater production volumes and enjoys more and more customer acceptance. Established EVs like Tesla compete against combustion engine cars, as a real alternative. These vehicles have a high driving range (>400 km), very good driving and charging performance. Government incentives and an increasing awareness for CO2 emissions may be additional volume drivers for electric cars in Europe and Worldwide. Nevertheless, the current generation of battery electric vehicles will probably be still too expensive to make it into comparable volumes with conventional technology.

The reduction in cost, especially in the next generation of BEVs from 2022 is therefore the development goal for all engineering faculties in BEVs and PHEVs.

A possibility to reduce costs on the electric drivetrain is suggested in this article. Integrated electric-drive-units (EDUs) are already widely in use. They integrate the electric machine, the transmission, the differential and in most cases the power inverter in one easy to install unit.

An EDU is characterized by its torque capability at the wheel(s), power output and maximum vehicle speed. For this research project we defined those data for the upper mid class and premium pass car segment for 2022. The scalability down to mid and compact class pass cars and even light duty and sports cars was an important project target.

We assumed a two ton rear wheel driven car with well dimensioned 5000 Nm axle torque. A trend for sophisticated BEVs, that we observe on the market, is torque vectoring. Each wheel can be driven and controlled separately to get a traction advantage in curves.

The EDU consists therefore of two drive systems, with ~ 200 kW and 2500 Nm on each side. The maximal vehicle speed was targeted to 240 km/h, to match usual specifications of premium combustion engine vehicles.

The system voltage of this EDU was chosen to be in the 800 Volt range. We see advantages in the higher voltage to reduce weight of conducting materials and reduce chip area in the inverter. Both effects have the potential to lower costs of inverter and wiring [3]. The charging power can be increased despite current limitations on the charge connector.

The e-machine costs can be decreased by reducing the size and thus the material costs, but also the torque output. To reach the required power the speed must be increased, like the following equations show.

$$P_{mech} = \omega * M; \quad M \sim d^2 * l; \quad \rightarrow \; Volume \sim \frac{1}{\omega}$$

(d: airgap diameter; l: lamination length)

An increase of factor 2 in machine speed results in a reduction of active machine material by half, maintaining the power capability. If special or expensive technologies in machine and transmission can be avoided there is a substantial cost saving in the machine. These relations

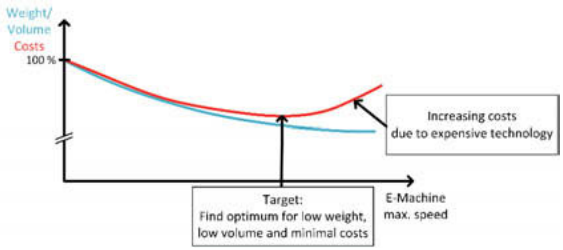

Fig. 1: Speed vs Cost

between speed and weight/volume/cost are shown in Fig. 1. We want to stay left of the point in speed, from where the costs are increasing again, because of special bearings, lamination material, windings etc.

When increasing machine speed, influence on transmission and inverter must be observed. The transmission should be simple and highly efficient. Shiftable two speed transmissions offer the possibility to select the most efficient operation points of the e-drive, but it also increases complexity, weight and costs.

A high-speed e-machine achieves the desired wheel torque and vehicle top velocity using a single speed transmission.

To fulfil high efficiency, the number of stages was limited to 2, which leads to a transmission ratio up to about 16:1. With this ratio the e-machine reaches about 30.000 rpm at vehicle top speed of 240 km/h.

Advantages in the most important properties efficiency, simplicity and costs lead us to use a two stage lay shaft transmission.

E-Machine

To reach a high-power density, a permanent magnet synchronous machine (PMSM) was chosen. Magnets with a reduced amount of expensive heavy rare earth materials like Dysprosium (Dy) and Terbium (Tb) are used to reduce the cost of this machine. These magnets are arranged in a simple single layer V-shaped structure as shown in Fig. 3.

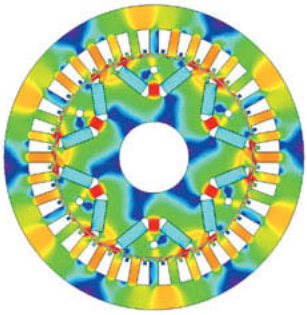

Fig. 3: Flux Density at Corner Point (peak operation)

Fig. 2 left: Mechanical Simulation (von Mises stress) at 36000 rpm, Right: Current Density in the Conductors of One Slot at Maximum Rotation Speed

One of the first concerns regarding high-speed machines is the mechanical strength of the rotor, which is linked to its maximum peripheral speed. The current design reaches a maximum speed of 155 m/s, exceeding most automotive e-machines (< 120 m/s) but still below maximum possible speeds above 200 m/s reported in [1]

Different FEM analysis and optimization tools were used to achieve a robust and efficient design (Fig. 2). To reduce the high-frequency losses in the windings, a distributed round wire winding was preferred to a hairpin winding due to prevented skin effect.. Fig. 22 shows the FEM simulated current density in the conductors and it can be seen that additional proximity losses can be avoided by lead placement in the slot.
Iron losses are the predominant losses in an electrical machine at high rotation speeds. To reduce these, a 0,2mm lamination NO20 was selected.

A 3-pole-pair machine was chosen as the best compromise between an optimal magnetic circuit and a moderate maximum electrical frequency of 1500 Hz.

To reduce the high-frequency losses in the windings, a distributed round wire winding was preferred to a hairpin winding. Thin wires are used to prevent skin effect even at the maximum

speed. However, the influence of copper wires on one another and flux leakages across the slot lead to an inhomogeneous current density distribution in the wires and result in increased Joule losses [1]. Closed stator slots help reducing these losses by canalizing the magnetic flux and thus reducing the flux crossing the slot. The wires are also pushed away from the airgap, i.e. towards the outer diameter, where they are less affected by flux leakage. Fig. 2 shows the FEM simulated current density in the conductors.

Cooling

A direct oil cooling system, like the one integrated in the AVL COUP-E 800 V electric vehicle [3] was implemented to efficiently dissipate the losses of the machine. The coolant is pumped through the stator slots in the axial direction to directly cool the windings. The oil is kept inside the stator because of closed slots. This solution saves the effort of an additional airgap tube and at the same time significantly reduces the airgap width, the cogging torque and the torque ripple.

With the direct cooling concept, the continuous power output of this small but powerful machine can be drastically improved compared to water jacket cooling.

Direct cooling improves efficiency in low to medium load conditions, due to low copper temperatures.

There is no rotor cooling required. NO20 lamination and segmented magnets ensure low rotor losses and the low stator surface temperature in the airgap avoids heats radiation from stator to rotor.

Performance

Fig. 4 shows the efficiency map of the machine. The limits of this machine can be scaled for various applications. On the motor test bench and on the chassis tester the EDU showed excellent power ability up to 240 kW per motor for 10 sec. As shown the magnetic limit is given with 273 kW, which can be reached for short time with boosted current.

Thanks to the applied measures to reduce the high-frequency losses, the machine offers a large high-efficiency operating region above 95%.

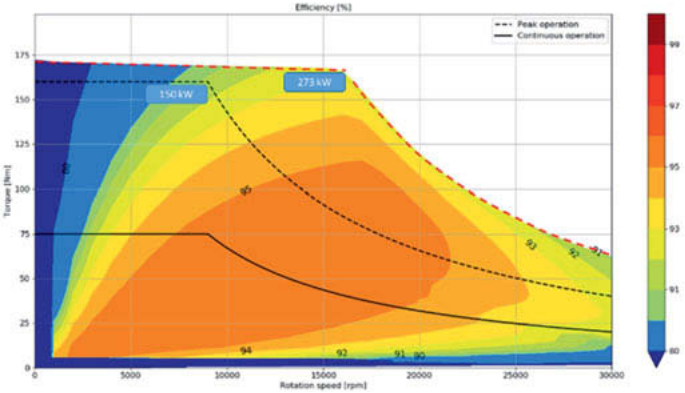

Fig. 4: High-speed e-machine efficiency map at 80°C copper and magnet tempera-

Inverter

The focus of the inverter development was to find a solution that meets the requirements for current and frequency of the eMotor and also enabling high efficiency and high power density.

To achieve this, new wide bandgap Silicon Carbide (SiC) power modules are a perfect fit. The SiC power stage has considerably lower switching losses than state-of-the art IGBT solutions. This allows to increase the switching frequency while still achieving higher efficiency. Increasing the switching frequency also made it possible to reduce the package size, particularly the commutation cell and EMC Filter. The sweet spot for this application was found at a switching frequency of 15 kHz. The inductance of the commutation cell can be simulated during the mechanical concept phase to find the best solution to reduce it as much as possible. A low value for the commutation inductance is necessary to be able to increase dV/dt of the power switches' gate drive to further increase efficiency.

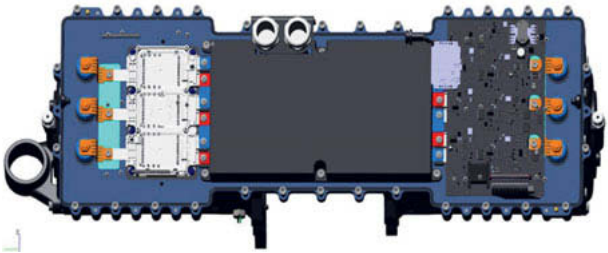

Fig. 5: Integrated Dual Inverter

Another advantage that enables high power density is that SiC modules are smaller than IGBT modules with the same power (amperage) specification, because the die size is smaller and the thermal conductivity is better. For this design the power stage is capable of a phase current up to 520 Arms to fit the e-machines and a DC voltage up to 820 V. The higher costs for SiC modules are reimbursed on system level by enabling a very compact inverter package and increasing the range.

The two power stages share a common DC-Link capacitor. The dual inverter can control the two e-machines independently from each other and enables thereby torque vectoring.

The two independent controls are synchronized with an inverter internal signal. A differential LVDS interface was selected for this to be immune against common mode noise. The electrical design includes safety related monitoring and control functions as defined in the technical safety requirements of typical automotive traction inverters.

Transmission

Fig. 6 shows the double transmission. It contains two single-speed, two stage layshaft transmissions integrated into one housing. Together with the two motors and two independent torque command paths it is suited for efficient torque vectoring.

Lubrication and cooling are key parameters for high speed helical gears.

Fig. 6: Layout of Dual Single Speed, Two Stage Trans-

Splash lubrication cannot be used if the pitch line velocity exceeds 20 m/s due to the fact that drag losses will increase drastically with speed, which reduces the transmission efficiency and increases the oil sump temperature. Therefore, pressurized or forced lubrication must be implemented for proper cooling and lubrication of gears and bearings.

The advantage of the forced lubrication system is increased control over the oil flow rate to each component as well as higher efficiency due to the dry sump which reduces the drag losses of rotating components.

There are important parameters that need to be considered for a functioning forced lubrication system. These parameters are listed below. Only the gear design and the position of the lubricant's nozzle will be discussed here.

- Gear design
- Gear surface distress

- Lubricant selection and its properties
- Cooling and thermal behavior of components
- Position and type of the lubricant‘s nozzle

Gear design parameters play an important role in high speed transmission and particularly on the lubrication and cooling of gears. Some of these parameters are: pitch line velocity, helix angle, axial meshing velocity, face width, pressure angle and surface roughness.

Pitch line velocity is the linear speed at the pitch diameter of a gear. This is the key parameter to decide on lubrication method.

Helix angle is another important parameter in high speed gears because it has direct effect on the transmission noise level. Small errors in gear design can generate noise and reduce passenger comfort. To decrease the transmission noise, the gear total contact ratio has to be increased. A high contact ratio will reduce the peak-to-peak transmission error. The total contact ratio consists of transverse and overlap/face contact ratios.

Transverse contact ratio depends on gear module, pressure angle and tooth proportion. Tooth proportion itself depends on addendum and dedendum factors. For normal gears the addendum factor is approximately 1.25 and the dedendum factor is 1. However, in this project these factors are increased to improve the transverse contact ratio. Moreover, the pressure angle on the 1st stage of gears is reduced to 14° to increase the transverse contact ratio. A lower pressure angle leads to a lower tooth load capacity and higher tooth temperatures which causes the oil film thickness to reduce. Therefore, more attention should be paid to lubrication of the 1st stage gears.

The overlap/face contact ratio depends on the helix angle and the gear width. A helix angle of 35° is used in this project. High helix angles generate higher axial forces that must be supported by a bearing. However, higher helix angle also leads to lower axial meshing velocity. Air and oil trapped in the gear mesh will pump out at lower speeds which means less friction heating and lower temperature of gear tooth.

Using higher helix angles makes it possible to decrease the gear face width. A small face width means that trapped air and oil travel less distance which in turn leads to less frictional heating and lower gear tooth temperature.

Position of lubricant’s nozzle is another important factor that affect the gears lubrication and cooling. Nozzles can be placed in a way that they spray oil into the in-mesh or out-mesh or both. The general theory is that spraying oil into the in-mesh is good for gear lubrication and

spraying oil into the out-mesh improves the gears cooling. However, packaging and available space to position the spray nozzles can limit the choice of spraying oil into the in-mesh or out-mesh only and moreover, the choice of positioning the spray nozzles also depends on gear manufacturer experience.

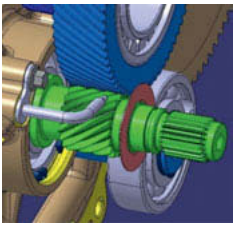

Fig. 8: Nozzle position on the 1st Stage

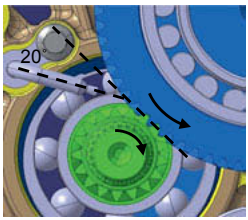

Fig. 7: Nozzle Position on the 1st Stage

Another factor that needs to be considered for spraying the oil on gears is the oil flow rate and oil pressure. A High flow rate and pressure might be needed for gears with high rotational speed to make sure that oil can reach the gear tooth face and not to be deflected by the movement of accelerated air caused by rotation of the gears.

To decide on the nozzle size and the oil flow rate, the total heat produced by gears should be calculated. The power loss of the helical gears is around 1.5% to 2% and knowing the input power to the gears the power loss can be calculated. It is important that oil covers the gear tooth surface for short time interval before it is being slung off.

Fig. 8 and Fig. 7 show the spray nozzle for the 1st stage (input) gears. The angle of the spray nozzle is set to 20° to provide the best oil coverage on the tooth of the driven gear. Moreover, as can be seen from Fig. 8, the spray nozzle is located on the right side of the gear and this is because of the nature of helical gears that pushes the oil to one side. By locating the nozzle on the right side, the rotation of the input shaft gears will push the oil across the gear tooth face.

Bearings for high speed application

The bearing cage becomes one of the main concerns at high rotational speeds. If the cage design and material are not suited, the cage can expand and touch the bearing outer race and become destroyed. The accelerations and decelerations on the other hand generate high

stresses in the bearings especially in the cage. Other challenges for high speed applications are leakage from sealed bearings which can destroy grease and bearings raceways and operating temperature that can reach up to 180˚C requires special attention to the bearing material.

SKF has developed a new design for their sealed bearing allowing up to 1.6 million ndm. The cage has been redesigned to reduce the stress and power loss. Polymer material is used to be able to withstand high centrifugal forces. Special attention is paid to the type of grease used in the sealed bearings to avoid overheating and keep the losses to a minimum. The type of seal and its material has been reviewed to ensure sufficient cleanliness. Extensive testing has been performed by SKF to verify the lifetime of the design and the results has shown considerable improvement of the bearing power loss and the speed capacity.

System Test Results

E-Motor tests have been performed on the motor test bench. Results show a torque output which even exceeds the simulated values. The motor reaches 188 Nm at 2000 rpm and lies over 180 Nm up to 11000 rpm. The peak power was reached at 14000 rpm with 243 kW for 10 sec. The rotor strength has been confirmed in a spinning test at 33000 rpm with a plastic deformation of only 3 µm, which fulfilled the design targets.

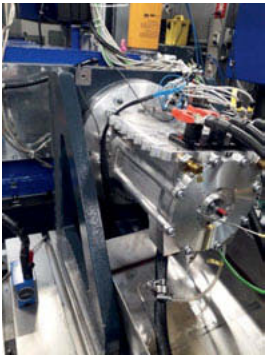

Fig. 9: High Speed E-Motor on Testbench

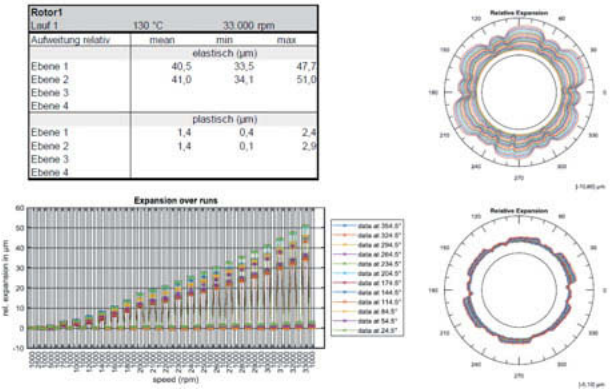

Fig. 10: Spinning Test Results

On EDU level the performance of 2x200kW pk for 10 sec could be measured. The ongoing test bench run confirmed also an excellent system efficiency of 93% in the best points tested so far. This is from DC power input to torque/power at wheels.

Even though the lubrication concept relies on pressurized lubrication system and dry sump, still sprayed oil on gears and bearings need to be collected and guided to the pump intake. The transparent housing shows this process clearly.

Tests revealed that collected oil at the transmission sump is aeriated (air bubble mixed with oil) which leads to problem for oil pump like noise and loss of pressure. To address this issue ring gear of the final drive and the 1st stage gear wheel are shielded off from the main transmission. Moreover, the oil pump pickup point is optimized so that less air enters it and constant supply of oil can be assured under different driving condition.

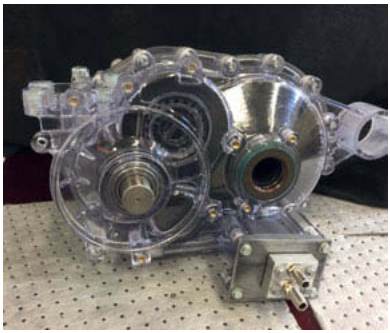

Fig. 11: Transmission in Transparent Housing

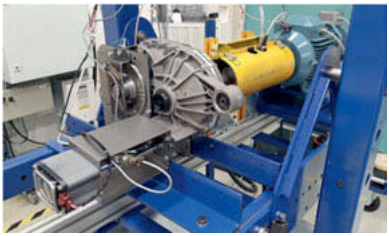

Fig. 12: Transmission on Dyno Testbench

During the function test pump operation (audible noise or unexpected pressure drop), oil sump condition (foaming and aeriation), bearings temperature, oil leakage through the slinger and other sealing and sealed bearing grease leakage at high speed were observed.

Vehicle Integration

After thorough testing of the EDU the e-axle will be built into a technology demo vehicle.

Functional integration requires to introduce a TQ-vectoring interface, The HV supply voltage is boosted from the battery with a dedicated DCDC converter (Boost Converter). A boost strategy sets the voltage depending on speed, load and system efficiency.

The direct oil cooling uses an oil/water heat exchanger. Coolant pump and transmission oil supply is map controlled.

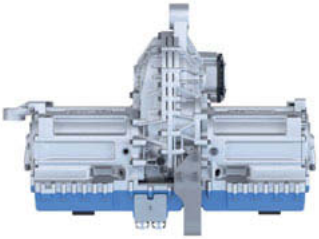

Fig. 13:
Complete High Speed E-Axle

Fig. 12:
High Speed E-Axle Integrated in Vehicle14

Conclusions

Our high-speed EDU was designed for a max. speed of 30.000 rpm and 160 Nm at the e-motor. Roller bearings and standard silicon sheet metal were used to operate at high speed. The magnets use reduced rare earth materials. Its small size lowers costs in the motor, saves material resources and supports integration into various vehicles. Scalability can be realized by using a single motor config, e-motor length reduction and others.

The transmission is kept simple with its single speed configuration. Lubrication of the gear mesh and the touchless shaft sealings solve the main challenges for high speed. Sophisticated roller bearings of the latest generation are used in the motors and first stage of transmissions.

The high-speed e-motor marks a contribution to technologies that enable future success of a higher volume electro-mobility with lower resource usage.

References

[1] A. Engstle, M. Deiml, A. Angermaier and W. Schelter, “800 Volt für Elektrofahrzeuge eine applikationsgerechte Spannungslage,” 2013.

[2] D. Gerada, A. Mebarki, N. L. Brown, C. Gerada, A. Cavagnino and A. Boglietti, “High-Speed Electrical Machines: Technologies, Trends, and Developments,” IEEE Transactions on Industrial Electronics, vol. 61, no. 6, pp. 2946-2959, 2014.

[3] M. Popescu and D. G. Dorrell, “Skin effect and proximity losses in high speed brush-less permanent magnet motors,” in IEEE Energy Conversion Congress and Exposition, Denver, 2013.

[4] A. Engstle, M. Deiml, M. Schlecker and A. Angermaier, “Entwicklung Eines Heckgetriebenen 800-V-Elektrofahrzeugs,” ATZ - Automobiltechnische Zeitschrif, 2012.

Elektroantriebe der nächsten Generation

Next Generation Electric Drives

Dr. Stephan Demmerer,
ZF-Friedrichshafen AG, Friedrichshafen

Kurzfassung

Effizienz ist einer der wichtigsten Treiber für zukünftige Technologien. Andererseits ist Leistung ein wichtiges Verkaufsargument für Fahrzeuge. Wie kann man beide Ziele zugleich erfüllen? ZF präsentiert ein Bündel von Technologien für zukünftige elektrische Antriebe, die diese Ziele erreichen: e||Connect ist der elektrische Antrieb von ZF mit einem Entkopplungselement zur Verringerung der Schleppverluste. e2Drive ist der 2-Gang-Antrieb von ZF zur gleichzeitigen Verbesserung von Fahrleistung und Effizienz. Mit 800 Volt Technologie und Siliziumcarbid-Halbleitern wird ein Fahrzeug schnellladefähig, so dass auf längeren Fahrten die Batterie schnell wieder nachgeladen werden kann. Zukünftige elektrische Antriebe sind eine Kombination mehrerer fortschrittlicher Technologien. Eine harmonische Integration werden zusätzliche Aspekte für zukünftige elektrische Antriebe sein.

Abstract

Efficiency is one of the most important drivers for future technologies. At the same time, performance is an exciting selling point for vehicles. How to pay for both targets? ZF presents a bundle of technologies for future electric drivelines meeting those goals: e||Connect is ZF's electric drive with a decoupling element to lower drag losses. e2Drive is ZF's 2-speed approach to simultaneously enhance driving performance and efficiency. With 800 V and Silicon Carbide semiconductor inverters, the fast charging driveline can supplement an efficient electric drive. Future electric drives are a combination of several advanced technologies. A harmonic integration and design will be additional aspects for future electric drives.

Introduction

ZF is a global technology company and supplies systems for passenger cars, commercial vehicles, and industrial technology, enabling the next generation of mobility. With its comprehensive technology portfolio, the company offers integrated solutions for established vehicle manufacturers, mobility providers, and start-up companies in the fields of transportation and mobility. ZF continually enhances its systems in the areas of digital connectivity and automation in order to allow vehicles to see, think and act.

In 2019, ZF achieved sales of €36,5 billion. The company has a global workforce of 148.000 employees with approximately 240 locations in 41 countries. ZF invested seven percent of its sales in research and development.

Founded in 1915, ZF has evolved from a supplier specializing in aviation technology to a global technology company.

Electric and electrified drives are an essential lever for rapidly reducing emissions from local traffic. True to the slogan of “ZF electrifies everything”, ZF Group offers purely electric and hybrid solutions for all vehicle segments, from bicycles to 40-ton trucks, from tractors to race cars.

ZF is the innovator for driveline technology. First generations of purely electric drives are in the market, but the future will bring enhanced technology for eMobility. Some prospects will be given in the following pages.

e||Connect

Efficiency is the most important driver for future technologies. The range of a vehicle is defined by the size of the battery and the energy consumption of the vehicle. The battery is heavy and is very expensive. Future electric drives must be as efficient as possible in order to save electric energy and allow small battery sizes. Additionally, performance should be maintained, or even enhanced. e||Connect is a technology to fulfill both requirements: performance and efficiency.

Today's electric drives have a constant ratio and a permanent connection between electric motor and wheels, which results in continuous, synchronous rotation. There is no clutch or separating element between the electric motor and the wheels.

A four-wheel drive battery electric vehicle (4WD BEV) configuration with 2 electric drives, one at the front axle and one at the rear axle, does not need all the installed power all the time. In normal driving situations, the power of one electric motor is enough to run the car. Full power is only needed in acceleration phases, on gradients, in towing situations, or during high-speed driving modes. This leads to the idea to disconnect one axle drive, as it is common in conventional 4WD drivelines, to avoid drag losses.

The drag losses of the mechanics and the electric drag losses, caused by the rotating magnets in the rotor, are much higher than in conventional drivelines. In one of our electric drives, we reduce the drag losses by 90%. Depending on the vehicle, overall consumption, and the driving behavior, range can be increased up to 10%.

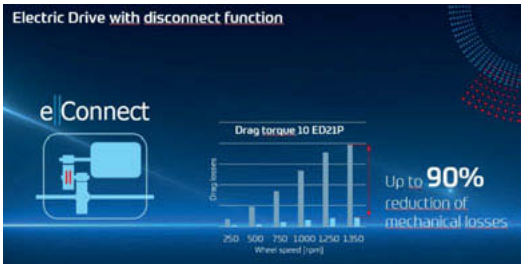

Fig. 1: Disconnect function reduces drag losses up to 90%. Quick and comfortable reconnect supplies full torque within imperceptible time.

The technical challenge is to simultaneously connect quickly and imperceptibly. The driver does not want to feel an interruption of requested torque. The car should behave exactly like a car without this disconnect function. Only the range should be enhanced. This technical task can be managed by a close cooperation between electric motor and mechanical dog clutch. In the disconnected situation when a torque request comes from the driver, the electric motor must accelerate within milliseconds (ms) to the target rotational speed, followed by the clutch closing actuation. Depending on the actual speed of the vehicle, we can manage this operation between 50 and 250 ms.

e2Drive

The disconnect function is one step to increasing efficiency for a 4WD configuration. Another step to increasing efficiency is a multispeed electric drive. With a two-speed gearbox and an optimized electric motor layout, the efficiency and the performance of a vehicle can be improved. Let's first have a look on performance and then on efficiency:

Performance

Fig. 2: Performance can be enhanced with a 2-speed gearbox.

With a 2-speed gearbox it is possible to have a higher first gear ratio to increase acceleration, and/or the gradeability. Especially with a trailer, this can be an advantage.

With a lower second gear ratio, top speed can be increased. So, it is possible to have a wider range to use the power and the torque of the electric motor.

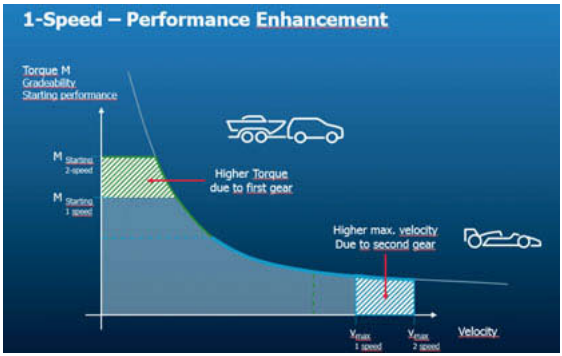

Fig. 3: Higher first gear ratio and lower second gear ratio spreads the usage of an e-motor.

Efficiency

Efficiency is the energy-quotient of mechanical output over electrical input of an electric drive. The goal is to run as long as possible on one battery charge. To calculate the value of a new technology, we can imagine reducing battery size while keeping the distance driven constant. In our case, we could save about 5% of electrical energy, which means that we can use a 5% smaller battery to keep the range of that vehicle. In use cases with large batteries, 5% saving is a significant number and a good business case for 2-speed technology.

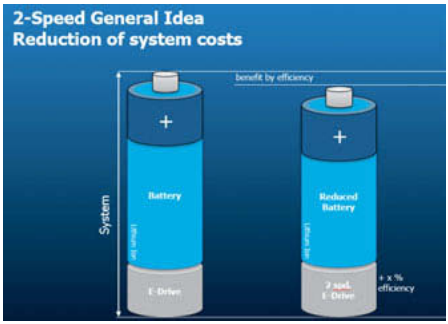

Fig. 4: Higher efficiency leads to savings in the battery.

There are two effects to save energy with a two-speed electric drive. First, it is possible to shift to a more efficient working point. The best point in the efficiency map is typically at medium range of rotation. With a higher first gear and a lower second gear it is possible to run, on average, with less energy consumption in a certification cycle. Especially for highway driving it will be much better. In our demo vehicle, we could achieve a 1,7% range extension by this effect during the Worldwide Harmonized Light Vehicles Test Procedure cycle.

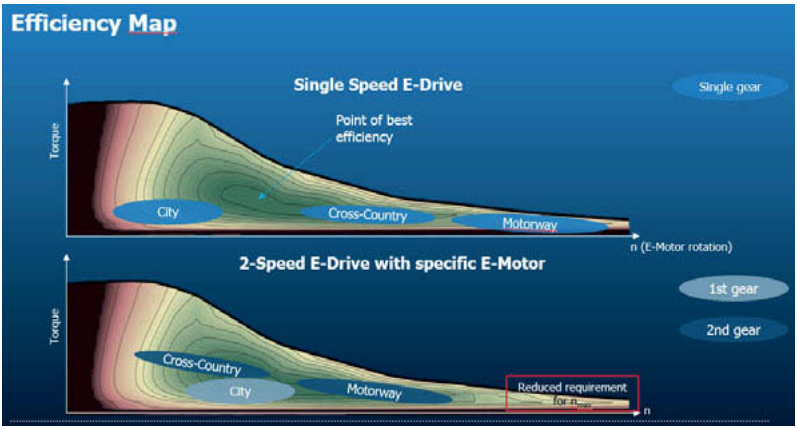

Fig. 5: The design of an e-motor can be trimmed to higher efficiency at lower rpms. High rpms can be avoided with a second gear.

The second effect has more influence: it is a new layout for the electric motor. Since we have a second gear and thereby lower rpms at maximum speed, we can completely avoid these fields of operation. This means, it is possible to design an electric motor in such a way, that we can have even higher efficiency around the best point by losing efficiency at maximum speed. With this effect, we could achieve an additional 3% range extension in our demonstration vehicle. In total, we achieved an improvement of about 4,7%. [1]

Fig. 6: Demonstration vehicle of ZF: by replacing a single speed drive by a 2-speed drive, 4,7% range extension could be achieved. [1]

Future Electric Axle Drive Shapes

First generation electric axle drives are in the market now. They typically have the appearance of a prototype design without obvious signs of higher-level integration. ZF, with its in-house development of all components, has the opportunity to introduce higher integration. Looking at highly developed automatic transmissions, with many generations, it is obvious, that the development of electric axle drives will have higher integration in future. Regarding the positive effect of disconnect and 2-speed transmissions, the mechanical gearbox will be extended and equipped with actuators and controls.

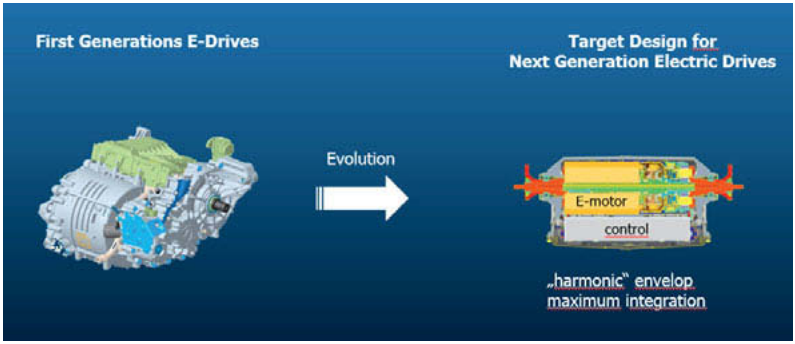

Fig. 7: Future generations of electric axle drives will be highly integrated and shaped like an automatic transmission.

Plug-In hybrid transmissions show us the development path for electric axles: high integration of electronic controls and the inverter combined with an integrated hydraulic concept, which handles actuation, lubrication, and cooling within one system. The coaxial shape has a positive effect on noise, vibration, and harshness. The challenges are to keep the system as small as possible, to place the drive in the limited installation space between the wheels, and to leave enough length for the side shafts. In other words, system development and highest integration are the challenges for future electric drives.

800V and Silicon Carbide (SiC)

Common voltage levels are approximately 400V. Depending on the state of charge, the voltage level operates between 300 and 400V. 400V is generally a peak voltage. Nevertheless, the e-mobility community is talking about the 400V class. The power of this voltage class is limited by the current, since power = Voltage x Current. When current meets resistance, losses are the result, which ends up as heat. Heat destroys the isolation and leads to short circuit and the end of electronics and electric parts:

Power = Voltage x Current

Current => Losses => Heat => destroyed isolation => short circuit => damage

At a certain level of power, it is necessary to increase the voltage due to limitations of the current. High power is demanded for heavy vehicles, like trains or trucks and buses. So, heavy commercial vehicles are using 650V voltage level to provide 200 – 400 kilowatts (kW) power for one single drive. This 650V voltage is the nominal voltage level. The maximum voltage is thereby up to 800V. The passenger car community is talking about 800V technology, which is the same as for commercial vehicles. Nominal voltage level in both cases is around 650V.

The 800V level is driven by the aspect of charging time. Overnight charging is not a problem, but the goal is to reduce charging time on highways down to a minimum. With 800V, the charging time can be halved. A 5 minute stop can then be used to recharge for about 170 km driving range (Fig. 8)

The 800V voltage level will relieve the problem of range limitations for battery electric vehicles. Electric drives must be 800V compatible to operate with the battery in the vehicle. So, the future is electric drives with 800V, at least for higher power applications and for vehicles with higher ranges.

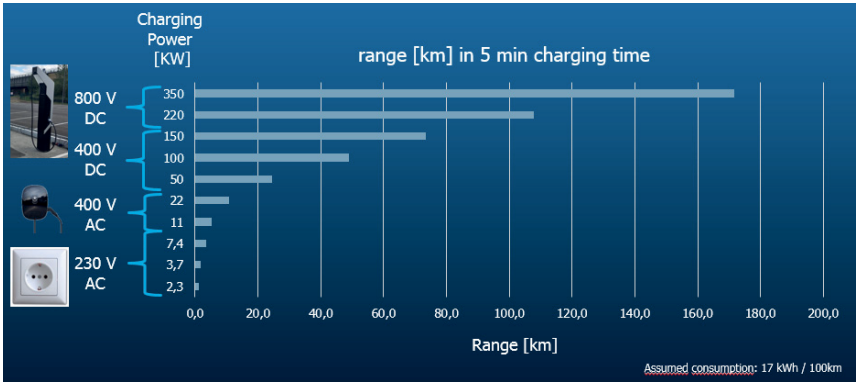

Fig. 8: Charged energy in 5 minutes, measured in range of a vehicle with 17 kWh/100km consumption

How to design an 800V drive?

The e-motor has a different number of windings and an isolation concept, which fulfills the 800V requirements. The key to the change is the inverter.

400V inverters normally are based on silicon insulated-gate bipolar transistor (Si – IGBT) semiconductor technology. The more efficient SiC Metal–oxide–semiconductor field-effect transistor (Mosfet) Technology is much more expensive; so, it is not common to implement such technology. The situation is different at 800V voltage level: The material must be thicker and thereby the losses with Si-IGBTs are much higher. The benefits of the SiC-technology versus Si are higher. The range can be extended by more than 5% with SiC-Mosfets compared to Si-IGBTs.

SiC Mosfets can switch faster than Si-IGBTs. Losses occurring during the shifting time (see Fig. 9)

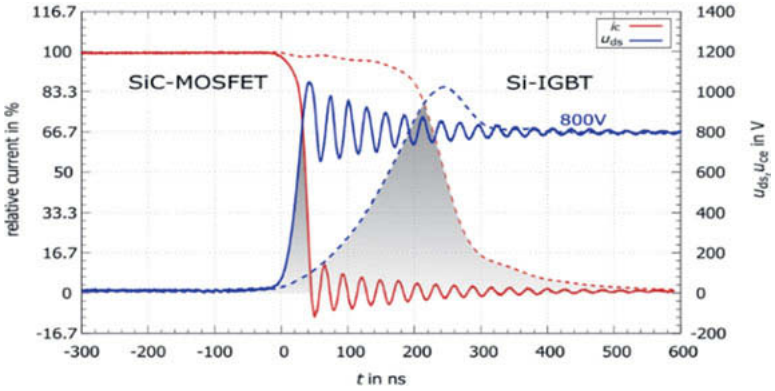

Fig. 9: Measured switching time for SiC (solid) and Si (dotted).
The grey areas between voltage and current represents the switching losses.
Si has much higher losses, due to slower switching. SiC has higher oscillations due to faster switching.

Future electric drives at 800V voltage level will operate with a SiC inverter due to much lower losses. The faster switching possibility enables a wide field of different operating frequencies. This opens the door for system optimization between inverter, electric motor, and transmission.

Electric Drives of Tomorrow

Electric vehicles will become common on the roads. They will be used like conventional cars today. Not only small distances, but larger distances with higher velocities must be operated with battery electric cars. So, battery size will stay high and so will the weight and the costs of the battery.

Disconnect and 2-speed technology are a promising business case due to their energy saving potentials. However, the range will still be an issue for long distance driving. Fast charging is the key to tackle that disadvantage. 800V technology is an enabler for fast charging. So, 800V and 2-speed technology are a combination that fulfill the same requirements of a multi-purpose vehicle as we know it from today's habits. System development of all three components can lead to the highest efficiency.

Finally, the electric drive with more gears and more power must be installed on the axle between the wheels. The requirements for that limited installation space lead to highest integration. The boundaries between the three key elements will be removed and we will end up with an integrated design. A modular kit will cover the different power levels, but keep the synergy.

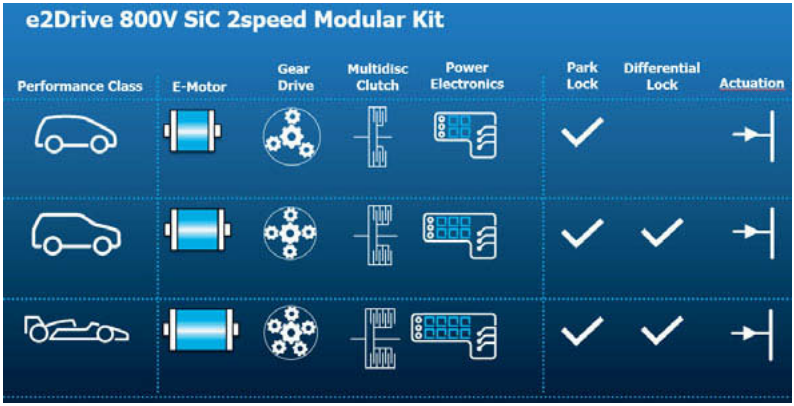

Fig. 10: Modular kit for a future electric drive with 2-speed and 800V technology

Literature:

[1] Dr. Stephan Demmerer, Efficiency of electric axle drive systems – Potential of multi-speed-drives, VDI-Bericht 2354, Bonn, 10.-11. Juli 2019, p.279-286

Coupled topology optimization of an electric drive

Dr.-Ing. **Steffen Rothe**, Dr.-Ing. **Bettina Schröder**,
Dr.-Ing. **Georg Lührs**, Volkswagen AG, Baunatal

Zusammenfassung

Bei der Entwicklung von elektrischen Antrieben mit permanenterregten Synchronmaschinen spielt der minimale Einsatz des Magnetmaterials sowie der Wirkungsgrad und die Effizienz eine große Rolle zur Erreichung der Kostenziele. Um sowohl kosteneffiziente als auch wirkungsgradeffiziente Rotortopologien für elektrische Antriebe zu entwickeln, wurde das Forschungsprojekt “Topologische Optimierung für einen energieeffizienten elektrischen Fahrzeugantrieb bei verbesserter Magnetmaterialnutzung – TOPMAGNET“ mithilfe des Bundesministeriums für Wirtschaft (BMWi) gegründet. Ziel dieses Projektes ist die Entwicklung eines numerischen Optimierungsalgorithmus sowie dessen Anwendung um derartige Rotortopologien herzuleiten. Für die Auslegung des elektrischen Antriebs ist es einerseits wichtig alle elektromagnetischen Anforderungen und andererseits die mechanischen Festigkeitsanforderungen zu erfüllen. Daher ist ein Kernelement die Kopplung beider physikalischer Felder im Optimierungsalgorithmus. Mit dem entwickelten Algorithmus wird ein optimiertes Rotordesign erzeugt und über eine integrierte Werkzeugkette bewertet. Anschließend wird ein Prototyp aufgebaut und experimentell vermessen. Abschließend werden die Simulations- und Messergebenisse miteinander verglichen.

Abstract

In order to develop efficient rotor topologies for electrical drives the cooperative research project “Topological Optimization of an Energy Efficient Electrical Drive with Improved Magnetic Material Usage – TOPMAGNET” was founded with support of the BMWi. Within this project an innovative numerical optimization algorithm is derived and used to create a rotor design with reduced magnet material. The functioning and the performance of an electric drive is mainly characterized be the interaction of electromagnetic and mechanical properties. Hence, the key element of the derived algorithm is the coupling of those fields. With the optimization result at hand a rotor design is developed and validated using a specialized tool chain, taking into account the distinct demands of an electrical drive. Furthermore, a prototype is set up and tested experimentally. Finally, the simulation and experimental results are compared and evaluated.

1. Motivation

Topology optimization is originated and well established in the field of structural mechanics, in order to develop lightweight but reliable as well as stable designs. In general with the help of topology optimization an optimal material distribution in a given design domain can be derived. The advantages are the use of a systematic design approach in early design phases, where the domain and boundary conditions are applied and the algorithm delivers a first idea or even a completely new and not intuitive design. In this paper the method of topology optimization is applied to a permanent magnet electrical machine. The main goal is the identification of highly efficient magnet-iron-air structures in the rotor. Thus the algorithm has to take into account the optimization of three different materials - iron, magnet and air. The coupling of these three materials in the topology optimization can be found in [1]. In the literature the application of topology optimization in the field of electromagnetics received increasing popularity in the recent years. In [2] and [3] a multi-material topology optimization is used to optimize a rotor considering magnet, iron and air material within a genetic algorithm. [4-7] deal with the topology optimization of permanent magnet synchronous machines with the aim of reducing the cogging torque, the electromotive force, noise and vibration. In addition uncertainties are taken into account and a variance-based optimization is performed resulting in a robust design. [8] deals with an electric motor using topology optimization and the mathematical concept of topological derivatives. An electromagnetic topology optimization using an on/off method is applied to a synchronous motor improved with the help of a filtering process in [9]. All the mentioned publications have in common that topology optimization is only applied to electromagnetic field problems. For a good performance of an electrical drive the optimization algorithm has to consider on the one hand electromagnetic demands, on the other hand the mechanical durability plays an important role. Both goals, however, have contradictory design criteria. Thus, the key element of the topology optimization algorithm is to couple mechanical and electromagnetic objectives. The coupling of different physical fields within the topology optimization can be found in [10]. In this book electromechanical systems are investigated and optimized. In [11] an electromagnetic-mechanical coupled topology optimization algorithm is developed and applied to electrical machines, which is similar to the algorithm presented in this paper. The transformation of topology optimization results to geometries is treated in [12]. The challenging tasks thereby are the continuous material distributions and their transformation to a producible geometry.

During the design process high attention is paid to the optimal distribution of high-priced magnet material in the rotor, see Fig. 1. Instead of using an experienced-based approach nowadays numerical optimization methods are used to find the best design, changing the number and arrangement of magnets as well as the form and pattern of the air cavities. For a given magnet arrangement often a shape optimization, based on a parametric CAD model, is used

to determine the cavities' shape. Nonetheless, creating such a model can be a cumbersome as well as time-consuming task and the optimal design can only be found if the geometric parameters represent the optimal geometry. Therefore, the choice of the parameters describing the geometry is an essential part of the optimization process. Additionally, a lot of different designs have to be computed which is a time-consuming task as well. Instead of describing the geometry with certain parameters topology optimization offers the possibility to generate completely new and not intuitive designs without any restrictions in the geometry's description.

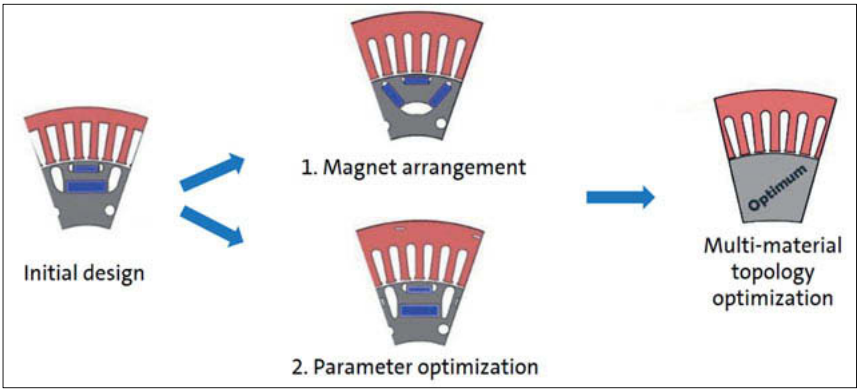

Fig. 1: Optimization of permanent magnet synchronous motors

2. Outline

Since for the optimization of the rotor lamination manifold demands have to be taken into account, Chapter 3 presents a concept of a coupled electromagnetic-mechanical topology optimization algorithm. First, in a general scheme the optimization algorithm which aims at reducing cost intensive magnet material in the rotor lamination is depicted. Therein, the input parameters and variables as well as the physical problem - consisting of distinct operating points of an electric drive - are defined. Additionally, the basic structure of the objective function and the corresponding constraints are formed. In the forthcoming, the individual aspects are substantiated and a limited number of challenges in the implementation are addressed.

Chapter 4 presents and evaluates the result of the optimization algorithm. Therefore, the characteristic electromagnetic and mechanical properties of the obtained topology are compared to the ones which can be derived if a mass-produced e-Golf drive is taken into account.

Due to the extraordinary results, Chapter 5 illustrates the manufacture of a prototype based on the optimized rotor lamination topology.

Chapter 6 focusses on the comparison between the simulated and experimentally determined electromagnetic characteristics and thus enables a final evaluation of the optimized rotor topology.

Finally, Chapter 7 summarizes the main results and gives a short outlook of further applications of the presented optimization algorithm.

3. Multi-Material Topology Optimization for an e-Drive

In Fig. 2 the concept of the coupled electromagnetic-mechanical topology optimization is shown. For the optimization different inputs have to be generated. First of all the geometry of the stator and the winding areas have to be defined as well as the material data. The electric current for the different operating points needs to be given too. Since topology optimization in general depends on starting values, appropriate initial values for the design variables have to be set.

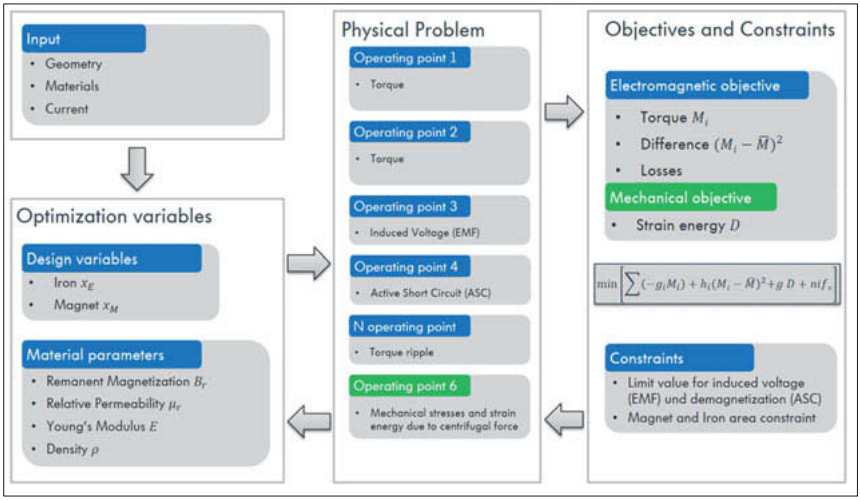

Fig. 2: Topology optimization concept

Performing a multi-material optimization, two design variables – one for magnet and one for iron - are necessary, which are coupled with a classical SIMP approach to the material parameters B_r, E, ρ and the nonlinear material function $\mu_r(B)$. One challenge in the topology optimization is the mesh dependency and the occurrence of thinner and more branched structures with increasing number of finite elements. A solution for this problem is the application of a Helmholtz filter to the design variables, see [13]. With the help of such a filtering technique

small holes are eliminated and smoother structures can be derived, which improves the topology optimization results concerning the manufacturability.

The underlying physical problem consists of different operating points of the electric drive. Two operating points describe the torque-speed characteristics. One operating point represents the electromotive force (EMF) and a fourth operating point computes a simplified active short circuit incorporating the demagnetization of magnets. Including the torque ripple requires the computation of different rotor positions leading to a certain number of different operating points. These different rotor positions are used in addition for the computation of the eddy current iron losses in the rotor and stator. For all operating points distinct electromagnetic finite element simulations have to be performed. In order to incorporate the mechanical strength, the stresses and strains in the rotor due to the centrifugal force are computed.

The optimization procedure requires an objective function which is minimized by the algorithm. This objective function may consist of different weighted components. In this paper the torque and torque ripple are chosen for the electromagnetic part and the strain energy is defined as a component of the objective function for the mechanical part. A further objective is obtained, if the iron losses are taken into account as well. Besides the objective function, constraints are necessary to fulfill the machine requirements. The EMF has to be restricted as well as the demagnetization of the magnets in the active short circuit. For the reduction of the magnet and iron area constraints are added too. Finally, the optimization concept is available and describes the significant machine behavior of a permanent magnet synchronous machine.

With this process at hand the rotor lamination of an electric drive is optimized. The main goal therein is the reduction and optimal distribution of the high-priced magnet material. For the evaluation of the optimization result a reference machine is defined. The optimized machine should fulfill the same performance properties and all other requirements of the reference machine but with reduced magnet material. A mass-produced Volkswagen e-Golf is defined as the reference machine for the optimization, see Fig. 3.

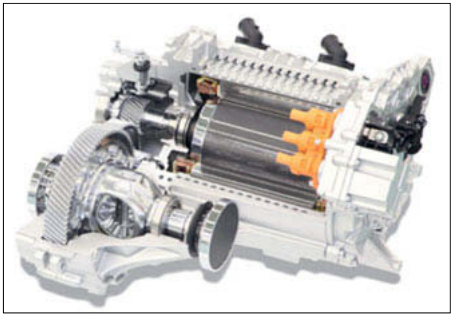

Fig. 3: e-Golf electric drive

During optimization studies it turned out to be efficient to perform a two-step optimization procedure, see Fig. 4. In the first step a coupled electromagnetic-mechanical multi-material optimization is performed changing the magnet, iron and air structures in the rotor domain. In this step all the main optimization demands are incorporated except the torque ripple. One main influence on the optimization convergence and result are the starting values. Thus a promising geometry can accelerate the optimization process and leads to better results in the end. The result of the first step of the optimization process is the magnet's shape and position.

In a second optimization only the iron and air structures are optimized now incorporating the torque ripple. The iron air structures at the outer rotor edge have a major influence on the torque ripple due to the proximity to the air gap. With the help of the optimization the torque ripple can be reduced by 70% in a significant operating point of the machine. Moreover the torque ripple after the optimization is lower than the torque ripple of the reference machine, if unskewed rotors are considered, see Fig. 5.

After this step a parameter variation is carried out to find the optimal thickness of the iron bar between the magnets, which was not a part of the design area. A minimal thickness reduces the magnetic flux leakage but can lead to a reduced strength of the rotor. Thus, a trade-off between these two demands has to be found.

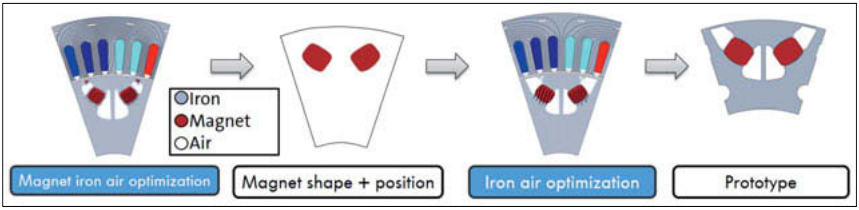

Fig. 4: Two-step optimization procedure

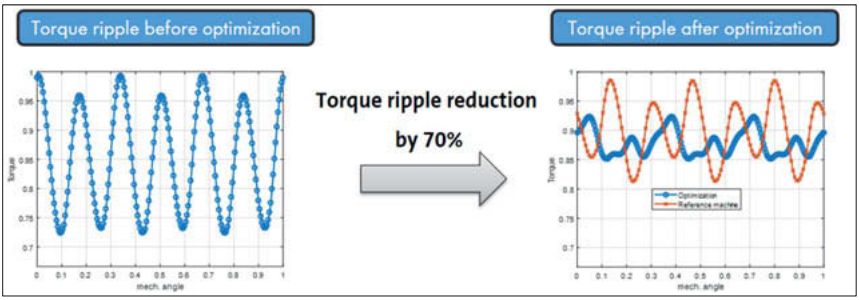

Fig. 5: Torque ripple comparison without skewing

In the final step the optimal skewing angles are derived using an evolutionary algorithm. Symmetric skewing is used and a pareto plot between the torque ripple and the mean torque in a specific operating point is derived, see Fig. 6. Out of this investigation optimal skewing angles are chosen and the torque ripples are on an equal level compared to the reference

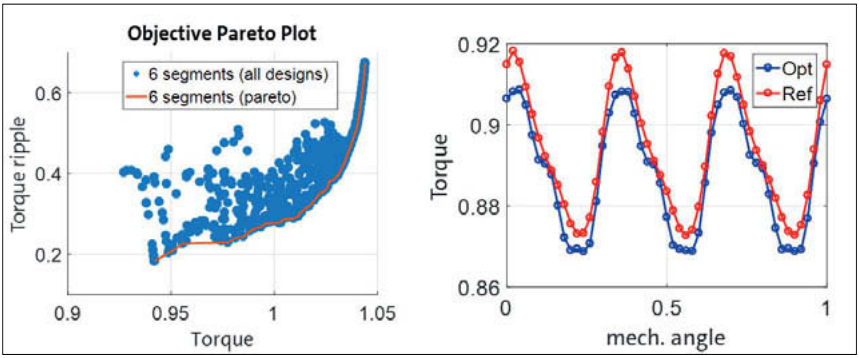

Fig. 6: Skewing angle optimization

machine. It can be recognized that skewing affects the torque ripple of the reference machine more than the optimized rotor.

4. Simulation and Validation of the optimized rotor design

Before a prototype can be built up the final rotor topology has to be constructed suitable for production. Afterwards, this geometry is evaluated according to electromagnetic and mechanical demands. Concerning, the latter the major load of the rotor lamination is the centrifugal force. In order to proof the durability of the rotor a static overload analysis is performed. The resulting von Mises stresses are shown in Fig. 7 (left). The rotor

Fig. 7: Normed von Mises stress (left), normed speed torque characteristic (right)

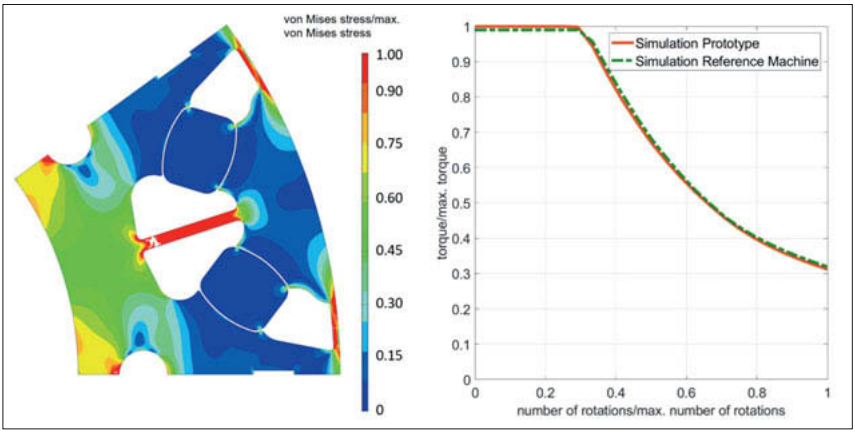

lamination shows high stresses in the bar between the two magnets, nevertheless, the stresses are moderate in most areas of the rotor lamination and fulfill the mechanical durability requirements. The torque speed characteristics in Fig. 7 (right) shows the equivalence between the reference machine and the optimized prototype. A more detailed comparison between the e-Golf drive and the proposed prototype is shown in Table 1, where also the electromotive force, the weights of the individual parts and the torque ripple are evaluated. Due to the necessity that the geometry has to be suitable for production, the magnets are constructed symmetrically and the rotor lamination is adjusted in accordance. This increases the torque ripple slightly. Nevertheless, all quantities of the optimized rotor are on a similar level as the reference machine - except the magnetic weight which is roughly 19% lower.

Table 1: Comparison between reference machine and prototype

Parameters	Difference (Reference machine/Prototype)
Torque @ base speed	0.8%
Torque @ max. speed	-2.2%
EMF (effective voltage)	-2.0%
Magnet weight	-19.2%
Iron weight	1.5%
Torque ripple (peak2peak)	0.3%

5. Construction of a Prototype for Experimental Testing

Due to the extraordinary simulative results obtained for the optimized rotor lamination, a prototype is set up. In this context an e-Golf drive is used, where a new rotor with the improved rotor lamination is inserted. Thus, as much parts as possible are kept original to identify the influence of the rotor lamination. Even the rotor shaft is identical to the one used in a mass-produced e-Golf. An almost identical process chain for the rotor assembly is the consequence.

Fig. 8: Finalized rotor package

In the first step the rotor laminations are manufactured. Therefore, electric steel sheets with bonding varnish are cut by a laser in accordance with the optimized geometry. Afterwards, the individual sheets are stacked as well as oriented to gain different packages with a defined height. The connection between the individual sheets is achieved by applying a defined preload together with a curing in the oven. In the second step the magnets are inserted into the laminated packages. The geometry of the rotor lamination and the magnets is design in such a way that a gap between both parts prevails. Hence, their correct assembly is guaranteed and production tolerances are taken into account. Because of this gap, however, a movement of the magnets within the rotor lamination during operation is possible. Using glue the magnets' position is fixed. The type, the amount and the kind of application of the glue is determined via experiments. Therein, distinct variants are analyzed. Furthermore, the force needed to get a magnet out of a laminated package is measured and compared, leading to a defined amount of glue. The finalized package, see Fig. 8, is achieved, if the magnets are inserted

and glued and the package height is measured. The third step of the rotor assembly is characterized by stacking the individual packages in such a way that they are twisted relatively to each other, see Fig. 9 (left). Moreover, the balancing disks are placed and screwed, creating an assembly as shown in Fig. 9 (left). This is heated in an oven, while the rotor shaft is cooled with nitrogen. Exploiting proper devices the shaft and the tower can then be assembled. If the rotor has cooled down, it is balanced and magnetized. Finally, the magnetic field at the outer

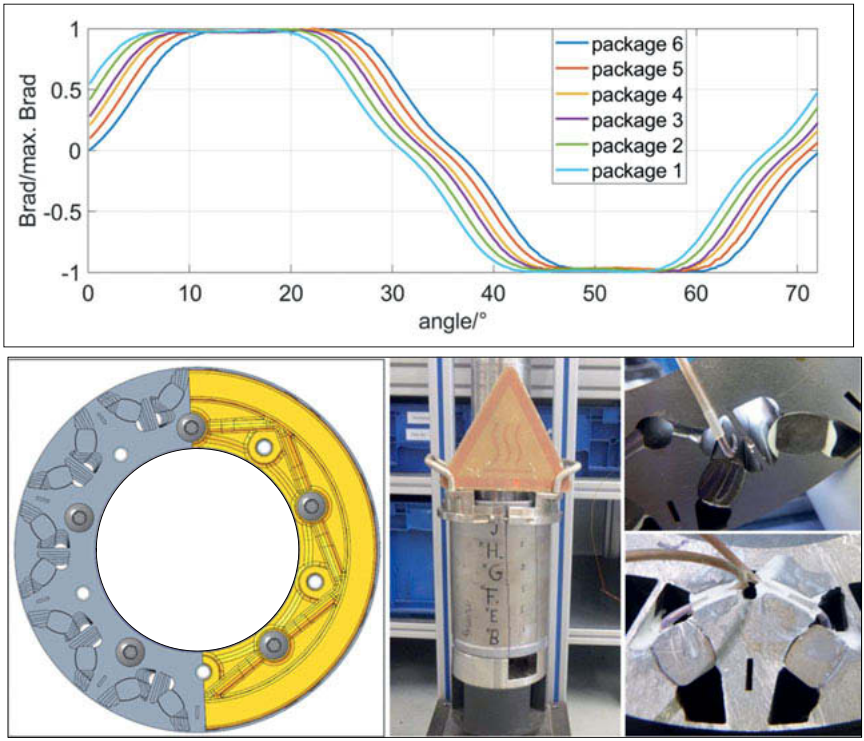

Fig. 9: Skewed packages (left), package tower (middle), thermal sensors (right)

surface in the middle of each laminated package in radial direction is measured. The corresponding normed results are presented in Fig. 10 for one pole. The offset between the individual lines represents the obtained skewing angle. Accordingly, the electromagnetic properties can be evaluated. Apart from this standard prototype assembly of an optimized rotor, a thermal assembly is established to determine the temperature evolution within the improved rotor. Therefore, individual magnets - at distinct axial and radial positions of the rotor - are equipped with temperature sensors as depicted in Fig. 9 (right) and the rotor shaft is furnished with a telemetry unit. With the standard, the telemetry, and a mass-produced assembly distinct

experiments are performed to assess, on the one hand the simulation in general and the optimization result in specific.

6. Comparison between Simulation and Experimental Results

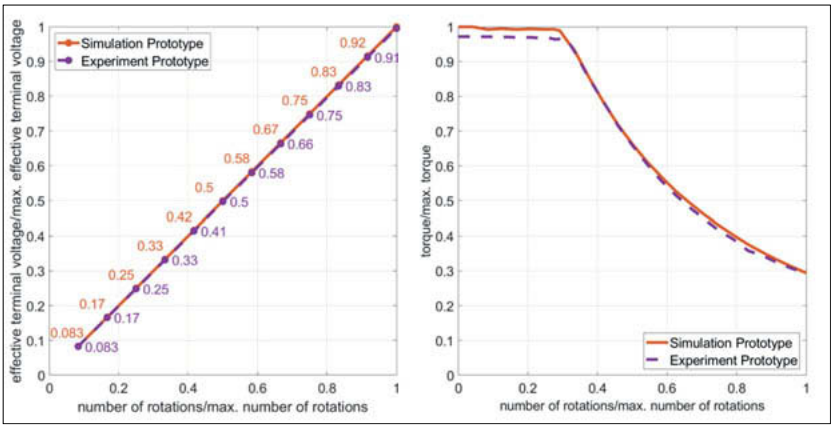

Fig. 7: Normalized effective terminal voltage (left), normalized speed torque characteristic (right)

In order to validate the fundamental simulation parameters such as, the rotor's skewing angle and the material parameters of the magnets as well as of the electric steel sheets the electromotive force is examined numerically as well as experimentally. For the latter, the electric drive equipped with the optimized rotor is fitted to a universal test bed. This is furnished with an external electric drive which on the one hand enables the application of a defined output torque and on the other hand permits that a prescribed number of rotations can be applied to the rotor shaft of the test specimen. If the second option is exploited and the optimized electric drive is operated currentless at room temperature, the electromotive force can be characterized by measuring the effective terminal voltage. This procedure is performed for different numbers of rotations. Analogously, a simulation is carried out. Therein, the rotor's skewing angle determined by the surface measurement in Fig. 10 is taken into account. Furthermore, a variety of measurements is performed to get the material characteristics of the magnets and the electric steel sheet used in the simulation. The simulation and experimental results are depicted in Fig. 11 (left). For the different numbers of rotations, hardly any differences in the effective terminal voltage between simulation and experiment can be recognized. The same is true if the course of the terminal voltage is evaluated. Hence, the utilized fundamental simulation parameters are correct and no further adaptation has to be performed. In the second step the speed torque characteristic is determined numerically and experimentally. For the latter, again a prescribed number of rotations is applied to the test specimen. Additionally, the

electric drive equipped with the optimized rotor is connected to a universal inverter which enables the application of different current feeds. The maximal available output torque can thus be detected taking into account the machine's current and voltage limit. In order to acknowledge correct material parameters, for the simulation a machine temperature of about 70°C at the magnets is assumed. This value is chosen due to the thermal measurements depicted in Fig. 12, carried out with the telemetry rotor

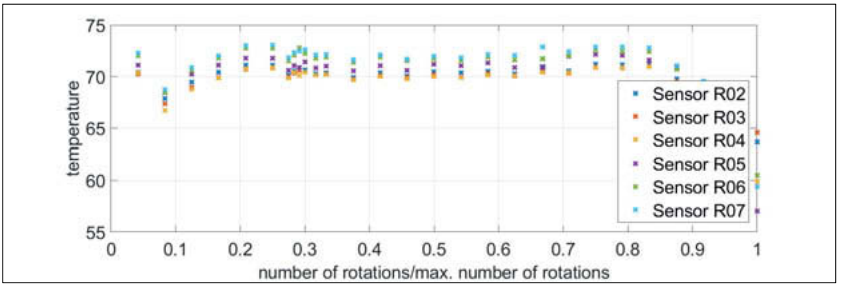

Fig. 8: Temperature evolution over number of rotations

shown in Fig. 9 (right). The emanating speed torque characteristic is depicted in Fig. 11 (right) together with the respective simulation results. In the latter appearing losses are taken into account. In general a good agreement between simulation and experiment can be observed. The differences, less than 3%, stem from the differences between the 2D simulation and the 3D prototype. Moreover, the applied current feed in the experiment deviates from the one in the simulation. Chapters 4 and 5 show that the electromagnetic as well as the mechanical properties of the optimized rotor are equivalent to those of a mass-produced one, although about 19% less magnet material is used.

7. Summary and Outlook

In this paper a multi-material topology optimization algorithm dealing with the coupling of electromagnetics and mechanics is presented. This algorithm is applied to the rotor of a permanent magnet synchronous machine, leading to an optimized topology with 19% less magnet material. The optimized rotor geometry possesses the same speed torque characteristics as the mass-produced e-Golf which is considered as reference drive. This could be demonstrated using simulations as well as by experiments. Moreover the prototype shares the same good efficiency as the reference drive. Thus, the prototype shows the high potential of the topology optimization algorithm. Additionally, the optimized rotor proves that free magnet shapes can be superior to the classical rectangular shapes. The key aspect is the coupling of the mechanical and electromagnetic fields to derive an optimal trade-off between the concurrent demands

of those physics. The optimization algorithm allows not only the reduction of magnet material. Furthermore, it would also be possible to increase the performance and maintain the magnet material. An inclusion of other physical fields like the heat equation would embody a further improvement of the algorithm. All in all the presented algorithm helps to develop efficient electric drives for the future mobility in a shorter time.

8. References

[1] Tasche, M.: Entwicklung neuer Methoden zur Optimierung und Auslegung elektromagnetischer Vorgänge. Universität Kassel Dissertation. 2014

[2] Ishikawa, Takeo; Xie, Peijie; Kurita, Nobuyuki: Topology Optimization of Rotor Structure in Permanent Magnet Synchronous Motors Considering Ease of Manufacturing. IEEJ Journal IA 4, (2015) 4, S. 469–475

[3] T. Sato, K. Watanabe and H. Igarashi: Multimaterial Topology Optimization of Electric Machines Based on Normalized Gaussian Network. IEEE Trans. Magn., 51 (2015) 3, pp. 1-4

[4] Putek, Piotr; Paplicki, Piotr; Palka, Ryszard: Low Cogging Torque Design of Permanent Magnet Machine Using Modified Multi-Level Set Method With Total Variation Regularization. IEEE Trans. Magn. 50 (2014) 2, S. 657–660

[5] Putek, Piotr; Paplicki, Piotr; Pulch, Roland; Maten, E. Jan W. ter; Günther, Michael; Pałka, Ryszard; Lahaye, Domenico: Multi-objective topology optimization of a permanent magnet machine to reduce electromagnetic losses and cogging torque. JAE 53 (2015), S. S203-S212

[6] Putek, Piotr; Pulch, Roland; Bartel, Andreas; ter Maten, E Jan W; Günther, Michael; Gawrylczyk, Konstanty M.: Shape and topology optimization of a permanent-magnet machine under uncertainties. J.Math.Industry 6 (2016) 1, S. 37.

[7] Putek, Piotr A.; Maten, E. Jan W. ter; Günther, Michael; Sykulski, Jan K.: Variance based Robust Optimization of a Permanent Magnet Synchronous Machine. IEEE Trans. Magn. 54 (2018) 3, S. 1–4

[8] Gangl, Peter; Amstutz, Samuel; Langer, Ulrich: Topology Optimization of Electric Motor Using Topological Derivative for Nonlinear Magnetostatics. IEEE Trans. Magn. 52 (2016) 3, S. 1–4

[9] Watanabe, Kota; Suga, Takao; Kitabatake, Shinya: Topology Optimization Based on the ON/OFF Method for Synchronous Motor. IEEE Trans. Magn. 54 (2018) 3, S. 1–4

[10] Dede, Ercan M.; Lee, Jaewook; Nomura, Tsuyoshi: Multiphysics Simulation. London: Springer London 2014

[11] Back, A.: Neuer Ansatz zur Optimierung permanenterregter Synchronmaschinen. Universität Kassel Dissertation. 2019

[12] Drüner, Luise; Brabetz, Ludwig; Ayeb, Mohamed: Post-Processing of Multimaterial Topology Optimization Results of Permanent Magnet Electrical Machines. IEEE 28th International Symposium on Industrial Electronics (ISIE) (2019), S. 372–377, Vancouver, BC, Canada

[13] Lazarov, B. S.; Sigmund, O.: Filters in topology optimization based on Helmholtz-type differential equations. Int. J. Numer. Meth. Engng. 86 (2011) 6, S. 765–781.

Design optimization of battery systems by multiphysics simulation

B. Pohle, **M. Clauß**, **J. R. Schwarz**, **E. Schwiederik**,
IAV GmbH, Stollberg;
D. Lasuen,
IAV S.A.S.U, Guyancourt, France

Abstract: IAV has developed a multiphysics simulation approach to optimize the design of batteries. In 2014 IAV started battery technology development of bipolar Li-Ion battery system named EMBATT Chassis-embedded Energy (www.embatt.de). The target of the approach is to design more efficient battery systems to reach electric driving distances up to 1000 km. The disruptive technology is focused on system to cell level and dissolving of interfaces. This paper concentrates on simulation methods and tools to optimize cell design and safety aspects of the batteries.

The first step of the optimization takes place into the cell itself, using electrochemical simulation to define preoptimized characteristics of the electrodes like thickness and porosity. The next step is a simulation for the design optimization of electrical connection inside and outside of the cell to reduce the power losses and effects of cooling. The last step is related to the investigation of the development of cell-to-cell thermal propagation inside a battery pack to reach the expected safety level. This multiphysics simulation approach (electrochemical, electric and thermal) allows increasing the battery system development, efficiency and making it cheaper for our customers by the reduction of prototypes and tests in early development stages.

Keywords: lithium-ion, EMBATT, bipolar battery, multiphysics simulation, thermal propagation

1. Introduction

The multiphysics simulation in Li-Ion batteries is combining different physical quantities e.g. electrical, chemical, thermal and mechanical simulation. All of these quantities have influence on others. The simulation results shown in this paper are applied to a planar bipolar battery developed at IAV, called EMBATT. Compared to state-of-the-art batteries, the technology of EMBATT allows maximizing the volume utilization at system level. Thanks to the absence of modules organization with standard cell shapes (cylindrical, prismatic or pouch, which lead to high free space) and a chassis-embedded technology that uses the vehicle chassis as battery housing.

The main component of EMBATT, as shown on figure 1, is the bipolar plate with the active material. The electrode foils are assembled to a stack. Each bipolar plate has on one side the anode, and on the other side the cathode. All electrochemical cells must be isolated from each other with a sealing to prevent ion flux. The electrical connection to the outside is made of two metal endplates (HV+, HV-). With this structure organization, it is possible to connect the cells in series to get a higher system voltage and very flat design.

The traction system voltage is the consequence of the unitary cells voltage multiplied by the number of cells in the stack. The energy scale factor is the active area of the cell and voltage level

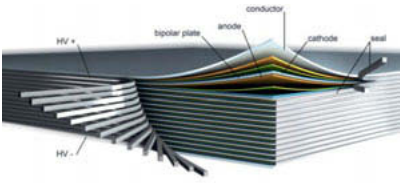

Figure 1 Bipolar Battery

Aims of the technology are:

- Energy density on system level of 500 Wh/l
- System costs about 100 €/kWh
- Internal resistance 1/3 smaller as current systems

Completely new platform concepts, manufacturing equipment, coating processes and simulation approaches are in development.

2. Electrochemical Simulation

2.1 Theory

State of the Art battery simulations use mostly an equivalent circuit model with RC- components to simulate the cell. The disadvantage of the RC models is the missing simulation of the dynamic chemical processes inside in the cell. Electrochemical simulation allows defining more precisely the chemical properties of a battery cell and simulating more accurately the processes inside the cell. The theory of electrochemical simulation was define from Newman- Fuller-Doyle [1,2]. The cell is divided into three regions Anode, Separator and Cathode. The simulation is based on the calculation of lithium concentration in the particles of active material, in the electrolyte and at the interaction between them. Simulating the concentration of lithium in the particles makes it possible to calculate the over potential of the cell with the Butler–Volmer equation and the open circuit voltage from the specific material. The reactions inside of the cell during charging and discharging processes are reversible processes of diffusion and intercalation of lithium ions in the porous electrodes and separator [5].

$$MLi_z + vLi^+ + vze^- \rightleftharpoons MLi_{x+v} \quad [2.1]$$

$$MLi_y \rightleftharpoons MLi_{x-v} + vLi^+ + vze^- \quad [2.2]$$

The electrochemical model (ECM) exists in different complexities. The most used models are the SPM (single particle model) [3], eSPM (extended single particle model and p2d (pseudo 2d model). SPM is zero dimension model to calculate the lithium concentration for the whole electrode with only one particle, eSPM is an extension which includes the electrolyte dynamics in the anode, cathode and separator. The p2d is a pseudo 2d model (one-dimensional) with more than one particle in each electrode. Figure 2 shows the p2d model with five particles in each electrode and separator is divided in three sectors. The full cell has in the sum 13 calculations nodes. All other regions between the nodes are interpolated. For simplification purpose, the particles have a spherical geometry. Every active material has a specific particle radius. For the calculation is used a mean value of the specific material. The two lower circles show a detail of a particle. These are subdivided into five regions. It is necessary to calculate the diffusion of the lithium inside of the particle. The left and right borders of a cell are the current collectors from anode and cathode.

The current flow inside the cell is constant. It is changing from an electron current to an ion current and backwards.

It is also possible to simulate in the two or the three dimensions of the cell. The basis is the p2d model with some modifications. With this simulation, it is possible to simulate state of the art active material and electrolytes.

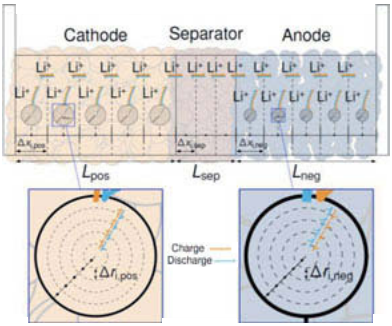

Figure 2 P2D Model of a Battery Cell

2.2 Simulation

Figure 3 shows the results of the simulation of lithium concentration in the cell with different discharge times and constant discharge current for the whole time. The simulation is carried out with the IAV ECM Tool and a p2d Model. The structure of the model is comparable with the Figure 2. The active material combination in all simulation is:

- Anode material: Graphite (C6)
- Cathode material: NCM 111
- Electrolyte is a combination of EC/DEC (1:1) and LiPF6

The nominal concentration of the electrolyte in steady state is 1 mol/L (t = 0 s). The cell is divided into three regions a = Anode, s = Separator and c = Cathode. The thickness of the layers is the distance of the three region. The concentration of lithium is falling in the anode and rising at the cathode during a discharge process. The electrodes have a porous structure (~30 %) and the electrolyte is distributed within the whole electrode. During this discharge process, the lithium ions de-intercalate from the anode in the electrolyte. The ions move to the cathode where a reverse process is started. The lithium ions intercalate in the particle of the cathode. That cause for concentration difference in the Figure 3.

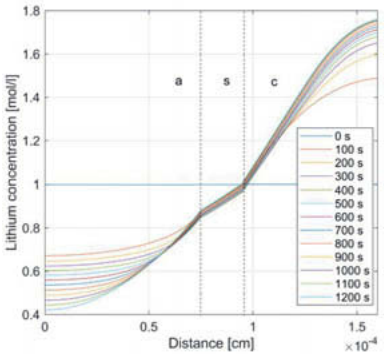

Figure 3 Lithium concentration in the cell during discharging

An application of this simulation is the optimization of the charge profile for a minimum charge time and minimum impact on cell ageing. Any active material has a specific maximal lithium concentration; this is limiting the intercalation in the particles. The optimisation target is a minimization of a concentration difference to the reference of 1 Mol/L. This implies a reduction of dimensions of the particle radius for a faster intercalation. With these adaptions, it is possible to reach a faster diffusion from lithium ions.

During the utilization of the cell, the electrodes and the electrolyte components change their characteristics. An example of the cell aging process is the reduction of the maximal possible lithium concertation in the electrodes. For example, particles are changing their structure. The diffusion inside of a particle reduces or the transition from the electrolyte to particle is limited due to creation of thin layers of reactions products.

All simulations were carried out at room temperature. A vehicle integration is necessary to simulate a wide range from -40 °C to 60 °C. The impact of temperature on the model is defined with some parameters which limit for example the diffusion and the conductivity from the electrolyte and the diffusion in the active material. A lower temperature means a lower diffusion process. This is limiting the maximal operating charge and discharge current. The temperature dependence is a part of the simulation model.The simulation of Figure 3 shows a comparison with two commercial tools. The input simulation parameter have the same basis with dimension of area, electrode thickness and active material combination.

The choice of the active material is comparable to that of Figure 3. The Figure 4 shows the cell voltage from one cell with a random driving cycle profile of a passenger car. The test starts at SOC of 50 % and room temperature. The discharge time is up to 2600 s and stops at 13 % SOC. The correlation between the three graphs is high. Some differences could be seen at low SOC values, mostly due to the slightly different open-circuit voltage of the active material of each tool.

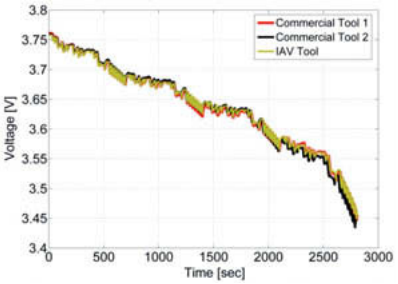

Figure 4 Comparison with different simulation tools

IAV own developed tool has shown sufficiently accurate results to apply it for material optimization, compared to existing tools on the market. The next step of our multiphysics simulation approach is to simulate the electrical behaviour of the cell to increase the level of details of our simulations. The validation of the model starts with the post mortem analysis of real cells to determine the most important values, for examples thickness of the active material. Another intention of this simulation is the implementation of simplified on-line model to improve accuracy of BMS models.

3. Electrical Simulation

The next step of multiphysics simulation approach requires understanding of the flow of current in electrode foils. Today, battery cells are equipped with some coated metal foils as voltage tap. Aluminium is use for the cathode and copper for the anode. Every chemical element has a characteristic potential to the standard hydrogen potential (electrochemical series). In Bipolar batteries cannot use this standard setup due to the dissolving of aluminium and copper induced by the different electrochemical series. A bipolar battery requires the use of a material with higher electrochemical series of both active materials.

Conductive polymer foil can be seen as an alternative solution since it works with both voltage areas of the anode and cathode. The disadvantage of a polymer foil is the low electrical conductivity in all dimensions (X = 150 S/m, Y = 56 S/m, Z = 5 S/m). This polymer foil is provided from our partner Leibniz Institute of Polymer Research Dresden (IPF).

The goal of the simulation is to evaluate the voltage drop of the polymer foil considering an anisotropic conductivity from the cell. This will allow an optimization of the current flow inside the cell and the definition of the necessary electrical conductivity to reduce the losses inside the cell. Designing a bipolar battery requires the definition of two load cases. While a standard battery cell requires only one load case because the current is flowing on one single point only, the stacked architecture of the bipolar battery requires the consideration of the following cases:

Case 1: High current flow (until 300 A) through the cell in orthogonal to plan direction

In a bipolar cell, the electrical conductivity can be low, but the area is large. The calculation can be estimated with the Ohm's law.

Case 2: Balancing of the cells in plane direction

The balancing between cells appears when small potential differences are observed between cells. The reasons of this unbalanced state is mostly due to the variation of the production and to the variation of ageing of the cells. During balancing phases, the current is low with 100 mA. The important values are the in-plane conductivity of the foil and its thickness. The calculation of the voltage drop of the foil requires a two dimensional simulation.

The structure of the simulated cell is shown at Figure 5.Our simulations are related to the second load case. This case is relevant for the dimensioning of the polymer foil. The difference between the electrical conductivity of a metal foil and a polymer foil is 10^6 S/m. The cell consists of three active material parts, conducting foil and contacts. The active material has a thickness of 150 µm, it is simplified and modelled as a resistive loss with 1 mOhm. The value of this loss is calculated with the electrochemical simulation model detailed in chapter 2. The current input and output is defined in opposite side of the bipolar cell. A metallic material is used for the contacts to ensure a solid connection to the outside of the cell. The trickiness is the same as the conducting foil within 100 µm. This setup represents the worst-case scenario with the maximum voltage drop since the current flows over the longest way between the contacts.

The conducting foil represents the polymer foil. The thickness of this foil is thicker to conventional current collector thickness about 20 µm. This was the first version of the foil. The on-going research working at thinner foil up to the conventional ones. Due to the extrusion process to produce the polymer foil, it has different electrical conductivity in X and Y dimension. The conductivity of the polymer is modified with conductive additives with a defined concentration. It is possible to increase the conductivity but the polymer material then cannot be extruded to a foil. An example of this is the highly filled plastics bipolar plates used for fuels cells.

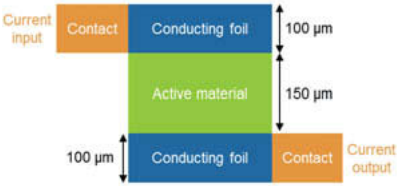

Figure 5 Structure of Battery Cell for electrical simulation

The simulation is built up in different stages as shown in Figure 6. The first simulation step, highlighted in yellow circle, is a mathematical one-dimensional simulation considering an isotropic conductivity with the Ohm's law. The boundary conditions of the equations used in our model are only valid for flat designs. Our model uses a simplification of the current output, by replacing the small the terminal (orange part of Figure 6 up-middle and up-right), with a larger surface over the complete length of the cell (orange part of Figure 6 up-left). The next steps, highlighted in green and blue, are simulated using JMAG. This tool is originally used to simulate electromagnet circuits for electrical motors and solenoids in two- and three-dimensions. All simulations are using a three dimensional model. The first step is to build up an equivalent simulation with a current tap and isotropic conductivity. The tool JMAG has no embedded option to implement this anisotropy. An alternative is to define two different areas as geometric equivalent circuit model, each with a different conductivity. A small area with a high conductivity and a larger area with a small conductivity. Figure 7 shows structure of the anisotropic conductivity. The implementation consists of 11 areas with a high and low conductivity (the small area is not directly visible). The vertical lines in the figure define the separated areas. The combination of these conductivities results in the total conductivity of the polymer foil.

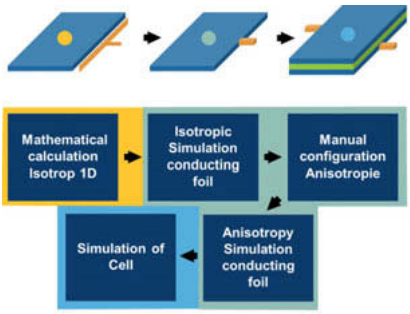

Figure 6 Simulation development of anisotropic conductivity

The final simulation model is made out of a combination of the structure shown on Figure 5 and the anisotropic conductivity with all-important parts (contacts, active material, current collector). The results of electrical simulation from load case two is shown on Figure 7. The figure shows the voltage drop from one tap to the other. The cell is depicted from the top view. The maximum voltage difference in this simulation is up to 16 V for an active area of 1.5 m² and current of 100 mA. The bottom tab with the blue colour is the ground potential (0 V). The top tab with the red colour is the highest potential (16 V). Our aim is to reach homogeneous SOC distribution during balancing and 100 mV voltage drop would be a first target. This makes it necessary to modify the conductivity of the polymer foil in plan direction.

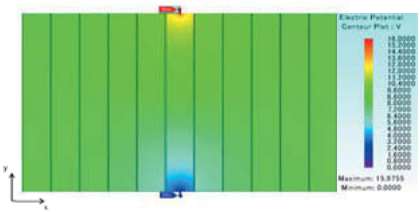

Figure 7 result anisotropy simulation of the Cell

One possible modification is the addition of a thin metal coating on the surface of the polymer foil. This thin metal layer with significantly higher conductivity reduces the voltage drop. With some studys is the polymer foil modified with a thin nickel layer on both sides. The isotropy of conductivity increases in plan direction with a higher conductivity by factor 5.

The ideal conductivity for the bipolar battery with a polymer foil has not been identified yet. This electrical simulation offers the possibility to use new innovative materials to evaluate the feasibility and performance of different concepts, including the anisotropic properties of the materials

4. Thermal Propagation Simulation

The two first steps of our multiphysics simulation describe, first, the chemical processes involved inside the cell, then, the electrical conductivity of different material combinations. The last step of our simulation process is related to the simulation of the cell-to-cell thermal propagation. For the simulation are used some prismatic PHEV 2 cells. The cells are assembled in a module. The homologation of a cell or a full battery system requires carrying out some critical safety-related tests based on several regulation like:

- UN38.3 Transportation tests
- United Nations Economic Commission for Europe (UNECE) R100
- Global Technical Regulation (GTR Nr.20)

In the regulations are defined many different tests. These tests are divided in three parts, mechanical, electrical and thermal. Mechanical test can be, for example, crush or vibration tests. Electrical tests can be short circuit or overcharge and thermal tests are over-temperature and the thermal propagation. Similar test are defined in different regulations, with different boundary conditions.

For homologation in the European Union, the UNECE R100 is compulsory. The global regulations of the UN38.3 and GTR are partially assumed in the regional standards. The thermal propagation test is actually not implanted in the ECE regulation. It is defined in Global Technical Regulation (GTR) No. 20, related to electrical vehicle as a passenger car and heavy-duty vehicles. In other regulations, this test is planned to be implemented for 2021. The thermal propagation test is realized by simulating a cell with an internal short circuit, which leads to a thermal runaway situation. The thermal propagation to the next cells is observed. Most of used cells today have a flammable liquid electrolyte. At vehicle level, the test is passed if the emergency time to leave the car (egress time) for the passengers is lower than five minutes.

Using thermal propagation simulation allows to optimize the mechanical design of the battery housing, the module design and the cell material for a safer system to reach faster homologation with less prototypes.

The Figure 8 shows a simplified model of a one-dimensional thermal model with four cells. The cells are simplified to a thermal mass with mean values of thermal capacity and conductivity. It is also possible to simulate the cell with all active layers, but the complexity increases dramatically.

All cells are coupled together. The thermal transfer modes of the heat are the convection, radiation and conduction in all simulations. The whole model does not consider flame propagation simulation. The thermal conduction is split into three types: cell-to-cell, cell-to-busbar and cell-to-housing. These five heat transfers have different order of magnitudes. The most significant ones are the conduction transfers, which represent about 90 %. The radiation transfers are low due the small cell surface observed (5 %) and the convection is least about a closed box. About 55 % of the released energy from the cell is transferred as cell-to-cell conduction. The distance between the cells is very limited and has a good thermal connection. The next most influencing transfer is cell-to-housing conductive transfer (24 %). The housing of the battery system is produced with metal (high thermal conductivity) and the cooling system has a good connection to the housing.

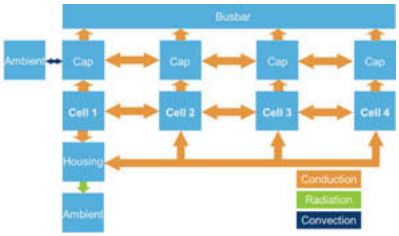

Figure 8 Thermal 1D Model of cell module

The released energy in a thermal propagation case is 10 times higher than the stored electrical energy. The higher energy is justified with the Arrhenius equation [8] of the chemical reaction. The active material and the components from the electrolyte have some decomposition over a critical temperature.

An example of a simulation is show at Figure 9. This simulation shows the thermal propagation of a model composed of 3 cells in the first 1000 s. The simulation model is based on Figure 8. The figure describe the cell temperature and pressure progress over the time. All cells have an overpressure valve integrated. The implementation of the valve is different depending on the cell type: pouch-cells use pouch pack sealing, while round- and prismatic cells use perforated thin metal plate.

In most cases, if the temperatures of the cell gets higher than 50 °C the deposition of electrolyte and a gas formation start. The inner cell pressure grows up to a critical value and the valve opens at around 1.6 – 1.8 bar and releases the gases. The gases are flammable and toxic, and must be safely drained of the outside of the battery pack and car in the later application.

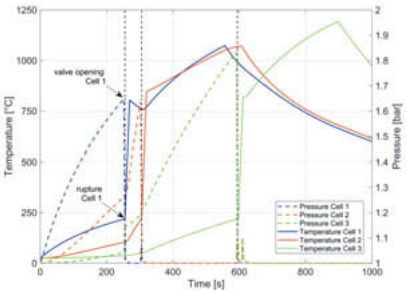

Figure 9 Thermal progress of cell temperatur

The thermal runaway is starting at a temparature of around 240 °C. The first cell valve opens after 250 s. The moment define the start of the 5 minutes delay allowed by the regulation. The temperature is rising from 250 °C up to 800 °C. The rupture of the cell two is 50 s after the first cell. The maximum temperature is more than 1000 °C of both cell before the cell three comes to rupture. At this temperature level, the aluminium components start melting. The simulation allows the implementation of thermal insulators and alternative materials to reduce the maximum temperature.

4. Conclusion

This paper gives an overview of the opportunities offered by our multiphysics simulation approach to optimize battery design. The simulation starts from the inside of the cell with the electro chemistry, to simulate the dynamical properties of a cell with a higher precision. The accuracy of the simulation model has been validated with two other commercial tools. The next simulation stage is the electrical simulation, with alternative bipolar foil with anisotropic conductivity. Finally, the last simulation stage is focused on thermal propagation and the investigation on levers to meet upcoming safety related regulations. Most of our simulations were focused on bipolar battery concept, but can be adapted to a variety of materials, geometries and requirements.

5. Acknowledgement

We would like to thank our project partners Thyssenkrupp System Engineering and Fraunhofer IKTS, together with all other project partners. We would also like to thank the European regional developing fund of saxony, the Ministry for education and research and the Ministry for economy affairs and energy for funding this project.

7. References

[1] Marc Doyle, Thomas F. Fuller, and John Newman. Modeling of galvanostatic charge and discharge of the lithium/polymer/insertion cell. Journal of The Electrochemical Society, 140(6):1526–1533, 1993.

[2] Thomas F. Fuller, Marc Doyle, and John Newman. Simulation and optimization of the dual lithium ion insertioncell. Journal of The Electrochemical Society, 141(1):1–10, 1994

[3] Kinson C. Kam, Apurva Mehta, John T. Heron, and Marca M. Doeff. Electrochemical and physical properties of ti-substituted layered nickel manganese cobalt oxide (nmc) cathode materials. Journal of The Electrochemical Society, 159(8):A1383–A1392, 2012

[4] Thanh-Son Dao, Chandrika P. Vyasarayani, and John McPhee. Simplification and order reduction of lithiumion battery model based on porous-electrode theory. Journal of Power Sources, 198:329 – 337, 2012

[5] E. Prada, D. Di Domenico, Y. Creff, J. Bernard, V. Sauvant-Moynot, and F. Huet. Simplified electrochemical and thermal model of lifepo4-graphite li-ion batteries for fast charge applications. Journal of The Electrochemical Society, 159(9):A1508–A1519, 2012

[6] Larsson, F.; Mellander, B.-E. Abuse by external heating, overcharge and short circuiting of commercial lithium-ion battery cells- J Electrochemical Society 2014, 161, A1611-1617

[7] James G. Quintiere, Sean B. Crowley, Richard N. Walters, Richard E. Lyon, and David Blake Fire Hazards of Lithium Batteries, 2016, NTIS), Springfield, Virginia 22161

[8] Fredrik Larsson, Petra Andersson, Bengt-Erik Mellander 1 Lithium-Ion Battery Aspects on Fires in Electrified Vehicles on the Basis of Experimental Abuse Tests, Batteries 2016, 2(2), 9

8. Glossary

BMS *Battery Management System*

DEC *Diethyl carbonate*

EC *Ethylene carbonate*

ECM *Electro chemical model*

EMBATT *CHASSIS EMBEDDED ENERGY*

eSPM *extended Single particle model*

GTR Global Technical Regulation

HV *High Voltage*

IAV *Ingenieurgesellschaft Auto und Verkehr*

IKTS *Fraunhofer Institute for Ceramic Technologies and Materials*

IPF *Leibniz Institute of Polymer Research Dresden*

NCM *Lithium nickel cobalt manganese oxide*

P2D *Pseudo-two-Dimensional*

SOC *State of Charge*

SPM *Single particle model*

UN *United Nations*

UNECE *United Nations Economic Commission for Europe*

A new generation of thermal fluid technology for high performance charging of electric vehicles

How new thermal fluids can enhance battery performance in EVs

Dr. **Volker Null**, Shell Global Solutions (Deutschland) GmbH, Hamburg

Zusammenfassung

Batterieladezeit ist eine der Hauptsorgen von Konsumenten, die überlegen ein EV zu kaufen. Der Trend zu immer kürzeren Batterieladezeiten macht ein leistungsfähigeres Thermomanagement erforderlich. Mit CFD Modellierungen untersuchten wir, wie sich konventionelle Kühlkonzepte mit Glykol/Wasser mit immersiven Kühldesigns vergleichen. Mit einem Partner entwickelten wir einen einzigartigen Demonstrator für Batteriemodule, um eine neue Generation Fluide zu untersuchen und um die CFD Modellierung mit experimentellen Daten zu validieren. Die Sicherheitsperformance neuer Fluide wurde auf Modulebene erfolgreich mit Partnern in der Industrie durch Heizdrahttest und Nagelpenetration bestätigt. Diese neue Generation von Thermal Fluiden hat das Potential, die Systemintegration mit anderen Komponenten neu zu denken und effektivere Ingenieurslösungen für die nächste Generation von elektrischen Fahrzeugen zu finden.

Abstract

Battery charging time is one of the top concerns of consumers who consider buying an EV. The trend to ever shorter time for recharging of batteries will require a step change in thermal management performance. We studied how conventional cooling concepts with water/glycol compare to immersive cooling designs with CFD modelling. With a partner we developed a unique battery module demonstrator to assess a new generation of thermal fluids and to validate CFD modelling with experimental data. The safety performance of the new fluids was tested at module level successfully in collaboration with industry partners in nail penetration and heat wire tests. This new generation of thermal fluids offers the potential to rethink system integration with other components and to find more effective engineering solutions for the next generation of electric vehicles.

Introduction

By 2050, more than 50% of passenger car vehicles are likely to use EV architectures and most will have lithium ion batteries. The dominant charging option will probably be domestically focussed and be sufficient to meet the needs of most drivers. But this may be impractical for some people, especially those for whom off-road parking is not an option, and it does not satisfy the needs of people undertaking longer-range driving for whom high-power, fast charging on the go will be required. Also, many EV buyers crave a fast charging experience similar to an ICE vehicle even if their actual requirements may not need fast charging in most cases.

An increased rate of charging demands an increase in the charging current and/or the voltage. Because the batteries have a significant internal resistance, the waste heat that high current charging generates is substantial: sometimes 20 kW or more. If this heat cannot dissipate effectively, the individual battery cells will be exposed to too high a temperature and suffer irreversible deterioration. Very careful thermal management is, therefore, essential to avoid this and hold local cell temperature at 50°c or lower.

Consequently, EV battery management systems are sophisticated and can monitor temperatures of individual cells and control charging rates to cap peak temperatures. Overall rates of charging are thus influenced by temperature excursions within individual cells such that charging rates and charging times can be slowed considerable.

The simplest and cheapest cooling technologies utilise air, but these are becoming obsolete as the demand for increased energy density rise. More advanced thermal management schemes are appearing that use water/glycol mixtures [1, 2], phase change materials or immersive coolants [3, 4].

Tesla has opted for a water/glycol system in which the coolant passes through a snake-like series of pipes in intimate contact with about 11% of the cell surfaces. This has proved effective enough to support Tesla´s supercharging scheme but is limited by the thermal resistance created by the pipe walls between the cell surface and the coolant [5].

The phase-change materials utilised in some systems are an effective means of taking up heat when they change from solid to liquid state. However, solid phase-change material is limited by its melting temperature so may be unsuitable for thermal management. It could melt at high ambient temperatures without any heat from the battery and thus fail to control cell temperature level and uniformity effectively. Evaporative cooling is another means of phase change material. While this is used in some of the current battery thermal management systems, it has been observed that the pressure may rise significantly, thus leading to leaks and loss of thermal fluid or gas respectively.

Immersive cooling is under development for the next generation of electric vehicles. Here a fluid with good dielectric properties surrounds the individual battery cells to provide intimate heat transfer. It has already been shown that immersive cooling can help to increase power and energy density ratios and significantly enhance cell durability. Furthermore, enhanced immersive cooling using a non-flammable, hydrofluoroether is being used in current Formula E racing applications.

Development of next generation thermal fluid for immersive thermal management

Shell is currently developing thermal fluid technology aimed to match the needs for immersive cooling utilizing Shell proprietary Gas-to-Liquid base oil technology (GTL). In this synthetic process, methane is converted to liquid GTL products.

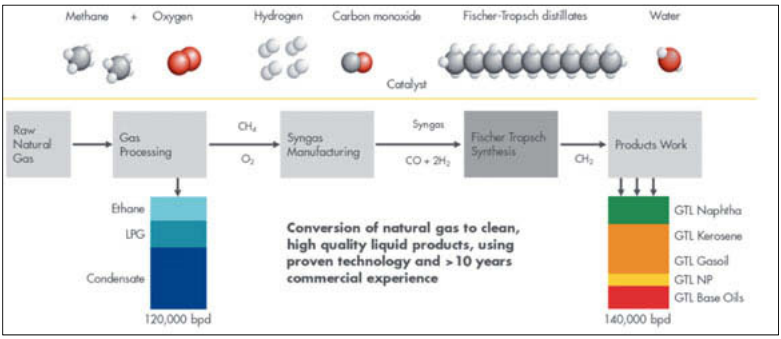

Fig. 1: Shell Gas-to-Liquid process to convert natural gas (Methane) into GTL products

Methane is reacted with oxygen to create synthesis gas, then the synthesis gas is converted in a Fischer-Tropsch process into longchain hydrocarbons. Finally, the longchain hydrocarbons are hydrocracked and hydroisomerized and then distilled into a wide range of liquid GTL products, including feedstocks for the chemical industry, transport fuels and high purity base oils. Fig. 1 gives an overview of the Gas-to-Liquid process.

The use of GTL base oil technology provides significant performance benefits for the development of thermal fluids. GTL base oils are virtually free of Sulphur and are therefore intrinsically non-corrosive. They also respond very well to antioxidants and allow to formulate thermal fluids with outstanding oxidative and thermal stability. This can result in thermal fluids with greatly extended service life and fill-for-life performance.

Comparison of different fluid technologies for immersive cooling

Conventional water/glycol coolants are conductive for electric current and are no option for immersive cooling. Several types of dielectric fluids are suitable for immersive cooling technologies. Important criteria for the fluid selection are thermodynamic properties, material compatibility weight and flammability. Cost is also an important factor to enable implementation of this promising technology. Fig. 2 shows the ranking of hydrofluoroether, silicon oil and the GTL based Shell Thermal Fluid E5 TM in five key criteria. As non-flammable fluid, the hydrofluoroether ranks best in flammability performance and falls behind in the other four criteria. Silicon oil is another fluid option, it ranks medium in all five parameters. The GTL based Shell Thermal Fluid E5 TM ranks medium in flammability and best in the other four performance criteria.

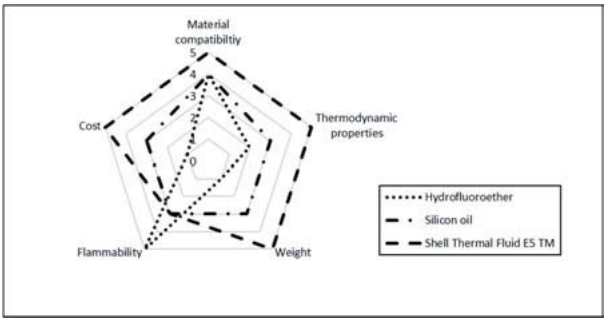

Fig. 2: Comparison of different fluid types for immersive cooling technology against five key requirements. 5 = best, 0 = worst

The lower density of the GTL based Shell Thermal Fluid E5 TM compared to hydrofluoroether results in much lower weight of the fluid. With an estimated volume of eight Litres fluid for the battery pack per car, the resulting weight is 14,4 kg for hydrofluoroether and 6,4 kg for Shell Thermal Fluid E5 TM. In direct comparison, the GTL based Shell Thermal Fluid E5 TM saves 8 kg in weight.

Good material compatibility of the fluid is another key requirement, especially with elastomeric seals, gaskets etc. and various metals. The interaction between the fluid and material is twofold. Firstly, it is important that the fluid has minimal impact on the material properties and the material retains its intended functional performance. Secondly the material may impact the fluid and it is equally important that the fluid retains its dielectric properties. The compatibility

of Shell Thermal Fluid E5 TM 410 has been successfully tested with many material types such as several metals and polymer types in lab testing.

CFD modelling of indirect and direct cooling systems

At fluid level, water/glycol (e.g. Shell HD Coolant GF Pre-Diluted) has better thermodynamic properties than dielectric fluids such as hydrofluoroether and Shell Thermal Fluid E5 TM 410 as shown in Table 1.

Table 1: Comparison of physical and thermodynamic properties of Water/Glycol 50/50, hydrofluoroether [6] and Shell Thermal Fluid E5 TM 410

Property	Method	Unit	Water/Glycol 50/50	Hydrofluoroether	Shell Thermal Fluid E5 TM 410
Kinematic viscosity @ 20°C	ISO 3104	mm2/s	4,5	0,7	19,4
Pour Point	ISO 3016	°C	-35	-38	<-60
Density @ 20°C	ISO 12185	kg/m3	1080	1660	805
Vapour pressure @ 25°C		kPa		6	0,00002
Flash point PM	ISO 2719	°C	111	-	190
Thermal conductivity @ 25°C	calculated	W/m*K	0,38	1,14	0,143
Specific heat capacity @ 25°C	ASTM D1269mod	J/kg*K	3,31	1,14	2,1
Electrical conductivity @25°C	ASTM D2624 / IEC 60247	nS/m	50000	0,5	0,001

In order to assess the cooling effectiveness of indirect systems with water/glycol and direct systems with dielectric fluids it is important to compare at system level. Computer fluid dynamic modelling (CFD) is widely used for this purpose.

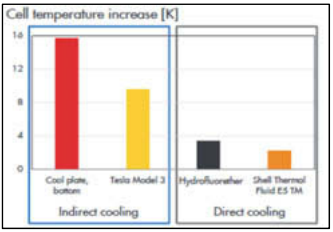

Fig. 3: Temperature differences between cell and fluid inlet from single cell CFD modelling for indirect cooling with glycol water 50/50 and for direct cooling comparing hydrofluoroether and Shell Thermal Fluid E5 TM 410 [6]

Hermann and Boehm [7] modelled and tested these GTL fluids alongside other fluids in immersive battery designs in a comparative study for ultrafast charging with conventional and modified indirect system. The CFD modelling results with single cylindrical cells in these set-

ups are shown in Fig. 3. The results demonstrate the much more effective cooling of immersive designs resulting in significantly lower temperature difference between the maximum cell temperatures and the inlet temperature of the fluid. In this comparative study the GTL based Shell Thermal Fluid E5 TM 410 was reported with superior thermodynamic and cooling performance [7].

Shell assessed the cooling performance at module level with cylindrical cells with bottom cooling using glycol/water (50/50) coolant against an immersive design with Shell Thermal Fluid E5 TM. The heat generated by the cells was calculated with an electrochemical model at 2C charging rate. The modelled differences between maximum cell and inlet temperatures are shown in Fig. 4 for different flow rates. These results demonstrate that direct cooling is much more effective than indirect cooling and show also the excellent cooling performance of the GTL based Shell Thermal Fluid E5 TM.

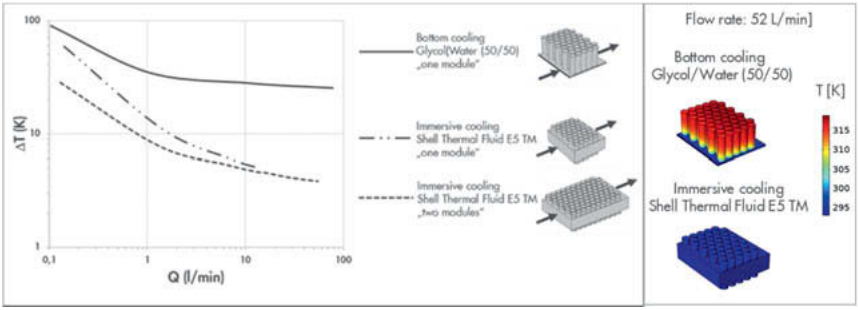

Fig. 4: Temperature differences between cell and fluid inlet at 2C charging rate (left) and temperature distribution (right) for modules with bottom cooling with Glycol/Water and immersive cooling with Shell Thermal Fluid E5 TM obtained by computed charging rates and coupled with a CFD model.

The results for bottom cooling with glycol water show, that is impossible to reach sufficiently low temperature levels, even at very high flow rates. Immersive cooling with Shell Thermal Fluid E5 TM is much more effective. With two modules combined to a small battery pack, the temperature can be controlled well at moderate flow rates. The temperature distribution within the cells of the module was found much more homogeneous and narrower. This can lead to longer battery life and better performance retention with immersive cooling.

New battery demonstrator rig to validate CFD modelling

A new battery demonstrator test rig with pouch cells in a module with tab cooling [8] has been developed and designed together with a partner and has recently been installed at the battery test stand at the Shell Technology Centre Hamburg. Equipped with several temperature sensors, it is used to gain experimental temperature profiles under different fluid flow conditions. The computational chemistry group at the Shell Technology Centre Bangalore computes with a single particle model the voltage and current profiles and models the temperature profile of the cells to validate the CFD model for this module design (Fig. 5).

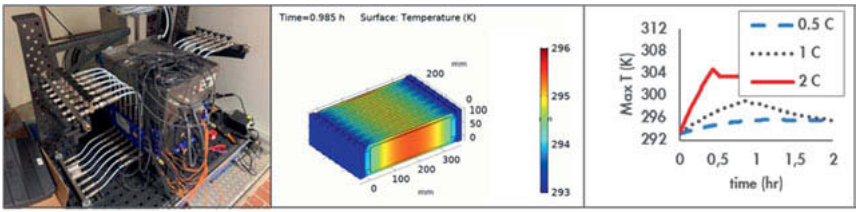

Fig. 5: Battery module test rig at Shell Technology Centre Hamburg (left) and temperature profile obtained with CFD model and coupled voltage and current particle (middle and right)

Abuse tests with the new thermal fluid types

The Shell Thermal Fluid E5 TM 410 consists of hydrocarbons and can start burning when ignited at fluid temperatures above the flash point. It is therefore mandatory to assess the safety performance of the fluid in battery modules under abuse conditions. Thermal runaway was triggered by nail penetration and in a second experiment by heating wire in one cell each of a battery pack consisting of two modules filled with Shell Thermal Fluid E5 TM 410 under static conditions (no oil flow) .Successful 'Pass' results were obtained in both experimental set-ups, that means no propagation to neighbouring cells and no toxic materials formed [9]. The maximum cell surface temperature at neighbour cells was measured as max 70°C in both experiments. Other OEMs also confirmed the safety performance of Shell Thermal Fluid E5 TM 410 under abuse conditions in their respective module designs. Some of these modules were equipped with pouch cell types.

These results confirm, that battery modules can be engineered to mitigate the fire and safety risks when using hydrocarbon based thermal fluids.

Potential to simplify the cooling circuit

The excellent cooling performance of Shell Thermal Fluid E5 TM 410 and the 'Pass' results in abuse tests make these fluids potent candidates for immersive battery cooling and beyond. This approach could allow to reach a new level of performance and to rethink vehicle integration for the next generation of electric vehicles with greatly improved performance and faster re-charging times.

One single fluid might be used to firstly cool the battery system, then the inverter and subsequently also the e-motor (Fig. 6). The heated fluid would then release the heat energy in a heat exchanger and be pumped again into the cooling circuit.

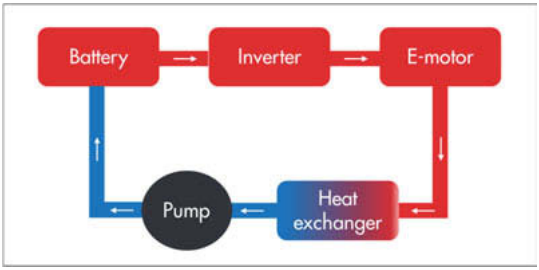

Fig. 6: Single cooling circuit one fluid for direct battery, inverter and e-motor cooling

Conclusions

Fast charging performance of battery systems needs to improve significantly to meet end customer expectations. Faster charging means higher currents, which then generates more waste heat and consequently requires more effective thermal management of the battery. Current battery cooling with glycol/water coolant can not sufficiently control the battery temperatures which then can lead to reduced battery life. Direct cooling offers a superior solution for fast charging of EV batteries.

Glycol/water is conductive and therefore not suitable for direct contact with the electrical system. Shell started to develop a new generation of thermal fluids which are intended for direct cooling technologies.

Conventional cooling concepts with water/glycol were evaluated against immersive cooling designs with CFD modelling. This demonstrated the superior cooling performance of immersive designs under fast charging conditions. It showed also a more homogeneous and narrower temperature distribution of the battery cells, which can lead to longer battery life.

In order to address safety performance of direct cooled batteries with hydrocarbon fluids, Shell collaborated with industry partners to test the performance at module level in heating wire and nail penetration tests. The data show, that successful 'Pass' results can be obtained with different module types and cell formats in these critical tests. This confirms that engineering solutions can be realized to fully exploit the potential of the new fluid types.

The use of thermal fluids for e-motor and inverter cooling offers the potential to combine these systems in a cycle with the battery system. This can enable automotive engineers to rethink vehicle integration and to reach a new level of performance for the next generation of electric vehicles with much shorter recharging times.

References

[1] S. Rajadurai, S. Ananth, Battery Thermal Management in Electrical Vehicle - Review Article. International Journal of Innovative Science, Engineering & Technology 2020, 7: 290-306

[2] Z. Shang, H. Qi, X. Liu, C. Ouyang, Y. Wang, Structural optimization of lithium-ion battery for improving thermal performance based on a liquid cooling system. International Journal of Heat and Mass Transfer 2019, 130: 33-41

[3] S. Wang, W. Wu, K. Chen, S. Hong, Y. Lai, A critical review of battery thermal performance and liquid based battery thermal management. Energy Conversion and Management 2019, **182:** 262-281

[4] Y. Deng, C. Feng, J. E, H. Zhu, J. Chen, M. Wen, et al. Effects of different coolants and cooling strategies on the cooling performance of the power lithium ion battery system: A review. Applied Thermal Engineering 2018, **142:** 10-29

[5] C. Zhao, W. Cao, T. Dong, F. Jiang, Thermal behavior study of discharging/charging cylindrical lithium-ion battery module cooled by channeled liquid flow. International Journal of Heat and Mass Transfer 2018, **120:** 751-762

[6] Novec: 3M™ Novec™ 7300 Engineered Fluid. Technical Data Sheet

[7] P. Herrmann, A. Boehm, Next Generation Module for Ultra Fast Charging. VDI Wissensforum 2019

[8] H. Heimes, A. Kampker, A. Mohsseni, F. Maltoni, J. Biederbeck, Cell Tab Cooling System for Battery Life Extension. 18th IEEE ITHERM Conference 2019**:** 1125

[9] H. Kastler, Effective Battery Design and Integration of Cylindrical Cells for High Power Applications. 18th CTI SYMPOSIUM in Berlin 2019

VDI Wissensforum

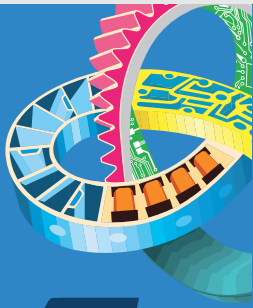

International Conference
EDrive

ISBN 978-3-18-092373-4